

The Commonwealth of Massachusetts
Energy Facilities Siting Board

EFSB 21-02

**DIRECT PREFILED TESTIMONY OF
JOHN HINCKLEY, Q.E.P.**

ON BEHALF OF INTERVENOR SAVE THE PINE BARRENS

EXHIBIT STPB-JH-1

September 29, 2022

TABLE OF CONTENTS

I.	Introduction.....	3
II.	Purpose of Testimony	4
III.	Analysis of Potential Air Emissions and Dispersion Due to a Thermal Runaway Event at the Proposed Facility	5
	A. Scope of Analysis	5
	B. Review of Thermal Runaway Events at Other Facilities.....	9
	C. Review of EFSB Docket Documents.....	10
	D. Air Pollutant Literature Review.....	12
	E. Potential Thermal Runaway Event Emissions Information.....	12
	F. Meteorological Data Review	14
IV.	Professional Opinions.....	16
V.	Conclusion	17

1 **I. Introduction**

2 **Q. Please state your name.**

3 A. My name is John Hinckley.

4 **Q. Please state your occupation, current place of employment, and business**
5 **address.**

6 A. I am a Senior Managing Consultant with ALL4 LLC (ALL4), a nationally
7 recognized environmental consulting firm with expertise in air quality and other
8 environmental media. My business address is 2393 Kimberton Road, Kimberton, PA
9 19442, but I usually work remotely in Vermont.

10 **Q. Please describe your educational background and relevant work experiences.**

11 A. I earned a B.S. in Natural Resources from the University of Vermont in 1994 and
12 an M.S. in Environmental Science & Engineering from the University of Virginia in
13 1998. I am certified as a Qualified Environmental Professional (“Q.E.P.”) in the area of
14 air pollution control by the Institute for Professional Environmental Practice (“IPEP”). I
15 also have specialized training from the U.S. EPA Air Pollution Training Institute and in
16 air quality modeling. I have over 22 years of experience in air emissions permitting, air
17 dispersion modeling, accidental emissions release modeling, air toxics evaluations, air
18 emissions reporting (including greenhouse gas reporting), and air pollution control
19 technology assessments. My curriculum vitae is attached to my testimony as Exhibit 1.

20 **Q. Have you previously testified in any formal hearing before regulatory**
21 **bodies?**

1 A. I have testified in in two New York State Department of Environmental
2 Conservation (“NYSDEC”) adjudicatory hearings, two Massachusetts Department of
3 Environmental Protection (“MassDEP”) adjudicatory hearings, two Vermont
4 Environmental Court proceedings, and in at least five Vermont Act 250 District
5 Commission hearings.

6 **II. Purpose of Testimony**

7 **Q. Are you aware of Cranberry Point Energy Storage LLC’s (“Cranberry**
8 **Point”), pending petition before the Energy Facilities Siting Board (“Siting Board”)**
9 **to construct a battery energy storage system (“BESS”) facility in the Town of**
10 **Carver Massachusetts (the “Project” or “Facility”), docket EFSB21-02?**

11 A. Yes.

12 **Q. What is the purpose of your testimony?**

13 A. I am providing this testimony to the Siting Board to present my analysis and
14 expert opinions concerning ambient (*i.e.*, outdoor) air pollution produced by potential
15 emergency thermal runaway events (*i.e.*, fires) at the Facility.

16 **Q. How is your testimony organized?**

17 A. My testimony is provided in Section III below with supporting information in the
18 attached exhibits. Section III testimony is organized into the following sections:

- 19 1. Summary of recent thermal runaway events at other facilities.
20 2. Comments on documents submitted to the Siting Board.

- 1 3. Review of literature sources addressing emissions from lithium-ion battery
- 2 fires.
- 3 4. Description of potential air pollutant emissions from thermal runaway events.
- 4 5. Summary of local meteorological data and prevailing wind patterns.

5 **Q. Are you presenting any exhibits in addition to your testimony and the**
6 **curriculum vitae you previously identified?**

7 A. My list of exhibits and curriculum vitae are as follows:

- 8 1. Curriculum Vitae
- 9 2. EFSB Petition and Analysis (EFSB Exhibit 2)
- 10 3. Draft Emergency Response Plan (EFSB Exhibit 16)
- 11 4. Table 1: Thermal Runaway Event Summary
- 12 5. Table 2: Emissions Summary Table
- 13 6. Thermal Runaway Event Emissions Literature Sources
- 14 7. Figure 1 – Stand Alone Wind Rose
- 15 8. Figure 2 – Wind Rose Superimposed on Study Area
- 16 9. Figure 3 – Proximity to Plymouth Municipal Airport

17 **III. Analysis of Potential Air Emissions and Dispersion Due**
18 **to a Thermal Runaway Event at the Proposed Facility**

19 **A. Scope of Analysis**

20 **Q. What were you and ALL4 asked to do?**

21 A. ALL4 was asked by Save the Pine Barrens (“STPB”) to evaluate potential air
22 quality impacts (Evaluation) resulting from air pollutants (or “air emissions”) that may be

1 released during a thermal runaway event at the proposed Facility, specifically a 150
2 megawatt (MW)/300 megawatt-hour (MWh) standalone BESS to be located in the Town
3 of Carver, MA.

4 **Q. What did you consider to be a thermal runaway event?**

5 A. For the purposes of this testimony, a thermal runaway event was assumed to be an
6 unintended (*i.e.*, emergency) event where lithium-ion batteries overheat and ignite,
7 thereby releasing various air pollutants (to be described later in this testimony) at levels
8 that can potentially be injurious to human health.

9 **Q. What did your Evaluation include?**

10 A. As part of the Evaluation, ALL4 conducted five analyses:

- 11 1. **Summary of Thermal Runaway Events at Other Facilities.** Developed a
12 summary table of recent thermal runaway events including, but not limited to,
13 the, facility location, facility size, dates when the event occurred, approximate
14 duration of thermal runaway event, and Internet sources.
- 15 2. **Review of documents submitted to the EFSB.** Reviewed and commented on
16 certain documents uploaded to the EFSB docket.
- 17 3. **Review of Thermal Runaway Event Literature.** Compiled and reviewed
18 literature describing the air pollutants that are potentially released during
19 lithium-ion battery combustion.
- 20 4. **Thermal Runaway Event Air Emissions.** Using information developed from
21 the literature review, ALL4 developed a list of air pollutants that could be
22 released during a thermal runaway event and that are regulated by MassDEP

1 and/or by the U.S. Environmental Protection Agency (U.S. EPA) as hazardous
2 air pollutants (HAP) and criteria pollutants for other types of air pollution
3 sources (*e.g.*, manufacturing plants, power plants). Refer to Table 2 (Exhibit
4 5) for a summary of these air pollutants.

5 **5. Meteorological Data Analysis.** Evaluated prevailing wind patterns. ALL4
6 compiled meteorological data from the Plymouth Municipal Airport from the
7 last five complete calendar years (2017 to 2021) to characterize prevailing
8 wind patterns (*i.e.*, wind speed and wind direction) at the Facility.

9 **Q. Could you explain in more detail why you performed these five tasks?**

10 A. As I will explain in my testimony, I found little to no data or analysis in the
11 documents submitted by Cranberry Point to the EFSB about the potential air pollutants
12 that could be released at the Facility in the event of a thermal runaway event. I therefore
13 had to develop an understanding of that potential risk, in the absence of data and analysis
14 from Cranberry Point.

15 I began by simply doing some recent historical research to see if other thermal
16 runaway events had occurred at facilities like this one to develop an understanding of
17 some of the characteristics of those events. As I will testify, I identified several recent
18 events, which varied in their characteristics.

19 Having established that thermal runaway events have occurred in the recent past, I
20 then analyzed certain of Cranberry Point's submissions into the EFSB docket, to
21 determine the data and analyses that Cranberry Point has presented to the EFSB
22 concerning a potential thermal runaway event. As I will testify, while I identified some

1 general statements acknowledging that a thermal runaway event could cause the release
2 of air pollutants, I did not see an extended discussion, analysis, or supporting data to
3 sufficiently understand the characteristics including the spatial extent of such an event.

4 Because of that lack of data and analysis, my next step was to review the available
5 literature to identify the air pollutants that could potentially be emitted if a thermal
6 runaway event were to occur at the Facility. I was most interested in and am limiting my
7 testimony to those pollutants that have been shown to cause adverse health effects by
8 being listed as either criteria pollutants, HAPs, or air toxics under either or both U.S.
9 EPA or MassDEP regulations.

10 Following that, I used the results of my literature review to create a list of the
11 potential air pollutants that could be released if a thermal runaway event were to occur at
12 the Facility. Refer to Table 2 (Exhibit 5) for the list of air pollutants.

13 Finally, I compiled meteorological data from the nearest suitable location to the
14 proposed site of the Facility. In this case, that was the Plymouth Municipal Airport. I
15 compiled that data to develop an understanding of how the air pollutants I identified for
16 my air pollutants list could potentially disperse if a thermal runaway event were to occur.

17 **Q. Why did you choose to do these five tasks?**

18 A. As described in more detail below, Cranberry Point's submission to the EFSB
19 acknowledges that a thermal runaway event could release air pollutants but does little to
20 explain or quantify the potential air quality risks to surrounding areas during thermal
21 runaway events. This highlights an unknown risk factor that the EFSB should consider
22 when evaluating Cranberry Point's petition. Therefore, the five tasks I described above

1 were undertaken to help understand and explain the nature of this potential risk and the
2 reasons why the EFSB should closely evaluate the data provided by Cranberry Point and
3 consider whether it is sufficient for the EFSB’s decision-making.

4 **B. Review of Thermal Runaway Events at Other Facilities**

5 **Q. What thermal runaway information did ALL4 compile?**

6 A. ALL4 compiled information concerning the characteristics of thermal runaway
7 events that have occurred at four similar facilities within the past three years. Please note
8 that this list is not intended to be exhaustive and additional thermal runaway events may
9 have occurred within this timeframe, which ALL4 did not identify. Details concerning
10 that research are set forth below; please refer to Table 1 (Exhibit 4) with documentation
11 for the sources of that information.

Facility	Location	Facility Size	Date	Duration
AES Corporation	Chandler, Arizona	10 MW	April, 2022	13 days
Neoen	Victoria, Australia	300 MW	July, 2021	Approximately 3 days
APS-Energy Storage Systems	Surprise, Arizona	2 MW	April 19, 2019	No specifics identified, appears to have been contained in less than one day.
Vista Energy Storage Facility	Moss Landing, California	300 MW	February 13, 2022 and September 4, 2022	Appears to have been contained in less than one day.

12

1 **C. Review of EFSB Docket Documents**

2 **Q. What did you learn from the documents you reviewed in the EFSB docket?**

3 A. My review focused on the EFSB Petition and Analysis (Exhibit 2) and the Draft
4 Emergency Response Plan (Exhibit 3). Both documents address air pollutant emissions
5 from the Facility. My comments regarding Exhibit 2 and Exhibit 3 are provided below.

6 **Exhibit 2.** Section 4.1 addresses air pollutant emissions and states the “*Project*
7 *will contribute near zero emissions. In fact, the Project may displace conventional*
8 *generation facilities and thereby reduce emission of carbon, particulates, and other*
9 *pollutants.*” While this statement may be accurate for normal operating conditions, the
10 document does not include, or reference corresponding information quantifying expected
11 air pollutant emissions that could potentially be released during a thermal runaway event,
12 which is not a normal operating condition.

13 **Exhibit 3.** The top of page 11 discusses the potential quantities and types of air
14 pollutants that may be released during a thermal runaway event. Page 11 states that:
15 “*There are five major risks posed by lithium-ion battery failures. They are electric shock,*
16 *arc flash, fire, explosion, and the by-product from off-gassing. During failure, a lithium-*
17 *ion battery may emit tens to hundreds of liters of off gas, and larger failures may emit*
18 *thousands of liters of gas.*” Page 11 also states “*Lithium-ion batteries release flammable*
19 *and toxic chemicals when subjected to electrical or physical damage, including fire.*
20 *Chemicals release can also pose an inhalation hazard.*”

21 The types of air emissions are ***partially*** identified in the middle of page 11 as
22 hydrogen, carbon, monoxide, carbon dioxide, methane, ethane, and other flammable

1 hydrocarbons. I say “partially” because the document does not say that it includes all
2 possible emissions that could be released. Further, Exhibit 3 provides the “typical
3 composition” that an off-gassing event “may” include.

4 Page 12, bullet (6), second sub-bullet describes the location of the closest
5 neighbor and provides a setback (*i.e.*, safety) distance of 650. “...*the closest proposed*
6 *battery enclosures are approximately 650' away, and are **sufficiently distant** such that*
7 *smoke or off-gas from the battery container are not expected to pose a risk.*” (emphasis
8 added) I was unable to identify information supporting the basis for the safety distance of
9 650 feet. Thus, while the document states that these neighbors are “sufficiently distant,” it
10 does not provide the information that was that was used to determine that 650 feet is an
11 adequate distance for the neighbors during a thermal runaway event.

12 Page 12, bullet (7) states that “*Full firefighter protective gear shall be worn in*
13 *any response to a fire and/or explosion event or any indication a fire may be present.*
14 *This shall include proper use of Self-Contained Breathing Apparatus (SCBA).*” While
15 SCBA gear may be worn for protection from many other types of fires (*e.g.*, burning
16 buildings), the requirement to wear SCBA gear suggests that the level of air pollutant
17 emissions that could be released during a thermal runaway event poses a potential
18 inhalation risk..

19 The last paragraph of page 15 to first paragraph of page 16 states “*Following*
20 *partial or complete consumption of the system by fire, batteries may continue to emit low*
21 *levels of flammable gases and dangerous levels of toxic gases for an extended period of*
22 *time. Continuous monitoring of gas levels in and around the incident location is*

1 *recommended to be conducted and use of mechanical ventilation may be utilized to*
2 *manage gas levels. Full firefighter PPE and SCBA shall be utilized until gas levels are*
3 *confirmed to be at a safe level.” This quote underscores the possibility that air pollutant*
4 *emissions may not be released over a short period of time and that their levels should be*
5 *monitored in ambient air following an event. I was unable to identify any documents that*
6 *describe monitoring equipment or protocols to be followed if such an event were to*
7 *occur.*

8 **D. Air Pollutant Literature Review**

9 **Q. What literature did you review concerning potential air pollutants that may**
10 **result from a thermal runaway event?**

11 A. There are many studies that have been performed to identify the types and
12 quantities of air pollutants released by lithium-ion batteries, which can be extrapolated to
13 thermal runaway events at battery storage facilities. Studies have been published by a
14 range of sources such as the U.S. Naval Research Laboratory (“U.S. NRL”), U.S.
15 Department of Energy (“U.S. DOE”), Tsinghua University (Beijing, China), and the
16 Energy and Environmental Science Journal (Royal Society of Chemistry). I have
17 included 13 documents that address potential thermal runaway emissions that are
18 collectively called Exhibit 6.

19 **E. Potential Thermal Runaway Event Emissions Information**

20 **Q. What did you use this literature to determine?**

1 A. As previously mentioned, I found it notable that Cranberry Point did describe
2 emissions related to a thermal runaway event in the EFSB docketed documents that I
3 reviewed. Therefore, I used my literature review to create a list of potential air pollutants
4 that could be released if such an event were to occur. Given this is based on a literature
5 review and that certain Facility documents such as Safety Data Sheets (SDS) were not
6 available at the time of my review, I cannot say with certainty either that all these
7 pollutants would be released or that other pollutants that I have not identified would not
8 be released. I believe that this list is nonetheless useful to highlight the importance of
9 having such a list and why the absence of one in Cranberry Point's documents is both
10 notable and of relevant to the EFSB's decision-making process. These documents were
11 used to develop the emissions information described below and summarized in Table 2
12 (Exhibit 4).

13 **Q. Please describe the air pollutants list you created.**

14 A. The air pollutants that could be released during a thermal runaway event are
15 particulate or gaseous in nature. The air pollutant list developed by ALL4 is limited to air
16 pollutants that are regulated by the U.S. EPA and MassDEP for other facilities that are
17 subject to Federal and Commonwealth of Massachusetts air pollution control regulations
18 respectively. While U.S. EPA and MassDEP do not necessarily regulate thermal runaway
19 emissions from battery storage facilities, these air pollutants are regulated from other
20 types of facilities (*e.g.*, fossil power plants, manufacturing plants, and
21 colleges/universities) and are regulated because they can adversely affect human health.

1 The emissions information includes criteria pollutants¹ and HAP² that are
2 regulated by both U.S. EPA and MassDEP and air toxics³ that are regulated only by
3 MassDEP. Refer to Table 3 (Exhibit 5) for the list of air pollutants and their respective
4 pollutant category and the primary reference used for that pollutant.

5 While I am not myself an expert in the potential adverse health effects of these
6 pollutants, the U.S. EPA and other regulatory agencies provide such information. The
7 U.S. EPA's Health Effects Notebook for Hazardous Air Pollutants can be accessed
8 through this link: [https://www.epa.gov/haps/health-effects-notebook-hazardous-air-](https://www.epa.gov/haps/health-effects-notebook-hazardous-air-pollutants)
9 pollutants.

10 **F. Meteorological Data Review**

11 **Q. Please describe the meteorological data that you developed.**

12 A. ALL4 developed meteorological data in a format suitable for air dispersion
13 modeling (*i.e.*, air quality modeling), which is required by MassDEP in some
14 circumstances for certain emissions sources.

15 **Q. Why did you develop that data?**

16 A. It is my understanding that air quality modeling has not been performed, nor has
17 any regulatory agency such as MassDEP required it to be performed. But even in the

¹ Available at: <https://www.epa.gov/criteria-air-pollutants/naaqs-table>

² Available at: [https://www.epa.gov/haps/initial-list-hazardous-air-pollutants-](https://www.epa.gov/haps/initial-list-hazardous-air-pollutants-modifications)
modifications

³ <https://www.mass.gov/service-details/massdep-ambient-air-toxics-guidelines>

1 absence of such a requirement, understanding the prevailing wind patterns by evaluating
2 meteorological data helps to show where air pollutants would potentially travel if a
3 thermal runaway event were to occur. This meteorological data in tandem with the air
4 pollutants list helps to illustrate that if a thermal runaway event were to occur at the
5 Facility, air pollutants could travel in all directions away from the Facility.

6 **Q. Where did you get these data?**

7 A. ALL4 processed meteorological data from the closest weather recording station
8 that can be considered representative of the weather conditions at the Facility. Therefore,
9 ALL4 developed surface hourly weather data (“Surface Data”) from the Plymouth
10 Municipal Airport surface observation station, located approximately 3.1 miles from the
11 Facility. Refer to Exhibit 8 for a map showing the proximity of the Plymouth Municipal
12 Airport to the Facility. As customary for air dispersion modeling, ALL4 processed upper
13 air data from the Gray, Maine upper air station (“Upper Air Data”).

14 **Q. Please describe the quality of these data.**

15 A. Data was available for at least 90% of the five-year period; therefore, 43,848
16 hours of data were developed. This level of data availability is suitable for determining
17 prevailing wind speeds and directions.

18 **Q. What did you do with these data?**

19 A. ALL4 used the Surface Data to develop a Wind Rose. A Wind Rose is a graphical
20 representation of wind speed and direction. As shown in Exhibit 7 and Exhibit 8 wind
21 speed and direction are illustrated with pie wedges. The direction the wind is blowing
22 towards is indicated by the narrow end of the wedge.

1 **Q. What did those Wind Roses show?**

2 A. As shown in both figures, wind blows from all directions; however, there are
3 three prevailing wind directions: from the southwest to the northeast, from the northeast
4 to the southwest, and from the west-northwest towards the east-southeast. According to
5 Exhibit 8, wind speeds range from approximately one mile per hour (mph) to greater than
6 25 mph. The approximate time when there is no observable wind speed (i.e., calms) is
7 1.38% of the time; therefore, there are measurable winds approximately 98.6% of the
8 time.

9 Exhibit 8 shows the wind rose superimposed on an aerial image of the Facility
10 location and the surrounding area. The surrounding area includes residential areas,
11 cranberry bogs, and the Carver Elementary School. Given that measurable winds occur
12 most of the time and given the diversity of wind directions; it is likely that some
13 emissions generated by a thermal runaway event would be transported outside of the
14 Facility's property boundary.

15 **IV. Professional Opinions**

16 **Q. What, if any, professional opinions have you formed about the Facility?**

17 A. Based on my analysis, I have several opinions regarding potential thermal
18 runaway events at the Facility.

19 First, Cranberry Point has acknowledged that air pollutants would be released if a
20 thermal runaway event were to occur at the Facility. However, Cranberry Point has not
21 provided sufficient information (e.g., data, analysis of data) to thoroughly understand the

1 extent of inhalation risk in the areas surrounding the Facility. In particular, I could not
2 determine from Cranberry Point's submissions all the specific pollutants that may be
3 released, the emissions rates for those pollutants, and the extent to which those pollutants
4 could travel offsite and into surrounding areas that include residential populations,
5 cranberry bogs, and at least one school during a thermal runaway event.

6 Second, any significant thermal runaway event will likely result in the release of
7 air pollutants that have been classified by U.S. EPA and/or MassDEP as impactful to
8 human health. Therefore, given the meteorological data that was evaluated, a thermal
9 runaway event would bring with it the potential that emissions that are known to impact
10 human health may travel offsite.

11 Third, there is reason to be concerned with the lack of data and analysis provided
12 by Cranberry point about air pollutants released during a potential thermal runaway
13 event. Based both on recent historical events and Cranberry Point's own submissions
14 that: (1) the risk of a thermal runaway event is not zero; (2) a thermal runaway event
15 brings with it the risk of a fire and the release of air pollutants; (3) such an event could
16 release air pollutants at levels that workers and emergency responders at the Facility
17 would need to wear SCBA equipment, and (4) the safety distance of 650 feet could not be
18 verified. I believe the Siting Board should be aware of and should consider this lack of
19 information during its decision-making process in this proceeding.

20 **V. Conclusion**

21 **Q. Does this conclude your direct testimony?**

- 1 A. Yes, but I reserve the right to supplement this testimony if any additional
- 2 information becomes available due to later-filed discovery responses or other materials.

Affidavit of John Hinckley

I, John Hinckley, affirm under the pains and penalties of perjury that:

1. I am testifying in the Energy Facilities Siting Board's proceeding docketed as number EFSB21-02;
2. This prefiled testimony was prepared by me or at my direction, under my supervision and control; and
3. The information contained in this prefiled testimony is true and accurate to the best of my knowledge and belief at the time I signed this affidavit.



John Hinckley

EXHIBIT 1



JOHN HINCKLEY, QEP SENIOR MANAGING CONSULTANT

CREREDENTIALS

- ◆ M.S., Environmental Science & Engineering, University of Virginia, 1998
- ◆ B. S., Natural Resources, University of Vermont, 1994
- ◆ U.S. EPA Air Pollution Training Institute, North Carolina State University (2002-2003)
- ◆ AERMOD Training (2018)
- ◆ Member, Institute for Professional Environmental Practice (IPEP)
- ◆ Member, Air and Waste Management Association (AWMA)
- ◆ Qualified Environmental Professional (2003 - present)

PROFESSIONAL EXPERIENCE

- ◆ **May 2020-Present:** ALL4, Kimberton, PA – Senior Project Manager
- ◆ **March 2018-March 2020:** GeoInsight, Inc., Manchester, NH – Associate/Air Compliance Specialist
- ◆ **July 1998-March 2018:** RSG, Inc., White River Junction, VT – Director

TECHNICAL EXPERTISE

- ✓ New/modified source air permit application preparation;
- ✓ Air emissions dispersion modeling for criteria pollutants and air toxics using the AERMOD modeling system;
- ✓ Pollution Control Technology Assessments including BACT/LAER and Vermont HMSER;
- ✓ Federal air quality regulations including, NSPS and NESHAPs;
- ✓ State level air toxics evaluations including New Hampshire Env-A 1400, Vermont HMSER; and New York Part 212;
- ✓ Accidental release modeling using SLAB, DEGADIS, and ALOHA;
- ✓ Mobile source emissions estimation with MOVES and dispersion modeling with AERMOD; and
- ✓ Vermont Act 250 Permitting.

PROFESSIONAL OVERVIEW

Mr. John Hinckley possesses over 22 years of air quality consulting experience focusing on air emissions permitting, air dispersion modeling (including accidental release modeling), and air pollution control technology assessments. Mr. Hinckley has worked with a variety of clients in the institutional (education, public health), renewable energy (biomass, biogas, landfill gas to energy, renewable natural gas), forest products, manufacturing, hot mix asphalt, aggregate, dimension stone, concrete and ski area sectors from Maine to Alaska. Mr. Hinckley's primary interest and career work focuses on helping clients understand how to design and operate their facilities in compliance with complex federal and state air pollution control regulations. His experience with emissions estimation, pollution control technology assessments, and air dispersion modeling are used to evaluate regulatory applicability and to develop compliance solutions. He has guided clients through feasibility studies for new facilities, evaluating facility design and operation requirements, resolving odor and dust nuisance issues, responding to federal/state enforcement actions, permitting first-of-their-kind projects, evaluating safety from accidental releases of air emissions, and providing litigation support and expert testimony.



JOHN HINCKLEY, QEP
SENIOR MANAGING CONSULTANT

PROJECT HISTORY

Compressor Station Peer Review. Town of Weymouth, MA. Senior Project Manager: *Performed peer review of a proposed natural gas-fired compressor station on behalf of Town of Weymouth, MA. Reviewed emissions calculations, air dispersion modeling, and pollution control technology evaluation prepared for the compressor station's permit application. Conducted independent air dispersion modeling evaluation of start-up emissions using U.S. EPA AERMOD model. Performed accidental release modeling evaluation using U.S. EPA ALOHA model. Prepared prefiled testimony and provided expert witness testimony at MassDEP Boston separately for air permit application review and accidental release modeling.*

Consent Decree Representation for Massachusetts Industrial Facility. Confidential Industrial Client: Provided technical assistance to an industrial Massachusetts facility that was sued by the Massachusetts Attorney General. Provided on-site representation in meetings between the Facility and the Massachusetts Attorney General. Assisted facility with an emission control evaluation for pollution control equipment selection. Reviewed and commented on draft consent decrees.

Enforcement Action Representation for Massachusetts Industrial Facility. Confidential Industrial Client: Provided technical assistance to an industrial Massachusetts facility that was inspected and later received a Letter of Deficiency from U.S. EPA Region 1. Assisted the facility with emissions testing and equipment changes to comply with federal air pollution control requirements. Participated in meeting with the Facility and U.S. EPA at the Region 1 office in Boston, MA.

Consent Decree Representation for New Hampshire Commercial Facility: Provided technical assistance to a New Hampshire commercial facility to comply with a consent decree with the New Hampshire Department of Environmental Services (NHDES). Assisted with meetings at the NHDES office in Concord, pollution equipment improvements, and source emission testing.

Consent Decree Representation for Massachusetts Industrial Facility. Confidential Industrial Client: Provided technical assistance to an industrial Massachusetts facility that was sued by the Massachusetts Attorney General. Provided on-site representation in meetings between the Facility and the Massachusetts Attorney General. Assisted facility with an emission control evaluation for pollution control equipment selection. Reviewed and commented on draft consent decrees.

Enforcement Action Representation for Massachusetts Industrial Facility. Confidential Industrial Client: Provided technical assistance to an industrial Massachusetts facility that was inspected and later received a Letter of Deficiency from U.S. EPA Region 1. Assisted the facility with emissions testing and equipment changes to comply with federal air pollution control requirements. Participated in meeting with the Facility and U.S. EPA at the Region 1 office in Boston, MA.

Consent Decree Representation for New Hampshire Commercial Facility: Provided technical assistance to a New Hampshire commercial facility to comply with a consent decree with the New Hampshire Department of Environmental Services (NHDES). Assisted with meetings at the NHDES office in Concord, pollution equipment improvements, and source emission testing.



JOHN HINCKLEY, QEP
SENIOR MANAGING CONSULTANT

Nuclear Power Plant Cooling Tower. Evaluation, Riverkeeper, Buchanan, NY, Senior Project Manager: Retained by Riverkeeper (New York State non-profit) to evaluate the feasibility of permitting cooling towers for the 2000-megawatt Indian Plant Energy Center (IPEC) in Buchanan, NY. Evaluated emissions control from mist eliminators, estimated emissions, and performed air dispersion modeling to demonstrate that Riverkeeper's proposed cooling tower design would meet the National Ambient Air Quality Standards (NAAQS) for fine and coarse particulate matter. Modeling findings were affirmed by the New York State Department of Environmental Conservation (NYSDEC). Provided expert witness testimony on three occasions at NYSDEC headquarters in Albany, NY.

Permitting and Representation for Hot Mix Asphalt Plant and Rock Crushing Plants. Graniteville, VT. Senior Project Manager: Provided air permitting, air dispersion modeling, emissions control, and expert witness testimony for North East Materials Group, for its hot mix asphalt plant and rock crushing plants in Graniteville, VT. Provided expert testimony at Act 250 District Commission hearings in Vermont Environmental Court Proceedings.

Permitting and Representation for Hot Mix Asphalt Plant. Irasburg, VT. Senior Project Manager: Provided air permitting, emissions control, and expert witness testimony for J. Hutchins, Inc. for its hot mix asphalt plant and rock crushing plant in Irasburg, VT. Provided expert testimony at Act 250 District Commission hearing.

Hot Mix Asphalt Plant Peer Review. Permitting, Mediation. Colchester, VT. Senior Project Manager: Involved as intervenor, then facility consultant, then mediator regarding odor and dust issues regarding the FW Whitcomb Construction Company. Initially hired by neighboring commercial office complex to evaluate and identify a solution to odors generated by a hot mix asphalt plant. Worked with the neighbor and Whitcomb to design odor control equipment for the hot mix plant. Was later hired by Whitcomb to provide air permitting services for additional equipment changes. Recently represented Whitcomb to work with neighbor as part of mediation to resolve additional odor issues.

Permitting and Representation of Hot Mix Asphalt Plant and Rock Crushing Plants. Graniteville, VT. Senior Project Manager: Have provided air permitting, air dispersion modeling, emissions control, and expert witness testimony for North East Materials Group (NEMG) for their hot mix asphalt plant and rock crushing plant in Graniteville, VT. Provided expert testimony in separate Vermont Environmental Court Proceedings.

Bulk Heated Storage Tank Peer Review. Senior Managing Consultant: Assisted the City of South Portland, Maine with evaluating a proposed odor control system for bulk heated storage tanks located at Global Companies, LLC's (Global) petroleum storage and distribution facility in South Portland. ALL4 was retained by the City of South Portland, Maine to evaluate the potential effectiveness of the equipment and to address South Portland citizen's concerns regarding the equipment. Prepared findings report and testified at public hearings.

EXHIBIT 2

**COMMONWEALTH OF MASSACHUSETTS
ENERGY FACILITIES SITING BOARD**

Petition of Cranberry Point Energy Storage, LLC,)
Pursuant to G.L. c. 164, § 69J ¼ for Approval to) EFSB 21-02
Construct a 150 MW Battery)
Energy Storage System in Carver, MA)

**PETITION OF CRANBERRY POINT ENERGY STORAGE, LLC
FOR APPROVAL OF 150 MW BATTERY ENERGY STORAGE PROJECT**

NOW COMES Cranberry Point Energy Storage, LLC (“Cranberry Point”, the “Company” or the “Applicant”), pursuant to G.L. c. 164, § 69J ¼, seeking approval from the Energy Facilities Siting Board (the “Siting Board” or “EFSB”) to construct a 150 megawatt (“MW”)/300 megawatt-hour (“MWh”) standalone battery energy storage system (“BESS”) to be located in the Town of Carver (the “Town” or “Carver”) (the “Cranberry Point Energy Storage Project” or the “Project”).

G.L. c. 164, § 69J ¼ states that the Siting Board shall approve construction of a generating facility where the applicant has demonstrated that: (i) the description of the proposed generating facility and its environmental impacts are substantially accurate and complete; (ii) the description of the site selection process used is accurate; (iii) the plans for the construction of the proposed generating facility are consistent with current health and environmental protection policies of the Commonwealth and with such energy policies as are adopted by the Commonwealth for the specific purpose of guiding the decisions of the Board; (iv) such plans minimize the environmental impacts consistent with the minimization of costs associated with the mitigation, control, and reduction of the environmental impacts of the proposed generating facility; and (v) the construction of the proposed near zero greenhouse gas emission-generating facility on balance contributes to a reliable, low-cost, diverse, clean regional energy supply with minimal environmental impacts.

As detailed herein, the Project is contractually committed to meeting the capacity needs of Massachusetts as determined by ISO-New England, Inc. (“ISO-NE”), is located in an area that allows for easy interconnection adjacent to an existing NSTAR Electric Company d/b/a Eversource Energy (“Eversource”) substation, is consistent with current health, safety and environmental regulations and policies, and is designed to minimize environmental impacts. As such, the Project is consistent with the requirements for approval of the Project under the Siting Board requirements.

In support of the Application, the Company states as follows:

1. The Siting Board Has Jurisdiction over the Proposed Project

The Siting Board has jurisdiction to review and approve “generating facilities” pursuant to G.L. c. 164, § 69J ¼, defined as “any generating unit designed for or capable of operating at a gross capacity of 100 MW or more, including associated buildings, ancillary structures, transmission and pipeline interconnections that are not otherwise facilities, and fuel storage facilities.” The Project is a standalone energy storage system, in that it is not designed as a co-located or a hybrid installation with renewable energy generation onsite. The Project is the first of its kind in Massachusetts and proposes to: (1) have a nameplate capacity of 150 MW; (2) be connected to the ISO-NE administered transmission system and (3) to participate in the ISO-NE wholesale market and the ISO-NE Forward Capacity Market (“FCM”).

While the Siting Board’s statutes and regulations do not explicitly define what constitutes a “generating unit,” “generation,” or a “generating facility”, the Siting Board has, in the past, looked to definitions in Section 1 of Chapter 164 when a particular term is not defined in G.L. c. 164 § 69G. Chapter 164 defines generation as “the act or process of transforming other forms of energy into electric energy or the amount of electric energy so produced.” Relatedly, a “generation facility” is defined as a “plant or equipment used

to produce, manufacture or otherwise generate electricity and which is not a transmission facility, or an energy storage system procured by a distribution company for support in delivering energy services to end users.”¹ Cranberry Point Energy Storage meets these definitions. Cranberry Point is a BESS, which is defined as “a commercially available technology that is capable of absorbing energy, storing it for a period of time and thereafter dispatching the energy.”² Cranberry Point was not procured by a distribution company for support in delivering energy services to end users. Rather, Cranberry Point is a BESS that can participate in the ISO-NE marketplace as a Generator Asset, which is defined in the ISO-NE Tariff as a “device (or a collection of devices) that is capable of injecting real power onto the grid.”³ Because Cranberry Point will function as a generator, it is a “generating facility” subject to Siting Board review. Cranberry Point has been designed to participate in ISO-NE’s Forward Capacity Market (“FCM”) and will contribute to system reliability with its 150 MW of capacity in Southeast Massachusetts within ISO-NE’s Southeast New England (“SENE”) capacity zone. The Project, located in ISO-NE’s Southeast Massachusetts (“SEMSS”) load zone will also participate in the Day-Ahead and Real-Time energy markets as well as ISO-NE’s ancillary services markets and will mitigate instability on the grid that could result from intermittent resources, congestion, fluctuations in system demand and other system contingencies. From a wholesale electricity market standpoint, the Project will operate much like a generator in that it will act as a source of wholesale electricity and provide wholesale services in the same manner as other resources, *i.e.*, by dispatching electricity into the marketplace.

¹ G.L. c. 164 § 1.

² *Id.*

³ ISO-NE Tariff § “Generator Asset.”

ISO-NE has implemented a technology-neutral market construct, meaning that a resource participating as a BESS must register under existing market constructs. Specifically, a storage facility registers as a dispatchable Generator Asset to manage injection capability for the provision of capacity energy, reserves, primary frequency response, blackstart, and reactive power. A BESS, like other resources, also has the ability to participate in the ISO-NE FCM by qualifying as a Generating Capacity Resource. A BESS can also offer as a Limited Energy Resource, which allows it to lower its maximum dispatch limit at any time during the current operating hour or future hours to save the facility's energy for a future period, while continuing to provide reserves up to its full capability. Essentially, under ISO New England's market rules, a BESS acts as and is modeled a generator when dispatching electricity into the marketplace.

The size of the Project, at 150 MW, exceeds the Siting Board's 100 MW jurisdictional threshold. Moreover, given Cranberry Point's intended participation in the wholesale electricity markets and ISO-NE's characterization of storage facilities as Generator Assets under the market rules, this Project qualifies as a "generating unit" or a "generating facility," and its operation should be considered to be "generation" over which the Siting Board's exercise of jurisdiction is appropriate.

2. ISO-NE has Determined a Need for Resources Such as Standalone Battery Energy Storage Systems

The Project critically supports ISO-NE in meeting the future capacity needs of the SENE zone, which is comprised of Northeastern Massachusetts, Greater Boston, Southeastern Massachusetts, and Rhode Island. Pertinent to this matter, on February 8, 2021, Cranberry Point participated in ISO-NE's Forward Capacity Market Auction ("FCA 15") and ISO-NE selected Cranberry Point to provide capacity to serve the SENE zone starting in 2024.

The projects selected by ISO-NE align with power system transmission constraints and signal areas of the system with a potential shortfall. The clearing prices in FCA 15 reveal the different values across the region based on the individual capacity needs for each zone. The clearing price in the SENE zone, where this Project will be located, is \$3.98 kW-month. ISO-NE noted that FCA 15 included nearly 600 MW of energy storage capacity target for 2024-2031, of which 150 MW was committed to from the Project.

3. Project Has Minimal Environmental Impacts

The Project has significantly fewer environmental considerations and impacts for EFSB review than traditional generation projects. The Project will generate near zero air emissions, and will not impact water resources, will not impact rare species, and will not interfere with heritage agricultural uses. Additionally, it is not anticipated that the Project will damage any sensitive archaeological resources. All predicted noise levels from the Project are within the Massachusetts Department of Environmental Protection (“MDEP”) noise regulation standards. Similarly, traffic impacts due to initial construction and occasional on-site maintenance will all be minimal, especially as the site location is adjacent to a substation on property owned by Eversource and in an area where BESS is allowed pursuant to a 2018 Town Board meeting (see Exhibit CP-1, Exhibit CP-2, attached). Any required traffic changes during construction have been discussed with the Town and will be addressed in accordance with the requirements set forth in the Town of Carver’s Site Plan Review and Special Permit for the Project. The Project will be remotely monitored; traffic to the Project Site will be limited to regularly scheduled site inspections.

4. The Project Site Selection is Preferred

The Project site was chosen given its proximity to its existing transmission lines and Eversource substation, as well as its remote location. Specifically, the size of the lot, at

approximately 6 acres, meets the requisite land area needed for a project of the size proposed. Second, as the lot is more than 400 feet from the nearest residence, there is minimal, if any, economic or environmental impact on the surrounding community. Third, the lot is readily available for lease. Fourth, the lot is adjacent to infrastructure with available transmission interconnection capabilities. Fifth, the location of the Project is in an area where the Company could readily obtain a Site Plan Review and Special Permit, with minimal impact on the environment. Sixth, the location is in close proximity to retiring nuclear and fossil-fuel generation facilities and potential offshore wind interconnection points onshore which, combined with significant market advantages including but not limited to, energy price volatility and compensation mechanisms available for providing ancillary services, etc., enhancing the viability of a project of this size and scope. In fact, the Project Site allows sufficient physical and electrical space to add new enclosures of batteries in the future to maintain the system's capacity.

5. Consistency with Massachusetts Energy Policies and Initiatives

In addition to being nearly emissions-free and environmentally consistent with current laws and regulations, the Project may displace conventional non-renewable generation facilities and thereby further reduce emissions of carbon, particulates, and other air pollutants. For example, the Project represents approximately 10 percent of the capacity of the nearby retiring Mystic gas plant and is sited near other Mystic units that are slated to retire in the coming years.⁴ As such, the Project will also promote the Commonwealth of Massachusetts's energy storage and clean energy goals. For example, in its *State of Charge*, Massachusetts Energy Storage Initiative, a copy of which is attached hereto as Attachment 1 and in subsequent initiatives and mandates,

⁴ <https://www.exeloncorp.com/newsroom/statement-regarding-the-retirement-of-mystic-generating-station-in-2024>

the Commonwealth intends to enhance the efficiency, affordability, resiliency and cleanliness of the electric grid by modernizing the way that electricity is generated and delivered. Massachusetts established the Energy Storage Initiative in 2015, with the goal of “advancing energy storage” by:

- *Attracting, supporting and promoting* storage companies in Massachusetts;
- *Accelerating the development of* early commercial storage technologies;
- Expanding markets for storage technologies, and *valuing storage benefits* to clean energy integration, grid reliability, system wide efficiency, and peak reduction; and
- Recommending and developing policies, regulations and programs that help achieve those objectives.

As demonstrated below, the Project is anticipated to qualify to participate in the Commonwealth’s Clean Peak Standard as well as the initiatives established in the Global Warming Solutions Act.

WHEREFORE, Cranberry Point Energy Storage, LLC respectfully requests that the Energy Facilities Siting Board approve this Application, with conditions as required to be met by the Town of Carver pertaining to its Site Plan Review and Special Permit and its Order of Conditions.

Respectfully submitted,

Cranberry Point Energy Storage, LLC

By its attorneys,



Andrew O. Kaplan
Paul K. Connolly
Jared S. des Rosiers
Kayla J. Grant
Pierce Atwood LLP
100 Summer Street
Boston, Massachusetts 02110

Dated: August 27, 2021

**COMMONWEALTH OF MASSACHUSETTS
ENERGY FACILITIES SITING BOARD**

**Petition of Cranberry Point Energy Storage, LLC for Approval to
Construct a 150 MW Battery Energy Storage System in Carver, MA
Docket No. EFSB 21-02**



Submitted by:
Cranberry Point Energy Storage, LLC

Prepared by:

PIERCE ATWOOD LLP
100 Summer Street
Boston, MA 02110

AECOM
250 Apollo Drive
Chelmsford, MA 01824

ENERGY SAFETY RESPONSE GROUP
36 Plymouth Drive South
Glen Head, NY 11545

August 27, 2021

ANALYSIS IN SUPPORT OF PETITION

Table of Contents

SECTION 1.0	THE PROJECT	1
1.1	PROJECT OVERVIEW	1
1.2.	HOW THE PETITION IS STRUCTURED	2
1.3	PROJECT TEAM	3
SECTION 2.0	SITE DESCRIPTION.....	5
2.1	TOWN OF CARVER ZONING APPROVALS	10
SECTION 3.0	PROJECT DESCRIPTION	11
3.1	PROJECT DEVELOPMENT SCHEDULE	13
3.2	BATTERY TECHNOLOGY AND LOCATION	15
SECTION 4.0	ENVIRONMENTAL IMPACTS AND MITIGATION MEASURES	17
4.1	AIR QUALITY.....	17
4.2	EMISSIONS	18
4.3	WATER RESOURCES.....	19
4.4	WETLANDS	20
4.5	STORMWATER	21
4.6	SOLID AND HAZARDOUS WASTE	22
4.7	VISUAL	22
4.8	NOISE.....	25
4.9	LOCAL AND REGIONAL LAND USE	27
SECTION 5.0	BATTERY SAFETY.....	32
5.1	SAFETY STANDARDS	32
5.2	MITIGATION	33
5.3	HAZARD CONTROL.....	34
5.4	LOCAL COORDINATION.....	35
SECTION 6.0	ARCHAEOLOGICAL AND HISTORICAL	36
SECTION 7.0	ALTERNATE SITES ANALYSIS	37
SECTION 8.0	CONSISTENCY WITH COMMONWEALTH POLICIES.....	40
8.1	CONSISTENCY WITH POLICIES OF THE COMMONWEALTH	40
8.2	ENERGY STORAGE INITIATIVE.....	40
8.3	CLEAN PEAK STANDARD	41
8.4	GLOBAL WARMING SOLUTIONS ACT.....	42

Attachments

- Attachment 1: State of Charge Report
Attachment 2: Clean Peak Energy Standard Guidelines
Attachment 3: Clean Peak Energy Standard 225 CMR 21.00

Exhibits

- Exhibit CP-AJS-1 Testimony of Allyson J. Sand
Exhibit CP-CQ-1 Testimony of Christopher Quaranta
Exhibit CP-PNS-1 Testimony of Polly N. Shaw
Exhibit CP-PR-1 Testimony of Lt. Paul Rogers
Exhibit CP-TJK-1 Testimony of Thomas J. Keough
- Exhibit CP-1 Town of Carver 2018 Annual Town Meeting Warrant
Exhibit CP-2 Town of Carver 2018 Annual Town Meeting Minutes
Exhibit CP-3 Carver Site Plan Review and Special Permit
Exhibit CP-4 Carver PB June 22 2021 Meeting Minutes
Exhibit CP-5 Carver Conservation Commission Order of Conditions
Exhibit CP-6 Carver Conservation Commission Meeting Minutes
Exhibit CP-7 Expanded ENF
Exhibit CP-8 Wetland Delineation Report
Exhibit CP-9 Stormwater Report
Exhibit CP-10 Acoustic Assessment
Exhibit CP-11 Draft Emergency Response Plan
Exhibit CP-12 Project Notification Form
Exhibit CP-13 MHC Response Letter

SECTION 1.0 THE PROJECT

1.1 PROJECT OVERVIEW

Cranberry Point Energy Storage, LLC (the “Applicant” or the “Company” or “Cranberry Point”) proposes to construct a 150 MW/300 MWh battery energy storage system with ancillary structures (*i.e.*, transformers, substation, low voltage/medium voltage equipment) to be located at 31R Main Street, in Carver, Massachusetts. Currently, the Project is designed to utilize lithium-ion batteries, which will be located in approximately 116 above-ground enclosures on an approximately 6-acre parcel of undeveloped land that is currently under an Option to Lease with the Company.

The Project will interconnect adjacent to an Eversource substation (No. 276), via a new 115 kV three-breaker ring bus, which will tap into the existing transmission line #127, requiring the installation of two (2) new dead-end structures between existing structures. In terms of site access, there are two main points of ingress/egress. The existing approximately 530-foot long gravel access driveway from Main Street to the Project will be improved to a width of 20 feet. An existing gravel access road of approximately 20-foot wide and 25-foot long will be extended further south on the East side of the Project Site to allow for emergency vehicle access.

The Project will store electricity, during times of oversupply, and dispatch the electricity, during times of peak demand onto the electric grid. This function will serve as a valuable addition to the electricity system by lower-cost energy generated during off-peak periods to meet peak demand, provide flexibility to optimize the use of other clean, intermittent renewable resources, and defer future traditional generation and transmission projects while avoiding and even offsetting their environmental impacts.

The Project critically supports ISO-NE in meeting the future capacity needs of the SENE zone, which is comprised of Northeastern Massachusetts, Greater Boston, Southeastern Massachusetts, and Rhode Island. On February 8, 2021, ISO-NE as part of its most recent Forward Capacity Market Auction (“FCA 15”), selected Cranberry Point to ensure

there are adequate power system resources available to provide New England with sufficient capacity to meet peak demand needs from 2024-2031.

The projects selected by ISO-NE align with power system transmission constraints and signal areas of the system with a potential shortfall. The clearing prices in FCA 15 reveal the different values across the region based on the individual capacity needs for each zone. The clearing price in the SENE zone, where this Project will be located, was \$3.98 kW-month. ISO-NE noted that FCA 15 included nearly 600 MW of energy storage capacity for 2024-2025, of which 150 MW was committed by the Project.

1.2. HOW THE PETITION IS STRUCTURED

There are eight sections that make up the Company's Siting Board application including the Project Overview. Collectively, they demonstrate that Cranberry Point's proposed Project meets or exceeds the statutory requirements, pursuant to G.L. c. 164 § 69J ¼.

Specifically, Sections 2 and 3 provide details about the Project's site. Testimony on these sections will be offered by Allyson J. Sand, the Development Lead for the Project.

Section 4 details the testing and analysis that was completed by AECOM, on behalf of the Company, to demonstrate that the Project will have minimal impact on the environment, including, but not limited to, surrounding water, wetlands, stormwater, solid and hazardous waste, air quality, noise, or emissions. Thomas J. Keough, Senior Wetland Scientist and Permitting Specialist at AECOM will testify on these matters.

Section 5 describes the extraordinary safety testing, evaluations, analyses, and planning that the Company has undertaken to ensure that the Project is constructed and operated in a safe and secure manner. These include, but are not limited to, meeting extensively with the Carver Fire Department ("CFD") to design the Project Site and retaining retired New York City Fire Department Lieutenant Paul Rogers, who helped to develop the safety and building code standards for lithium-ion battery installations. Testimony on the Project's safety will be offered by Lieutenant Rogers, the co-founder of Energy Safety Response Group ("ESRG") and

Christopher Quaranta, Director of Engineering and Construction for the Project.

Section 6 discusses the Archaeological & Historical analysis and is sponsored by the testimony of Thomas J. Keough.

Section 7 details the Site Selection process, including information about alternative sites that were considered, but for a variety of reasons, ultimately not chosen. In addition to Ms. Sand, Mr. Keough will sponsor this section.

Section 8 outlines each of the Commonwealth's policies designed to promote energy storage and how this Project will help propel the Commonwealth to meeting those policy goals and will be sponsored by the testimony of Polly N. Shaw.

1.3 PROJECT TEAM

The Plus Power team, led by seasoned executives from the renewables and energy storage industry, is accelerating the deployment of transmission-connected battery storage throughout the United States, including the development of the Cranberry Point Energy Storage Project.

With a mission to facilitate the changing energy landscape, Plus Power focuses on standalone battery energy storage systems that foster grid flexibility by providing capacity, energy and ancillary services as more renewable generation enters wholesale energy markets.

In addition, the Company has retained the following entities for environmental, safety and legal services.

1.3.1 AECOM

AECOM is an approximately 54,000-person engineering and environmental consulting firm based internationally, including offices in and around the greater Boston area. For the Cranberry Point Energy Storage Project, AECOM's role is lead environmental consultant for the necessary federal, state, regional, and local permitting, as well as performing studies that include, but are not limited to biological resources, physical resources, cultural resources, and noise resources. AECOM is responsible for evaluation of environmental

impacts and provided environmental support for the Petition.

1.3.2 ESG

ESRG co-founder Paul Rogers led New York City's development of the then-most stringent fire codes in the nation for battery energy storage systems as supervisor of NYC Fire Department's premier HazMat team. Mr. Rogers has also played a pivotal role in the design and evolution of the ensuing National Fire Protection Association (NFPA) 855 national standard for BESS, and he is a member of the International Fire Code Action Committee for BESS. Co-founder Nick Warner similarly advises on six UL standards related to BESS, as well as NFPA and ICC codes for fire safety and BESS deployment. Co-founder Tom Benson also sits on the NFPA 855 committee, bringing over 20 years of fire investigation including extensive BESS safety review. Many of ESRG's senior consultants served in the NYC, Boston, and Phoenix Fire Departments.

1.3.3 PIERCE ATWOOD LLP

Pierce Atwood LLP is a full-service law firm, representing a broad range of utilities, developers, and other stakeholders before federal and state agencies. Pierce Atwood clients include energy storage developers, solar, wind and biomass companies, developers of natural gas-fired generation facilities, electric and natural gas utilities, hospitals, global governmental agencies and industrial facilities.

SECTION 2.0 SITE DESCRIPTION

The Project is located on two undeveloped, primarily wooded properties (Map 61, Lots 7 and 10) at 31R Main Street in Carver, Massachusetts (see Figure 1.1-1).

Figure 1.1-1 | Site Locus



The approximate 6-acre area of the Project (the "Project Site") that will be leased from the current landowner is part of two larger parcels, one of which is 21.5 acres and the other is 12.5 acres. (see Figure 1.1-7 and Figure 1.1-8).

Figure 1.1-7 | Site Layout Map

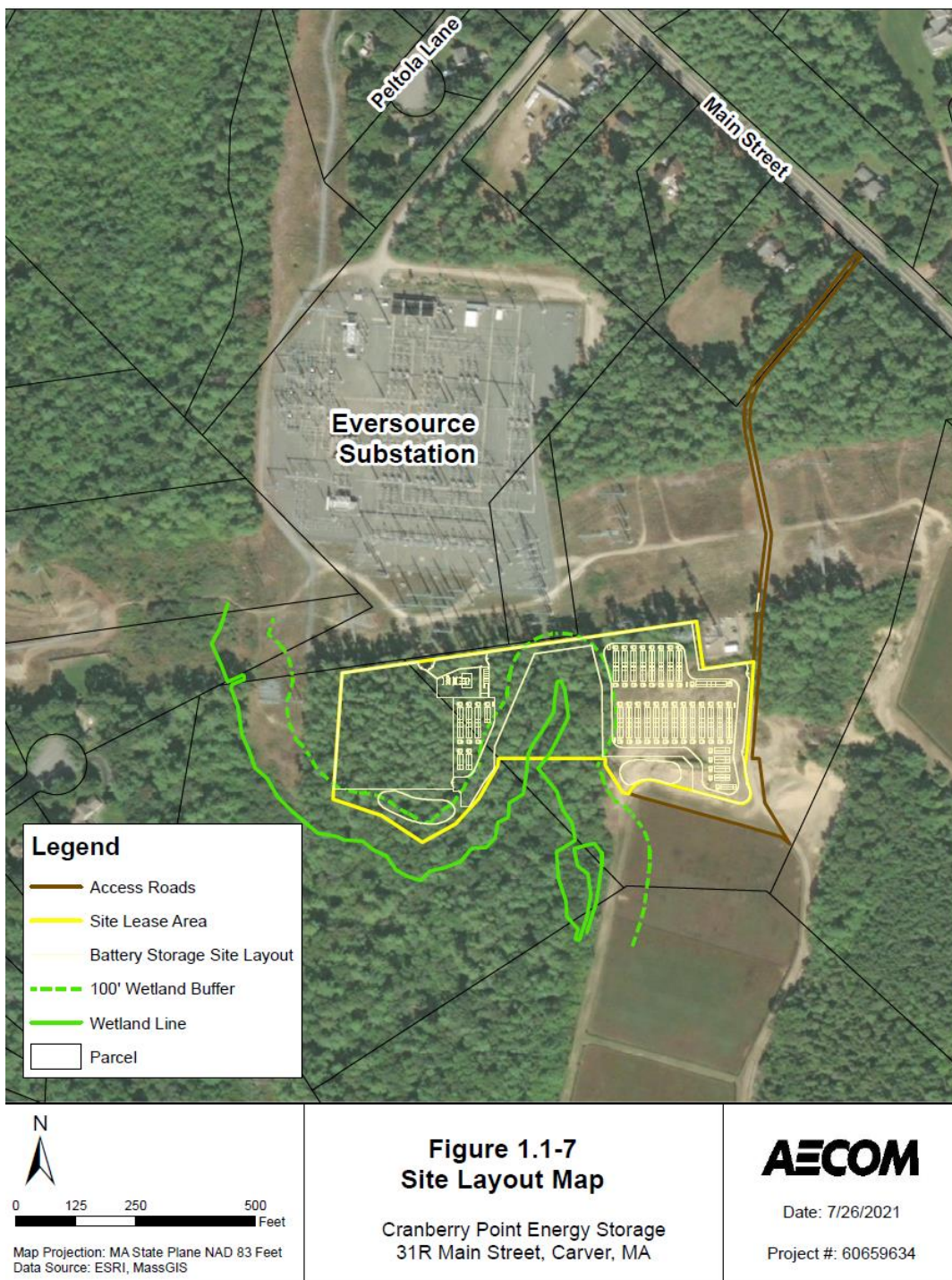
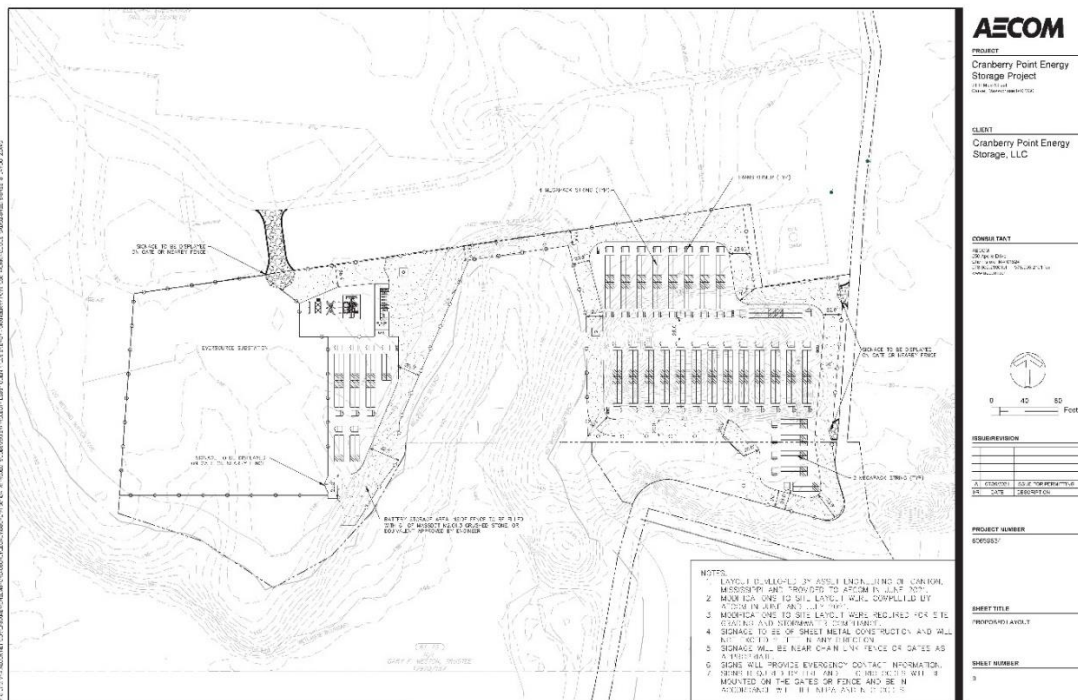


Figure 1.1-8 | Proposed Layout Map



An Eversource Substation (Station No. 726) and electrical transmission/distribution lines are located within a right-of-way ("ROW") just north of the Project Site (see Figure 2).

Figure 2 | Aerial Rendering



The Project Site also includes existing unimproved roads to access a cell tower, to the northeast of the Project, and cranberry bogs to the south (see Figure 1.1-7 above). Electrical transmission and distribution lines are also located to the north and west of the Project Site within an additional ROW (see Figure 2 above). Residential properties are not located within 400 feet of the proposed Project Site boundaries.

Although wetlands and commercial cranberry bogs are located to the south and east of the Project Site, they will not be impacted by the construction or operation of the Project.

The wooded areas are dominated by softwoods (pines) and mixed hardwoods (maples and oaks). Understory species consist of a mix of saplings, shrubs, and herbaceous species. Topography slopes gently in a southerly direction towards the wetland and cranberry bogs. A large Palustrine Forested (PFO) wetland was delineated south of the Project Site.

A Palustrine Emergent (PEM)/Scrub-Shrub (PSS) wetland is located within the electrical transmission line ROW to the west of the site. All these areas of PFO and PEM/PSS wetland are contiguous and considered one large wetland area. Vegetation within the Bordering Vegetated Wetland include an overstory of trees consisting of red maple (*Acer rubrum*) and yellow birch (*Betula alleghaniensis*) a shrub understory dominated by pepperbush (*Clethra alnifolia*), spicebush (*Lindera benzoin*) and highbush blueberry (*Vaccinium corymbosum*) with an herbaceous understory of cinnamon fern (*Osmundastrum cinnemomea*), skunk cabbage (*Symplocarpus foetidus*), Massachusetts fern (*Parathelypteris simulate*) and sphagnum moss. Hydric soil containing both shallow and deep organic soil and hydrologic indicators including soil saturation at the surface and a water table less than 12 inches below the surface were encountered.

Wetlands Protection Act ("WPA") regulations (310 CMRS 10.02(2)(b) establish a 100-foot buffer zone that extends from Bordering Vegetated Wetland ("BVW"). The buffer zone itself is not a jurisdictional resource area under the WPA; however, it is a resource area pursuant to Chapter 1 of the Carver Wetlands Protection Bylaw (Chapter 9). In addition, the Town of Carver

Wetlands Protection Bylaw provides a 65-foot setback from wetlands that restricts the construction of any structure or impervious surface within 65 feet of a wetland. The Project will not result in any direct wetland impacts, and no Project facilities are located within the 65-foot setback.

Based on the Federal Emergency Management Agency (“FEMA”) Flood Insurance Rate Map (“FIRM”) panel No. 25023C0343J (July 17, 2012), the Project Site is located outside of the flood hazard areas subject to the 100-year flood/inundation by the 1% annual chance flood. Therefore, the Project Site does not contain any areas of Bordering Land Subject to Flooding (“BLSF”).

According to Massachusetts Natural Heritage and Endangered Species Program (“NHESP”) Atlas (August 1, 2017, 14th Edition), the Project Site is not located within an area of Estimated Habitats of Rare Wildlife or an area of Priority Habitats of Rare Species. There are no certified vernal pools located on or near the site.

Two cranberry bogs are located to the south of the Project Site, within the remaining southern portion of the eastern parcel (parcel 61/7) and also within an off-site parcel (parcel 61/8) to the south. Based on review of United States Geological Survey historical topographical maps from 1893 to the present and historic aerial photographs from 1960 to the present, it appears the northern portion of the bog located within the southern extent of the remaining portion of the Project area parcel (parcel 61/7) is an “upland bog” since there has historically been an upland area (upland lobe) that is surrounded by wetland to the south, east and west. The far southern bog (the southernmost bog) located off-site on parcel 61/8 appears to have potentially been former wetland; however, the far northernmost portion of the bog (the “upland bog” area) located on the site of the Project area appears to have been mostly upland. The proposed Project Site is not located within a current or former bog.

2.1 TOWN OF CARVER ZONING APPROVALS

On March 26, 2019, the Town of Carver Planning Board awarded the Applicant a Site Plan Review and Special Permit, allowing for the construction and operation of the Project, subject to limited conditions (see Exhibit CP-3 attached). The vote was four in favor and one opposed. On June 22, 2021, the Project's Minor Modification Application was approved by the Town of Carver's Planning Board (see Exhibit CP-4, attached). Additionally, on February 6, 2019, the Company received an Order of Conditions from the Carver Conservation Commission (see Exhibit CP-5, attached). Per the December 2, 2020 letter from the Carver Conservation Commission (see Exhibit CP-6, attached), no additional conditions were necessary as a result of the minor modifications made to the Projects design.

SECTION 3.0 PROJECT DESCRIPTION

The description below is based on the Project layout as it is currently designed as of the date of this filing. As battery technology evolves, the exact quantity and dimensions of the equipment listed below that will be utilized for the Project may change. However, the Company will maintain strict adherence to the requirements as to the environment, and other conditions required in the Company's permits and certifications.

The Project involves the construction of a 150 MW lithium-ion battery energy storage system ("BESS") that will contain lithium-ion battery modules built into approximately 116 individual enclosures that will be supported by concrete slabs and pier foundations and surrounded by crushed stone. The BESS itself will be constructed using an assembly of subcomponents that include battery enclosures manufactured by Tesla, oil-filled step-up transformers, medium voltage circuit breakers, and associated electrical control and interconnection equipment. The entire BESS will be electrically connected to a Project Substation (described in more detail below), which includes a single large Power Transformer, circuit breaker, and interconnection structures that are used to match up to the electrical interface of the Eversource grid. Lastly, the Project will include an Eversource-owned switchyard that will electrically allow Eversource and ISO-NE to either connect, disconnect, or bypass the Project based on market and grid conditions, as required.

Within the Project's BESS, groups of two battery enclosures will connect to their own 3,000 kVA transformer to form an AC "string". Lithium-ion battery cells, which are hermetically sealed, are combined electrically in a series of parallel arrangement within each battery module. Each enclosure will have approximately 22 inverter and 15 battery modules to provide the necessary power and energy required from each enclosure. Enclosures in the current design are 23.5 feet long, 5.4 feet wide, and stand 8.3 feet tall atop one-foot concrete pad foundations. Every two enclosures will be installed back-to-back, creating a string that will be approximately

11-feet wide. The concrete pad foundation will also include empty space for the future installation of additional battery equipment to address the time-based degradation of the initial installation, which is further detailed below in Section 3.2.

The rows of enclosures in the current Project design are spaced 8 feet apart and the transformers are spaced 3 feet from the first and last enclosures in each row. Per this design, there will be a total of approximately 58 standard step-up transformers that are approximately 4-feet by 5-feet and approximately 8-feet high.

The physical layout of the proposed Project has two separate areas of development within the Project Site, including an east and west battery storage area to ensure no wetland impacts and to mitigate the need to cut the nearby forest. The eastern storage area is the larger of the two areas and is connected to the western side via a proposed vehicle access path at the northern edge of the Project Site. Within the approximately 6-acre Project Site, 4,217 square feet includes impervious surfaces such as concrete slabs and drilled piers. The remaining 213,583 square feet within the proposed fenced-in area will be surfaced with an approximate 12-inch-thick layer of crushed stone and approximately 13,051 square feet of crushed stone within the driveways.

As noted above, in addition to the battery system and transformers, the Project will include a small substation within the fenced area ("Project Substation") with low voltage/medium voltage equipment, protective relays, circuit breakers, and other ancillary electrical equipment, all of which will be supported by concrete pads. All of this equipment will be secured by the installation of a chain link fence and, with prohibitive signage, will be monitored by security cameras. Within the fenced Project Substation, all equipment will be placed on concrete pads and the area in between the concrete pads will be covered with gravel.

The Project will interconnect to Eversource's existing transmission line #127 via a new 115-kV three-breaker ring-bus ("Switchyard") to be located west of the Project Substation. It is anticipated this interconnection will be effectuated via an approximately 100-foot, aboveground

115-kV line directly from the Cranberry Point Project Substation to the Switchyard ring-bus.

Said interconnecting line, and the two new dead-end structures, will not cross any public ways and will be entirely located on the Project Site and Eversource's right-of-way.

A total of three access gates (points of ingress/egress) are proposed for the Project, two of which would be for normal use, with one additionally proposed emergency entrance within Eversource's existing transmission ROW to the north of the Project Site. A new approximately 16- to 20-foot-wide gravel access driveway that is approximately 530 feet in length is proposed to extend from an existing unimproved drive-way from Main Street that is currently used to access the cranberry bogs located to the south of the Project area. A second new 20-foot wide gravel access driveway that is approximately 25 feet in length is proposed to extend from the existing access road directly to the east storage area. A third new 20-foot wide gravel access driveway that is approximately 90 feet in length is proposed to extend from the existing road to the northern portion of the site to provide ingress/egress to the west storage area from the existing electrical substation. This driveway is proposed solely for emergency access purposes and must be approved by Eversource.

Permanent structural stormwater management control devices are proposed including two infiltration basins. These stormwater management control devices will collect and treat stormwater before discharge to the surrounding wetlands.

3.1 PROJECT DEVELOPMENT SCHEDULE

On August 16, 2021, an Expanded Environmental Notification Form ("ENF") was submitted to the Massachusetts Environmental Policy Act Office ("MEPA") (see Exhibit CP-7, attached). Relatively few remaining permits or applications are needed for the development of the Project.

The timeline for the remaining anticipated permits / approvals are as follows:

<u>Number</u>	<u>Permit/Review/Approval</u>	<u>Issuing Agency / Regulatory Authority</u>	<u>Status</u>
1	Site Plan Review and Special Permit	Town of Carver Planning Board	Awarded March 26, 2019 Extension approved March 23, 2021 Minor Modification Application approved June 22, 2021
2	Petition of Cranberry Point Energy Storage, LLC, Pursuant to G.L. c. 164, § 69J ¼ for Approval to Construct a 150-MW BESS (EFSB 21-02)	Massachusetts Energy Facilities Siting Board (EFSB)	Submitting August 2021
3	Expanded Environmental Notification Form (EENF) and Environmental Impact Report (EIR) pursuant to 309 CMR 11.03(7)(1)	Massachusetts Environmental Policy Act (MEPA) Office	Submitted Expanded Environmental Notification Form August 16, 2021
4	WPA Form 5 - Order of Conditions (SE# 126-579)	Carver Conservation Commission, Massachusetts Department of Environmental Protection Bureau of Resource Protection - Wetlands)	Awarded February 7, 2019
5	Certificate of Compliance	Carver Conservation Commission	Once construction is completed
6	National Pollutant Discharge Elimination System (NPDES) Stormwater General Permit	U.S. Environmental Protection Agency (EPA)	Application to be submitted prior to construction start

7	Project Notification Form (PNF)	Massachusetts State Historic Preservation Office (SHPO)	PNF submitted July 2, 2021
8	Building Permit	Town of Carver	Application to be submitted prior to construction start
9	Electrical Permit	Town of Carver	Application to be submitted prior to construction start
10	Certificate of Use and Occupancy	Town of Carver	Application to be submitted prior to construction start

3.2 BATTERY TECHNOLOGY AND LOCATION

Currently, the Project expects to use the Tesla Megapack enclosure as the proposed battery solution. The Tesla Megapack includes:

- DC Battery Module –
 - Quantity of 15, rated for ~89.4 KW (AC) for a 2-hour duration
- Powerstage (DC-AC Inverter) –
 - Quantity of 22, each rated for 71.5KVA

Each Megapack enclosure also includes equipment that provides ancillary functionality for heating and cooling (thermal management - heater, cooling pump and reservoir, cooling distribution system, and heat exchanger with fans); connection and disconnection (fuses, circuit breakers, switches); as well as an integrated controls and Battery Management System (“BMS”).

As any battery is used, it begins to degrade the total amount of electrical charge that it can store and release. For large grid-connected BESS installations, there are two typical approaches to solve for this standard process: either to (i) overbuild the Project with considerably more batteries to plan for the “theoretical” decline over the lifetime, or (ii) build the

Project such that sufficient physical and electrical space is available to add new enclosures of batteries in the future to maintain the system's capacity. Cranberry Point has chosen to implement the latter of those two approaches, which is often referred to as an augmentation of the BESS' total energy. The foundation areas for the Megapack enclosures will include open space where augmentation segments can be added to the existing equipment to increase its energy as the cells naturally decline, thereby enabling the full Project to continue to operate at its full capacity.

SECTION 4.0 ENVIRONMENTAL IMPACTS AND MITIGATION MEASURES

G.L. c. 164 § 69J ¼ requires the Siting Board to determine whether the plans for construction of the Project minimize the environmental impacts of the proposed Project consistent with minimization of costs associated with the mitigation, control, and reduction of the environmental impacts of the Project. To make this determination, the Siting Board assesses the impacts of the Project in eight areas prescribed by G.L. c. 164, § 69J ¼, including air quality, water resources, wetlands, solid waste, visual impacts, noise, local and regional land use, and health. Several of these environmental considerations are not at issue or are mitigated by the very nature of the Project. For instance, there are no air impacts from carbon, nitrogen oxides, sulfur dioxide, methane, nitrous oxide, or fine particulates associated with the Project, as energy storage systems using lithium-ion batteries produce near zero emissions. For purposes of completeness, the Company addresses each potential environmental impact below and demonstrates how it is not applicable to the Project or, alternatively, how the Project's environmental impact is minimal or non-existent.

4.1 AIR QUALITY

The Project will contribute near zero emissions. In fact, the Project may displace conventional generation facilities and thereby further reduce emission of carbon, particulates, and other air pollutants.

According to the U.S. EPA ("EPA"), emissions including, carbon dioxide, nitrogen oxides, sulfur dioxide, methane, nitrous oxide and fine particulates are products of combusting fossil fuels, as well as biogenic and other materials, and are the primary greenhouse gases ("GHG") emitted by human activities that are driving global climate change. Nitrogen oxides are also emitted by electric generating units and are precursors to the formation of ozone or smog, and fine particulates, and they also contribute to acid rain and other environmental and human health impacts. Additionally, sulfur dioxide is emitted by electric generating units especially in coal combustion; it produces acid rain and particulates that are associated with

other environmental and human health impacts.

The EPA estimated that in 2018, conventional power plants across the country emit more than 1.93 billion tons of CO₂. According to the EPA eGRID 2016 technical support documents, the CO₂ emissions from hydrogen, nuclear, purchased steam, solar, waste heat, water, wind, and energy storage are considered to be zero. Further, since energy storage has near zero emissions of any kind, the Project has no air impacts from the nitrogen oxides, sulfur dioxide, methane, and nitrous oxide and fine particulates that compose greenhouse gas emissions. Thus, from an air impacts perspective, BESS is superior as a unit. Depending on the generating sources on the electric grid that charge it, it can also be significantly superior as to air quality in performing services for the electric grid system to those performed by traditional generation. In sum, energy storage has a positive impact on air quality because storage helps replace traditional polluting generation and enables higher amounts of renewable energy on the grid.

4.2 EMISSIONS

G.L. c. 164, § 69J ¼ requires that a Petition include “either (a) evidence that the expected emissions from the Facility meet the technology performance standard in effect at the time of filing, or (b) a description of the environmental impacts, costs, and reliability of other fossil fuel generating technologies, and an explanation of why the proposed technology was chosen [over these alternatives].” As explained in further detail in Section 69J ¼, the purpose of the technology performance standards is to “streamline the [Siting Board’s] review of petitions to construct generating facilities that have state of the art environmental performance characteristics.”

A petition for approval must include an analysis of the proposed facility's expected emissions of the criteria and non-criteria pollutants listed in 980 CMR 12.03. If the expected emissions from a proposed generating facility meet the technology performance standards, the Petition does not need to include information regarding other fossil fuel technologies. Furthermore, applicants proposing the use of fuel types that do not contain pollutants specified in the technology performance standards and do not result in pollutants specified in the technology performance standards when burned, will not be required to provide modelling or testing results, guarantees, work papers or other similar documents with respect to those pollutants.

As discussed above in Section 4.1, the Project has near zero emissions, and there are no air impacts from criteria pollutants such as nitrogen oxides, sulfur dioxide, methane, and nitrous oxide and fine particulates. The Project also does not produce or burn fuel that produces non-criteria pollutants listed in 980 CMR 12.03(2). Because the emissions from a BESS is considered to be near zero, the Project satisfies, and arguably exceeds, the technology performance standards. Accordingly, information regarding other fossil fuel technologies is not required, nor are modelling or testing results, guarantees, work papers, or the like, as the "fuel type" the Company proposes to use does not contain or produce the pollutants specified in the technology performance standards. As explained throughout this Petition, the proposed technology was selected because of the economic, grid reliability, and environmental benefits that battery energy storage systems provide and the Project's contribution to the Commonwealth's clean energy and storage-specific objectives.

4.3 WATER RESOURCES

The Siting Board has historically based its determination regarding water supply upon a demonstration by the applicant of (1) an agreement for, or documentation of, an adequate water supply for the operational needs of the facility; (2) that the required water supply infrastructure exists, or can be constructed with minimal environmental impacts; and (3) that historical and

projected water withdrawals are within the permitted limits for the water supply source. Typical generation requires water for steam generation, cooling ponds, wash ponds, and for dust control. In locations where cooling ponds or outfalls to rivers or harbors are used, there is often an increase in temperature in the receiving water.

In almost all fossil fuel generating plants, ash management includes the use of settling basins, wash ponds or lagoons where the ash is pumped into the pond in slurry. After the ash settles, the water is pumped and treated before being reused. In coal-fired generating facilities, water is used for dust mitigation and equipment washing/maintenance.

A BESS does not require a source of on-site water. The only instance where water may be utilized at the Project Site would be in the rare occurrence of a thermal event. As was confirmed with the Carver Fire Department, in the unlikely event of a thermal event, a mobile water source would be used to transport water for fire suppression, should the CFD choose to utilize water. After construction of the Project, dust suppression is not required because of the limited number of visits to the site by maintenance workers. For these reasons, a BESS is superior to most other forms of electric generation with respect to water use.

4.4 WETLANDS

The Siting Board examines direct wetlands alteration, disturbance of wetland buffer zones or coastal wetland resource areas. Specifically, whether, and if so, how much of the Project footprint or site access would be located in or disturb wetlands.

The Massachusetts Wetlands Protection Act, G.L. c. 131 § 40, protects water-related lands such as wetlands, rivers and streams, floodplains, ponds, estuaries, and others and establishes procedures by which work is conducted in these areas. The implementation of Massachusetts wetland regulations is delegated to local conservation commissions. Any proposed activity which will remove, fill, dredge, alter, or build upon a protected area or within 100 feet of a protected area (the Buffer Zone), requires the filing of a Notice of Intent. The Carver Conservation Commission will make a determination on the Notice of Intent and issue a

permit in the form of an Order of Conditions. An Order of Conditions may confirm wetlands boundaries and permit proposed work, and includes conditions under which work will be carried out to minimize impacts to wetlands, wildlife, or to prevent pollution or flooding, and may include conditions for long-term operation and maintenance that will continue after the work is done. The Notice of Intent to obtain an Order of Conditions was submitted on January 18, 2019 (MDEP file number SE#126-579) and issued by the Carver Conservation Commission on February 6, 2019. See Exhibit CP-5 which includes a letter from the Carver Conservation Commission dated February 7, 2019.

There are wetlands to the south and west of the Project site as determined by AECOM in the Wetland Delineation Report dated November 9, 2018 (see Exhibit CP-8). There will be no direct impacts to the wetlands bordering the Project Site. While the Project Site falls within the 100-foot buffer zone of a wetland, in no instance will work be conducted within 65 feet from the delineated wetland and impacts to the buffer zone will be limited to tree removal and no impervious surfaces will be constructed within the Buffer Zone. In addition to the general conditions under the Massachusetts Wetlands Protection Act, all work associated with the Project will be performed in accordance with the Project's Order of Conditions.

4.5 STORMWATER

The Siting Board examines whether an applicant has a comprehensive plan for minimizing impacts resulting from stormwater-related discharges, i.e., runoff resulting from rainfall events and snow melt. MDEP has issued the Massachusetts Stormwater Handbook, as well as Stormwater Management Standards pursuant to the Wetlands Protection Act, G.L. c. 131 § 40, and the Massachusetts Clean Waters Act, G.L. c. 21, §§ 26-53, to promote increased stormwater recharge, the treatment of more runoff from polluting land uses, low impact development ("LID") techniques, pollution prevention, the removal of illicit discharges to stormwater management systems, and improved operation and maintenance of stormwater Best Management Practices ("BMPs").

As part of the Project's Order of Conditions, the Carver Conservation Commission found that work associated with the Project is subject to the Massachusetts Stormwater Standards and imposed conditions to address stormwater impacts. All work associated with the Project as it pertains to stormwater will be performed in compliance with the Order of Conditions.

To accommodate the change in runoff at the site by this Project, two infiltration basins with sediment forebays are proposed at both the eastern and western portions of the Project Site to collect and treat stormwater before discharge to the surrounding wetlands. Each infiltration basin was sized to store the amount of runoff associated with the 10-year, 24-hour storm. The structures were developed in accordance with Volume 2, Chapter 2 of the Massachusetts Stormwater Handbook. Both infiltration basins are proposed just outside of the fence lines to the battery storage areas, but outside of the 65-foot wetland setback area. Please refer to the Stormwater Report located as Exhibit CP-9 for further detail.

To protect infiltration basins from failing during a large storm, emergency spillways will be installed. The spillways will be designed to discharge just enough water so that the infiltration basin will not overflow. In addition, riprap will be used to prevent erosion at the weir discharge locations.

In conclusion, the installation of two infiltration basins with sediment forebays are designed to prevent a net increase in runoff from the site for the 10-year, 24-hour storm. The basins have also been designed to withstand larger rainfall events.

4.6 SOLID AND HAZARDOUS WASTE

The Project will produce neither solid nor hazardous waste during operations. During construction of the Project, solid waste will be transported offsite by the construction contractors in accordance with local, state and federal guidelines.

4.7 VISUAL

The visual impact of the Project is minimal due to the location and orientation of the Project Site, the existing tree cover on adjacent properties and the existing electrical

infrastructure to the north of the Project Site. As seen in Figure 3 below (and in Figure 2, above), the Project Site is located on a remote portion of land and the proposed western fence line of the Project is approximately 730 feet from the nearest occupied residence with a direct line of sight.

Figure 3 | Rendering looking West



A depiction of the future view, looking southeast towards the proposed Project Site, from said residence's backyard is included as Figures 4-1 and 4-2.

**Figure 4-1 | Rendering of View from Easternmost Residence on Atwood Street
(scale)**



**Figure 4-2 | Rendering of View from Easternmost Residence on Atwood Street
(no scale)**



The closest residence to the Project is approximately 400 feet west of the proposed Project fence line, but is shielded by forest, as is depicted in Figure 3, above.

As for visual impacts that could result from the construction of the Project, the Town of Carver limits construction to daylight hours of 7:00 a.m. to 4:30 p.m. As such, temporary lighting is not anticipated.

Moreover, permanent lighting within the Project Site will be pole-mounted. Carver zoning restrictions limit the height of those lighting poles to 15 feet. Accordingly, there should be no visual impact from those poles. As one of the conditions of the Site Plan Review and Special Permit, an approved lighting plan with a photometric analysis will be required before a building permit will be issued by the Town of Carver.

4.8 NOISE

The Project has minimal noise impacts to the surrounding community and complies with the MDEP's Noise Regulations and Policy.

1. State/Local Noise Policy/Regulations

The MDEP regulates noise under its Air Pollution Control regulations. Per the regulations, an "air contaminant" includes "any substance or man-made physical phenomenon in the ambient air space" and includes sound, and "air pollution" means the "presence . . . of one or more air contaminants . . . in such concentrations and of such duration as to . . . cause a nuisance . . . or unreasonably interfere with the comfortable enjoyment of life and property or the conduct of business." The MDEP regulations also prohibit "unnecessary emissions" of noise. The MDEP Division of Air Quality Control Policy Statement 90-001 (Feb. 1, 1990) interprets a violation of this noise regulation to have occurred if the sources cause either:

- An increase in the broadband sound pressure level of more than 10 A-weighted decibels (dBA) above the ambient, or
- A "pure tone" condition.

The ambient background level is defined as the L_{90} level as measured during proposed operating hours. A “pure tone” condition occurs when any octave band sound pressure level exceeds both of the two adjacent octave band sound pressure levels by 3 decibels (dB) or more.

These noise limits are MDEP policy and are applicable both at the property line and at the nearest noise sensitive areas (residences). In some circumstances, the policy limits can be “waived” by MDEP at property line locations when the adjacent land uses are not considered sensitive to elevated sound levels and are likely to remain so. The policy limits typically apply at the quietest period analyzed (*i.e.*, nighttime) unless the measurement location is associated with daytime use only. MDEP does not regulate the sound from construction activities or moving motor vehicles.

The permits issued by the Town of Carver do not contain noise requirements because the Town does not have a numerical decibel requirement. The Town of Carver will specify construction hours, which are currently expected to be from 7:00 a.m. to 4:30 p.m. Otherwise, no numerical decibel limits apply to construction activity.

2. Modeling Procedure and Results

Under normal conditions such as those present during the collection of ambient noise measurements, the modeled noise increase at the nearest residences are expected to be zero (0) to four (4) dBA above the ambient noise (see Exhibit CP-10). Moreover, all predicted noise levels from the proposed Project are within 10 dBA of the minimum measured background and will not exceed the MassDEP noise regulation standard at the property line.

Noise mitigation measures are not required for the Project because the predicted noise levels are within 10 dBA of the minimum measured background as required by DEP. As explained above, the rural Project Site minimizes noise impacts, and all predicted noise levels from the Project fall within the acceptable range of the MassDEP’s noise regulation standards.

4.9 LOCAL AND REGIONAL LAND USE

The Project Site consists of an approximately 6-acre portion of two larger parcels. While portions of the larger parcels are occupied by cranberry bogs, the proposed location of the BESS is not, and has not, been used for agricultural purposes. The anticipated changes to the acreage required to construct and operate the Project is as follows:

	<u>Existing</u>	<u>Change</u>	<u>Total</u>
Footprint of buildings	<u>0</u>	<u>+0.911 acres¹</u>	<u>0.911 acres</u>
Internal roadways	<u>0</u>	<u>+3.265 acres</u>	<u>3.265 acres</u>
Parking and other paved areas	<u>0</u>	<u>0</u>	<u>0</u>
Other altered areas	<u>0</u>	<u>+0.624 acres²</u>	<u>0.624 acres</u>
Undeveloped areas	<u>5.85</u>	<u>4.80 acres</u>	<u>5.85 acres</u>
	<u>acres</u>		
Total: Project Site Acreage	<u>5.85</u>	<u>4.80 acres</u>	<u>5.85 acres</u>
	<u>acres</u>		

1. Structure to house switchgear and controls.
2. Grading and grass areas for stormwater basins.

As reflected in the above table, the Project Site consists of approximately 6 acres of undeveloped uplands, of which 4.80 acres will be altered to accommodate the proposed BESS. In addition to the above changes, and as described above in Section 3.0, grading will be completed during the construction phase and grass areas will be added for stormwater infiltration basins.

The use of the land for the Project is consistent with the Town of Carver Master Plan, dated 2001 (the "Plan"). Under the Plan, Carver requires that land be used for economic development. The Project will provide a near zero emission source of electricity at times when that electricity will have the greatest economic value to the regional electric system. Moreover, the Project will improve grid reliability as intermittent renewables are added and traditional generation is retired in the Southeast Massachusetts load zone, improving current and future local business' access to reliable electricity. As such, the Project will improve the overall utilization and economics of resources supplying electric service to the grid.

Similarly, the addition of a BESS meets the Plan's objectives to add adequate infrastructure in cluster formations. Carver encourages developers to build infrastructure together with similar-situated purposes, so as not to construct infrastructure that interferes with the cranberry agriculture, on which Carver is reliant. This Project will be constructed next to a cell tower and adjacent to 345-kV, 230-kV and 115-kV transmission systems in Eversource's substation (No. 276) and adjacent electrical systems and lines. This selected location was carefully sought out and is consistent with the efforts preferred in the Section 1.3 Land Use Strategies of the Town Master Plan.

Moreover, the Project is consistent with the Southeastern Regional Planning and Economic Development District (the "SRPEDD"). The SRPEDD holds a responsibility for the region by enhancing the quality of life including economic opportunity and environmental quality. This refers to both preserving open land and maintaining a low unemployment rate.

As with the Town's Plan, the SRPEDD encourages development in areas that contain underutilized infrastructures (land, buildings, and other facilities). The Project's location is beneficial in that it is currently an undeveloped wooded area, however, infrastructure will be centrally located to interconnect with the existing 115-kV transmission system.

Additionally, the amount of land required for this Project is significantly less than would be necessary for a traditional generation plant of similar size (*i.e.*, 150 MW fossil fuel plant), which would require approximately 41 acres on average, as opposed to approximately 6 acres for development of the Project. This assumption was calculated by estimating the footprints of the following Massachusetts power plants: Pittsfield – 40 acres (154 MW), Mt. Tom – 86 acres (143 MW), Milford – 7 acres (148 MW), Exelon Medway – 53 acres (123.8 MW), Potter Station 2 – 65 acres (183 MW), Cleary Flood – 26 acres (133 MW) and Dighton – 12 acres (164.2 MW).

In generating stations that are oil-fired, vast areas of land are used to house large (~100,000 to ~500,000-gallon capacity) above-ground fuel storage tanks ("ASTs"). Since the fuel is liquid, the land immediately surrounding the ASTs is improved with containment berms to

contain 110% of the tank volume in the event of a breach in the tank. Filling the AST is typically accomplished by unloading fuel from offshore vessels/tankers or by pipeline. Smaller facilities may use over the road tank trucks to refuel their ASTs. This additional land is not needed for a BESS.

In generating stations that are fueled by natural gas, there is typically a restricted corridor that contains underground piping used to transport the natural gas. This corridor restricts most land use activities to maintain the integrity of the pipeline and to provide access for maintenance and or repair. This type of restricted corridor is also not required for a battery energy storage system.

In many cases, the transmission and distribution lines involve wetland crossing or work within the wetlands – these are not necessary to a significant degree for the Project. In addition, fossil fuel generating stations also require significant land for staging areas and employee parking and, although the generating stations are automated and do not require a large number of employees, a large portion of generating stations are paved.

Essentially, the Project will occupy a space approximately 12% the size of a traditional generation plant of the same MW output. The Project will not store fuel (coal, oil or other fuels); it does not contain any lagoons or wash ponds; it has limited restricted areas protecting underground utilities; and since the BESS Project is unmanned, there is no paved parking or sewer interconnections. All repairs are made on a carry-in and carry-out basis. In terms of decommissioning the Project Site, the Company will provide the Town of Carver with a bond per the requirements of the Site Plan Review and Special Permit (see Exhibit CP-3, attached). Based upon the above comparison of recent fossil-fuel fired generating facilities, the Cranberry Point Energy Storage Project's land use impacts associated with the BESS are significantly fewer, limited in location and easily mitigated.

Nonetheless, an erosion and sedimentation control program will be implemented to minimize potential temporary impacts to BVW and the 100-foot Buffer Zone during the

construction of the Project. The program incorporates BMPs specified in guidelines developed by the MDEP and presented in the Massachusetts Erosion and Sediment Control Guidelines for Urban and Suburban Areas: A Guide for Planners, Designers, and Municipal Officials (1997), River & Stream Crossing Standards (2011), U.S. Army Corps of Engineers (ACOE) document, Stream Crossing Best Management Practices (2015) and the EPA document, Developing Your Stormwater Pollution Prevention Plan: A Guide for Construction Sites (Office of Water Report EPA 833-B-09-002, February 2009). Proper implementation of the erosion and sedimentation control program will:

1. Minimize exposed soil areas through sequencing and temporary stabilization; and,
2. Place structures to manage stormwater runoff and erosion.

Non-structural practices to be used during construction include temporary stabilization, pavement sweeping along Main Street (if necessary), and dust control. These practices will be initiated as practicable in appropriate areas at the Project Site. Any areas of exposed sediment or stockpiles that will remain inactive for more than 14 days will be covered with a layer of straw mulch or plastic sheeting.

Structural erosion and sedimentation controls to be used on the site include erosion control barriers including silt fence, hay bales, and/or wattles or a combination of these materials.

Prior to any ground disturbance, an erosion control barrier will be installed at the downgradient limit of work. As construction progresses, additional barriers will be installed around the base of stockpiles and other erosion prone areas.

The following includes the key design and operation procedures for the Project in the approximate order of their implementation.

- Installation of soil erosion and siltation controls;
- Vegetation clearing and grubbing;
- New access driveway construction;

- Installation of concrete slab and pier foundations;
- Installation of battery storage system components and equipment; and,
- Installation of security fencing.

SECTION 5.0 BATTERY SAFETY

The Cranberry Point Energy Storage Project will be designed, constructed, and operated in a manner that will promote and maintain safety. The BESS will be designed in conformance with the Massachusetts Fire Code and associated National Fire Protection Association (“NFPA”) standards. As described in greater detail below, the Company has taken proactive and practical steps to ensure that the safety of the public, emergency responders, employees and others is adequately protected.

5.1 SAFETY STANDARDS

There are numerous and redundant safeguards built into the hardware and management systems of lithium-ion battery systems to help mitigate the risk of a thermal event. The Project will adhere to the premier national standard for stationary BESS installation (*i.e.*, the NFPA 855 code) (the “Code”).

Moreover, the design and operation of the Project will comply with international, national and state safety requirements standards, and best practices, including but not limited to the following.

- Battery design requirements, driven by safety standards from organizations such as UL or International Electrotechnical Commission (“IEC”)
 - *UL 1642 Standard for Lithium Batteries*
 - *UL 1741 Standard for Inverters, Converters, Controllers and Interconnection System Equipment for Use with Distributed Energy Resources*
 - *UL 1973 Standard for Batteries for Use in Light Electric Rail (LER) Applications and Stationary Applications*
 - *UL 9540 Standard for Energy Storage Systems and Equipment*
 - *UL 9540A Test Method for Evaluating Thermal Runaway Fire Propagation in Battery Energy Storage Systems*
 - *IEC 62619 Secondary cells and batteries containing alkaline or other non-acid electrolytes - Safety requirements for secondary lithium cells and batteries, for use in industrial application*
- Fire codes and National Fire Protection Association (“NFPA”) standards,

including:

- The Massachusetts Comprehensive Fire Safety Code (527 CMR 1.00);
- NFPA 1 *National Fire Code*;
- NFPA 855 *Energy Storage Systems Standard*.

5.2 MITIGATION

The Cranberry Point Energy Storage Project will utilize multiple redundant systems to prevent and manage battery short-circuiting, overcharging the BESS, overheating and thermal runaway, as described below.

To protect against battery short-circuiting and overcharging, the Project will use pyrotechnic fusing at various circuit integration levels to protect the low-voltage battery modules from faults triggered by overcurrent or the module-level battery management system (BMS). The power electronics have DC-side Solid State Circuit Breakers integrated into the battery enclosures, which, in part, measure the resistance between the ground and both poles. If the resistance drops below 1,000 Ω/V , a warning alarm is set off automatically and the applicable equipment is shut down.

To mitigate hazards due to overheating, the proposed battery enclosures are equipped with a thermal management system. This system operates by flowing a cooling liquid through a coolant loop which travels into each module to ensure that each cell is controlled thermally. The thermal management system undergoes a series of UL electrical tests (e.g., overcharging or short-circuiting battery cells), environmental tests (e.g., subjecting cells to external heating) and mechanical tests (e.g., dropping and/or physically damaging the cells). The testing is used to ensure that a single cell failure will not cascade to cause a thermal event outside of the battery enclosure.

Even with stringent testing, thermal events within a battery enclosure are possible. To mitigate such an event from cascading to more significant thermal activity outside of the enclosure, each enclosure has an automatic shut-down sequence that will occur should a

particular battery cell operate outside predetermined values of temperature, voltage and impedance. Additionally, a manual shutdown mechanism will be included in the Project design in the rare event that the system needs to be shut down on site by the CFD or an operations and maintenance professional.

If a thermal event does occur, and spreads beyond the incipient stage, the CFD will be notified automatically by an external fire detection system. This external fire detection system, which is separate from the thermal management system, utilizes thermal imaging cameras located outside of the enclosures, to detect heat rise within seconds of a battery enclosure reaching thermal runaway conditions.

Additionally, a Draft Emergency Response Plan (“ERP”) was prepared to reflect discussions with the CFD and the Company’s consultant, ESRG, and is included herein as Exhibit CP-11, attached.

5.3 HAZARD CONTROL

Battery technologies continue to evolve and be tested in accordance with similarly evolving codes and standards. Tesla battery systems have undergone rigorous testing in compliance with the standards outlined for the battery storage industry, including the national standard for stationary BESS installation, NFPA 855. This testing will be performed as part of the building permit process prior to construction of the Project pursuant to NFPA 855.

Per the manufacturer’s hazard mitigation analysis, unless there are conditions deemed at risk by the CFD within the immediate area of an enclosure with a thermal runaway event occurring, no water use is required or recommended, as the thermal event will end once the fuel sources within the enclosure (battery cells) are consumed. However, if the CFD does deem the use of water to be necessary, the manufacturer has indicated that there is no risk of electric shock for fire service personnel when applying water to lithium-ion battery fires. The use of water on an electrical system only presents a risk for very high voltages and even then, the risk is limited.

5.4 LOCAL COORDINATION

Cranberry Point has had numerous meetings with the CFD to discuss the proposed Project, including fundamental design components, emergency vehicle access, and emergency response plan development. Enclosures included in the proposed site design, as opposed to housing batteries within a building structure, present easier access and promote safety in the event of an emergency at the Project. The Project implemented several additional recommendations from the Carver Fire Department, including:

1. A ~20-foot access road around the Project, to allow fire truck access throughout the Project Site;
2. 8-foot spacing between battery enclosures; and
3. Coordinated emergency planning.

The Company incorporated this input and designed the Project accordingly. The Company also included the CFD recommendations on the parameters of the Emergency Response Plan (appended hereto as Exhibit CP-11, attached).

SECTION 6.0 ARCHAEOLOGICAL AND HISTORICAL

On July 1, 2021, Cranberry Point submitted a Project Notification Form (“PNF”) to the Massachusetts Historical Commission (“MHC”) for the proposed Project. On July 20, 2021, the MHC notified the Company that the Project Site is “in proximity” to several ancient Native American archaeological sites (19-PL-767; 19-PL-768). The MHC requested that an intensive (locational) archaeological survey (950 CMR 70) be conducted within archaeologically sensitive portions of the project impact area.

Cranberry Point is currently working with MHC to determine the extent of the archaeological survey. The Company will supplement this Application upon the completion of the archaeological survey. A copy of the PNF, as well as the MHC Response Letter, can be found attached as Exhibit CP-12 and Exhibit CP-13, respectively.

No part of the Project Site includes any historic structure, nor will any aspect of the Project be constructed within a historic district. Similarly, no part of the Project Site is listed in the State Register of Historic Places or the Inventory of Historic and Archaeological Assets of the Commonwealth.

SECTION 7.0 ALTERNATE SITES ANALYSIS

Cranberry Point conducted a comprehensive analysis to determine a suitable Massachusetts location for its 150 MWBESS.

The locations evaluated met specific requirements for a project of the size and scope under consideration. For example, the BESS had to be located (1) adjacent to infrastructure with available transmission capacity, (2) on a parcel of land greater than 1 acre and available for lease or sale, (3) in an area where construction and operation of the project would have minimal environmental impact or would not closely abut residences, (4) in ISO-NE's "SENE" zone, and (5) at a location on the grid where the Project could provide its maximum service potential to local electric reliability.

As such, Cranberry Point evaluated several alternative sites as well as a 'no-build' alternative.

No Build Alternative

Under the No-Build alternative, the Project would not be constructed. Failure to develop the Project would undermine ISO-NE's capacity requirements in the SENE zone. Without this Project, the SENE zone will face increasing volatility with the retirement of Mystic gas generation units, the recent retirement of the Plymouth nuclear plant, and the future on shoring of the Vineyard Wind and Mayflower Wind offshore projects. Moreover, because the Project is likely to defer and/or alleviate the need for additional electric transmission infrastructure in the area, the environmental benefits from the Project would not be realized. Therefore, the No-Build alternative was not considered further.

Alternative 1 – Carver (Preferred Alternative)

The proposed Carver BESS site is an approximately 6-acre site (250,000+ square foot) area located adjacent to and just south of the existing Eversource Carver Substation off Main Street in Carver, Massachusetts. This location was identified as the optimal solution for multiple reasons. First, the size of the lot, at approximately 6-acres, meets the requisite land area

needed for a project of the size proposed. Second, as the lot is more than 400 feet from the nearest residence, has no wetland intrusion, and no historical cranberry operations, there is minimal, if any, economic or environmental impact on the surrounding community. Third, the lot of land is readily available for lease. Fourth, the parcel is adjacent to infrastructure with available transmission capacity. Fifth, the location of the Project is in an area where the Company could readily obtain a Site Plan Review and Special Permit, with minimal impact on the environment, but for tree clearing on the western portion of the Project Site. Sixth, the location is in close proximity to retiring nuclear and fossil-fuel generation facilities and potential onland interconnection points for offshore wind, combined with significant market advantages including but not limited to, energy price volatility and compensation mechanisms available for providing ancillary services. All of these enhance the viability of a project of this size and scope.

Alternative 2 – Wakefield

The Wakefield BESS site is an approximately 2.24-acre (97,700+ square foot) area located adjacent to and just east of the existing Wakefield Substation off of Old Colony Drive in Wakefield, Massachusetts. The location within the Boston load center made the Wakefield site attractive, however, as compared to the Preferred Alternative, this location was not considered further. First, the site is densely forested and surrounded by Isolated and Bordering Vegetated Wetlands. Second, the site is located within 300 feet of the nearest residence. Third, this site was not known to be located near future offshore wind interconnection points or retiring generation. As such, the economics to develop a project at this location were not viable. Access to the site would have required significant tree clearing and filling an Isolated Wetland in order to construct the roadway. Given the constraints that this site would have on the project's development and economic viability, Wakefield was not considered further.

Alternative 3 – Falmouth

The proposed Falmouth BESS site is an approximately 2.42-acre (105,600+ square foot) area located adjacent to and northwest of the existing Falmouth Substation off of Stephens

Lane in Falmouth, Massachusetts. The Falmouth site is on a lower-voltage network near Cape Cod, which presented deliverability difficulties to the Boston load center when compared to the location and transmission network of the Preferred Site. From an interconnection perspective, a generation tie-line would have been required in order to connect to the nearest point of interconnection. Moreover, the site is located within 200 feet of the nearest residence, as well as within 200 feet of the Oak Grove cemetery. While the site is an active sand and gravel pit, and any tree removal required to construct the BESS project would be minimal, construction would result in impacts to an Isolated Wetland. When Falmouth was under consideration, it was not known to be located in an area where offshore wind projects were thought to tie into the existing onshore electrical grid or near retiring generation. Thus, given these issues, the Falmouth site was not considered further.

Conclusion

Of all the BESS sites considered, Alternatives 2 and 3 were excluded because of the significant environmental impacts (e.g., close proximity to Isolated Wetlands and residential neighborhoods. Additionally, Alternative 2 would result in significant tree clearing. The Preferred Alternative location was selected because of its proximity to a crucial inter-tie point for the 115-kV transmission systems, has no impact on wetlands, minimal tree-clearing needs, and is more than 400 feet of the nearest residence. Given the cost, siting constraints, land area requirements, environmental considerations and transmission analysis performed, the Preferred Alternative is ideally located for a large, grid-improving standalone BESS project in Massachusetts.

SECTION 8.0 CONSISTENCY WITH COMMONWEALTH POLICIES

8.1 CONSISTENCY WITH POLICIES OF THE COMMONWEALTH

The Project, if approved, would contribute 300 MWh of energy storage toward the goals delineated by the Commonwealth of Massachusetts in its *State of Charge* report and other initiatives and mandates. As discussed below, it is designed to enhance the efficiency, affordability, resiliency, and cleanliness of the electric grid by modernizing the way that electricity is generated and delivered.

8.2 ENERGY STORAGE INITIATIVE

As noted above, the Baker Administration launched the Energy Storage Initiative in May 2015 with the goal of advancing the energy storage segment of the Massachusetts clean energy industry by: 1) Attracting, supporting and promoting storage companies in Massachusetts; 2) Accelerating the development of early commercial storage technologies; 3) Expanding markets for storage technologies, and valuing storage benefits to clean energy integration, grid reliability, system wide efficiency, and peak demand reduction; and 4) Recommending the developing policies, regulations and programs that help achieve those objectives.

As part of the 2015 Energy Storage Initiative, the Department of Energy Resources (“DOER”) and Massachusetts Clean Energy Center partnered to conduct a study, the *State of Charge* (see Attachment 1, attached), to review the storage industry landscape, review economic development and market opportunities for energy storage, and evaluate potential policies and programs to support energy storage development in Massachusetts. DOER has implemented many of the 2016 *State of Charge* report’s recommendations to promote energy storage in the state.

The *State of Charge* report identified ratepayer cost benefits of energy storage associated with “reduced peak demand, deferred transmission and distribution investments, reduced GHG emissions, reduced cost of renewables integration, deferred new capacity

investments, and increased grid flexibility, reliability and resiliency.”⁵ The report also identified near and long term economic and workforce benefits to Massachusetts by implementing energy storage.⁶

An Act Relative to Energy Diversity, Chapter 188 of the Acts of 2016, directed the DOER to adopt targets to achieve the state’s energy storage goals. DOER adopted a 200 MWh energy storage target for Massachusetts Electric Distribution Companies (“EDCs”) to procure by January 1, 2020. An Act to Advance Clean Energy, signed into law by Governor Baker in 2018, subsequently revised that goal to a 1,000 MWh energy storage target to be achieved by December 21, 2025. As of February 15, 2020, Massachusetts EDCs reported only 108 MWh of installed energy storage. The Project would contribute 150 MWh of energy storage toward the Commonwealth’s 1,000 MWh goal, while posing minimal impact to the environment by not contributing to, and potentially reducing or displacing, GHG emissions.

8.3 CLEAN PEAK STANDARD

The Massachusetts Clean Peak Standard (“CPS”) is “designed to provide incentives to clean energy technologies that can supply electricity or reduce demand during seasonal peak demand periods established by DOER” (see Attachments 2 and 3, attached). According to DOER, Clean Peak Resources contribute to the Commonwealth’s environmental protection goals concerning air emissions, including those required by the Global Warming Solutions Act (“GWSA”),⁷ discussed below, by displacing non-renewable generating resources while reducing peak demand and system losses and increasing grid reliability.

Similar to the Massachusetts Renewable Portfolio Standard, the CPS requires a percentage of electricity delivered during peak hours to come from certain eligible Clean Peak

⁵ State of Charge: A Comprehensive Study of Energy Storage in Massachusetts, Emerging Technology Division (last accessed Oct. 8, 2020), available at <https://www.mass.gov/service-details/energy-storage-study>.

⁶ *Id.*

⁷ Global Warming Solutions Act, M.G.L. c. 21N, §§ 1-9.

Sources. Clean Peak Sources include Qualified RPS Resources, Qualified Energy Storage Systems, or Demand Response Resources that generate, dispatch, or discharge electricity into the electric distribution system during certain peak periods, or alternatively, reduce load on the system during those periods.⁸

The Project is uniquely positioned to satisfy the CPS. One of the many benefits of the Project is that it is “fully dispatchable,” capable of providing an energy source directly to the transmission system during peak load and can store electricity during off peak periods, whereas intermittent renewables and renewable-storage hybrid projects are unable to fully produce on demand and are limited in their charge and discharge by implementation rules of the federal Investment Tax Credit that they use in financing. Moreover, fully dispatchable BESS installations like the Project can perform additional grid services that are currently provided by traditional power plants, such as fast frequency response, virtual inertia, and black-start capabilities to prevent catastrophic failure or restart after an outage. Standalone BESS like the Project are thus the ideal clean facilities to achieve the objectives of the CPS because they displace non-renewable generating sources, thereby reducing air emissions, while reducing peak demand and increasing reliability.

8.4 GLOBAL WARMING SOLUTIONS ACT

The 2008 Global Warming Solutions Act (“GWSA”) required a 25% reduction in greenhouse gas (“GHG”) emissions from all sectors of the economy below the 1990 baseline emission level by 2020, and mandates at least an 80% reduction by 2050. The Executive Office of Energy and Environmental Affairs is working toward the development of the Massachusetts Decarbonization Roadmap to 2050 that will identify “strategies, policies, and implementation pathways for MA to achieve at least 80% GHG reductions by 2050, including multiple pathways

⁸ See 225 CMR 21.02, “Clean Peak Resource.”

to near zero emissions.”⁹ On January 21, 2020, Governor Baker announced the Commonwealth’s intent to pursue the more aggressive near zero target to further reduce emissions.

The GWSA requires that the Secretary of Energy and Environmental Affairs, in consultation with the MassDEP and DOER, adopt separate statewide GHG emissions limits for 2020, 2030, 2040, and 2050. On April 22, 2020, the Secretary established a 2050 statewide emissions limit of near zero greenhouse gas emissions defined as follows:

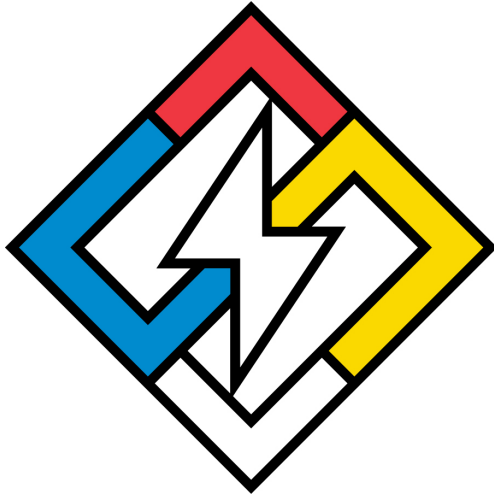
A level of statewide greenhouse gas emissions that is equal in quantity to the amount of carbon dioxide or its equivalent that is removed from the atmosphere and stored annually by, or attributable to, the Commonwealth; provided, however, that in no event shall the level of emissions be greater than a level that is 85 percent below the 1990 level.¹⁰

Approval of the Project would contribute to the Commonwealth’s achievement of important health, environmental, and energy policies, including meeting the Commonwealth’s 2050 near zero emissions goal under the GWSA. Battery storage facilities increase the energy efficiency of the electric grid with minimal environmental impacts. As described throughout this Petition, there is no waste produced by energy storage systems and no fuels emitted by the BESS. Furthermore, the system increases grid reliability during peak load times, and can perform other grid services, thereby offsetting the need for additional fossil-fuel fired peaking units, further reducing greenhouse gas emissions and limiting the environmental impacts of such projects.

⁹ See MA Decarbonization Roadmap, Massachusetts Executive Office of Energy and Environmental Affairs (last accessed Oct. 8, 2020), available at <https://www.mass.gov/info-details/ma-decarbonization-roadmap>.

¹⁰ *Determination of Statewide Emissions Limit for 2050*, Executive Office of Energy and Environmental Affairs (Apr. 22, 2020), available at <https://www.mass.gov/doc/final-signed-letter-of-determination-for-2050-emissions-limit/download>.

EXHIBIT 3



ESRG

ENERGY SAFETY RESPONSE GROUP

PLUS POWER - CRANBERRY POINT ENERGY STORAGE PROJECT: EMERGENCY RESPONSE PLAN (ERP)

Draft ERP 3 August 2021 Version 1.0

Summary

This document is an emergency response plan for the Plus Power - Cranberry Point Energy Storage Project located at 31R Main St., Carver, MA 02330.

This ERP provides information and instruction to guide first responders in preparing for and safely responding to an accident, fire, or other emergency associated with the Cranberry Point Energy Storage Project.

Life safety shall be the highest priority during any type of event.

Important Note on Document Status

This document will remain as a "DRAFT" and is subject to further update, and will be finalized upon completion of the construction and commissioning of the Cranberry Point Energy Storage Project

Paul Rogers

Paul.Rogers@energyresponsegroup.com

Plus Power - Cranberry Point Energy Storage Project: Emergency Response Plan (ERP)

Document Review, Issuance and Revisions

Reviewed by:

Paul Rogers, Principal Founder Energy Safety Response Group (ESRG) _____ Date: _____	Casey Grant, P.E., Senior Consultant Energy Safety Response Group (ESRG) _____ Date: _____
---	---

Issuance and Revision Summary:

Action	Version	Date	Description / Comment
Issuance	1.0	3 August 2021	Initial issuance of draft document for review.
Revision			
Revision			
Revision			

Note: The information in this ERP is subject to change while in draft status, potentially due to modifications to equipment or other factors affecting the design of the system.

Table of Contents

1) *Site Overview* 2

2) *Emergency Contacts*..... 3

3) *Site Map*..... 4

4) *System Specific Fire Protection & Safety Controls* 7

5) *Potential Hazards*..... 10

6) *Potential Site-Specific Hazards* 11

7) *Required Personal Protective Equipment*..... 12

8) *Emergency Response Recommendations* 13

9) *Specific Recommendations (By Type of Emergency)* 14

10) *System Specific Fire Protection & Safety Controls* 17

Appendix A – Safety Data Sheets (SDS)..... 18

Appendix B – Site Specific Signage, hazards, placarding: (Example Signs) 19

Appendix C – Proposed Site Layout..... 20

Appendix D – Subject Matter Expert (SME) Incident Response 21

Appendix E – ESS Information Card (EIC) 23

Plus Power - Cranberry Point Energy Storage Project: Emergency Response Plan (ERP)

1) Site Overview

Project Owner:

Applicant – Cranberry Point Energy Storage, LLC (developed by Plus Power, LLC)

Owner – Cranberry Point Energy Storage, LLC

Site Area – 186,436 SF

Current Use – Undeveloped; wooded (Cranberry bogs to the south of Project Site)

Proposed Use – Battery Energy Storage System

Site Location:

31R Main St., Carver, MA 02330; located next to Eversource substation.

Equipment on Site:

- Major equipment on site will consist of up to 128 cabinet style enclosures containing lithium-ion batteries. PCS and thermal management systems are integrated into the battery enclosure and not separate equipment. Included are 58 MV step up transformers.
- 150MW/300MWh system located in Carver, MA that will be interconnecting to the Eversource grid at 115kV, adjacent to a large substation.
- BESS equipment on site will consist of up to 1.0 MW and 3.0 MWh battery energy storage system (BESS) free-standing enclosures. Each BESS battery enclosure has up to 20 modules, thermal management units, an AC auxiliary power distribution system, a DC power distribution system. The output voltage of each enclosure is approximately 480 VAC.
- The AC output of the inverter (PCS) is connected to the low side of the medium voltage transformer. The high side of the medium voltage transformer is connected to the electric grid.
- None of the enclosures are intended to be entered.
- Only onsite personnel present will be for maintenance purposes.
- No onsite disconnect outside of the BESS inverter local disconnect.
- Responder Knox box location: At the Northern entrance gate near the cell tower (TBD). It contains the following information: TBD

Plus Power - Cranberry Point Energy Storage Project: Emergency Response Plan (ERP)

2) Emergency Contacts

Local & State Emergency Response Agencies:

Emergency: 911

Carver Fire Department:

Address: 99 Main St., Carver, MA 02330

Phone: 508-866-3440 (non-emergency)

- Deputy Chief Eric Germaine
- Assistant Deputy Chief Jesse Boyle (code enforcement officer)

<https://carverfire.org/company/chief-officers/>

Carver, MA Police Department:

Address: 112 Main Street, Carver, Massachusetts, 02330

Phone: 508-866-2000

Local Hospital: Beth Israel Deaconess Hospital in Plymouth, 275 Sandwich St, Plymouth, MA 02360 - 24 hr emergency room

Local Trauma Center: South Shore Hospital, 55 Fogg Rd, South Weymouth, MA 02190 - Level II Trauma Center

Local Burn Center: Massachusetts General Hospital 55 Fruit St GRB 1300, Boston, MA 02114 (likely would transport aeromedical unless conditions prevented)

BESS Emergency Call Center: Tesla for the BESS emergency

Available 24/7: 1-650-681-6060

Subject Matter Expert (SME) Chris Quaranta, Director - Engineering & Construction, Plus Power (until NOC or O&M contract in place; additional SME to be determined)

Plus Power - Cranberry Point Energy Storage Project: Emergency Response Plan (ERP)

3) Site Map

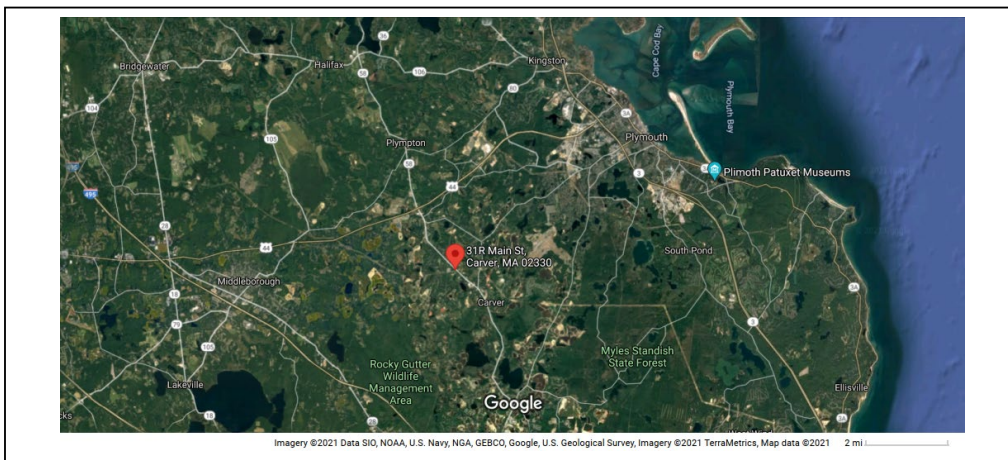


Figure 1 – Cranberry Point Energy Storage Project

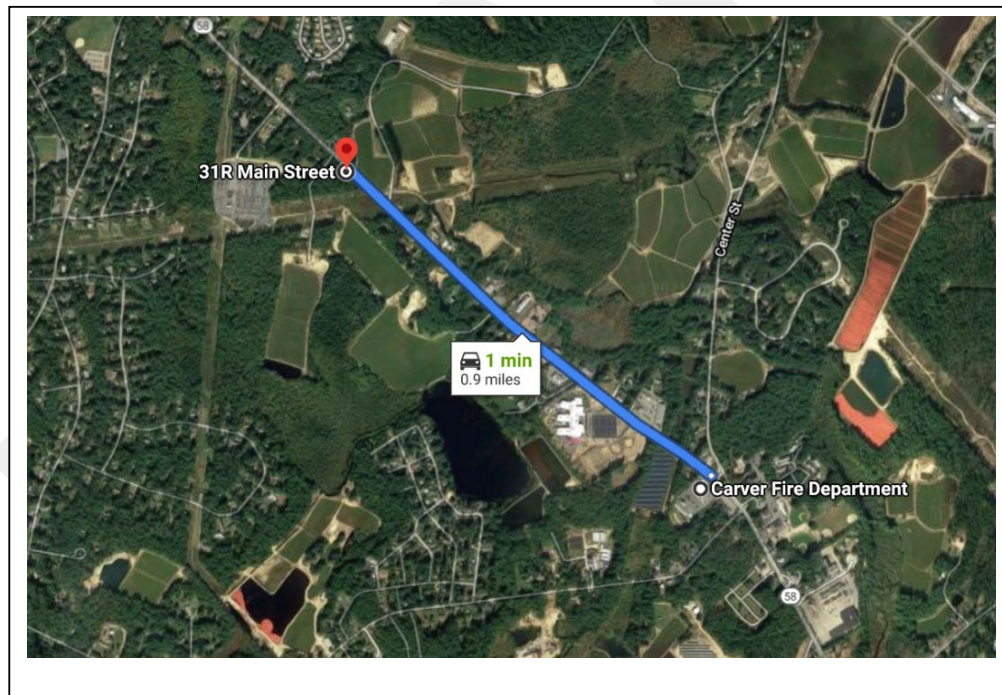


Figure 2 – Carver, MA Fire Department Response Distance

Plus Power - Cranberry Point Energy Storage Project: Emergency Response Plan (ERP)



Figure 3 – Conceptual Drawing



Figure 4 – Conceptual Drawing

Plus Power - Cranberry Point Energy Storage Project: Emergency Response Plan (ERP)



Figure 5 – East Side of Site Looking South (view as of 13/Jul/2021)



Figure 6 – Southwest View towards Cell Tower (view as of 13/Jul/2021)



Figure 7 – North of Site – View to the West of Eversource Substation (view as of 13/Jul/2021)

Plus Power - Cranberry Point Energy Storage Project: Emergency Response Plan (ERP)

4) System Specific Fire Protection & Safety Controls

4.1) Condition Monitoring & Alarming:

Conditions inside the Tesla Megapack system are continuously measured for temperature, current, state of charge, and voltage sensor information, and can be accessed remotely through the Network Operations Center (NOC). Although the data is also available on the LCD screen on each enclosure, the screen on the exterior of the unit **shall not be approached when risk of fire or explosion exists.**

Fire detection for each BESS unit consists of Battery Management System (BMS) data available through the NOC and an external multi-spectrum infrared camera for the site. Upon detection of an overtemperature or fire incident, the alarm condition will be transmitted to a Network Operations Center and a Central Monitoring Station that will in turn send an alarm to the Carver FD Dispatch Center. The following is an example of a typical infrared camera mounted to a pole for exterior detection of heat and fire events emanating from a Megapack Unit:

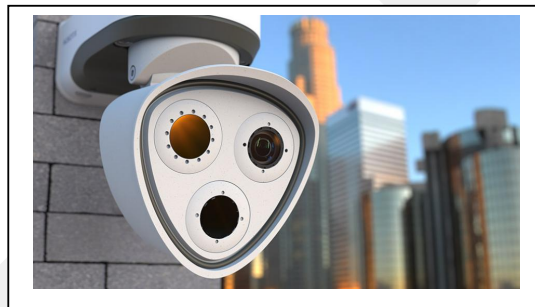


Figure 8 – Example of Thermal Camera for Fire Detection

4.2) Considerations for Incidents and Emergencies

4.2.1) Incidents

For inverter faults, isolation faults, and internal loss of communication that prevent the safe operation of the system, Tesla's monitoring system will automatically alert the Tesla NOC to initiate a corrective action remotely or to dispatch an in-person field visit. The project will also have an O&M provider and 24/7 NOC in place prior to the system going live, which will also be monitoring these conditions.

4.2.2) Emergencies

4.2.2.1) Thermal Runaway/Fire

For the Tesla Megapack, testing has shown that a propagating thermal runaway event due to internal causes is very unlikely due to physical internal separation elements and the battery module's design, which requires multiple co-located cells to go into runaway at the same time.

Plus Power - Cranberry Point Energy Storage Project: Emergency Response Plan (ERP)

External factors, including a large impact that damages many cells at once or a pro-longed exposure to an intense external fire, could create a propagating thermal runaway event that may spread throughout the entire enclosure.

In such a case, it is likely that all battery modules will consume themselves. **In the event of a fire, the design approach is for the Megapack contents to be fully consumed based upon data from UL 9540A installation level tests.**

If a propagating thermal runaway occurs, over-temperature faults isolate the concerned Megapack by first disconnecting the affected battery module, and then opening the AC contactors. All faults are monitored passively by the Tesla computer system which then will be relayed to the NOC that will review and act accordingly. This NOC is TBD prior to commissioning.

While testing has shown that the system performs in a safe and controlled manner, fully consuming itself slowly over a period of a few hours, without explosive bursts, deflagrations, or unexpected hazards, the decision to apply external suppression to the troubled enclosure and adjacent units is **ultimately at the discretion of the incident commander.**

4.2.2.2) Explosion / Deflagration Control

Tesla utilizes over-pressure vents and a proprietary sparker system to manage potential deflagration.



Figure 9 – Tesla Megapack – View 1

Plus Power - Cranberry Point Energy Storage Project: Emergency Response Plan (ERP)



Figure 10 – Tesla Megapack – View 2

Tesla's proprietary sparker system prevents a dangerous buildup of gases within the enclosure by combusting flammable off-gases during a runaway event.

The vents mitigate the effects of over-pressure by directing all gases, smoke, and flame out of the top of Megapack and ensure the front doors remain shut for the safety of nearby exposures and personnel. The vents are passive and are not actuated or controlled. Their rubber seals are designed to release over-pressure events (including arc flash events) or melt out during thermal runaway events.

Co-located with the vents are one-way "umbrella" valves that help exhaust and disperse runaway gases to help minimize gas concentrations inside the enclosure.

Emergency responders and others may observe a continual sparking within cabinets at certain locations. This is a normal operational feature of the unit, i.e., the "sparker system", which is part of the automatic safety system to prevent a dangerous build-up of gases within the enclosure.

The sparker system is always on and is powered by internal battery power, and thus will remain operational even during loss of grid power or if an external shutdown is triggered for the battery equipment. If an event were to occur under these conditions, the sparker system and corresponding overpressure vents would still operate as described.

Plus Power - Cranberry Point Energy Storage Project: Emergency Response Plan (ERP)

5) Potential Hazards

There are five major risks posed by lithium-ion battery failures. They are electric shock, arc flash, fire, explosion, and the by-product from off-gassing. During failure, a lithium-ion battery may emit tens to hundreds of liters of off gas, and larger failures may emit thousands of liters of gas.

Indicators which may provide insight into what is happening or about to happen during an incident may include:

- **Electrical equipment** – Electrical equipment shall always be treated as energized. Associated hazards include electric shock, arc flash, and fire.
- **Overhead power lines** – Overhead power lines shall always be treated as energized. Associated hazards include electric shock, arc flash, and fire. For locations see facility site plan, Appendix C.
- **BESS electrical equipment** – BESS electrical equipment including batteries shall always be treated as energized. A BESS does not have a single point of disconnect to electrically isolate all components from each other. There are disconnects that will de-energize select parts of the system, but the batteries themselves will remain energized.
- **BESS battery fire** – Battery fires present unique hazards, including stranded energy and re-ignition risk.
- **BESS off-gassing** – Lithium-ion batteries release flammable and toxic chemicals when subjected to electrical or physical damage, including fire. Chemicals released can also pose an inhalation hazard.
- **BESS explosion/deflagration** – Although the approach that is taken with the Tesla Megapack mitigates the buildup of gases by burning them from the outset of any potential release, responders should be aware that unexpected situations may arise and a safe standoff distance from the troubled enclosure is recommended.
- **Water run-off** – Water run-off could be considered contaminated, and all efforts should be taken to minimize unnecessary firefighting water contamination of the surrounding environment. Robust drainage and water run-off features are included in the design of the facility to capture credible worst case water discharge. Two water runoff containment areas, known as infiltration basins are provided. One will be installed in the Western Storage area, and one will be installed in the Eastern Storage area. The basins are designed to provide water quality treatment and to control the peak discharge from 2-year and 10-year storms. In the

Typical composition of off-gassing event may include:

- **High concentrations (>10%)**
 - Hydrogen
 - Carbon Monoxide
 - Carbon Dioxide
- **Lower Concentrations (<10%)**
 - Methane
 - Ethane
 - Other flammable hydrocarbons

Plus Power - Cranberry Point Energy Storage Project: Emergency Response Plan (ERP)

event of a fire or emergency the basins are designed to capture and contain water runoff from potential cooling efforts to the BESS units adjacent to the troubled enclosure that may be smoking or burning. The design specifically avoids runoff towards the adjacent Cranberry Bogs. It is not anticipated, nor advised, that special extinguishing agents such as foam should be used throughout the incident. A plan, similar to an electrical substation Spill Prevention, Control, and Countermeasure (SPCC) will be put in place to contain and remove from the site runoff from these areas throughout the life of the incident.¹

6) Potential Site-Specific Hazards

- **Residential Exposures** - Potential site risks to the local community are minimal due to the remote location and nature of the site. Private residences in the vicinity are remote with the closest residence approximately 400 feet to the west of the project site's fence line. However, the closest proposed battery enclosures are approximately 650' away, and are sufficiently distant such that smoke or off-gas from the battery container are not expected to pose a risk.
- **Electrical Substation** – The BESS project is in the vicinity is an Eversource Carver Substation. The exposure threat between these facilities is minimal. If necessary, protective measures should be taken for the electrical substation. This includes taking requisite protective measures, including sufficient standoff distances, using fog patterns for hose lines with only potable water, and other precautions for energized electrical equipment.
- **Adjacent Buildings and Structures** - Nearby is a Cell Tower and service structures, and these are normally not occupied but may contain its own battery system and electrical equipment. The outside of these structures should be monitored and cooled should it be necessary.
- **Wetlands and Cranberry Bogs** – Nearby wetlands require special consideration for firefighting water discharge control. The BESS project is located outside of the 100' buffer zone for run-off. The nearest cranberry bog is located approximately 60' to the South of the nearest BESS unit.
- **Surrounding Wooded Area** – The BESS project location will be cleared approximately 50 ft from BESS project and maintained free of foliage and growth. Access roads are indicated in the Appendix in Figure C1. The access pathways throughout the Project site will be gravel/crushed stone. Emergency access path is planned from Eversource's existing Carver substation to the north of the site.

¹ Additional Information on water runoff containment can be found in the Stormwater Report produced by AECOM Environmental Engineers for the Cranberry Point Energy Storage Project.

Plus Power - Cranberry Point Energy Storage Project: Emergency Response Plan (ERP)

7) Required Personal Protective Equipment

Full firefighter protective gear shall be worn in any response to a fire and/or explosion event or any indication a fire may be present. This shall include proper use of Self-Contained Breathing Apparatus (SCBA).

If no fire or explosion risk is present, AR protective clothing to protect against arc flash and shock shall be worn. Jewelry such as necklaces shall be removed to avoid contact with any electrical hazard.

DRAFT

Plus Power - Cranberry Point Energy Storage Project: Emergency Response Plan (ERP)

8) Emergency Response Recommendations

Initiation of emergency response shall be activated per current protocol. If there is any threat or potential threat to life or safety, 911 shall be called immediately to summon the aid of public safety responders. An initial scene assessment shall be conducted from all sides (360-degree scene size-up) if possible, and a clear concise assessment shall be given to incoming responders. Hazards and facility safety concerns such as high voltage areas or other electrical concerns shall be announced to all responders. The scene assessment shall include the following in plain language (No code or terms):

- Where the incident is located,
- What has happened,
- What is occurring,
- Any injuries or unaccounted for individuals,
- What the needs/resources should be requested.

An Incident Command System (ICS) shall be established immediately and shall include designation of roles. The primary command post location will be at a to-be-determined location . If public safety is summoned to the incident, the ICS shall be a Unified Incident Command System.

Onsite staff and visitors shall immediately go to a designated muster point for accountability, which will be the command post location unless designated differently by Incident Command. Incident Command shall designate the individual in charge of accountability. Accountability shall be reported as soon as possible. If available, another individual shall control any traffic and guide first responders into the scene.

At the same time as these activities are occurring the Emergency Contact shall immediately establish available data from the Battery Management System (BMS) and communicate this to the appropriate incident command individual.

Plus Power - Cranberry Point Energy Storage Project: Emergency Response Plan (ERP)

9) Specific Recommendations (By Type of Emergency)

9.1) Fire

When sensors within the BESS enclosures (e.g., BMS) detect conditions that indicate a fire, an audible alarm will sound, and a visual strobe will flash on the enclosure exterior. Smoke and flame may be visible from the outside of the BESS enclosure. Fire growth can be slow, fast, or ultra-fast (e.g., deflagration) in nature.

The batteries in this facility are designed to NOT spread if a specific unit fails and begins to burn. The primary approach is to protect exposures as needed and let the unit burn itself out.

A safe stand-off distance shall be maintained between individuals and the BESS enclosure exhibiting fire conditions. Staging of personnel and equipment shall be on the angles of the BESS enclosure, to stay out of the potential blast radius of any doors or other potential projectiles. Attempt to extinguish the fire only if imminent threat to life safety exists.

If there is no immediate threat to life safety:

Unless there is an immediate threat to life safety or similar threat, a defensive fire attack should be used.

1. **Allow the BESS to burn in a controlled fashion** until all fuel sources inside are depleted.
2. A defensive approach should be considered utilizing water to cool and protect adjacent exposures and mitigate the spread of fire to areas outside of the fenced installation. Remove or protect adjacent vegetation through routine maintenance program to avoid providing an additional fuel source which may aid the spread of fire.
3. Remember that even after the BESS is isolated from the electric grid there will still be considerable stored energy in the batteries that poses a potential electric shock hazard to anyone in the nearby vicinity.

Chemicals released during a fire or explosion will be in a gaseous form and primarily pose an inhalation hazard. A fog pattern from a handline or monitor nozzle may be an effective way to control the off-gassing event on the exterior of the battery container from migrating to unwanted areas. However, if water is used in extinguishing flames, these gases can become acids which may cause skin irritation.

******** WARNING *****
The risk of battery re-ignition and/or secondary ignition remains present for hours or even days after the smoke/flame was initially detected. Even if a lithium-ion battery fire has been extinguished, there is still a risk of re-ignition.***

Water curtains or hose streams may be applied to adjacent exposures for cooling purposes. If any indicators are present of damage or heat to an adjacent system, the BMS data shall be closely monitored for the adjacent system and relayed to the appropriate individual within the Incident Command System.

Following partial or complete consumption of the system by fire, batteries may continue to emit low levels of flammable gases and dangerous levels of toxic gases for an extended period of time. Continuous monitoring of gas levels in and around the incident location is recommended to be

Plus Power - Cranberry Point Energy Storage Project: Emergency Response Plan (ERP)

conducted and use of mechanical ventilation may be utilized to manage gas levels. Full firefighter PPE and SCBA shall be utilized until gas levels are confirmed to be at a safe level. A Firewatch shall be performed for a minimum of 24 hours after any fire incident.

The initial Fire Department water supply will be from fire apparatus and water tankers (tenders) for shuttling water to the site. Secondary water sources if needed include local bogs and ponds.

9.2) Deflagration/Explosion

Tesla Megapacks are designed to minimize the potential of a deflagration or explosion occurring. Still, a safe stand-off distance shall be maintained between individuals and the BESS enclosure exhibiting fire conditions. Staging of personnel and equipment shall be on the angles of the BESS enclosure, to stay out of the potential blast radius of any doors or other potential projectiles. Attempt to extinguish the fire only if imminent threat to life safety exists.

Lithium batteries off-gas when heated or when subjected to electrical or physical damage. These gasses can accumulate inside the battery container at levels above the Lower Explosive Limit (LEL). While it is highly cautioned against that an enclosure door be opened during an off-gassing or fire event, should the need arise, the following precautions shall be taken:

- The responder, if preparing to open any door or compartment, shall stand to the side to eliminate the risk of being directly in the path of the blast pressure if an explosion were to occur.
- Gas monitoring should be continuously conducted, and gas meters shall be affixed to all responders to warn of potential atmospheric risks.
- Gas readings outside the battery cabinet, if the doors remain closed, should not be considered indicative of conditions inside the enclosure.
- Any ignition source inside or near the BESS enclosure can potentially cause the flammable gasses to ignite and/or explode.

9.3) Electric Shock

All BESS systems and related electrical equipment shall always be treated as energized (Energetic Hazardous Material).

Even though a battery may look to be destroyed by fire and/or other means, there is great potential that the battery still has stranded energy and remains energized. De-energization of the system or any removal of the battery or battery component shall only be performed by a trained and competent individual with appropriate PPE.

Note: ESRG strongly advises against the fire department attempting to overhaul the Megapack enclosure as there are considerations for handling damaged batteries requiring equipment and expertise not readily available. Once the scene is secured, these actions may be undertaken by trained experts under close supervision.

Plus Power - Cranberry Point Energy Storage Project: Emergency Response Plan (ERP)

9.4) Arc Flash

All BESS systems and related electrical equipment shall always be treated as energized (Energetic Hazardous Material).

Qualified PPE and training is required when working or accessing equipment within an Arc Flash Boundary. In general, when in direct proximity of the battery enclosure, wear non-melting or untreated natural fiber long-sleeve shirt, long pants, safety glasses, hearing protection, and leather gloves. AR plant clothing is also acceptable. Maintain arc flash boundary until completion of any particular task.

******* CAUTION *******
Always treat the batteries as Energetic Hazardous Material, as they will maintain their state of charge (SOC) long after being isolated.

Arc Flash Boundary for Tesla Megapack Batteries at 100% SOC: (TBD during the engineering design process)

9.5) Chemical Release

The BESS site perimeter should not be entered during a fire or off-gassing event unless there is an imminent threat to life safety, at which time only properly trained and equipped public safety personnel may enter. This entry shall be with full firefighter protective gear to include self-contained breathing apparatus (SCBA). The entry in this situation shall be at the sole discretion of the officer in charge (OIC).

Chemicals consumed during a thermal runaway event will produce copious amounts of smoke. However, if water is used in extinguishing flames, these gasses can become acids which may cause skin irritation.

9.6) Drainage and Water Run-Off

The area surrounding the BESS project includes wetlands and cranberry bogs, and special attention should be given to water run-off from firefighting efforts. The facility has significant drainage capabilities built into the site location as mentioned in section 5 of this ERP (Water run-off). A containment and removal plan, similar to an electric utility substation SPCC is to be employed prior to commissioning.

Plus Power - Cranberry Point Energy Storage Project: Emergency Response Plan (ERP)

10) System Specific Fire Protection & Safety Controls

10.1) Site Alarm Panel

To be determined.

10.2) Audible Alarm

To be determined. The purpose will be to alert any person in the immediate area of the facility.

10.3) Emergency Stop (E-Stop)

To be determined. These are located at multiple locations in and near the facility, and specifically at _____.

It should be noted that there is no delay in the activation of the emergency stop button (E-Stop). **Always treat the batteries as Energetic Hazardous Material as the batteries will maintain their state of charge (SOC) and are energized up to the switchgear.**

The following summarizes the E-Stops for this facility. (Note: Additional information on E Stop design and location will be provided, along with the process for remote activation via the NOC as the plan nears finalization.)

- Installation E-Stop Conceptual Design – These are located at _____. The purpose is to **disconnect the inverter from the grid.**
- Battery Enclosure E-Stops – These are located on each battery enclosure. The purpose is to **open contacts and isolate individual Megapack units.**

Power isolation and shut-off should be conducted in coordination with the facility SME (see Appendix D). The following is excerpted from the Tesla ERP for Emergency Power Shutoff:

- 1) If an external E-stop button or remote shutdown contact to Megapack is present, engage it.
- 2) If Megapack is serviced upstream by an external AC breaker or disconnect, open the breaker or disconnect.
- 3) Only if safe to do so, open the customer interface bay door to access the AC breaker, remove the DC lockout key, and apply Lock Out, Tag Out (LOTO) if needed.

******* CAUTION *******
Always treat the batteries as Energetic Hazardous Material, as they will maintain their state of charge (SOC) long after the activation of E-Stops.

Plus Power - Cranberry Point Energy Storage Project: Emergency Response Plan (ERP)

Appendix A – Safety Data Sheets (SDS)

If the information is available and able to be shared, insert SDS(s) for the TESLA Megapack and any other hazardous materials or processes that are important to the local emergency responders.

DRAFT

Plus Power - Cranberry Point Energy Storage Project: Emergency Response Plan (ERP)

Appendix B – Site Specific Signage, hazards, placarding: (Example Signs)



Figure B1 – Example of ESS Signage



Figure B2 – Example of Danger Signage

Plus Power - Cranberry Point Energy Storage Project: Emergency Response Plan (ERP)

Appendix C – Proposed Site Layout

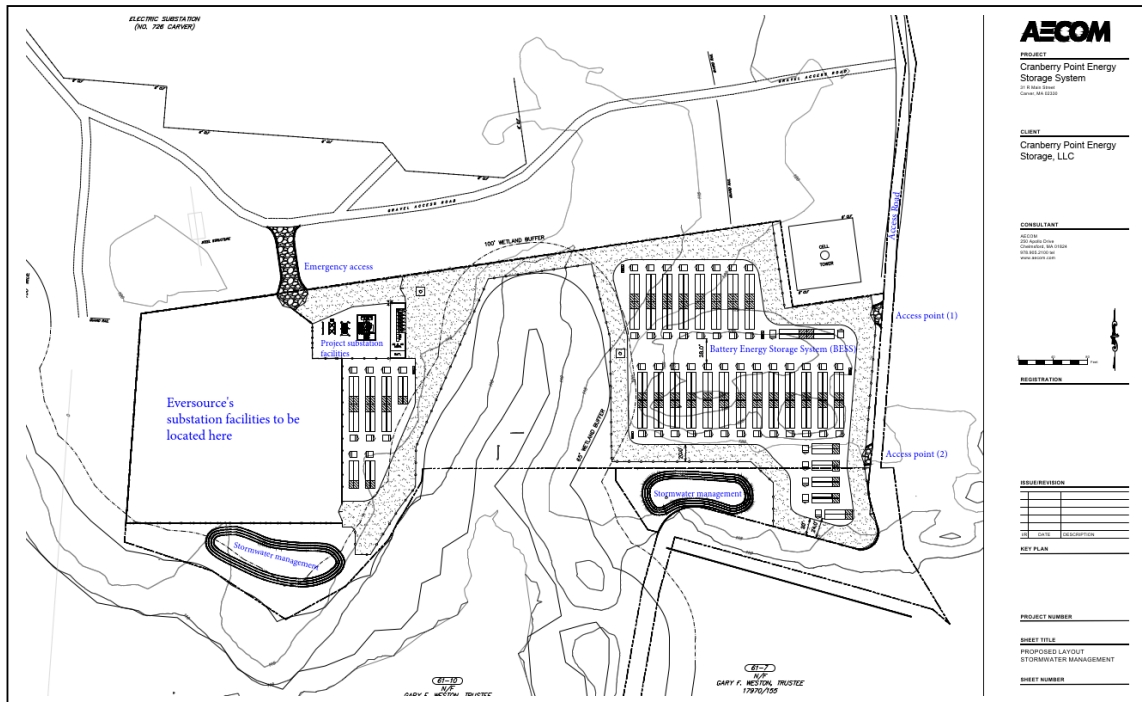


Figure C1 – Proposed Site Layout

DRAFT

Plus Power - Cranberry Point Energy Storage Project: Emergency Response Plan (ERP)

Appendix D – Subject Matter Expert (SME) Incident Response

The following information outlines Plus Power’s plan for responding to an incident at the BESS installation site. Response is based on one or more qualified Subject Matter Experts (SMEs) responding to the site to support the local fire department and other emergency responders. This covers initial alarm activation, representative response, representative qualifications, anticipated actions, transition of command, recovery and/or decommissioning process.

D-1) Notification. Plus Power will be utilizing Tesla’s Network Operations Center that operates 24/7 monitoring the safety and health of the BESS Installation. Based on remote monitoring, when certain thresholds are reached an alert signal will be sent to a Central Station that in turn transmits to the Carver Fire Department Dispatch Center. As per response protocols that will be developed in conjunction with the local fire department, an alarm will be generated for response.

D-2) SME Response. Plus Power will dispatch a representative (SME) to the scene within time frames acceptable to the local fire department. The representative that responds to the scene will have the following background and duties:

- A working knowledge of the energy storage system and the safety concerns of lithium-ion batteries;
- Fire Service operational familiarity;
- Specific familiarity with the ERP, design, and fire protection as pertains to the BESS installation;
- SME will interpret this information for the IC at the site;
- Upon arrival SME will confer with the IC and assist in the development of a tactical action plan; and
- SME will remain available to advise all stakeholders on the risks posed by the system.

D-3) Responsibility. Plus Power SME Representative will assume responsibility for securing the scene, assuming the fire has been contained, or will provide guidance based on available data and expertise on how to contain the fire or event. The Plus Power Representative will also:

- Determine whether a hazmat mitigation effort is necessary and will coordinate with hazmat partners to perform work if necessary; and
- Will coordinate with the local fire department, if necessary, to establish a fire watch and isolate any other affected parts of the system.

D-4) Scene Coordination. Upon securing the scene Plus Power personnel will coordinate with Tesla remotely to:

- Isolate the affected system if not already accomplished;
- Assess the condition of adjacent systems;
- Return the system to operation if safe to do so and with consultation of fire department command;
- Establish a perimeter around the installation ensuring the fenced area is secure;

Plus Power - Cranberry Point Energy Storage Project: Emergency Response Plan (ERP)

- Begin the process of determining how to render safe the affected system and/or return it to service;
- Alternatively, begin the process of safely decommissioning the system by making the appropriate notifications and beginning to develop a recovery plan; and
- Determine next steps for performing a fire investigation and which parties should be notified.

D-5) Restoration Work. Tesla Megapack strategy of allowing the troubled unit to consume itself serves to limit the amount of stranded energy that would need to be dissipated during the restoration phase of the event.

During restoration, investigation, and disposal, the SME will:

- Work with stakeholders to determine what degree of restoration may be performed with respect to continuity of operations, spoliation of evidence, and overall safety;
- Act as investigator for Plus Power or help begin and facilitate investigation process; and
- Work with hazmat and disposal partners following completion of the investigation to ensure the system is properly secured and to determine the appropriate course of action for disposing of the system.

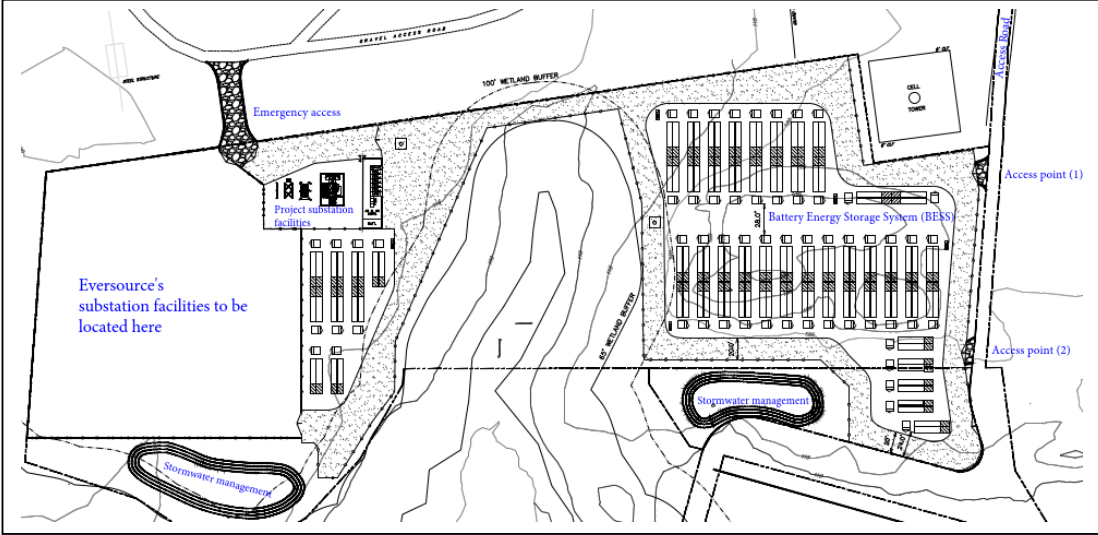
Plus Power - Cranberry Point Energy Storage Project: Emergency Response Plan (ERP)

Appendix E – ESS Information Card (EIC)

This section provides the fundamental site information that is important for emergency responders to an emergency incident at Cranberry Point Battery Energy Storage Project.


ESS Information Card (EIC)
Cranberry Point Battery Energy Storage Project
31R Main St., Carver, MA 02330

Local & State Emergency Response Agencies: Emergency: 911
Facility Emergency Contact Phone Number: **Plus Power**



Facility Overview

Provide color coding in above drawing for all key features (with a legend) that are important for emergency responders, such as BESS, nearby exposures, access roads, water supply locations, rendezvous points, drainage etc.



Typical Battery Energy Storage Unit (multiple on-site)

EIC Sheet 1 of 2

Plus Power - Cranberry Point Energy Storage Project: Emergency Response Plan (ERP)

ESS Information Card (EIC)	
Cranberry Point Battery Energy Storage Project	
31R Main St., Carver, MA 02330	
EVENT: Fire: Include key ERP details	EVENT: Deflagration/Explosion: Include key ERP details
EVENT: Electric Shock: Include key ERP details	EVENT: Arc Flash: Include key ERP details
EVENT: Chemical Release: Include key ERP details	EVENT: Water Run-Off: Include key ERP details
Communications: Include key ERP details	Emergency Stop: Include key ERP details
Alarms: Include key ERP details	Key Contacts: Include key ERP details

EIC Sheet 2 of 2

EXHIBIT 4

Table 1
Thermal Runaway Event Summary
Save The Pine Barrens - MA

Facility	Location	Facility Size	Date	Duration	Sources (Partial List)
AES Corporation	Chandler, Arizona	10 MW	April, 2022	13 days (April 18- May 1)	1) https://santansun.com/2022/05/12/chandler-fire-learns-much-from-lithium-battery-fire/ 2) https://www.power-eng.com/energy-storage/batteries/cause-of-battery-storage-fire-in-arizona-under-investigation/ 3) https://www.datacenterdynamics.com/en/news/4mw-of-aes-lithium-batteries-burn-in-chandler-arizona/
Neoen	Victoria, Australia	300 MW	July, 2021	Approximately 3 days	1) https://www.datacenterdynamics.com/en/news/300mw-tesla-megapack-battery-storage-site-in-australia-catches-fire/ 2) https://www.bestmag.co.uk/teslas-lithium-ion-megapack-causes-three-day-fire-during-test-australian-300mw-ess/ 3) https://www.theguardian.com/australia-news/2021/aug/02/tesla-big-battery-fire-in-victoria-burns-into-day-three 4) https://cleantechica.com/2022/05/13/heres-what-tesla-learned-from-last-years-megapack-fire-in-australia/#:~:text=Experts%20at%20Fisher%20Engineering%20and,within%20the%20Megapack's%20battery%20modules
APS-Energy Storage System	Surprise, Arizona	2 MW	April, 19 2019	Not specifics identified, appears to have been contained in less than one day.	1) https://www.power-eng.com/energy-storage/aps-probe-2019-battery-fire-caused-by-thermal-runaway/ 2) https://fsri.org/research-update/report-four-firefighters-injured-lithium-ion-battery-energy-storage-system 3) https://www.greentechmedia.com/articles/read/lg-chem-battery-cell-mcmicken-arizona-fire
Vistra Energy Storage Facility	Moss Landing, California	300 MW	February 13, 2022 and September 4th (very similar events at the same facility)	Appears to have been contained in less than one day	1) https://www.saurenergy.com/ev-storage/the-top-5-lithium-ion-battery-mishaps-and-lessons-therein#:~:text=On%20the%20evening%20of%20February,took%20place%20n%20September%202021. 2) https://www.energy-storage.news/investigation-begins-into-overheating-incident-at-worlds-biggest-battery-storage-facility/

EXHIBIT 5

Table 2
Air Pollutants Summary Table
Save The Pine Barrens - MA

Chemical Name	CAS#	Hazardous Air Pollutant (HAP)	MassDEP Air Toxic	Criteria Pollutant	Reference
		(Y/N)	(Y/N)	(Y/N)	
1,3-Butadiene	106990	Y	Y		Naval Research Lab 2014 - Table 15
1,4-Dioxane	123911	Y	Y		Naval Research Lab 2014 - Table 15
Benzene	71432	Y	Y		Naval Research Lab 2014 - Table 13
Carbon Monoxide	630080			Y	Naval Research Lab 2014 - Table 13
Carbon Tetrachloride	56235	Y	Y		Naval Research Lab 2014 - Table 14
Carbonyl Sulfide	463581	Y	Y		Naval Research Lab 2014 - Table 13
Chlorobenzene	108907	Y	Y		Naval Research Lab 2014 - Table 14
Chromium (metal)	7440473	Y	Y		Lithium Battery Chemistry
Ethanol	64175	N	Y		Fernandes 2018 - Figure 6
Ethylbenzene	100414	Y	Y		Naval Research Lab 2014 - Table 15
Formaldehyde	50000	Y	Y		Combustion Biprodukt
Hydrogen Chloride	7647010	Y	Y		Naval Research Lab 2014 - Table 14
Hydrogen Fluoride	7664393	Y	Y		Anderrson 2013 - Table 7 & 16
Methanol	67561	Y	Y		Fernandes 2018 - Figure 6
Nitrogen dioxide	1102440			Y	Ribiere 2012
Particulate matter	-			Y	Wang 2020
Phosphoric Acid	7664382	N	Y		Naval Research Lab 2014 - Table 15
Styrene	100425	Y	Y		Naval Research Lab 2014 - Table 15
Sulfur dioxide	7446095			Y	Naval Research Lab 2014 - Table 14
Sulfuric Acid	7664939	N	Y		Naval Research Lab 2014 - Table 14
Tetrahydrofuran	109999	N	Y		Naval Research Lab 2014 - Table 14
Toluene	108883	Y	Y		Naval Research Lab 2014 - Table 15

EXHIBIT 6



Investigation of fire emissions from Li-ion batteries

Petra Andersson, Per Blomqvist, Anders Lorén and Fredrik Larsson

SP Technical Research Institute of Sweden

Investigation of fire emissions from Li-ion batteries

Petra Andersson, Per Blomqvist, Anders Lorén and
Fredrik Larsson

Abstract

Investigation of fire emissions from Li-ion batteries

This report presents an investigation on gases emitted during Lithium-ion battery fires. Details of the calibration of an FTIR instrument to measure HF, POF_3 and PF_5 gases are provided as background to the minimum detection limits for each species. The use of FTIR in tests has been verified by repeating experiments reported in the literature. The study reports on gases emitted both after evaporation and after ignition of the electrolyte fumes. Tests were conducted where electrolyte is injected into a propane flame and the influence of the addition of water is studied. Finally three types of battery cells were burnt and emission of fluorine and/or phosphorous containing species quantified.

Key words: Lithium-ion battery fires, toxic gases, FTIR

SP Sveriges Tekniska Forskningsinstitut
SP Technical Research Institute of Sweden

SP Report 2013:15
ISBN 978-91-87461-00-2
ISSN 0284-5172
Borås 2013

Contents

Abstract	3
Contents	4
Förord / Preface	6
Sammanfattning / Summary	7
1 Introduction	8
2 FTIR instrumentation	10
3 Fundamental Chemistry of LiPF₆	12
4 Pre-study of fluorinated emission products	13
4.1 Production of calibration gases	13
4.2 Calibration of FTIR	13
4.2.1 HF	13
4.2.2 POF ₃	14
4.2.3 PF ₅	15
4.3 Stability of POF ₃	18
4.3.1 Room temperature	18
4.3.2 Elevated temperature	19
4.4 Heating tests with the Cone Calorimeter	19
4.4.1 Evaporation tests of pure components	20
4.4.2 Evaporation tests with mixtures of components	22
4.4.3 Combustion tests	23
5 Burner tests with electrolyte	26
5.1 Electrolyte – salt solutions	27
5.2 Tests conducted	27
5.3 Test Results	29
6 Fire tests with batteries	48
6.1 Batteries tested	48
6.1.1 Cell preparation	49
6.2 Experimental apparatus	49
6.3 Experimental procedure	51
6.4 Results	51
6.4.1 Video	51
6.4.2 HRR and gas measurements	55
6.5 Discussion	62
7 Conclusions	64
8 References	65
Appendix A Tests conducted in burner	A1
Appendix B Results from battery cell tests	B1
Appendix C Photos from cell experiments	C1

Förord / Preface

This work has been sponsored by Brandforsk, Brandforsk project number 402-111 and FFI project number 35755-1 which is gratefully acknowledged.

Several persons have contributed to the work including technical staff at Fire technology, Sven Ove Vendel and Brith Månsson.

Input from the reference group consisting of Ulf Lundström, Trafikverket, Thomas Mohlen, Scania, Bengt-Erik Mellander, Chalmers and Patrik Roth, Atlas Copco is also acknowledged.

Sammanfattning

Rapporten beskriver tests som har gjorts på elektrolyt i Litium-jon batterier. Elektrolyten blandades till baserat på litteratordata och injicerades i en propanflamma. Olika blandningsförhållanden användes och även vatten sprutades in. Gaser från branden samlades in och analyserades med hjälp av en FTIR. Projektet inleddes med att FTIRen kalibrerades upp för att kunna mäta HF, POF₃ och PF₅.

Försöken visade att det var möjligt att använda FTIR för att mäta dessa gaser. Dock visade det sig i ett tidigt skede av projektet att PF₅ är så pass reaktiv att den inte finns tillräckligt länge för att detekteras. Däremot visade sig POF₃ finnas med i samtliga försök. POF₃ är en gas som potentiellt är mycket giftig, eventuellt giftigare än HF. Influensen av vatten som sprutades in i flammorna med avseende på emitterade gaser undersöktes. Det gick dock inte att påvisa någon effekt på vilka gaser som emitteras av att spruta in vatten.

Projektet avslutades med att battericeller som kan finnas i elhybrider eldades och gaserna analyserades. I dessa försök mättes HF men ingen POF₃. Detta berodde dock sannolikt på att vi hamnade under detektionsgränsen för POF₃ i dessa försöken.

Samtliga resultat extrapoleras och jämfördes med rapporterade emissionsdata från mätningar gjord på en helbilsbrand. Extrapolationen gav värden i samma storleksordning som de storskaliga bränderna.

1 Introduction

Batteries are used in more and more applications and are seen as an important solution to meet the climate goals for the automotive sector. Several types of batteries are used today and more are developed over time.

One of the most common types of batteries today is lithium-ion (Li-ion) batteries due to their high energy and power densities. Li-ion also offers long life time. Li-ion batteries have, however, some safety drawbacks. Compared to many other battery technologies, Li-ion batteries have a smaller region of stability, regarding temperatures and cell voltage. Li-ion batteries can undergo a thermal runaway resulting in gassing and fire, and potentially even explosion. A thermal runaway can be the result if a Li-ion cell is exposed to increased temperatures, typically starting from 120-150 °C. Other types of abusive conditions, e.g. overcharge or deformation can also result in venting of gasses and thermal runaway reactions. The Li-ion cell has an organic based electrolyte which enables its high energy and power densities, but it is also flammable.

Another feature of Li-ion batteries is the potential for emitting toxic gases. So far it is HF (Hydrogen Fluoride) that has gained most interest as this is a very toxic gas. Other gases that can pose a danger include the chemical species in the oxidation and thermal breakdown of the initial LiPF_6 salt solution. Most likely PF_5 , POF_3 and HF are of greatest concern but also the fluorinated phosphoric acids can be of interest since they will give HF and phosphoric acid when completely reacted with water. The toxicity of all these gases is not fully established. The Swedish Work Environment Authority has exposure limits for total fluorides, HF and phosphoric acid but lacks data for the rest of the substances¹.

The NGVⁱ for total fluorides are 2 mg/m³ and HF has a TGVⁱⁱ of 2 ppm. NIOSH (National Institute for Occupational Safety and Health, USA) states that HF has a IDLH (Immediately Dangerous to Life and health) value of 30 ppm. No exposure limits are given for PF_5 and POF_3 , however their chlorine analogues, PCl_5 and POCl_3 have NGV values of 0.1 ppm. The toxicity might, however, differ between the chlorine and fluorine species and there is no general rule like “fluorine is always more toxic”. But, still, the limits are low and gases evolved from battery fires are certainly of great concern to both the fire fighters, people in the vehicles and in the close vicinity of the fire. Both of these gases are very reactive and very few measurements have been performed on these gases in the literature. Yang, Zhuang and Ross² report measurements conducted using TGA (Thermal Gravimetry Analysis) and FTIR (Fourier transform Infra Red) on pure LiPF_6 salt and salt solved in EC, PC, DMC and EMC but so far little or none work has been published on emissions of these gases from fire scenarios.

One important aspect for Li-ion batteries is the possibility to extinguish a fire in them. Several different types of advice are available such as using copious amounts of water or sand or letting the battery burn. There are, however, several situations when it is not possible to allow a battery fire to continue, e.g. if someone is trapped in a car. It is, therefore, important to investigate different extinguishing means together with the toxic gases emitted during extinguishment.

The work presented in this report includes calibration of an FTIR equipment to be used to measure HF, POF_3 and PF_5 to analyse smoke from fire tests. The technique developed is

ⁱ ”Nivågränsvärde” Mean value threshold in a working environment

ⁱⁱ ”Takgränsvärde” Maximum allowed concentration in a working environment

then used in different heating and combustion conditions in different scales. The impact of water on the combustion gases is also investigated.

2 FTIR instrumentation

The instrument used for analysis of the emission products in the fire tests reported here was an FTIR spectrometer. Fourier transform infrared spectroscopy (FTIR) is a general technique used to obtain an infrared spectrum of absorption from a solid, liquid or gas. An FTIR spectrophotometer uses an interferometer to simultaneously collect spectral data over a wide spectral range, in the form of an interferogram, which is different from classical dispersive spectroscopy, which sequentially collects data at each wavelength. A Fourier transform is a mathematical algorithm used to convert the raw data into a spectrum, corresponding to the spectrum resulting from a classical scanning dispersive spectrometer. The use of an interferometer gives two main advantages in comparison with the traditional dispersive spectroscopy: First, all wavelengths are collected in principal simultaneously. Second, the interferometer throughput is higher compared to dispersive methods which gives a higher signal.

The measurement system used here consisted of an FTIR spectrometer, a gas cell, sampling lines, filters for removing particulates before the gas cell and a pump that continuously drew sample gas through the cell. The system is specified in Table 1.

Table 1 Specification of the FTIR measurement system.

Instrumentation	Specification
Spectrometer	Thermo Scientific Antaris IGS analyzer (Nicolet)
Spectrometer parameters	Resolution: 0.5 cm ⁻¹ Spectral range: 4800 cm ⁻¹ – 650 cm ⁻¹ * Scans/spectrum: 10 Time/spectrum: 12 seconds Detector: MCT
Gas cell	Volume: 0.2 litres Path length: 2.0 m Temperature: 180°C** Cell pressure: 650 Torr**
Primary filter	M&C ceramic filter heated to 180 °C
Secondary filter	M&C sintered steel filter heated to 180°C***
Sampling tubing	4/6 mm diameter PTFE tubing heated to 180°C. The length of the tubing was 1.5 m in the Cone calorimeter tests and 8.5 m in the battery tests.
Pump	Sampling flow: 3.5 l/min

* The spectral range used in the initial pre-study was 4000 cm⁻¹ – 650 cm⁻¹.

** In the initial pre-study and calibration the cell temperature was 170 °C and the pressure was ~740 Torr.

*** A 37 mm diameter planar filter (PTFE) heated to 130°C was used in the initial pre-study.

Photos of the FTIR measurement system connected to the Cone calorimeter are shown in Figure 1.

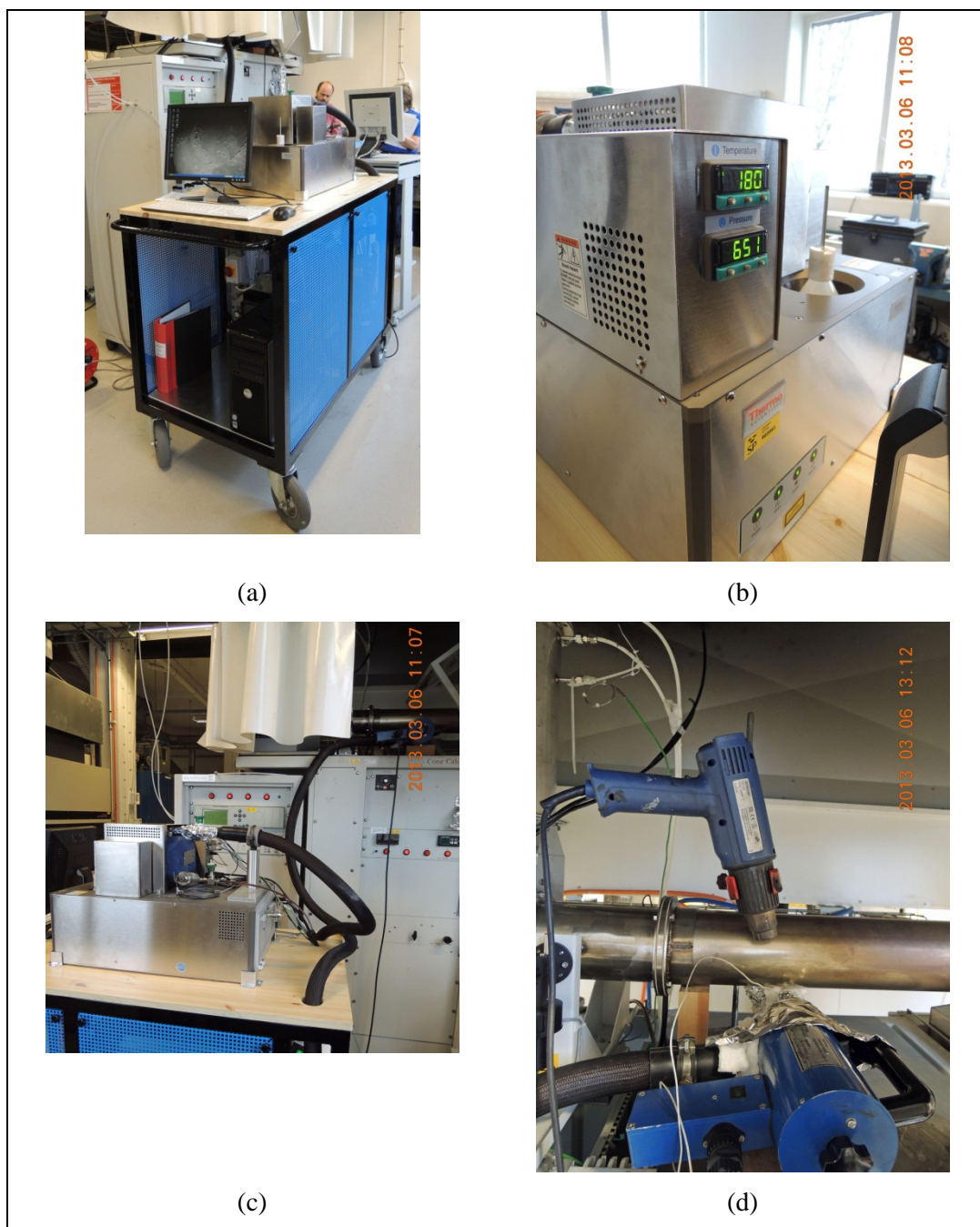


Figure 1 Photos of the FTIR instrumentation. (a) Overview of the measurement set-up. (b) The Antaris FTIR spectrometer. (c) The connection of the incoming sample gas to the measurement cell. (d) The primary filter with the heating device (blue in front) and heating of incoming connection with a heating gun.

3 Fundamental Chemistry of LiPF_6

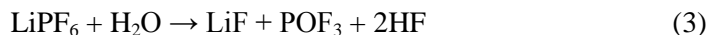
When heated in a dry and inert environment LiPF_6 decomposes to lithium fluoride (LiF) and phosphorous pentafluoride ($\text{PF}_5(\text{g})$)².



In contact with moisture/water PF_5 reacts to form phosphorous oxyfluoride and hydrogen fluoride.²



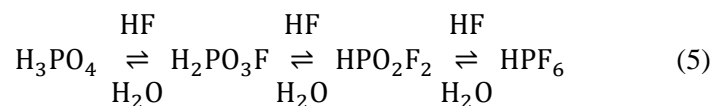
When heated in moisture/water LiPF_6 can directly form LiF, POF_3 and HF.²



PF_5 also react with HF to form hexafluorophosphoric acid (HPF_6)³:



Phosphorous oxyfluoride (POF_3) can react to form several fluorinated phosphoric acids, monofluorophosphoric acid ($\text{H}_2\text{PO}_3\text{F}$), difluor-phosphoric acid (HPO_2F_2) hexafluorophosphoric acid (HPF_6), and phosphoric acid (H_3PO_4)⁴. The fluorinated phosphoric acids can react with water and yield HF and form phosphoric acid as a final product. [4]:



4 Pre-study of fluorinated emission products

In order to be able to study the fluorinated emission products emitted during a potential battery fire the FTIR to be used in the experiments had to be calibrated. The measuring method was then also verified by conducting experiments on electrolyte and salt solutions that were heated. The full calibration methodology is described below.

4.1 Production of calibration gases

The FTIR instrument contained a basic factory calibration for HF. This calibration was, however, improved during the project to include more spectral information and a wider concentration range. The calibration of HF was made using a dynamic dilution system where a water solution of HF was injected into a heated stream of nitrogen.

In addition was the FTIR calibrated for PF₅ and POF₃. Calibration gas mixtures were prepared for this purpose by dilution of PF₅ (99%, ABCR) and POF₃ (99%, ABCR) in nitrogen atmosphere using gasbags (Flexfoil, SKC). Extra effort was put into pre-conditioning the bags so they were free of water adsorbed to the walls. This was necessary to be able to prepare the highly reactive PF₅ mixture. The concentrations produced for the POF₃ calibration were: 25 ppm, 100 ppm, 200 ppm, 300 ppm and 416 ppm. While the PF₅ concentrations were 108 and 200 ppm, respectively.

4.2 Calibration of FTIR

The FTIR used had a calibration for a number of components when delivered from factory. These components included *e.g.* CO₂, CO and HF. It was seen that the factory calibration was not sufficiently accurate for the intended use of the instrument and the instrument was recalibrated during the course of this project. The settings of the FTIR instrument were changed somewhat (see Table 1) for the recalibration, which meant that measurements made before the recalibration could only be evaluated semi-quantitatively using recalibration data. This was not a problem, however, as the new calibration data was used in the evaluation of the project data.

4.2.1 HF

The instrument was recalibrated for HF during the project to include the full spectral band of HF and to include a wide concentration range *i.e.* 18 ppm to 1245 ppm. The quantification limit (LOQ) for HF was calculated to 2 ppm.

The spectral band at 520 ppm for HF (together with water) in nitrogen is seen in Figure 2. There are two branches of peaks for HF. The branch at the higher wavenumbers is clearly seen in the figure whereas the branch at lower wavenumbers contains interference from water bands.

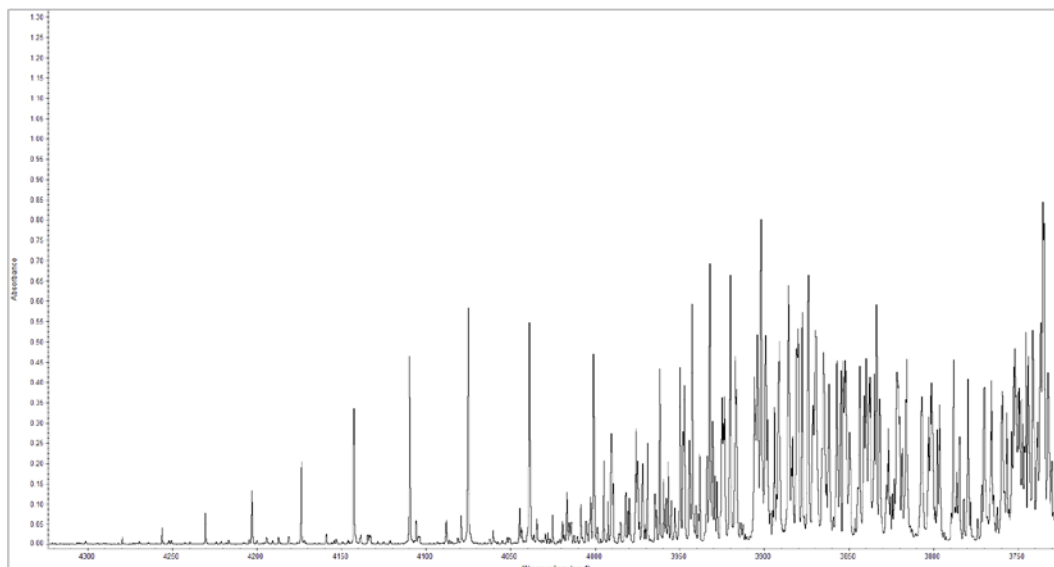


Figure 2 Spectra of 520 ppm HF and 2.9 % H₂O in N₂.

4.2.2 POF₃

Tests were conducted to record the spectral bands of POF₃ as a basis for calibration of the FTIR. An important part of the calibration work was further to investigate the stability of POF₃ under the conditions used for calibration (see section 4.3). This initial work was conducted before the FTIR was recalibrated.

A spectrum of POF₃ (116 ppm) is shown in Figure 3. Several distinctive absorption bands can be seen (together with some water that was present in the bag). These bands can be seen more clearly in Figure 4, where the spectral range of interest is shown.

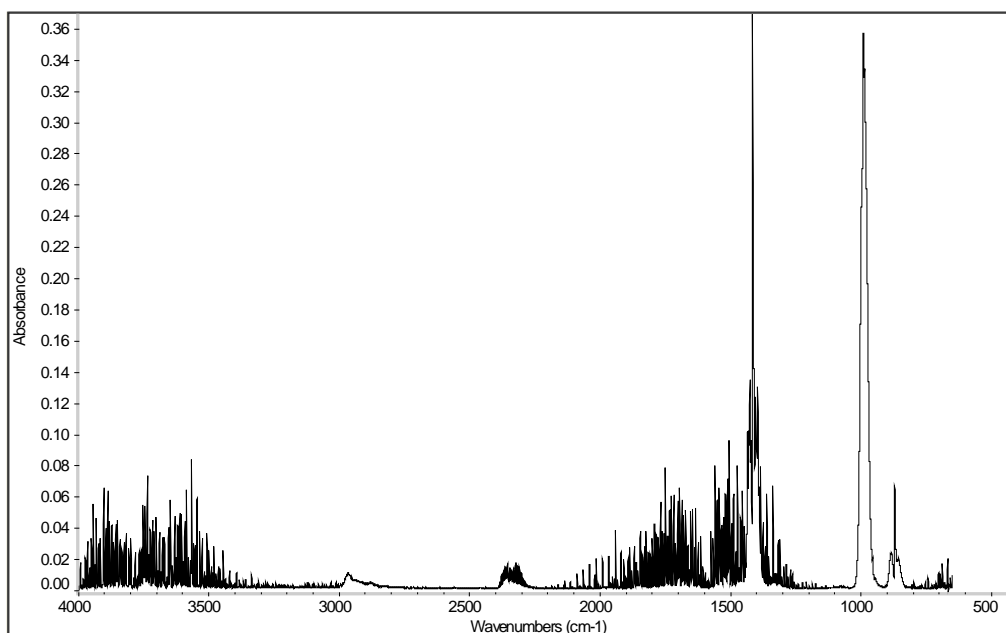


Figure 3 Spectra of 116 ppm POF₃ in N₂.

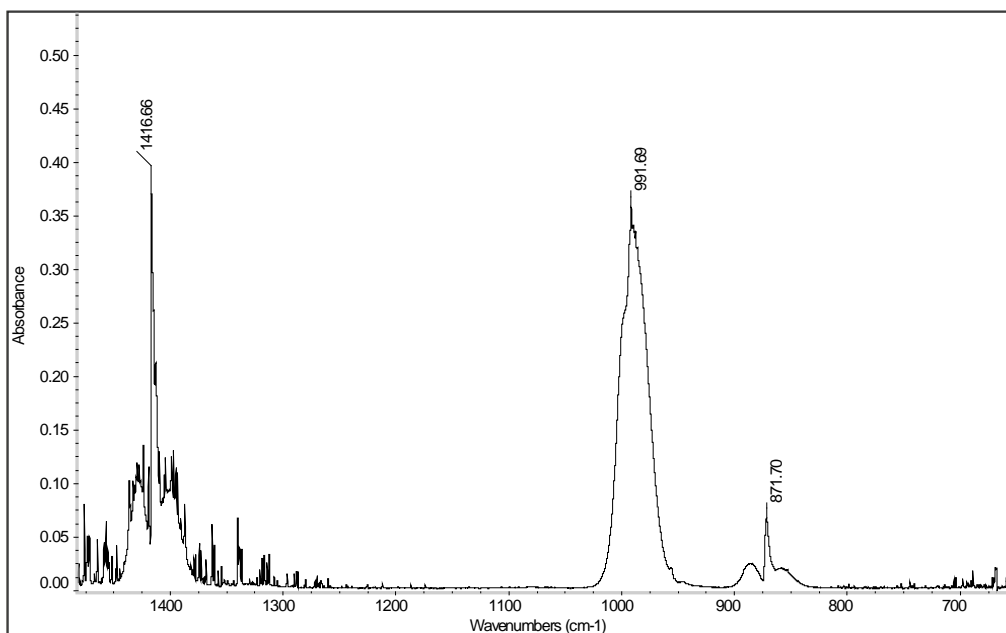


Figure 4 Spectral bands of POF₃ (from 116 ppm POF₃ in N₂).

Three spectral bands are shown centred around the wavenumbers 871 cm⁻¹, 991 cm⁻¹ and 1416 cm⁻¹. These bands are from P-F symmetrical stretches, P-F asymmetrical stretches and P-O stretches. The two latter vibrations are the strongest. The spectral information of POF₃ is summarized in Table 2.

Table 2 Spectral band positions for POF₃.

Band position (cm ⁻¹)	Absorptivity (abs/ppm.m)	Type of band [2]
1416	0.00159	P-O stretch
991	0.00154	P-F asymmetrical stretch
871	0.00029	P-F symmetrical stretch

A quantitative calibration was made for POF₃ using flushed gas bags where known volumes of POF₃ gas were injected into a known volume of nitrogen gas. The concentrations produced for the calibration were: 25 ppm, 100 ppm, 200 ppm, 300 ppm and 416 ppm. Spectral regions around 871 cm⁻¹ and 1416 cm⁻¹ were used for a CLS (classical least squares) calibration and water was included as an interfering component. The quantification limit (LOQ) for POF₃ was calculated to 6 ppm.

4.2.3 PF₅

It was found that the gas bags used needed to be dried by flushing with N₂ in order to remove any remaining water. Water was unwanted as hydrolysis of PF₅ could be expected. Figure 5 shows the FTIR spectrum of a non-flushed gas bag where the nominal concentration of PF₅ was 108 ppm. This spectrum shows, however, no significant spectral bands apart from those of POF₃ and HF. (Spectral bands of water, some CO₂ and a small contamination of HCl are additionally shown.)

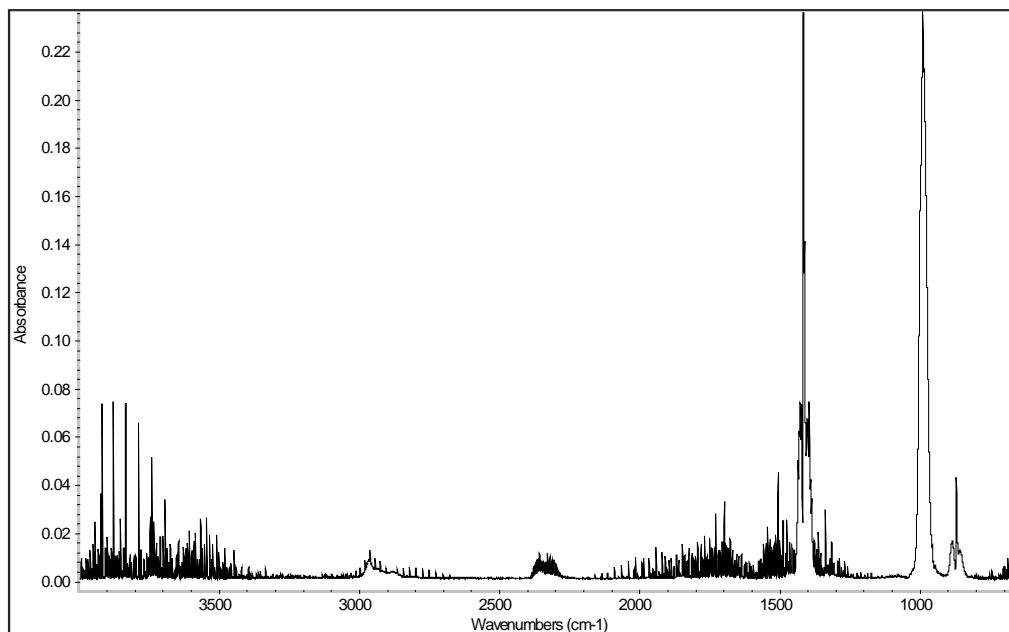


Figure 5 Spectra of 108 ppm PF₅ in argon (bag not flushed – contained water).

The explanation found was that the PF₅ added to the bag was hydrolysed by the small amounts of water that was present in the bag, to form the decomposition products POF₃ and HF.

The bags were subsequently thoroughly dried before adding PF₅. A spectrum from the content of a gas bag flushed with N₂ is shown in Figure 6. Only very small remains of water can be seen here.

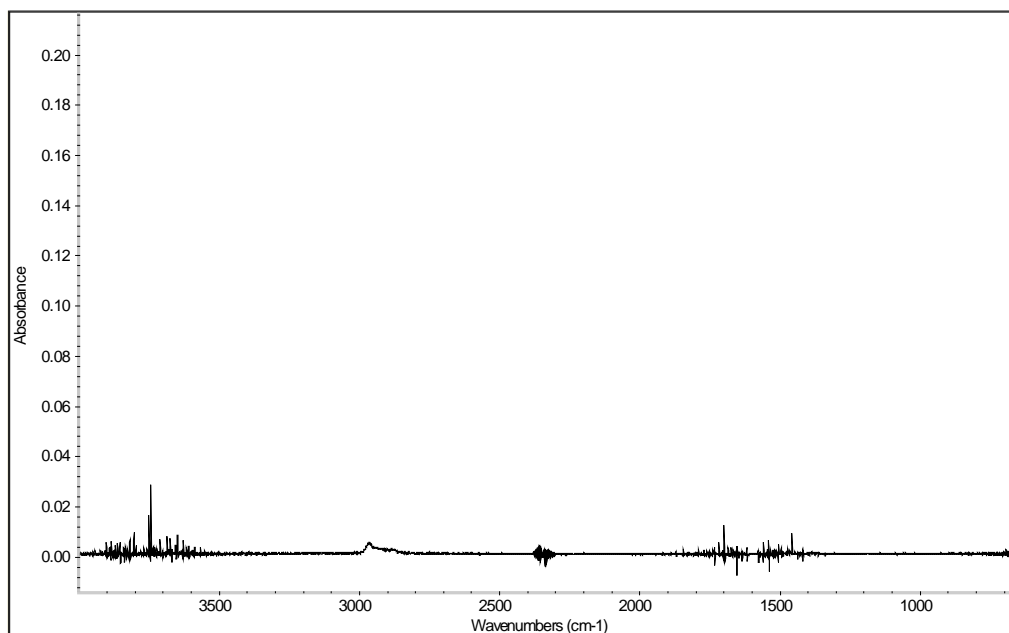


Figure 6 Spectra of gas content in gas bag flushed with dry N₂.

By using flushed bags it was possible to locate the spectral bands of PF₅. Figure 7 shows a spectrum of nominally 200 ppm PF₅ in N₂. However, also here the bands of POF₃ and HF can be seen together with the bands of PF₅. It is clear from this that PF₅ is very unstable and decomposes easily. The interesting spectral range for PF₅ is magnified in Figure 8.

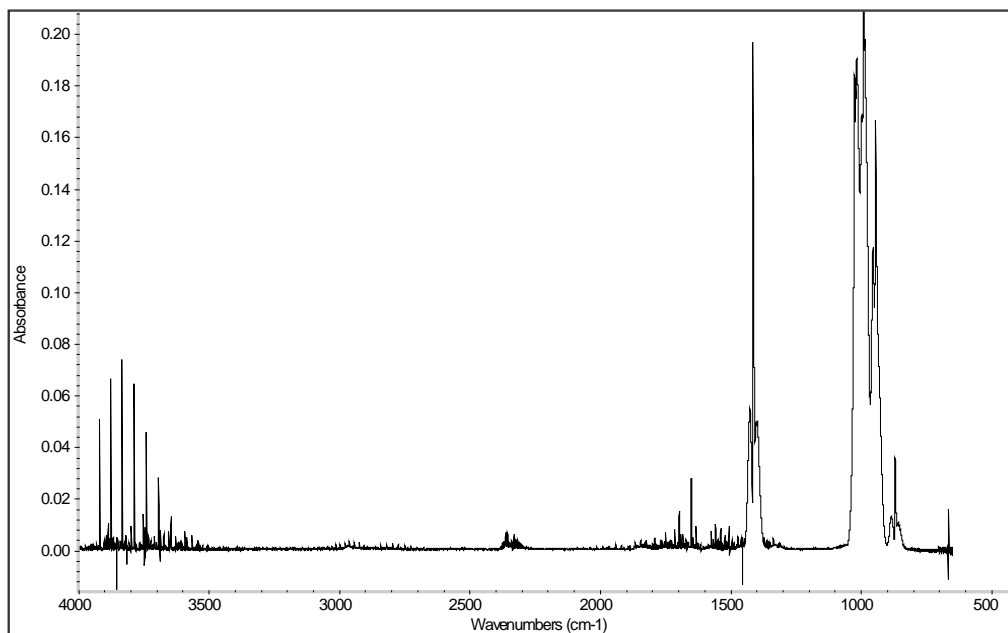


Figure 7 Spectra of 200 ppm PF₅ in dry N₂ (bag flushed).

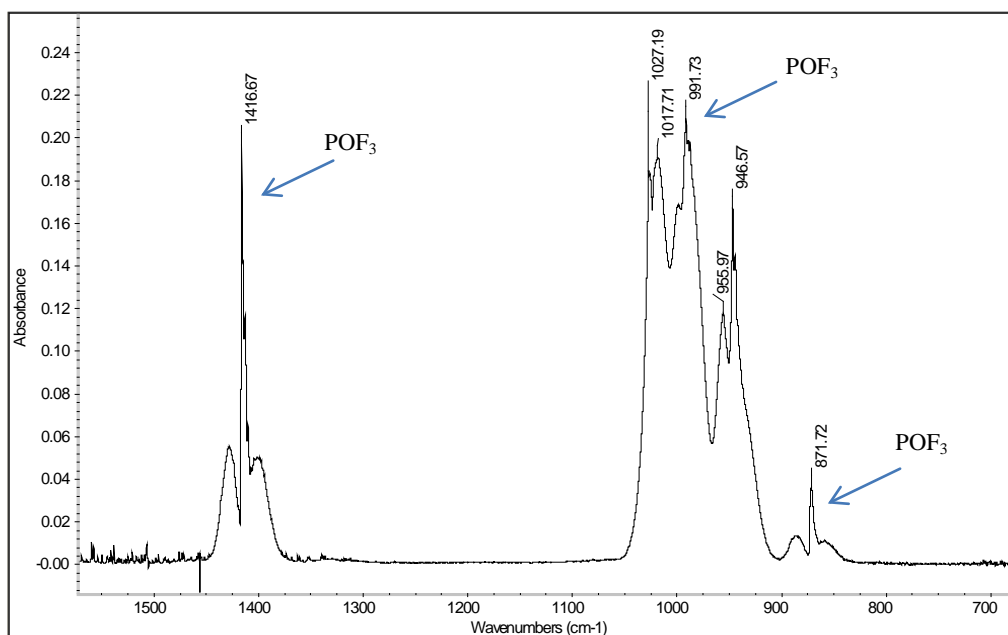


Figure 8 Spectral bands of PF₅ (from 200 ppm PF₅ in dry N₂).

The spectral bands of POF₃ are seen in Figure 8 at 871 cm⁻¹ (P-F symmetrical stretch), 991 cm⁻¹ (P-F asymmetrical stretch) and 1416 cm⁻¹ (P-O stretch). Remaining bands are from PF₅ or additional decomposition products of PF₅. PF₅ has two stretching modes according to Yang et al. [2]. These are most probably the bands at 1017.71 cm⁻¹ and 946.57 cm⁻¹. The remaining two bands found, 1027 cm⁻¹ and 996 cm⁻¹, must thus originate from unidentified decomposition products of PF₅. The bands found that were not from POF₃ are listed in Table 3.

Table 3 Spectral band positions found from PF₅ and decomposition products.

Band position (cm ⁻¹)	Type of band
1017	PF ₅ : PF stretching [2]
946	PF ₅ : PF stretching [2]
1027	Band from unknown decomposition product
956	Band from unknown decomposition product
1416	POF ₃ : P-O stretch
991	POF ₃ : P-F asymmetric stretch
871	POF ₃ : P-F symmetric stretch

4.3 Stability of POF₃

The stability of POF₃ at both room temperature and at an elevated temperature was investigated. It was important to have this information to be sure that the calibration mixtures prepared in gas bags were stable and to see if any significant decomposition would take place in the heated sampling and measurement system.

4.3.1 Room temperature

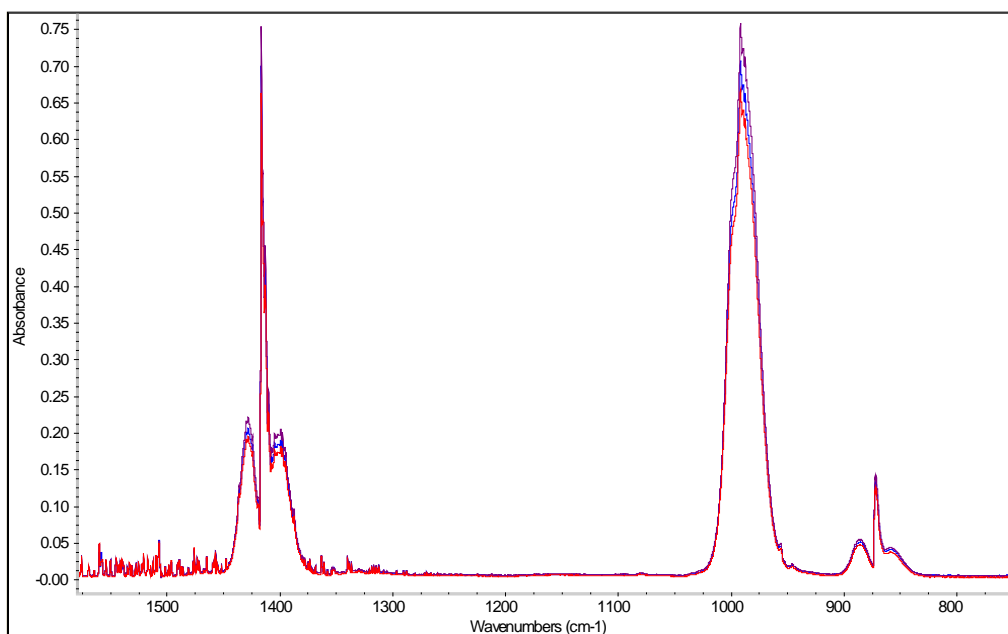


Figure 9 Spectra of ~200 ppm POF₃ measured in 3 separate Flexfoil bags at 8 min (blue), 16 min (brown) and 33 min (red) after preparation.

The investigation showed that POF₃ is very stable at room temperature in a gas bag diluted with N₂, which makes it possible to prepare quantitative calibration standards. Figure 9 shows the spectra of ~200 ppm POF₃ from three different gas bags, stored for various length of time before measurement. A very limited decomposition can be seen for the standard stored 33 minutes before measurement.

4.3.2 Elevated temperature

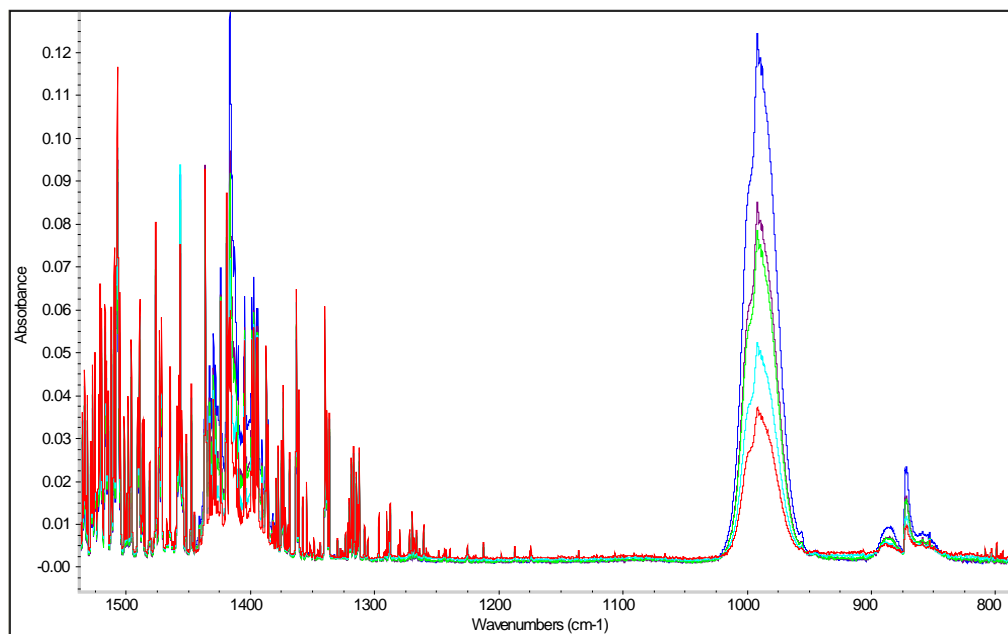


Figure 10 Series of spectra of 41 ppm POF₃ kept at 170°C in the FTIR gas cell for 0 min (blue), 8 min (brown), 10 min (green), 21 min (magenta) and 31 min (red).

The half-life for POF₃ in N₂ at 170 °C is about 15 minutes according to the measurements shown in Figure 10, which means that there is no significant decomposition taking place in the measurement system during the ~10 s response time of the FTIR measurement set-up.

4.4 Heating tests with the Cone Calorimeter

Yang et al [2] have studied the thermal stability of LiPF₆ salt and of solutions of LiPF₆ in prototypical Li-ion battery solvents by thermogravimetric analysis (TGA) and on-line FTIR. They showed that in the presence of water the decomposition products formed were POF₃ and HF. No new products were observed in 1 molar solutions of LiPF₆ in EC, DMC and EMC. In the evaporation tests that are reported below it was investigated whether the same type of decomposition products could be found in tests where the electrolyte was heated in an open container with radiative heating in a Cone calorimeter. Further, combustion tests were conducted where the vapour was ignited to investigate how combustion would change the type of decomposition products.

The sample was placed in a small (~40 mm diameter) steel container under the heating cone of the Cone calorimeter as can be seen in Figure 11. The irradiation of the sample was in the range of 10-15 kW/m². The FTIR was connected to the exhaust duct of the Cone calorimeter. Separate tests were conducted with only solvents (DME and PC), the pure LiPF₆ salt, and saturated solutions of LiPF₆ salt and solvents. Leftovers from the tests can be seen in Figure 12. The FTIR measurement system is described in Section 2.



Figure 11. Open container placed underneath cone heater and ignited



Figure 12. Leftovers in cake-cup after test

4.4.1 Evaporation tests of pure components

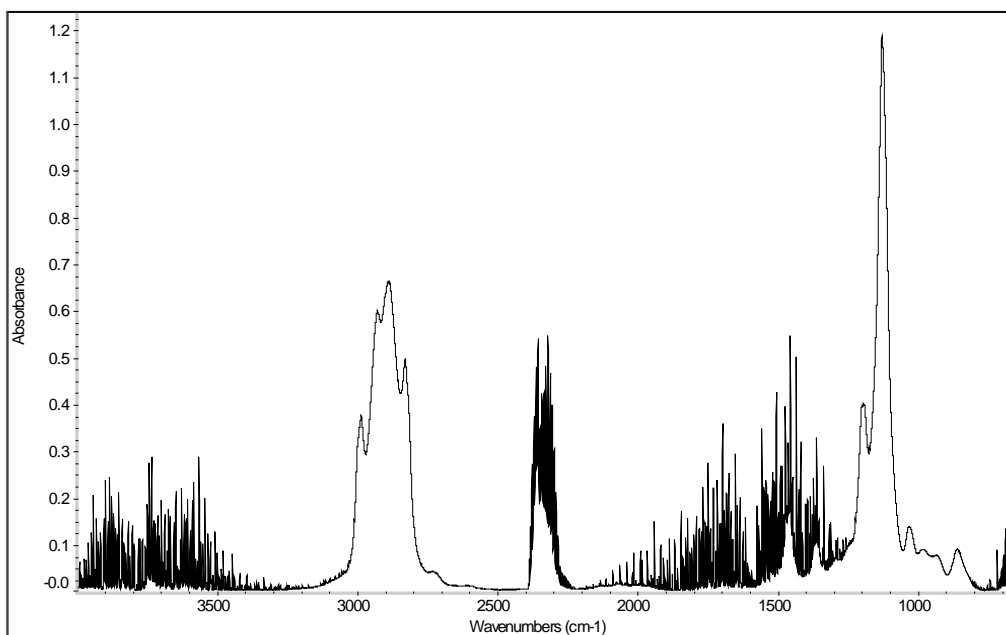


Figure 13 Spectra of Dimethoxyethane (DME) evaporated in the Cone Calorimeter.

Figure 13 shows a spectrum of DME when evaporating from heating in the cone calorimeter with absorption bands around 1100 cm^{-1} and 2900 cm^{-1} . The highest distinctive peak is located at 1129 cm^{-1} .

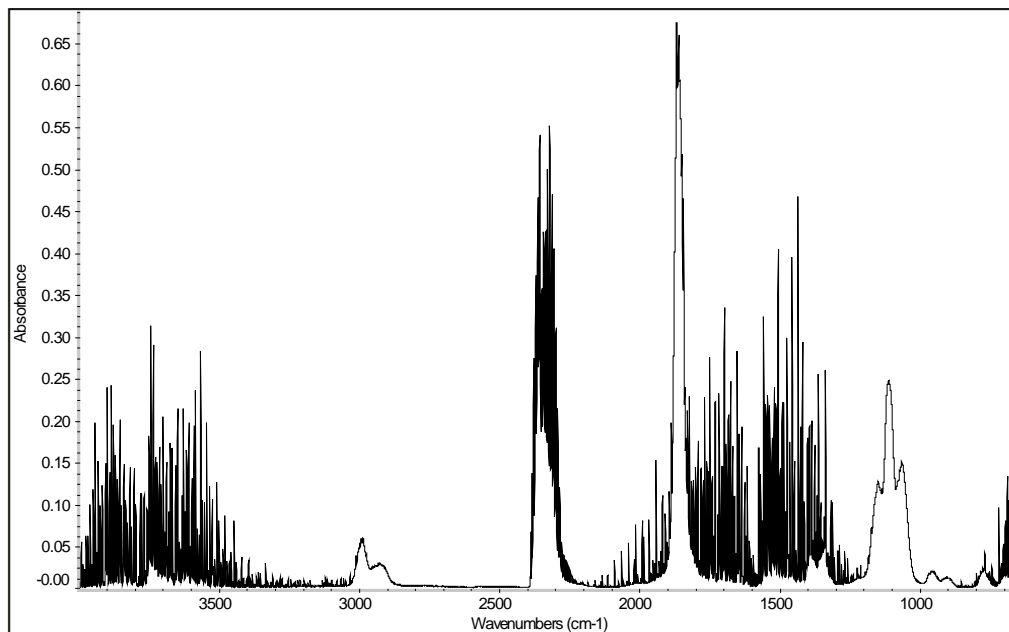


Figure 14 Spectra of Propylene carbonate (PC) evaporated in the Cone Calorimeter.

Figure 14 shows a spectrum of PC when evaporating from heating in the cone calorimeter with absorption bands around 1100 cm^{-1} , 1850 cm^{-1} and 2950 cm^{-1} . The two highest distinctive peaks are located at 1114 cm^{-1} and 1867 cm^{-1} .

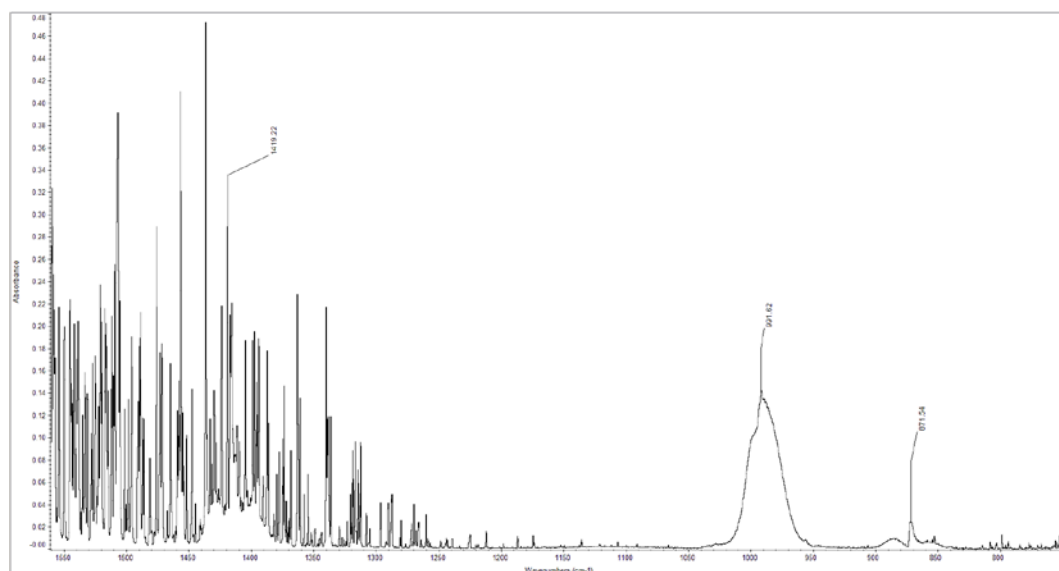


Figure 15 Spectral bands of evaporation products from Lithium hexafluoride.

Figure 15 show the spectral bands of POF_3 in a test where pure LiPF_6 salt was thermally decomposed in the cone calorimeter. HF could only be qualitatively identified here (not shown) as severe interference of water made quantification impossible in the region up to 4000 cm^{-1} which was the highest wavenumber measured in these early tests.

There are no traces of PF_5 or any decomposition products apart from POF_3 in the spectral range shown in Figure 13.

4.4.2 Evaporation tests with mixtures of components

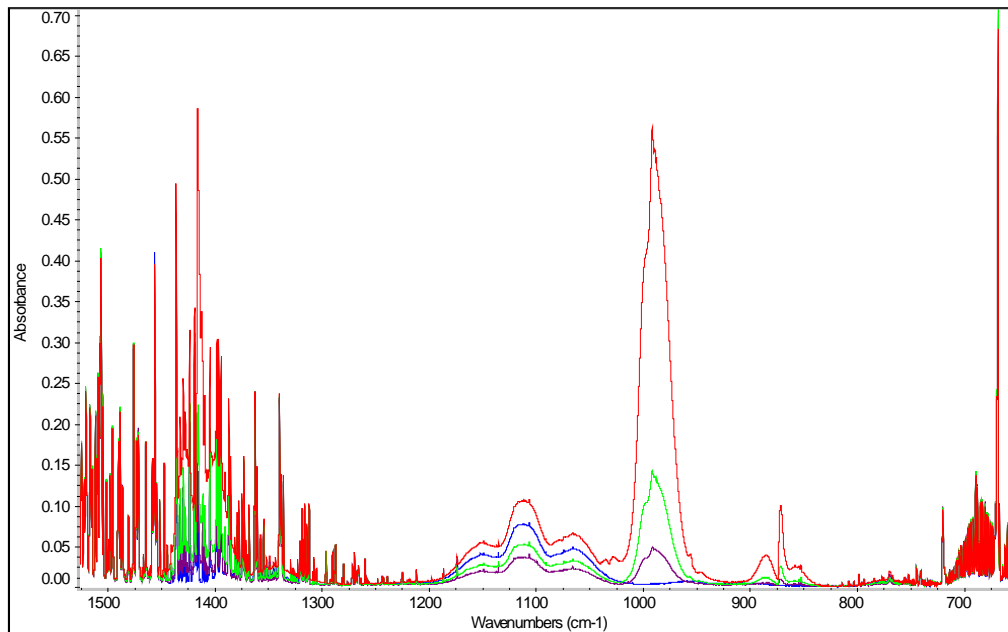


Figure 16 Series of spectra from evaporation test with LiPF₆ mixed in Polypropylene carbonate (PC). Spectra measured at 57 s (brown), 82 s (green), 157 s (red) and 257 s (blue) after start of heat exposure.

Spectra from an evaporation test with a saturated solution of LiPF₆ salt in PP are shown in Figure 14 above. The spectral band from the solvent is shown around 1100 cm⁻¹ together with the three bands of POF₃ at 871 cm⁻¹, 991 cm⁻¹ and 1416 cm⁻¹. It can be seen from the overlaid spectra that the emission of POF₃ ends before the solvent is totally evaporated (see blue spectrum from 257 s in Figure 14).

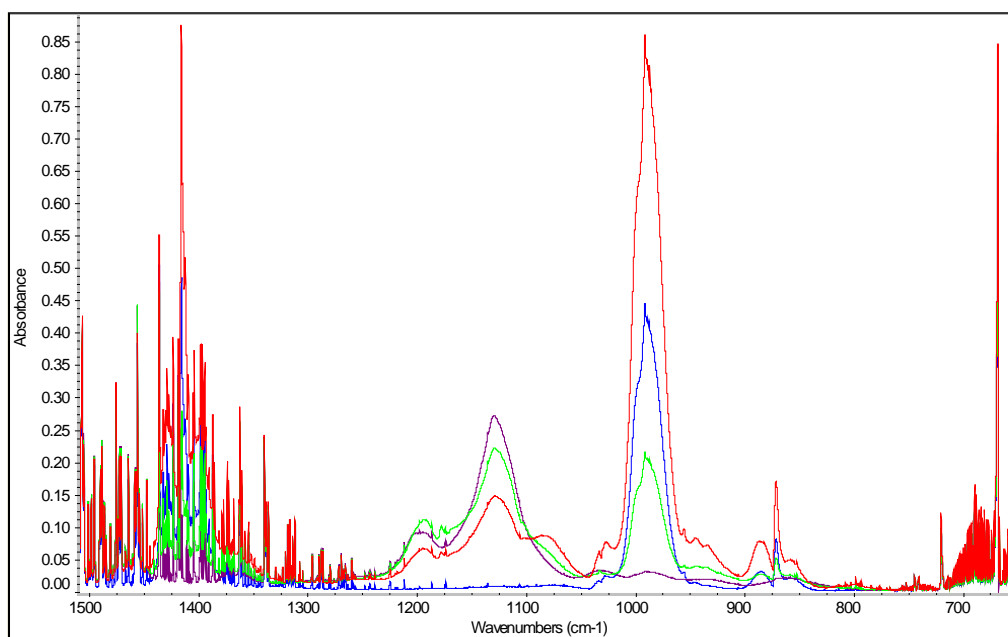


Figure 17 Series of spectra from evaporation test with LiPF₆ mixed in Dimethoxyethane (DME). Spectra measured at 30 s (brown), 67 s (green), 117 s (red) and 155 s (blue) after start of heat exposure.

Figure 17 shows a series of spectra from an evaporation test with a saturated solution of LiPF_6 salt in DME. Also here the spectral band from the solvent is shown around 1100 cm^{-1} together with the three bands of POF_3 at 871 cm^{-1} , 991 cm^{-1} and 1416 cm^{-1} . Here it can be seen from the overlaid spectra that the emission of POF_3 continues after that the solvent is totally evaporated (see blue spectrum from 155 s in Figure 15). This is the opposite behaviour compared to the solution of LiPF_6 salt in PC. One cannot, however, draw any conclusion from this as the emission behaviour of POF_3 here might be an effect of the saturation degree of the two mixtures.

4.4.3 Combustion tests

Test where saturated solutions of LiPF_6 salt in DME respective PC, were ignited in the cone calorimeter are reported below. In these tests the same level of external radiative heat flow was used as for the evaporation tests discussed above ($10\text{-}15\text{ kW/m}^2$). However, in these tests the electric spark igniter was used to ignite the evaporated fumes over the sample container.

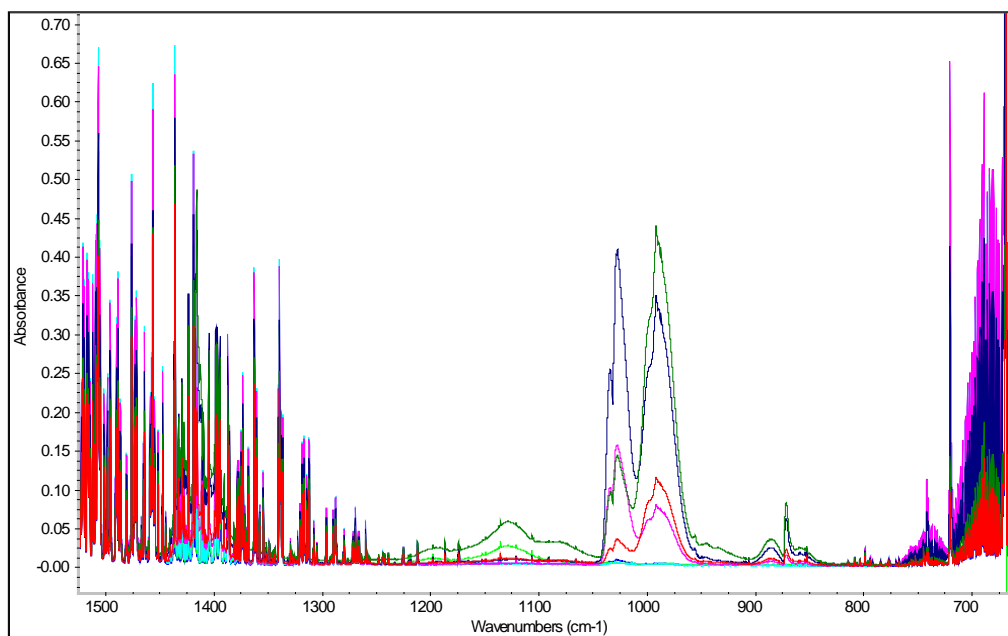


Figure 18 Series of spectra from fire test with LiPF_6 mixed in Dimethoxyethane [DME]. Spectra measured at 5 s (light green), 29 s (aqua), 42 s (pink), 54 s (black), 67 s (dark green), 79 s (red) and 104 s (blue) after start of heat exposure. Ignition at 2 s after start. Flame-out at 95 s.

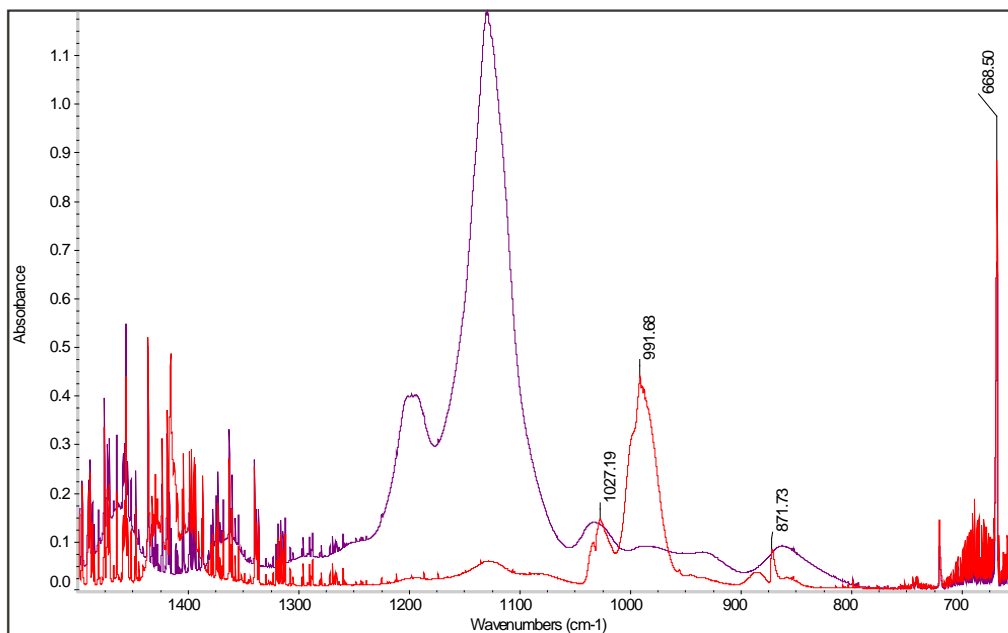


Figure 19 Spectra from the fire test with LiPF_6 mixed in DME at 67 s from start of test (red). Overlaid by spectra from evaporation test with DME (purple).

A series of spectra (overlaid) are shown in Figure 18 from the tests with LiPF_6 salt in DME. One can clearly see the characteristic spectral features of POF_3 during the period of combustion (2-95 s). Also HF was seen in the spectrum during this period (not shown above). The spectral band from the solvent is shown only in the first few spectra and in the spectrum from 67 s (see Figure 19). The combustion efficiency must have decreased at this time but extinction was not recorded until 95 s.

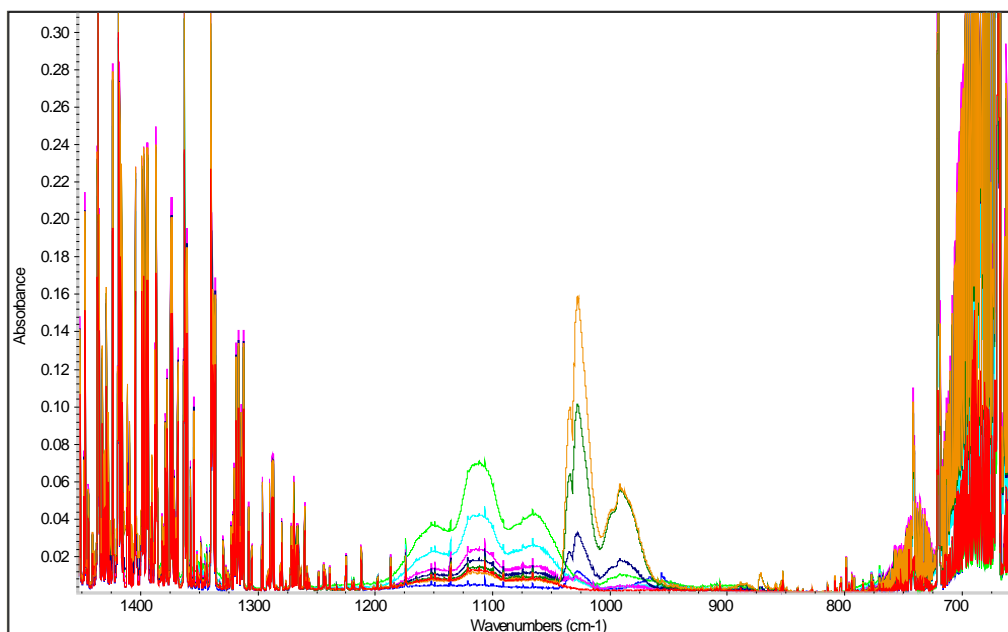


Figure 20 Series of spectra from fire test with LiPF_6 mixed in Polypropylene carbonate (PC). Spectra measured at 28 s (red), 53 s (light green), 78 s (aqua), 90 s (pink), 103 s (black), 116 s (dark green), 128 s (orange) and 190 s (dark blue) after start of heat exposure. Ignition at 1 min 11 s after start. Flame-out at 170 s.

Figure 20 shows a series of spectra (overlaid) from the tests with LiPF_6 salt in PC. The spectral bands of POF_3 (the band at 992 cm^{-1} can be clearly seen in the figure) were seen in the spectra during the period of combustion (71-170 s). Also HF was seen as in the

spectra during this period (not shown above). The spectral band from the solvent is clearly shown in the spectra before combustion.

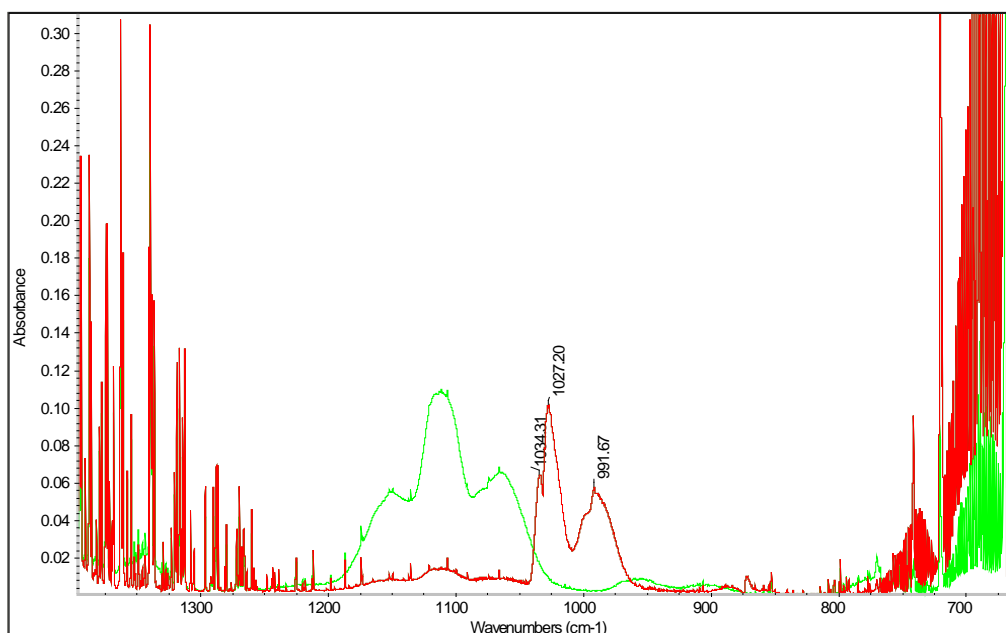


Figure 21 Spectra from the fire test with LiPF_6 mixed in Polypropylene carbonate at 116 s from start of test (red). Overlaid by spectra from evaporation test with Polypropylene carbonate (light green).

Figure 21 shows the spectrum collected at 116 s into the combustion test with LiPF_6 salt in PC. The spectra of pure PC has been overlaid. Also here one can see two additional peaks which do not originate from POF_3 , one at 1027 cm^{-1} and one at 1034 cm^{-1} .

The combustion tests with electrolyte solvents of LiPF_6 salt showed that HF and also POF_3 are present in the combustion effluents. This is an important finding. Further, unidentified spectral absorption bands indicate the presence of an additional, possibly fluorine containing, decomposition product.

5 Burner tests with electrolyte

Tests were conducted by using a small propane burner about 2 cm in diameter in which electrolyte salt solutions were introduced through needles or on a spoon as seen in Figure 21. The amount of propane inserted was controlled by a variable area flow-meter. Two different amounts of propane were used, i.e. 7 scale points on the flow meter scale and 5 scale points. The Heat Release Rate (HRR) was measured in all tests. The HRR was found to be 4.8 kW for the 7 scale point case (referred to as the “normal case” below) and 3.2 kW for the 5 scale point case (referred to as the “lower case” below). The amount of electrolyte inserted was controlled by two HPLC pumps.

The Heat Release Rate from the fire was measured by using Oxygen Consumption Calorimetry in the cone calorimeter hood. In some experiments the cone heater and load cell was used. FTIR measurement were made in all tests. The FTIR measurement system is described in Section 2. A schematic of the cone calorimeter is provided in Figure 20.

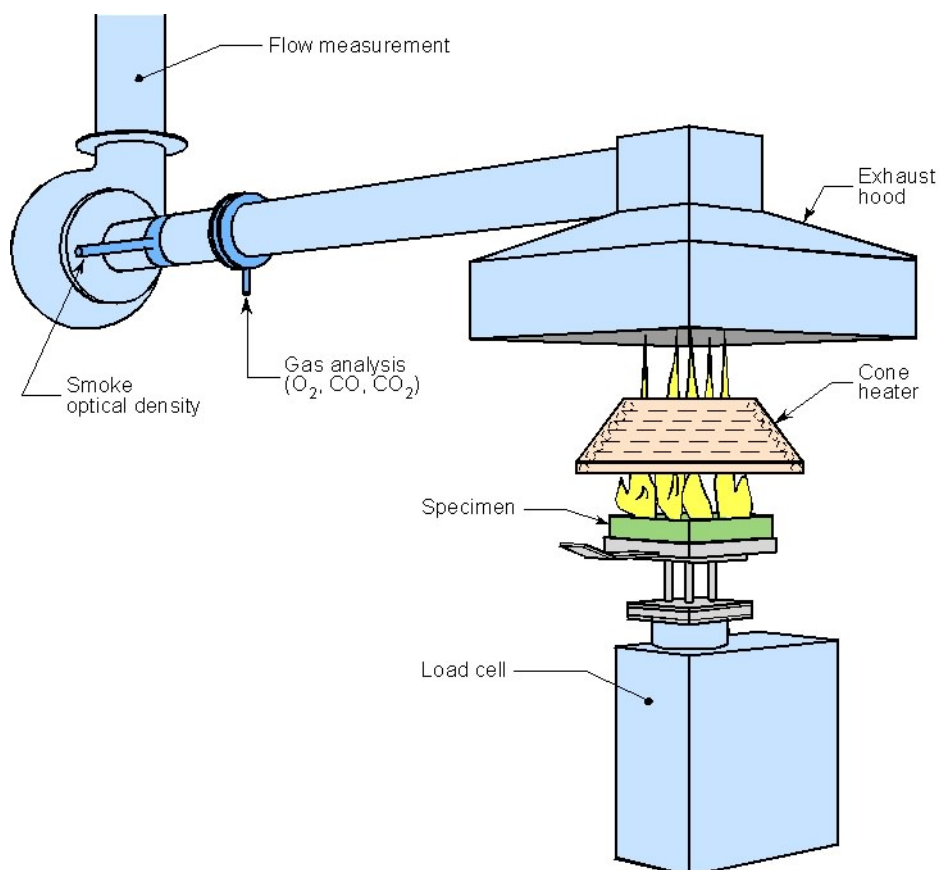


Figure 22 The cone calorimeter. The heater and load cell was not used in the major part of the tests.

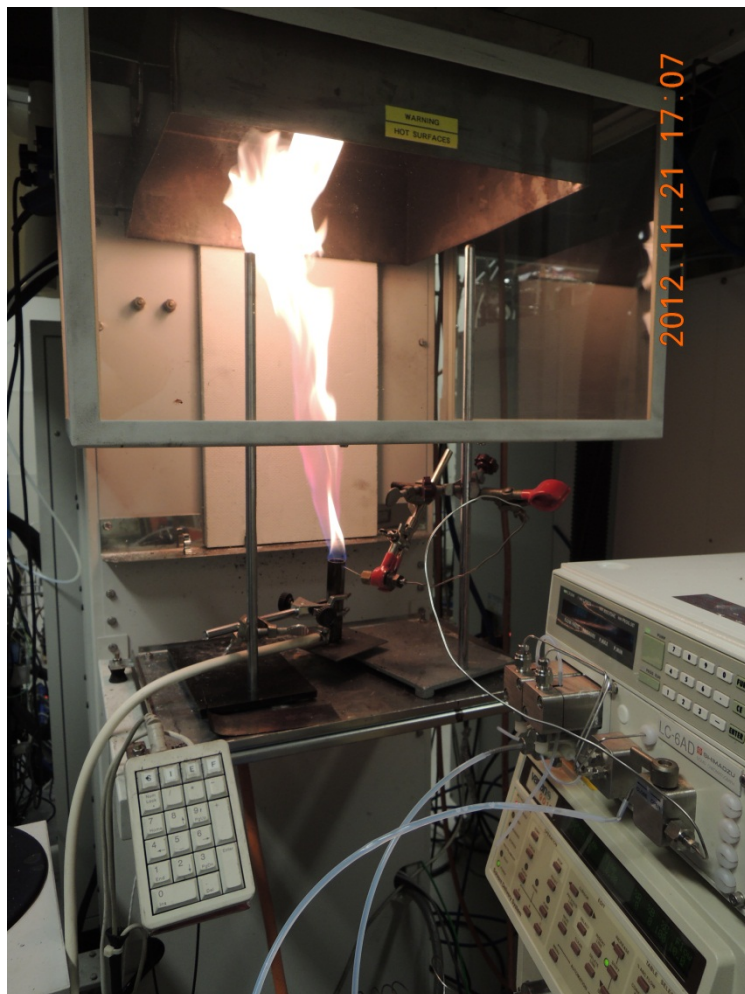


Figure 23 Experimental set-up with the needle inserted in the burner.

5.1 Electrolyte – salt solutions

Solutions of LiPF_6 (99 %, Sigma-Aldrich) were prepared by dilution in dimethylcarbonate (DMC, 99% Sigma-Aldrich) and 1,2-dimethoxy ethane (DME, 99% Sigma-Aldrich). The DMC solutions were 1.0 M and 0.4 M respectively and the DME solution was 0.4 M.

5.2 Tests conducted

Tests were conducted in two batches. In the first batch it turned out that the needles became clogged with the salt and it was difficult to produce a spray. Custom made needles were therefore ordered and a new batch of tests was conducted with the new needles.

Tests conducted in the first batch are listed in Table 4. Further description of the test procedures and results is provided in Appendix A. In this batch the propane flow was the same in all tests. The way the solvent and salt were introduced into the flame was varied and the amount was varied. Due to difficulties with achieving a stable spray and clogging of the needles it was not possible to conduct any tests where water was introduced together with salt and solvent.

Table 4 Tests conducted in first batch.

Test nr	Type of test	Fuel	Comment
1	burner	Propane only	Initial test to determine propane HRR
2	Burner + needle	Propane and 5.9 ml/min DME	DME works not as spray but as a beam, possibility that all DME not burnt
3	Burner + Needle	Propane and 5.9 ml/min DME	Needle in bottom of burner instead of top
4	Burner + Needle	Propane and 5.9 ml/min DME	Needle inserted outside of burner
5	Burner + spoon	Propane and 2.4 ml/min DMC	Not a very successful attempt
6	Burner + Needle	Propane and 12 ml/min DMC	and later 5 ml/min
7	Burner + Needle	Propane and 20 ml/min DMC	Interrupted as holder melted
8	Burner + Needle	Propane and 20-18 ml/min DMC	Burner placed a bit lower under the collecting hood
9	Burner + Needle	Propane and DMC 18 ml/min	
10	Burner + Needle	Propane and DMC 18 ml/min with 1 M salt	
11	Burner + needle	Propane and DME 18 ml/min	
12	Burner + needle	Propane and DME 18 ml/min with 0.4 M salt	
13	Burner + Needle	Propane and DMC 18 ml/min 1 M salt	
14	Burner + Spoon	Propane and DMC 1.8 ml/min	
15	Burner + spoon	Propane and DMC 1.8 ml/min + 1M salt	
16	Burner + spoon	Propane and DME 1.8 ml/min + 0.4 M salt	
17	cakecup	DMC + salt 1:1	No external heating, did not burn very well
18	cakecup	DME + salt 1:1	No external heating, did not burn very well

The tests conducted in the second batch are presented in Table 5, additional information about the test procedures can be found in appendix A. The tests were conducted using the same burner as used in the first batch of tests. Two different propane flows were used, 7 and 5 scale points on the flow meter, resulting in a HRR of 4.8 and 3.2 kW respectively. These HRR levels were in the same order of magnitude as the HRR resulting from the electrolyte burning. Most of the tests were conducted on DMC. The salt concentration in the DMC was varied together with the amount of DMC introduced into the flame. In

addition some tests were conducted where water was introduced into the flame. The duration of these tests was however, limited because despite careful design of needles that were custom made for this project we encountered problems with creating a stable spray for long periods of time.

Table 5 Tests conducted in second batch.

Test nr	Injection	Other conditions
20	none	Normal propane 7 sp
21	none	Normal propane and water 7 - 8 min and 10 - 11 min
22	15 ml/min 2 min 1 M = 30 ml M	Normal propane 7 sp DMC
23a	15 ml/min 4.5 min 0.4M = 27 ml M	Normal propane during 3 minutes, lower during 1.5 min DMC
23b	15 ml/min 3 min 0.4M = 18 ml M uncertainty for the 15 ml/min, according to HRR only about half	5 skd propane DMC
24	10 ml/min 3 min 1 M (initial 5 minutes injection problematic)	7 sp propane, short while at end with water injection DMC
25	15 ml/min 1 M 2:45 = 41 ml M	7 sp propane DMC
26a	15 ml/min 1 M 1:45	7 sp propane DMC
26b	Cleaning system with water	
26c	15 ml/min 1 M 1:30	7 skd propane, water at end DMC
27	1 M salt in DMC in cakecup	
28	0.4 M salt in DME in cakecup	

5.3 Test Results

Results from tests where LiPF₆ salt was injected in the first test batch are presented in Figure 22 - Figure 36. For these tests is HRR presented together with an indication of when different injections were conducted by means of coloured lines in the graphs. In addition are graphs presented with HRR on the left axis and the HF concentration in the exhaust duct on the right hand side axis. Finally one graph is presented for each of these tests where the HF concentration in the exhaust duct is given on the left hand side axis and the POF₃ concentration in the duct on the right hand side axis.

When studying the graphs it is important to remember that the concentrations presented are concentrations in the exhaust duct. These depend on the gas flow in the exhaust duct and the amount of salt and electrolyte introduced into the flame. They should not be considered as the concentration in the vicinity of a burning vehicle but are only presented here as concentrations in order to evaluate changes in amount produced due to changes in flame composition etc.

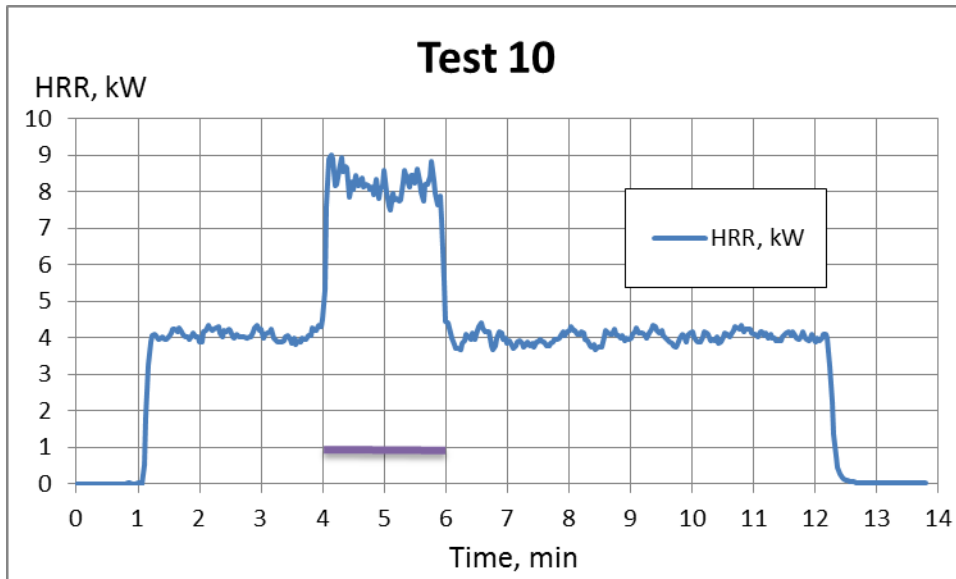


Figure 24 Heat Release Rate (HRR) from test 10. DMC and salt injection (18 ml/min with 1 M salt) indicated as a purple line between time 4 and 6 minutes.

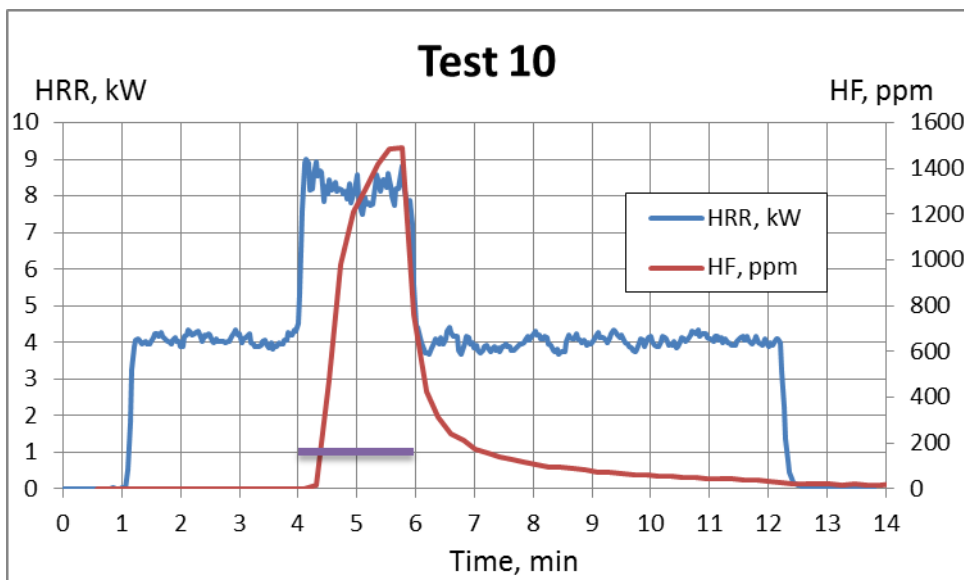


Figure 25 HRR and HF concentration during Test 10. DMC and salt injection (18 ml/min with 1 M salt) indicated as a purple line between time 4 and 6 minutes.

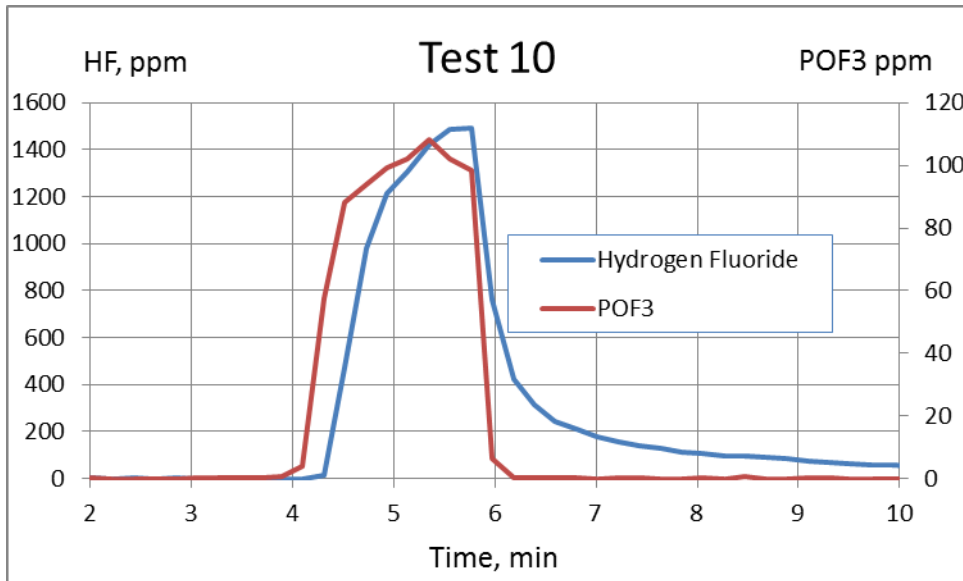


Figure 26 HF and POF₃ concentration as a function of time for test 10. DMC with salt was injected during time 4 to 6 minutes.

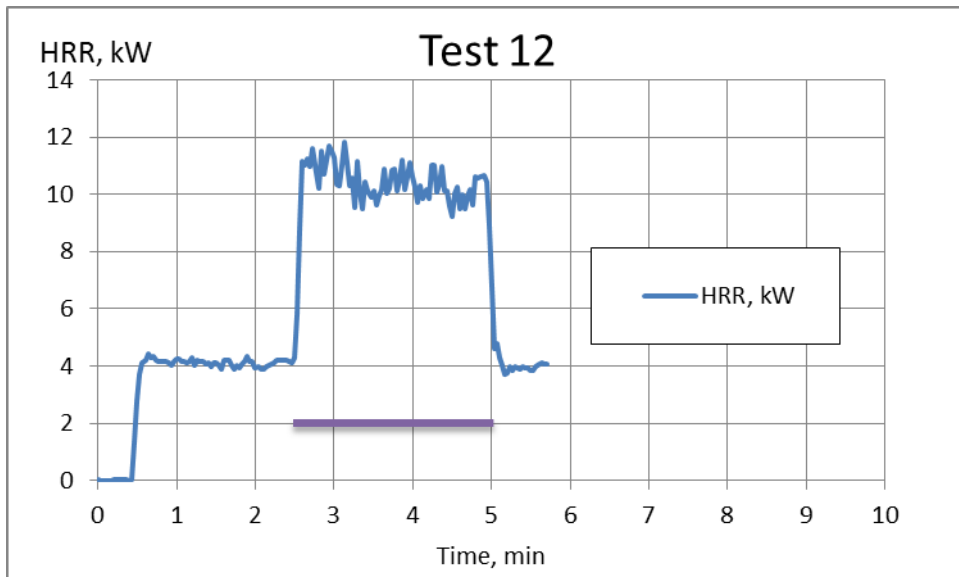


Figure 27 HRR as function of time for test 12. The time period under which DMC with salt was introduced into the flame is indicated with a purple line (2.5 minutes – 5 minutes).

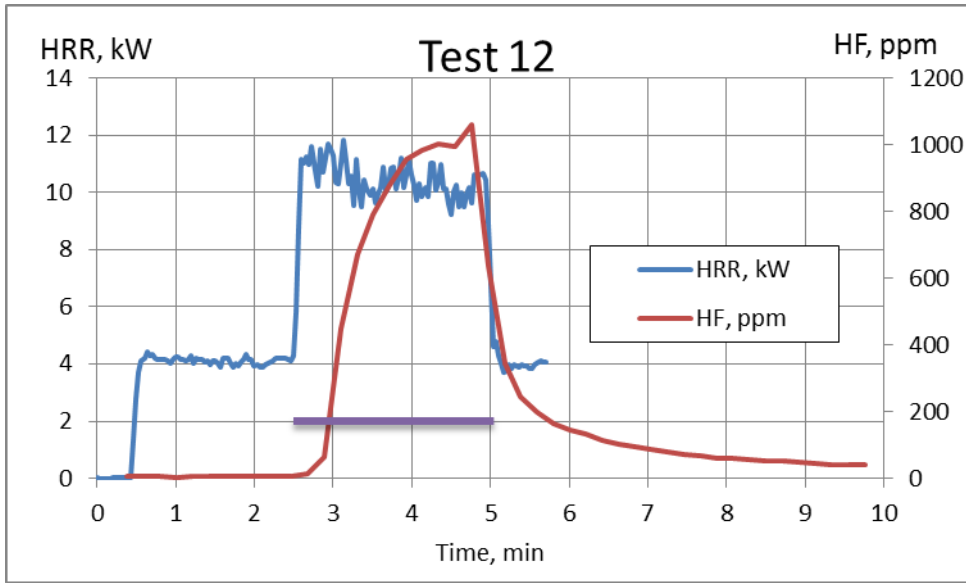


Figure 28 HRR and HF concentration as function of time for test 12. The time period under which DMC with salt was introduced into the flame is indicated with a purple line (2.5 minutes – 5 minutes).

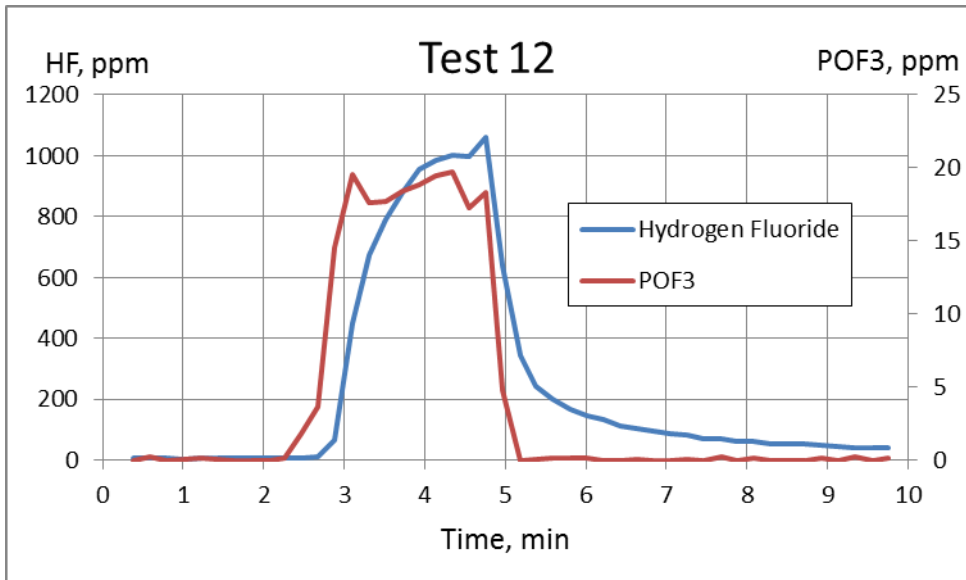


Figure 29 HF and POF₃ concentration as a function of time for test 12. DME with salt was injected during time 2.5 to 5 minutes.

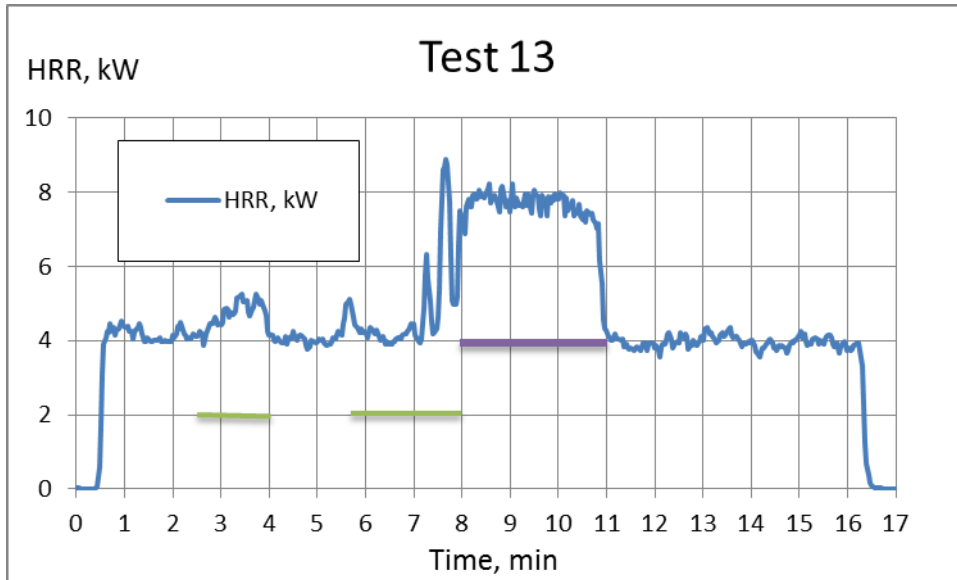


Figure 30 HRR as function of time for test 13. Initial spray attempt with DMC starting at 2:30 had to be interrupted at 4:00 due to difficulties with spray. Second period of pure DMC at time 5:40 until 8:00, both DMC periods indicated with green line in figure. The time period under which DMC with salt was introduced into the flame is indicated with a purple line (8 minutes – 11 minutes).

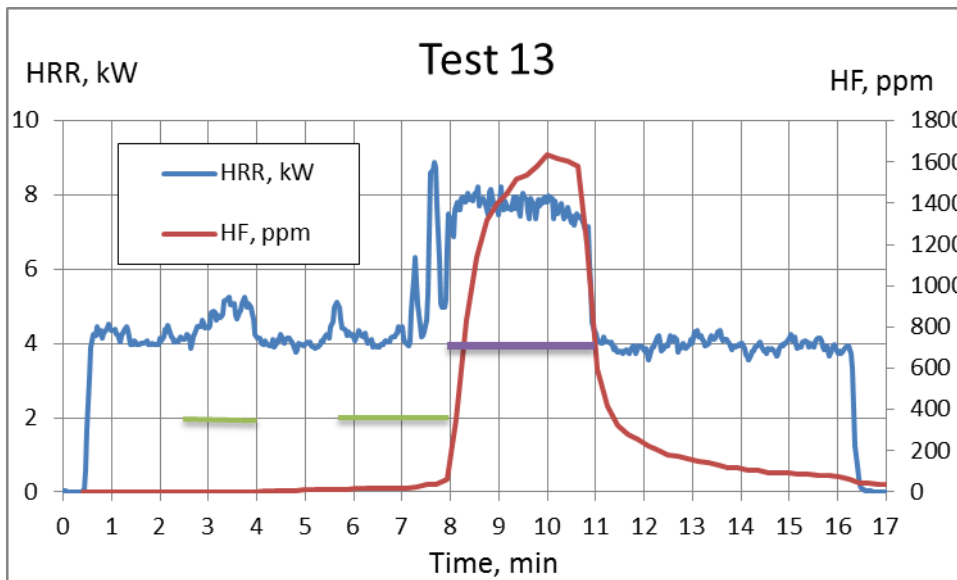


Figure 31 HRR and HF concentration as function of time for test 13. Initial spray attempt with DMC starting at 2:30 had to be interrupted at 4:00 due to difficulties with spray. Second period of pure DMC at time 5:40 until 8:00, both DMC periods indicated with green line in figure. The time period under which DMC with salt was introduced into the flame is indicated with a purple line (8 minutes – 11 minutes).

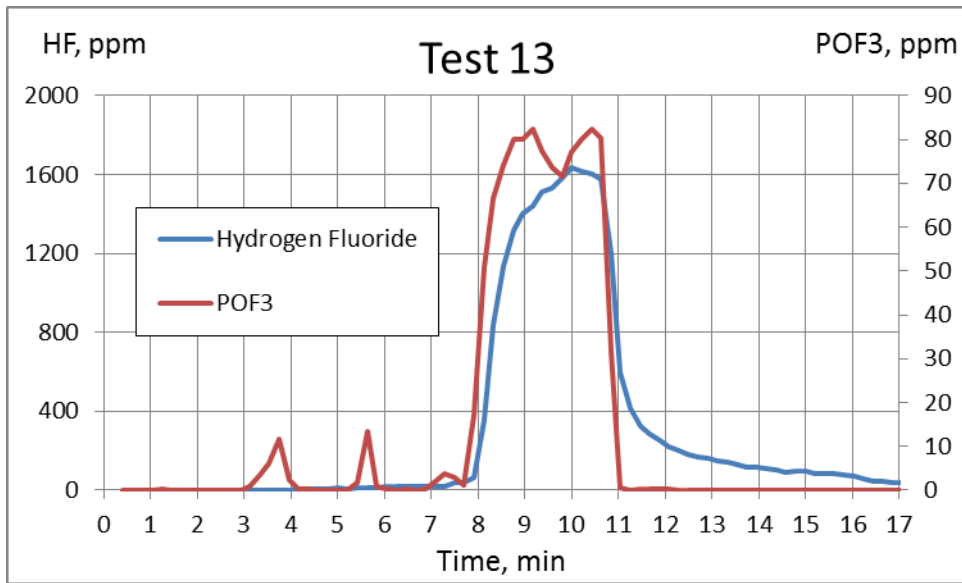


Figure 32 HF and POF₃ concentration as a function of time for test 13. DMC with salt was injected during time 8 to 11 minutes.

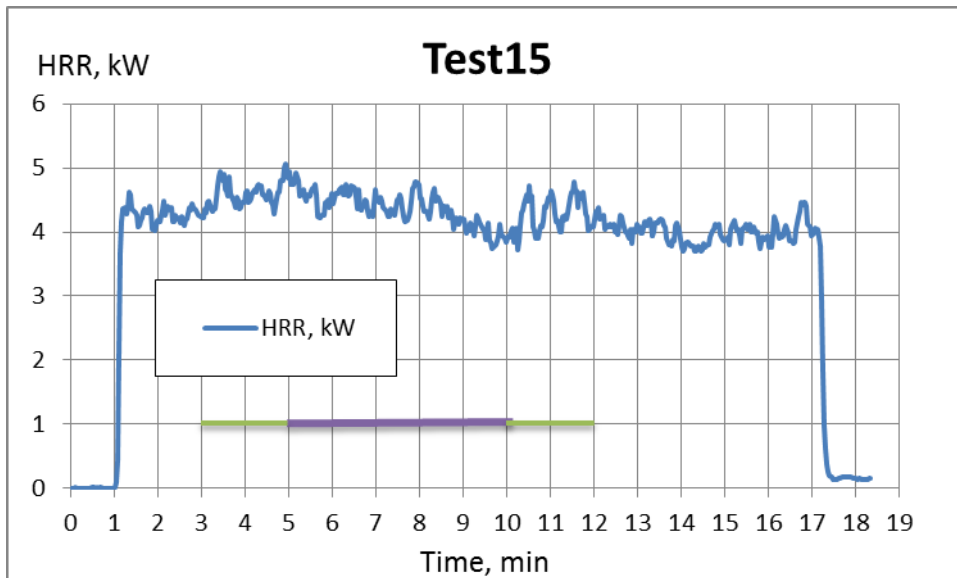


Figure 33 HRR as a function of time for test 15. DMC and salt was inserted through a needle onto a spoon in the flame during time 5 minutes to 10 minutes, DMC only was injected between times 3 and 5 minutes and 10 and 12 minutes.

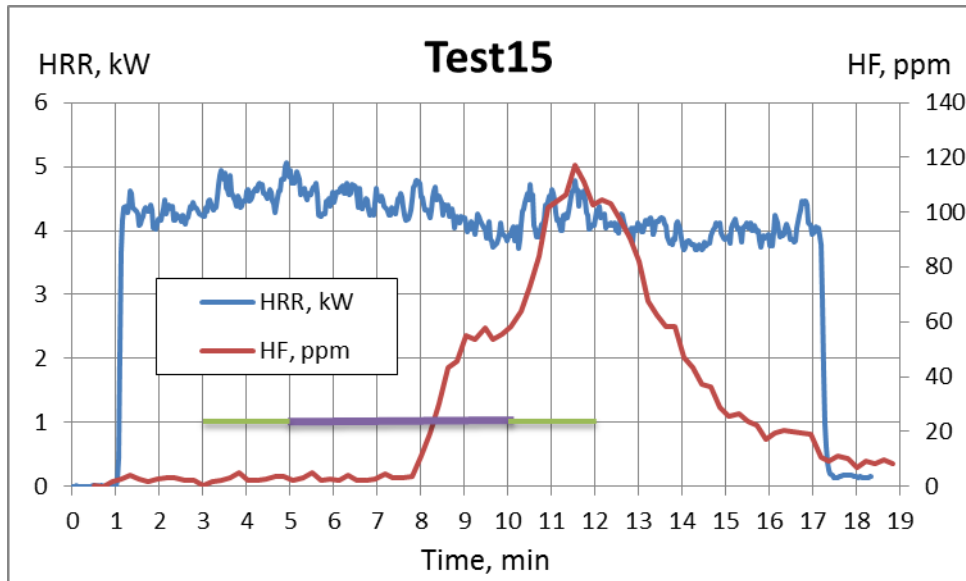


Figure 34 HRR and HF concentration as a function of time for test 15. DMC and salt was inserted through a needle onto a spoon in the flame during time 5 minutes to 10 minutes.

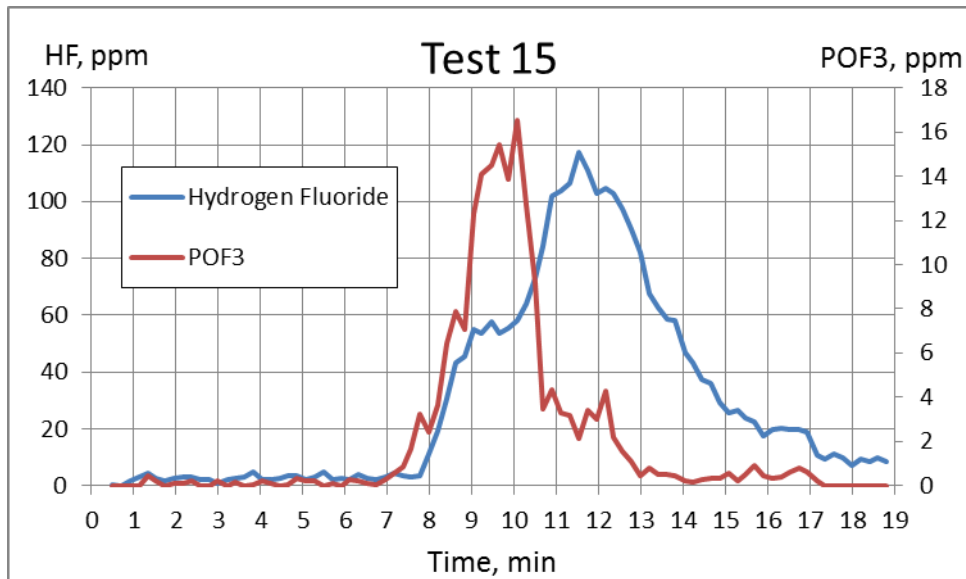


Figure 35 HF and POF₃ concentration as a function of time for Test 15. DMC and salt was inserted through a needle onto a spoon in the flame during time 5 minutes to 10 minutes.

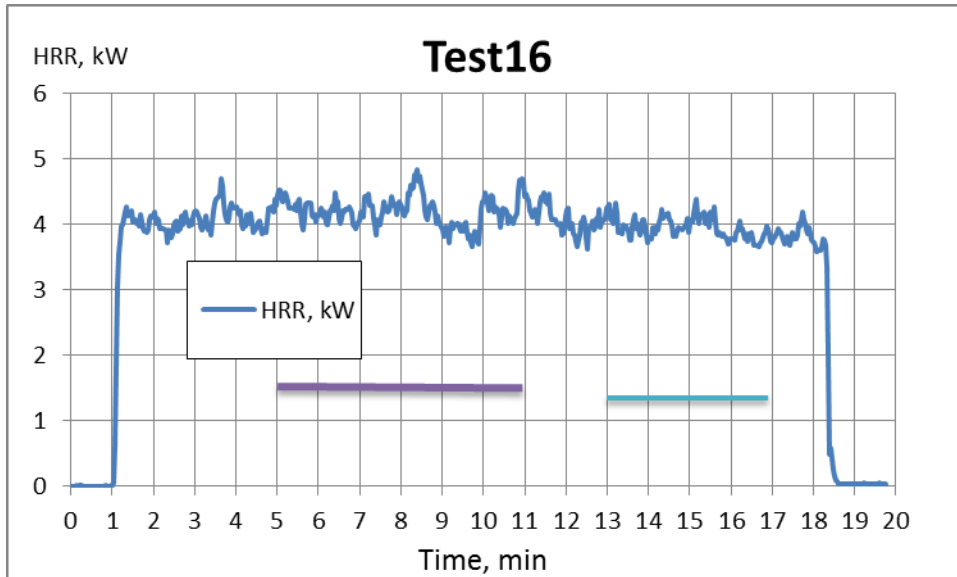


Figure 36 HRR as a function of time for test 16. DME and salt was inserted through a needle onto a spoon in the flame during time 5 minutes to 11 minutes. During time 13 to 17 minutes water was inserted to the spoon instead.

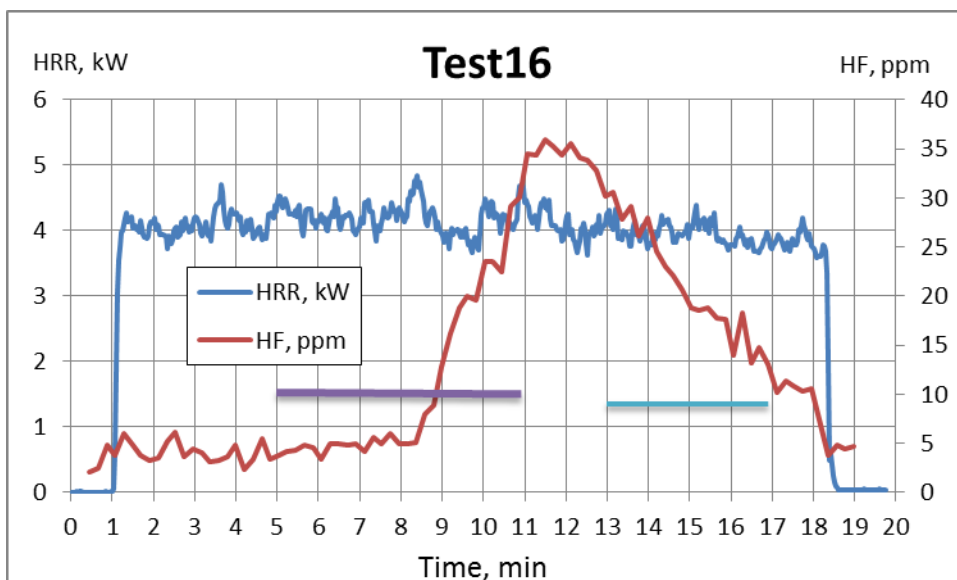


Figure 37 HRR and HF concentration as a function of time for test 16. DME and salt was inserted through a needle onto a spoon in the flame during time 5 minutes to 11 minutes. During time 13 to 17 minutes water was inserted to the spoon instead.

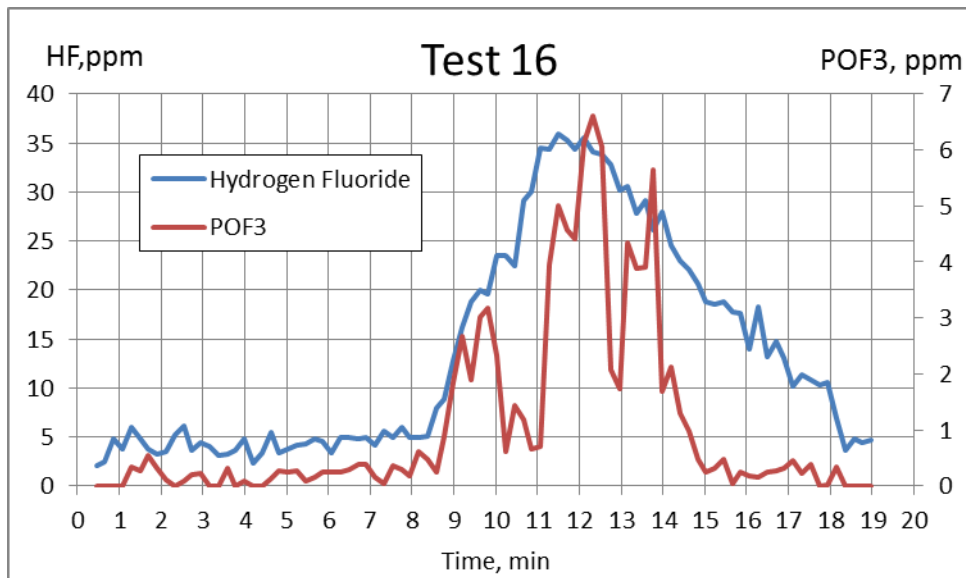


Figure 38 HF and POF₃ concentration as a function of time for Test 16. DME and salt was inserted through a needle onto a spoon in the flame during time 5 minutes to 11 minutes. During time 13 to 17 minutes water was inserted to the spoon instead. Note that the concentration of POF₃ measured here was below the limit of quantification.

The FTIR measurements showed that both HF and POF₃ were always present in the combustion effluents when electrolytes were burning. The measured concentration of HF was always significantly higher than POF₃, often about 20 times higher.

Test 10-16 all shows that the POF₃ seems to appear a bit earlier than HF, this is particular apparent in test 15. It is known that losses of HF occurs in the measurement system and especially in the sampling filter⁵. The effect is most significant at measurements of low concentrations as the proportion captured in the filter in such cases is high compared to the total amount HF sampled through the filter. An effect of HF-losses in the filter is an initial increased response time (until the sampling system is saturated) that can be significant especially in measurements of low concentrations. The filter was exchanged before test 14 but as test 14 was interrupted the filter can be considered as being new for test 15.

Selected filter used in the measurements reported below (test 22-test 27) were analysed for total fluorine content. The analysis results showed that the amounts lost in the filter were low, normally around 5 % on weight basis.

Test results from the second batch of tests are presented in Figure 37 - Figure 53. The result are presented for the tests where solvent and salt was introduced into the flame. For all tests the HRR curve is presented including the HRR from the propane. Different injections are indicated with different colours in the figures, i.e. green for solvent only, purple for salt and solvent, and different blue colours for water and alcohol.

An example of how the flame look liked when salt was injected is given in Figure 39.

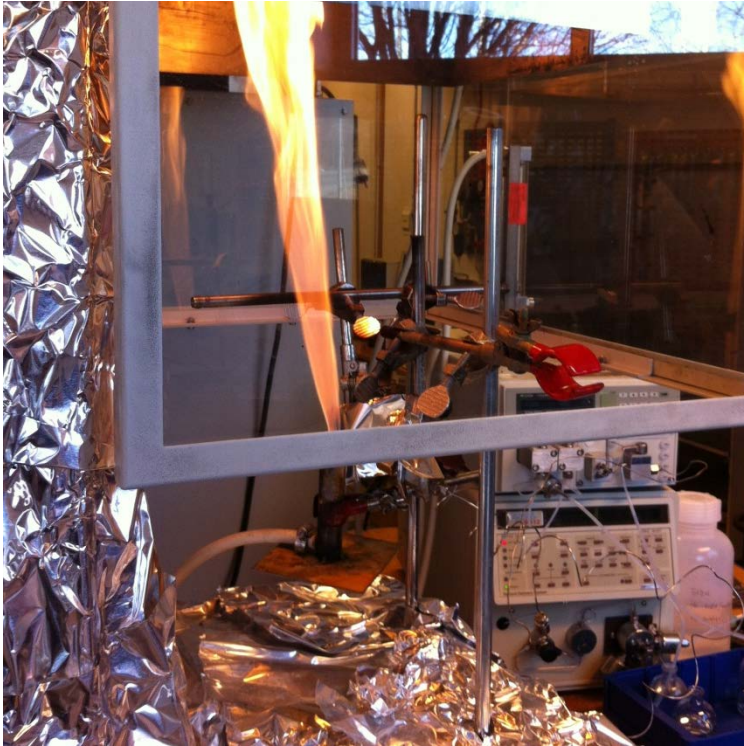


Figure 39 Example of flame when electrolyte and salt is injected, test 25

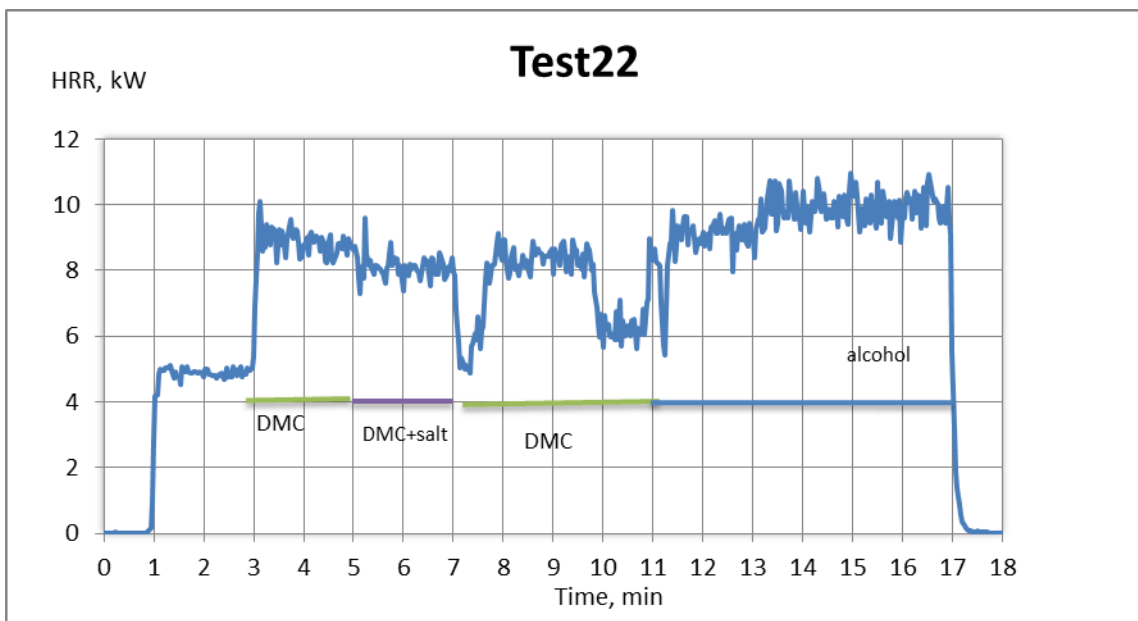


Figure 40 HRR as a function of time for test 22. The different injections period are indicated with a green line for pure DMC, purple line for DMC + salt and a blue line for cleaning with alcohol at the end of the test.

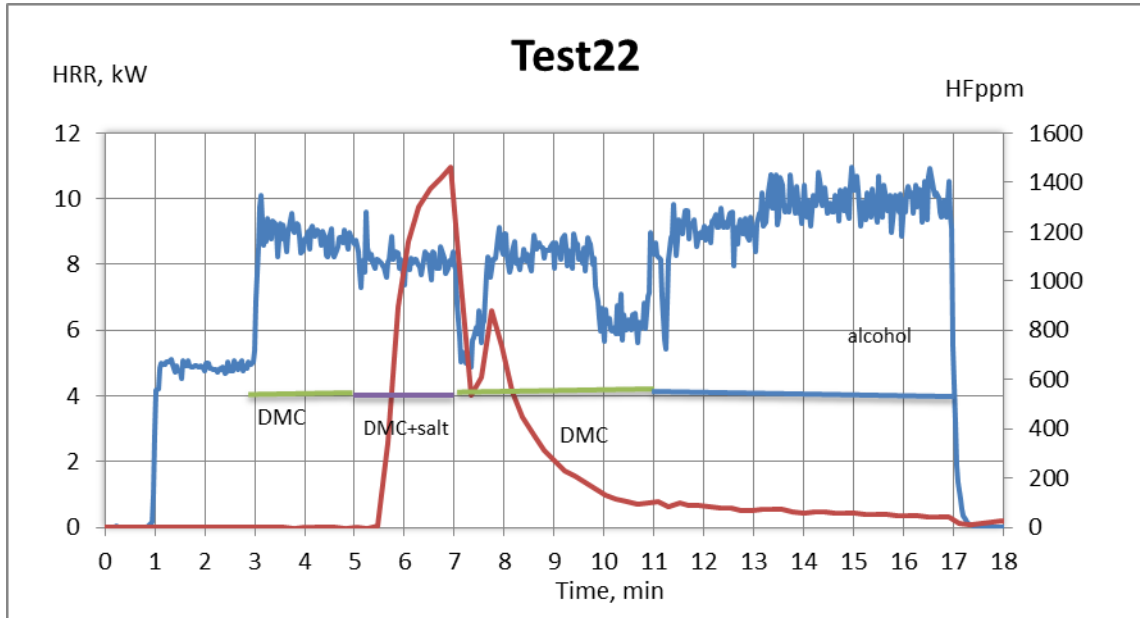


Figure 41 HRR and HF concentration as a function of time for test 22. The different injections period are indicated with a green line for pure DMC, purple line for DMC + salt and a blue line for cleaning with alcohol at the end of the test.

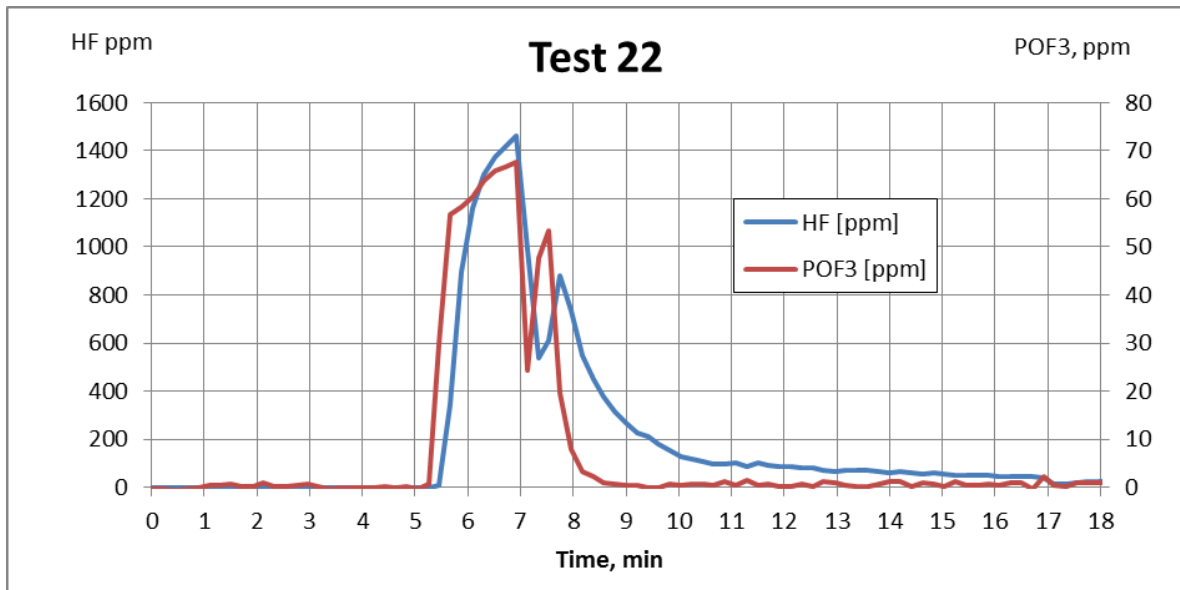


Figure 42 HF and POF₃ concentration as a function of time for test 22. DMC with salt was injected under time 5-7 minutes.

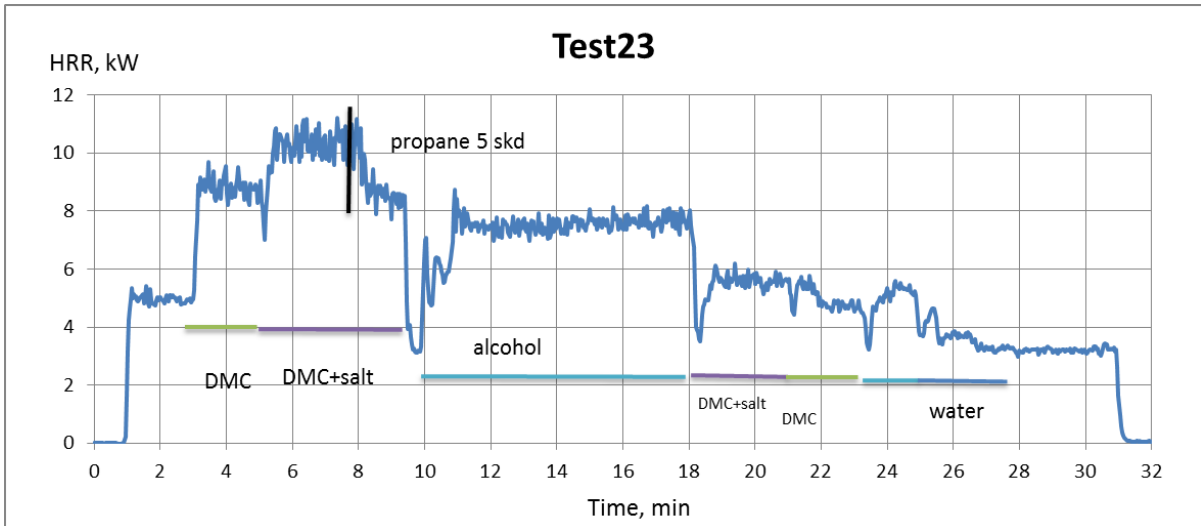


Figure 43 HRR as a function of time for Test 23. The different injections are indicated as green line for DMC only, purple line for DMC with salt (5 minutes until 9:30 and then again 18 until 21 minutes), light blue for alcohol and darker blue for water.

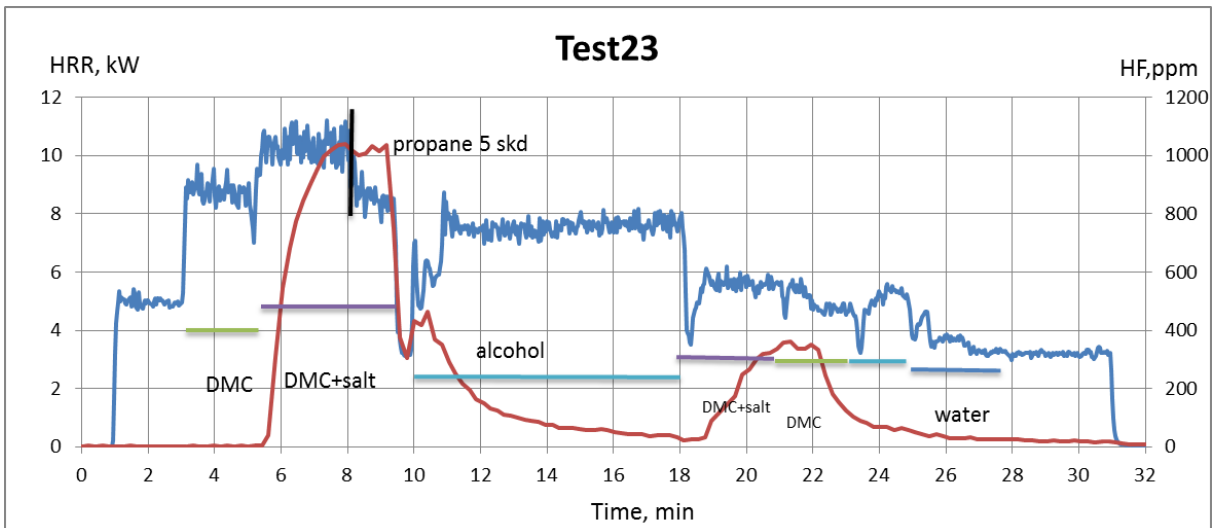


Figure 44 HRR and HF concentration as a function of time for Test 23. The different injections are indicated as green line for DMC only, purple line for DMC with salt, light blue for alcohol and darker blue for water.

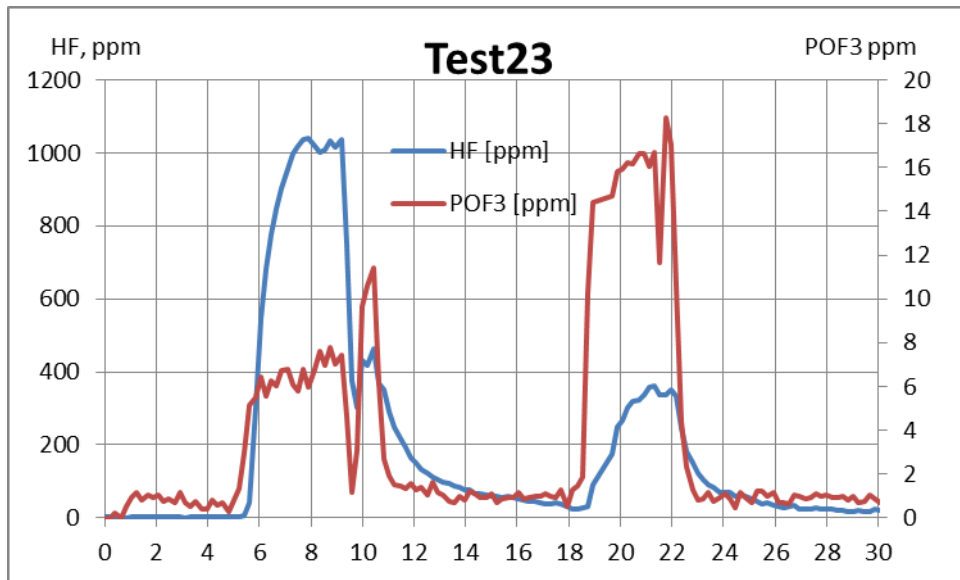


Figure 45 HF and POF₃ concentration in exhaust gases as a function of time for test 23. DMC + salt was injected during time 5 minutes until 9:30 and then again between time 18 and 21 minutes.

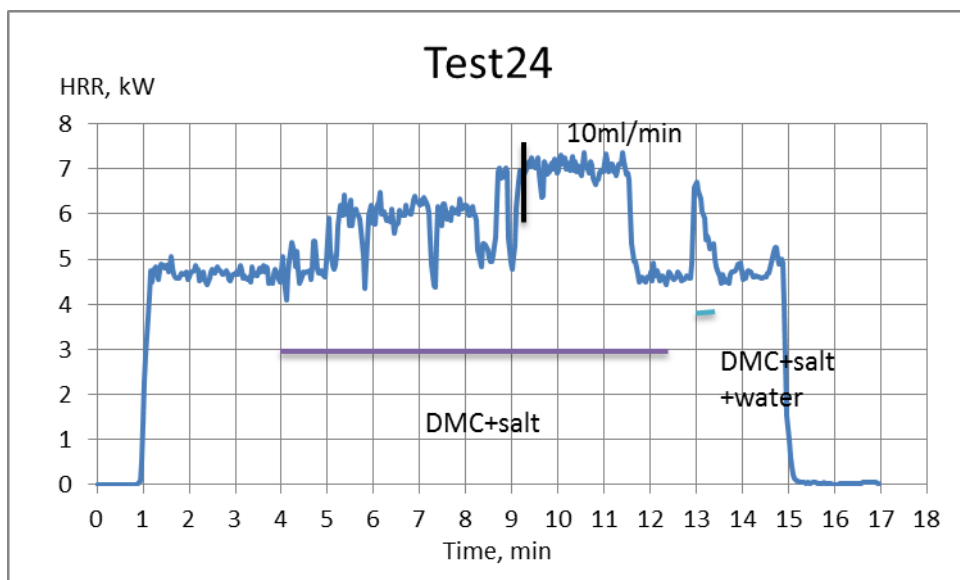


Figure 46 HRR as a function of time for test 24. DMC and salt was injected during time 4 minutes until 12:30, the spray did not work correctly until time 9:15.

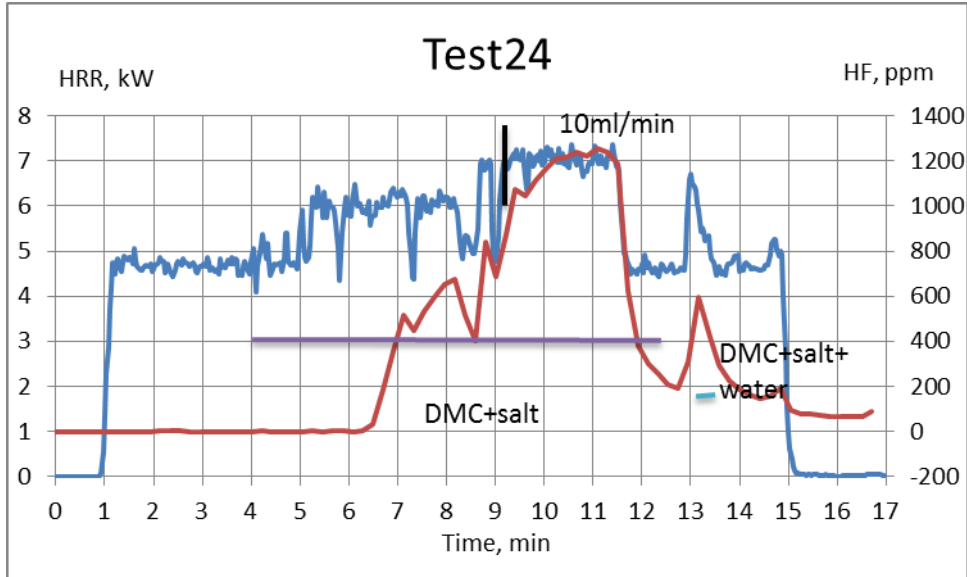


Figure 47 HRR and HF concentration as a function of time for test 24. DMC and salt was injected during time 4 minutes until 12:30, the spray did not work correctly until time 9:15.

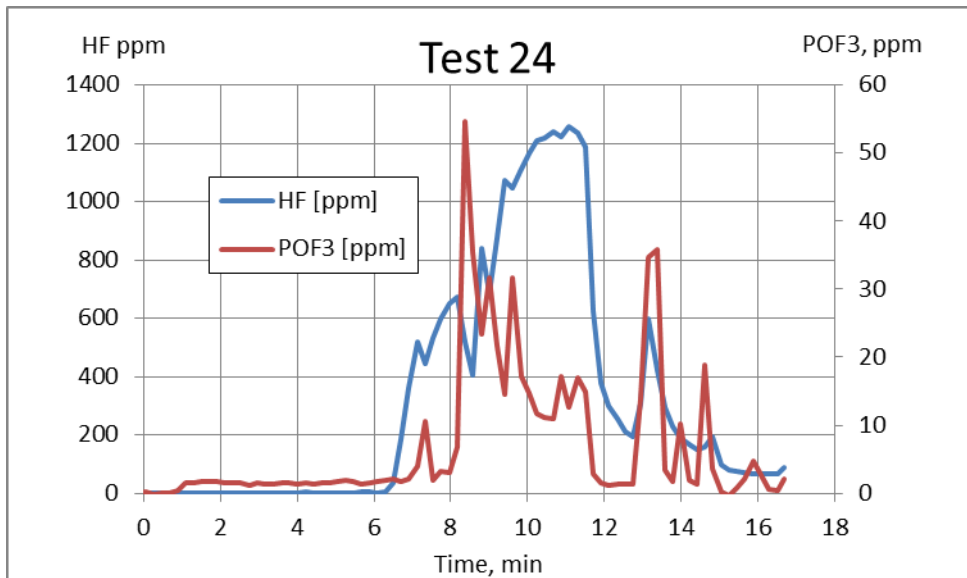


Figure 48 POF₃ and HF concentration as a function of time for test 24. DMC and salt was injected during time 4 minutes until 12:30, the spray did not work correctly until time 9:15.

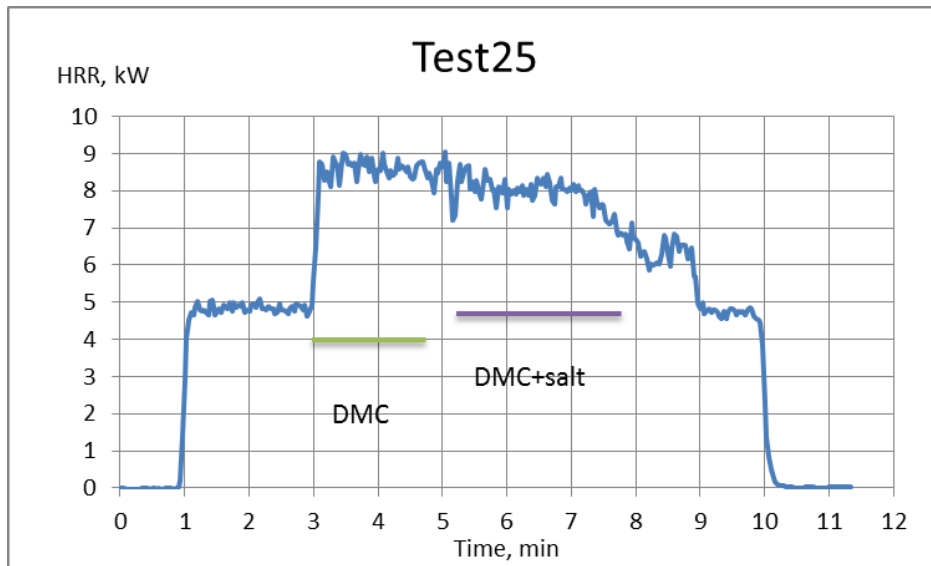


Figure 49 HRR as a function of time for test 25.

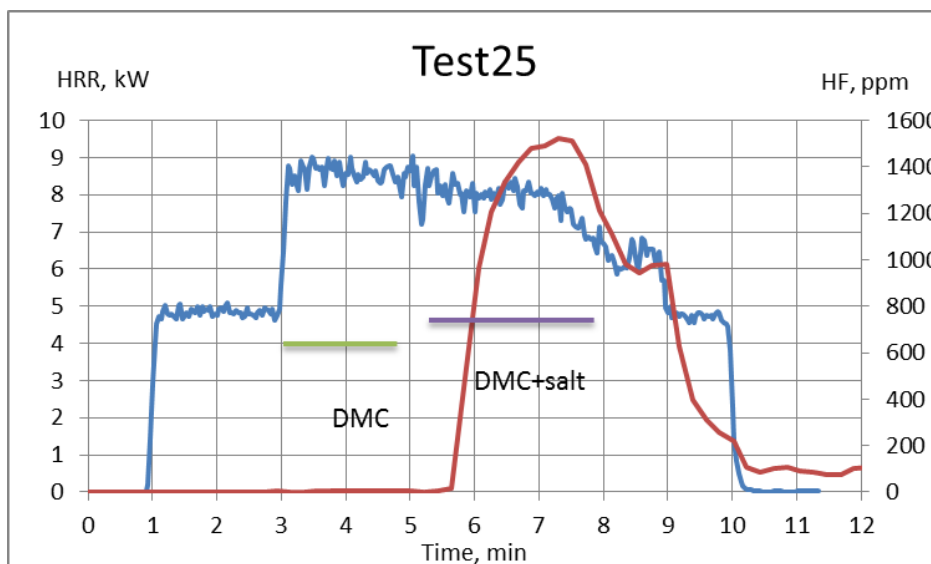


Figure 50 HRR and HF concentration as a function of time for test 25.

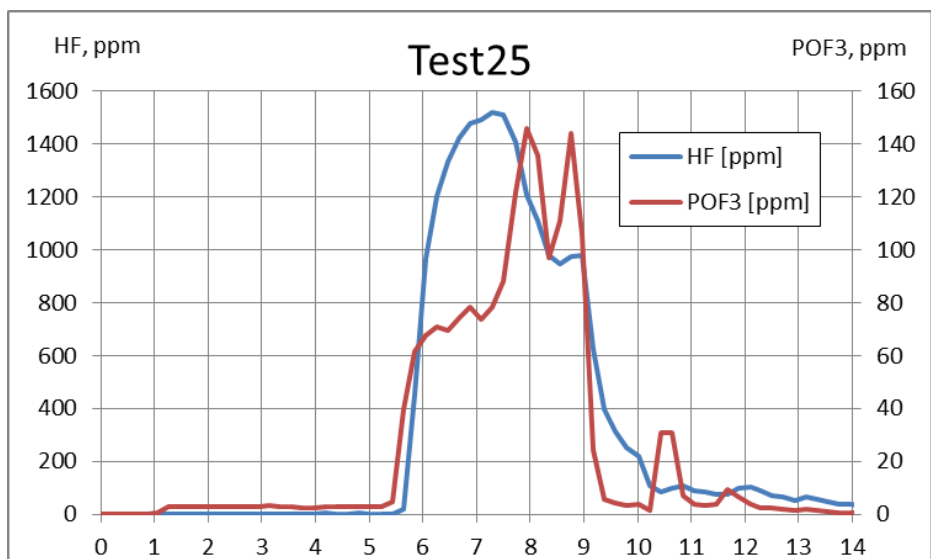


Figure 51 HF and POF₃ concentration as a function of time for test 25.

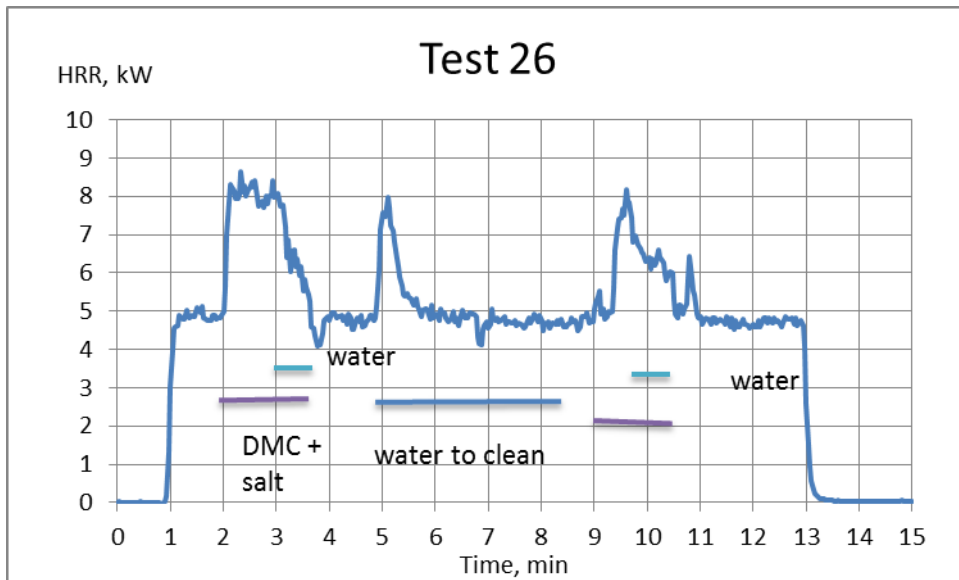


Figure 52 HRR as a function of time for test 26. DMC and salt injection indicated as purple line at time 2 until 3:40 and then at time 9 minutes until 10:30. Water injection into flames by water spray bottle indicated as light blue line from time 3 minutes until 3:40 and then from time 9:50 until time 10:30. Water was injected through the needle between time 5 minutes and 8:30 to clean the system.

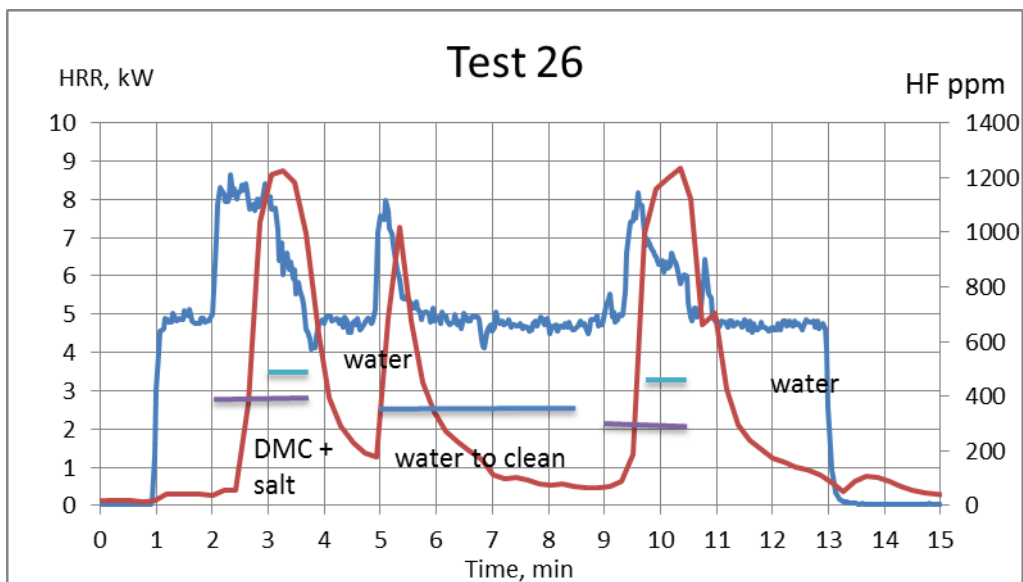


Figure 53 HRR and HF concentration as a function of time for test 26. DMC and salt injection indicated as purple line at time 2 until 3:40 and then at time 9 minutes until 10:30. Water injection into flames by water spray bottle indicated as light blue line from time 3 minutes until 3:40 and then from time 9:50 until time 10:30. Water was injected through the needle between time 5 minutes and 8:30 to clean the system.

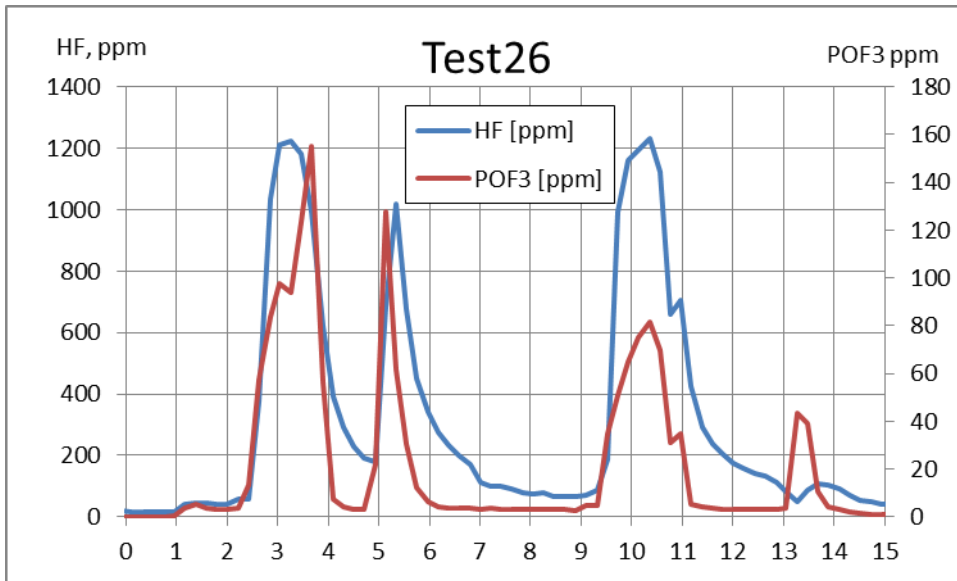


Figure 54 HF and POF₃ concentration as a function of time for test 26.

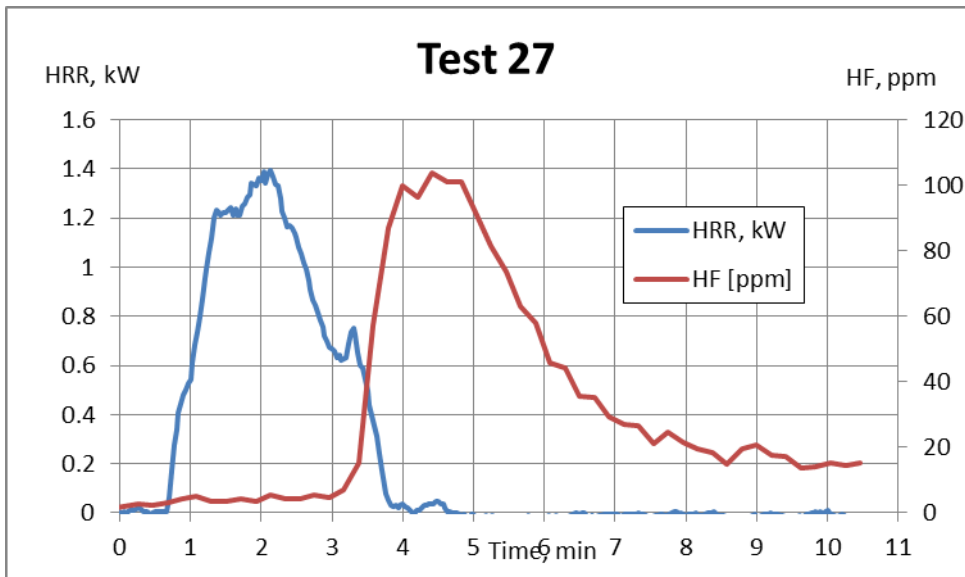


Figure 55 HRR and HF concentration for the cakecup test. Heat radiation applied 10-15 kW/m². Ignited about 15 s after heat application started.

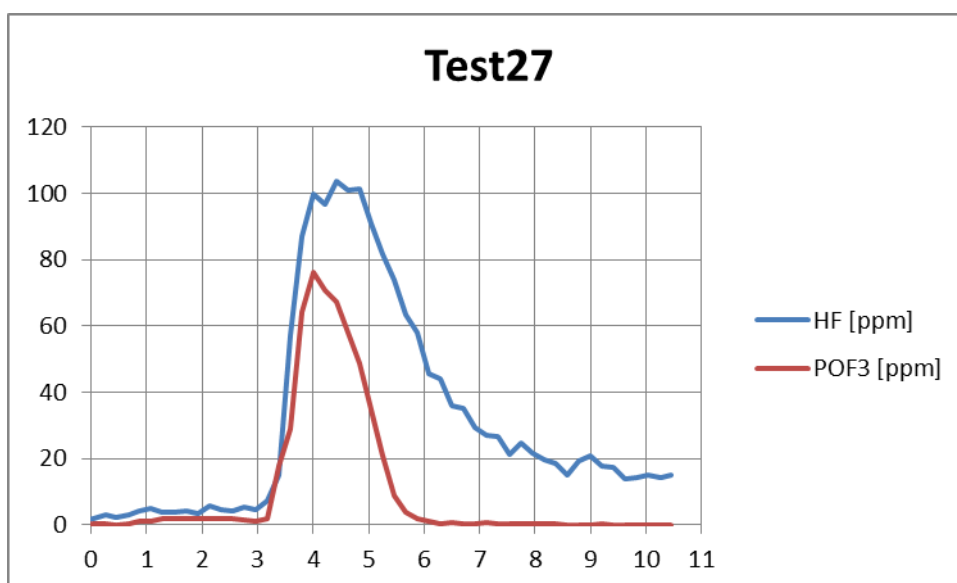


Figure 56 HF and POF₃ concentration as a function of time for test 27, test where the electrolyte was heated in a cakecup and ignited by a igniter.

Test 27 shows a different behaviour than the other tests. Unfortunately there was no electrolyte available to explore this further as this was the last test. This could indicate a potential for that toxic gases are produced especially at the end of a fire. This could also reflect that the salt is burnt later than the electrolyte solvent.

The test results from the burner tests in the second batch are summarized in Table 6. The table contains the amount of salt injected expressed as mass of F (grams) based on pump speed, Molar concentration of solution and time sprayed into the flame. This value contains some uncertainty due to uncertainties in conjunction with the pumps and the fact that the spray was not always a spray but more of a beam. The gases produced are expressed as the amount HF and POF₃ in grams, these values are then recalculated into mass of F in grams. The HF values contains also the fluorine content found in the filters analysed after the tests. This value was added to the HF content despite we do not know whether the fluorine is in the form of HF or any other fluorine specie.

Table 6 Results from tests conducted in second batch.

Test nr	Amount salt injected as F (g)	Amount HF (g)	Amount POF ₃ (g)	Amount HF as F (g)	Amount POF ₃ as F (g)	Missing F (g)	HF/POF ₃ by mass
22	3.4	2.5	0.5	2.3	0.3	0.8	5
23a	3.1	2.8	0.1	2.6	0.1	0.4	23
23b	1.7	0.8	0.2	0.8	0.1	0.8	4
	HRR compensated 0.9	0.8	0.2	0.8	0.1	0.0	4
24	3.4	4.2	0.5	4.0	0.3	-0.9	8
25	6.3	3.7	1.4	3.5	0.8	2.0	3
26a	4.0	1.4	0.6	1.3	0.3	2.3	2
26b	Cleaning system with water	0.8	0.3	0.7	0.1	-0.8	
26c	1.7	1.6	0.4	1.5	0.2	0.0	4

The results in Table 6 shows that not all F is captured in the measurements. This can be due to that some of the F is not present as HF or POF₃ but some other species such as phosphoric acid. We see also that we over-predict the amount of F in two cases, one case where the system was not injected with salt, this was probably due to some remains of salt in the pumps or the filters used to protect the needles from clogging. And one case where time was spent in the beginning of the test to get the spray working with salt. The response time of the FTIR analysis makes it difficult to exclude this initial amount of salt into the system in the calculations unfortunately.

6 Fire tests with batteries

Tests were also conducted on battery cells and batteries used for automotive applications and laptops. Water was added to the flames in one test in order to investigate the influence of water addition to the HF production.

6.1 Batteries tested

The cells in test 1-5 were commercially available pouch cells for automotive applications. The cell is a power optimized cell with a cathode chemistry of LiFePO₄, lithium ion phosphate (commonly abbreviated LFP).

The cells in test 6 were commercially available cylindrical cells (of type 26650). The cell is an energy optimized type of LFP, and have been used in e.g. electric vehicles.

The laptop battery pack in test 7 consisted of 2 commercially available battery packs for laptops. Each laptop pack consisted of 6 cells, in which 3 were in series and 2 in parallel, often denoted as 3s2p. The laptop battery pack differs from the other tested cells in several aspects. Firstly, it has a different Li-ion chemistry, which has a higher nominal cell voltage (3.7 V vs 3.2 V for LFP). Secondly, it is a commercially complete battery pack including electronics, plastic housing, electrical connector to laptop, etc. Thirdly, it has a higher pack voltage due to the fact that three cells are connected in series inside the battery pack, increasing the voltage by a factor 3 (to 11.1 V).

All cells were unused. However, the laptop pack was less than 6 months old. The LFP type 1 cells used in tests 1-5 were approximately 1-2 years old and the LFP type 2 cells in test 6 were approximately 2-3 years old.

Table 7 Fire tests with batteries conducted under the hood of the SBI-equipment.

Test no	Cell type	State of Charge, SOC (%)	Nominal capacity (Ah)	No of cells	Total weight (g)
1	LFP type 1, pouch	100 %	35 Ah	5	1 227.9
2	LFP type 1, pouch	100 %	35 Ah	5	1 229.7
3	LFP type 1, pouch	100 %	35 Ah	5	1 229.3
4	LFP type 1, pouch	0 %	35 Ah	5	1 228.6
5	LFP type 1, pouch	50 %	35 Ah	5	1 227.6
6	LFP type 2, cylindrical	100 %	28.8 Ah	9	734.8
7	Laptop battery pack	100 %	33.6 Ah*	2 x (3x2)	639.0

* Corresponding value, rated at each battery pack is 5.6 Ah with 11.1 V.

6.1.1 Cell preparation

All battery cells were charged/discharged to the selected state of charge (SOC) level, using an ordinary power aggregate for labs as well as Digatron battery test equipment. The laptop batteries were fully charged by putting them into a laptop computer.

The five cells, in tests 1-5, were carefully fastened together with steel wire. The poles (tabs) were cut on all cells but one.

The cells in test 6 had originally welded tabs on its poles which after charging were physically removed. The nine cells were placed inside a box, which had steel net at the bottom and top and walls made of a silica board. These specifications were safety precautions in order to avoid possible projectiles.

The laptop pack, which consisted of two identical laptop packs were placed inside a steel net and fastened on the burner grid in order to prevent possible projectiles.

6.2 Experimental apparatus

The tests were conducted in the Single Burning Item apparatus, EN13823, that is normally used for classification of building materials according to the European Classification scheme. This apparatus was chosen as it has a suitable extraction flow for the tests conducted.

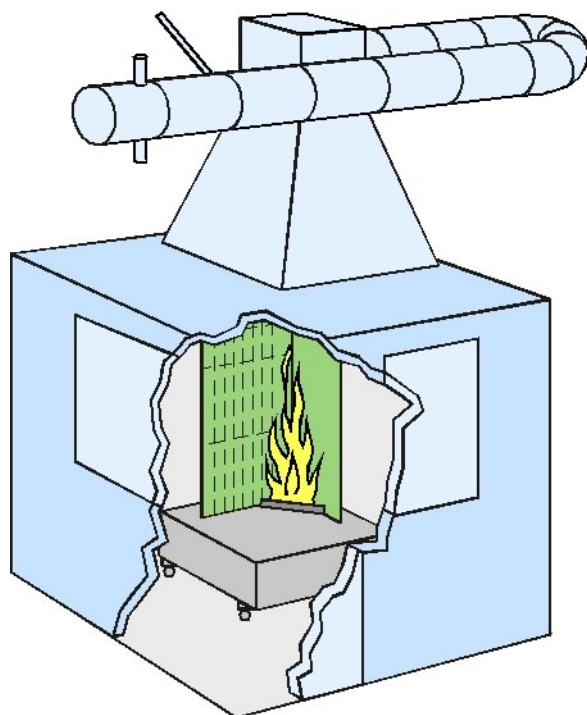


Figure 57 The SBI apparatus.

The cells or batteries were placed on a small table with the table top consisting of wires. A propane burner was placed underneath the batteries/cells.



Figure 58 Experimental set-up test 1-5.



Figure 59 Experimental set-up test 6.



Figure 60 Experimental set-up test 7.

6.3 Experimental procedure

In all tests a premeasuring time of 5 minutes was used for the HRR before the gas supply to the burner was turned on. All tests were video-recorded, video recordings started 1 minute before the burner. FTIR measurements started 2 minutes before the burner. The tests were conducted over two days with tests 1-5 the first day and tests 6-7 the second day. Both days started with a blank test where only the burner was used and HRR and FTIR gases were measured. The HRR from the burner was 14-15 kW. The burner HRR was subtracted from the results.

6.4 Results

In tests 1-3 outbursts of rapid vented gases could be seen. In principle there was one outburst per cell in tests 1-3 with had 100% SOC. In tests 4-5 with lower SOC, no outbursts could be observed. Outbursts could be seen in tests 6-7. The laptop battery pack in test 7 showed rapid venting in several directions and probably had the most energized venting of the seven tests.

In the seven tests, the orientation of the cells were different due to the different battery types (pouch, cylindrical, complete pack). This could potentially have affected the results, since some gases might have been missed by the hood collecting the gases. Also the extent to which gases are mixed in a limited space could have an impact on the results. It was not possible to determine the magnitude of these aspects in these tests. The cells in tests 1-5 were however all oriented which provide for a good comparison between these tests. The other two tests can be considered more as examples of possible scenarios.

All tests were photographed. Photos can be found in appendix C.

6.4.1 Video

All tests were captured on video. Below is the comment to the post-analysis of those videos. Note that the “video time” is 1 minute after the reference time. In other words, the

reference time 01:00 corresponds to 00:00 in video time. Video time is used in the tables below.

Table 8 Comment to test 1 from video analyses.

Video time (min:sec)	Comment
00:00	Video start
01:20	LPG fire beginnings
02:05	Cell material/vented material is clearly started to burn on the long sides
02:42-57	Outburst 1, 2 angles: ~ 45,100 deg Lighter flame colors (real or due to camera)
05:41-49	Outburst 2
05:53-04	Outburst 3, large flame on the right side from 110-190 deg
06:04-06:49	Venting flame at left side, burning for a relative long time
06:49-59	Outburst 4
07:34-40	Outburst 5
18:25	LPG flames end

Table 9 Comment to test 2 from video analyses.

Video time (min:sec)	Comment
00:00	Video start
01:05	LPG fire beginnings
02:13-19	Outburst 1
02:20-03:11	Burning
05:26-35	Outburst 2, 3 angles: ~ 0 (little), 80 (more), 120(more) deg
05:56-01	Outburst 3
06:01	Maybe an smaller outburst
06:29-41	Outburst 4 (3 angles as above in No.2)
07:06-17	Outburst 5
18:07	LPG flames end

Table 10 Comment to test 3 from video analyses.

Video time (min:sec)	Comment
00:00	Video start
01:10	LPG fire beginnings
02:04-12:06	Outburst 1 (left side 45deg, right side 120 deg (most @ right))
02:31-40	Some smoke from back of cell pack
03:05-09	Outburst 2 (both left and right side)
	More smoke from back of cell pack
05:50-02	Outburst 3 (most on left side, left ~30 deg, right ~ 145 deg) Lighter white-orange color than LPG flame colors
06:24-44	Outburst 4 (most left side, ~40 deg) Incl darker smoke
06:44 – 07:00	Clear cell fire along the long-sides, incl darker smoke
> 07:00	Person with handhold water mist makes entrance
07:13-07:23	Smaller outburst 5 (most left side)
07:41-07:53	Smaller outburst 6 (both sides)
07:40	Water mist on Pulsed by hand (~1 sec per puls) In flames above cell (cell is primarily not touched)
09:02-09:12	No water mist applied during this time, might have been longer time period
~ 09:45	Water mist off
11:15-56	Water mist on, into flames above cell
12:02-30	Water mist on, onto cell
12:43-44	Water mist on, onto cell, one pulse
13:45 – 14:03	Water mist on, into flames above cell
18:10	LPG flames end

Table 11 Comment to test 4 from video analyses.

Video time (min:sec)	Comment
00:00	Video start
01:15	LPG fire beginnings
	No outbursts could be seen
33:22	LPG flames end

Table 12 Comment to test 5 from video analyses.

Video time (min:sec)	Comment
00:00	Video start
01:12	LPG fire beginnings
	No outbursts could be seen
28:04	LPG flames end

Table 13 Comment to test 6 from video analyses.

Video time (min:sec)	Comment
00:00	Video start
01:20	LPG fire beginnings
05:56	Outburst 1 fast (max 0,5 sec), straight upwards
05:57-09	Probably cell venting which is burning
06:13-14	Outburst 2 little longer (0,5-1 sec), straight upwards
06:19-20	Outburst (0,5 sec), straight upwards
06:20-06:40	Probably burning from cell vent
06:46-47	Outburst 3 (1 sec), straight upwards
06:47-55	Burning from cell vent
06:58	Probably burning from cell vent
07:14	Outburst 4, straight upwards
07:14-07:24	Burning from cells
07:24	Outburst 5 very rapidly (~ 100 ms), straight upwards
07:26->	Outburst 6, straight upwards Burning and outburst, ventilation, a lot of activity, hard to
07:26:07:41	Burning over complete battery pack
07:41	Outburst 7 very rapidly, straight upwards
07:41-08:01	Burning from cells
08:01	Outburst 8 very rapidly, straight upwards
08:13	Outburst 9, not straight upwards but upwards to the right
08:15/16	Maybe outburst
08:18	Clear outburst 10 (1 sec), not straight upwards but upwards to the left
08:28	Outburst 11 , straight upwards
08:41-50	Clear outburst 12 (9 sec), not straight upwards but upwards to the left
08:45-53	Maybe outburst 13, long, straight upwards-little right
~07:00 - 10:00	Fire from battery cells (pack) almost finished at 10:00
10:00-12:45	Some flames from time to time, some black smoke
12:45-18:32	Less intense than above, and from time to time: some flames from time to time, some black smoke
18:32	LPG flames end

Table 14 Comment to test 7 from video analyses.

Video time (min:sec)	Comment
00:00	Video start
01:20	LPG fire beginnings
02:25	Small fire in left pack, likely in plastics – yellow flames (same as LGP flames)
03:24	One short flame
03:33	One short flame
03:34-39	Outburst 1 (4-5 sec)
03:43	One short flame
03:46-48	Outburst 2 (2-3 sec)
03:54	One short flame
03:58-01	Outburst 3 (2-3 sec)
04:04-08	Outburst 4 (3-4 sec)
04:12-14	Outburst 5 (2-3 sec)
04:15-19	Outburst 6 (4 sec), maybe several
04:22-23	Outburst 7 (2 sec), can have been multiple, last 20 sec
04:35-38	Outburst 8 (2-3 sec)
04:56-57	Outburst 9 (1 sec)
05:02-03	Outburst 10 (1 sec)
> 06:00	Light smoke
06:50-07:00	10 sec white smoke
> 07:00	Light smoke
18:14	LPG flames end

6.4.2 HRR and gas measurements

The results from the HRR measurements are summarized in Table 15. The HRR curves are presented in Figure 58 for test 1, 2 and 3, Figure 61 for test 4 and 5 and Figure 62 for test 6 and 7 respectively. Figure 59 indicates when outbursts of gases could be observed from the video while Figure 60 shows the HRR results from test 3 together with indications of when water mist was sprayed into the flames. Even if the maximum HRR was about the same for test 1, 2, 3 and 7, the test performance was quite different with large flames and material sprouting out from the laptop cells.

Table 15 Summary of results from the fire tests.

Test no	Weight loss (g)	Max heat release (kW)	Total heat release (kJ)
1	346	48	6826
2	342	44	6645
3	341	42	7130
4	353	9.5	7356
5	354	14	7460
6	145	26	2409
7	258	50	3036

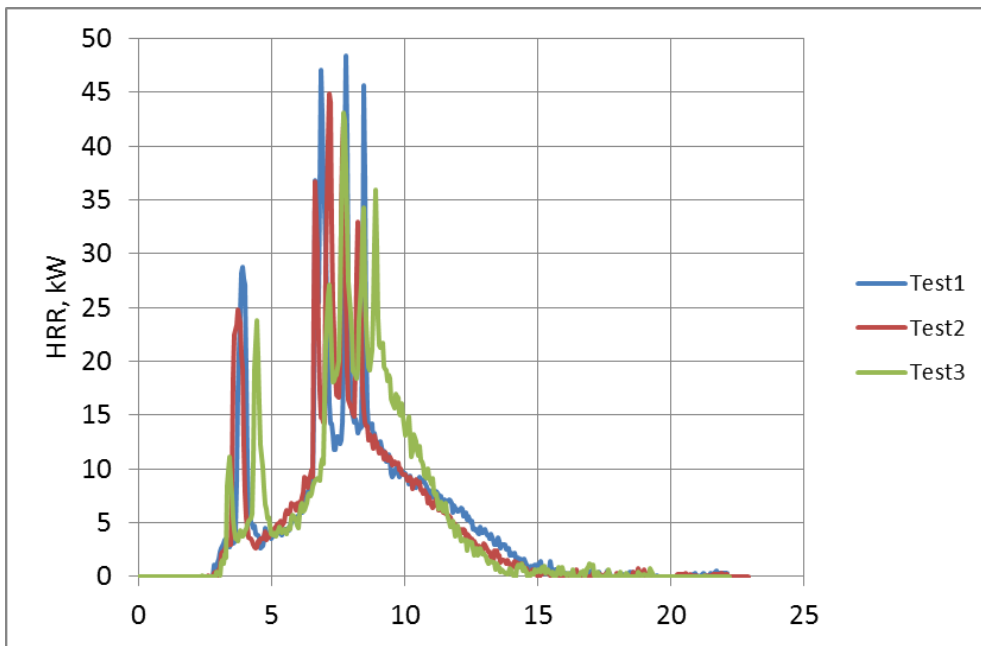


Figure 61 HRR measurements from test 1-3.

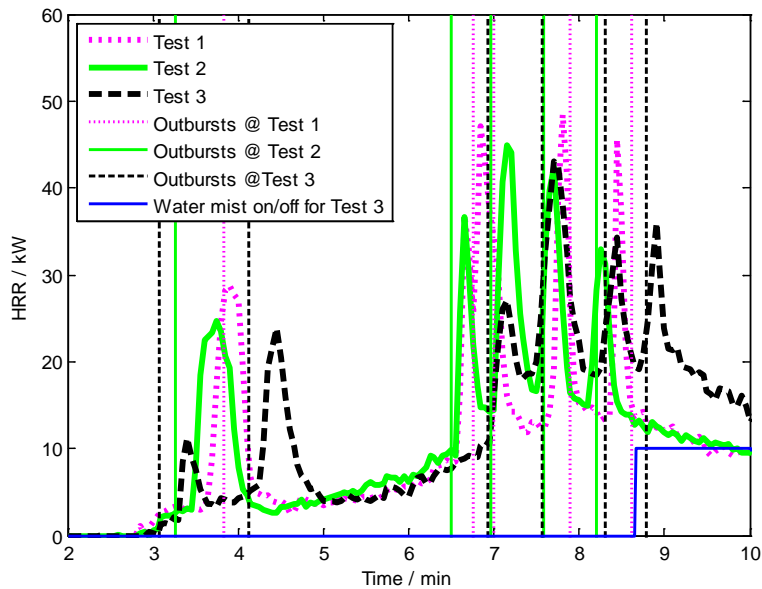


Figure 62 HRR measurements with outbursts as noted in the videos marked together with water mist injection for test 3.

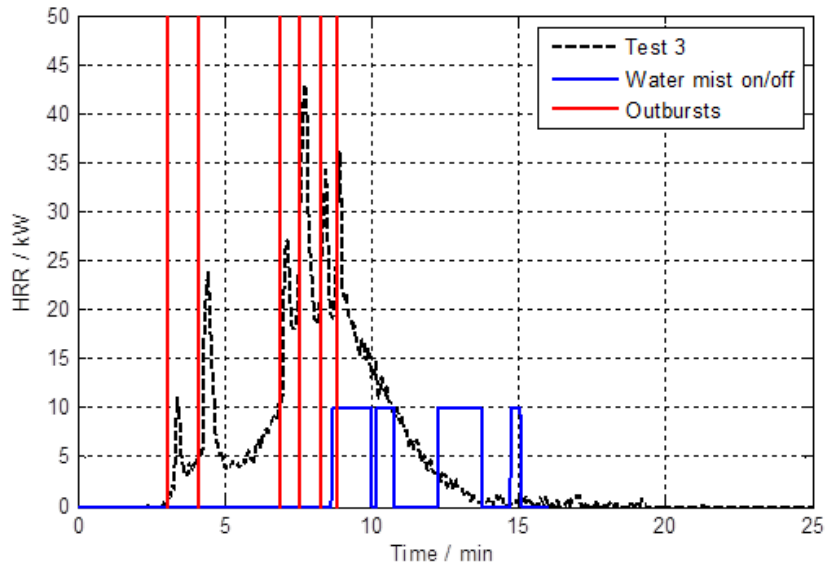


Figure 63 Water mist injection for test 3.

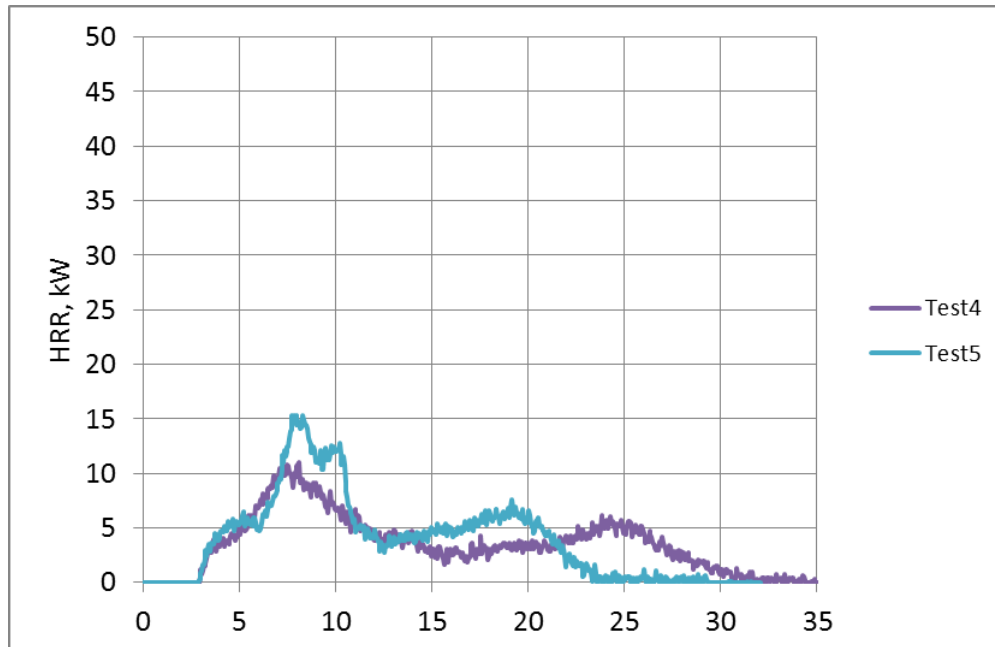


Figure 64 HRR measurements from test 4-5.

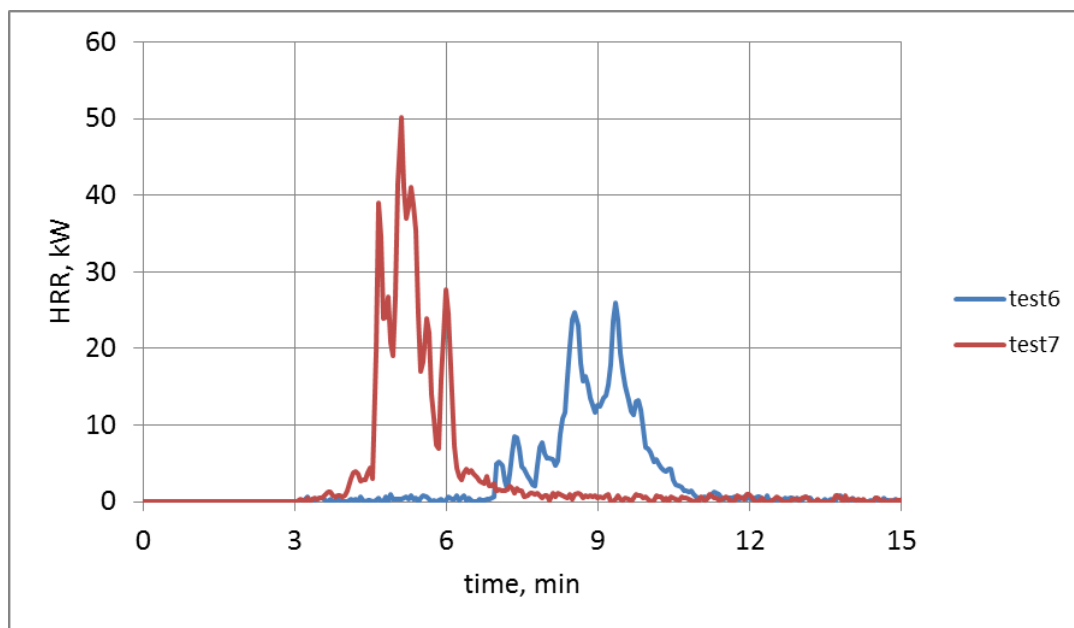


Figure 65 HRR measurements from test 6 and 7.

The FTIR measurements show production of HF in all tests, but POF_3 could not be detected. The measured concentrations of HF were generally quite low but well above the detection limits. Maximum concentrations in tests 1-2 were about 15 ppm and the duct flow was decreased before remaining tests to increase the HF concentration in the duct. The maximum concentration in the remaining tests were in the range 30 - 50 ppm.

The high dilution in the exhaust duct means that POF_3 might have been produced but not detected by the FTIR. Assuming that the ratio between HF and POF_3 concentration was 20 as seen in the spray-tests with the cone calorimeter, that would correspond with maximum POF_3 -concentrations below 1 ppm in tests 1-2 and 2.5 ppm in tests 3-5 which is below the quantification limit (6 ppm) for the FTIR.

The amount of HF produced during tests 1-5 is presented in Table 16. It is clear that the low concentration of HF resulted in a very large relative loss of HF in the sampling filters. In addition is the HF production presented together with the HRR in Figure 65- Figure 69 for test 1-5. The delay of HF compared to HRR seen in the production curves below is most probably influenced by retention in the filter. More results can be found in Appendix B.

From Table 15 it is evident that the total amount of HF produced is lower for the fully charged cells than those cells with a lower SOC. This could be due to the rapid outbursts of gases during these tests so that parts of the gases might not have been collected, but as the Total Heat Release (THR) from the tests are in the same order of magnitude then it seems that most of the gases were captured. Alternatively, the prolonged fire duration allowed more HF to be produced as it might give a chance for a more complete burning, or else it has something to do with how the Fluorine is available in the battery at different SOCs. It has not been possible to explore this further at this stage.

Table 15 also show that despite the larger peak in production rate of HF in test 3 where water was introduced into the flame, the total amount of HF was still the same.

Table 16 Results of HF analysis with FTIR from test 1-5.

Test no	Max production rate (g/s)	Total amounts from FTIR (g)	Total amounts from filter (g)	Total amounts (g)	Total yields (mg/g)
1	0.0088	3.2	1.7	4.9	14
2	0.0077	3.9	2.4	6.3	18
3	0.0154	4.2	1.5	5.7	17
4	0.0102	9.7	1.6	11.3	32
5	0.0164	12.0	1.9	13.9	39

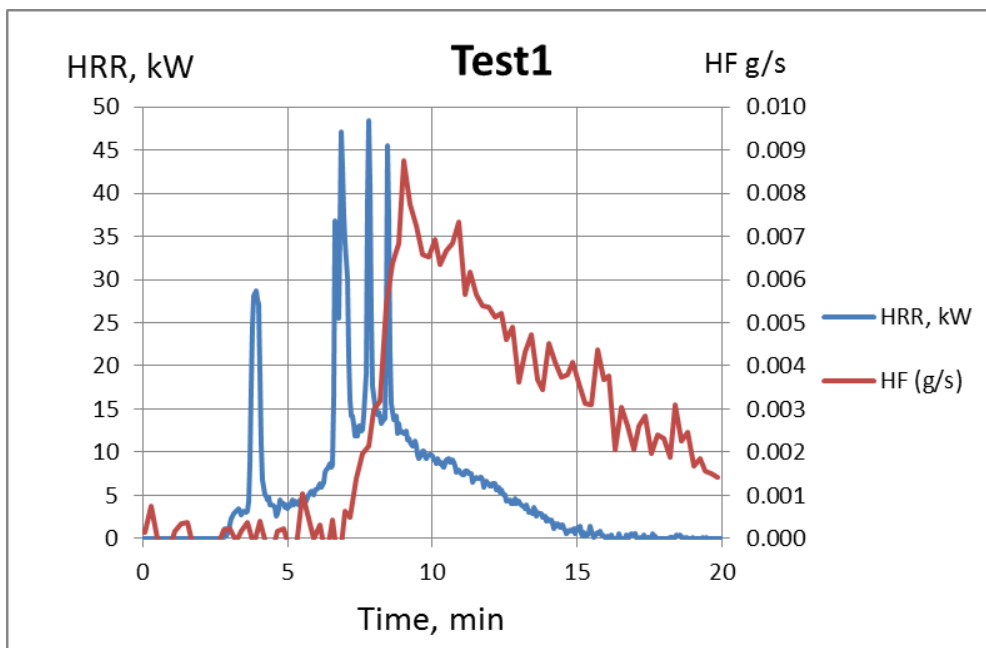


Figure 66 HRR and HF production as a function of time for test 1. The HF production only includes the readout from the FTIR so HF that is captured in the filter is not included.

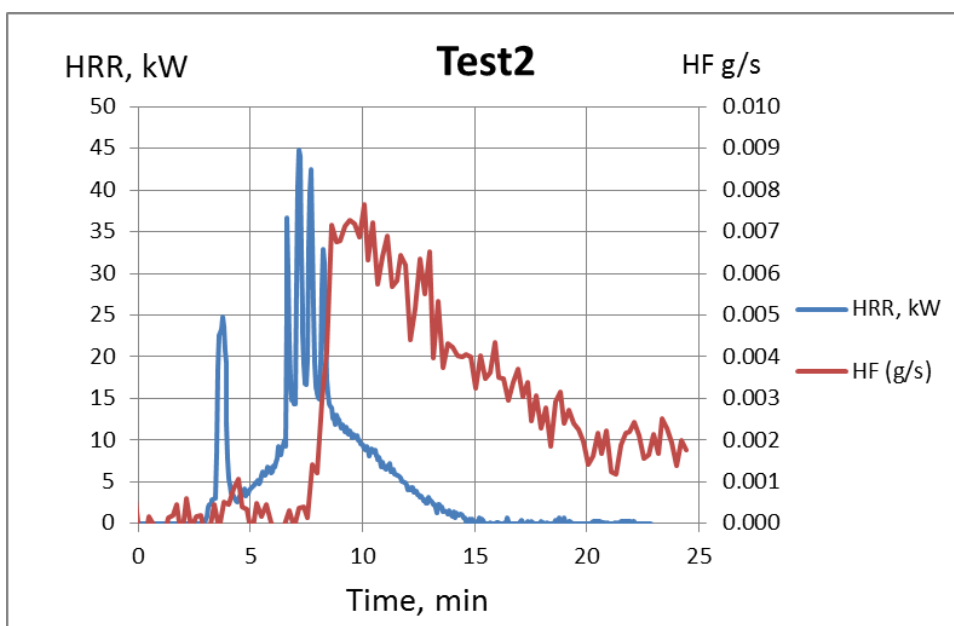


Figure 67 HRR and HF production as a function of time for test 2. The HF production only includes the readout from the FTIR so HF that is captured in the filter is not included.

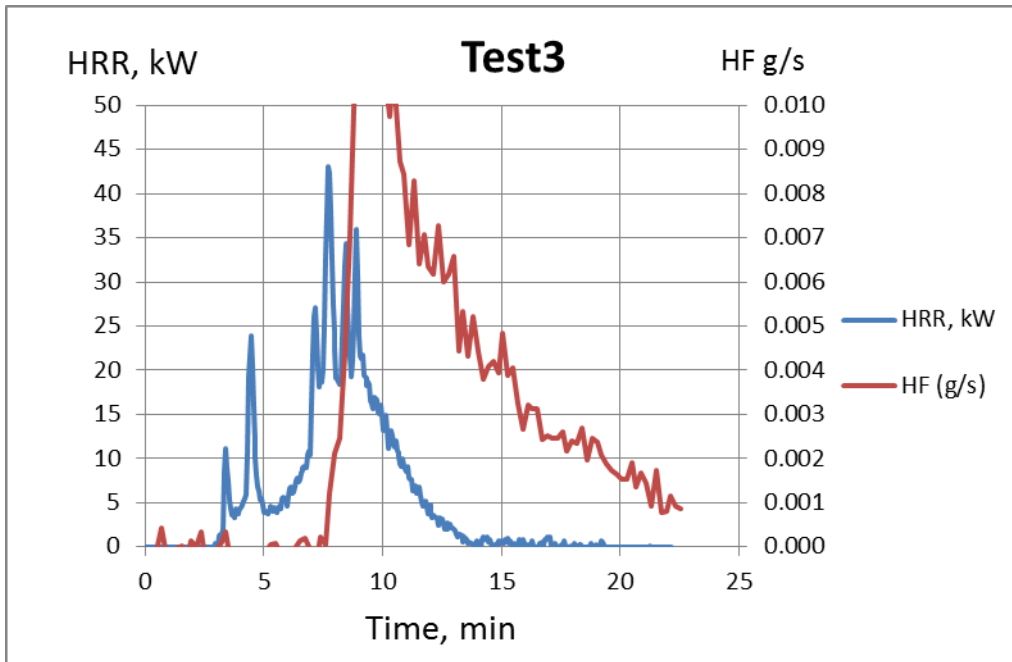


Figure 68 HRR and HF production as a function of time for test 3. The HF production only includes the readout from the FTIR so HF that is captured in the filter is not included.

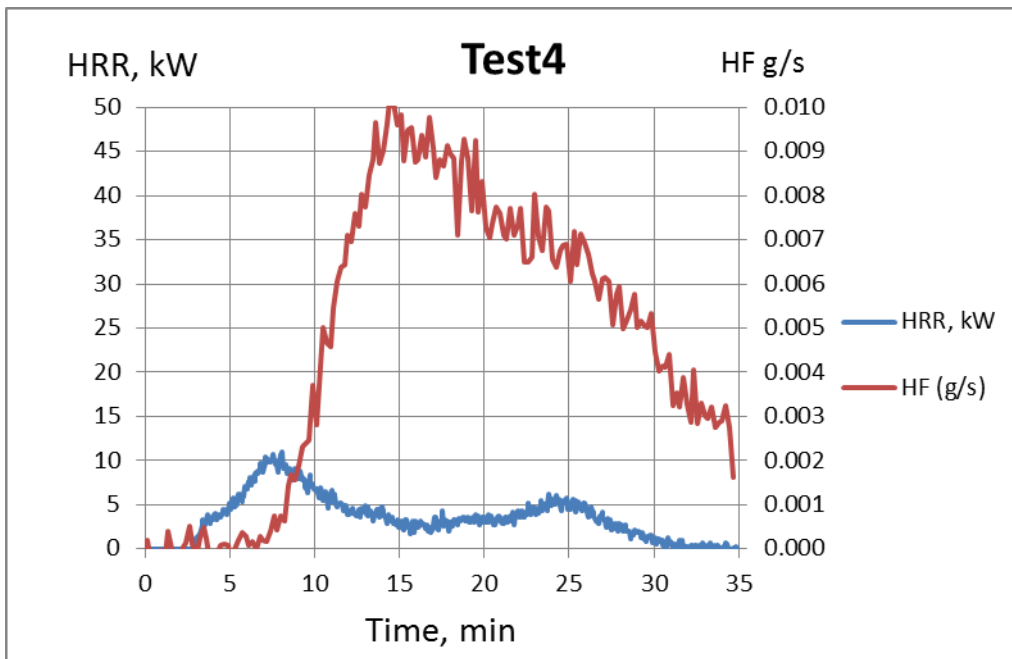


Figure 69 HRR and HF production as a function of time for test 4. The HF production only includes the readout from the FTIR so HF that is captured in the filter is not included.

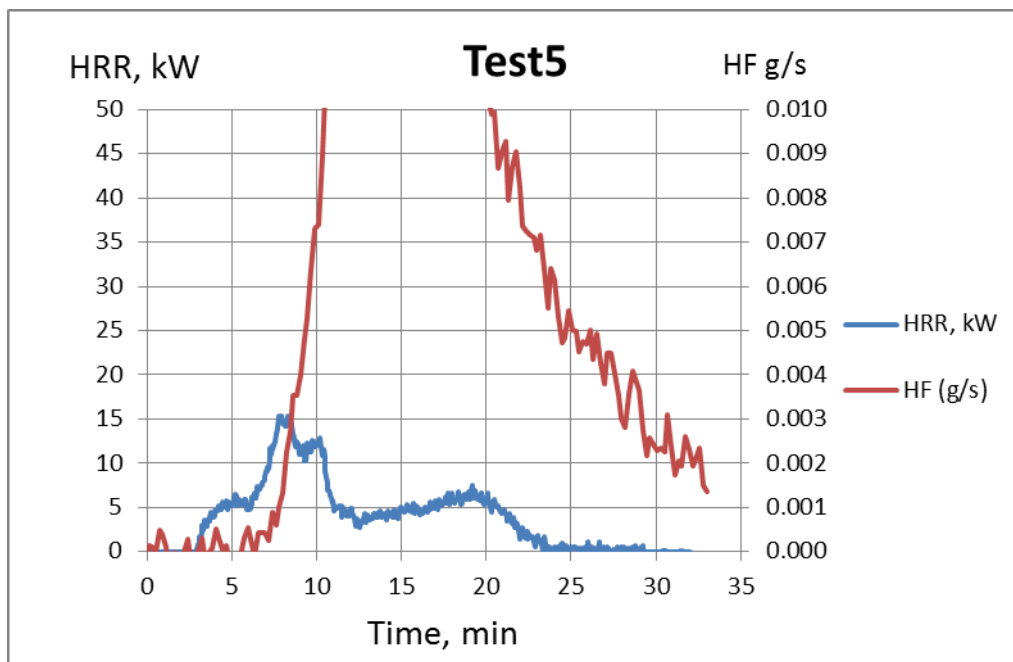


Figure 70 HRR and HF production as a function of time for test 5. The HF production only includes the readout from the FTIR so HF that is captured in the filter is not included.

The results from test 6 and 7 are available in Table 17 and Figure 70. As seen the yields of HF is much lower for the laptop cells, in fact the HF detected online was below the determined detection limit. Partly this is because the burnable mass in the laptop cells is also the plastic around the battery. But this does not explain all the difference. One plausible explanation is that the laptop cells exploded with liquid splashed on the walls in the equipment and some slat might have been missed there.

Table 17 Results of HF analysis with FTIR from test 6-7.

Test no	Max production rate (g/s)	Total amounts from FTIR (g)	Total amounts from filter (g)	Total amounts (g)	Total yields (mg/g)
6	0.0029	1.2	1.0	2.2	15
7	0.0011	Not detected	1.9	1.9	7.3

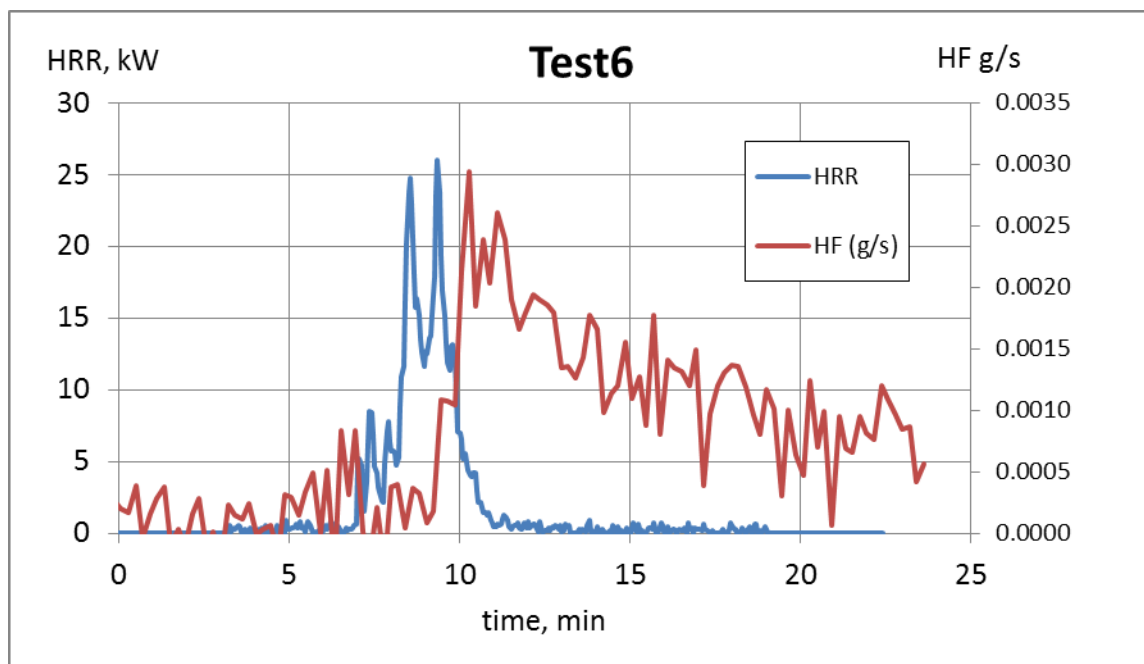


Figure 71 HRR and HF production as a function of time.

6.5 Discussion

Looking at the results from these reduced scale tests alone the emission data can be difficult to interpret. An important aspect in this context is a comparison with emission data from a traditional car fire. Emission data from a complete vehicle fire is scarce. Lönnermark and Blomqvist⁶ have made measurements both on a full scale fire and parts of a vehicle like door panels, dashboard etc. The vehicle tested in the full scale fire was a medium class model from 1998. No HF could be detected in these tests either in the small-scale tests or in the full scale test but significant amounts of HCN (NGV 1.8 ppm, TGV 3.6 ppm), HCl (TGV 5 ppm) and SO₂ (NGV 2 ppm, TGV 5ppm).

Recently Lecocq, Bertana, Truchot and Mairlair reported emission data from both a full-scale fire of a fully charged Electric Vehicle (EV) and a full-scale fire of a similar Diesel vehicle fully gassed⁷. This showed an initial peak of HF produced for both vehicles. This peak was higher than the amount of HF produced later in the fire stage when the battery started to burn in the EV but the amount of HF produced by EVs were at least twice the amount from the Diesel vehicles. The amounts reported are presented in Table 18. The initial HF peak might have been caused by the AC liquid.

The battery cells tested in this study were power optimized cells that one could find in a plug-in hybrid electric vehicle (PHEV). A typical PHEV could have 432 cells (9.7 kWh, 345.6 VDC nom, 108s4p, cell: 7Ah, 3.2 V nominal). This means that the emissions reported in the battery cell tests should be multiplied with a factor of $432/5 = 86.4$ to reflect a case where the complete battery is consumed in a fire. This results in a value of 400-1200 g HF depending on SOC with a low value for a high SOC. This is in the same order of magnitude as the valued reported by Leqocq et. al. (657 and 919 respectively) as presented in Table 18.

Similar, if the result from the burner tests are extrapolated to the amount of HF one would get if the entire amount of electrolyte in a vehicle is consumed in a fire, one ends up in a

large variation of values, 1200 – 2800 g of HF. These values are on the high end and higher than the value measured in the cell tests and larger than the values reported by Leqocq et. al. However, considering the large extrapolation done here going from a small number of completely different fire scenario the differences are not that big. In the burner test the electrolyte was introduced in a pure state and it had to go into the flame. In the vehicle test one cannot be 100% sure that all electrolyte is consumed, in addition, we do not know what kind of vehicle it was in the full vehicle test, this might differ from the assumptions on power etc. that was made in the extrapolation.

Table 18 Comparison with complete vehicle fire emissions.

Study/vehicle	HF (g)	HCN (g)	HCl (g)	SO2 (g)
Lönnermark/Blomqvist	No HF detected	170	1400	540
Leqocq et al. Diesel1	621	167	1990	
Leqocq et al. EV1	1540	113	2060	
Leqocq et al. Diesel2	813	178	2140	
Leqocq et al. EV2	1470	148	1930	
This study, cell tests	400-1200 depending on SOC, high SOC gives low amount of HF			
This study, burner tests	1200-2800			
This study, cakecup test	950			

The experimental results in this study could not show any significant change in the constitution of gases emitted if water is used as an extinguishing media. The battery cell experiment showed a higher concentration of HF produced during the actual spraying with water but the total amount HF was still the same. No change could be observed in the burner tests due to introduction of water.

7 Conclusions

The work presented here shows that it is possible to use FTIR to measure HF and POF_3 online in fire tests including Li-ion batteries at different scales.

POF_3 was detected in all the small scale tests using pure electrolyte. However, no POF_3 was detected in the tests on cells. The detection limit for POF_3 was 6 ppm. Extrapolating from the small scale tests to the cells tests one ends up at concentrations below 6 ppm, which probably explains why no POF_3 was detected in these tests.

It is an important finding that POF_3 is emitted from a battery fire as this will increase the toxicity of the fire effluents. The amount of POF_3 is shown to be significant, 5-40 % of the HF emissions on a weight basis.

No PF_5 could be detected in any of the tests. The reason for this is probably the high reactivity of this specie. This was also demonstrated by the difficulty to produce a calibration gas mixture for PF_5 .

There was no apparent experimental evidence that using water had a significant impact on the amount of HF produced if water is used as an extinguishing media. The use of water to extinguish a battery fire has the potential to shift the chemistry to favour the production of HF over POF_3 . The toxicity of POF_3 is not known but substances similar to POF_3 are highly toxic, more toxic than HF. Therefore shifting the chemistry to favour the production of HF over POF_3 may be toxicologically favourable. More information is needed to resolve this issue especially as POF_3 can be emitted under other cell venting situations and not only fires.

Extrapolating the results from these experiments one ends up in the same order of magnitude in amount of HF as reported in the few available complete EV vehicle burns. This is an indication that the small scale experiments conducted in this project provide useful information to analysing the risks associated with emissions from Li-ion batteries in fires and the impact of water application during the fire.

8 References

- ¹ Hygiensiska gränsvärden AFS 2011:1, 8 Hygieniska gränsvärden, AFS 2011:18 Hygieniska gränsvärden Arbetsmiljöverkets föreskrifter och allmänna råd om hygieniska gränsvärden, ISBN 78-9 91-7 7930-5 559-8 ISSN 650-3163 ARBETSMILJÖVERKET 112 79 Stockholm
- ² Yang, H., Zhuang, G. V. and Ross, P. N. Jr, "Thermal Stability of LiPF₆ salt and Li-ion battery electrolytes containing LiPF₆, Journal of Power sources 161 (2006) 573-579
- ³ Xiang-Guo Teng, Fa-Qiang Li, Pei-Hua Ma, Qi-Du Ren and Shi-You Li "Study on thermal decomposition of lithium hexafluorophosphate by TG-FT-IR coupling method". Thermochimica Acta, 2005, 436, 30-34
- ⁴ Kirk-Othmer Encyclopedia of Chemical Technology, John Wiley & Sons, 1994, Vol. 11.
- ⁵ ISO 19702:2006, Toxicity testing of fire effluents -- Guidance for analysis of gases and vapours in fire effluents using FTIR gas analysis
- ⁶ Lönnermark AN, Blomqvist, P., Emissions from an automobile fire, Chemosphere 62, 1043-1056, 2006.
- ⁷ Lecocq, A., Bertana, M., Truchot, B., Marlair, G., "Comaprison of the Fire Consequences of an Electric Vehicle and an Internal Combusion Engine Vehicle", FIVE 2012, September 27-28 2012 Chicago USA

A1

Appendix A Tests conducted in burner

Tests conducted are listed in Table 1. Each of the tests are then presented in tables (test procedure) and figures.

Table 1 Tests conducted

Test nr	Type of test	Fuel	Comment
1	burner	Propane only	Initial test to determine propane HRR
2	Burner + needle	Propane and 5.9 ml/min DME	DME works not as spray but as a beam, possibility that all DME not burnt
3	Burner + Needle	Propane and 5.9 ml/min DME	Needle in bottom of burner instead of top
4	Burner + Needle	Propane and 5.9 ml/min DME	Needle inserted outside of burner
5	Burner + spoon	Propane and 2.4 ml/min DMC	Not a very successful attempt
6	Burner + Needle	Propane and 12 ml/min DMC	and later 5 ml/min
7	Burner + Needle	Propane and 20 ml/min DMC	Interrupted as holder melted
8	Burner + Needle	Propane and 20-18 ml/min DMC	Burner placed a bit lower under the collecting hood
9	Burner + Needle	Propane and DMC 18 ml/min	
10	Burner + Needle	Propane and DMC 18 ml/min with 1 M salt	
11	Burner + needle	Propane and DME 18 ml/min	
12	Burner + needle	Propane and DME 18 ml/min with 0.4 M salt	
13	Burner + Needle	Propane and DMC 18 ml/min 1 M salt	
14	Burner + Spoon	Propane and DMC 1.8 ml/min	
15	Burner + spoon	Propane and DMC 1.8 ml/min + 1M salt	
16	Burner + spoon	Propane and DME 1.8 ml/min + 0.4 M salt	
17	cakecup	DMC + salt 1:1	No external heating, did not burn very well
18	cakecup	DME + salt 1:1	No external heating, did not burn very well

A2

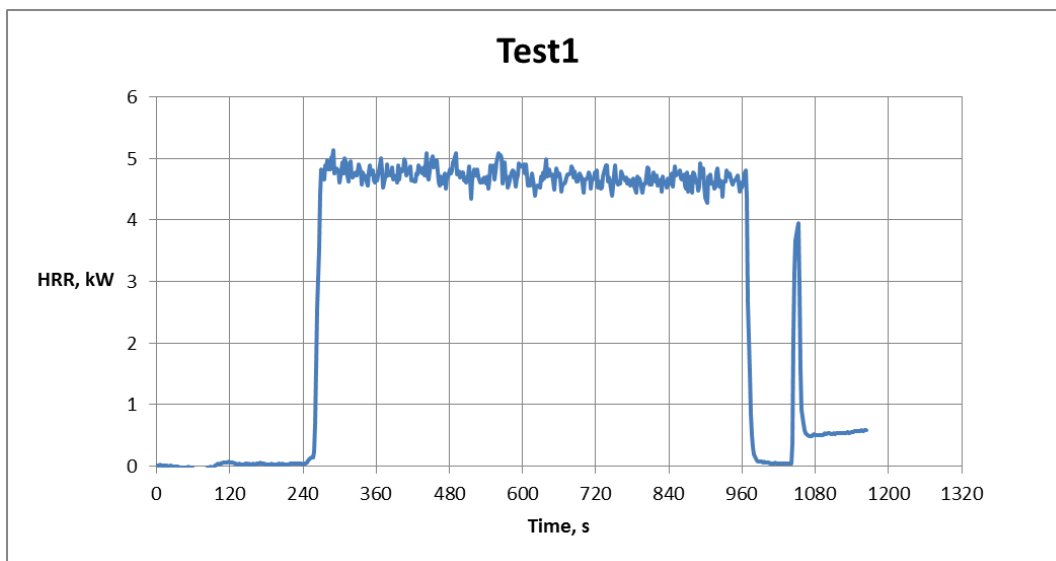


Figure 1 HRR from test 1, propane burner at 7 sp.

Table 2 Test procedure test 2

Time Min:sec	Comment
0	FTIR and HRR measurement started
1:00	Burner with 7 sp propane started
1:34	First numbers from FTIR available
6:00	Start DME injection 5.9 ml/min, DME works not as spray but as a beam, possibility that all DME not burnt

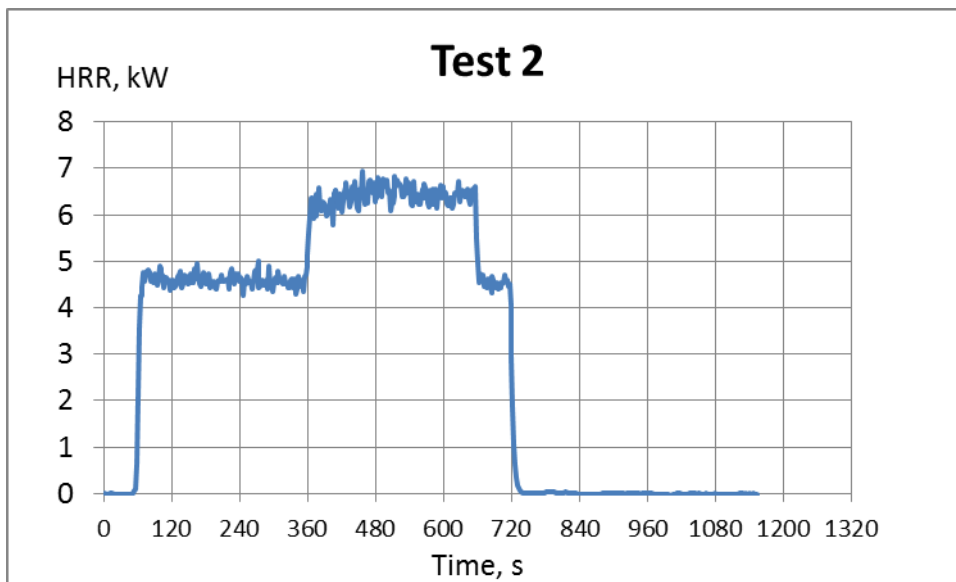


Figure 2 HRR from test 2

Table 3 Test procedure test 3

Time Min:sec	Comment
0	FTIR and HRR measurements started
1:00	Burner with 7 sp propane started
1:30	First numbers from FTIR available
6:00	Start DME injection 5.9 ml/min, Needle inserted in bottom of burner instead
8:00	test was interrupted as the spray hit the burner

A3

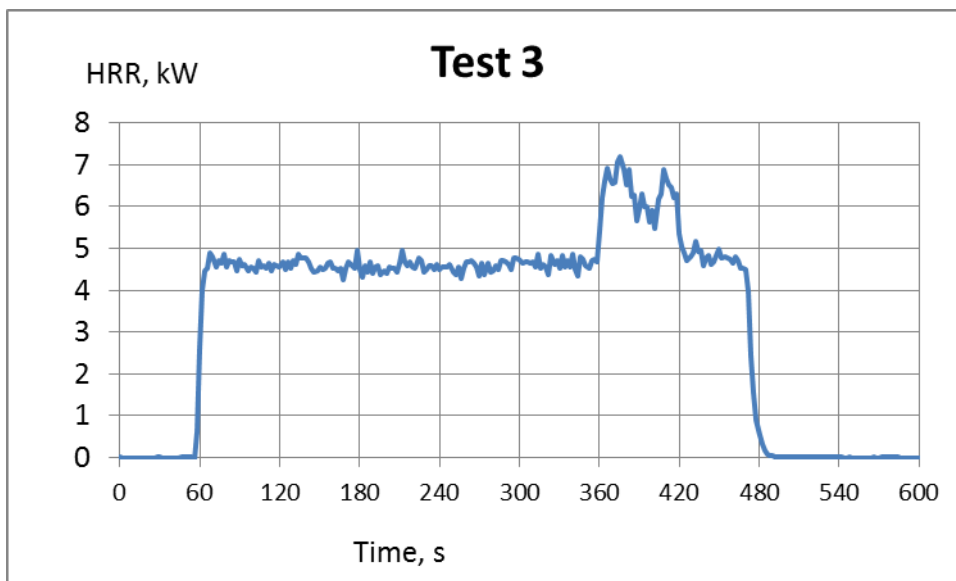


Figure 3 HRR from test 3

Table 4 Test procedure test 4

Time Min:sec	Comment
0	FTIR and HRR measurement started
1:00	Burner with 7 sp propane started
1:33	First numbers from FTIR available
4:00	Start DME injection 5.9 ml/min, Needle placed outside of burner

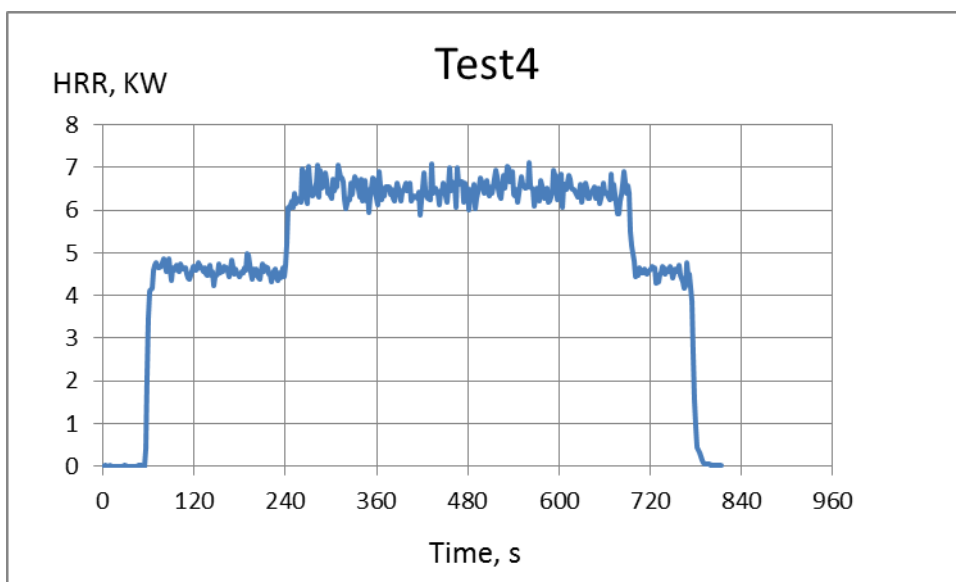


Figure 4 HRR from test 4

Table 5 Test procedure test 5

Time Min:sec	Comment
0	FTIR and HRR measurement started
1:03	First numbers from FTIR available
2:00	Burner start
10:30	Start DMC injection 2.4 ml/min onto spoon placed in flame
	Not a successful attempt

A4

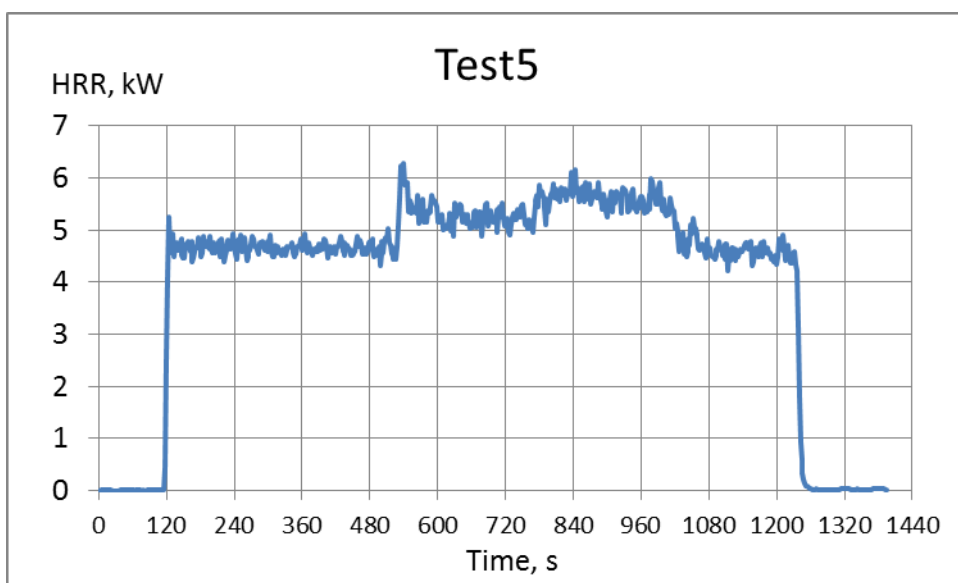


Figure 5 HRR from test 5

Table 6 Test procedure test 6

Time Min:sec	Comment
0	FTIR and HRR measurement started
1:00	Burner (propane) start
1:23	First numbers from FTIR available
6:00	Start injecting DMC 12 ml/min onto spoon
6:45	Injection interrupted
7:30	Injection started again flow 5 ml/min
8:00	Injection interrupted
8:57	Flame extinguished
10:09	Flame lit again
10:30	Injection 5 ml/min
12:00	Injection ended and flame turned off

A5

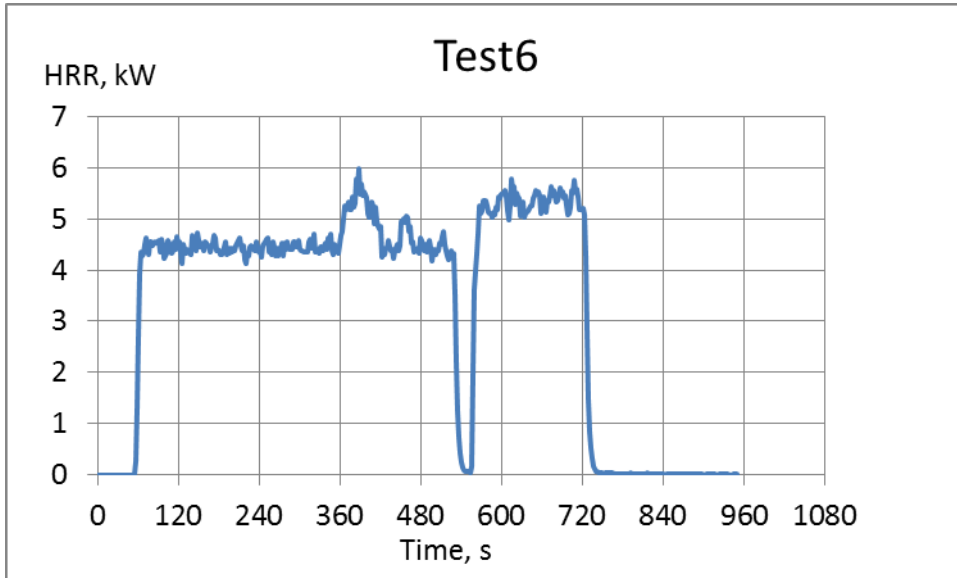


Figure 6 HRR from test 6

Table 7 Test procedure test 7

Time Min:sec	Comment
0	FTIR and HRR measurement started
0:41	First numbers from FTIR available
1:10	Burner start
6:00	Start injecting DMC 20 ml/min spray
7:45	Injection interrupted as holder melted
10:00	Burner off

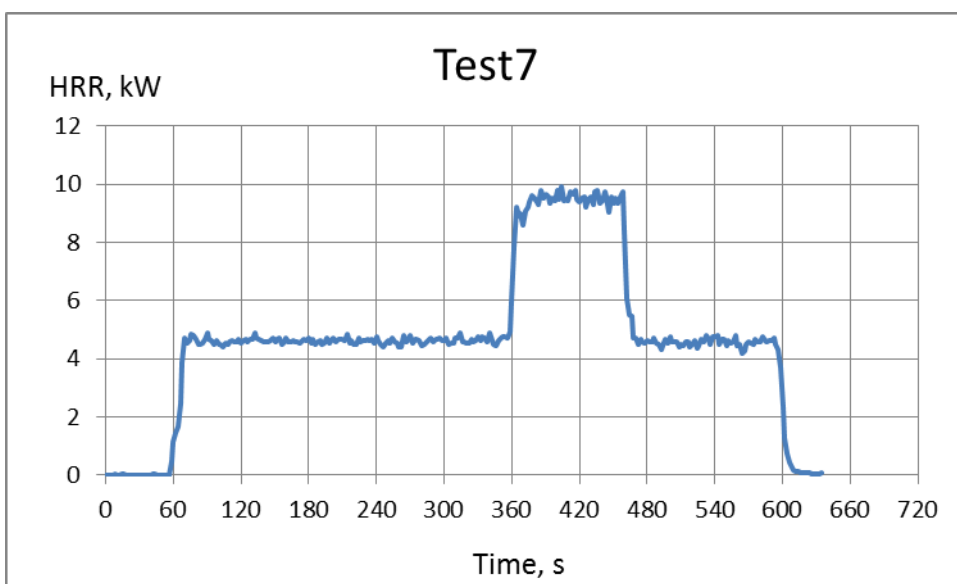


Figure 7 HRR from test 7

A6

Table 8 Test procedure test 8

Time Min:sec	Comment
0	FTIR and HRR measurement started
0:44	First numbers from FTIR available
1:00	Burner start, burner placed lower in relation to collecting hood
6:00	Start injecting DMC 20 ml/min spray
8:30	Start decreasing injection until 18 ml/min
9:30	Injection off

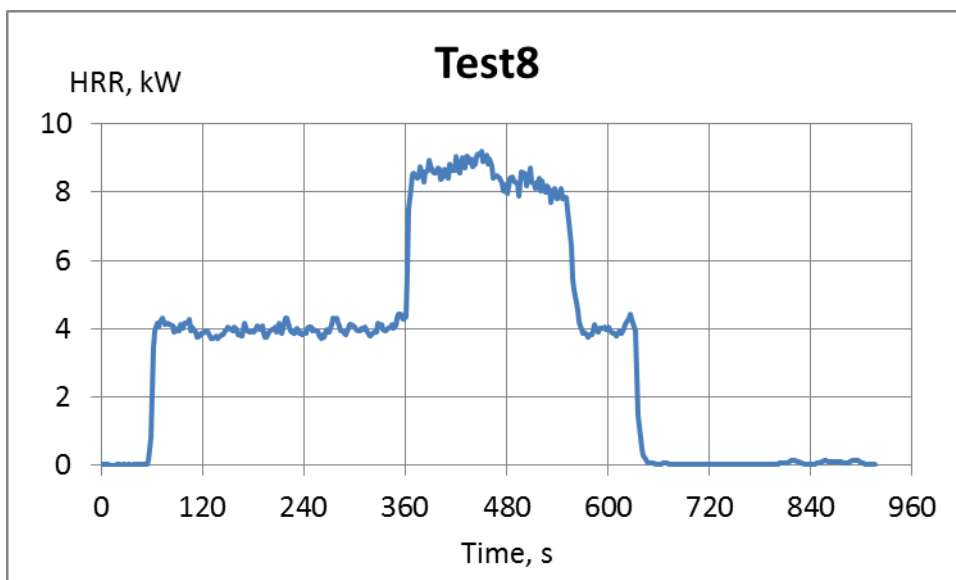


Figure 8 HRR from test 8

Table 9 Test procedure test 9

Time Min:sec	Comment
0	FTIR and HRR measurement started
0:33	First numbers from FTIR available
1:00	Burner start
4:00	Start injecting DMC 18 ml/min spray
7:00	DMC off
10:30	Burner off

A7

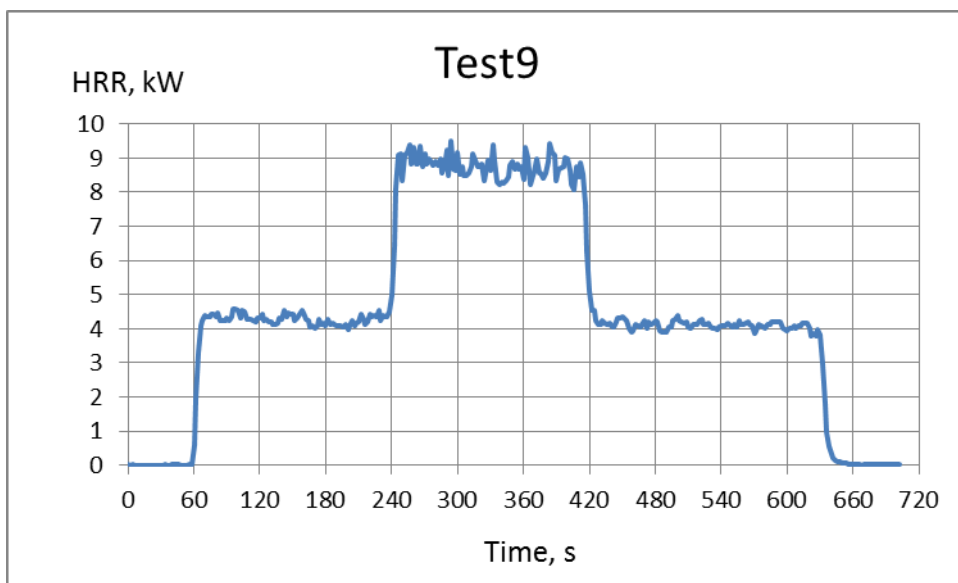


Figure 9 HRR from test 9

Table 10 Test procedure test 10

Time Min:sec	Comment
0	FTIR and HRR measurement started
0:54	First numbers from FTIR available
1:09	Burner start
4:00	Start injecting DMC + salt 18 ml/min spray
6:00	DMC off
12:20	Burner off

Table 11 Test Procedure test 11

Time Min:sec	Comment
0	FTIR and HRR measurement started
0:59	First numbers from FTIR available
1:00	Flame start
4:00	Start injecting DME 18 ml/min, flame turns purple, salt still available in system!
8:40	Stop spray
13:55	Start injecting DME again after cleaning of hoses
15:30	Stop injection
16:43	Burner off

A8

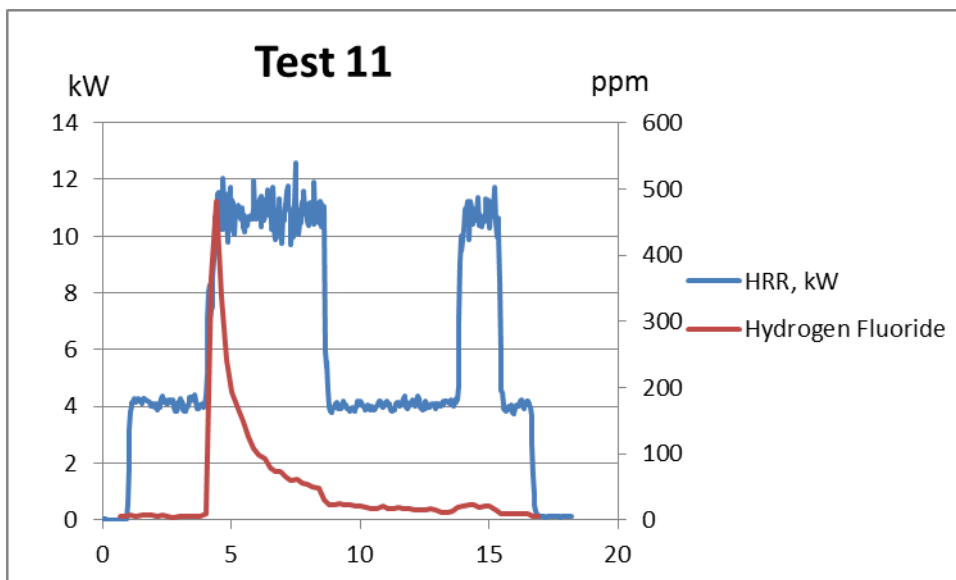


Figure 10 HRR and HF concentration test 11

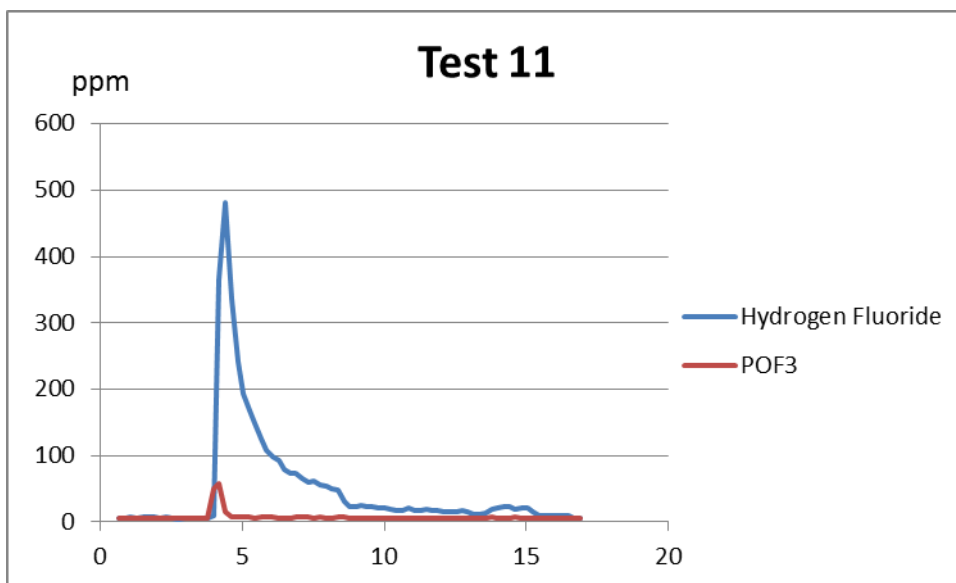


Figure 11 HF and POF₃ concentration test 11

Table 12 Test procedure test 12

Time Min:sec	Comment
0	FTIR and HRR measurement started
0:30	Flame start
0:43	First numbers from FTIR available
2:30	Start injecting DME 18 ml/min + 0.4 M salt
5:00	Stop spray
10:00	Burner off

A9

Table 13 Test procedure test 13

Time Min:sec	Comment
0	FTIR and HRR measurement started
0:30	Flame start
0:45	First numbers from FTIR available
2:30	Start injecting DMC + 1 M salt 18 ml/min
3:20	Flow increased to 20 ml/min
4:00	Stop spray due to no spray
5:40	Injection clean DMC
7:00	Gets spray
8:00	Start salt + DMC injection
11:00	Injection end
16:22	Burner off

Table 14 Test procedure test 14

Time Min:sec	Comment
0	FTIR including numbers on screen
3:00	HRR measurement started
3:30	Flame start
5:30	Start injecting DMC + 1 M salt 1.8 ml/min in spoon
7:15	Interrupted due to stop in needle

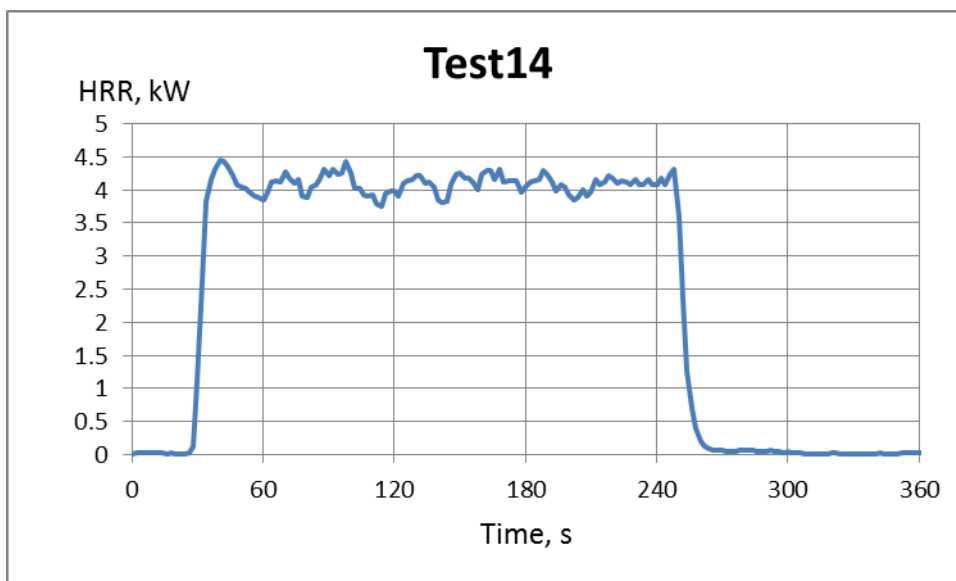


Figure 12 HRR test 14

Table 15 Test procedure test 15

Time Min:sec	Comment
0	FTIR and HRR measurement started
0:48	First numbers from FTIR available
1:05	Flame start
3:00	Start injecting DMC 1.8 ml/min onto spoon
5:00	Start injecting DMC + salt 1.8 ml/min onto spoon
10:00	Start injecting DMC 1.8 ml/min onto spoon
11:00	Injecting water instead, come through white plug in opening
15:15	Stop injection
17:15	Burner off

A10

Table 16 Test procedure test 16

Time Min:sec	Comment
0	FTIR and HRR measurement started
0:45	First numbers from FTIR available
1:07	Flame start
3:00	Start injecting DMC 1.8 ml/min onto spoon
5:05	Start injecting DMC + salt 1.8 ml/min onto spoon
11:15	Start injecting DMC 1.8 ml/min onto spoon
13:00	Injecting water instead
16:50	Stop injection
	Burner off

Table 17 Test procedure test 17

Time Min:sec	Comment
0	FTIR and HRR measurement started
0:47	First numbers from FTIR available
2:30	Light the 2g DMC + 2 g salt in open cup
3:40	Fire extinguishes itself
5:27	Light the 2g DMC + 2 g salt in open cup
6:40	Fire extinguishes itself
10:00	end

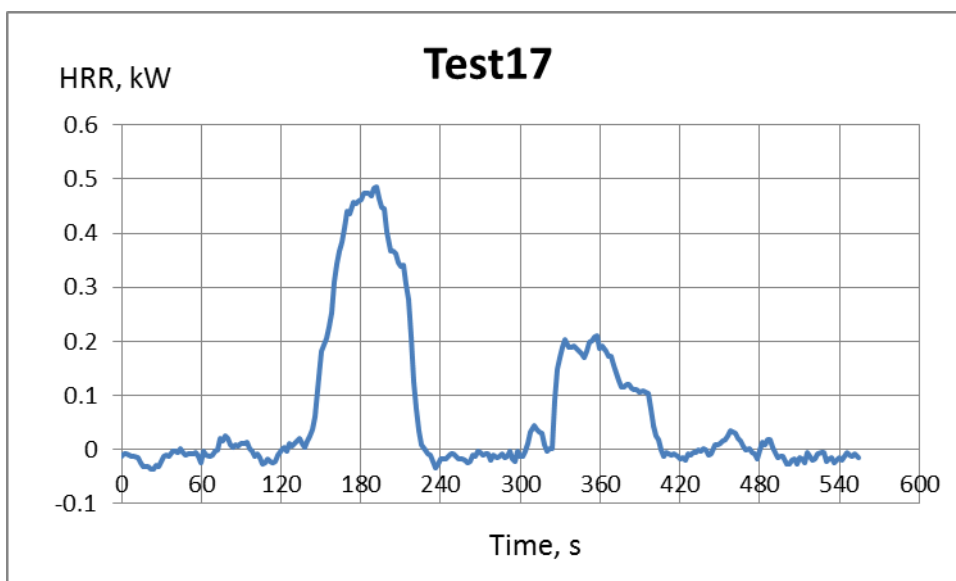


Figure 13 HRR test 17

Table 18 Test procedure test 18

Time Min:sec	Comment
0	FTIR and HRR measurement started
0:62	First numbers from FTIR available
6:50	Light the 2g DMC + 2 g salt in open cup
7:30	Fire extinguishes itself
10:48	Light the 2g DMC + 2 g salt in open cup
11:50	Fire extinguishes itself
10:00	end

A11

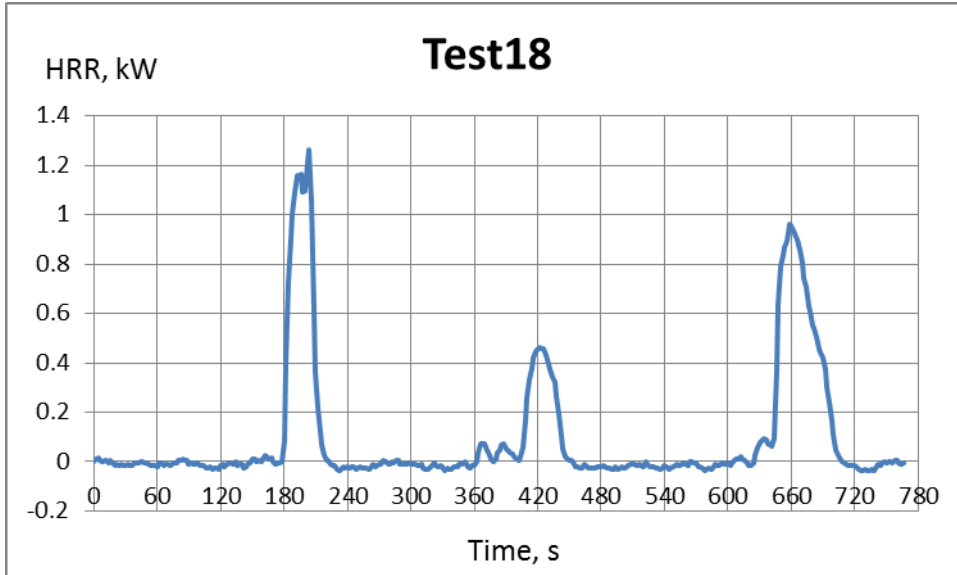


Figure 14 HRR from test 18

No test 19 was conducted

Table 19 Test procedure test 20

Time Min:sec	Comment
0	HRR measurement started
1:30	FTIR measurements start
1:59	FTIR values available
2:30	Start propane 7 skd
7:30	Stop propane

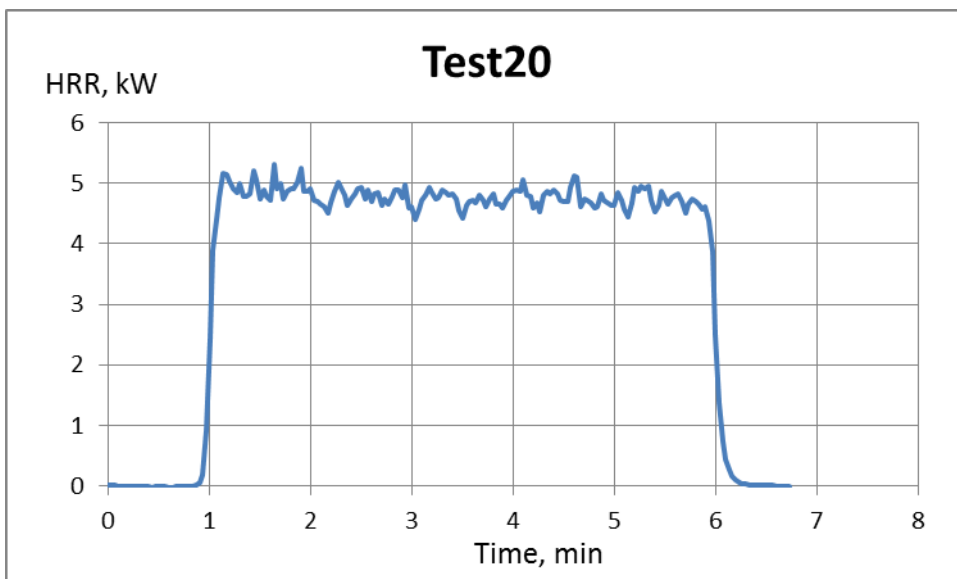


Figure 15 HRR from test 20 Propane only gave a mean HRR of 4.78 kW

A12

Table 20 Test procedure test 21

Time Min:sec	Comment
0	FTIR measurement started
0:28	FTIR values available
4:00	Start HRR measurements
5:00	Flame start
7:00-8:00	Spray water into flame
10:00-11:00	Spray water into flame
13:00	Stop flame

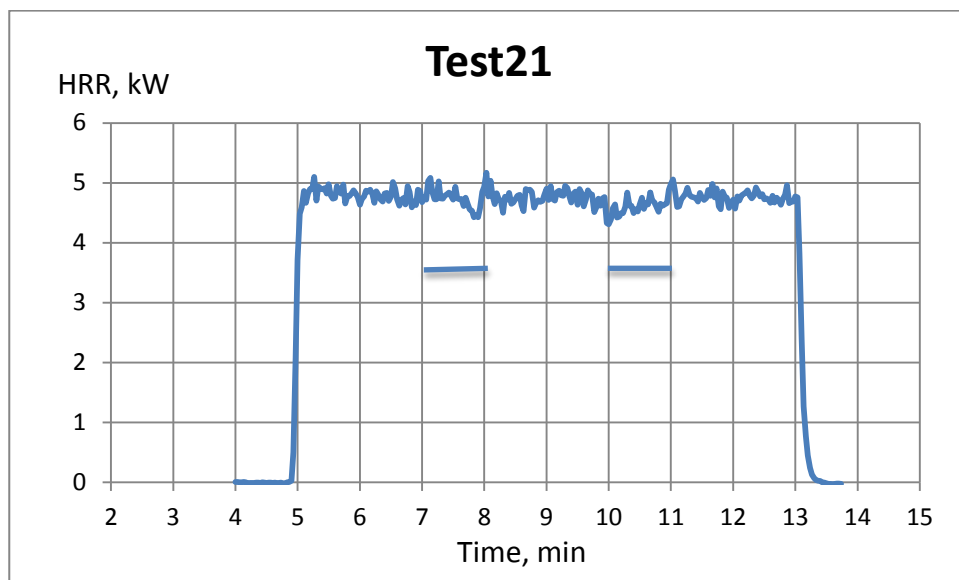


Figure 16 HRR from test 21. Propane + water injection by spraybottle. Sprayinjection of water marked in figure with horisontal lines

Table 21 Test procedure test 22

Time Min:sec	Comment
0	FTIR measurement started
0:25	First numbers from FTIR available
2:00	Start HRR measurements
3:00	Start propane flame
5:00	Start injecting DMC 15 ml/min
7:00	Start injecting DMC with salt 1 M
9:00	DMC only, spray not OK until 9:40
13:00	Injecting ethanol
19:00	Stop flame, inject water through needle

A13

Table 22 Test procedure test 23

Time Min:sec	Comment
0	FTIR measurement started
0:40	First numbers from FTIR available
2:00	Start HRR measurements
3:00	Start propane flame
5:00	Start injecting DMC 15 ml/min
7:00	Start injecting DMC with salt 0.4 M
10:00	Propane decreased to 5 skd
11:30	Pump stopped
12:00	Injecting ethanol
20:00	Injecting DMC and salt 0.4 M
23:00	Injecting DMC only
25:00	Injecting ethanol only
27:00	Injecting water only
30:00	Propane only
33:00	Stop flame

Table 23 Test procedure test 24

Time Min:sec	Comment
0	FTIR measurement started
0:27	First numbers from FTIR available
2:00	Start HRR measurements
3:00	Start propane flame
6:00	Start injecting DMC 15 ml/min with salt problematic
11:15	Decreased to 10 ml/min
14:25	DMC finished
15:00	Start again
15:05	Started injecting weater also, stop in system directly
17:00	Stop flame

Table 24 Test procedure test 25

Time Min:sec	Comment
0	FTIR measurement started
0:37	First numbers from FTIR available
2:00	Start HRR measurements
3:00	Start propane flame 7 skd
5:00	Start injecting DMC 15 ml/min
7:00	Start injecting DMC with salt 1 M
10:00	Spary became beam, turned injection off
12:00	Stop flame

A14

Table 25 Test procedure test 26

Time Min:sec	Comment
0	FTIR measurement started
0:38	First numbers from FTIR available
2:00	Start HRR measurements
3:00	Start propane flame 7 skd
4:00	Start injecting DMC 15 ml/min with salt 1 M
5:00	Water spray into flame
5:40	Spray became beam
7:00	Injecting water through needle for cleaning
11:00	Start injecting DMC 15 ml/min with salt 1 M
11:50	Water spray into flame
12:30	Spray became beam
15:00	Stop flame

Table 26 Test procedure test 27

Time Min:sec	Comment
0	FTIR measurement started
0:30	First numbers from FTIR available
2:00	Start HRR measurements
2:30	Cakecup with 1 M DMC placed into Cone calorimeter
2:47	Radiation starts, immediate ignition
5:45	Flames extinguish themselves
11:45	End heat exposure

Test28

0.4M salt in DME in cakecup, 15 kW/m² radiation applied as heating, spark placed above surface
 Ignition about 13 s after heat radiation started.
 The electrolyte burned up and then new was added at 7 minutes 35 s.

Unfortunately the FTIR program ceased to work during this test.

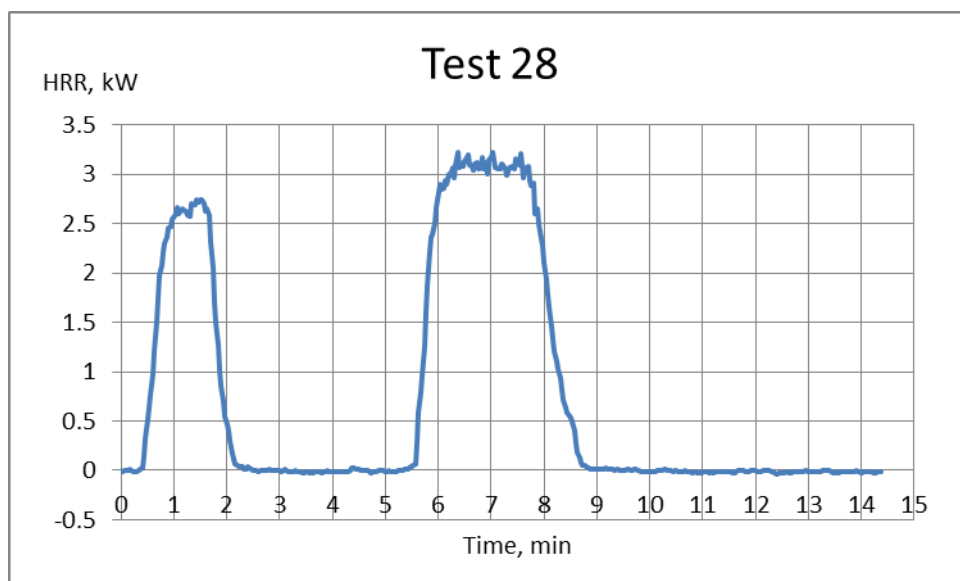


Figure 17 HRR test 28

A15

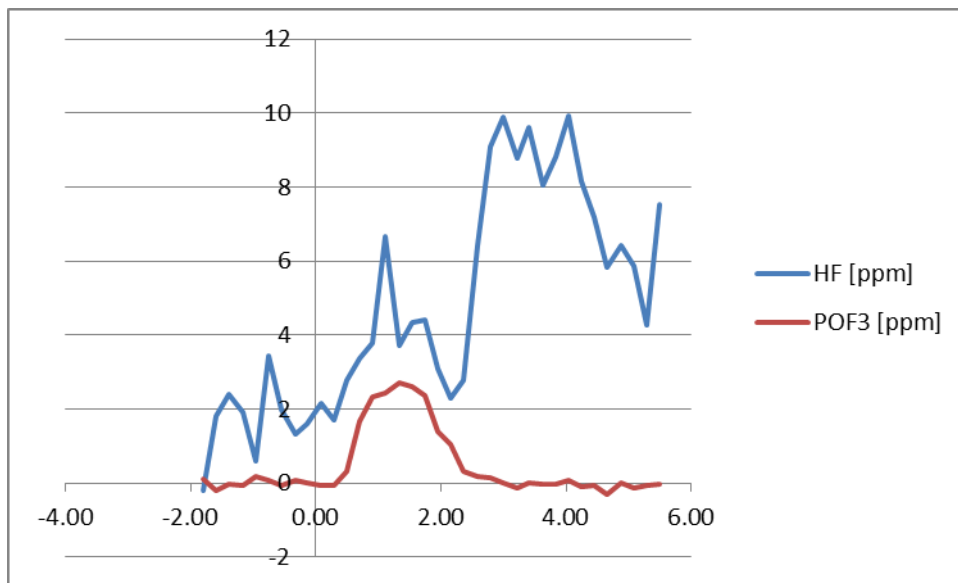


Figure 18 HF and POF₃ test 28

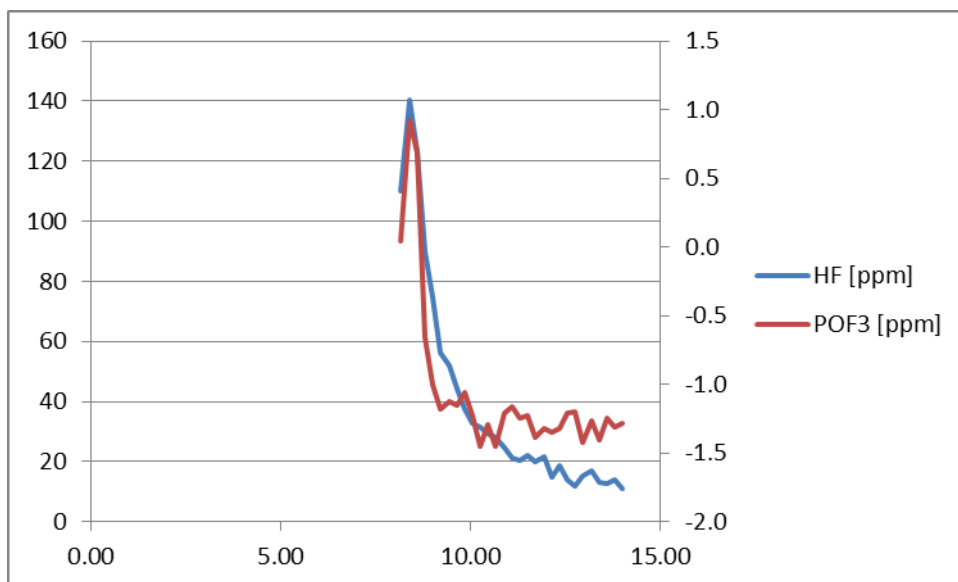


Figure 19 HF and POF₃ test 28

B1

Appendix B Results from batterycell tests

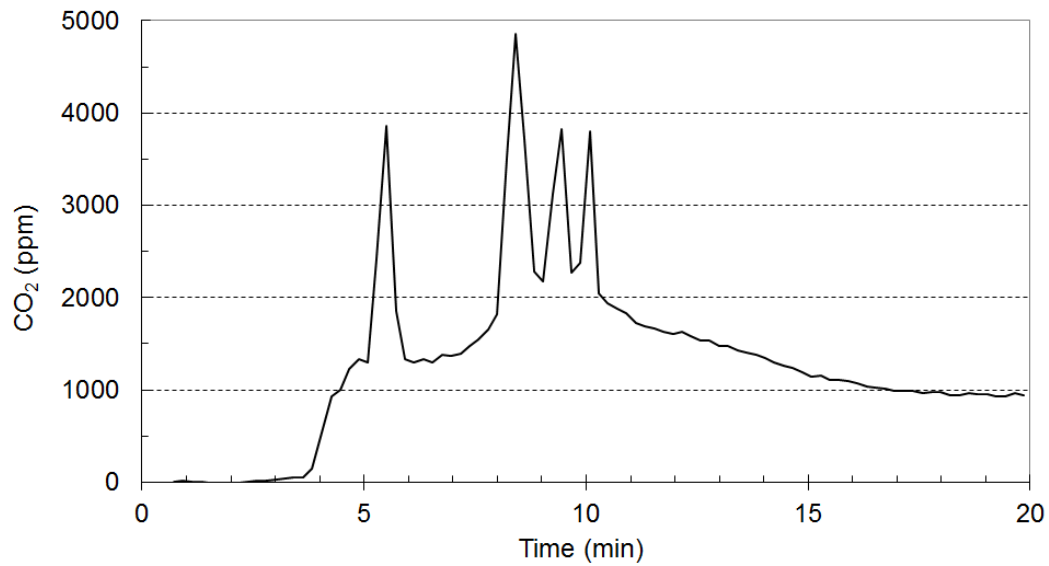


Figure 1 Concentration of CO₂ measured by FTIR in Test 1.

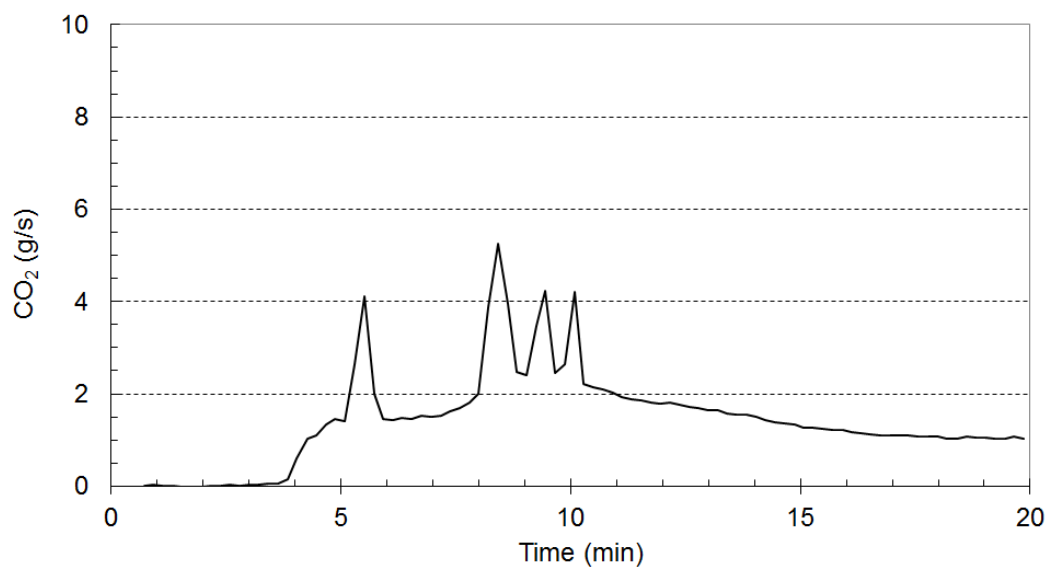


Figure 2 Production rate of CO₂ measured by FTIR in Test 1.

B2

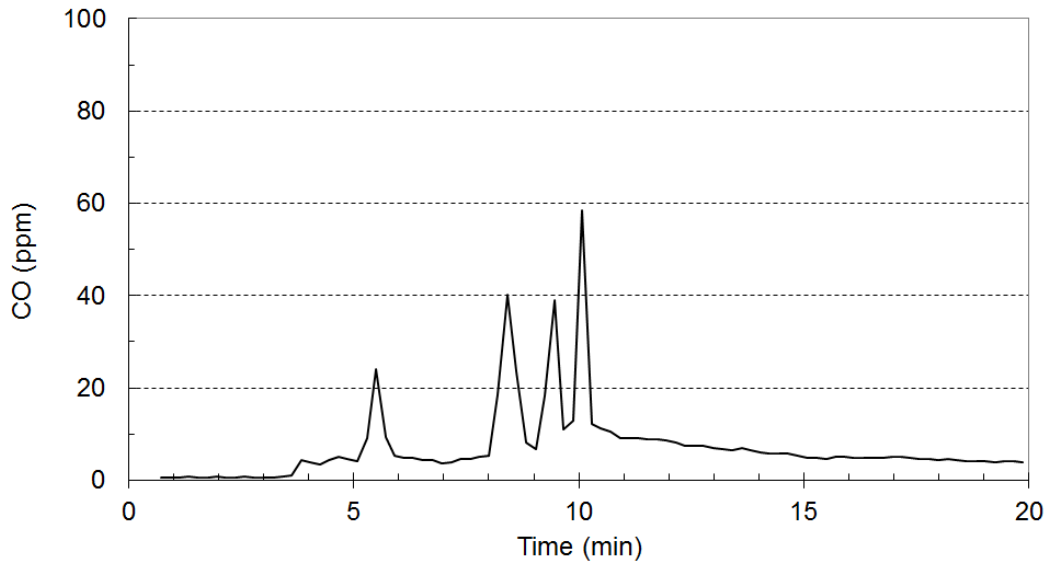


Figure 3 Concentration of CO measured by FTIR in Test 1.

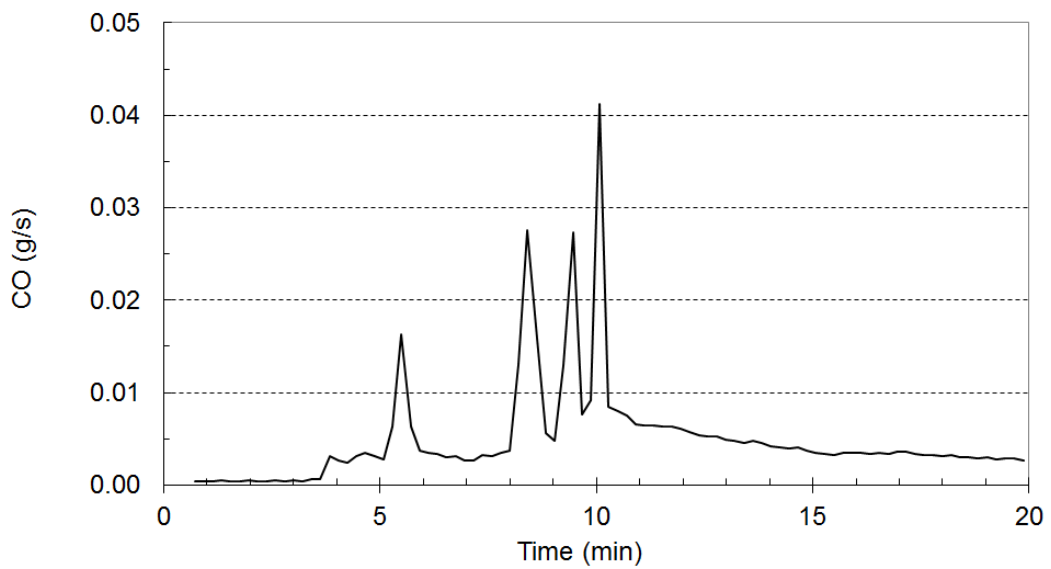


Figure 4 Production rate of CO measured by FTIR in Test 1.

B3

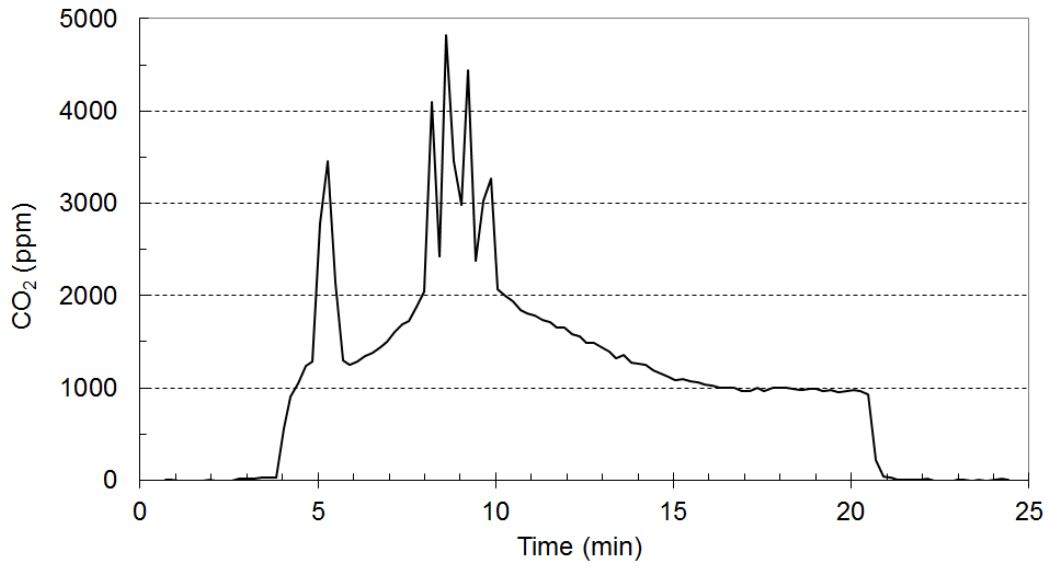


Figure 5 Concentration of CO₂ measured by FTIR in Test 2.

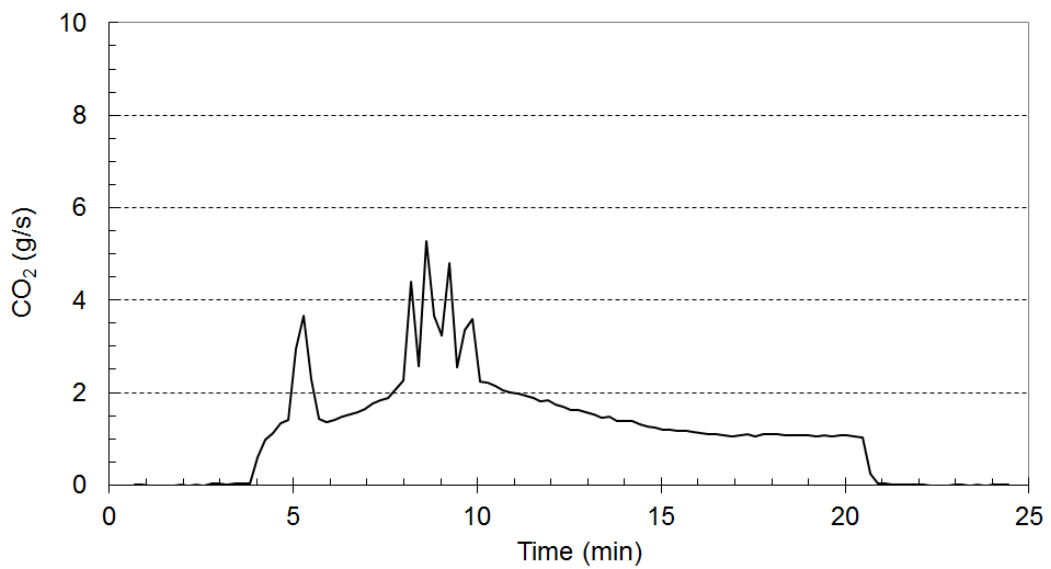


Figure 6 Production rate of CO₂ measured by FTIR in Test 2.

B4

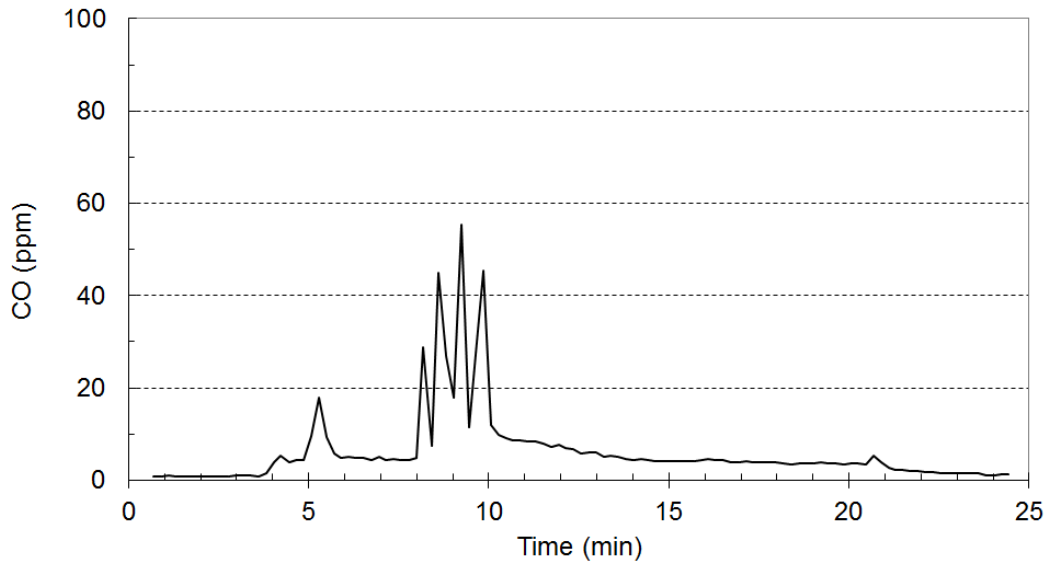


Figure 7 Concentration of CO measured by FTIR in Test 2.

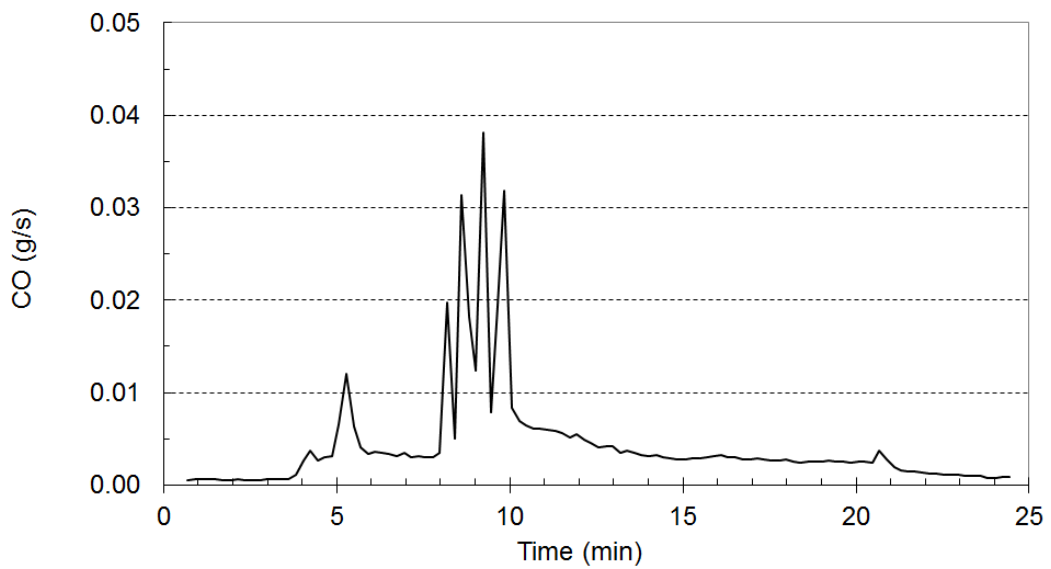


Figure 8 Production rate of CO measured by FTIR in Test 2.

B5

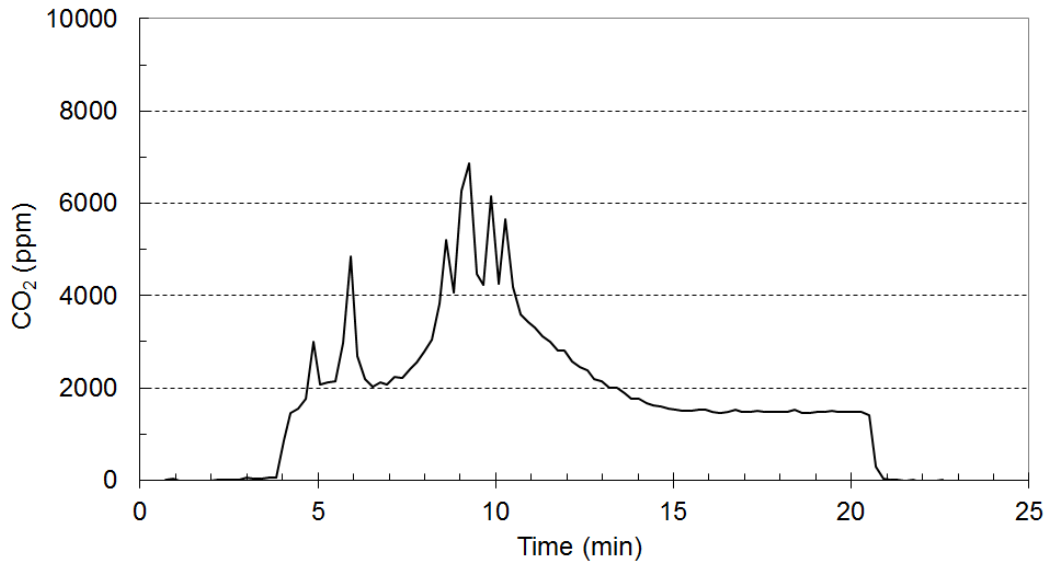


Figure 9 Concentration of CO₂ measured by FTIR in Test 3.

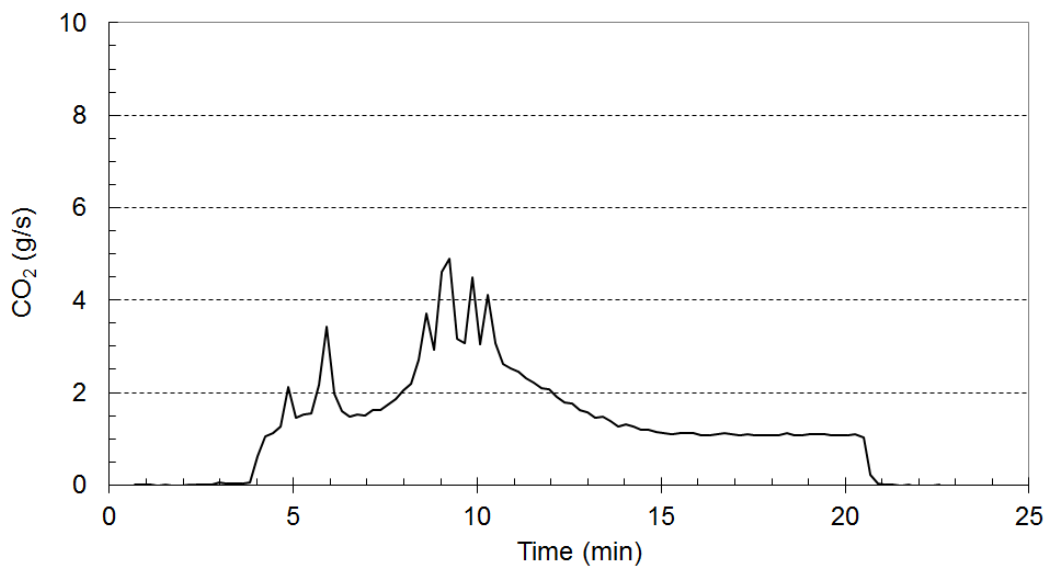


Figure 10 Production rate of CO₂ measured by FTIR in Test 3.

B6

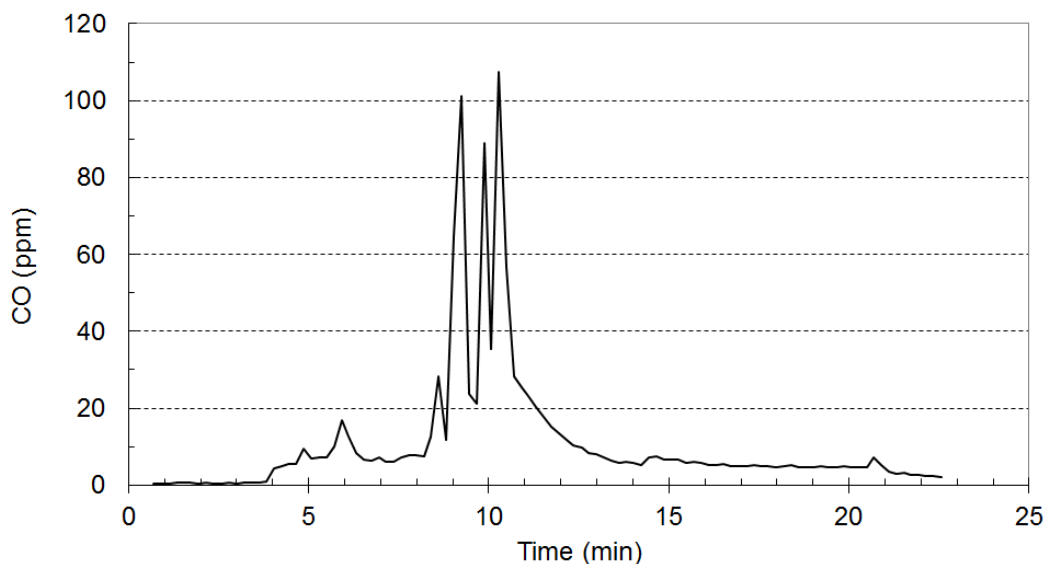


Figure 11 Concentration of CO measured by FTIR in Test 3.

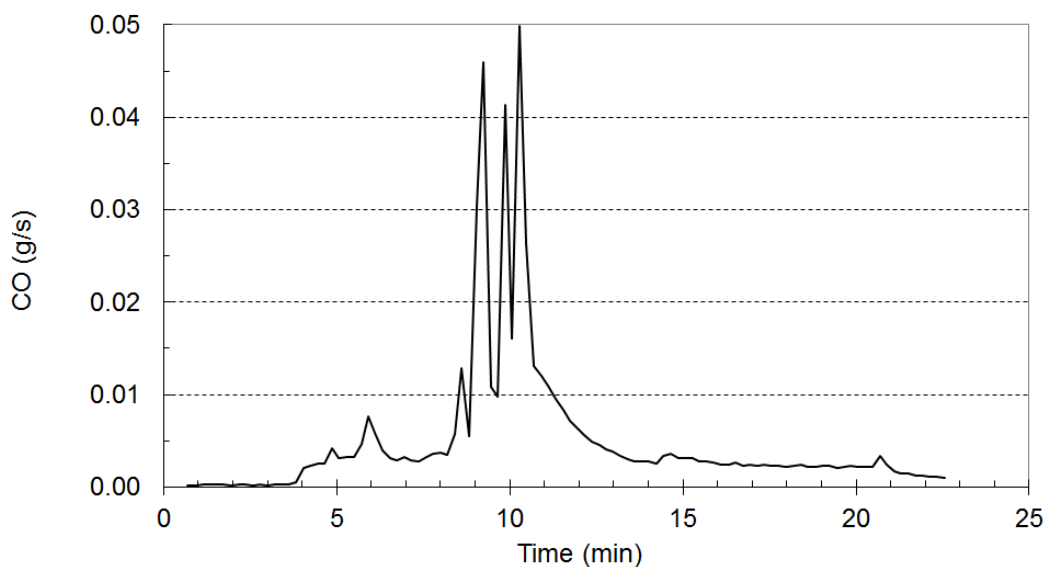


Figure 12 Production rate of CO measured by FTIR in Test 3.

B7

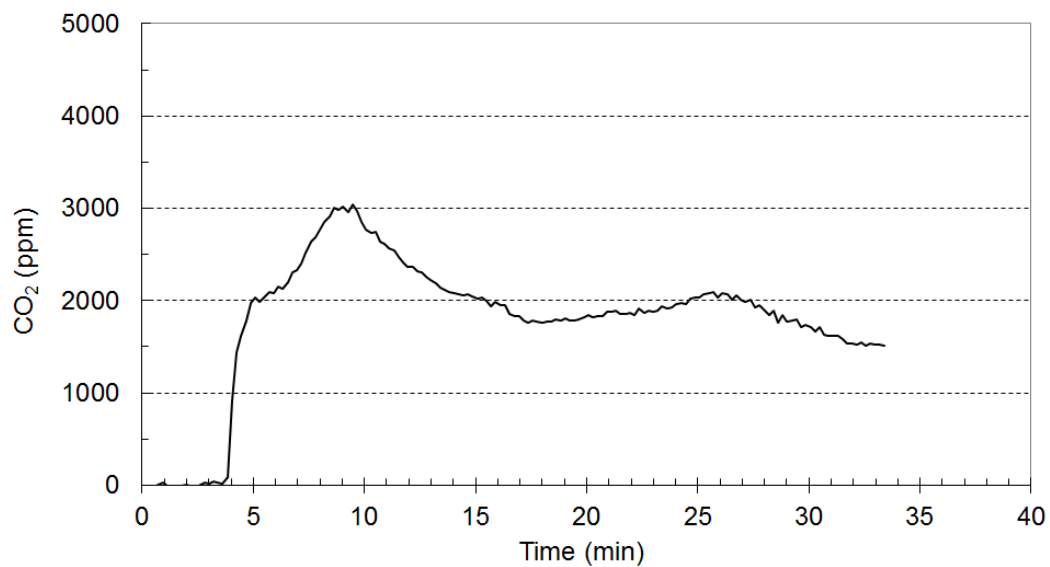


Figure 13 Concentration of CO₂ measured by FTIR in Test 4.

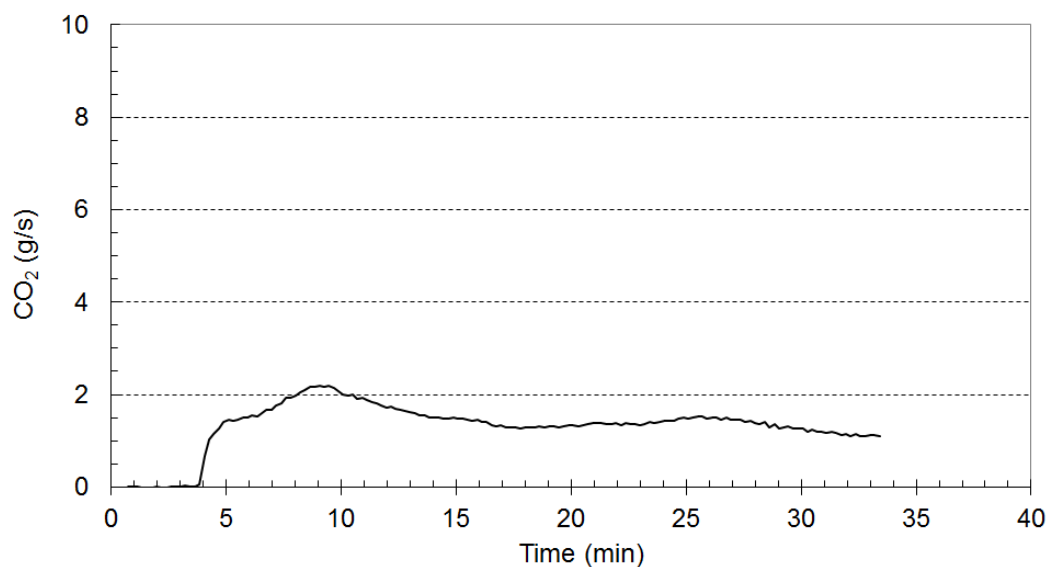


Figure 14 Production rate of CO₂ measured by FTIR in Test 4.

B8

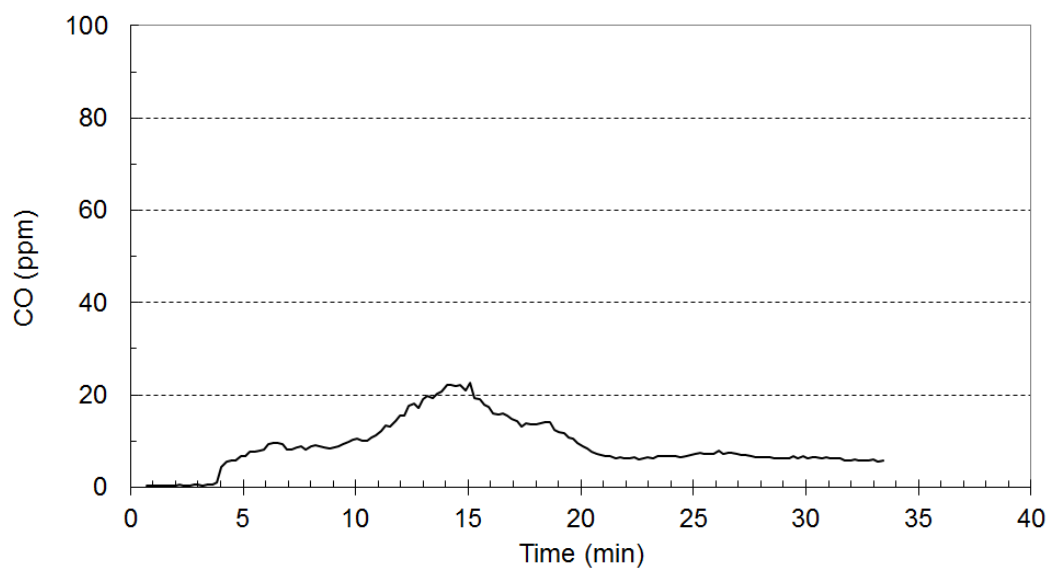


Figure 15 Concentration of CO measured by FTIR in Test 4.

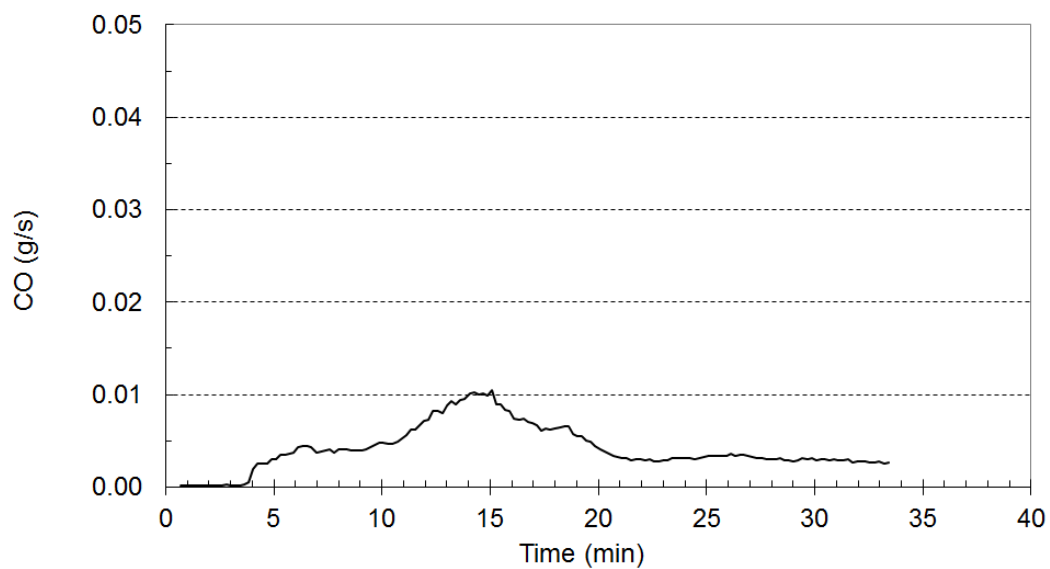


Figure 16 Production rate of CO measured by FTIR in Test 4.

B9

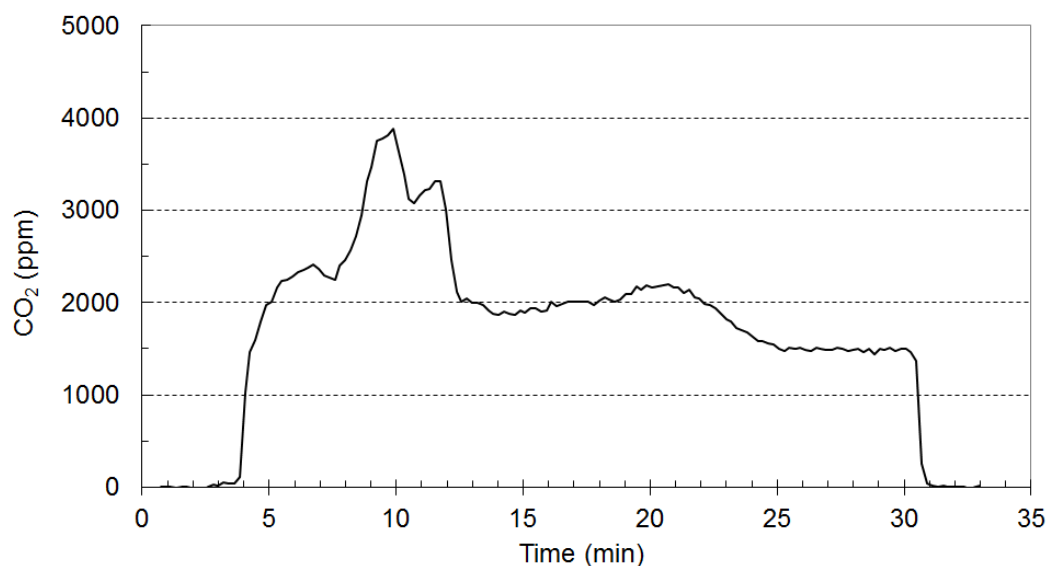


Figure 17 Concentration of CO₂ measured by FTIR in Test 5.

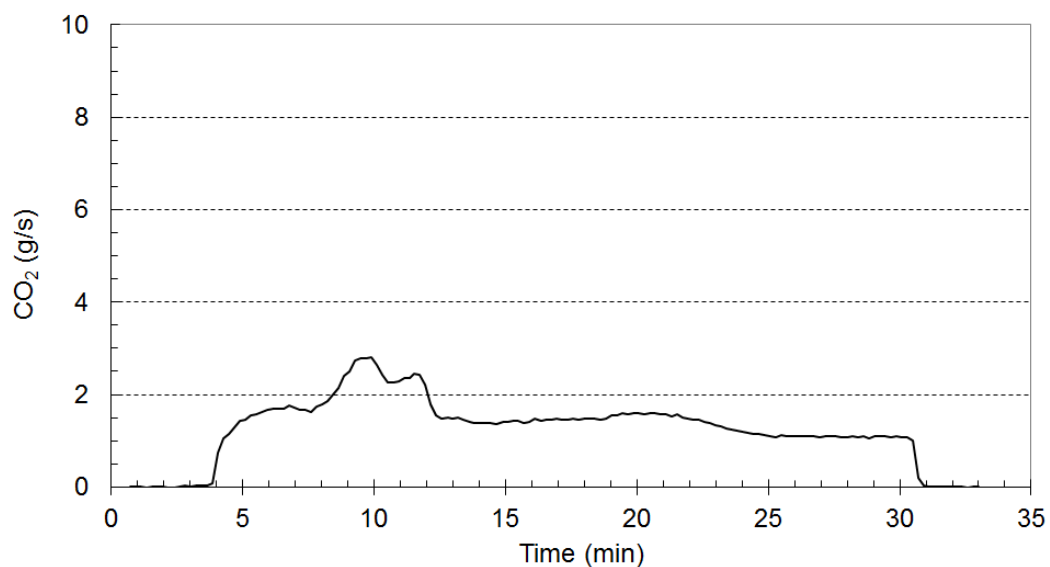


Figure 18 Production rate of CO₂ measured by FTIR in Test 5.

B10

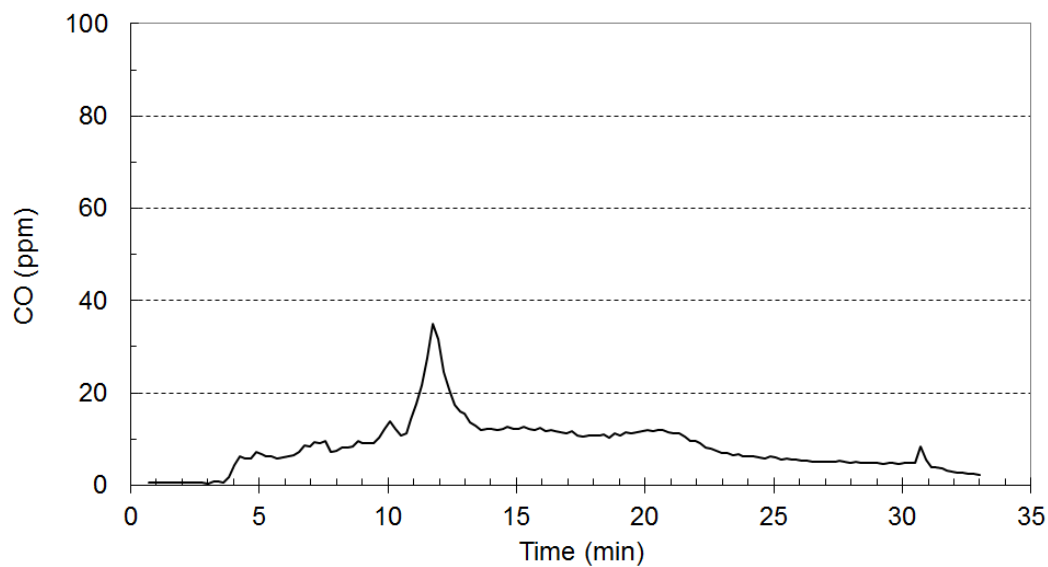


Figure 19 Concentration of CO measured by FTIR in Test 5.

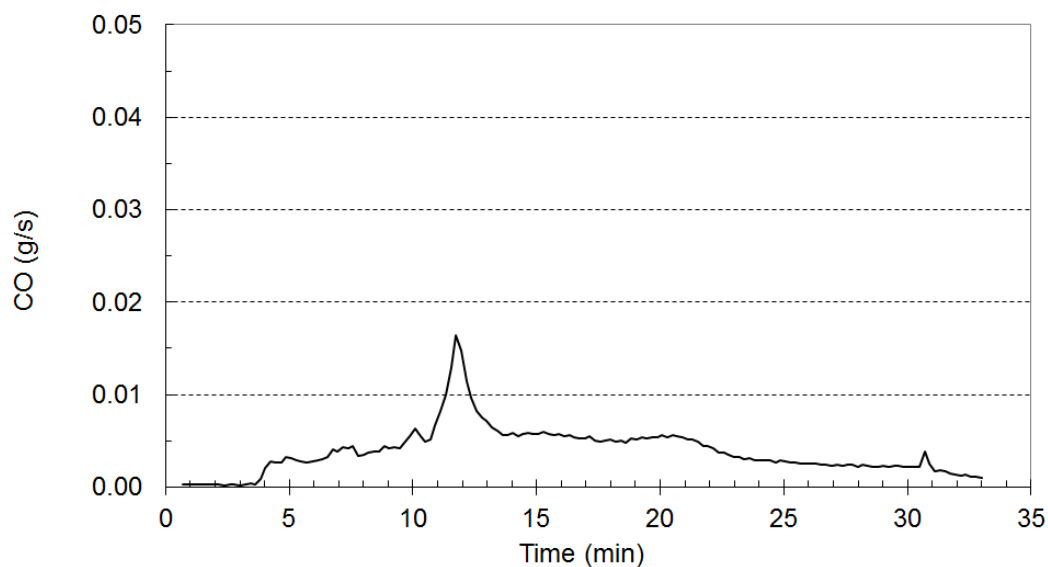


Figure 20 Production rate of CO measured by FTIR in Test 5.

B11

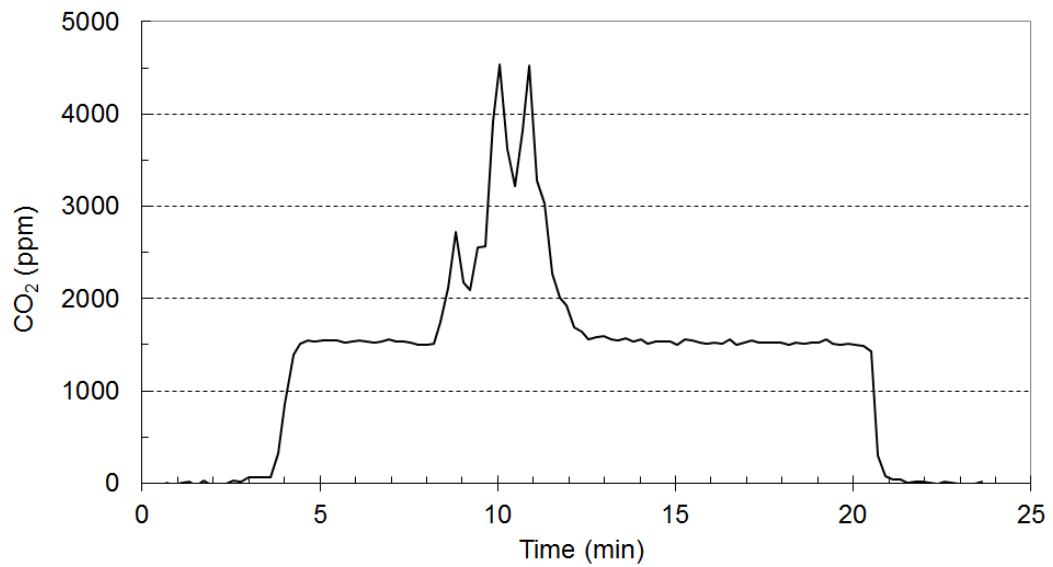


Figure 21 Concentration of CO₂ measured by FTIR in Test 6.

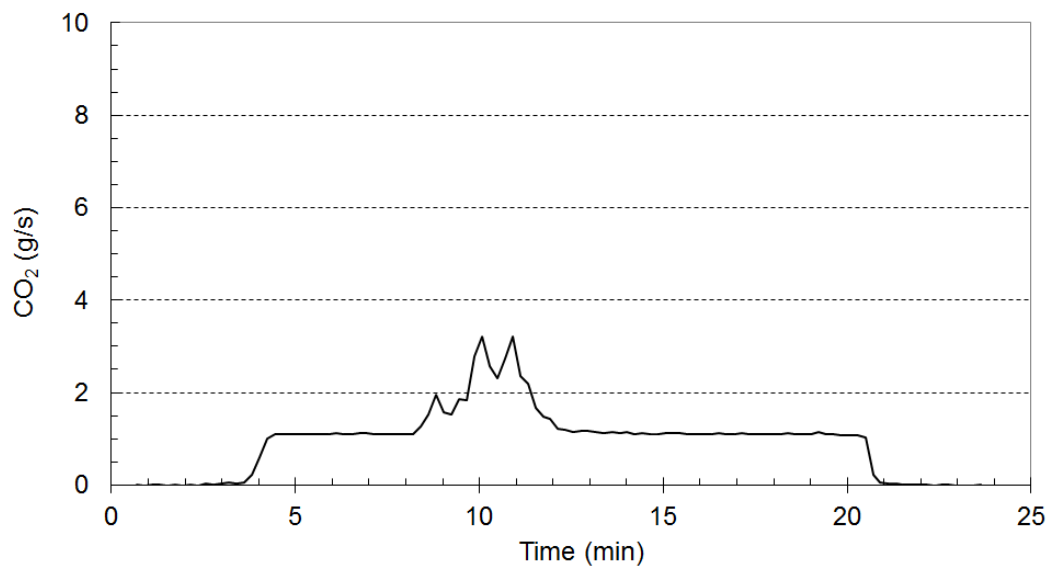


Figure 22 Production rate of CO₂ measured by FTIR in Test 6.

B12

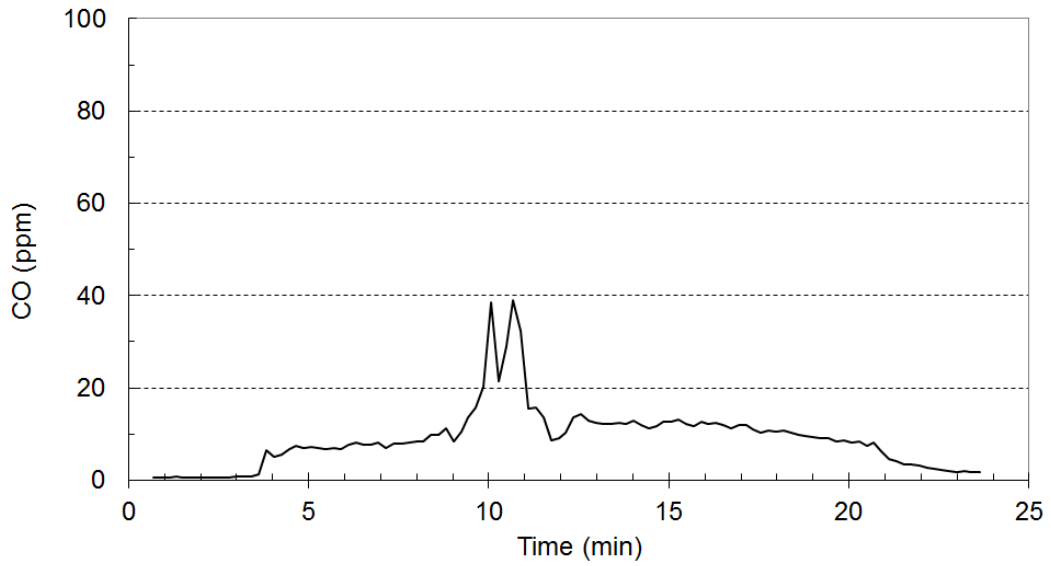


Figure 23 Concentration of CO measured by FTIR in Test 6.

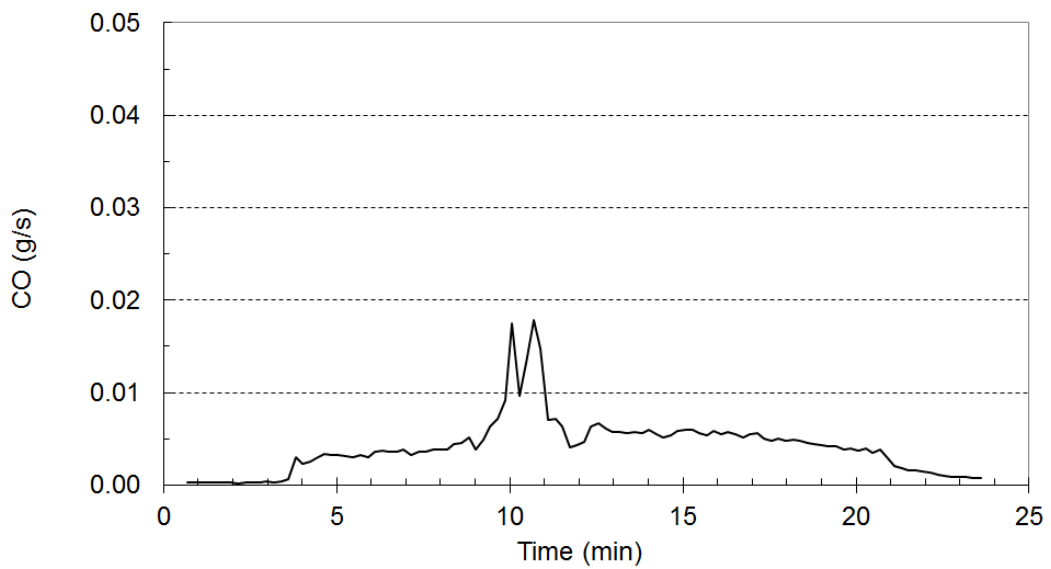


Figure 24 Production rate of CO measured by FTIR in Test 6.

B13

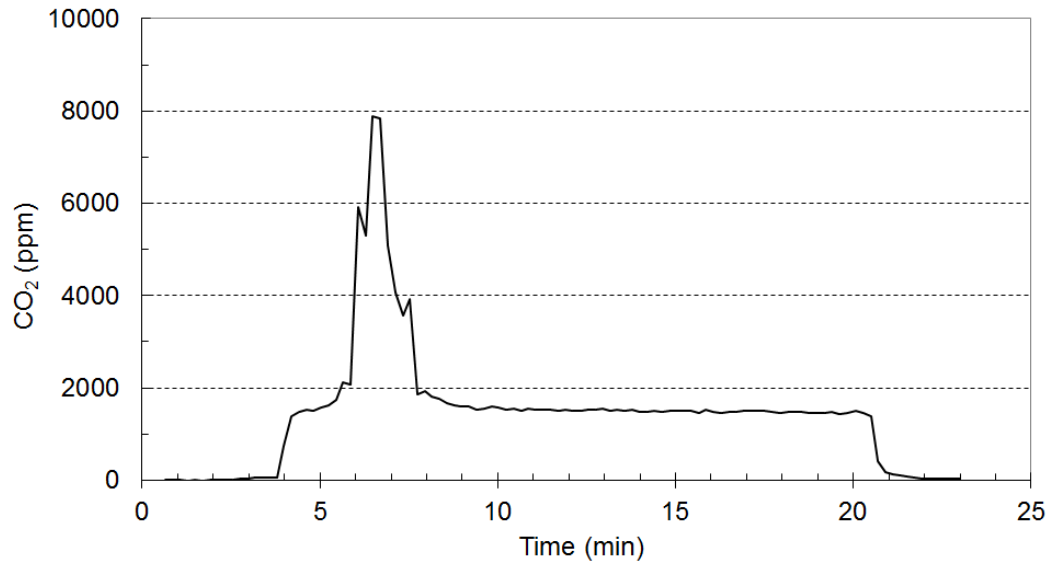


Figure 25 Concentration of CO₂ measured by FTIR in Test 7.

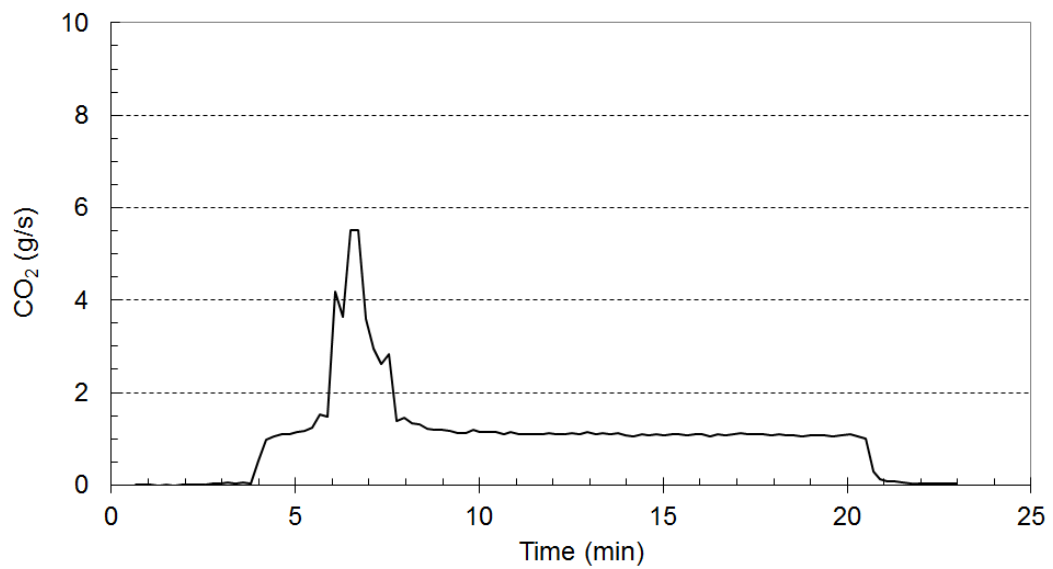


Figure 26 Production rate of CO₂ measured by FTIR in Test 7.

B14

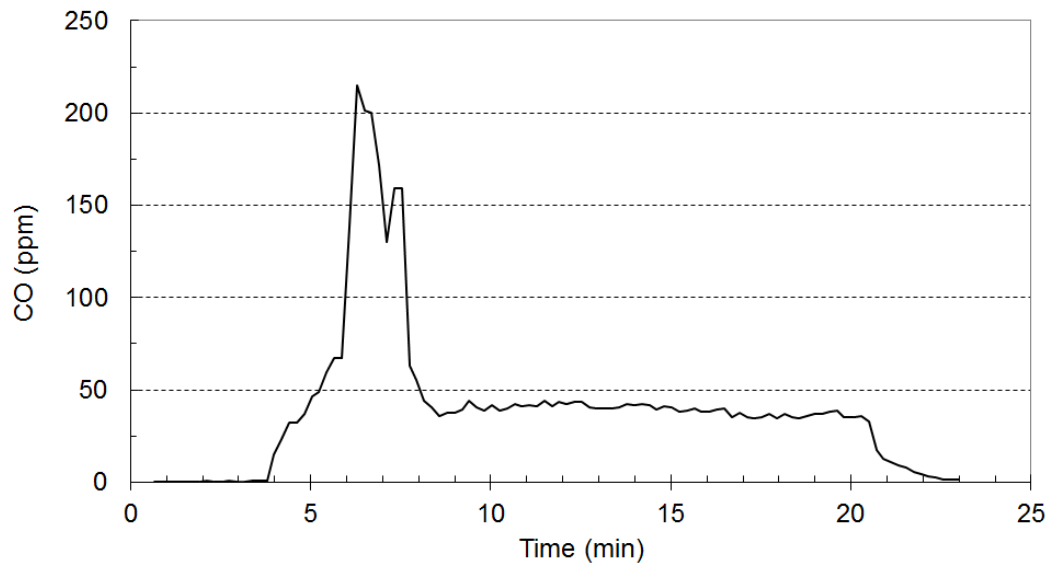


Figure 27 Concentration of CO measured by FTIR in Test 7.

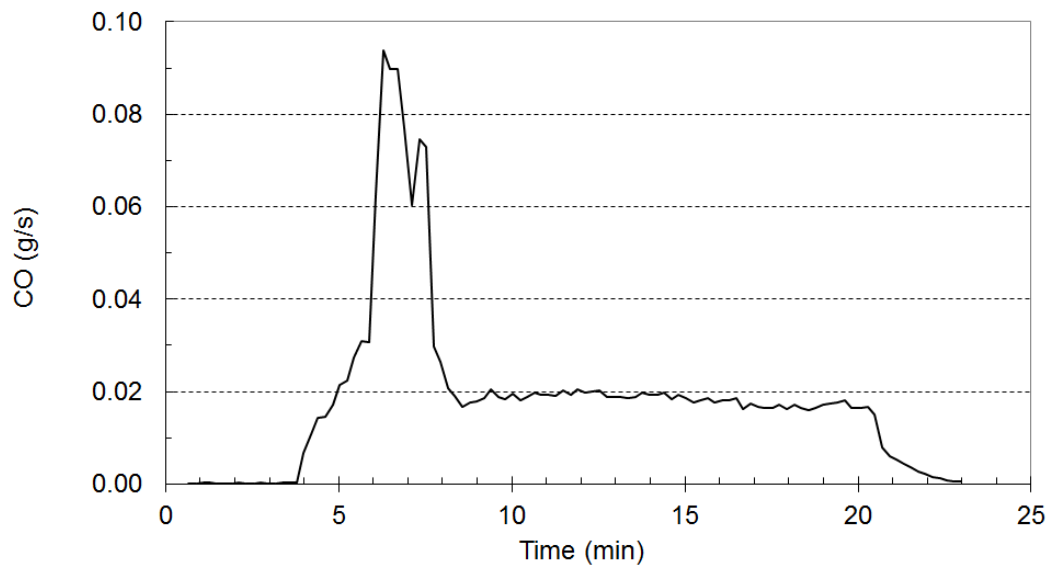


Figure 28 Production rate of CO measured by FTIR in Test 7.

Table 1 Results of CO₂ analysis with FTIR from test 1-5.

Test no	Total amounts with burner contribution subtracted (g)	Total yields (mg/g)
1	599	488
2	610	496
3	646	525
4	553	450
5	653	532

B15

Table 2 Results of CO analysis with FTIR from test 1-5.

Test no	Max production rate (g/s)	Total amounts (g)	Total yields (mg/g)
1	0.041	6.0	4.9
2	0.038	6.2	5.0
3	0.050	6.7	5.4
4	0.011	8.4	6.8
5	0.016	7.6	6.2

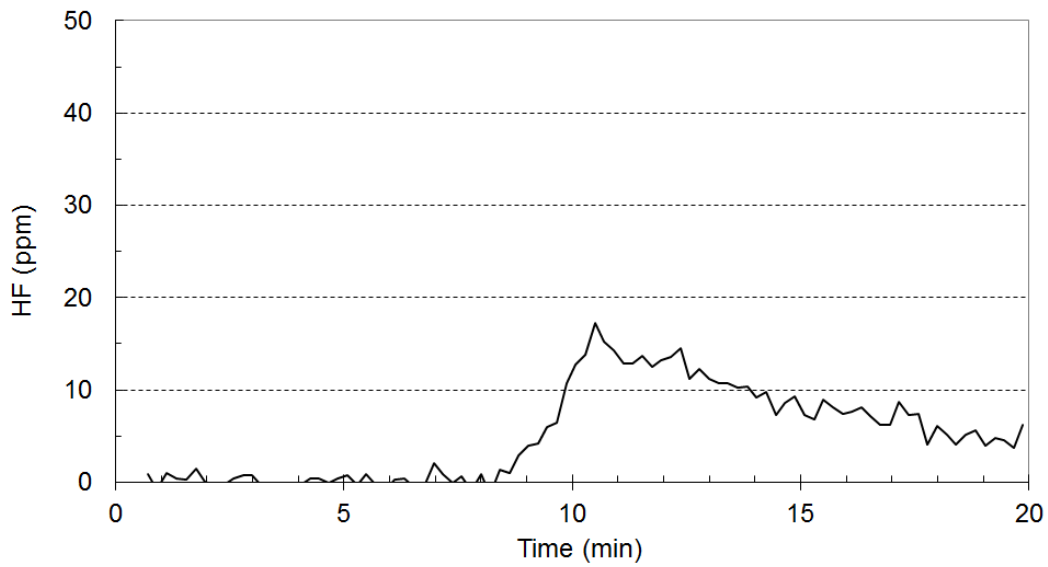


Figure 29 Concentration of HF measured by FTIR in Test 1.

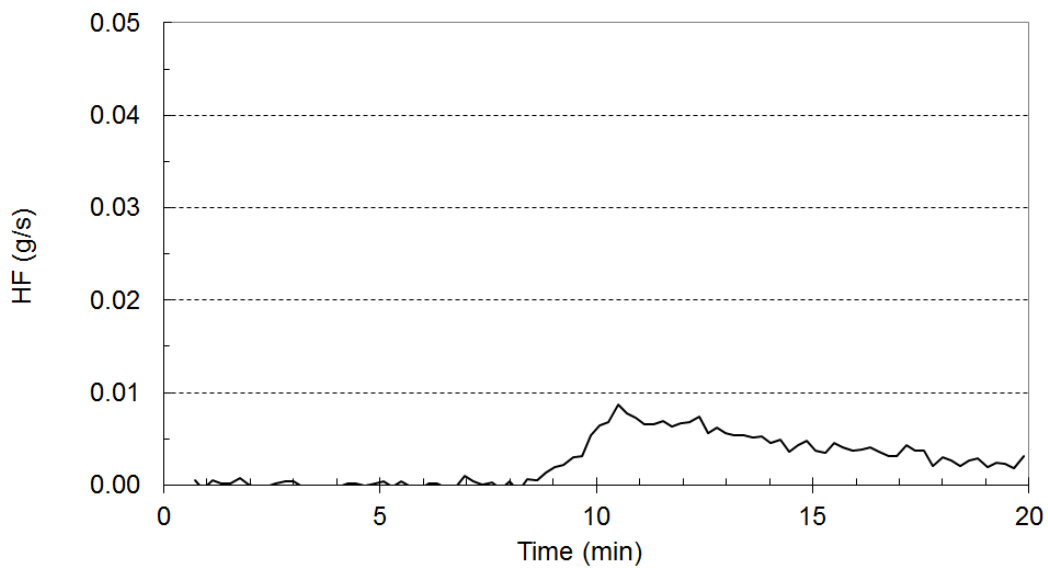


Figure 30 Production rate of HF measured by FTIR in Test 1.

B16

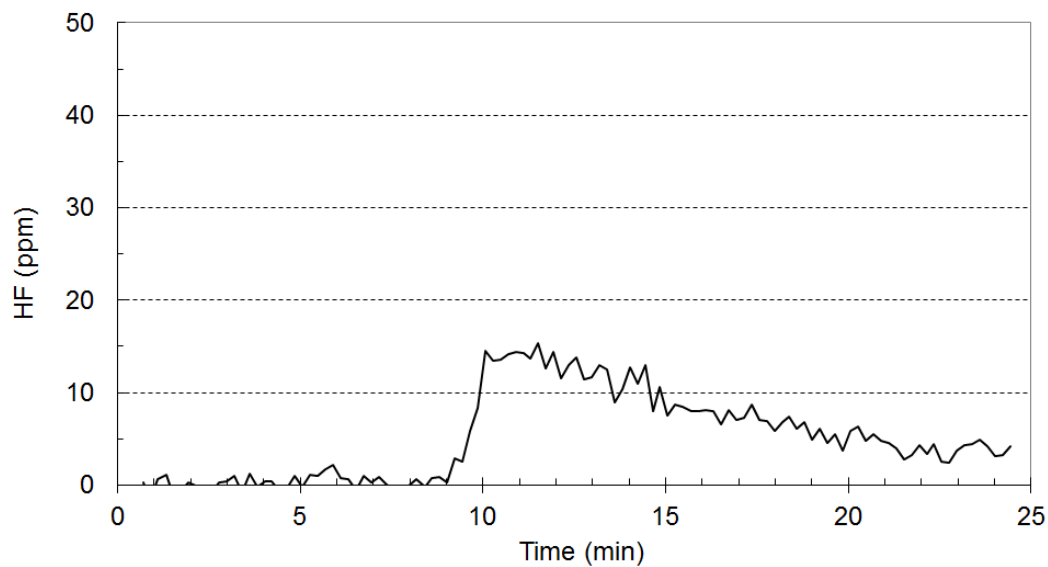


Figure 31 Concentration of HF measured by FTIR in Test 2.

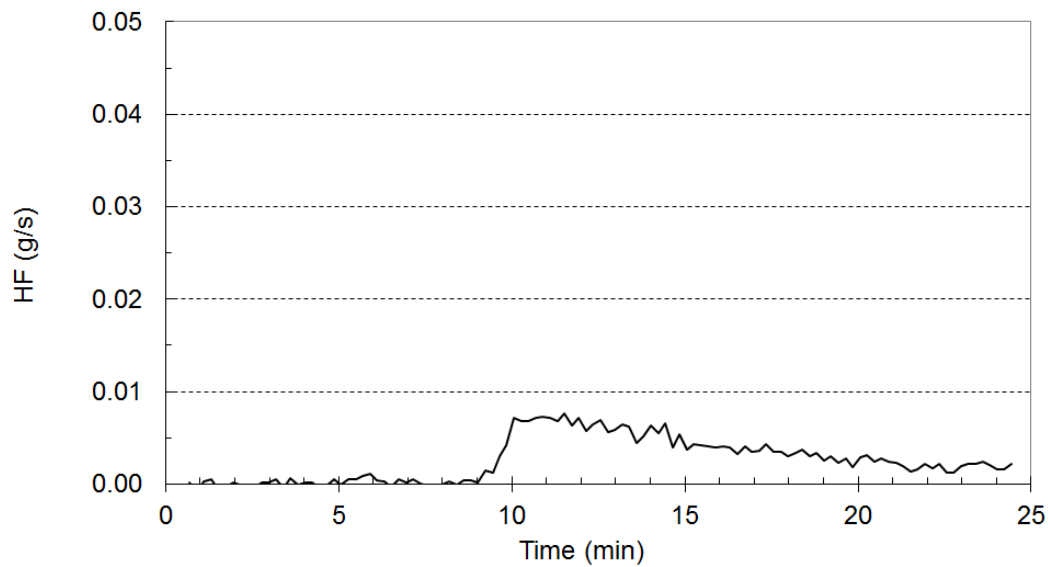


Figure 32 Production rate of HF measured by FTIR in Test 2.

B17

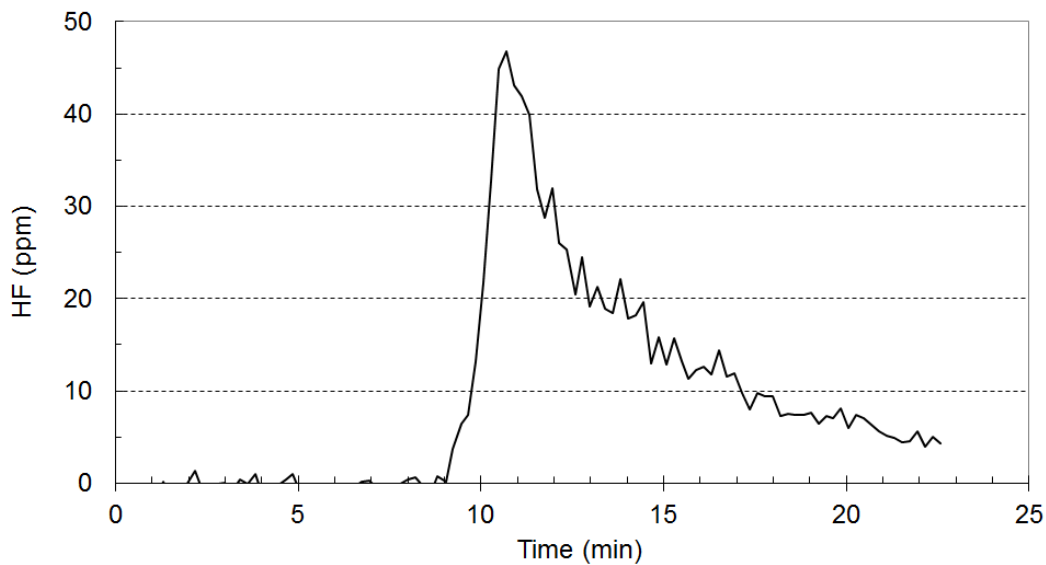


Figure 33 Concentration of HF measured by FTIR in Test 3.

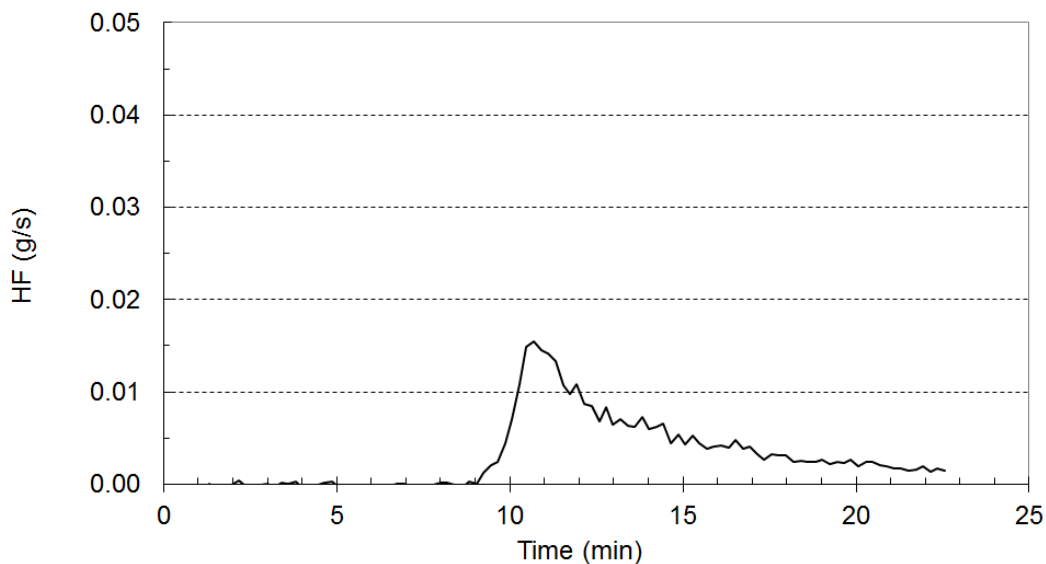


Figure 34 Production rate of HF measured by FTIR in Test 3.

B18

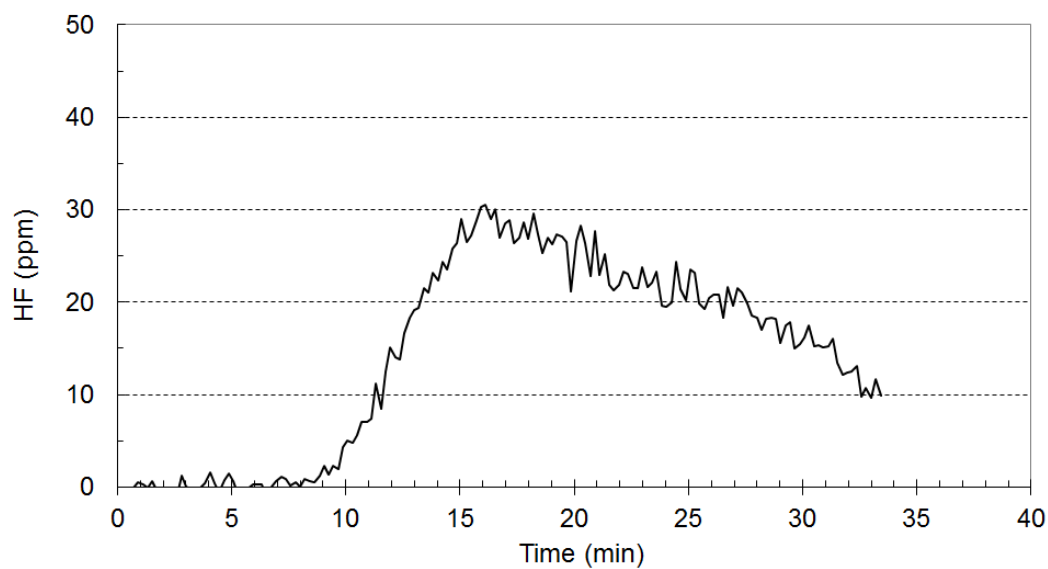


Figure 35 Concentration of HF measured by FTIR in Test 4.

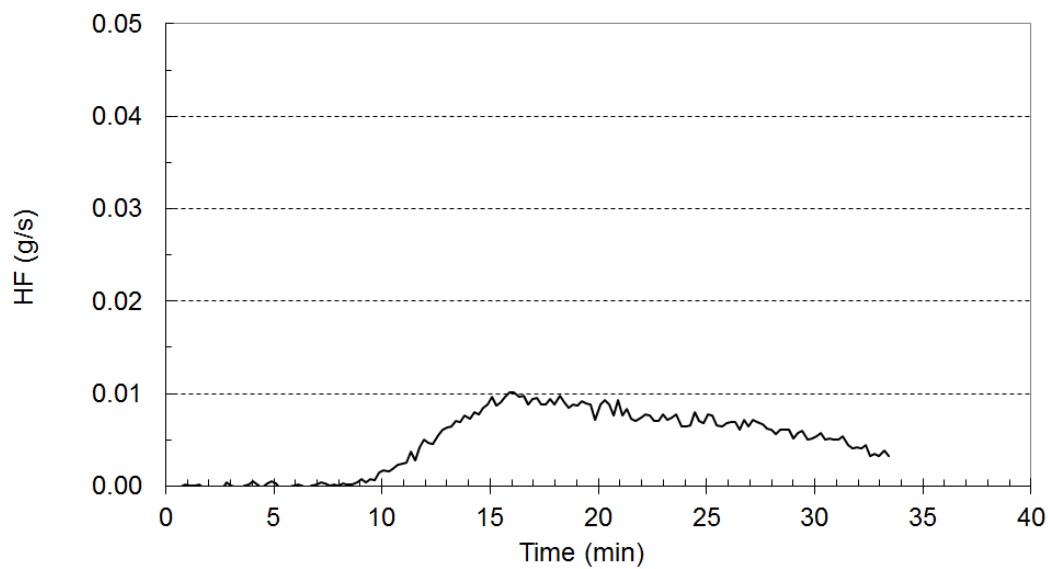


Figure 36 Production rate of HF measured by FTIR in Test 4.

B19

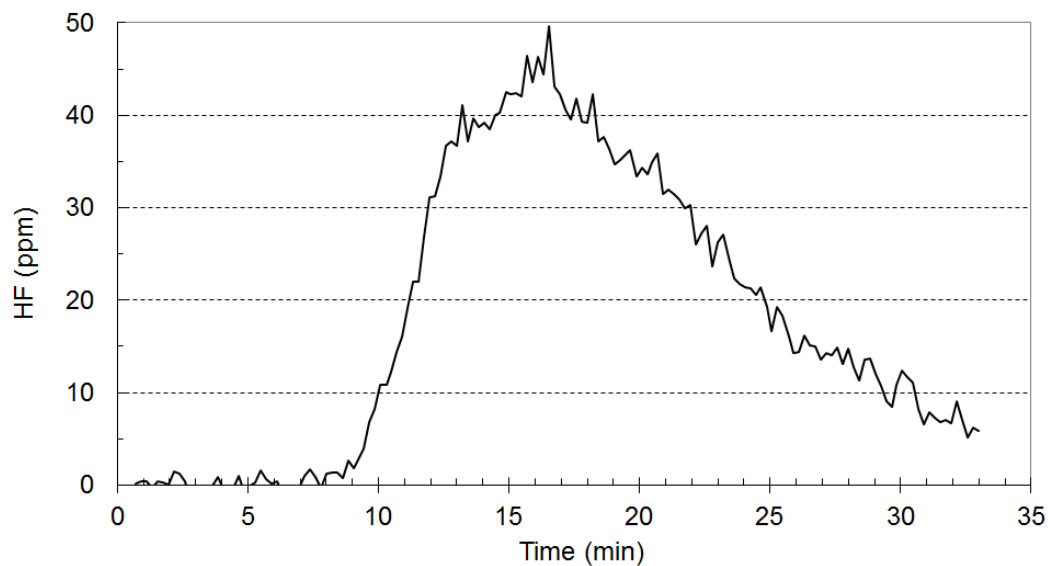


Figure 37 Concentration of HF measured by FTIR in Test 5.

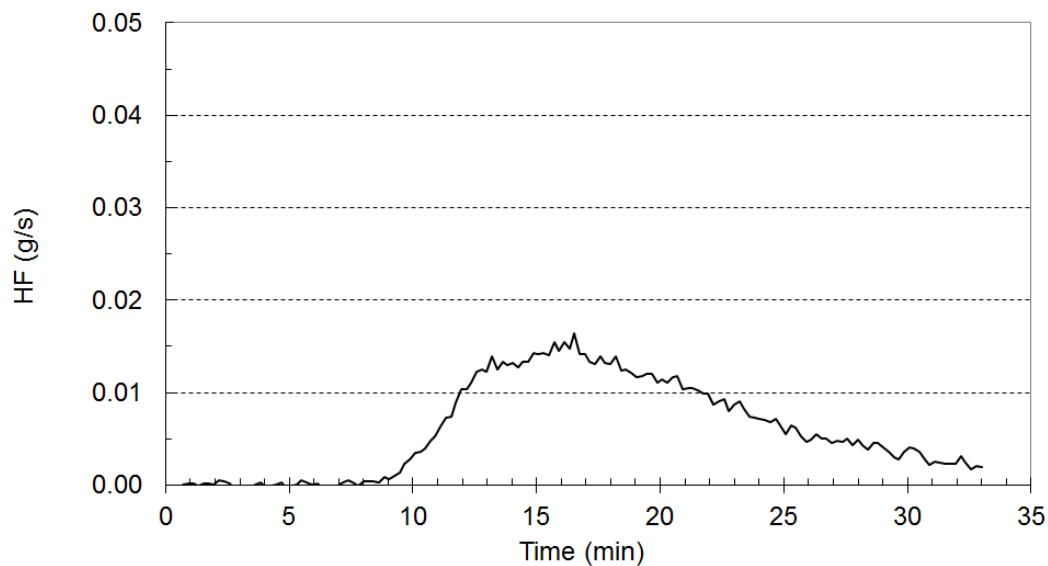


Figure 38 Production rate of HF measured by FTIR in Test 5.

B20

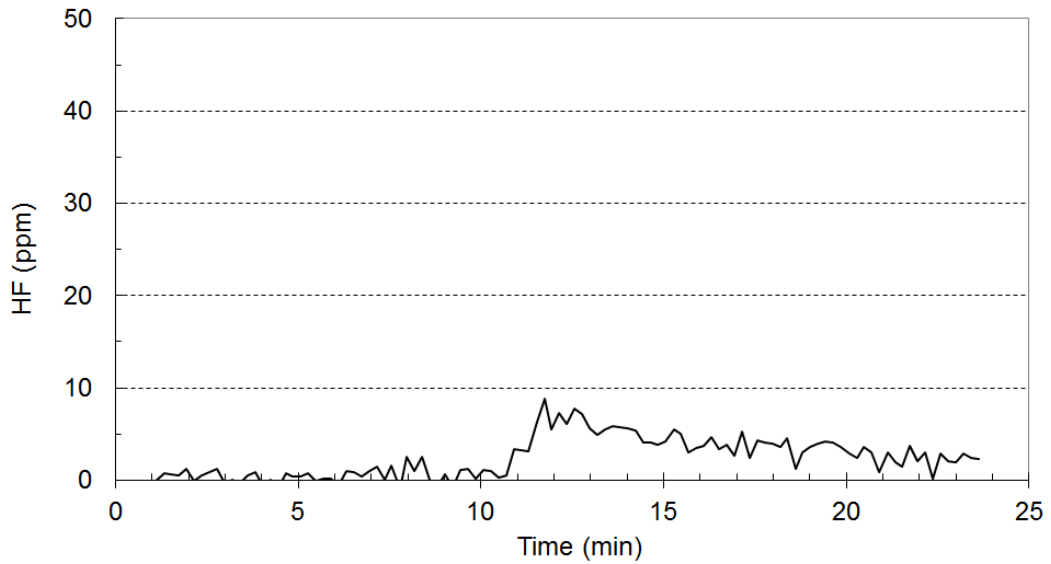


Figure 39 Concentration of HF measured by FTIR in Test 6.

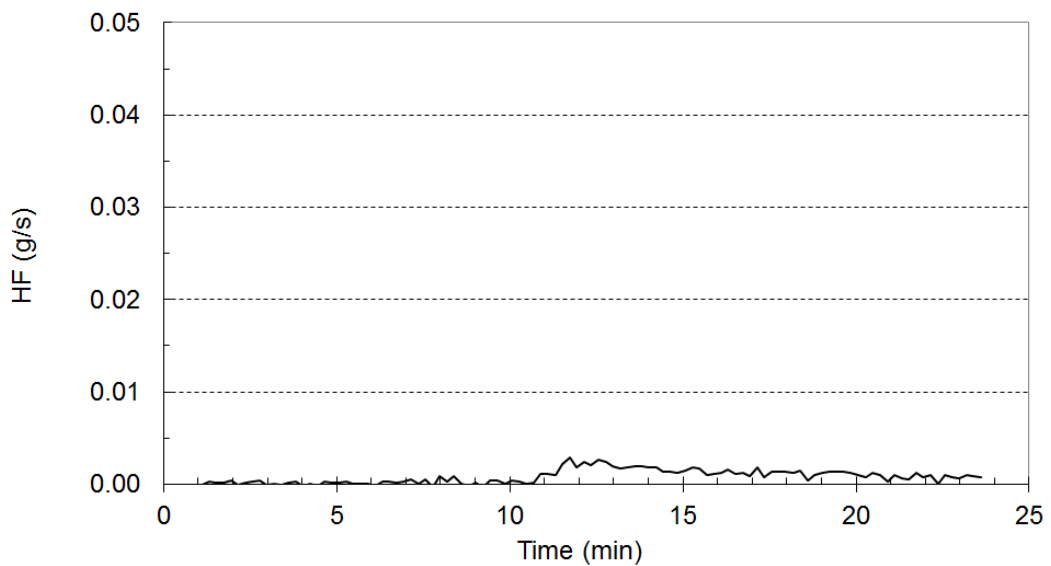


Figure 40 Production rate of HF measured by FTIR in Test 6.

B21

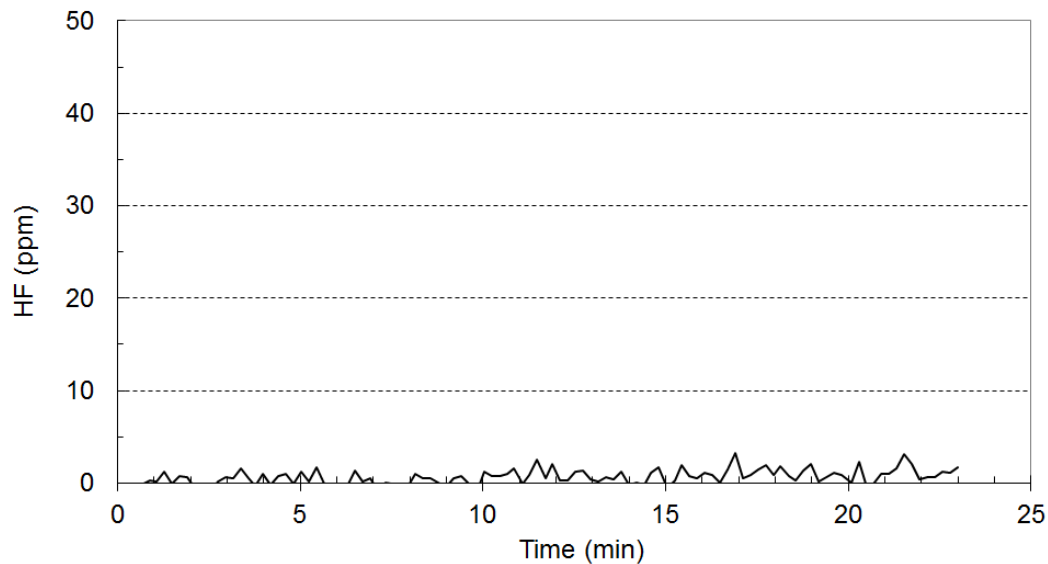


Figure 41 Concentration of HF measured by FTIR in Test 7.

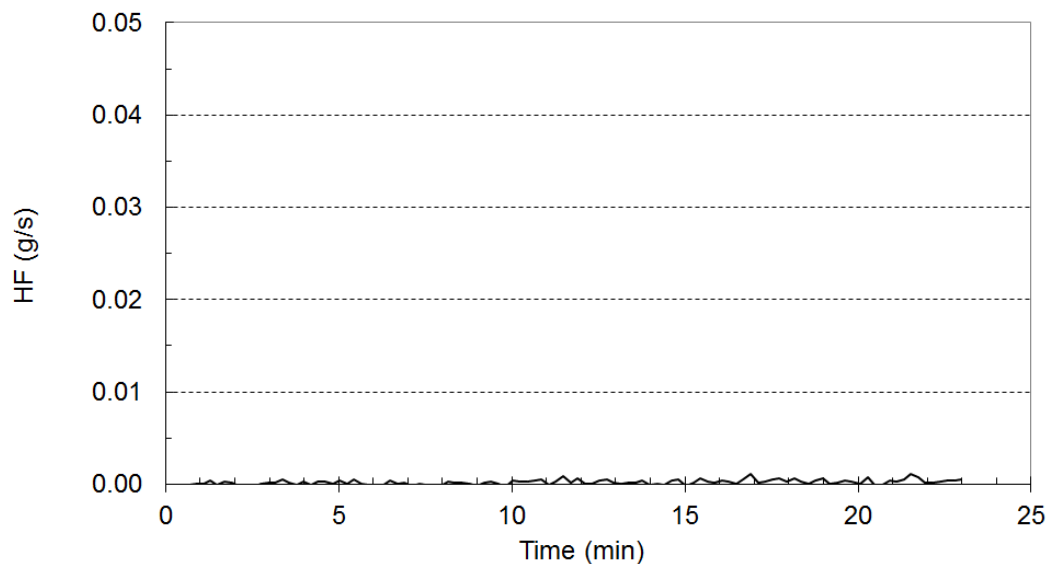


Figure 42 Production rate of HF measured by FTIR in Test 7.

C1

Appendix C Photos from cell experiments



Figure 1 Burner during blank test 1

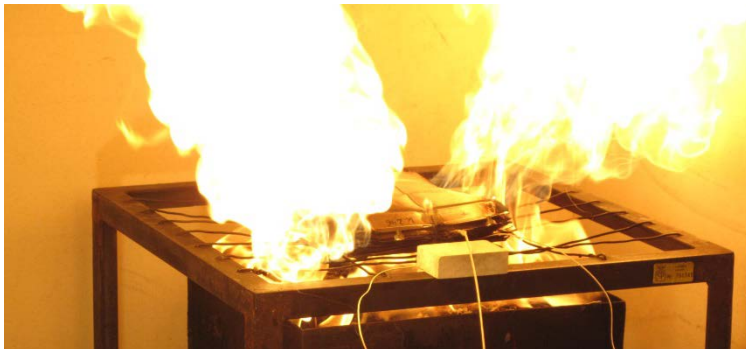


Figure 2 Typical outburst test 1



Figure 3 Later stage of fire Test 1

C2



Figure 4 Outburst example test 2



Figure 5 Close up of test 2.



Figure 6 After test 2

C3



Figure 7 Applying water test 3



Figure 8 Applying water test 3

C4



Figure 9 Applying water test 3



Figure 10 Cells for test 6 in their test container

C5



Figure 11 Test 6



Figure 12 Test 6

C6



Figure 13 Laptop cells in their container placed on burner before test 7



Figure 14 Outburst example test 7



Figure 15 Outburst example test 7

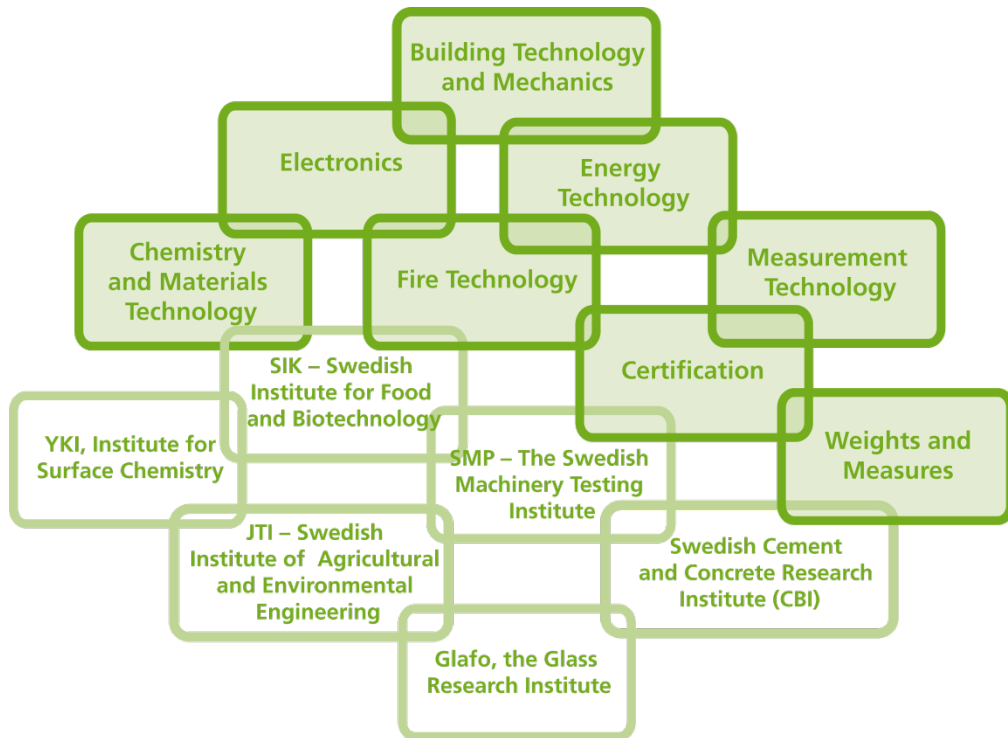
C7



Figure 16 Outburst example test 7

SP Technical Research Institute of Sweden

Our work is concentrated on innovation and the development of value-adding technology. Using Sweden's most extensive and advanced resources for technical evaluation, measurement technology, research and development, we make an important contribution to the competitiveness and sustainable development of industry. Research is carried out in close conjunction with universities and institutes of technology, to the benefit of a customer base of about 9000 organisations, ranging from start-up companies developing new technologies or new ideas to international groups.



SP Technical Research Institute of Sweden

Box 857, SE-501 15 BORÅS, SWEDEN
Telephone: +46 10 516 50 00, Telefax: +46 33 13 55 02
E-mail: info@sp.se, Internet: www.sp.se
www.sp.se

Fire Technology
SP Report 2013:15
ISBN 978-91-87461-00-2
ISSN 0284-5172

More information about publications published by SP: www.sp.se/publ



PUBLIC DOCUMENT

112(g) Case-by-Case MACT Analysis for the Lithium Ion Battery Plant

BASF Corporation – Elyria, Ohio

April 9, 2014

www.erm.com



The world's leading sustainability consultancy

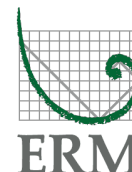


TABLE OF CONTENTS

EXECUTIVE SUMMARY		E-1
1	INTRODUCTION	1
1.1	FACILITY BACKGROUND	1
1.2	PROCEDURAL REQUIREMENTS FOR A CASE-BY-CASE MACT DETERMINATION	2
1.3	OVERVIEW OF BASF CASE-BY-CASE MACT ANALYSIS METHODOLOGY	3
2	LITHIUM ION BATTERY CASE-BY-CASE MACT CONSIDERATIONS	5
2.1	LIB PLANT PROCESS OVERVIEW	5
2.2	LIB PLANT AIR CAPTURE AND FLOW SCHEMES	8
2.3	LIB PLANT EMISSION CALCULATIONS	10
3	EVALUATION OF AVAILABLE CONTROL TECHNOLOGIES	14
3.1	SUMMARY OF AVAILABLE CONTROL TECHNOLOGIES	15
3.1.1	Baghouse/Fabric Filter	16
3.1.2	Electrostatic Precipitator	17
3.1.3	Cyclone	18
3.1.4	Extended Media	18
3.2	DATA AVAILABLE FROM THE USEPA CONTROL TECHNOLOGY CENTER	19
4	EVALUATION OF SIMILAR SOURCES	21
4.1	SIMILAR SOURCES WITHIN THE LIB INDUSTRY	22
4.2	SUMMARY OF CONTROL TECHNOLOGY DETERMINATIONS DOCUMENTED IN USEPA'S RACT/BACT/LAER CLEARINGHOUSE FOR SIMILAR SOURCES	24
4.3	REGULATIONS FOR SIMILAR SOURCES	26

5	CASE-BY-CASE MACT DETERMINATION	29
5.1	<i>IDENTIFIED CONTROL TECHNOLOGY THAT ACHIEVES THE MAXIMUM DEGREE OF HAP EMISSION REDUCTION</i>	29
5.2	<i>PROPOSED EMISSION LIMITATION</i>	29
5.3	<i>DISCUSSION OF OTHER ASPECTS OF CASE-BY-CASE MACT</i>	30
5.3.1	<i>Identification of Fabric Filter as MACT</i>	30
5.3.2	<i>Form of the Proposed Emission Limitation</i>	30
5.4	<i>PROPOSED OPERATIONAL/MONITORING STANDARDS</i>	32
6	CONCLUSIONS	34
	<i>APPENDIX A - CASE-BY-CASE MACT REGULATIONS</i>	<i>A-1</i>
	<i>APPENDIX B - SIMILAR SOURCE SEARCH RESULTS</i>	<i>B-1</i>
	<i>APPENDIX C - RBLC SEARCH RESULTS</i>	<i>C-1</i>
	<i>APPENDIX D - CONTROL EQUIPMENT DESIGN DOCUMENTATION</i>	<i>D-1</i>

LIST OF FIGURES

Figure 1. Process flow diagram for the BASF Lithium Ion Battery Plant. 7

LIST OF TABLES

Table 1. Information Requirements to Support a Case-by-Case MACT Determination as Described in 40 CFR §63.43(e) 3

Table 2. Summary of Emission Points..... 6

Table 3. PM Capture and Filter Design Parameters for HAP-containing Process Equipment..... 9

Table 4. Summary of LIB Plant Potential Uncontrolled and Controlled Emissions..... 12

Table 5. Summary of PM and PM-HAP Control Technologies and Control Efficiencies..... 15

Table 6. Gas-to-Cloth Design Ratios for Pulse-jet Fabric Filters 17

Table 7. Similar Sources at Permitted Battery Material Manufacturers and Battery Assembly Facilities..... 23

Table 8. Summary of Control Technology Determinations Found in RBLC for Similar Sources 26

Table 9. Summary of PM and PM-HAP Emission Standards 28

EXECUTIVE SUMMARY

This document serves as the BASF Corporation's (BASF) 112(g) case-by-case maximum achievable control technology (MACT) analysis and application for its lithium ion battery (LIB) plant at the Elyria, Ohio, facility. The Ohio Environmental Protection Agency (OEPA) requested that BASF conduct a case-by-case analysis to propose a MACT emission limit or standard because the LIB plant is a new major source of hazardous air pollutants (HAP) and not specifically regulated or exempted from regulation under another subpart of 40 CFR Part 63.

The analysis was conducted in accordance with the requirements specified in 40 CFR Part 63, §63.40 through §63.44. Various sources of information were investigated to ensure that all possible control strategies were identified that could feasibly be applied to the LIB plant operations to achieve the maximum degree of emissions reduction. The relevant information sources used in this analysis included sources recommended by OEPA and other industry resources.

Review of the available information with respect to control technologies concludes that a new baghouse/fabric filter will operate with a higher control efficiency than a wet scrubber or cyclone, and as good, if not better, than a new electrostatic precipitator (ESP). Further consideration of control technology for this case-by-case MACT could then be limited to either a fabric filter or ESP.

To evaluate the control technologies employed by similar sources, a nationwide control technology search was conducted. The nationwide control technology search included review of available air permits for facilities identified to have manufacturing operations similar to the LIB plant (i.e., battery material manufacturers and battery assemblers in the electric drive vehicle and hybrid-electric vehicle industry). As part of this search, the RACT/BACT/LAER Clearinghouse (RBLC) database also was queried for all PM determinations made within the past 5 years. These two searches both lead to the conclusion that the best controlled similar source employs a fabric filter. A detailed review of the promulgated MACT standards in 40 CFR Part 63 revealed that no similar source must achieve a greater degree of HAP emission reduction than identified in the nationwide control technology review.

In accordance with 40 CFR 63.43(e), BASF proposes to use fabric filters for particulate matter (PM) and PM-HAP emission control on all LIB plant process operations except the kilns. PM emissions from the kilns are

inherently low and therefore, no additional control is proposed for the kilns. The proposed emission limitation for the LIB plant takes the form of an equipment/operational standard. This approach to a proposed emission limitation is consistent with, and supported by, both the regulatory history of case-by-case MACT and specific instructions from the OEPA. Several specific operational/monitoring standards also are proposed to demonstrate continuous compliance with the proposed equipment/operational standard.

1 INTRODUCTION

This document serves as the BASF Corporation's (BASF) 112(g) case-by-case maximum achievable control technology (MACT) analysis and application for its lithium ion battery (LIB) plant at the Elyria, Ohio, facility. This analysis is being submitted in conjunction with the permit to install (PTI) applications (initial application A0045081 and two subsequent applications A0046796 and A0047014), previously submitted for the LIB plant to the Ohio Environmental Protection Agency (OEPA). Standards promulgated pursuant to Section 112(g) of the Clean Air Act Amendments of 1990 (CAAA) regulate constructed (i.e., new) and reconstructed major sources of HAPs and consist of five standards under 40 CFR Part 63, §63.40 through §63.44. Appendix A contains the text of these standards. Section 63.43 requires that an application for a case-by-case MACT determination be submitted to the permitting authority as part of the construction permitting process.

1.1 FACILITY BACKGROUND

BASF began construction on the new Elyria, Ohio, cathode material manufacturing operations on November 28, 2011. The new operations were designed to produce nickel/manganese/cobalt (NMC) cathode material for lithium ion batteries. Construction of the new operations, i.e., the LIB plant, was accomplished through a cooperative agreement between BASF Catalysts LLC and the United States Department of Energy (US DOE) established to support the anticipated growth in the LIB industry and, more specifically, the electric drive vehicle and hybrid-electric vehicle industry. Construction of the LIB plant, which included a single kiln unit, was completed on June 11, 2012. In June 2013, construction of a second kiln unit began. The expected completion date for construction of the second kiln unit is December 2014, and the anticipated startup date of operation of the second kiln is January 2015.

The cathode materials manufacturing process consists of state-of-the-art operations, including: metal carbonate process operations, metal hydroxide process operations, mixed materials process operations, and cleanup operations. Collectively, the operations are equipped with 13 fabric filtration systems that were designed and are operated to achieve the highest degree of control affordable for particulate matter (PM) and hazardous air pollutants (HAPs) (nickel, manganese, and cobalt compounds). Although these filters operate to produce very low air

pollutant emissions, emission reductions achieved through use of the control devices installed as part of the LIB plant construction are not considered federally enforceable, and therefore, potential emissions must be based on uncontrolled emissions from the operations. The resulting potential HAP emission rate for the LIB plant is above the HAP major source threshold of 25 ton/year of any combination of HAPs. As such, the LIB plant is considered a new major source of HAP.

1.2 ***PROCEDURAL REQUIREMENTS FOR A CASE-BY-CASE MACT DETERMINATION***

The OEPA requested that BASF conduct a case-by-case analysis to propose a MACT emission limit or standard because the LIB plant is a new major source of HAP and not specifically regulated or exempted from regulation under a standard issued pursuant to Sections 112(d), 112(h), or 112(j) of the CAAA that has been incorporated in another subpart of Part 63.

The requirements for a 112(g) case-by-case MACT analysis are described in 40 CFR § 63.43(e). Under that section, an application for a MACT determination must specify a control technology selected by the owner or operator that, if properly operated and maintained, will meet the MACT emission limit or standard as proposed by the applicant and approved by OEPA according to the principles set forth in 40 CFR § 63.43(d).

For a new source, MACT is defined as the emission limitation which is not less stringent than that achieved in practice by the best controlled similar source and which reflects the maximum degree of deduction in emissions that is achievable by the constructed or reconstructed major source. In accordance with § 63.43(d)(3), the MACT standard may be determined to be a specific design, equipment, work practice, or operational standard, or a combination thereof, if it is not feasible to prescribe or enforce an emission limitation.

Table 1 lists the information that is required to be submitted in a case-by-case MACT analysis, to the extent needed to support a proposed MACT emission limit or standard. Table 1 also shows the location that such information is provided in BASF documents.

In addition to the 112(g) case-by-case MACT requirements, §63.43(c)(4) specifies that BASF must comply with all applicable requirements of Subpart A of 40 CFR Part 63 with respect to operation of the LIB plant.

These requirements, which are known as the MACT general provisions, are found in §§ 63.1 through 63.16. As an example, BASF will prepare a startup, shutdown, and malfunction plan for the LIB plant in accordance with § 63.6(e)(3).

Table 1. Information Requirements to Support a Case-by-Case MACT Determination as Described in 40 CFR §63.43(e)

Application Requirement	Location of Requirement Content
(i) The name and address of the major source	PTI Applications
(ii) A brief description of the major source and identification of any listed source category or categories in which it is included	PTI Applications
(iii) The expected commencement date for the construction	PTI Applications and this MACT Analysis
(iv) The expected completion date for construction	PTI Applications and this MACT Analysis
(v) The anticipated date of start-up	PTI Applications and this MACT Analysis
(vi) The HAP(s) emitted by the source and the estimated emission rate for each such HAP	PTI Applications and this MACT Analysis
(vii) Any federally enforceable emission limitations applicable to the constructed major source	PTI Applications
(viii) The maximum and expected utilization of the source and the associated uncontrolled emission rates for that source	PTI Applications
(ix) The controlled emissions for the source in tons per year at expected and maximum utilization	PTI Applications and this MACT Analysis
(x) A recommended emission limitation for the constructed or reconstructed major source consistent with the principles set forth in §63.43(d)	This MACT Analysis
(xi) The selected control technology to meet the recommended MACT emission limitation	This MACT Analysis
(xii) Supporting documentation, including identification of alternative control technologies considered by the applicant to meet the emission limitation	This MACT Analysis
(xiii) Any other relevant information required pursuant to 40 CFR 63 Subpart A	This MACT Analysis

1.3

OVERVIEW OF BASF CASE-BY-CASE MACT ANALYSIS METHODOLOGY

Defining MACT is generally a two-step process: 1) identify a control technology that represents the highest control achieved in practice by the best-controlled similar source, and 2) determine whether stricter controls are achievable in light of costs, non-air quality health and environmental

impacts, and energy requirements. BASF's case-by-case MACT analysis is based on this process and entails first identifying the emission control which is achievable in theory at the LIB plant and achieved in practice by the best controlled similar source and then using the information to determine MACT (i.e., the maximum degree of reduction in emissions of HAP that is achieved in practice).

Section 2 of this report describes the LIB plant and the operations within the plant. This information is presented to assist the reader in understanding the MACT concept of "similar source" and to assist in determining technically feasible control technologies. Section 3 presents an evaluation of control technologies used in practice for similar sources, and Section 4 identifies sources similar to the LIB plant and the emission control technologies utilized by those similar sources. Section 5 presents the proposed MACT control technology and operational standards of the control technology in order to demonstrate continued compliance.

2 *LITHIUM ION BATTERY CASE-BY-CASE MACT CONSIDERATIONS*

2.1 *LIB PLANT PROCESS OVERVIEW*

The BASF LIB plant (cathode material manufacturing process) consists of 15 process operations identified as Cathode-1 through Cathode-15. These operations have the potential to emit PM, including inorganic solid phase metal HAPs. Raw materials consist of mixed metal powders, and the end product is a dry powder material that is packaged in drums or bags. The manufacturing process begins with receipt of raw materials (non-HAP metal carbonate and HAP metal hydroxide). The raw materials are milled, mixed, and then chemically combined in one of two kilns. The resulting chemical is a HAP compound (cobalt compound/manganese compound/nickel compound) that is again milled and blended before packaging. Once the raw materials are introduced, the entire manufacturing process takes place in a closed system.

Process equipment within the LIB plant were designed and constructed to achieve maximum recovery of valuable raw materials and products from all operations. The mills and blenders are specifically designed to minimize dust generation and maximize material recovery. Except for the two kilns, all process equipment are served by a dust filter (the LIB plant includes 13 such filters).

Table 2 lists the process operations, the identification numbers of the associated primary and secondary control devices, and the associated stacks. (Process descriptions in this table are considered trade secret information). A total of 7 stacks are used to discharge emissions from the 15 processes. As identified in Table 2, air streams from Cathode-1 through Cathode-7 are combined after control and prior to being discharged to the atmosphere through Stack A1, air streams from Cathode-9 and Cathode-13 are combined after control and prior to being discharged through Stack A2, and air streams from Cathode-11 and Cathode-12 are combined after control and prior to being discharged through Stack A9. All other stacks serve individual processes.

Table 2. Summary of Emission Points

Process Operation	Description ^(a)	Dust Collector	After Filter	Stack
Cathode-1		DF-1		A1
Cathode-5		DF-5	AF-2	
Cathode-3		DF-3	AF-1	
Cathode-2		DF-2	AF-3	
Cathode-4		DF-4		
Cathode-6		DF-6		
Cathode-7		DF-7		
Cathode-9		DF-12, DF-8	AF-4	A2
Cathode-13		DF-8	AF-7	
Cathode-10		DF-9	AF-5	A3
Cathode-8				A4
Cathode-14				A6
Cathode-11				
Cathode-11		DF-10	AF-6	A9
Cathode-12				
Cathode-15		DF-13	AF-8	A10

a. The process descriptions are considered trade secret information.

Figure 1 presents a schematic of the process flow through the LIB plant. (The process descriptions in Figure 1 are considered trade secret information). Raw materials (the non-HAP material and the precursor material) enter the process on the left side of the schematic and are processed from left to right. The numerous low-flow dust filters, as well as the after filters, are shown connected to process operations identified in Table 2. As illustrated in Figure 1, the LIB plant consists of a large number of enclosed and intricately-connected processes.

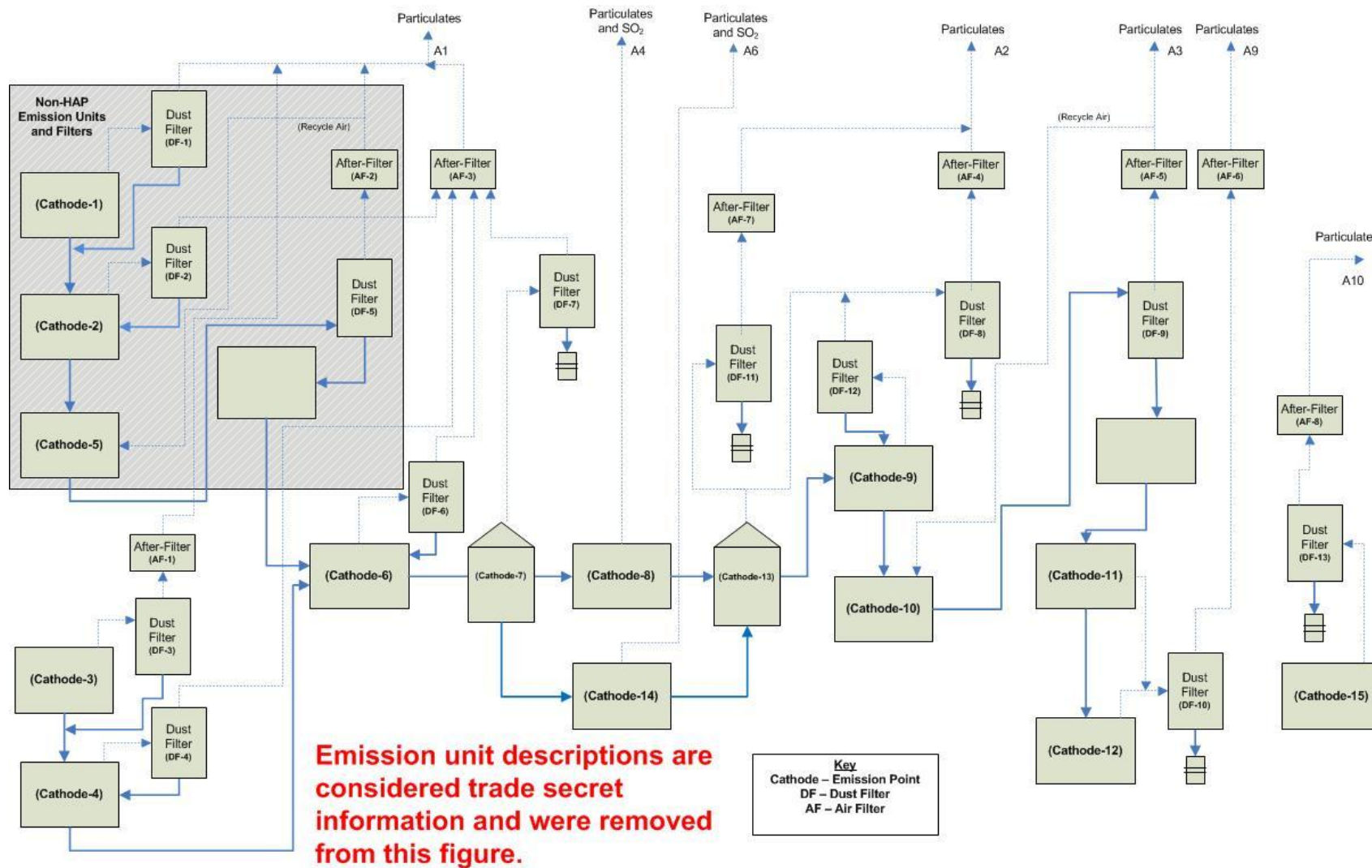


Figure 1. Process flow diagram for the BASF Lithium Ion Battery Plant.

2.2

LIB PLANT AIR CAPTURE AND FLOW SCHEMES

Process equipment are constructed as fully-enclosed units to completely eliminate fugitive loss of raw or process materials. Material transfer between equipment units takes place through enclosed pipe or conveyors. Table 3 describes the properties of the capture systems that have been incorporated into the LIB plant operations. A large portion of the LIB plant is occupied by the sagger conveyor system that receives raw material for delivery to the two kilns and transports processed material to the unloading station after the kilns. The sagger conveyor system is located within a three-story housing that operates under negative pressure and functions as a permanent total enclosure (PTE) to capture all escaping air for delivery to various fabric filtration systems. The two kilns are isolated from the PTE by kiln entry and exit point airlocks that prevent the air in the housing from entering the either kiln.

The two mills are the largest individual processes from an air volume standpoint. These mills (Cathode-5 and Cathode-10) incorporate state-of-the-art high-efficiency cyclones/collection vessels as intermediate product capture devices to separate most of the material from the air stream prior to passing through the filters. A majority of the air stream exiting the mill filters is recycled back to the mills to maintain sufficient flow of dry air through the mills to avoid moisture uptake by the process material. The only air added to the recycle loop is fresh dry air used to flush seal gaps around rotating parts of the mill and a small amount as entrained air with the process material. The balance of added air and recycle air results in less than 10 percent of the air stream exiting the mill filters that must be vented to the atmosphere to maintain the required recycle air flow rate.

Minimum air flows are maintained from all other process equipment to all filters (air flow rates through individual filters range from 30 cubic feet per minute [cfm] to 2,350 cfm), so as to minimize dust entrainment in the airstream and minimize the air-to-cloth ratios (as shown in Table 3), ultimately maximizing the degree of control. All of the separated material is either returned directly to the process from which it originated or collected in a plastic-lined drum for reuse in subsequent processing. To further prevent potential material loss, all process equipment equipped with a dust filter, except the non-HAP metal carbonate unloading operation, are exhausted through a subsequent in-line after filter prior to being discharged to the atmosphere. These after filters, some of which are high efficiency particle air (HEPA) filters, were added to the HAP-containing processes to provide a continuous secondary layer of control should a malfunction of a primary control/recovery device occur.

Table 3. PM Capture and Filter Design Parameters for HAP-containing Process Equipment

Process Operation	Equipment Description	Equipment Discharge/Transfer Mechanism	Source of Exhaust Air	Filter Design Air-to-Cloth ratio
Cathode-1	Not in HAP service			
Cathode-5	Not in HAP service			
Cathode-3	Standard fully-enclosed Supersack handling bin (off-the-shelf)	Attached via hard pipe to Cathode-4	Induced draft acting as an inductor to assist in material transfer	4.0
Cathode-2	Not in HAP service			
Cathode-4	Standard fully enclosed hopper with rotary discharge valve (off-the-shelf)	Hard pipe/short screw conveyor to Cathode-6	Displaced air during Cathode-3 operation	1.8
Cathode-6	Standard fully-enclosed mixer (off-the-shelf)	Hard pipe to Cathode-7 feed hopper/short screw conveyor	Small induced draft to clear mixer	1.8
Cathode-7	Three-story PTE for containing sagger conveyor (loading, unloading, cleaning) and kiln airlock (field constructed)	Dropped via hard pipe to Cathode-9	Induced draft to maintain negative pressure in housing; multiple pick-up points	1.9
Cathode-9	Standard fully-enclosed crusher (off-the-shelf)	Hard pipe to enclosed feed bin equipped with short screw conveyor; rotary valve discharge to Cathode-10.	Displaced air when transferring material to Cathode-10	1.9
Cathode-13	Three-story PTE for containing sagger conveyor (loading, unloading, cleaning) and kiln airlock (field constructed)	Dropped via hard pipe to Cathode-9	Induced draft to maintain negative pressure in housing; multiple pick-up points	1.9
Cathode-10	Standard, fully-enclosed mill (off-the-shelf)	Air conveyed to product collector for transfer via hard pipe to Cathode-11	Intermediate product conveying air	3.6
Cathode-8	Fully-enclosed indirect-heated dryer with airlock (field constructed)	Inlet and outlet airlocks to accommodate sagger conveyor	Airlock exhaust and small induced draft to maintain negative pressure in kiln	none
Cathode-14	Fully-enclosed indirect-heated dryer with airlock (field constructed)	Inlet and outlet airlocks to accommodate sagger conveyor	Airlock exhaust and small induced draft to maintain negative pressure in kiln	none
Cathode-11	Standard fully enclosed hopper with screw discharge (off-the-shelf)	Hard pipe to Cathode-12	None	1.8
Cathode-12	Fully-enclosed packaging station (off-the-shelf)	Material is completely packaged prior to transfer	Small induced draft to clear enclosure	1.8
Cathode-15	Central Vacuum Unit (off-the-shelf)	Dust is collected in receiver bin	Vacuum unit	2.2

2.3 LIB PLANT EMISSION CALCULATIONS

Table 4 presents a summary of uncontrolled and controlled potential PM and HAP emissions for each LIB plant processes as well as each stack after air streams are combined. (Process descriptions in this table are considered trade secret information). These emission rates were originally presented in the LIB plant PTI applications cited in Section 1 of this report. Potential uncontrolled emissions are based on uncontrolled AP-42 emission factors for metallic mineral processing, while annual controlled mass emissions (ton/yr) are calculated after applying an assumed control efficiency of 99%, taking into account only the control achieved by the primary dust filters (pulse-jet fabric filters).ⁱ

As noted above, the calculated values presented in Table 4 are to allow comparison to the values originally presented in the LIB plant PTI. These values are for illustration only, and caution is warranted when attempting to extrapolate the calculated results for other uses. The primary reason for this caution is that the calculated values present an indication of the outlet conditions from the controlled processes, but the values themselves are not completely accurate. The algebraic relationship between hourly mass inlet and outlet loadings inherently produce higher calculated control efficiencies with higher inlet mass rates. Additionally, consistency of results between this calculated efficiency and a calculated outlet concentration cannot be maintained between identical fabric filtration systems. This is because for a given combination of filter design and dust loading, the overall efficiency of a fabric filter is more likely to vary with inlet particulate mass loading (i.e., pounds per hour) whereas the outlet particle concentration (i.e., grains per cubic foot) from a fabric filter is nearly constant.ⁱⁱ

The algebraic anomaly around control efficiency calculations can be demonstrated by comparing the controlled emission rates for Cathode-5 and Cathode-10 in Table 4. The fabric filters associated with these two processes (DF-5 and DF-9, respectively) are identical in all ways (i.e., manufacturer, design, fabric filter bag model), and the inlet concentrations

ⁱ Compilation of Air Pollutant Emission Factors, AP-42, Fifth Edition (8/82). Volume I, Section 11.24: Metallic Minerals Processing

ⁱⁱ *Stationary Source Control Techniques Document for Fine Particulate Matter*, Air Quality Strategies and Standards Division, U.S. EPA, October 1998. <http://www.epa.gov/ttn/catc1/dir1/finepmtech.pdf>

are nearly the same. Because DF-5 and DF-9 are based on the exact same design criteria (air-to-cloth ratio), the outlet PM concentrations for the units should be the same. However, using the controlled PM emission rates (based on 99% control) and air flow rates provided in Table 4 for DF-5 and DF-9 results in a calculated PM concentration of 0.0043 gr/dscf for DF-5 and 0.0054 gr/dscf for DF-9. As per the USEPA document cited above, the outlet concentration of DF-9 should be the same as that for DF-5 (because the filter designs are the same), and the control efficiency of DF-9 should be higher than that of DF-5 (because the inlet mass loading is twice as high in DF-9 as in DF-5).

Controlled concentrations (grains per dry standard cubic foot [gr/dscf] of gas) are calculated based on the annual controlled mass emissions and the outlet gas flow rates reported in Table 4. Due to the conservative nature of the emission factors and assumed control efficiency, both the uncontrolled and controlled emissions are higher than would actually be expected. This is especially true for the mills that employ specially-designed high-efficiency cyclones/collection vessels for material separation prior to the dust collector (PM separation in these high-efficiency cyclones is likely not accounted for in the AP-42 emission factor that was established in 1982.) In addition, no additional control has been applied to account for performance of the after filters.

As seen in Table 4, the total uncontrolled HAP emission rate is 46.6 ton/year. The individual HAP component of the uncontrolled emission rate varies depending on the product formulation. The largest individual HAP metal component in the precursor material for any product is nickel, and the largest fraction of nickel in any product is 50 percent. The precursor material is added to the lithium carbonate at a ratio of approximately 7 to 3 (i.e., 70 % precursor). The calcination process that occurs within the kilns chemically combines the raw materials into a single compound. Although the new compound is less than 100 percent element HAP, the Clean Air Act of 1990 defines the metal-bearing HAP as the HAP compound. Thus, the entire quantity of material leaving the kiln is considered the HAP compound (i.e., a compound of nickel, cobalt, and manganese). Therefore, the largest single HAP uncontrolled emission rate is 46.3 ton/year of nickel compound, assuming continuous manufacturing of the product containing the largest ratio of nickel. This emission rate was calculated assuming the material HAP fraction in emissions from Cathode-3 and Cathode-4 are 50 percent nickel, emissions from Cathode-6 and Cathode-7 are 35 percent nickel, and emissions from the kilns and all subsequent process operations (i.e., Cathodes-8 through 14) are 100 percent nickel compounds.

Table 4. Summary of LIB Plant Potential Uncontrolled and Controlled Emissions

Process Operation	Description ^(a)	Potential Uncontrolled Emissions		Dust Collector ID	Controlled Emissions ^(b)		Outlet Gas Flow Rate (acfm)	Stack ID	Controlled Emissions at Outlet of Stack ^(b)			
		ton/yr			ton/yr				ton/yr		gr/dscf ^(c)	
		PM	HAP ^(d)		PM	HAP			PM	HAP	PM	HAP
Cathode-1		0.10	0	DF-1	0.0010	0	300	A1	0.24 ^(f)	0.0071	0.0019	0.0001
Cathode-5		22.9	0	DF-5	0.23	0	1,423 ^(e)					
Cathode-3		0.17	0.17 ^(g)	DF-3	0.0017	0.0017	300					
Cathode-2		0.32	0	DF-2	0.0032	0	1,300 ⁽ⁱ⁾					
Cathode-4		0.17	0.17 ^(g)	DF-4	0.0017	0.0017						
Cathode-6		0.26	0.18 ^(h)	DF-6	0.0026	0.0018						
Cathode-7		0.26	0.18 ^(h)	DF-7	0.0026	0.0018						
Cathode-9		0.62	0.62	DF-12 / DF-8	0.0062	0.0062	1,300	A2	0.0080	0.0080	0.0001	0.0001
Cathode-13		0.19	0.19	DF-8 / DF-11	0.0018	0.0018	116					
Cathode-10		44.5	44.5	DF-9	0.44	0.44	2,213 ^(e)	A3	0.44 ^(f)	0.44	0.0054	0.0054
Cathode-8		0.13	0.13 ^(j)	none	0.13	0.13	3,500	A4	0.13	0.13	0.0010	0.0010
Cathode-14		0.13	0.13 ^(j)	none	0.13	0.13	3,500	A6	0.13	0.13	0.0010	0.0010
Cathode-11		0.19	0.19	DF-10	0.0037	0.0037	2,350	A9	0.0037	0.0037	0.0042	0.0042
Cathode-12		0.19	0.19									
Cathode-15		0.002	0.002	DF-13	0.0015	0.0015	208	A10	0.0015	0.0015	0.0049	0.0049
TOTAL		70.2	46.6		0.96	0.73			0.96	0.73		

Footnotes for Table 4 are defined on the following page.

Footnotes for Table 4:

- a. **The process descriptions are considered trade secret information.**
- b. Controlled emissions account for dust filter control efficiency (99% was assumed), but do not account for additional reductions achieved in the after filters.
- c. The outlet grain loadings identified for each process operation do not represent the design loading for the associated control device; the outlet grain loadings were calculated based on the controlled emission rate, which was conservatively assumed to be 99% control, and the maximum air flow rate (see Subsection 2.3 for more detail.)
- d. Total HAP emissions include nickel/manganese/cobalt compounds.
- e. The majority of the air flow must be returned to the process (see Subsection 2.2 for more detail).
- f. Assuming 90% of the air flow is recycled to the mills, the controlled PM emission rate for stack A1 is 0.036 ton/yr and for stack A3 is 0.044 ton/yr.
- g. The precursor material loaded to the system in Cathode-3 is 100% total HAP with a maximum individual HAP content of 50% (nickel – see Subsection 2.3 on pg. 11 for more detail).
- h. The material processed in Cathode-6 and -7 has a maximum precursor content of 70% which results in a total HAP content of 70% and maximum individual HAP content of 35% (nickel – see Subsection 2.3 on pg. 11 for more detail).
- i. The air flow rate through the fabric filters associated with Cathodes-2, -4, -6, and -7 are regulated by individual pressure control loops that control the blower output to maintain the pressure set-point. The pressure set-points for Cathodes-2, -4, and -6 maintain maximum air flow rates of 30 acfm with the balance air flow through Cathode-7.
- j. The calcination process that occurs in the kilns chemically combines the raw materials into a single compound; as such, the material exiting the kiln is considered a single metal HAP compound based on the definition of metal-bearing HAP in the Clean Air Act of 1990 (see Subsection 2.3 on pg. 11 for more detail).

EVALUATION OF AVAILABLE CONTROL TECHNOLOGIES

In accordance with 40 CFR 63.43(d)(1) and (2) (reproduced in Appendix A), MACT requirements recommended by an applicant must not be less stringent than the emission control which is achieved in practice by the best controlled similar source. A case-by-case MACT analysis must define a control strategy, based upon available information, that can achieve the maximum degree of reduction in emissions of HAP. In the hierarchy of air pollution control strategies, therefore, a MACT control strategy would represent the ultimate degree of control achievable. An applicant must also determine whether stricter controls are achievable. This determination can be facilitated by reviewing emission control concepts established for similar sources by other regulatory programs such as New Source Review and New Source Performance Standards.

The following sections describe the various information sources investigated, as recommended by OEPA, to ensure that all possible control strategies were identified that could feasibly be applied to the LIB plant operations to achieve the maximum degree of emissions reduction. When reviewing information in this section, as well as Section 4 that follows, the reader should be cognizant of the original intention of U.S. Environmental Protection Agency (USEPA) with respect to data collection for a case-by-case MACT evaluation. While every effort was made to collect complete and relevant information, the use of the information is guided by USEPA's intention, as stated in the preamble to the final case-by-case MACT rule:

The EPA wishes to clarify that the requirement in §63.43(e)(2)(vi) to list emission rates is intended as background information to enable the permitting authority to identify the pollutants requiring MACT controls. The EPA recognizes that there is often a significant effort required to obtain precise estimates of HAP emission rates and speciations. The EPA does not intend in this paragraph to require a greater level of detail than is necessary for evaluating applicability and emission control issues. (61 FR 68393, December 27, 1996)

3.1

SUMMARY OF AVAILABLE CONTROL TECHNOLOGIES

The USEPA Clean Air Technology Center (CATC) website maintains Technical Bulletins and Air Pollution Technology Fact Sheets for a variety of control technologies. A review of the Technical Bulletins and Fact Sheets identified several technologies capable of controlling PM, PM with an aerodynamic diameter less than 10 microns (μm) (PM10), PM with an aerodynamic diameter less than 2.5 microns (PM2.5), and particle-phase HAP (PM-HAP) emissions.

Table 5 presents a summary of CATC-identified PM control technologies and the expected control efficiencies. Table 5 shows that a new baghouse/fabric filter will commonly operate with a control efficiency of 99% and greater. The same is shown for a new electrostatic precipitator (ESP). Table 5 also shows that a wet scrubber or cyclone will operate with a maximum control efficiency equal to the low range of control achieved by a fabric filter or ESP. Thus, one can conclude that further consideration of technology for this case-by-case MACT can be limited to either a fabric filter or ESP. (As concluded in Section 4, however, similar sources employ fabric filtration.) The following subsections provide additional discussion of fabric filters and, to a lesser extent, ESPs. A brief description of a cyclone is also included because the mills incorporate a high-efficiency cyclone as an integral part of the process. Finally, a description of extended media is included to describe the HEPA after filters.

Table 5. Summary of PM and PM-HAP Control Technologies and Control Efficiencies

Control Category	Control Type	Pollutant Removal Efficiency (%)		
		PM	PM10	PM2.5
Baghouse/Fabric Filter	Mechanical Shaker	Older existing equipment: 95 to 99.9 New equipment: 99 to 99.9		
	Pulse-Jet			
	Reverse-Air/Reverse-Jet			
Dry Electrostatic Precipitator (ESP)	Wire-Pipe	Older existing equipment: 90 to 99.9 New equipment: 99 to 99.9		
	Wire-Plate			
Wet ESP	Wire-Pipe	Older existing equipment: 90 to 99.9 New equipment: 99 to 99.9		
	Wire-Plate			
Wet Scrubber	Condensation			99+
	Impingement-Plate/Tray-Tower	50 to 99		
	Mechanically-Aided	80 to 99		
	Orifice	80 to 99		
	Packed-Bed/ Packed-Tower		50 to 95	
	Spray-Chamber/Spray-Tower	70 to 99		
	Venturi	70 to 99		
Cyclone	Conventional	70 to 90	30 to 90	0 to 40
	High Efficiency	80 to 99	60 to 95	20 to 70
	High Throughput	80 to 99	10 to 40	0 to 10

3.1.1 *Baghouse/Fabric Filter*ⁱⁱⁱ

A fabric filter unit consists of one or more isolated compartments containing rows of fabric bags or cartridges. PM-laden gas passes through the fabric where the particles are retained on the upstream face of the bags, and the cleaned gas stream is vented to the atmosphere. The filter operates by cycling between long periods of filtering and short periods of cleaning. During cleaning (either mechanical or with air), dust that has accumulated on the bags is removed from the fabric surface and deposited in a hopper. (In the LIB plant, this dust is recovered for reintroduction back into the process.)

Fabric filters collect PM with sizes ranging from submicron to several hundred microns in diameter at efficiencies generally in excess of 99 or 99.9 percent. The layer of dust, or dust cake, collected on the fabric is primarily responsible for such high efficiency, as it serves as a barrier that traps PM as they travel through the cake. Fabric filters are used where high-efficiency PM collection is required.

The major operating feature of fabric filters that distinguishes them from other gas filters, such as HEPA filters, is the ability to renew the filtering surface periodically by cleaning. Fabric filters are usually made of woven or (more commonly) needle-punched felts sewn to the desired shape, mounted in a plenum with special hardware, and used across a wide range of dust concentrations.

Pulse-jet cleaning of fabric filters can treat high dust loadings, operate at constant pressure drop, and occupy less space than other types of fabric filters. Because bags cleaned by pulse-jet do not need to be isolated for cleaning, pulse-jet cleaning fabric filters do not need extra compartments to maintain adequate filtration during cleaning. Also, because of the intense and frequent nature of the cleaning, they can treat higher gas flow rates with higher dust loadings. Consequently, fabric filters cleaned by pulse jet can be smaller than other types of fabric filters in the treatment of the same amount of gas and dust, making higher gas-to-cloth ratios achievable.^{iv}

ⁱⁱⁱ EPA Air Pollution Control Cost Manual, Sixth Edition, EPA/452/B-02-001, January 2002, http://www.epa.gov/ttnecat1/dir1/c_allchs.pdf

^{iv} Stationary Source Control Techniques Document for Fine Particulate Matter, Air Quality Strategies and Standards Division, U.S. EPA, October 1998. <http://www.epa.gov/ttnecat1/dir1/finepmttech.pdf>

Important process variables include particle characteristics, gas characteristics, and fabric properties. The most important design parameter is the air- or gas-to-cloth ratio and the usual operating parameter of interest is pressure drop across the filter system^v. The gas-to-cloth ratio has a major effect on particle collection mechanisms. This is a ratio of the volumetric flow rate of gas per unit of filtering area, and is usually expressed in the units of cubic feet per minute of gas per square foot of fabric [(ft³/min)/ft²]. Higher gas-to-cloth ratios allow for smaller fabric filters, but as the gas-to-cloth ratio increases, there is increased pressure drop, increased particle penetration, blinding of fabric, more frequent cleaning, and reduced bag life. Table 6 presents recommended gas-to-cloth design conditions for various industrial dusts.

Table 6. Gas-to-Cloth Design Ratios for Pulse-jet Fabric Filters

Dust	Gas-to-Cloth Ratio for Pulse-jet Felt Fabric (acfm/ft ² of net cloth area)
carbon black, graphite, fly ash, iron sulfate, lead oxide, soap, detergents, talc	5 to 6
alumina, bauxite, coal, cement, fertilizer, iron oxide, limestone, paint pigments, plastics, silica, starch	7 to 8
asbestos, clay, cosmetics, enamel frit, feldspar, gypsum, iron ore, lime, mica, paper, quartz, rock dust, sand, spices	9 to 11
cocoa, chocolate, feeds, grain, flour, leather dust, sawdust, slate, sugar	12 to 14

Source: Table 1.1, EPA Air Pollution Control Cost Manual, Sixth Edition, January 2002

3.1.2 *Electrostatic Precipitator*

An ESP is a PM control device that uses electrical forces to move the PM out of the flowing gas stream and onto collector plates. The PM is given an electrical charge by forcing them to pass through a corona, a region in which gaseous ions flow. The electrical field that forces the charged PM to move comes from electrodes maintained at high voltage in the center of the flow lane. Resistivity of the PM is a key factor influencing the successful use of an ESP, because the PM collected on the ESP plates or wires must be removed without re-entraining it into the gas stream. PM can become reentrained when the electrical charge is retained by the particle such as occurs when handling high-resistivity materials. This

^v EPA Air Pollution Control Cost Manual, Sixth Edition, EPA/452/B-02-001, January 2002, http://www.epa.gov/ttnecat1/dir1/c_allchs.pdf

difficulty can be lessened by conditioning the gas stream with water and through the use of a wet ESP, but these mitigations make the collected PM less amenable to re-introduction into the production process than particles collected from a dry control system.

3.1.3 *Cyclone*

Cyclones operate to separate PM from a gaseous stream through the use of centrifugal forces. Particle-laden gas is made to rotate in a decreasing diameter pathway forcing solids to the outer edge of the gas stream for deposition into the bottom of the cyclone. Because different-sized particles display differing inertial properties, cyclones can also be used to classify materials by particle size. Higher efficiency cyclones are designed to achieve high control of smaller particles, but come with higher pressure drops, which require higher energy costs to move the exhaust gas through the cyclone.

3.1.4 *Extended Media*

In addition to the PM control devices discussed above, extended media filters, such as HEPA and ultra-low penetration air (ULPA) filters, are utilized in situations where high collection efficiency of submicron PM is required, where toxic or hazardous PM cannot be cleaned from the filter, or where the PM is difficult to clean from the filter. HEPA and ULPA filters are installed as the final component in a PM collection system, downstream from other PM collection devices such as ESPs or baghouses.

HEPA filters are composed of a mat of randomly arranged fibers. The fibers are typically composed of fiberglass and possess diameters between 0.5 and 2.0 μm . The small fiber diameter and high packing density of the filter media allow for the efficient collection of submicron PM. HEPA and ULPA filters are generally not cleaned, because a dynamic cleaning system would likely prohibit the filter from maintaining its rated efficiency. The dust cake that forms on the filter media from the collected PM will increase its collection efficiency. After sufficient dust cake forms on the filter, however, the air flow rate will decrease to the point that prevents adequate air flow, and the filter must be replaced and properly disposed.

HEPA filters, as defined by the DOE standard adopted by most American industries, remove at least 99.97% of airborne particles 0.3 μm in diameter.^{vi}

3.2 *DATA AVAILABLE FROM THE USEPA CONTROL TECHNOLOGY CENTER*

The USEPA's Air Pollution Control Technology Center (APCTC) conducts third party verification of commercial-ready technologies that control stationary and mobile air pollution sources and mitigate the effects of indoor air pollutants. The APCTC has verified technologies in a range of categories, including:

- Baghouse filtration products
- Dust suppression and soil stabilization products
- Emulsified fuels
- Indoor air quality products
- Mobile sources devices
- Mobile sources fuels
- Mobile sources selective catalytic reduction
- Nitrogen oxide (NO_x) control technologies for stationary sources
- Outdoor wood-fired hydronic heaters
- Paint overspray arrestors
- Volatile organic compounds (VOCs) emission control technologies

The baghouse filtration products category is the only technology category tested that is relevant to the type of emissions (particle-phase) generated by the LIB plant operations. This program area was designed to evaluate the performance of particulate filters for fine-particle emission control. Performance testing of filtration performance was conducted by the APCTC during four separate rounds of testing: initial verifications conducted in 2000, a second round of verifications conducted in 2001, a third round in 2005 through 2007, and a final round in 2011 through 2012.

During each performance test, a small swatch of the fabric filter was tested in a test apparatus (i.e., not an actual baghouse in operation at an industrial facility). While the performance testing conducted on the fabric filter swatches do not directly translate to the efficiency of a particular

^{vi} <http://www.iaqsource.com/article.php/what-is-a-hepa-filter-and-what-is-not-a-hepa-filter/?id=20>

baghouse in practice, the results demonstrate continuous improvement in the performance of the verified fabrics over the past decade.^{vii} As such, fabric filters equipped with newer filter media will have a greater control efficiency than fabric filters equipped with older filter models.

The dust collectors at the LIB plant employ the latest in fabric filtration technology. As an example, the dust filters used for the mills (i.e., the largest contributors to the uncontrolled emission estimate at the LIB plant) are equipped with latest generation of filter media manufactured by the Donaldson Company, Inc. (Donaldson), Tetratex Extreme PTFE-Membrane (ePTFE). Donaldson actively participated in each round of the baghouse filtration products verification studies by the APCTC. In fact, three of the nine filter samples tested during the final round of verification studies were samples of Donaldson's Tetratex ePTFE filter technology. Each of these three filter samples resulted in measured concentrations below the detection limit of the study.

^{vii} The Evolution of Improved Baghouse Filter Media as Observed in the Environmental Technology Verification Program, Paper #176, presented at the Air & Waste Management Association 101st Annual Conference. June 2008. <http://www.epa.gov/etv/pubs/600etv08023.pdf>

EVALUATION OF SIMILAR SOURCES

In accordance with the principles of MACT determinations specified in 40 CFR 63.43(d), the MACT requirements shall not be less stringent than the emission control which is achieved in practice by the best controlled similar source. Similar source, as defined in §63.43, means a stationary source or process that has comparable emissions and is structurally similar in design and capacity to a constructed or reconstructed major source such that the source could be controlled using the same control technology.

The preamble to the 112(g) case-by-case MACT rule provides two criteria that should be used when determining if a source is considered similar: 1) whether the two sources have similar emissions, and 2) whether the source can be controlled with the same type of control technology. The preamble goes on to classify emission sources as one of five different types: 1) process vent or stack discharges, 2) equipment leaks, 3) evaporation and breathing losses, 4) transfer losses, and 5) operational losses. These five types of emission sources can serve as a general guide in identifying available control options while also considering the concentration and the type of constituents of a gas stream. USEPA also states that while two pieces of apparatus can be classified within the same emission source type, this does not automatically mean that the emission points can be controlled using the same type of control technology. In fact, the preamble explicitly states that “the EPA recognizes that control efficiencies across similar sources may be different. The permitting authority is expected to use its judgment in determining when operating conditions are comparable across emission units.”^{viii}

The following subsections summarize the evaluation of available information on emission controls that are achieved in practice by similar sources. Per USEPA guidance, this evaluation considered the following factors: the volume and concentration of emissions, the type of emissions, the similarity of emission points, and the effectiveness of controls relative to the effectiveness of those controls at the LIB plant, as well as other operating conditions.^v

^{viii} Federal Register, Volume 61, No. 250. Hazardous Air Pollutants: Regulations Governing Constructed or Reconstructed Major Sources, Final Rule. pgs. 68394 and 68395. December 27, 1996.

4.1

SIMILAR SOURCES WITHIN THE LIB INDUSTRY

Of the similar source evaluation factors identified by USEPA and listed above, BASF considers the type of emissions and the similarity of emission points as the most relevant factors. As noted earlier in this report, the US DOE is supporting growth in the LIB industry and tracks current process development. Because this development represents the activity of the most relevant similar sources to the LIB plant, a nationwide search was conducted to identify facilities with manufacturing operations similar to the LIB plant. Such facilities would potentially be considered in the same MACT source category as the LIB plant if one was listed by USEPA. Using the US DOE activity as a starting point, two general types of potentially similar facilities were identified: battery material manufacturers and battery assemblers. Appendix B presents a summary of the facilities identified in this search. The types of operations present at these facilities (i.e., raw material handling and processing/conditioning) were determined to represent the most valid comparison to the LIB plant operations. Table 7 lists the permitted battery material manufacturers and battery assembly facilities identified in the search and summarizes the types of operations present at each facility as well as the permitted control requirements, if available.

In all cases except one, the similar sources listed in Table 7 achieve PM control through the use of a fabric filter or HEPA filter or combination of both. Table 7 shows that sources within the LIB industry using a fabric filtration system achieve the highest degree of control.

Table 7. Similar Sources at Permitted Battery Material Manufacturers and Battery Assembly Facilities

Company	HAP Major or Minor Source?	Activity	Operations	Control Device	Emission Limit ^(a) (gr/dscf)
A123 Systems - Romulus, MI	minor	manufacture nano-iron phosphate cathode powder	receiving, handling, milling, mixing, and weighing	fabric filter	0.01
DOW-Kokam - Midland Battery Park, MI	minor	manganese oxide cathode / graphite LIB assembly	dry ingredient material handling and mixing	dust collectors and HEPA filters	0.001
EnerDel - Indianapolis, IN	synthetic minor	LIB assembly	mixers	fabric filter	0.03
EnerG2, Inc. - Albany, OR	minor	manufacture high energy density nano-carbon	milling	fabric filter	See footnote below. ^(b)
			product bagging	HEPA filter	
ERACHEM Comilog, Inc. - Riviera Beach, MD	minor	manufacture manganese carbonates	milling, classifier, material handling and transfer, and roaster/calciner,	fabric filter	0.03
LG Chem Michigan Incorporated - Holland, MI	minor	manganese-based cathode material LIB assembly	material metering and mixing	fabric filter	0.001 to 0.003
BASF Corporation - Troy, MI	minor	manufacture nickel metal hydride battery material	bulk bag unloading, mixing	fabric filter and HEPA filter	0.005
Rockwood Lithium - Kings Mountain, NC	synthetic minor	manufacture Li ₂ CO ₃ and LiOH	material handling	fabric filter	not applicable (subject only to state PM emission limits based on process weight rate)
Toda America - Battle Creek, MI	minor	manufacture NMC cathode material	raw material handling and mixing, intermediate handling and mixing, and calcination mixing	fabric filter	0.001 to 0.03
			calcination process	wet scrubber	0.001

a. The Michigan PM emission limits are provided in units of lb PM/1,000 lb exhaust. Emission limits were converted to units of gr/dscf using the conversion provided by the Michigan Department of Environmental Quality.

b. The activated carbon process is subject to an overall annual emission limit of 2.6 ton PM/yr. PM emissions from any air contaminant source (other than fuel burning and fugitive emission sources) may not exceed 0.1 gr/scf.

4.2

***SUMMARY OF CONTROL TECHNOLOGY DETERMINATIONS
DOCUMENTED IN USEPA'S RACT/BACT/LAER CLEARINGHOUSE
FOR SIMILAR SOURCES***

The case-by-case MACT definition of similar source encompasses sources that may exist in other source categories, and, therefore, this evaluation of similar sources must look beyond the LIB industry itself. The USEPA CATC was consulted to aide in this endeavor.

The USEPA maintains a database of control technology determinations made throughout the United States. This database represents the largest compendium available in the field of air pollutant source requirements and control capabilities, and is a useful resource when conducting a nationwide case-by-case MACT analysis. As part of this nationwide control technology search, therefore, the RACT/BACT/LAER Clearinghouse (RBLC) database was queried for all PM determinations from January 1, 2008 to present (longer than a 5-year period). The query returns information for any process that has a PM determination. Each process could include several records for other pollutants as well; therefore, the number of records returned in any query may not all be related to PM. A total of 5,918 records were obtained from the query, downloaded into an Access database, and filtered to list only PM records (approximately 48% of the total records) and exclude records for operations that are not similar to the LIB plant.

Two separate screening methods were employed to evaluate the RBLC records for operations that are similar to the LIB plant. For both of these methods, all records for fuel combustion sources, such as coal, oil, or natural gas-fired boilers, were excluded from further consideration. There are no fuel combustion sources associated with the LIB plant; therefore, these records were removed because they failed the "similar design" criteria. Fuel combustion sources would produce larger volumes of air (i.e., combustion gases) than produced in the LIB plant, and the particulate will be much smaller than found in the LIB plant operations. This initial filtering removed approximately two thirds of the records. The remaining 1,050 PM records were evaluated using both of the following two methods:

1. Filter the PM records by industrial source category (i.e., SIC code) and use engineering judgment and general knowledge of the processes to exclude those not similar to the LIB plant. These records were removed because they failed the "similar design" and/or "similar capacity" criteria. Records excluded using this

method were related to sources such as large material processing and handling sources (e.g., cement and lime kilns), because they are much larger, both in gas volumes and particulate mass loadings, than the types of sources at the LIB plant.

2. Identify the records that report throughput capacity data and exclude all records that have reported hourly or annual throughputs more than 10 times greater than the hourly or annual LIB plant throughput rates. These records were removed because they failed the “similar capacity” criteria.

Appendix C provides additional documentation on the RBLC records review and the two separate methods employed to screen the records that are not similar. The review identified 58 records (sources) that are potentially similar to the LIB plant. The review was unable to fully assess whether these 58 records would be considered similar sources to the BASF LIB plant operations because the RBLC does not contain all of the information needed to assess the previously-stated USEPA evaluation factors (i.e., the volume and concentration of emissions, the type of emissions, the similarity of emission points, and the effectiveness of controls). Nonetheless, the records were evaluated in this assessment because they primarily include material handling processes and other operations with capacities that would be expected to be similar to the LIB plant capacities. Records were obtained from the following Standard Industrial Classification (SIC) groups:

- 2816 - Inorganic Pigments
- 2819 - Industrial Inorganic Chemicals, Not Elsewhere Classified
- 2895 - Carbon Black
- 2899 - Chemicals and Chemical Preparations, Not Elsewhere Classified
- 3211 - Flat Glass
- 3274 - Lime
- 3295 - Minerals and Earths, Ground or Otherwise Treated
- 3312 - Steel Works, Blast Furnaces (Including Coke Ovens), and Rolling Mills
- 3321 - Gray and Ductile Iron Foundries
- 3325 - Steel Foundries, Not Elsewhere Classified
- 3624 - Carbon and Graphite Products

Table 8 presents a summary of these 58 RBLC control technology determinations. Every similar RBLC record that identifies a control technology specifies a baghouse (fabric filter) as the control device

employed by the source. This leads one to conclude that the best controlled similar source employs a fabric filter. Therefore, evaluation of these similar sources yields the same conclusion as derived by review of the LIB industry sources, i.e., the best controlled similar source employs a fabric filter.

Table 8. Summary of Control Technology Determinations Found in RBLC for Similar Sources

Control Type	Total Number of Records	Type of Limit				
		gr/dscf		lb/hr	lb/ton	ton/yr
		0.005	0.01			
No additional control	1			1		
Operating practice	2			2		
Baghouse	55	29	6	13	7	3
TOTAL	58	29	6	13	7	3

4.3

REGULATIONS FOR SIMILAR SOURCES

USEPA has promulgated a variety of control technology standards in recent years for area sources (facilities emitting less than 10 tons per year of any one HAP and less than 25 tons per year total HAP) and major sources (facilities emitting 10 tons per year or more of any one HAP and 25 tons per year or more total HAP). The LIB plant is a major source of HAP based on the uncontrolled emissions of PM-HAP metals; however, the LIB plant does not meet the applicability requirements for any source category that has currently been selected by USEPA for regulation.

The control technology standards promulgated in 40 CFR Part 63 were reviewed to determine whether any promulgated standard is relevant to the LIB plant. Of the 133 NESHAPs promulgated in Part 63 (Subparts F through 7H), only 25 are major source MACT standards that include a standard for PM emissions or a specific metal HAP. The majority of these 25 standards relate to the metallurgical industry or fuel burning sources, which are not similar to the emission units at the LIB plant based on the volume and concentration of emissions and the dissimilarity of emission points. Excluding these source categories, the following list identifies the remaining major source categories with PM standards:

- Lime Manufacturing
- Mineral Wool Production
- Brick and Structural Clay Products Manufacturing
- Clay Ceramics Manufacturing

- Portland Cement Manufacturing
- Asphalt Processing and Asphalt Roofing Manufacturing
- Wool Fiberglass Manufacturing
- Taconite Iron Ore Processing
- Phosphoric Acid

Table 9 presents a summary of the PM emission standards for new units with numeric emission standards for PM under these potentially similar major source categories. Table 9 shows PM grain loading standards ranging from 0.02 to 0.04 gr/dscf and PM emission rates ranging from 0.02 to 0.42 lb/ton product. While the emission units identified in these remaining source categories are not necessarily similar to the LIB plant (e.g., lime and cement manufacturing operations will have much larger design capacities than the LIB plant processes), they aide in understanding USEPA's MACT determinations for source categories involving PM-HAPs.

PM or specific metal HAP standards also exist for 15 area (i.e., non-major) sources. While the LIB plant is defined as a major source of HAP based on uncontrolled emissions, the similar sources identified above in Section 4.2 are minor sources of HAP. Those similar sources that use as feedstock, generate as a byproduct, or produce as a product any one of the urban metal HAP (i.e., arsenic, cadmium, chromium, lead, manganese, or nickel) are subject to the Chemical Manufacturing Area Source (CMAS) rule in Subpart VVVVVV (6V).

Table 9. Summary of PM and PM-HAP Emission Standards

Source Category	40 CFR 63 Subpart	Emission Rate (lb/ton product)	Grain Loading (gr/dscf)
Lime Manufacturing	AAAAA	0.10 (kilns/lime coolers)	0.02 (material handling)
Mineral Wool Production	DDD	0.10 (cupola)	--
Brick and Structural Clay Products Manufacturing	JJJJJ	0.12 (tunnel kiln)	--
Clay Ceramics Manufacturing	KKKKK	0.42 (< 10 ton/hr) or 0.12 (>10 ton/hr) (tunnel kiln)	--
Portland Cement Manufacturing	LLL	0.02	--
Asphalt Processing/ Asphalt Roofing Manufacturing	LLLLL	0.08 (mineral-surfaced) or 0.8 (smooth-surfaced)	--
Wool Fiberglass Manufacturing	NNN	0.5 (furnace)	--
Taconite Iron Ore Processing	RRRRR	--	0.005 (crushing/handling) 0.006 (furnace)
Phosphoric Acid	AA	0.060 (dryer)	0.040 (calciner)

Under the CMAS rule, the affected source is the facility-wide collection of chemical manufacturing production units (CMPU) and applies to all process vents within a CMPU. If metal HAP emissions from all process vents within a CMPU are greater than or equal to 400 pounds per year, the facility must reduce collective uncontrolled emissions of total metal HAP by at least 95 percent by weight by routing emissions from a sufficient number of the metal process vents through a closed-vent system to any combination of control devices. This required degree of control is less stringent than is achievable through the LIB plant design.

In conclusion, none of the identified rules promulgated under 40 CFR 63 present an emission limit that is more stringent than the degree of control achieved by the best controlled similar source.

5 *CASE-BY-CASE MACT DETERMINATION*

5.1 *IDENTIFIED CONTROL TECHNOLOGY THAT ACHIEVES THE MAXIMUM DEGREE OF HAP EMISSION REDUCTION*

As stated throughout this document, 40 CFR 63.43(d) specifies the manner in which a case-by-case MACT analysis must be conducted. In adhering to those specifications, two separate nationwide reviews were conducted to identify the maximum degree of HAP emissions reduction that is achieved at a similar source. While recognizing the limitations noted by USEPA in attempting to identify similar sources, as well as the maximum degree of HAP emission reduction that is achieved in practice, the results of this case-by-case MACT analysis are irrefutable and consistent between the two nationwide searches performed – the best controlled source similar to the LIB plant employs a fabric filter. This conclusion is corroborated by review of data available from the USEPA APCTC.

5.2 *PROPOSED EMISSION LIMITATION*

Pursuant to 40 CFR 63.43(e), an application for a MACT determination must specify a control technology that, if properly operated and maintained, will meet the MACT emission limitation or standard as determined according to the principles set forth in paragraph (d) of that section.

As demonstrated in various sections of this report, a properly designed (appropriate gas-to-cloth ratio) and operated (within the manufacturer's specified pressure drop across the filter system) fabric filter will have an extremely high PM collection efficiency and is considered MACT for the LIB plant. In accordance with 40 CFR 63.43(e), therefore, BASF proposes to use fabric filters for PM and PM-HAP emission control on all LIB plant process operations except the kilns. PM emissions from the kilns are inherently low (0.13 ton/yr and 0.0010 gr/dscf) and control is unnecessary; therefore, no additional control is proposed for the kilns.

Appendix D provides supporting documentation of the manufacturer's equipment specifications for the control equipment and associated blowers at the LIB plant.

5.3 *DISCUSSION OF OTHER ASPECTS OF CASE-BY-CASE MACT*

5.3.1 *Identification of Fabric Filter as MACT*

The data presented in Table 5 demonstrate that fabric filters and ESPs can achieve comparable levels of control. Data presented in Table 7 and Table 8 (i.e., other battery material production permits and the RBLC determinations), however, demonstrate that in practice fabric filters are used at similar sources to achieve the highest degree of HAP emission control. These evaluations of similar sources clearly dictate that fabric filters be considered the MACT control technology.

5.3.2 *Form of the Proposed Emission Limitation*

The proposed emission limitation for the LIB plant takes the form of an equipment design and operational standard. An appropriately designed and operated fabric filter will achieve the highest degree of HAP emission control. Specifications for fabric filters employed at the LIB plant have/will include the appropriate air-to-cloth ratio needed to achieve this HAP emission control. The actual form of the proposed equipment design and operational standard may be specified as follows:

- Process equipment shall be designed, installed, and operated to minimize HAP emissions through the use of closed-pipe conveyance, equipment enclosures, and/or permanent total enclosures with all HAP-laden air from bins and enclosures routed to a fabric filter control device.
- HAP-laden air from all process operations, except for the kilns (Cathode-8 and Cathode-14), shall be routed to a pulse-jet fabric filter control device designed with an air-to-cloth ratio of no more than 5 acfm/ft² of cloth area.
- Fabric filters shall be operated and maintained in accordance with the manufacturer's recommendations, instructions, and operating manual(s).
- Equipment to continuously monitor the pressure drop across each fabric filter shall be properly installed and maintained; this equipment shall be operated when the associated process equipment is in operation, including periods of startup and shutdown. The acceptable pressure drop shall be based upon the manufacturer's specifications.

This approach to a proposed emission limitation is consistent with, and supported by, both the regulatory history of case-by-case MACT and

specific instructions from the OEPA. As stated in OEPA's letter to BASF's Site Director, dated September 30, 2013:

[T]he proposed standard may be an emissions limitation, or if it is not feasible to prescribe or enforce an (*numeric*) emission limitation, the proposed standard may be the employment of a specific design, a work practice, an operational standard, or a combination. (*italic text added*)

This concept is mirrored in both the 112(g) and 112(j) procedures promulgated at 40 CFR 63.43(d)(3) and 40 CFR 63.53(b)(3), respectively. Several important factors must be considered when determining whether a numeric emission limitation can be prescribed or is enforceable. The first of these considerations is USEPA's expressed recognition that direct transfer of control equipment performance from one source to another is not always possible. As declared in the case-by-case MACT preamble:

[t]he EPA recognizes that control efficiencies across similar sources may be different. The permitting authority is expected to use its judgment in determining when operating conditions are comparable across emission units. (61 FR page 68395, Dec 27, 1996)

A second factor to be considered is the inherently low emission rates produced by the process operations in the LIB plant. The high degree of control, coupled with the enclosed processes and low air flow rates will yield very low mass emission rates for processes equipped with control devices. These low rates were previously presented in Table 4 of this report. Generation of these low emission rates will represent an extreme challenge to source testing efforts, making such tests potentially meaningless. This is somewhat witnessed by the observation by the USEPA's APCTC verification test on filter fabrics during which the fabric used by the two LIB plant mills produced results that were below the detectable limit of the test equipment. (This observation was presented previously in Section 3.2 of this report.) USEPA's observation, coupled with the need to perform up to 15 separate emission tests at the LIB plant, makes enforcement of a numeric emission limitation a technical challenge and economically-costly venture. Although not equipped with control devices, the kilns operate with inherently low emissions as well, producing similar compliance demonstration challenges.

Finally, several of the processes in the LIB plant are intermittent operations. For example, the Central Vacuum Unit (Cathode-15) is only

operated during periods of maintenance or after an upset of process equipment. As such, the operation of this process is not regular or predictable, and a numeric emission limit for this process operation is likewise not feasible.

5.4 ***PROPOSED OPERATIONAL/MONITORING STANDARDS***

The following operational standards are proposed to demonstrate continuous compliance with the equipment/operational emission limitation identified above. These proposed MACT standards include operation, monitoring, and recordkeeping requirements for the LIB plant.

1. HAP-laden air from the process operations listed above shall be vented to their respective fabric filter when the process equipment is in operation.
2. Discharges from the fabric filters listed above shall be vented to an after filter whenever the process equipment is in operation.
3. Equipment to continuously monitor the pressure drop across each fabric filter shall be properly installed, operated, and maintained when the controlled process equipment are in operation, including periods of startup and shutdown. The pressure drop across each fabric filter shall be recorded on a daily basis.
4. The monitoring equipment shall be installed, calibrated, operated, and maintained in accordance with the manufacturer's recommendations, instructions, and operating manual(s), unless any modifications are deemed necessary. The acceptable pressure drop shall be based upon the manufacturer's specifications.
5. Whenever the monitored value for the pressure drop deviates from the limit or range established in accordance with this permit, an investigation of the cause of the deviation shall be promptly conducted, and records of the following information for each investigation shall be maintained:
 - a. the date and time the deviation began;
 - b. the magnitude of the deviation at that time;
 - c. the date the investigation was conducted;
 - d. the name(s) of the personnel who conducted the investigation; and
 - e. the findings and recommendations.

6. In response to each required investigation to determine the cause of a deviation, prompt corrective actions shall be conducted to bring the operation of the control equipment within the acceptable range specified in this permit, unless it is determined that corrective action is not necessary and the reasons for that determination and the date and time the deviation ended are documented. Records of the following information for each corrective action taken shall be maintained:
 - a. a description of the corrective action;
 - b. the date corrective action was completed;
 - c. the date and time the deviation ended;
 - d. the total period of time (in minutes) during which there was a deviation;
 - e. the pressure drop readings immediately after the corrective action was implemented; and
 - f. the name(s) of the personnel who performed the work.

Investigation and records required by this paragraph do not eliminate the need to comply with the requirements of OAC rule 3745-15-06 if it is determined that a malfunction has occurred.

CONCLUSIONS

The BASF LIB plant sited at the Elyria, Ohio, facility has been designed to satisfy a growing demand for new energy technology. The plant incorporates state-of-the-art equipment and environmental control strategies that maximize material usage and recovery.

In part because this industry represents a relatively new source category, USEPA has not developed standards specific to the source category, and a new major source of HAP in the industry must apply for a case-by-case MACT determination. This analysis satisfies this case-by-case MACT requirement. BASF will comply with the proposed case-by-case MACT by implementing the equipment/operational emission limitations specified in this analysis. The HAP emission limitation at the BASF LIB plant is the use of fabric filters with design specifications that will achieve the highest degree of HAP emission control. A nationwide search of similar facilities, including other known cathode material manufacturing facilities, yielded results demonstrating that no more stringent emission limitation is achieved at any similar source.

Establishing numeric emission limitations on the operations at the LIB plant is not technically feasible from an enforcement standpoint, nor is it economically feasible to incur the costs associated with testing the large number of process operations in order to demonstrate compliance with an emission limit while yielding undetectable amounts of HAPs. The LIB plant in Elyria, therefore, will operate under equipment design and operational conditions that produce the maximum degree of HAP emission control achievable in practice.

APPENDIX A - CASE-BY-CASE MACT REGULATIONS

40 CFR Part 63--National Emission Standards for Hazardous Air Pollutants for Affected Source Categories

Subpart B--Requirements for Control Technology Determinations for Major Sources

§63.40 Applicability of §§63.40 through 63.44.

(a) Applicability. The requirements of §§63.40 through 63.44 of this subpart carry out section 112(g)(2)(B) of the 1990 Amendments.

(b) Overall requirements. The requirements of §§63.40 through 63.44 of this subpart apply to any owner or operator who constructs or reconstructs a major source of hazardous air pollutants after the effective date of section 112(g)(2)(B) (as defined in §63.41) and the effective date of a title V permit program in the State or local jurisdiction in which the major source is (or would be) located unless the major source in question has been specifically regulated or exempted from regulation under a standard issued pursuant to section 112(d), section 112(h), or section 112(j) and incorporated in another subpart of part 63, or the owner or operator of such major source has received all necessary air quality permits for such construction or reconstruction project before the effective date of section 112(g)(2)(B).

(c) Exclusion for electric utility steam generating units. The requirements of this subpart do not apply to electric utility steam generating units unless and until such time as these units are added to the source category list pursuant to section 112(c)(5) of the Act.

(d) Relationship to State and local requirements. Nothing in this subpart shall prevent a State or local agency from imposing more stringent requirements than those contained in this subpart.

(e) Exclusion for stationary sources in deleted source categories. The requirements of this subpart do not apply to stationary sources that are within a source category that has been deleted from the source category list pursuant to section 112(c)(9) of the Act.

(f) Exclusion for research and development activities. The requirements of this subpart do not apply to research and development activities, as defined in §63.41.

§63.41 Definitions.

Terms used in this subpart that are not defined in this section have the meaning given to them in the Act and in subpart A.

Affected source means the stationary source or group of stationary sources which, when fabricated (on site), erected, or installed meets the definition of "construct a

major source" or the definition of "reconstruct a major source" contained in this section.

Affected States are all States:

- (1) Whose air quality may be affected and that are contiguous to the State in which a MACT determination is made in accordance with this subpart; or
- (2) Whose air quality may be affected and that are within 50 miles of the major source for which a MACT determination is made in accordance with this subpart.

Available information means, for purposes of identifying control technology options for the affected source, information contained in the following information sources as of the date of approval of the MACT determination by the permitting authority:

- (1) A relevant proposed regulation, including all supporting information;
- (2) Background information documents for a draft or proposed regulation;
- (3) Data and information available for the Control Technology Center developed pursuant to section 113 of the Act;
- (4) Data and information contained in the Aerometric Informational Retrieval System including information in the MACT data base;
- (5) Any additional information that can be expeditiously provided by the Administrator; and
- (6) For the purpose of determinations by the permitting authority, any additional information provided by the applicant or others, and any additional information considered available by the permitting authority.

Construct a major source means:

- (1) To fabricate, erect, or install at any greenfield site a stationary source or group of stationary sources which is located within a contiguous area and under common control and which emits or has the potential to emit 10 tons per year of any HAP's or 25 tons per year of any combination of HAP, or
- (2) To fabricate, erect, or install at any developed site a new process or production unit which in and of itself emits or has the potential to emit 10 tons per year of any HAP or 25 tons per year of any combination of HAP, unless the process or production unit satisfies criteria in paragraphs (2)(i) through (vi) of this definition.
 - (i) All HAP emitted by the process or production unit that would otherwise be controlled under the requirements of this subpart will be controlled by emission

control equipment which was previously installed at the same site as the process or production unit;

(ii)(A) The permitting authority has determined within a period of 5 years prior to the fabrication, erection, or installation of the process or production unit that the existing emission control equipment represented best available control technology (BACT), lowest achievable emission rate (LAER) under 40 CFR part 51 or 52, toxics--best available control technology (T-BACT), or MACT based on State air toxic rules for the category of pollutants which includes those HAP's to be emitted by the process or production unit; or

(B) The permitting authority determines that the control of HAP emissions provided by the existing equipment will be equivalent to that level of control currently achieved by other well-controlled similar sources (i.e., equivalent to the level of control that would be provided by a current BACT, LAER, T-BACT, or State air toxic rule MACT determination);

(iii) The permitting authority determines that the percent control efficiency for emissions of HAP from all sources to be controlled by the existing control equipment will be equivalent to the percent control efficiency provided by the control equipment prior to the inclusion of the new process or production unit;

(iv) The permitting authority has provided notice and an opportunity for public comment concerning its determination that criteria in paragraphs (2)(i), (2)(ii), and (2)(iii) of this definition apply and concerning the continued adequacy of any prior LAER, BACT, T-BACT, or State air toxic rule MACT determination;

(v) If any commenter has asserted that a prior LAER, BACT, T-BACT, or State air toxic rule MACT determination is no longer adequate, the permitting authority has determined that the level of control required by that prior determination remains adequate; and

(vi) Any emission limitations, work practice requirements, or other terms and conditions upon which the above determinations by the permitting authority are applicable requirements under section 504(a) and either have been incorporated into any existing title V permit for the affected facility or will be incorporated into such permit upon issuance.

Control technology means measures, processes, methods, systems, or techniques to limit the emission of hazardous air pollutants through process changes, substitution of materials or other modifications;

(1) Reduce the quantity of, or eliminate emissions of, such pollutants through process changes, substitution of materials or other modifications;

(2) Enclose systems or processes to eliminate emissions;

(3) Collect, capture or treat such pollutants when released from a process, stack, storage or fugitive emissions point;

(4) Are design, equipment, work practice, or operational standards (including requirements for operator training or certification) as provided in 42 U.S.C. 7412(h); or

(5) Are a combination of paragraphs (1) through (4) of this definition.

Effective date of section 112(g)(2)(B) in a State or local jurisdiction means the effective date specified by the permitting authority at the time the permitting authority adopts a program to implement section 112(g) with respect to construction or reconstruction or major sources of HAP, or June 29, 1998 whichever is earlier.

Electric utility steam generating unit means any fossil fuel fired combustion unit of more than 25 megawatts that serves a generator that produces electricity for sale. A unit that co-generates steam and electricity and supplies more than one-third of its potential electric output capacity and more than 25 megawatts electric output to any utility power distribution system for sale shall be considered an electric utility steam generating unit.

Greenfield suite means a contiguous area under common control that is an undeveloped site.

List of Source Categories means the Source Category List required by section 112(c) of the Act.

Maximum achievable control technology (MACT) emission limitation for new sources means the emission limitation which is not less stringent than the emission limitation achieved in practice by the best controlled similar source, and which reflects the maximum degree of deduction in emissions that the permitting authority, taking into consideration the cost of achieving such emission reduction, and any non-air quality health and environmental impacts and energy requirements, determines is achievable by the constructed or reconstructed major source.

Notice of MACT Approval means a document issued by a permitting authority containing all federally enforceable conditions necessary to enforce the application and operation of MACT or other control technologies such that the MACT emission limitation is met.

Permitting authority means the permitting authority as defined in part 70 or 71 of this chapter.

Process or production unit means any collection of structures and/or equipment, that processes assembles, applies, or otherwise uses material inputs to produce or store an intermediate or final product. A single facility may contain more than one process or production unit.

Reconstruct a major source means the replacement of components at an existing process or production unit that in and of itself emits or has that potential to emit

10 tons per year of any HAP or 25 tons per year of any combination of HAP, whenever:

- (1) The fixed capital cost of the new components exceeds 50 percent of the fixed capital cost that would be required to construct a comparable process or production unit; and
- (2) It is technically and economically feasible for the reconstructed major source to meet the applicable maximum achievable control technology emission limitation for new sources established under this subpart.

Research and development activities means activities conducted at a research or laboratory facility whose primary purpose is to conduct research and development into new processes and products, where such source is operated under the close supervision of technically trained personnel and is not engaged in the manufacture of products for sale or exchange for commercial profit, except in a de minimis manner.

Similar source means a stationary source or process that has comparable emissions and is structurally similar in design and capacity to a constructed or reconstructed major source such that the source could be controlled using the same control technology.

§63.42 Program Requirements Governing Construction or Reconstruction of Major Sources.

(a) Adoption of program. Each permitting authority shall review its existing programs, procedures, and criteria for preconstruction review for conformity to the requirements established by §§63.40 through 63.44, shall make any additions and revisions to its existing programs, procedures, and criteria that the permitting authority deems necessary to properly effectuate §§63.40 through 63.44, and shall adopt a program to implement section 112(g) with respect to construction or reconstruction of major sources of HAP. As part of the adoption by the permitting authority of a program to implement section 112(g) with respect to construction or reconstruction of major sources of HAP, the chief executive officer of the permitting authority shall certify that the program satisfies all applicable requirements established by §§63.40 through 63.44, and shall specify an effective date for that program which is not later than June 29, 1998. Prior to the specified effective date, the permitting authority shall publish a notice stating that the permitting authority has adopted a program to implement section 112(g) with respect to construction or reconstruction of major sources of HAP and stating the effective date, and shall provide a written description of the program to the Administrator through the appropriate EPA Regional Office. Nothing in this section shall be construed either:

(a)(1) To require that any owner or operator of a stationary source comply with any requirement adopted by the permitting authority which is not intended to

implement section 112(g) with respect to construction or reconstruction of major sources of HAP; or

(a)(2) To preclude the permitting authority from enforcing any requirements not intended to implement section 112(g) with respect to construction or reconstruction of major sources of HAP under any other provision of applicable law.

(b) Failure to adopt program. In the event that the permitting authority fails to adopt a program to implement section 112(g) with respect to construction or reconstruction of major sources of HAP with an effective date on or before June 29, 1998, and the permitting authority concludes that it is able to make case-by-case MACT determinations which conform to the provisions of §63.43 in the absence of such a program, the permitting authority may elect to make such determinations. However, in those instances where the permitting authority elects to make case-by-case MACT determinations in the absence of a program to implement section 112(g) with respect to construction or reconstruction of major sources of HAP, no such case-by-case MACT determination shall take effect until after it has been submitted by the permitting authority in writing to the appropriate EPA Regional Administrator and the EPA Regional Administrator has concurred in writing that the case-by-case MACT determination by the permitting authority is in conformity with all requirements established by §§63.40 through 63.44. In the event that the permitting authority fails to adopt a program to implement section 112(g) with respect to construction or reconstruction of major sources of HAP with an effective date on or before June 29, 1998, and the permitting authority concludes that it is unable to make case-by-case MACT determinations in the absence of such a program, the permitting authority may request that the EPA Regional Administrator implement a transitional program to implement section 112(g) with respect to construction or reconstruction of major sources of HAP in the affected State of local jurisdiction while the permitting authority completes development and adoption of a section 112(g) program. Any such transitional section 112(g) program implemented by the EPA Regional Administrator shall conform to all requirements established by §§63.40 through 63.44, and shall remain in effect for no more than 30 months. Continued failure by the permitting authority to adopt a program to implement section 112(g) with respect to construction or reconstruction of major sources of HAP shall be construed as a failure by the permitting authority to adequately administer and enforce its title V permitting program and shall constitute cause by EPA to apply the sanctions and remedies set forth in the Clean Air Act section 502(I).

(c) Prohibition. After the effective date of section 112(g)(2)(B) (as defined in §63.41) in a State or local jurisdiction and the effective date of the title V permit program applicable to that State or local jurisdiction, no person may begin actual construction or reconstruction of a major source of HAP in such State or local jurisdiction unless:

(c)(1) The major source in question has been specifically regulated or exempted from regulation under a standard issued pursuant to section 112(d), section 112(h) or section 112(j) in part 63, and the owner and operator has fully complied with all procedures and requirements for preconstruction review established by that standard, including any applicable requirements set forth in subpart A of this part 63; or

(c)(2) The permitting authority has made a final and effective case-by-case determination pursuant to the provisions of §63.43 such that emissions from the constructed or reconstructed major source will be controlled to a level no less stringent than the maximum achievable control technology emission limitation for new sources.

§63.43 Maximum Achievable Control Technology (MACT) Determinations for Constructed and Reconstructed Major Sources.

(a) Applicability. The requirements of this section apply to an owner or operator who constructs or reconstructs a major source of HAP subject to a case-by-case determination of maximum achievable control technology pursuant to §63.42(c).

(b) Requirements for constructed and reconstructed major sources. When a case-by-case determination of MACT is required by §63.42(c), the owner and operator shall obtain from the permitting authority an approved MACT determination according to one of the review options contained in paragraph (c) of this section.

(c) Review options. (1) When the permitting authority requires the owner or operator to obtain, or revise, a permit issued pursuant to title V of the Act before construction or reconstruction of the major source, or when the permitting authority allows the owner or operator at its discretion to obtain or revise such a permit before construction or reconstruction, and the owner or operator elects that option, the owner or operator shall follow the administrative procedures in the program approved under title V of the Act (or in other regulations issued pursuant to title V of the Act, where applicable).

(c)(2) When an owner or operator is not required to obtain or revise a title V permit (or other permit issued pursuant to title V of the Act) before construction or reconstruction, the owner or operator (unless the owner or operator voluntarily follows the process to obtain a title V permit) shall either, at the discretion of the permitting authority:

(c)(2)(i) Apply for and obtain a Notice of MACT Approval according to the procedures outlined in paragraphs (f) through (h) of this section; or

(c)(2)(ii) Apply for a MACT determination under any other administrative procedures for preconstruction review and approval established by the permitting authority for a State or local jurisdiction which provide for public participation in the determination, and ensure that no person may begin actual construction or reconstruction of a major source in that State or local jurisdiction

unless the permitting authority determines that the MACT emission limitation for new sources will be met.

(c)(3) When applying for a permit pursuant to title V of the Act, an owner or operator may request approval of case-by-case MACT determinations for alternative operating scenarios. Approval of such determinations satisfies the requirements of section 112(g) of each such scenario.

(c)(4) Regardless of the review process, the MACT emission limitation and requirements established shall be effective as required by paragraph (j) of this section, consistent with the principles established in paragraph (d) of this section, and supported by the information listed in paragraph (e) of this section. The owner or operator shall comply with the requirements in paragraphs (k) and (l) of this section, and with all applicable requirements in subpart A of this part.

(d) Principles of MACT determinations. The following general principles shall govern preparation by the owner or operator of each permit application or other application requiring a case-by-case MACT determination concerning construction or reconstruction of a major source, and all subsequent review of and actions taken concerning such an application by the permitting authority:

(d)(1) The MACT emission limitation or MACT requirements recommended by the applicant and approved by the permitting authority shall not be less stringent than the emission control which is achieved in practice by the best controlled similar source, as determined by the permitting authority.

(d)(2) Based upon available information, as defined in this subpart, the MACT emission limitation and control technology (including any requirements under paragraph (d)(3) of this section) recommended by the applicant and approved by the permitting authority shall achieve the maximum degree of reduction in emissions of HAP which can be achieved by utilizing those control technologies that can be identified from the available information, taking into consideration the costs of achieving such emission reduction and any non-air quality health and environmental impacts and energy requirements associated with the emission reduction.

(d)(3) The applicant may recommend a specific design, equipment, work practice, or operational standard, or a combination thereof, and the permitting authority may approve such a standard if the permitting authority specifically determines that it is not feasible to prescribe or enforce an emission limitation under the criteria set forth in section 112(h)(2) of the Act.

(d)(4) If the Administrator has either proposed a relevant emission standard pursuant to section 112(d) or section 112(h) of the Act or adopted a presumptive MACT determination for the source category which includes the constructed or reconstructed major source, then the MACT requirements applied to the constructed or reconstructed major source shall have considered those MACT

emission limitations and requirements of the proposed standard or presumptive MACT determination.

(e) Application requirements for a case-by-case MACT determination. (1) An application for a MACT determination (whether a permit application under title V of the Act, an application for a Notice of MACT Approval, or other document specified by the permitting authority under paragraph (c)(2)(ii) of this section) shall specify a control technology selected by the owner or operator that, if properly operated and maintained, will meet the MACT emission limitation or standard as determined according to the principles set forth in paragraph (d) of this section.

(e)(2) In each instance where a constructed or reconstructed major source would require additional control technology or a change in control technology, the application for a MACT determination shall contain the following information:

(e)(2)(i) The name and address (physical location) of the major source to be constructed or reconstructed;

(e)(2)(ii) A brief description of the major source to be constructed or reconstructed and identification of any listed source category or categories in which it is included;

(e)(2)(iii) The expected commencement date for the construction or reconstruction of the major source;

(e)(2)(iv) The expected completion date for construction or reconstruction of the major source;

(e)(2)(v) The anticipated date of start-up for the constructed or reconstructed major source;

(e)(2)(vi) The HAP emitted by the constructed or reconstructed major source, and the estimated emission rate for each such HAP, to the extent this information is needed by the permitting authority to determine MACT;

(e)(2)(vii) Any federally enforceable emission limitations applicable to the constructed or reconstructed major source;

(e)(2)(viii) The maximum and expected utilization of capacity of the constructed or reconstructed major source, and the associated uncontrolled emission rates for that source, to the extent this information is needed by the permitting authority to determine MACT;

(e)(2)(ix) The controlled emissions for the constructed or reconstructed major source in tons/yr at expected and maximum utilization of capacity, to the extent this information is needed by the permitting authority to determine MACT;

(e)(2)(x) A recommended emission limitation for the constructed or reconstructed major source consistent with the principles set forth in paragraph (d) of this section;

(e)(2)(xi) The selected control technology to meet the recommended MACT emission limitation, including technical information on the design, operation, size, estimated control efficiency of the control technology (and the manufacturer's name, address, telephone number, and relevant specifications and drawings, if requested by the permitting authority);

(e)(2)(xii) Supporting documentation including identification of alternative control technologies considered by the applicant to meet the emission limitation, and analysis of cost and non-air quality health environmental impacts or energy requirements for the selected control technology; and

(e)(2)(xiii) Any other relevant information required pursuant to subpart A.

(e)(3) In each instance where the owner or operator contends that a constructed or reconstructed major source will be in compliance, upon startup, with case-by-case MACT under this subpart without a change in control technology, the application for a MACT determination shall contain the following information:

(e)(3)(i) The information described in paragraphs (e)(2)(i) through (e)(2)(x) of this section; and

(e)(3)(ii) Documentation of the control technology in place.

(f) Administrative procedures for review of the Notice of MACT Approval. (1) The permitting authority will notify the owner or operator in writing, within 45 days from the date the application is first received, as to whether the application for a MACT determination is complete or whether additional information is required.

(f)(2) The permitting authority will initially approve the recommended MACT emission limitation and other terms set forth in the application, or the permitting authority will notify the owner or operator in writing of its intent to disapprove the application, within 30 calendar days after the owner or operator is notified in writing that the application is complete.

(f)(3) The owner or operator may present, in writing, within 60 calendar days after receipt of notice of the permitting authority's intent to disapprove the application, additional information or arguments pertaining to, or amendments to, the application for consideration by the permitting authority before it decides whether to finally disapprove the application.

(f)(4) The permitting authority will either initially approve or issue a final disapproval of the application within 90 days after it notifies the owner or operator of an intent to disapprove or within 30 days after the date additional information is received from the owner or operator; whichever is earlier.

(f)(5) A final determination by the permitting authority to disapprove any application will be in writing and will specify the grounds on which the disapproval is based. If any application is finally disapproved, the owner or operator may submit a subsequent application concerning construction or reconstruction of the same major source, provided that the subsequent application has been amended in response to the stated grounds for the prior disapproval.

(f)(6) An initial decision to approve an application for a MACT determination will be set forth in the Notice of MACT Approval as described in paragraph (g) of this section.

(g) Notice of MACT Approval. (1) The Notice of MACT Approval will contain a MACT emission limitation (or a MACT work practice standard if the permitting authority determines it is not feasible to prescribe or enforce an emission standard) to control the emissions of HAP. The MACT emission limitation or standard will be determined by the permitting authority and will conform to the principles set forth in paragraph (d) of this section.

(g)(2) The Notice of MACT Approval will specify any notification, operation and maintenance, performance testing, monitoring, reporting and record keeping requirements. The Notice of MACT Approval shall include:

(g)(2)(i) In addition to the MACT emission limitation or MACT work practice standard established under this subpart, additional emission limits, production limits, operational limits or other terms and conditions necessary to ensure Federal enforceability of the MACT emission limitation;

(g)(2)(ii) Compliance certifications, testing, monitoring, reporting and record keeping requirements that are consistent with the requirements of §70.6(c) of this chapter;

(g)(2)(iii) In accordance with section 114(a)(3) of the Act, monitoring shall be capable of demonstrating continuous compliance during the applicable reporting period. Such monitoring data shall be of sufficient quality to be used as a basis for enforcing all applicable requirements established under this subpart, including emission limitations;

(g)(2)(iv) A statement requiring the owner or operator to comply with all applicable requirements contained in subpart A of this part;

(g)(3) All provisions contained in the Notice of MACT Approval shall be federally enforceable upon the effective date of issuance of such notice, as provided by paragraph (j) of this section.

(g)(4) The Notice of MACT Approval shall expire if construction or reconstruction has not commenced within 18 months of issuance, unless the permitting authority has granted an extension which shall not exceed an additional 12 months.

(h) Opportunity for public comment on the Notice of MACT Approval. (1) The permitting authority will provide opportunity for public comment on the Notice of MACT Approval, including, at a minimum:

(h)(1)(i) Availability for public inspection in at least one location in the area affected of the information submitted by the owner or operator and of the permitting authority's initial decision to approve the application;

(h)(1)(ii) A 30-day period for submittal of public comment; and

(h)(1)(iii) A notice by prominent advertisement in the area affected of the location of the source information and initial decision specified in paragraph (h)(1)(i) of this section.

(h)(2) At the discretion of the permitting authority, the Notice of MACT Approval setting forth the initial decision to approve the application may become final automatically at the end of the comment period if no adverse comments are received. If adverse comments are received, the permitting authority shall have 30 days after the end of the comment period to make any necessary revisions in its analysis and decide whether to finally approve the application.

(i) EPA notification. The permitting authority shall send a copy of the final Notice of MACT Approval, notice of approval of a title V permit application incorporating a MACT determination (in those instances where the owner or operator either is required or elects to obtain such a permit before construction or reconstruction), or other notice of approval issued pursuant to paragraph (c)(2)(ii) of this section to the Administrator through the appropriate Regional Office, and to all other State and local air pollution control agencies having jurisdiction in affected States.

(j) Effective date. The effective date of a MACT determination shall be the date the Notice of MACT Approval becomes final, the date of issuance of a title V permit incorporating a MACT determination (in those instances where the owner or operator either is required or elects to obtain such a permit before construction or reconstruction), or the date any other notice of approval issued pursuant to paragraph (c)(2)(ii) of this section becomes final.

(k) Compliance date. On and after the date of start-up, a constructed or reconstructed major source which is subject to the requirements of this subpart shall be in compliance with all applicable requirements specified in the MACT determination.

(l) Compliance with MACT determinations. (1) An owner or operator of a constructed or reconstructed major source that is subject to a MACT determination shall comply with all requirements in the final Notice of MACT Approval, the title V permit (in those instances where the owner or operator either is required or elects to obtain such a permit before construction or

reconstruction), or any other final notice of approval issued pursuant to paragraph (c)(2)(ii) of this section, including but not limited to any MACT emission limitation or MACT work practice standard, and any notification, operation and maintenance, performance testing, monitoring, reporting, and recordkeeping requirements.

(l)(2) An owner or operator of a constructed or reconstructed major source which has obtained a MACT determination shall be deemed to be in compliance with section 112(g)(2)(B) of the Act only to the extent that the constructed or reconstructed major source is in compliance with all requirements set forth in the final Notice of MACT Approval, the title V permit (in those instances where the owner or operator either is required or elects to obtain such a permit before construction or reconstruction), or any other final notice of approval issued pursuant to paragraph (c)(2)(ii) of this section. Any violation of such requirements by the owner or operator shall be deemed by the permitting authority and by EPA to be a violation of the prohibition on construction or reconstruction in section 112(g)(2)(B) for whatever period the owner or operator is determined to be in violation of such requirements, and shall subject the owner or operator to appropriate enforcement action under the Act.

(m) Reporting to the Administrator. Within 60 days of the issuance of a final Notice of MACT Approval, a title V permit incorporating a MACT determination (in those instances where the owner or operator either is required or elects to obtain such a permit before construction or reconstruction), or any other final notice of approval issued pursuant to paragraph (c)(2)(ii) of this section, the permitting authority shall provide a copy of such notice to the Administrator, and shall provide a summary in a compatible electronic format for inclusion in the MACT data base.

§63.44 Requirements for Constructed or Reconstructed Major Sources Subject to a Subsequently Promulgated MACT Standard or MACT Requirement.

(a) if the Administrator promulgates an emission standard under section 112(d) or section 112(h) of the Act or the permitting authority issues a determination under section 112(j) of the Act that is applicable to a stationary source or group of sources which would be deemed to be a constructed or reconstructed major source under this subpart before the date that the owner or operator has obtained a final and legally effective MACT determination under any of the review options available pursuant to §63.43, the owner or operator of the source(s) shall comply with the promulgated standard or determination rather than any MACT determination under section 112(g) by the permitting authority, and the owner or operator shall comply with the promulgated standard by the compliance date in the promulgated standard.

(b) If the Administrator promulgates an emission standard under section 112(d) or section 112(h) of the Act or the permitting authority makes a determination under section 112(j) of the Act that is applicable to a stationary source or group of sources which was deemed to be a constructed or reconstructed major source

under this subpart and has been subject to a prior case-by-case MACT determination pursuant to §63.43, and the owner and operator obtained a final and legally effective case-by-case MACT determination prior to the promulgation date of such emission standard, then the permitting authority shall (if the initial title V permit has not yet been issued) issue an initial operating permit which incorporates the emission standard or determination, or shall (if the initial title V permit has been issued) revise the operating permit according to the reopening procedures in 40 CFR part 70 or part 71, whichever is relevant, to incorporate the emission standard or determination.

(b)(1) The EPA may include in the emission standard established under section 112(d) or section 112(h) of the Act a specific compliance date for those sources which have obtained a final and legally effective MACT determination under this subpart and which have submitted the information required by §63.43 to the EPA before the close of the public comment period for the standard established under section 112(d) of the Act. Such date shall assure that the owner or operator shall comply with the promulgated standard as expeditiously as practicable, but not longer than 8 years after such standard is promulgated. In that event, the permitting authority shall incorporate the applicable compliance date in the title V operating permit.

(b)(2) If no compliance date has been established in the promulgated 112(d) or 112(h) standard or section 112(j) determination, for those sources which have obtained a final and legally effective MACT determination under this subpart, then the permitting authority shall establish a compliance date in the permit that assures that the owner or operator shall comply with the promulgated standard or determination as expeditiously as practicable, but not longer than 8 years after such standard is promulgated or a section 112(j) determination is made.

(c) Notwithstanding the requirements of paragraphs (a) and (b) of this section, if the Administrator promulgates an emission standard under section 112(d) or section 112(h) of the Act or the permitting authority issues a determination under section 112(j) of the Act that is applicable to a stationary source or group of sources which was deemed to be a constructed or reconstructed major source under this subpart and which is the subject of a prior case-by-case MACT determination pursuant to §63.43, and the level of control required by the emission standard issued under section 112(d) or section 112(h) or the determination issued under section 112(j) is less stringent than the level of control required by any emission limitation or standard in the prior MACT determination, the permitting authority is not required to incorporate any less stringent terms of the promulgated standard in the title V operating permit applicable to such source(s) and may in its discretion consider any more stringent provisions of the prior MACT determination to be applicable legal requirements when issuing or revising such an operating permit.

Clean Air Act Section 112(d)(2) and 112(d)(3)

Definition of MACT for New Sources

The definition of MACT for new sources is found in section 112(d)(2) and (3) of the Clean Air Act:

(2) STANDARDS AND METHODS. – Emissions standards promulgated under this subsection and applicable to new or existing sources of HAPs shall require the maximum degree of reduction in emissions of the HAPs subject to this section (including a prohibition on such emissions, where achievable) that the Administrator, taking into consideration the cost of achieving such emission reduction, and any non-air quality health and environmental impacts and energy requirements, determines is achievable for new or existing sources in the category or subcategory to which such emission standard applies, through application of measures, processes, methods, systems or techniques including, but not limited to, measures which –

(A) reduce the volume of, or eliminate emissions of, such pollutants through process changes, substitution of materials or other modifications,

(B) enclose systems or processes to eliminate emissions,

(C) collect, capture or treat such pollutants when released from a process, stack, storage or fugitive emissions point,

(D) are design, equipment, work practice, or operational standards (including requirements for operator training or certification) as provided in subsection (h), or

(E) are a combination of the above.

None of the measures described in subparagraphs (A) through (D) shall, consistent with the provisions of section 114(c), in any way compromise any United States patent or United States trademark right, or any confidential business information, or any trade secret or any other intellectual property right.

(3) NEW AND EXISTING SOURCES. – The maximum degree of reduction in emissions that is deemed achievable for new sources in a category or subcategory shall not be less stringent than the emission control that is achieved in practice by the best controlled similar source, as determined by the Administrator.

APPENDIX B - SIMILAR SOURCE SEARCH RESULTS

Table B-1. Summary of Facilities Reviewed to Identify Sources Similar to BASF LIB Plant Operations

Company	Description	Types of Emission Units in Permit	Emission Limit Range	Control Requirements
1. A123 Systems - Romulus, MI	Manufacturer of nano-iron phosphate cathode powder and electrode coatings; fabrication of battery cells and modules; and assembly of complete battery pack systems for hybrid and electric vehicles.	Receiving and handling of battery powder raw materials (with dust collector). Milling of processed battery powders (with dust collector). Anode and cathode battery powder mixing and weighing (with dust collector).	0.02 lb PM/ 1,000 lb exhaust	<ul style="list-style-type: none"> The permittee shall not operate any EU unless the fabric filter is installed, maintained, and operated in a satisfactory manner, including monitoring the pressure drop for the fabric filter on a continuous basis. Monthly VE readings for each EU.
2. DOW Energy Materials - Midland, MI	Manufacturer of NMC cathode material.	Operations do not require an air permit under Michigan regulations.		
3. DOW-Kokam - Midland Battery Park	Produce manganese oxide cathode / graphite lithium-ion batteries for hybrid and electric vehicles.	Anode and binder dry ingredient material handling and mixing, and anode coating storage and manufacturing tanks controlled by dust collectors, HEPA filters, N2 blanketing system, and pipe-away PRVs. Cathode dry ingredient material handling and mixing, and cathode coating storage and manufacturing tanks controlled by dust collectors, HEPA filters, N2 blanketing system, and pipe-away PRVs.	0.002 lb PM/ 1,000 lb exhaust 0.001 lb PM/ 1,000 lb exhaust	<ul style="list-style-type: none"> Shall not operate dry material operations unless dust collectors and HEPA filters are installed, maintained, and operated in a satisfactory manner, including continuous pressure drop monitoring. Monthly VE readings for each EU.
4. DOW-Kokam - Lee's Summit Battery Park	Produce manganese oxide cathode / graphite lithium-ion batteries for hybrid and electric vehicles.	Operations do not require an air permit under Missouri regulations.		

Company	Description	Types of Emission Units in Permit	Emission Limit Range	Control Requirements
5. EnerDel - Indianapolis, IN	Produce lithium-ion cells and packs for hybrid and electric vehicles. Primary lithium chemistries include: manganese spinel cathode and lithium titanate anode for high power applications, as well as manganese spinel cathode and amorphous carbon for high energy applications.	Facility-wide limit of 100 ton PM/yr, 10 ton individual HAP/yr, and 25 ton total HAP/yr to avoid major source status. The PM emissions from the mixers EU7A, EU7C, and EU7E shall not exceed a combined emission rate of 2.26 lb/hr.	0.03 gr/dscf	<ul style="list-style-type: none"> • Shall operate baghouse (Dust Collector #1) at all times when EU7A, EU7C, and EU7E are not completely covered. • Daily pressure drop readings across the baghouse (Dust Collector #1) • Daily VE notations of Dust Collector #1 stack exhaust.
6. EnerG2, Inc. - Albany, OR	Produce high energy density nano-carbon for ultracapacitors.	Permit Notice Information: The EnerG2 facility will manufacture activated carbon particles and use baghouses and a thermal oxidizer to control air pollutants. A small natural gas-fired boiler will be used to provide steam heat for the manufacturing processes. Milling (controlled by fabric filter) and product bagging (controlled by HEPA) during the carbon manufacturing processes.	0.1 gr/dscf	
7. ERACHEM COMILOG, INC. - Riviera Beach, MD	Produce manganese chemical derivatives designed for Specialties and Electronics applications, as well as for the Agrochemical industry. Portfolio includes high purity oxides, anhydrous salts, specialty metallurgical products and reduced ore.	Milling, classifier, material handling and transfer, and roaster/calciner.	0.03 gr/dscf	Exhaust gases from must vent through the dust collector before discharging to the atmosphere.
8. Johnson Controls - Holland, MI	Produce nickel-cobalt-metal battery cells and packs, as well as production of battery separators (by partner Entek) for hybrid and electric vehicles.	According to the Michigan Department of Environmental Quality, this facility recently submitted a permit application but a permit has not yet been issued.		

Company	Description	Types of Emission Units in Permit	Emission Limit Range	Control Requirements				
9. LG Chem Michigan Incorporated - Holland, MI	Produce lithium-ion polymer battery cells for the GM Volt using a manganese-based cathode material and a proprietary separator.	Anode and cathode material metering and mixing controlled by a dust collector and activated carbon.	0.002 to 0.005 lb PM/ 1,000 lb exhaust	<ul style="list-style-type: none"> • Shall not operate EUs unless dust collector is installed, maintained, and operated in a satisfactory manner, including continuous pressure drop monitoring. • Monthly VE readings for each EU. <p>Other emission limits:</p> <ul style="list-style-type: none"> • 12-month rolling manganese emissions limit of 125 lb/yr. • 12-month rolling nickel emissions limit of 30 lb/yr. • 12-month rolling cobalt emissions limit of 24 lb/yr. • 12-month rolling emission limit for each individual HAP of 8.9 ton/yr. • 12-month rolling emission limit for total HAPs of 22.4 ton/yr. 				
10. NEI Corporation - Somerset, NJ	Manufacturer of NMC cathode material.	An Open Public Records Act request was submitted to the New Jersey Department of Environmental Protection (NJDEP) for any air permits issued to NEI Corporation. According to the NJDEP, no air permits have been issued to NEI Corporation.						
11. BASF Corporation - Troy, MI	Manufacturer of NiMH battery material.	<table border="1"> <tr> <td data-bbox="791 820 1352 873">Manganese sulfate and/or nickel sulfate bulk bag unloader. HEPA filter system.</td> </tr> <tr> <td data-bbox="791 873 1352 927">Manganese sulfate and/or nickel sulfate solution mixing tank. HEPA filter system.</td> </tr> <tr> <td data-bbox="791 927 1352 980">Cobalt sulfate and/or nickel sulfate bulk bag unloader. HEPA filter system.</td> </tr> <tr> <td data-bbox="791 980 1352 1027">Cobalt sulfate and/or nickel sulfate solution mixing tank. HEPA filter system.</td> </tr> </table>	Manganese sulfate and/or nickel sulfate bulk bag unloader. HEPA filter system.	Manganese sulfate and/or nickel sulfate solution mixing tank. HEPA filter system.	Cobalt sulfate and/or nickel sulfate bulk bag unloader. HEPA filter system.	Cobalt sulfate and/or nickel sulfate solution mixing tank. HEPA filter system.	0.01 lb PM/ 1,000 lb exhaust	<ul style="list-style-type: none"> • Shall not operate any EU unless HEPA filter system is installed, maintained, and operated in a satisfactory manner. • Monthly VE readings for each EU.
Manganese sulfate and/or nickel sulfate bulk bag unloader. HEPA filter system.								
Manganese sulfate and/or nickel sulfate solution mixing tank. HEPA filter system.								
Cobalt sulfate and/or nickel sulfate bulk bag unloader. HEPA filter system.								
Cobalt sulfate and/or nickel sulfate solution mixing tank. HEPA filter system.								

Company	Description	Types of Emission Units in Permit	Emission Limit Range	Control Requirements
12. Rockwood Lithium - Kings Mountain, NC	Produce battery-grade lithium carbonate and lithium hydroxide.	<p>Lithium hydroxide materials handling operation; lithium hydroxide materials handling operation; controlled by fabric filter (1,808 square feet of filter area).</p> <p>Subject only to state PM emission limits based on process weight rate.</p> <p>Facility-wide limit of 100 ton PM/yr, 10 ton individual HAP/yr, and 25 ton total HAP/yr to avoid major source status.</p>		<ul style="list-style-type: none"> Shall perform periodic inspections and maintenance (I&M) of fabric filter as recommended by the manufacturer and perform an annual (for each 12 month period following the initial inspection) internal inspection of each bagfilter system.
13. Toda America - Battle Creek, MI	Manufacturer of NMC cathode material.	<p>Raw material handling and mixing (with fabric filter).</p> <p>Calcination mixer controlled by a fabric filter</p> <p>Intermediate material handling and mixing (with fabric filter).</p> <p>Calcination process (with wet scrubber).</p>	<p>0.001 to 0.05 lb PM/ 1,000 lb exhaust</p> <p>0.001 lb PM/ 1,000 lb exhaust</p> <p>0.01 to 0.033 lb PM/ 1,000 lb exhaust</p> <p>0.001 lb PM/ 1,000 lb exhaust</p>	<ul style="list-style-type: none"> The permittee shall not operate Line 1 or 2 dry material operations unless the fabric filters are installed, maintained, and operated in a satisfactory manner, including but not limited to maintaining a pressure drop range across each fabric filter according to the manufacturer's specifications. Install, calibrate, maintain, and operate a device to monitor the pressure drop for each fabric filter on a continuous basis. The permittee shall not operate the lines unless the wet scrubbers are installed, maintained, and operated in a satisfactory manner, including continuously monitoring the scrubber liquid flow rate and maintaining it at a minimum of 0.22 gal/min. Monthly VE readings. <p>Other emission limits:</p> <ul style="list-style-type: none"> 12-month rolling nickel emissions limit of 145 lb/yr.

APPENDIX C - RBLC SEARCH RESULTS

The USEPA maintains a database of control technology determinations made throughout the United States. This database represents the largest compendium available in the field of air pollutant source requirements and control capabilities, and is a useful resource when conducting a case-by-case MACT analysis. The RBLC database was queried for all PM determinations from January 1, 2008 to present (a full 5 year period, plus the remainder of 2013). The query returns information for any process that has a PM determination. Each process could include several records for other pollutants as well; therefore, the number of records returned in any query may not all be related to PM. A total of 5,918 records were obtained from the query, downloaded into an Access database, and filtered to list only PM records (approximately 48% of the total records) exclude records for operations that are not relevant to the LIB plant.

Two separate screening methods were employed to evaluate the RBLC records for operations that are similar to the LIB plant. For both of these methods, all records for fuel combustion sources, such as coal, oil, or natural gas-fired boilers, were excluded from further consideration. There are no fuel combustion sources associated with the LIB plant; therefore, these records were removed because they failed the “similar design” criteria. Fuel combustion sources would produce larger volumes of air (i.e., combustion gases) than produced in the LIB plant, and the particulate will be much smaller than found in the LIB plant operations. This initial filtering removed approximately two thirds of the records. The remaining 1,050 PM records were evaluated using both of the following two methods:

1. Filter the PM records by industrial source category (i.e., SIC code) and use engineering judgment and general knowledge of the processes to exclude those not similar to the LIB plant. These records were removed because they failed the “similar design” and/or “similar capacity” criteria. Records excluded using this method were related to sources such as large material processing and handling sources (e.g., cement and lime kilns), because they are much larger, both in gas volumes and particulate mass loadings, than the types of sources at the LIB plant.
2. Identify the records that report throughput capacity data, and exclude all records that have reported hourly or annual throughputs more than 10 times greater than the hourly or annual LIB plant throughput rates. These records were removed because they failed the “similar capacity” criteria.

The first method was to filter the records by SIC group as presented in Table C-1 and then use general knowledge of the processes to exclude those not similar to the LIB plant. Once filtered by SIC group, additional records within SIC groups were excluded as appropriate (e.g., fuel burning processes). Table C-2 presents a detailed summary of the records potentially relevant to the LIB plant operations.

Table C-1. Summary of SIC Categories Identified in RBLC PM Records from January 1, 2008 to Present

SIC Code	SIC Description	Does SIC Represent a Similar Source?	Why Not?
0	(miscellaneous)	No	Wrong pollutant; Boilers
28	(chemical plant cooling tower)	No	Pollutant is mist
147	(lime silos at precipitated calcium carbonate plant)	No	Pollutant is mist
173	(fuel combustion)	No	High flow
242	(fuel combustion)	No	High flow
262	(fuel combustion)	No	High flow
361	(fuel combustion)	No	High flow
491	(fuel combustion and cooling towers)	No	Pollutant is mist
493	(fuel combustion)	No	High flow
701	(fuel combustion)	No	High flow
971	(fuel combustion)	No	High flow
1011	Iron Ores	No	High flow
1311	Crude Petroleum and Natural Gas	No	Wrong pollutant
1321	Natural Gas Liquids	No	No PM
1382	Oil and Gas Field Exploration Services	No	No PM
1474	Potash, Soda, and Borate Minerals	No	Boiler
1731	Electrical Work	No	NA
1771	Portland Cement	No	High flow
2032	Canned Specialties	No	Wrong pollutant
2046	Wet Corn Milling	No	Wet PM
2075	Soybean Oil Mills	No	Wet PM
2079	Shortening, Table Oils, Margarine, and Other Edible Fats and Oils, Not Elsewhere Classified	No	VOC/acid
2421	Sawmills and Planing Mills, General	No	Large PM
2493	Reconstituted Wood Products	No	Large PM
2611	Pulp Mills	No	Wrong pollutant
2621	Paper Mills	No	High flow
2711	Newspapers: Publishing, or Publishing and Printing	No	VOC
2813	Industrial Gases	No	Wrong pollutant
2816	Inorganic Pigments	Potentially	
2819	Industrial Inorganic Chemicals, Not Elsewhere Classified	Potentially	
2821	Plastics Materials, Synthetic Resins, and Nonvulcanizable Elastomers	No	Boilers; heaters
2822	Synthetic Rubber (Vulcanizable Elastomers)	No	Large PM
2869	Industrial Organic Chemicals, Not Elsewhere Classified	No	Boilers; generators
2873	Nitrogenous Fertilizers	No	High flow

SIC Code	SIC Description	Does SIC Represent a Similar Source?	Why Not?
2895	Carbon Black	Potentially	
2899	Chemicals and Chemical Preparations, Not Elsewhere Classified	Potentially	
2911	Petroleum Refining	No	High flow
3011	Tires and Inner Tubes	No	Wrong pollutant
3211	Flat Glass	No	High flow
3241	Cement, Hydraulic	No	High flow
3251	Brick and Structural Clay Tile	No	High flow
3274	Lime	Potentially	
3295	Minerals and Earths, Ground or Otherwise Treated	Potentially	
3296	Mineral Wool	No	Condensables/wet PM
3312	Steel Works, Blast Furnaces (Including Coke Ovens), and Rolling Mills	No	High flow
3313	Electrometallurgical Products, Except Steel	No	High flow
3321	Gray and Ductile Iron Foundries	No	High flow
3325	Steel Foundries, Not Elsewhere Classified	No	Fugitives
3334	Primary Production of Aluminum	No	High flow/acid
3341	Secondary Smelting and Refining of Nonferrous Metals	No	High flow/acid
3351	Rolling, Drawing, and Extruding Of Copper	No	Oily
3365	Aluminum Foundries	No	High flow
3511	Steam, Gas, and Hydraulic Turbines, and Turbine Generator Set Units	No	High flow
3624	Carbon and Graphite Products	Potentially	
3711	Motor Vehicles and Passenger Car Bodies	No	VOC
3713	Truck and Bus Bodies	No	VOC
3724	Aircraft Engines and Engine Parts	No	Specialty
4226	Special Warehousing and Storage, Not Elsewhere Classified	No	NA
4812	Radiotelephone Communications	No	NA
4911	Electric Services	No	NA
4922	Natural Gas Transmission	No	NOx
4923	Natural Gas Transmission and Distribution	No	NOx
4925	Mixed, Manufactured, or Liquefied Petroleum Gas Production and/or	No	NA
4931	Electric and Other Services Combined	No	NA
4939	Combination Utilities, Not Elsewhere Classified	No	Generators
4952	Sewerage Systems	No	Wrong pollutant
4953	Refuse Systems	No	High flow
4961	Steam and Air-Conditioning Supply	No	NA
5052	Coal and Other Minerals and Ores	No	Pollutant is mist
7011	Hotels and Motels	No	NA
8221	Colleges, Universities, and Professional Schools	No	Boilers
9711	National Security	No	NA

NA = not applicable
 NOx = nitrogen oxides
 PM = particulate matter
 VOC = volatile organic compounds

Table C-2. Summary of RBLC Records Potentially Relevant to the LIB Plant Operations

SIC Code	Facility Description	Process Name	Control Method Description	Emission Limit	Emission Limit Unit	Percent Efficiency (a)
2816	Titanium Dioxide Pigment Manufacturing	No. 7 Pigment Grinding Feed Bin (AK-107)	Baghouse	0.005	gr/dscf	
2816	Titanium Dioxide Pigment Manufacturing	No. 7 Pigment Grinding Feed Bin (AK-107)	Baghouse	0.01	gr/dscf	
2816	Titanium Dioxide Pigment Manufacturing	No. 7 Pigment Grinding Feed Bin (AK-107)	Baghouse	0.01	gr/dscf	
2819	Activated Carbon Production Facility	Carbon Production	Fabric filter	0.01	gr/dscf	
2819	Activated Carbon Production Facility	Carbon Production	Fabric filter	0.01	gr/dscf	
2819	Activated Carbon Production Facility	Carbon Production	Fabric filter	0.01	gr/dscf	
2895	Furnace Carbon Black Production	Carbon Black Production Units 3 and 4	Main Unit Filter Baghouse	3.01	lb/hr	
2895	Furnace Carbon Black Production	Carbon Black Production Units 3 and 4	Baghouse	3.01	lb/hr	
2899	A proposed manufacturing complex consists of an acrylamide plant, a powder plant, a diallyldimethylammoniumchloride (DADMAC) plant, a specialty products plant, an emulsion plant, a polyamine plant, a dimethylamineoethylacrylate (ADAM) plant, a chloromethy	ATBS Plant - Silos, Hoppers, Bagging Operations	No additional control	0.01	lb/hr	
2899	A proposed manufacturing complex consists of an acrylamide plant, a powder plant, a diallyldimethylammoniumchloride (DADMAC) plant, a specialty products plant, an emulsion plant, a polyamine plant, a dimethylamineoethylacrylate (ADAM) plant, a chloromethy	Powder Plant - Process Sources	Good equipment design and proper operations. Fueled by natural gas or propane	0.51	lb/hr	
2899	A proposed manufacturing complex consists of an acrylamide plant, a powder plant, a diallyldimethylammoniumchloride (DADMAC) plant, a specialty products plant, an emulsion plant, a polyamine plant, a dimethylamineoethylacrylate (ADAM) plant, a chloromethy	Powder Plant - Process Sources	Good equipment design and proper operations. Fueled by natural gas or propane	0.41	lb/hr	
2899	A proposed manufacturing complex consists of an acrylamide plant, a powder plant, a diallyldimethylammoniumchloride (DADMAC) plant, a specialty products plant, an emulsion plant, a polyamine plant, a dimethylamineoethylacrylate (ADAM) plant, a chloromethy	Powder Plant Packaging/Loading Areas	Dust Filters	0.1	lb/hr	

SIC Code	Facility Description	Process Name	Control Method Description	Emission Limit	Emission Limit Unit	Percent Efficiency (a)
2899	A proposed manufacturing complex consists of an acrylamide plant, a powder plant, a diallyldimethylammoniumchloride (DADMAC) plant, a specialty products plant, an emulsion plant, a polyamine plant, a dimethylamineoethylacrylate (ADAM) plant, a chloromethy	Powder Plant Packaging/Loading Areas	Dust filters	0.11	lb/hr	
3274	Lime manufacturing plant. Dolomitic lime is produced from limestone containing 30 to 45% magnesium carbonate.	Dust Load-out System	Baghouse with 99.5% capture efficiency. Mechanical enclosure for conveying equipment.	8.1	ton/yr	
3274	Lime manufacturing plant. Dolomitic lime is produced from limestone containing 30 to 45% magnesium carbonate.	Lime Load-Out, Screening, Transfer, Storage	Baghouses (2) which shall achieve 99.5% capture efficiency.	3.32	ton/yr	
3274	Lime manufacturing plant. Dolomitic lime is produced from limestone containing 30 to 45% magnesium carbonate.	Product Transfer, Processed Stone, Conveying at Kiln	Baghouse	1.23	ton/yr	
3295	The Carbo Ceramics, Inc. facility in McIntyre, GA is engaged in the production of ceramic pellets for use in the natural gas mining industry. The major raw materials are alumina-rich clay, water, and bauxite.	Alumina-Rich Clay, Water, and Bauxite	Addition of a baghouse to control PM emissions as required in 40 CFR 60 Subpart NSPS UUU.	0.01	gr/dscf	99
3295	Pyramax Ceramics plans to construct a manufacturing facility for the production of proppant beads for use in the oil and gas industry. The major raw material is clay. The clay is mixed with chemicals and then fired in a kiln to produce ceramic beads.	Material Handling	Baghouse	0.005	gr/dscf	99
3295	Pyramax Ceramics plans to construct a manufacturing facility for the production of proppant beads for use in the oil and gas industry. The major raw material is clay. The clay is mixed with chemicals and then fired in a kiln to produce ceramic beads.	Material Handling	Baghouse	0.005	gr/dscf	99

SIC Code	Facility Description	Process Name	Control Method Description	Emission Limit	Emission Limit Unit	Percent Efficiency (a)
3295	Pyramax Ceramics plans to construct a manufacturing facility for the production of proppant beads for use in the oil and gas industry. The major raw material is clay. The clay is mixed with chemicals and then fired in a kiln to produce ceramic beads.	Material Handling	Baghouse	0.005	gr/dscf	99
3624	Graphite Electrode Manufacturing Facility	Cleaning and Inspection	Baghouse	0.005	gr/dscf	
3624	Graphite Electrode Manufacturing Facility	Graphitizing Process (Gulper System, Dust Bins)	Baghouse	0.005	gr/dscf	
3624	Graphite Electrode Manufacturing Facility	Graphitizing Process (Gulper System, Dust Bins)	Baghouse	0.005	gr/dscf	
3624	Graphite Electrode Manufacturing Facility	Graphitizing Process (Gulper System, Dust Bins)	Baghouse	0.005	gr/dscf	
3624	Graphite Electrode Manufacturing Facility	Machining and Shipping	Baghouse	0.005	gr/dscf	
3624	Graphite Electrode Manufacturing Facility	Insulating Media Receiving	Baghouse	0.005	gr/dscf	
3624	Graphite Electrode Manufacturing Facility	Mill, Mix, and Extrusion Process Including Mixers	Baghouse/Dry Fume Scrubber	0.005	gr/dscf	
3624	Graphite Electrode Manufacturing Facility	Cleaning and Inspection	Baghouse	0.005	gr/dscf	
3624	Graphite Electrode Manufacturing Facility	Cleaning and Inspection	Baghouse	0.005	gr/dscf	
3624	Graphite Electrode Manufacturing Facility	Machining and Shipping	Baghouse	0.005	gr/dscf	
3624	Graphite Electrode Manufacturing Facility	Machining and Shipping	Baghouse	0.005	gr/dscf	
3624	Graphite Electrode Manufacturing Facility	Mill, Mix, and Extrusion	Baghouse	0.005	gr/dscf	
3624	Graphite Electrode Manufacturing Facility	Rebake Load and Unload/Graphitizing Preparation	Baghouse	0.005	gr/dscf	
3624	Graphite Electrode Manufacturing Facility	Rebake Load and Unload/Graphitizing Preparation	Baghouse	0.005	gr/dscf	
3624	Graphite Electrode Manufacturing Facility	Bake Load and Unload and Baked Electrode Cleaning Process	Baghouse	0.005	gr/dscf	

SIC Code	Facility Description	Process Name	Control Method Description	Emission Limit	Emission Limit Unit	Percent Efficiency (a)
3624	Graphite Electrode Manufacturing Facility	Mill, Mix, and Extrusion	Baghouse	0.005	gr/dscf	
3624	Graphite Electrode Manufacturing Facility	Insulating Media Receiving	Baghouse	0.005	gr/dscf	
3624	Graphite Electrode Manufacturing Facility	Mill, Mix, and Extrusion Process Including Mixers	Baghouse/Dry Fume Scrubber	0.005	gr/dscf	
3624	Graphite Electrode Manufacturing Facility	Mill, Mix, and Extrusion Process Including Mixers	Baghouse/Dry Fume Scrubber	0.005	gr/dscf	
3624	Graphite Electrode Manufacturing Facility	Rebake Load and Unload/Graphitizing Preparation	Baghouse	0.005	gr/dscf	
3624	Graphite Electrode Manufacturing Facility	Bake Load and Unload and Baked Electrode Cleaning Process	Baghouse	0.005	gr/dscf	
3624	Graphite Electrode Manufacturing Facility	Bake Load and Unload and Baked Electrode Cleaning Process	Baghouse	0.005	gr/dscf	
3624	Graphite Electrode Manufacturing Facility	Insulating Media Receiving	Baghouse	0.005	gr/dscf	
3624	Graphite Electrode Manufacturing Facility	Mill, Mix, and Extrusion	Baghouse	0.005	gr/dscf	

a. If blank, no efficiency was specified in the RBLC database record.

The second approach to reviewing the RBLC records involved reviewing available information to identify PM records for processes with similar capacity to the LIB plant. This approach began with filtering out all the non-PM records and records for fuel burning sources. These two refinements alone reduced the potentially relevant records from 5,918 to 1,050. The remaining 1,050 records contained records for cooling towers, boilers, and generators that were not removed by the initial filtering of fuel burning sources. These records were excluded and the remaining records numbered 922, just 15.5% of the initial query results.

These 922 records were then reviewed for available throughput data with which to compare the LIB plant capacity. The LIB plant material throughput rate is 0.35 ton/hr and 3,083 ton/yr. Of the 922 records, only 50% have throughput data of any kind, 28% have ton/hr throughput rates, and 5% have ton/yr throughput rates. For this review, similar capacity is conservatively considered to be a throughput rate within 10 times that of the LIB plant. Without considering the type of facility (e.g., plasma torch cutting operations would never be considered a similar source), only 5% of the facilities have hourly throughput rates within 10 times that of the LIB plant (12 records out of 256 with ton/hr throughput rates) and only 28% of the facilities have annual throughput rates within 10 times that of the LIB plant (14 records out of 50 with ton/yr throughput rates). These 26 remaining records with a throughput rate similar to that of the LIB plant include the following:

- 12 material handling storage area sources at an iron ore concentrate pelletizing plant that utilize bin vents for control,
- a batch mixer and material elevator at a flat glass plant that utilizes a baghouse for control,
- 3 plasma torch cutting operations at a specialty steel plant that utilize a baghouse for control,
- 7 process operations at an iron foundry and aluminum engine casting plant that utilize baghouses for control, and
- a stock house and 2 lime silos for pig iron production at a steel mill that use baghouses for control.

Because there are no storage area sources utilizing bin vents for control at the LIB plant, the 12 records associated with the iron ore concentrate pelletizing plant were not considered similar in design to the LIB plant process operations and were excluded from further evaluation. The remaining 14 records were identified with this approach as having a similar capacity to the LIB plant and are presented in Table C-3. These 14 records were compared to those identified in Table C-2. No duplicates exist between the two record sets. In addition, further review verified that the records identified in Table C-2 either have no throughput data available in the RBLC database or their throughput rates are at least 10 times greater than the LIB throughput rate. Therefore, the records in Table C-2 would not be identified by the search described above.

Both approaches to the RBLC data, using engineering knowledge of the industries and review of the capacities of the processes identified in the search, result in the observation that less than 1% of the query results (i.e., 58 records) contain a PM determination potentially relevant to the LIB plant.

Table C-3. Summary of RBLC Records with Similar Capacity to the LIB Plant Operations

SIC Code	Facility Description	Process Name	Throughput	Control Method Description	Emission Limit	Emission Limit Unit	Percent Efficiency
3211	Flat Glass Plant	Cullet Return, Elevator Bottom & Top; Batch Mixer	650 ton/yr	Baghouse	0.005	gr/dscf	none ^(a)
3312	Specialty Steel	Plasma Torch Cutting Operation	30,000 ton/yr	Baghouse	0.01	lb/hr	99.9
3312	Specialty Steel	Plasma Torch Cutting Operation	30,000 ton/yr	Baghouse	0.01	lb/hr	99.9
3312	Specialty Steel	Plasma Torch Cutting Operation	30,000 ton/yr	Baghouse	0.01	lb/hr	99.9
3321	Iron Foundry and Aluminum Engine Casting Plant	DeFlash, DeCore, DeGate Operations (4)	26,762 ton/yr	Baghouse	0.031	lb/ton	
3321	Iron Foundry and Aluminum Engine Casting Plant	Mold Cooling Line (4)	26,762 ton/yr	Baghouse	0.1	lb/ton	
3321	Iron Foundry and Aluminum Engine Casting Plant	Mold shakeout with duct burner (4)	26,762 ton/yr	Baghouse	0.17	lb/ton	
3321	Iron Foundry and Aluminum Engine Casting Plant	Mold shakeout with duct burner (4)	26,762 ton/yr	Baghouse	0.35	lb/ton	
3321	Iron Foundry and Aluminum Engine Casting Plant	Casting cooling tunnel (4)	26,762 ton/yr	Baghouse	0.09	lb/ton	
3321	Iron Foundry and Aluminum Engine Casting Plant	Casting cooling tunnel (4)	26,762 ton/yr	Baghouse	0.17	lb/ton	
3321	Iron Foundry and Aluminum Engine Casting Plant	Mold Cooling Line (4)	26,762 ton/yr	Baghouse	0.2	lb/ton	
3325	Pig Iron at Steel Mill	Stock House 2 Baghouse Vent	2,462 ton/yr	Fabric Filter	0.04	lb/hr	99.5
3325	Pig Iron at Steel Mill	Coke Battery 2 FGD Lime Silo Unloading	21,810 ton/yr	Fabric Filter	0.005	lb/hr	99.5
3325	Pig Iron at Steel Mill	Coke Battery 1 FGD Lime Silo Unloading	21,810 ton/yr	Fabric Filter	0.005	lb/hr	99.5

a. No efficiency was specified in the RBLC database record.

APPENDIX D - CONTROL EQUIPMENT DESIGN DOCUMENTATION

Table D-1. Index of Control Equipment and Location of Supporting Documentation

Process Operation	Appendix D Page #	Dust Collector	DF Filter ID	Manufacturer	DF Cloth Area (ft ²)	Blower ID	Outlet Gas Flow Rate (acfm)	Gas-to-Filter Area Ratio
Cathode-1	not in HAP service	DF-1	F21050	National Bulk Equipment	75	21060	300	4.0
Cathode-3	D-3	DF-3	F31020	National Bulk Equipment	75	31040	300	4.0
Cathode-5	not in HAP service	DF-5	F23010	Netzsch	377	23080	1423	3.8
Cathode-2	not in HAP service	DF-2	F21535	MAC Process, Inc.	17	61040	30	1.8
Cathode-4	D-5, D-9	DF-4	F32015	MAC Process, Inc.	17		30	1.8
Cathode-6	D-6, D-9	DF-6	F41020	Littleford Day, Inc.	17		30	1.8
Cathode-7	D-7, D-9	DF-7	F61030	MAC Process, Inc.	671		1300	1.9
Cathode-9	D-10	DF-12	F70025	MAC Process, Inc.	16	69050	30	1.9
Cathode-13	D-11	DF-8	F69040	MAC Process, Inc.	671		1300	1.9
Cathode-10	D-15	DF-11	F67350	Vac-U-Max	95	67355	116	1.2
Cathode-10	D-19	DF-9	F71030	Netzsch	614	71050	2213	3.6
Cathode-8								
Cathode-14								
Cathode-11	D-14	DF-10	F92010	MAC Process, Inc.	1342	92030	2350	1.8
Cathode-12								
Cathode-15	D-22	DF-13	F11910	Vac-U-Max	95	11930	208	2.2


National Bulk Equipment

Cathode-3

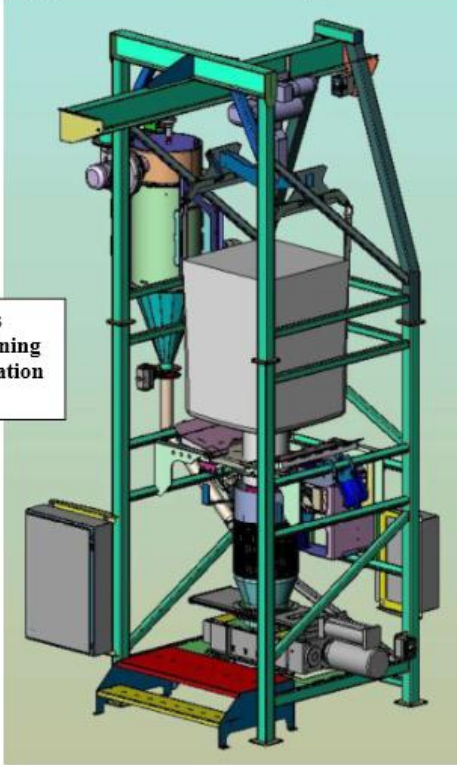
Dust Collector DF-3

Filter ID: F31020

Blower ID: 31040

**Forward Thinking. Real Results.**
NATIONAL BULK EQUIPMENT

Bulk Bag Unloader System Manual



NOTE: Be sure this document is used in training employees on daily operation of this machine.

BASF
CSO# E601060135
49-1SP-BBU

National Bulk Equipment
12838 Stainless Drive Holland, MI 49424
Phone: (616) 399-2220 Fax: (616) 399-7365
www.nbe-inc.com



- o Pneumatic Slide Gate: A 14" pneumatic gate is provided. The gate is designed to close during the empty bulk bag collapsing sequence. The gate is constructed in 304-2B stainless steel. Double acting air cylinders actuate the gate.
- o Dust Collection: The system includes an integral reverse pulse jet dust collector. It uses (1) one Chemco 12.5" diameter x 26" long standard pleated filter cartridge with a filtration surface area of 75 square feet. The cartridge is easily changeable and has NBE's exclusive diffusion cone for efficient reverse pulse cleaning. The dust collection system is powered by a 1 HP /460 VAC / 3 phase / 60 Hz inverter duty motor and includes a VFD located in the control panel. The American Fan unit is rated to 300 CFM @ 6" w.c. static pressure. The fan blade and housing are constructed in Aluminum (Stainless Steel is available). An analog DP transmitter is provided for the unit; a secondary unit is provided on the Precursor (BS31010) unit. An air flow sensor is provided to indicate if there is no air flow. There is an on/off switch on the control panel for the dust collection unit. It can be turned to the off position during equipment cleaning or maintenance. When it is turned to the off position it reverse pulses to clean the cartridge and the captured dust is reclaimed into the receiving hopper. The dust collector is mounted on the bulk bag unloader frame. The dust collection system is designed to collapse the bulk bag.
- o Controls: The enclosure is NEMA 4 type and all motor starters, VFD's, contactors, operator switches and an Allen Bradley CompactLogix PLC is supplied. The CompactLogix includes Ethernet IP communications. All Reliance motors supplied are in accordance with IEEE-841 requirements. The bulk bag unloader includes controls for the dust collector. The dust collector includes an On/Off switch for the fan and reverse pulse jet cleaning. A differential pressure transmitter is included and is mounted at the operator station. All devices within the control system conform to the BASF vendor list. An operator display is mounted on the operator enclosure and has been designed to adjust system variables and display equipment faults. The unit includes two separate enclosures; (1) has 460 VAC and the other is for the 24 VDC control voltage.
- o Operator Platform

MAC Process, Inc.

Cathode-4

Dust Collectors DF-4

Filter IDs: F32015

(5) GROUND LUGS (SEE DETAIL)

Filter area (17 ft²), flow rate (30 cfm), and design air-to-cloth ratio (1.8:1)

253.949

16

406.4

NOTES:

- ALL DIMENSIONS ARE IN INCHES WITH SECONDARY UNITS IN MILLIMETERS.
- 3/4" (19.05MM) FNPT, 60-90 PSI (4.1- 6.2 BARG) REGULATED CLEAN, DRY AIR REQUIRED. 1 SCFM VOLUME.
- 10 GA. 304 STAINLESS STEEL CONSTRUCTION.
- UNIT IS STRESSED FOR -17" Hg (-0.57 BAR).
- (2) 1/4" (6.35MM) FNPT DIFFERENTIAL PRESSURE GAUGE PORTS MUST HAVE PIPE PLUGS IF DIFFERENTIAL PRESSURE GAUGE IS NOT USED.
- TOP PLENUM REMOVABLE FOR ACCESS TO CARTRIDGE. DE-ENERGIZE TIMER CONTROL BEFORE WORKING ON UNIT. REMOVE BY UNBOLTING PLENUM FROM BAGHOUSE AND EXHAUST DUCT, DISCONNECT 3/4" (19.05MM) BRAIDED HOSE, AND LIFT OFF TOP PLENUM. (HEADER REMAINS ATTACHED TO HOUSING)
- (2) 1/4" (6.35MM) THICK WHITE EPDM CLOSED CELL SPONGE GASKETS PROVIDED TO SEAL TUBESHEET.
- NEMA 4 ENCLOSURE WITH TIMER CONTROL AND GOYEN SOLENOID VALVE, 24 VDC REQUIRED. (SOLENOID PRE-PLUMBED TO PULSE HEADER GOYEN DIAPHRAGM VALVE WITH 1/4" (6.35MM) POLY-FLO TUBING)
- UNIT INCLUDES (1) POUPLLET QP842 POLYESTER W/ PTFE TOP LOAD CARTRIDGE, PROVIDING 17 SQ. FT. OF MEDIA WITH AN AIR TO CLOTH RATIO OF 1.8:1 @ 30 CFM.
- 1/4" (6.35MM) WHITE EPDM CLOSED CELL SPONGE GASKET AND (1) SPARE PROVIDED FOR FLANGE CONNECTIONS.
- APPROX. WEIGHT: 50 LBS.
- S/N: 167824-002-1
- TAG: F32015
- STAINLESS STEEL TAG.

FINISH NOTES:

- INTERIOR PRODUCT CONTACT WELDS TO BE CONTINUOUS, GROUND SMOOTH TO CG24 GRIT FINISH.
- INTERIOR AND EXTERIOR STAINLESS STEEL SURFACES TO BE PICKLED.

SPECIAL ASSEMBLY AND TEST NOTES:

- FILTER TO BE BUBBLE TESTED AT 1/2 PSI (0.034 BARG)

14 STAINLESS STEEL TAG INFORMATION

MANUFACTURE: Mac Process, Inc.
 PLANT BUILT: SABETHA, KS
 YEAR BUILT: 2011
 MODEL: 19RTC1 STYLE II FILTER
 SERIAL NO.: 167824-002-1
 EQUIPMENT TAG NO.: F32015
 PURCHASE ORDER NO.: 4557726298
 DESIGN PRESSURE: +8.27 PSI (+0.57 BARG)
 -17" Hg (-0.57 BARG)
 DESIGN TEMPERATURE: 140°F (60°C)
 EMPTY WEIGHT: 50 LBS.

This print is certified to be dimensionally correct to ± 1/4 inch on all components, ± 1/2 on overall dimensions up to 120 inches and ± 1 1/2 on all dimensions greater than 120.

Mac Process, Inc.
 BY Michael L Herbster DATE 10/11

THIS MATERIAL IS THE PROPERTY OF MAC PROCESS INC. AND SHOULD NOT BE REPRODUCED, PUBLISHED OR DISCLOSED TO OTHERS WITHOUT AUTHORIZATION AND SHALL NOT BE USED IN ANY WAY AGAINST OR DETRIMENTAL TO MAC PROCESS INC., SABETHA, KANSAS.

macprocess schenckprocess group

19RTC1 STYLE II FILTER FOR BASF CORPORATION (ELYRIA, OH)

DRAWN BY MLH	DATE 03/24/11	UNLESS OTHERWISE SPECIFIED DIMENSIONS ARE IN INCHES TOLERANCES:	JOB NO. 167824	DRAWING NO. CM105936	REV. D
SCALE 1/8" = 1"	SEGMAL 1/16	FRACTION 3/16	OVERALL 3/16		

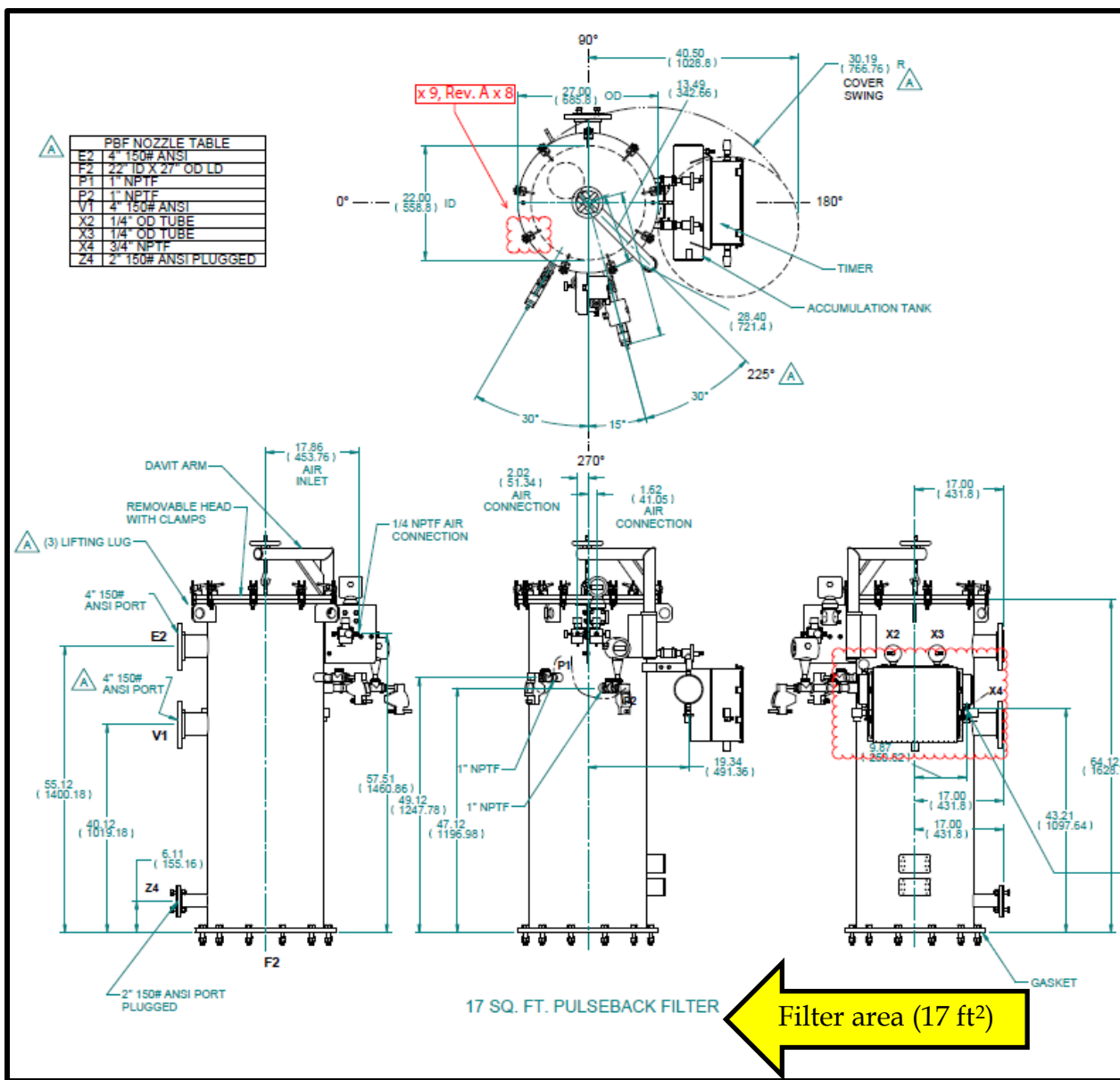
CM105936

Littleford Day, Inc.

Cathode-6

Dust Collector DF-6

Filter ID: F41020



MAC Process, Inc.

Cathode-7

Dust Collector DF-7

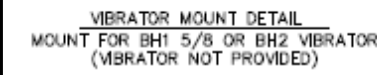
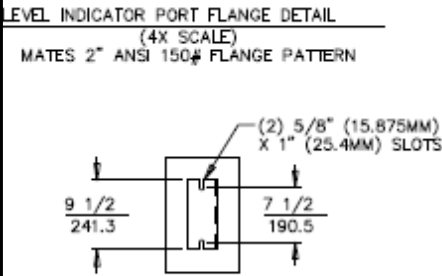
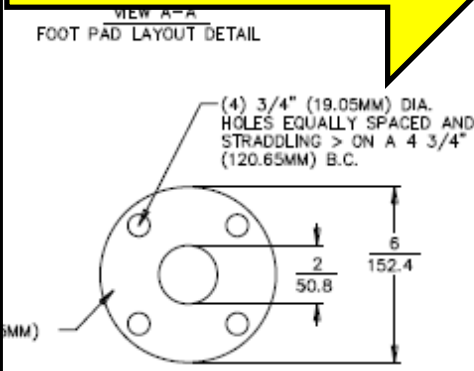
Filter ID: F61030

Filter area (671 ft²),
 flow rate (1,300 cfm), and
 design air-to-cloth ratio (1.9:1)

NOTES:

1. ALL DIMENSIONS ARE IN INCHES.
 2. PRIMARY FILTER CONSTRUCTED OF 304 STAINLESS STEEL AND SAFETY FILTER CONSTRUCTED OF CARBON STEEL.
 3. FILTERS STRESSED FOR -35" W.C. (-0.087BAR).
 4. - PRIMARY FILTER WITH (8) QP806 SPUNBOND POLYESTER W/ PTFE MEMBRANE (STAINLESS STEEL END CAPS AND CAGE) CARTRIDGES PROVIDING 671 SQ. FT. OF MEDIA WITH AN AIR TO MEDIA RATIO OF 1.9:1 @ 1300 CFM.
 - SAFETY FILTER WITH (2) PROTURA 254 CARTRIDGES PROVIDING 508 SQ. FT. OF MEDIA WITH AN AIR TO MEDIA RATIO OF 2.6:1 @ 1300 CFM.
 5. 1" (25.4MM) NPT CONNECTION FOR COMPRESSED AIR SUPPLY. 80-100 PSI (5.5-6.9 BARG), CLEAN DRY AIR REQUIRED. 1.7 SCF PER PULSE.
 6. NEMA 4 TIMER ENCLOSURE WITH 120 VAC SMART TIMER FOR PRIMARY FILTER TO BE MOUNTED ON SUPPORT STRUCTURE, PRE-WIRED AND TESTED. THEN REMOVED FOR SHIPPING. (NO REVERSE AIR PULSE CLEANING ON SAFETY FILTER)
 7. NEMA 4 GOYEN SOLENOID ENCLOSURE WITH 120 VAC SOLENOIDS MOUNTED ON PRIMARY FILTER HEADER AND PRE-PLUMBED TO GOYEN DIAPHRAGM VALVES WITH POLY-FLO TUBING.
 8. (2) 1/4" NPT DIFFERENTIAL PRESSURE GAUGE PORTS ON PRIMARY FILTER AND (2) 1/4" NPT DIFFERENTIAL PRESSURE PORTS ON SAFETY FILTER. PORTS MUST BE PLUGGED IF DIFFERENTIAL PRESSURE GAUGE IS NOT USED.
 9. 1/4" (6.35MM) WHITE EPDM CLOSED CELL SPONGE GASKET AND (1) SPARE PROVIDED FOR FLANGE CONNECTIONS
 10. 12" BUTTERFLY VALVE WITH 316SS DISC & STEM, WHITE EPDM SEAT AND MANUAL ACTUATOR.
 11. CARTRIDGES SHIPPED INSTALLED IN FILTERS.
 12. FIELD ASSEMBLY REQUIRED.
 13. APPROX. WEIGHT: 2260 LBS. (PRIMARY FILTER)
 610 LBS. (SAFETY FILTER)
 600 LBS. (PRIMARY FILTER STRUCTURE)
 3470 LBS. (TOTAL)
 14. S/N: 167824-003-2 (PRIMARY FILTER)
 167824-005-2 (SAFETY FILTER)
 167824-008-2 (FAN)
 15. TAG: F69040 (PRIMARY FILTER)
 F69045 (SAFETY FILTER)
 BL69050 (FAN)
 16. STAINLESS STEEL TAG REQUIRED.
- FINISH NOTES:
17. INTERNAL PRODUCT CONTACT WELDS ON PRIMARY FILTER TO CONTINUOUS, GROUND SMOOTH, TO CG24 GRIT FINISH.
 18. CARBON STEEL SURFACES TO BE SANDBLASTED TO SSPC-SP-10.
 19. PAINT: (CARBON STEEL SURFACES ONLY)
 - PRIMER: ZINC CLAD II (B69V3 & B69D11)
 - INTERMEDIATE COAT: MACROPOXY 646 (B58-600 & B58V600)
 - TOP COAT: COROTHANE II (B65-200 & B60V2)
 (COLOR: RAL-5015 (SKY BLUE))
 20. INTERNAL AND EXTERNAL STAINLESS STEEL SURFACES TO BE PICKLED.
 21. EXTERNAL REINFORCEMENT RIBS TO BE SKIP WELDED TO HOUSINGS. (CARBON STEEL RIBS TO HAVE CLEAR SILICONE CAULKING BETWEEN SKIP WELDS AFTER PAINTING, STAINLESS STEEL RIBS TO HAVE CLEAR SILICONE CAULKING BETWEEN SKIP WELDS AFTER PICKLING)

DM107269



MANUFACTURE: Mac Process, Inc.
 PLANT BUILT: SABETHA, KS
 YEAR BUILT: 2011
 MODEL: 2M2F8 MAC2FLO FILTER
 SERIAL NO.: 167824-003-2
 EQUIPMENT TAG NO.: F69040
 PURCHASE ORDER NO.: 4557726298
 DESIGN PRESSURE: +0.25 PSI (+0.017 BAR)
 -35" W.C. (-0.087 BAR)
 DESIGN TEMPERATURE: 180°F (82°C)
 EMPTY WEIGHT: 2260 LBS.

MANUFACTURE: Mac Process, Inc.
 PLANT BUILT: SABETHA, KS
 YEAR BUILT: 2011
 MODEL: 2M2F2 MAC2FLO FILTER
 SERIAL NO.: 167824-005-2
 EQUIPMENT TAG NO.: F69045
 PURCHASE ORDER NO.: 4557726298
 DESIGN PRESSURE: +0.25 PSI (+0.017 BAR)
 -35" W.C. (-0.087 BAR)
 DESIGN TEMPERATURE: 180°F (82°C)
 EMPTY WEIGHT: 610 LBS.

SPECIAL ASSEMBLY AND TEST NOTES:
 22. FILTERS TO BE BUBBLE TESTED AT 1/4 PSI (0.017 BARG)

This print is certified to be dimensionally correct to ± 1/4 inch on all components, ± 1/2 on overall dimensions up to 120 inches and ± 1 1/2 on all dimensions greater than 120.

Mac Process, Inc.
 BY Michael L Herbster
 DATE 12/16/11

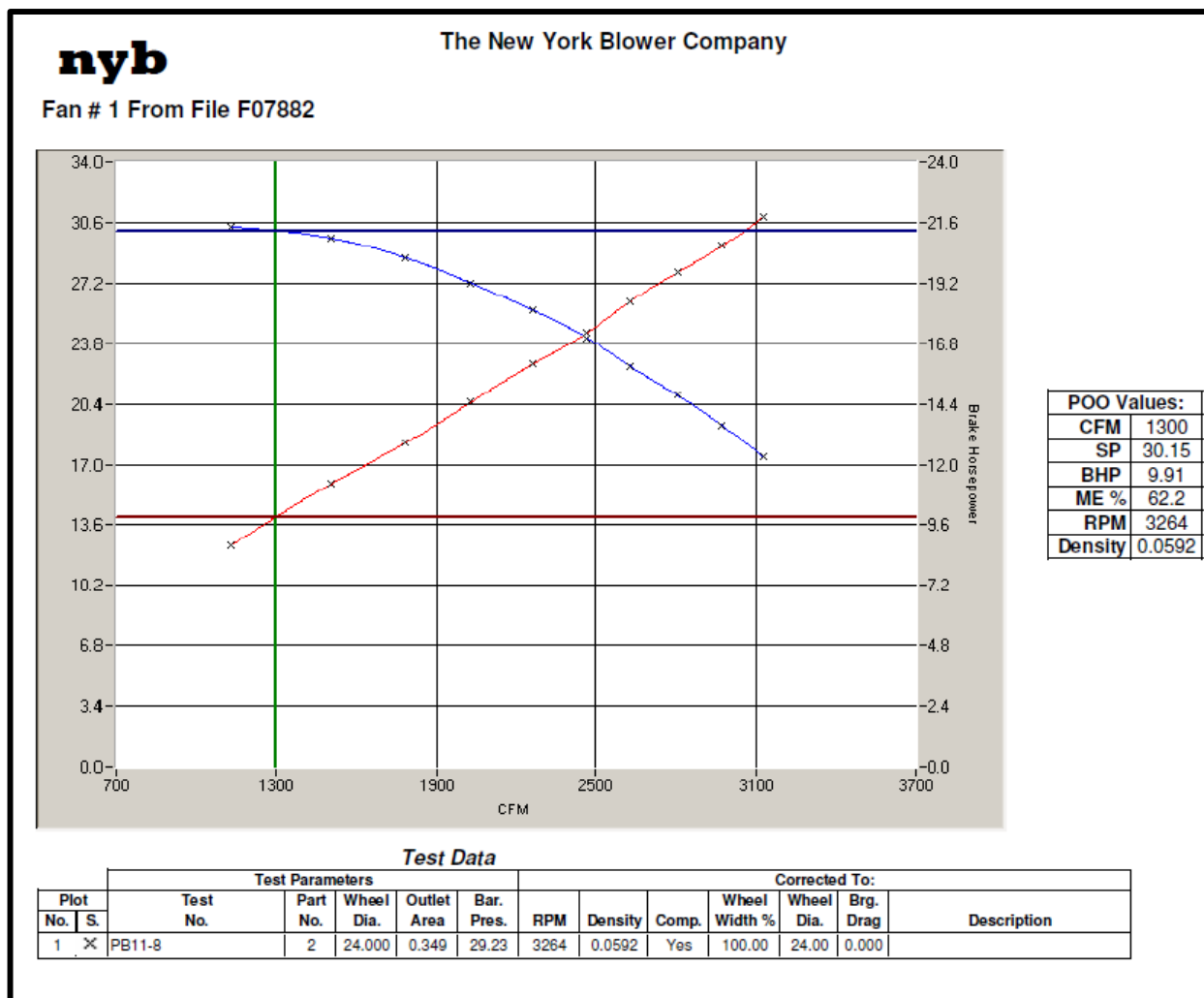
 schenckprocess group		THIS MATERIAL IS THE PROPERTY OF MAC PROCESS INC. AND SHOULD NOT BE REPRODUCED, PUBLISHED OR DISCLOSED TO OTHERS WITHOUT AUTHORIZATION AND SHALL NOT BE USED IN ANY WAY AGAINST OR DETRIMENTAL TO MAC PROCESS INC., SABETHA, KANSAS.	
2M2F8 MAC2FLO WITH 2M2F2 SAFETY FILTER FOR BASF CORPORATION (ELYRIA, OH)		JOB NO. 167824 DRAWING NO. DM107269 REV. D	
DRAWN BY MLH DATE 04/13/11 SCALE 1/16"=1"	CHECKED BY [blank] DATE [blank] DESIGNED BY [blank] DATE [blank]	APPROVED BY [blank] DATE [blank]	DATE 12/16/11

New York Blower Company

Cathodes-4, -6, and -7

Dust Collectors DF-4, DF-6, and DF-7

Blower ID: 61040

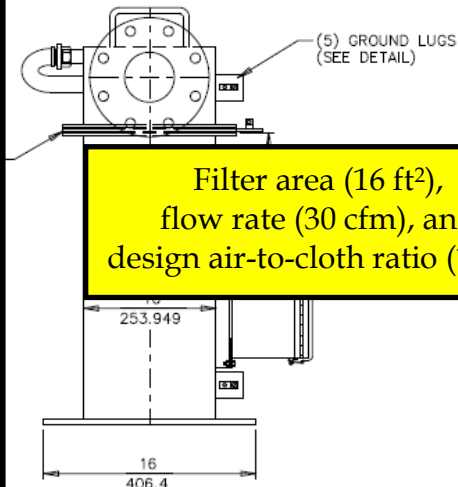


MAC Process, Inc.

Cathode-9

Dust DF-12

Filter ID: F70025



(5) GROUND LUGS
(SEE DETAIL)

Filter area (16 ft²),
flow rate (30 cfm), and
design air-to-cloth ratio (1.9:1)

253.949

16

406.4

NOTES:

1. ALL DIMENSIONS ARE IN INCHES WITH SECONDARY UNITS IN MILLIMETERS.
2. 3/4" (19.05MM) FNPT, 60-90 PSI (4.1- 6.2 BARG) REGULATED CLEAN, DRY AIR REQUIRED: 1 SCFM VOLUME.
3. 10 GA. 304 STAINLESS STEEL CONSTRUCTION.
4. UNIT IS STRESSED FOR -17" Hg (-0.57 BAR).
5. (2) 1/4" (6.35MM) FNPT DIFFERENTIAL PRESSURE GAUGE PORTS MUST HAVE PIPE PLUGS IF DIFFERENTIAL PRESSURE GAUGE IS NOT USED.
6. TOP PLENUM REMOVABLE FOR ACCESS TO CARTRIDGE. DE-ENERGIZE TIMER CONTROL BEFORE WORKING ON UNIT. REMOVE BY UNBOLTING PLENUM FROM BAGHOUSE AND EXHAUST DUCT, DISCONNECT 3/4" (19.05MM) BRAIDED HOSE, AND LIFT OFF TOP PLENUM. (HEADER REMAINS ATTACHED TO HOUSING)
7. (2) 1/4" (6.35MM) THICK WHITE EPDM CLOSED CELL SPONGE GASKETS PROVIDED TO SEAL TUBESHEET.
8. NEMA 4 ENCLOSURE WITH TIMER CONTROL AND GOYEN SOLENOID VALVE, 24 VDC REQUIRED. (SOLENOID PRE-PLUMBED TO PULSE HEADER GOYEN DIAPHRAGM VALVE WITH 1/4" (6.35MM) POLY-FLO TUBING)
9. UNIT INCLUDES (1) POLIPLLEET QN812 NOMEX W/ PTFE TOP LOAD CARTRIDGE, PROVIDING 16 SQ. FT. OF MEDIA WITH AN AIR TO CLOTH RATIO OF 1.9:1 @ 30 CFM.
10. 1/4" (6.35MM) WHITE SILICONE SPONGE GASKET AND (1) SPARE PROVIDED FOR FLANGE CONNECTIONS.
11. APPROX. WEIGHT: 50 LBS.
12. S/N: 167824-009-1
13. TAG: F70025
14. STAINLESS STEEL TAG.

FINISH NOTES:

15. INTERIOR PRODUCT CONTACT WELDS TO BE CONTINUOUS, GROUND SMOOTH TO CG24 GRIT FINISH.
16. INTERIOR AND EXTERIOR STAINLESS STEEL SURFACES TO BE PICKLED.

SPECIAL ASSEMBLY AND TEST NOTES:

17. FILTER TO BE BUBBLE TESTED AT 1/2 PSI (0.034 BARG)

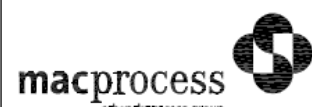
CM105939

This print is certified to be dimensionally correct to $\pm 1/4$ inch on all components, $\pm 1/2$ on overall dimensions up to 120 inches and $\pm 1 1/2$ on all dimensions greater than 120.

Mac Process, Inc.
 BY Michael L Herbster DATE 11/20/11

(14) STAINLESS STEEL TAG INFORMATION

MANUFACTURE: Mac Process, Inc.
 PLANT BUILT: SABETHA, KS
 YEAR BUILT: 2011
 MODEL: 19RTC1 STYLE II FILTER
 SERIAL NO.: 167824-009-1
 EQUIPMENT TAG NO.: F70025
 PURCHASE ORDER NO.: 4557726298
 DESIGN PRESSURE: +8.27 PSI (+0.57 BARG)
 -17" Hg (-0.57 BARG)
 DESIGN TEMPERATURE: 266°F (130°C)
 EMPTY WEIGHT: 50 LBS.



THIS MATERIAL IS THE PROPERTY OF MAC PROCESS INC. AND SHOULD NOT BE REPRODUCED, PUBLISHED OR DISCLOSED TO OTHERS WITHOUT AUTHORIZATION AND SHALL NOT BE USED IN ANY WAY AGAINST OR DETRIMENTAL TO MAC PROCESS INC., SABETHA, KANSAS.

19RTC1 STYLE II FILTER
 FOR
 BASF CORPORATION
 (ELYRIA, OH)

DRAWN BY	DATE	UNLESS OTHERWISE SPECIFIED DIMENSIONS ARE IN INCHES			JOB NO.	DRAWING NO.	REV.
MLH	03/24/11	TOLERANCES:	DECIMAL	FRACTION			
SCALE	1/8"=1"	±.005	±.01	±.01	167824	CM105939	D

MAC Process, Inc.

Cathode- 9 and Cathode -13

Dust Collector DF-8

Filter ID: F69040

Blower ID: 69050

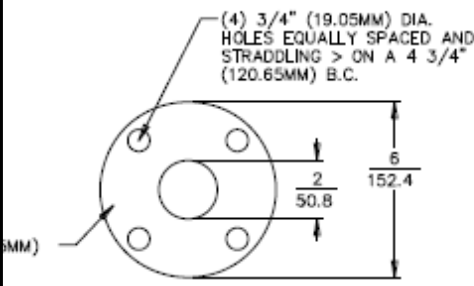
Filter area (671 ft²),
 flow rate (1,300 cfm), and
 design air-to-cloth ratio (1.9:1)

NOTES:

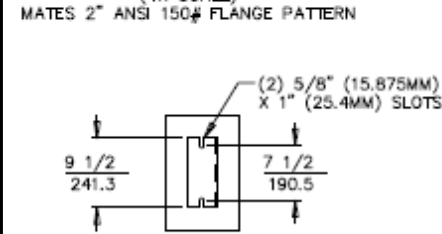
1. ALL DIMENSIONS ARE IN INCHES.
 2. PRIMARY FILTER CONSTRUCTED OF 304 STAINLESS STEEL AND SAFETY FILTER CONSTRUCTED OF CARBON STEEL.
 3. FILTERS STRESSED FOR -35" W.C. (-0.087BAR).
 4. - PRIMARY FILTER WITH (8) QP806 SPUNBOND POLYESTER W/ PTFE MEMBRANE (STAINLESS STEEL END CAPS AND CAGE) CARTRIDGES PROVIDING 671 SQ. FT. OF MEDIA WITH AN AIR TO MEDIA RATIO OF 1.9:1 @ 1300 CFM.
 - SAFETY FILTER WITH (2) PROTURA 254 CARTRIDGES PROVIDING 508 SQ. FT. OF MEDIA WITH AN AIR TO MEDIA RATIO OF 2.6:1 @ 1300 CFM.
 5. 1" (25.4MM) NPT CONNECTION FOR COMPRESSED AIR SUPPLY. 80-100 PSI (5.5-6.9 BARG), CLEAN DRY AIR REQUIRED. 1.7 SCF PER PULSE.
 6. NEMA 4 TIMER ENCLOSURE WITH 120 VAC SMART TIMER FOR PRIMARY FILTER TO BE MOUNTED ON SUPPORT STRUCTURE, PRE-WIRED AND TESTED. THEN REMOVED FOR SHIPPING. (NO REVERSE AIR PULSE CLEANING ON SAFETY FILTER)
 7. NEMA 4 GOYEN SOLENOID ENCLOSURE WITH 120 VAC SOLENOIDS MOUNTED ON PRIMARY FILTER HEADER AND PRE-PLUMBED TO GOYEN DIAPHRAGM VALVES WITH POLY-FLO TUBING.
 8. (2) 1/4" NPT DIFFERENTIAL PRESSURE GAUGE PORTS ON PRIMARY FILTER AND (2) 1/4" NPT DIFFERENTIAL PRESSURE PORTS ON SAFETY FILTER. PORTS MUST BE PLUGGED IF DIFFERENTIAL PRESSURE GAUGE IS NOT USED.
 9. 1/4" (6.35MM) WHITE EPDM CLOSED CELL SPONGE GASKET AND (1) SPARE PROVIDED FOR FLANGE CONNECTIONS
 10. 12" BUTTERFLY VALVE WITH 316SS DISC & STEM, WHITE EPDM SEAT AND MANUAL ACTUATOR.
 11. CARTRIDGES SHIPPED INSTALLED IN FILTERS.
 12. FIELD ASSEMBLY REQUIRED.
 13. APPROX. WEIGHT: 2260 LBS. (PRIMARY FILTER)
 610 LBS. (SAFETY FILTER)
 600 LBS. (PRIMARY FILTER STRUCTURE)
 3470 LBS. (TOTAL)
 14. S/N: 167824-003-2 (PRIMARY FILTER)
 167824-005-2 (SAFETY FILTER)
 167824-008-2 (FAN)
 15. TAG: F69040 (PRIMARY FILTER)
 F69045 (SAFETY FILTER)
 BL69050 (FAN)
 16. STAINLESS STEEL TAG REQUIRED.
- FINISH NOTES:
17. INTERNAL PRODUCT CONTACT WELDS ON PRIMARY FILTER TO CONTINUOUS, GROUND SMOOTH, TO CG24 GRIT FINISH.
 18. CARBON STEEL SURFACES TO BE SANDBLASTED TO SSPC-SP-10.
 19. PAINT: (CARBON STEEL SURFACES ONLY)
 - PRIMER: ZINC CLAD II (B69V3 & B69D11)
 - INTERMEDIATE COAT: MACROPOXY 646 (B58-600 & B58V600)
 - TOP COAT: COROTHANE II (B65-200 & B60V2)
 (COLOR: RAL-5015 (SKY BLUE))
 20. INTERNAL AND EXTERNAL STAINLESS STEEL SURFACES TO BE PICKLED.
 21. EXTERNAL REINFORCEMENT RIBS TO BE SKIP WELDED TO HOUSINGS. (CARBON STEEL RIBS TO HAVE CLEAR SILICONE CAULKING BETWEEN SKIP WELDS AFTER PAINTING, STAINLESS STEEL RIBS TO HAVE CLEAR SILICONE CAULKING BETWEEN SKIP WELDS AFTER PICKLING)

DM107269

MEW A-A
 FOOT PAD LAYOUT DETAIL



LEVEL INDICATOR PORT FLANGE DETAIL
 (4X SCALE)



VIBRATOR MOUNT DETAIL
 MOUNT FOR BH1 5/8 OR BH2 VIBRATOR
 (VIBRATOR NOT PROVIDED)

STAINLESS STEEL TAG INFO.

MANUFACTURE: Mac Process, Inc.
 PLANT BUILT: SABETHA, KS
 YEAR BUILT: 2011
 MODEL: 2M2F8 MAC2FLO FILTER
 SERIAL NO.: 167824-003-2
 EQUIPMENT TAG NO.: F69040
 PURCHASE ORDER NO.: 4557726298
 DESIGN PRESSURE: +0.25 PSI (+0.017 BAR)
 -35" W.C. (-0.087 BAR)
 DESIGN TEMPERATURE: 180°F (82°C)
 EMPTY WEIGHT: 2260 LBS.

MANUFACTURE: Mac Process, Inc.
 PLANT BUILT: SABETHA, KS
 YEAR BUILT: 2011
 MODEL: 2M2F2 MAC2FLO FILTER
 SERIAL NO.: 167824-005-2
 EQUIPMENT TAG NO.: F69045
 PURCHASE ORDER NO.: 4557726298
 DESIGN PRESSURE: +0.25 PSI (+0.017 BAR)
 -35" W.C. (-0.087 BAR)
 DESIGN TEMPERATURE: 180°F (82°C)
 EMPTY WEIGHT: 610 LBS.

SPECIAL ASSEMBLY AND TEST NOTES:
 22. FILTERS TO BE BUBBLE TESTED AT 1/4 PSI (0.017 BARG)

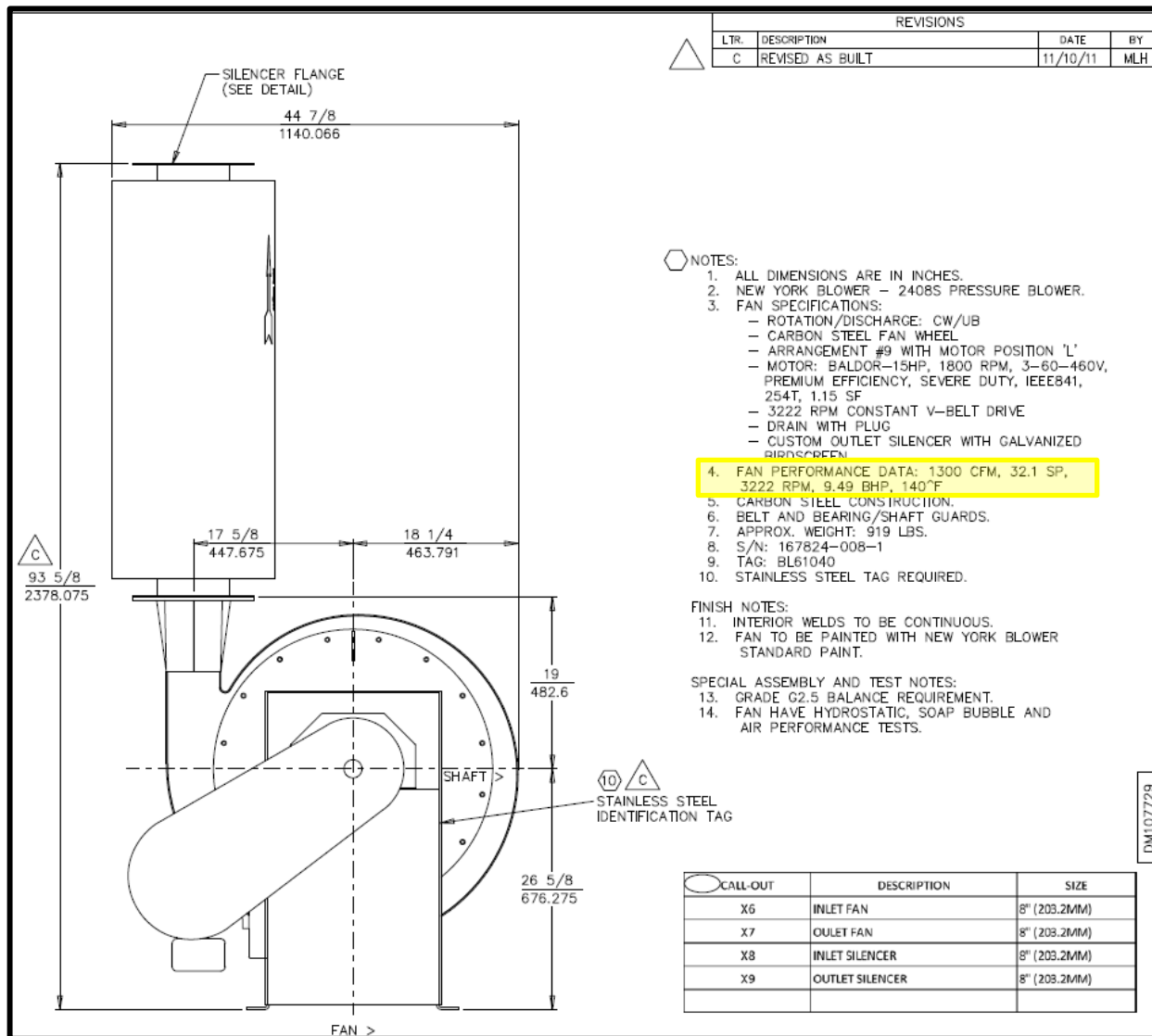
This print is certified to be dimensionally correct to ± 1/4 inch on all components, ± 1/2 on overall dimensions up to 120 inches and ± 1 1/2 on all dimensions greater than 120.

Mac Process, Inc.
 BY Michael L Herbster DATE 12/16/11

		THIS MATERIAL IS THE PROPERTY OF MAC PROCESS INC. AND SHOULD NOT BE REPRODUCED, PUBLISHED OR DISCLOSED TO OTHERS WITHOUT AUTHORIZATION AND SHALL NOT BE USED IN ANY WAY AGAINST OR DETRIMENTAL TO MAC PROCESS INC., SABETHA, KANSAS.	
macprocess schenckprocess group		2M2F8 MAC2FLO WITH 2M2F2 SAFETY FILTER FOR BASF CORPORATION (ELYRIA, OH)	
DRAWN BY MLH	DATE 04/13/11	UNLESS OTHERWISE SPECIFIED DIMENSIONS ARE IN INCHES DECIMALS FRACTIONS	JOB NO. 167824
SCALE 1/16" = 1"	DESIGNED BY CHECKED BY DATE	DRAWING NO. DM107269	REV. D

New York Blower Company

Blower ID: 69050



REVISIONS			
LTR.	DESCRIPTION	DATE	BY
C	REVISED AS BUILT	11/10/11	MLH

- NOTES:
- ALL DIMENSIONS ARE IN INCHES.
 - NEW YORK BLOWER - 2408S PRESSURE BLOWER.
 - FAN SPECIFICATIONS:
 - ROTATION/DISCHARGE: CW/UB
 - CARBON STEEL FAN WHEEL
 - ARRANGEMENT #9 WITH MOTOR POSITION 'L'
 - MOTOR: BALDOR-15HP, 1800 RPM, 3-60-460V, PREMIUM EFFICIENCY, SEVERE DUTY, IEEEE841, 254T, 1.15 SF
 - 3222 RPM CONSTANT V-BELT DRIVE
 - DRAIN WITH PLUG
 - CUSTOM OUTLET SILENCER WITH GALVANIZED BIRDSCREEN
 - FAN PERFORMANCE DATA: 1300 CFM, 32.1 SP, 3222 RPM, 9.49 BHP, 140°F
 - CARBON STEEL CONSTRUCTION.
 - BELT AND BEARING/SHAFT GUARDS.
 - APPROX. WEIGHT: 919 LBS.
 - S/N: 167824-008-1
 - TAG: BL61040
 - STAINLESS STEEL TAG REQUIRED.
- FINISH NOTES:
- INTERIOR WELDS TO BE CONTINUOUS.
 - FAN TO BE PAINTED WITH NEW YORK BLOWER STANDARD PAINT.
- SPECIAL ASSEMBLY AND TEST NOTES:
- GRADE G2.5 BALANCE REQUIREMENT.
 - FAN HAVE HYDROSTATIC, SOAP BUBBLE AND AIR PERFORMANCE TESTS.

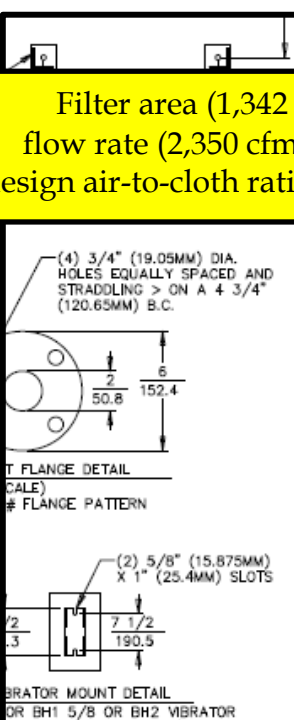
CALL-OUT	DESCRIPTION	SIZE
X6	INLET FAN	8" (203.2MM)
X7	OUTLET FAN	8" (203.2MM)
X8	INLET SILENCER	8" (203.2MM)
X9	OUTLET SILENCER	8" (203.2MM)

DM107729

MAC Process, Inc.
 Cathode-11 and Cathode -12
 Dust Collectors DF-10

Filter ID: F92010

Filter area (1,342 ft²),
 flow rate (2,350 cfm), and
 design air-to-cloth ratio (1.75:1)



(4) 3/4" (19.05MM) DIA. HOLES EQUALLY SPACED AND STRADDLING > ON A 4 3/4" (120.65MM) B.C.

T FLANGE DETAIL (SCALE) # FLANGE PATTERN

(2) 5/8" (15.875MM) X 1" (25.4MM) SLOTS

VIBRATOR MOUNT DETAIL (OR BH1 5/8 OR BH2 VIBRATOR (VIBRATOR NOT PROVIDED))

(15) STAINLESS STEEL TAG INFO.

MANUFACTURE: Mac Process, Inc.
 PLANT BUILT: SABETHA, KS
 YEAR BUILT: 2011
 MODEL: 4M2F16 MAC2FLO FILTER
 SERIAL NO.: 167824-010-1
 EQUIPMENT TAG NO.: F92010
 PURCHASE ORDER NO.: 4557726298
 DESIGN PRESSURE: +0.25 PSI (+0.017 BARG)
 -35" W.C. (-0.087 BAR)
 DESIGN TEMPERATURE: 180°F (82°C)
 EMPTY WEIGHT: 3160 LBS.

MANUFACTURE: Mac Process, Inc.
 PLANT BUILT: SABETHA, KS
 YEAR BUILT: 2011
 MODEL: 2M2F4 MAC2FLO FILTER
 SERIAL NO.: 167824-012-1
 EQUIPMENT TAG NO.: F92020
 PURCHASE ORDER NO.: 4557726298
 DESIGN PRESSURE: +0.25 PSI (+0.017 BARG)
 -35" W.C. (-0.087 BAR)
 DESIGN TEMPERATURE: 180°F (82°C)
 EMPTY WEIGHT: 1210 LBS.

NOTES:

- ALL DIMENSIONS ARE IN INCHES.
- PRIMARY FILTER CONSTRUCTED OF 304 STAINLESS STEEL AND SAFETY FILTER CONSTRUCTED OF CARBON STEEL.
- FILTERS STRESSED FOR 35" W.C. (0.087BAR).
- PRIMARY FILTER WITH (16) QP806 SPUNBOND POLYESTER W/ PTFE MEMBRANE (STAINLESS STEEL END CAPS AND CAGE) CARTRIDGES PROVIDING 1342 SQ. FT. OF MEDIA WITH AN AIR TO MEDIA RATIO OF 1.75:1 @ 2350 CFM.
- SAFETY FILTER WITH (4) PROTURA 254 CARTRIDGES PROVIDING 1016 SQ. FT. OF MEDIA WITH AN AIR TO MEDIA RATIO OF 2.31:1 @ 2350 CFM.
- 1" (25.4MM) NPT CONNECTION FOR COMPRESSED AIR SUPPLY. 80-100 PSI (5.5-6.9 BARG), CLEAN DRY AIR REQUIRED. 3.6 SCF PER PULSE.
- NEMA 4 TIMER ENCLOSURE WITH 120 VAC SMART TIMER FOR PRIMARY FILTER TO BE MOUNTED ON SUPPORT STRUCTURE, PRE-WIRED AND TESTED, THEN REMOVED FOR SHIPPING. (NO REVERSE AIR PULSE CLEANING ON SAFETY FILTER)
- NEMA 4 GOYEN SOLENOID ENCLOSURE WITH 120 VAC SOLENOIDS MOUNTED ON PRIMARY FILTER HEADER AND PRE-PLUMBED TO GOYEN DIAPHRAGM VALVES WITH POLY-FLO TUBING.
- (2) 1/4" NPT DIFFERENTIAL PRESSURE GAUGE PORTS ON PRIMARY FILTER AND (2) 1/4" NPT DIFFERENTIAL PRESSURE PORTS ON SAFETY FILTER. PORTS MUST BE PLUGGED IF DIFFERENTIAL PRESSURE GAUGE IS NOT USED.
- 1/4" (6.35MM) WHITE EPDM CLOSED CELL SPONGE GASKET AND (1) SPARE PROVIDED FOR FLANGE CONNECTIONS
- 12" BUTTERFLY VALVE WITH 316SS DISC & STEM, WHITE EPDM SEAT AND MANUAL ACTUATOR.
- CARTRIDGES SHIPPED INSTALLED IN FILTERS.
- FIELD ASSEMBLY REQUIRED.
- APPROX. WEIGHT: 3160 LBS. (PRIMARY FILTER)
1210 LBS. (SAFETY FILTER)
600 LBS. (PRIMARY FILTER STRUCTURE)
4970 LBS. (TOTAL)
- S/N: 167824-010-1 (PRIMARY FILTER)
167824-012-1 (SAFETY FILTER)
167824-015-1 (FAN)
- TAG: F92010 (PRIMARY FILTER)
F92020 (SAFETY FILTER)
BL92030 (FAN)
- STAINLESS STEEL TAG REQUIRED.

FINISHED NOTES:


- INTERNAL PRODUCT CONTACT WELDS ON PRIMARY FILTER TO CONTINUOUS, GROUND SMOOTH, TO CG24 GRIT FINISH.
- CARBON STEEL SURFACES TO BE SANDBLASTED TO SSPC-SP-10.
- PAINT: (CARBON STEEL SURFACES ONLY)
 - PRIMER: ZINC CLAD II (B69V3 & B69D11)
 - INTERMEDIATE COAT: MACROPOXY 646 (B58-600 & B58V600)
 - TOP COAT: COROTHANE II (B65-200 & B60V2) (COLOR: RAL-5015 (SKY BLUE))
- INTERNAL AND EXTERNAL STAINLESS STEEL SURFACES TO BE PICKLED.
- EXTERNAL REINFORCEMENT RIBS TO BE SKIP WELDED TO HOUSINGS. (CARBON STEEL RIBS TO HAVE CLEAR SILICONE CAULKING BETWEEN SKIP WELDS AFTER TO PAINTING, STAINLESS STEEL RIBS TO HAVE CLEAR SILICONE CAULKING BETWEEN SKIP WELDS AFTER PICKLING)

SPECIAL ASSEMBLY AND TEST NOTES:

- FILTERS TO BE BUBBLE TESTED AT 1/4 PSI (0.017 BARG)

This print is certified to be dimensionally correct to $\pm 1/4$ inch on all components, $\pm 1/2$ on overall dimensions up to 120 inches and $\pm 1 1/2$ on all dimensions greater than 120.

Mac Process, Inc.
 BY Michael L Herbster DATE 10/16/11



macprocess
a schenck process group

THIS MATERIAL IS THE PROPERTY OF MAC PROCESS INC. AND SHOULD NOT BE REPRODUCED, PHOTOCOPIED OR DISCLOSED TO OTHERS WITHOUT AUTHORIZATION AND SHALL NOT BE USED IN ANY WAY AGAINST OR DETRIMENTAL TO MAC PROCESS INC., SABETHA, KANSAS.

DRAWN BY: MLH DATE: 04/13/11 SCALE: 1/20"=1"	ALL DIMENSIONS UNLESS OTHERWISE SPECIFIED ARE IN INCHES DECIMALS: 1/16" FRACTIONS: 1/8" TOLERANCES: SEE SPEC	JOB NO.: 167824 DRAWING NO.: DM107270 REV.: E
--	---	---

ERM

D-14

BASF - ELYRIA, OHIO/GMS0221398-9 APRIL 2014

PUBLIC DOCUMENT

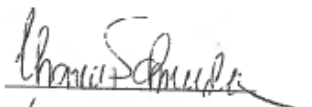
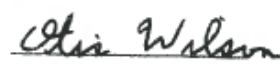

Vac-U-Max

Cathode-13

Dust Collectors DF-11

Filter ID: F67350

Blower ID: 67355

VAC-U-MAX	
69 William Street, Belleville, NJ 07109 (973) 759-4600 Fax (973) 759-6449 E-Mail: info@vac-u-max.com	
VAC-U-MAX QUALITY ASSURANCE INSPECTION CHECK LIST CENTRAL VACUUM SYSTEMS	
VAC-U-MAX Job #:	4240923
Customer:	BASF Corporation
Destination:	Elyria, Ohio
Purchase Order / Contract #:	4900110205
Equipment:	FSU 30 BIBO, VPU 5.0Hp
VAC-U-MAX Catalog #s:	Z71655/02A, 71655/01
BASF System Part #:	Filter Sagger Cleaning F67350 (VAC-U-MAX SYSTEM "A") Sub Assembly Part #s: BL67355, D67351, F67353
Assembled By:	Alan Zecca, Sr., Ruben Quijano: Mechanical Ed Orlando, Mike Diaz: Electrical
Engineering:	Jonathan Saenz: Mechanical Will Reigert: Electrical
Inspected By:	Thomas Schneider, VAC-U-MAX Otis Wilson, WORLEY PARSONS
Above referenced equipment has passed VAC-U-MAX, and Worley Parsons quality assurance and inspection and is approved for shipment. All pages of this report have been reviewed and accepted.	
VAC-U-MAX	WORLEY PARSONS
Thomas Schneider: 	Otis Wilson: 
Date: <u>1/19/2012</u>	Date: <u>19-Jan-2012</u>
	

11480 12/08 KU

INSPECTION CHECKLIST

GENERAL FUNCTION <i>(check as appropriate)</i> <input checked="" type="checkbox"/> ACCEPTED <input type="checkbox"/> REJECTED	THE SYSTEM FUNCTIONS AS SPECIFIED: <input checked="" type="checkbox"/> ON/OFF CIRCUITS <input checked="" type="checkbox"/> SOLENOIDS <input checked="" type="checkbox"/> PLC PROGRAMS AND TIMERS <input checked="" type="checkbox"/> FILTER CLEANING <input checked="" type="checkbox"/> DISCHARGE VALVES <input checked="" type="checkbox"/> LEVEL PROBES <input checked="" type="checkbox"/> DIAGNOSTIC INDICATORS <i>(vacuum gauges, delta-P gauges, etc.)</i> <input checked="" type="checkbox"/> VACUUM RELIEF VALVES <input type="checkbox"/> WARNING DEVICES AND INDICATORS <i>(audible alarms, stack or strobe lights, etc)</i> <input type="checkbox"/> OTHER:
CONSTRUCTION <input checked="" type="checkbox"/> ACCEPTED <input type="checkbox"/> REJECTED	MATERIAL: <input checked="" type="checkbox"/> CARBON/STAINLES 304 AND 316 FINISH: <input checked="" type="checkbox"/> WHITE POWDER COAT/BEAD BLAST WELDS <input checked="" type="checkbox"/> GENERAL PURPOSE CONSTRUCTION
RECEIVER / FILTER SEPARATORS <input checked="" type="checkbox"/> ACCEPTED <input type="checkbox"/> REJECTED	TYPE: <input checked="" type="checkbox"/> FREE STANDING BIBO RECEIVER SIZE: <input checked="" type="checkbox"/> 30" DIAMETER CONCENTRIC CONE INLET SIZE / TYPE: <input checked="" type="checkbox"/> 2.5" ANSI #150 OUTLET SIZE / TYPE: <input checked="" type="checkbox"/> 2.5" TUBE DISCHARGE VALVE: <input checked="" type="checkbox"/> DOUBLE WAFER VALVE COLLECTION CONTAINER: <input checked="" type="checkbox"/> CONTINUOUS BAGGING <div style="border: 2px solid yellow; padding: 2px;"> FILTER TYPE: <input checked="" type="checkbox"/> CARTRIDGE FILTER MEDIA: <input checked="" type="checkbox"/> POLYESTER WITH EPTFE MEMBRANE FILTER CLEANING: <input checked="" type="checkbox"/> CONTINUOUS PULSE </div>
POWER PACKAGE <input checked="" type="checkbox"/> ACCEPTED <input type="checkbox"/> REJECTED	TYPE: <input checked="" type="checkbox"/> ROTARY LOBE POSITIVE DISPLACEMENT PUMP <div style="border: 2px solid yellow; padding: 2px;"> BLOWER MODEL: <input checked="" type="checkbox"/> ROOTS URAI 33 </div> MOTOR: <input checked="" type="checkbox"/> IEEE841 RATED TEFC MOTOR MFG'R: <input checked="" type="checkbox"/> RELIANCE/BALDOR ELECTRIC HORSEPOWER: <input checked="" type="checkbox"/> 5.0 HP 230/480 VOLTS VACUUM RELIEF VALVE: <input checked="" type="checkbox"/> BREAKS AT 12" Hg INLET SIZE / TYPE: <input checked="" type="checkbox"/> 2.5" TUBE SECONDARY FILTER: <input checked="" type="checkbox"/> HEPA CARTRIDGE SOUND ENCLOSURE: <input checked="" type="checkbox"/> YES EXHAUST SILENCER: <input checked="" type="checkbox"/> DUAL EXHAUST SILENCER

Company: ROOTS Division
 Address: 16240 Port Northwest Drive, Houston, Texas 77041
 Ph: 832-590-2305/1-877-393-7668 Fax: 832-590-2326

ROOTS BLOWER PERFORMANCE REPORT : Program Version 6.13 Release Date 2/10/2010
 Program Mode: SELECTION Run Date: 11/28/2011

AMBIENT CONDITIONS:

Gas	AIR	
Relative Humidity	36%	
Molecular Weight	28.863	
k-Value	1.396	
Specific Gravity	.996	
Ambient Temperature	68	deg F
Ambient Pressure	14.33	PSIA
Elevation	700	feet

STANDARD CONDITIONS:

Pressure	14.7	PSIA
Temperature	68	deg F
Relative Humidity	36	%

SELECTED UNIT DETAIL: Model 33 URAI

	Design	Des/Max
Speed, RPM	2492	69.2%
System Inlet Volume, ICFM	128	
Actual Blower Inlet Volume, ICFM	128	+/-5 %
Standard Volume, SCFM	108	
Mass/Weight Flow, #/min	8.07	+/-5 %
System Inlet Temperature, deg F	68.0	
System Inlet Pressure, in Hg Vac	4.000	
Inlet Pressure Loss, PSI	0.000	
Blower Inlet Pressure, in Hg Vac	4.000	
Blower Discharge Pressure, PSIA	14.330	
Discharge Press. Loss, PSI	0.000	
System Discharge Pressure, PSIA	14.330	
Blower Diff. Press., PSI	1.956	16.3%
Power, BHP	1.57	+/-%
Temperature Rise, deg F	28.9	12.9%
Discharge Temperature, deg F	96.9	
System Discharge Volume, ACFM	116	
Relief Valve Setting, in Hg vac	12.0	77.4%
Power @ RV Setting, BHP	4.19	
Temp. Rise @ Relief Setting, deg F	140.7	62.5%
Disch. Temp @ Relief Setting, deg F	208.7	
V-Belt: Est. B10 Brg Life, hours	>99999999	
Coupling: Est. B10 Brg Life, hours	>99999999	
Est. Free Field Noise, dBA	77.7	

Measured as sound press. level per ISO 2151:2004E with +/-3 dBA tol.

Filter Sagger System F67350

VAC-U-MAX PART NO.	BASF PART NO.	QTY.	DESCRIPTION	PRICE
40125EPTFE		2	FLTR CRT 12DX26LG EPTFE	\$ 495.00 EA.

Mike Rectanus

From: Steve Wagoner <stevewagoner@vac-u-max.net>
Sent: Tuesday, April 08, 2014 10:16 AM
To: Mike Rectanus
Cc: Tony Branco
Subject: VAC-U-MAX filter area

4/8/14

Hi Mike,

Per our conversation this morning, I am confirming the filter area of our filter #40125EPPFE to be 47.5 sq ft.

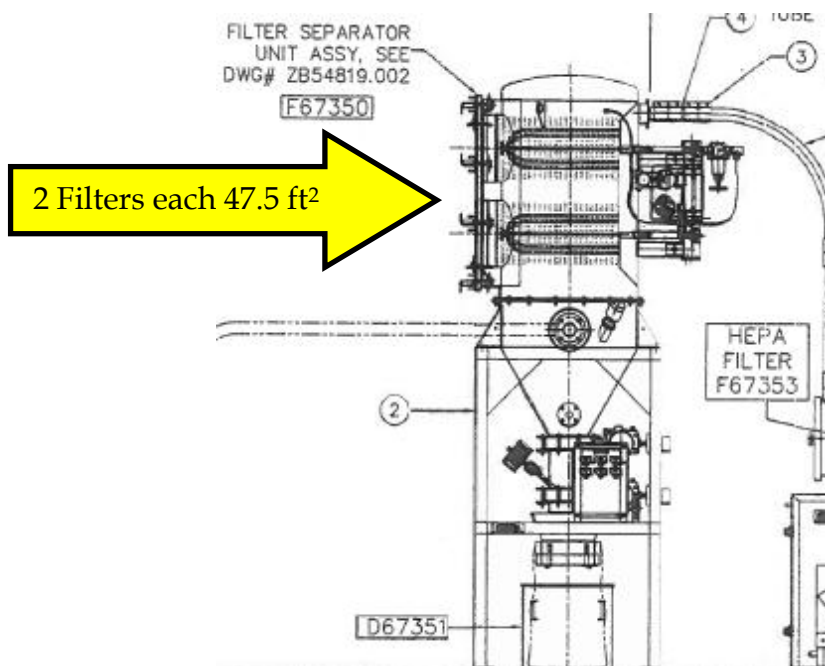
The material is an expanded PTFE.

Please feel free to contact us at anytime if you have further questions.

Steve Wagoner

Mechanical designer
VAC-U-MAX

This message is for the named person's use only.
 It may contain confidential, proprietary or legally privileged information. No confidentiality or privilege is waived or lost by any transmission errors. If you receive this message in error, please immediately delete it and all copies of it from your system, destroy any hard copies of it and notify the sender. You must not, directly or indirectly, use, disclose, distribute, print, or copy any part of this message if you are not the intended recipient. VAC-U-MAX and each of its subsidiaries each reserve the right to intercept and monitor all e-mail communications through its networks if legally allowed.
 Message transmission is not guaranteed to be secure.



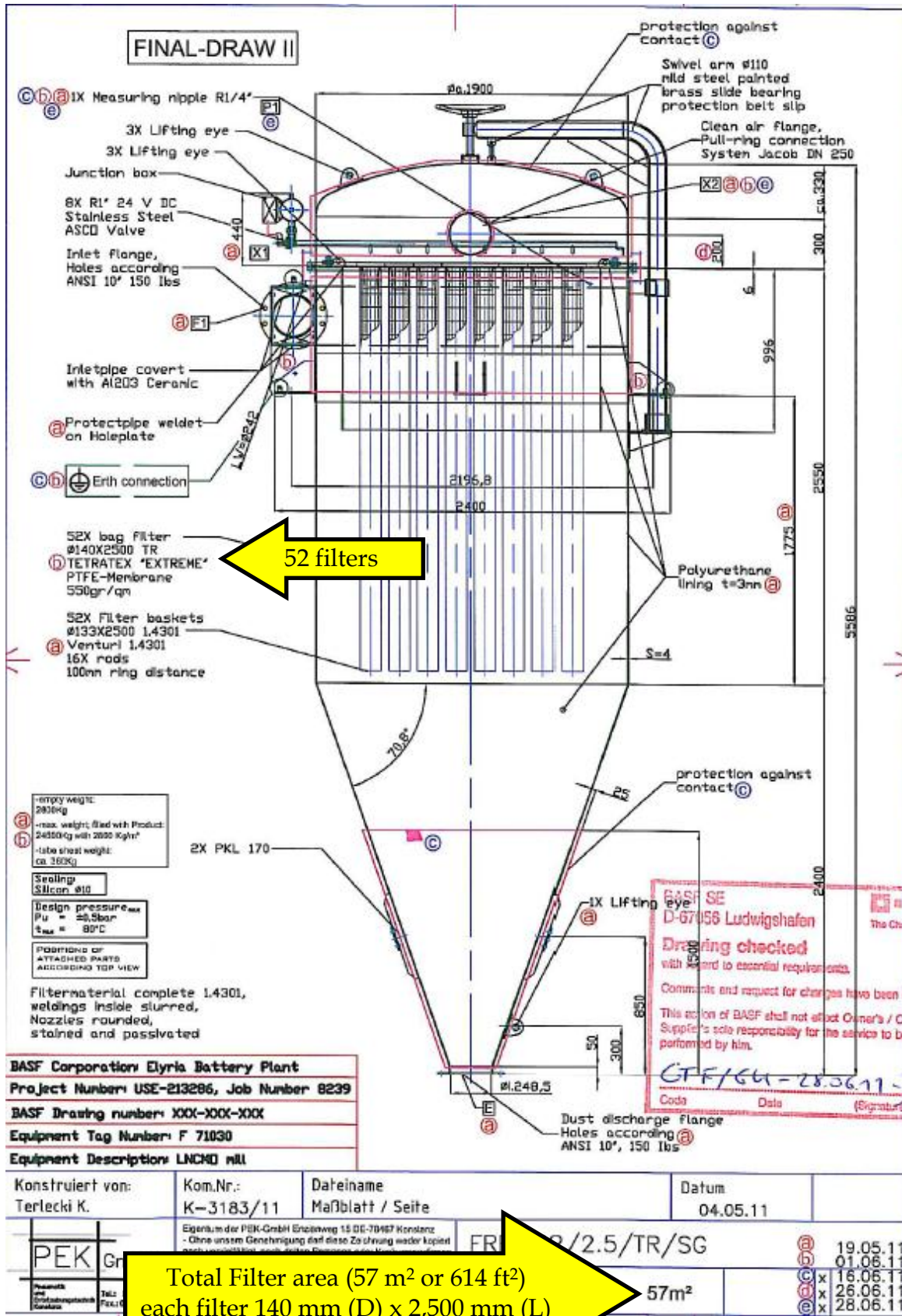
Netzsch

Cathode-10

Dust Collectors DF-9

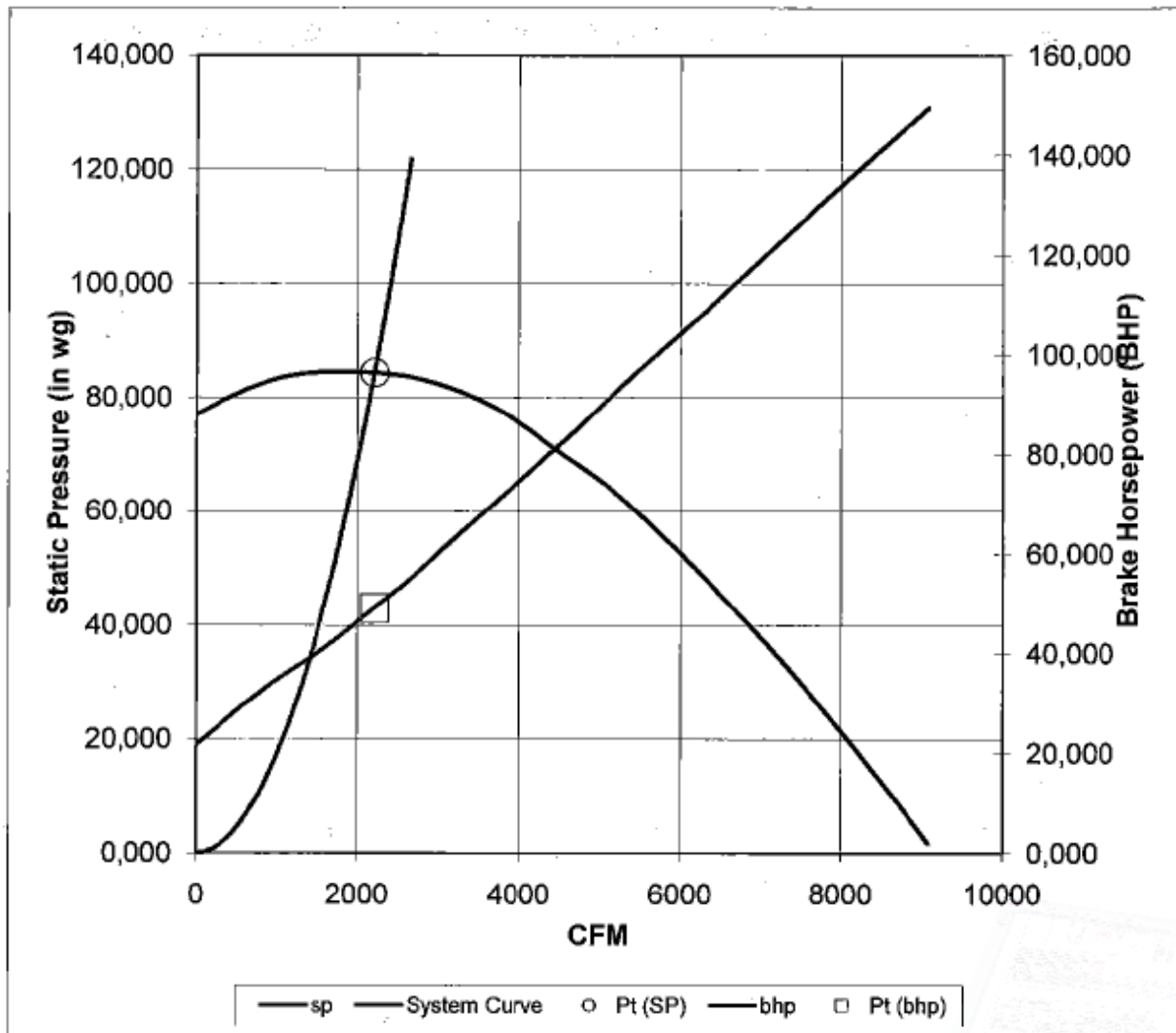
Filter ID: F71030

Blower ID: 71050



Performance Curve

Date:	25-Okt-11	File:	F11357-100	SB2
Performance		Cust. No.:	137964	
Options:		Customer:	NETZSCH-CONDOC MAHLTECHNIK	
			Rodenbacher Chassee 1	
		Product Line:	Type HP Pressure Blower	
		Size:	32010	
		Capacity:	Standard	
		CFM:	2.213	
		SP:	84,3	
		RPM:	3536	
Temperature:	70	BHP:	49,2	
Altitude:	N/A	Density:	0,075	
		Max Safe Speed:	3600	
Tag:	PID TAG NO BL71050 METZSCH-CONDOC MAT NO 737030 0530			




Vac-U-Max

Cathode-15

Dust Collectors DF-13

Filter ID: F11910

Blower ID: 11930

VAC-U-MAX	
69 William Street, Belleville, NJ 07109 (973) 759-4600 Fax (973) 759-6449 E-Mail: info@vac-u-max.com	
VAC-U-MAX QUALITY ASSURANCE INSPECTION CHECK LIST CENTRAL VACUUM SYSTEMS	
VAC-U-MAX Job #:	4240923
Customer:	BASF Corporation
Destination:	Elyria, Ohio
Purchase Order / Contract #:	4900110205
Equipment:	FSU 30 BIBO, VPU 7.5Hp
VAC-U-MAX Catalog #s:	Z71655/02B, 71655/04
BASF System Part #:	Filter Central Vacuum Unit F11910 (VAC-U-MAX SYSTEM "B") Sub Assembly Part #s: BL11930, D11910, F11920
Assembled By:	Alan Zecca, Sr., Ruben Quijano: Mechanical Ed Orlando, Mike Diaz: Electrical
Engineering:	Jonathan Saenz: Mechanical Will Reigert: Electrical
Inspected By:	Thomas Schneider, VAC-U-MAX Otis Wilson, WORLEY PARSONS
Above referenced equipment has passed VAC-U-MAX, and Worley Parsons quality assurance and inspection and is approved for shipment. All pages of this report have been reviewed and accepted.	
VAC-U-MAX	WORLEY PARSONS
Thomas Schneider: <i>Thomas Schneider</i>	Otis Wilson: <i>Otis Wilson</i> 
Date: <u>1/17/2012</u>	Date: <u>19-JAN-2012</u>

INSPECTION CHECKLIST

GENERAL FUNCTION <i>(check as appropriate)</i> <input checked="" type="checkbox"/> ACCEPTED <input type="checkbox"/> REJECTED	THE SYSTEM FUNCTIONS AS SPECIFIED: <input checked="" type="checkbox"/> ON/OFF CIRCUITS <input checked="" type="checkbox"/> SOLENOIDS <input checked="" type="checkbox"/> PLC PROGRAMS AND TIMERS <input checked="" type="checkbox"/> FILTER CLEANING <input checked="" type="checkbox"/> DISCHARGE VALVES <input checked="" type="checkbox"/> LEVEL PROBES <input checked="" type="checkbox"/> DIAGNOSTIC INDICATORS <i>(vacuum gauges, delta-P gauges, etc.)</i> <input checked="" type="checkbox"/> VACUUM RELIEF VALVES <input type="checkbox"/> WARNING DEVICES AND INDICATORS <i>(audible alarms, stack or strobe lights, etc)</i> <input type="checkbox"/> OTHER:
CONSTRUCTION <input checked="" type="checkbox"/> ACCEPTED <input type="checkbox"/> REJECTED	MATERIAL: <input checked="" type="checkbox"/> CARBON/STAINLESS 304 AND 316 FINISH: <input checked="" type="checkbox"/> WHITE POWDER COAT/BEAD BLAST WELDS <input checked="" type="checkbox"/> GENERAL PURPOSE CONSTRUCTION
RECEIVER / FILTER SEPARATORS <input checked="" type="checkbox"/> ACCEPTED <input type="checkbox"/> REJECTED	TYPE: <input checked="" type="checkbox"/> FREE STANDING BIBO RECEIVER SIZE: <input checked="" type="checkbox"/> 30" DIAMETER CONCENTRIC CONE INLET SIZE / TYPE: <input checked="" type="checkbox"/> 2.5" ANSI #150 OUTLET SIZE / TYPE: <input checked="" type="checkbox"/> 2.5" TUBE DISCHARGE VALVE: <input checked="" type="checkbox"/> DOUBLE WAFER VALVE COLLECTION CONTAINER: <input checked="" type="checkbox"/> CONTINUOUS BAGGING <div style="border: 2px solid yellow; padding: 5px;"> FILTER TYPE: <input checked="" type="checkbox"/> CARTRIDGE FILTER MEDIA: <input checked="" type="checkbox"/> POLYESTER WITH EPTFE MEMBRANE FILTER CLEANING: <input checked="" type="checkbox"/> CONTINUOUS PULSE </div>
POWER PACKAGE <input checked="" type="checkbox"/> ACCEPTED <input type="checkbox"/> REJECTED	TYPE: <input checked="" type="checkbox"/> ROTARY LOBE POSITIVE DISPLACEMENT PUMP <div style="border: 2px solid yellow; padding: 5px;"> BLOWER MODEL: <input checked="" type="checkbox"/> ROOTS URAI 45 </div> MOTOR: <input checked="" type="checkbox"/> IEEE841 RATED TEFC MOTOR MFG'R: <input checked="" type="checkbox"/> RELIANCE/BALDOR ELECTRIC HORSEPOWER: <input checked="" type="checkbox"/> 7.5 HP 230/460 VOLTS VACUUM RELIEF VALVE: <input checked="" type="checkbox"/> BREAKS AT 12" Hg INLET SIZE / TYPE: <input checked="" type="checkbox"/> 2.5" TUBE SECONDARY FILTER: <input checked="" type="checkbox"/> HEPA CARTRIDGE SOUND ENCLOSURE: <input checked="" type="checkbox"/> YES EXHAUST SILENCER: <input checked="" type="checkbox"/> DUAL EXHAUST SILENCER

Company: ROOTS Division
 Address: 16240 Port Northwest Drive, Houston, Texas 77041
 Ph: 832-590-2305/1-877-393-7668 Fax: 832-590-2326

ROOTS BLOWER PERFORMANCE REPORT : Program Version 6.13 Release Date 2/10/2010
 Program Mode: SELECTION Run Date: 11/28/2011

AMBIENT CONDITIONS:

Gas	AIR	
Relative Humidity	36%	
Molecular Weight	28.863	
k-Value	1.396	
Specific Gravity	.996	
Ambient Temperature	68	deg F
Ambient Pressure	14.33	PSIA
Elevation	700	feet

STANDARD CONDITIONS:

Pressure	14.7	PSIA
Temperature	68	deg F
Relative Humidity	36	%

SELECTED UNIT DETAIL: Model 45 URAI

	Design	Des/Max
Speed, RPM	2215	61.5%
System Inlet Volume, ICFM	229	
Actual Blower Inlet Volume, ICFM	229	+/-5 %
Standard Volume, SCFM	193	
Mass/Weight Flow, #/min	14.44	+/-5 %
System Inlet Temperature, deg F	68.0	
System Inlet Pressure, in Hg Vac	4.000	
Inlet Pressure Loss, PSI	0.000	
Blower Inlet Pressure, in Hg Vac	4.000	
Blower Discharge Pressure, PSIA	14.330	
Discharge Press. Loss, PSI	0.000	
System Discharge Pressure, PSIA	14.330	
Blower Diff. Press., PSI	1.956	19.6%
Power, BHP	2.64	+/-%
Temperature Rise, deg F	28.7	12.8%
Discharge Temperature, deg F	96.7	
System Discharge Volume, ACFM	208	
Relief Valve Setting, in Hg Vac	12.0	72.7%
Power @ RV Setting, BHP	7.21	
Temp. Rise @ Relief Setting, deg F	138.7	61.6%
Disch. Temp @ Relief Setting, deg F	206.7	
V-Belt: Est. B10 Brg Life, hours	>99999999	
Coupling: Est. B10 Brg Life, hours	>99999999	
Est. Free Field Noise, dBA	77.9	

Measured as sound press. level per ISO 2151:2004E with +/-3 dBA tol.

Filter Central Vacuum Unit F11910

VAC-U-MAX PART NO.	BASF PART NO.	QTY.	DESCRIPTION	PRICE
40125EPTFE		2	FLTR CRT 12DX26LG EPTFE	\$ 495.00 EA

Mike Rectanus

From: Steve Wagoner <stevewagoner@vac-u-max.net>
Sent: Tuesday, April 08, 2014 10:16 AM
To: Mike Rectanus
Cc: Tony Branco
Subject: VAC-U-MAX filter area

4/8/14

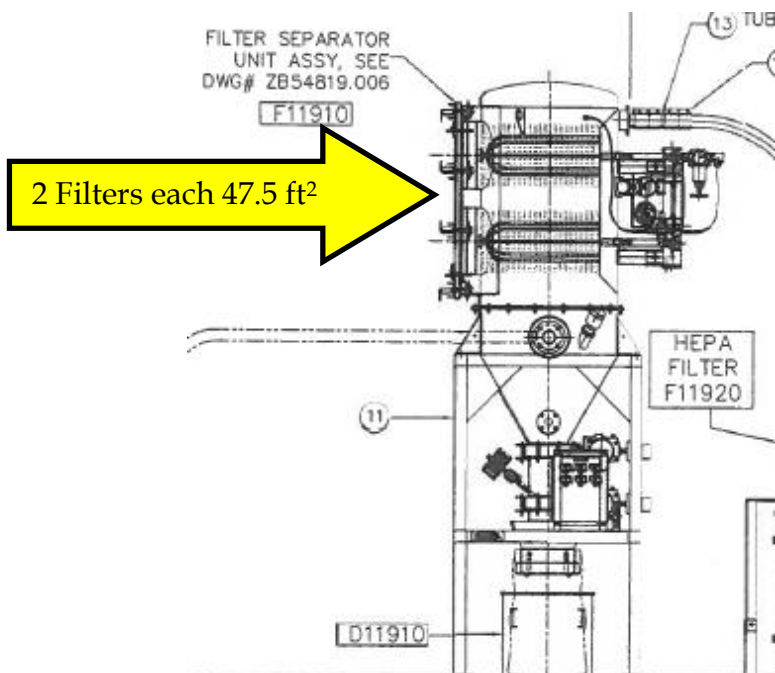
Hi Mike,

Per our conversation this morning, I am confirming the filter area of our filter #40125EPPFE to be 47.5 sq ft. The material is an expanded PTFE.

Please feel free to contact us at anytime if you have further questions.

Steve Wagoner
 Mechanical designer
VAC-U-MAX

This message is for the named person's use only. It may contain confidential, proprietary or legally privileged information. No confidentiality or privilege is waived or lost by any transmission errors. If you receive this message in error, please immediately delete it and all copies of it from your system, destroy any hard copies of it and notify the sender. You must not, directly or indirectly, use, disclose, distribute, print, or copy any part of this message if you are not the intended recipient. VAC-U-MAX and each of its subsidiaries each reserve the right to intercept and monitor all e-mail communications through its networks if legally allowed. Message transmission is not guaranteed to be secure.



**ERM has over 140 offices
across the following
countries and territories
worldwide**

Argentina	New Zealand
Australia	Panama
Belgium	Peru
Brazil	Poland
Canada	Portugal
China	Puerto Rico
Colombia	Romania
France	Russia
Germany	Singapore
Hong Kong	South Africa
Hungary	South Korea
India	Spain
Indonesia	Sweden
Ireland	Taiwan
Italy	Thailand
Japan	United Arab Emirates
Kazakhstan	UK
Malaysia	US
Mexico	Vietnam
The Netherlands	

ERM's Cincinnati Office

9825 Kenwood Road
Suite 100
Cincinnati, Ohio 45242
T: 513 830 9030
F: 513 830 9031

www.erm.com



Contents lists available at ScienceDirect

Journal of Power Sources

journal homepage: www.elsevier.com/locate/jpowsour



Identification and quantification of gases emitted during abuse tests by overcharge of a commercial Li-ion battery

Y. Fernandes^{a,b}, A. Bry^a, S. de Persis^{b,*}

^aCEA Le Ripault, BP 16, 37260 Monts, France

^bICARE, CNRS, University of Orléans, 1C, Avenue de la Recherche Scientifique, 45071 Orléans Cedex 2, France

HIGHLIGHTS

- The overcharge abuse test of a 35 cm³ commercial LFP cell is studied.
- A new analytical setup and a specific procedure have been established.
- Some species are produced after the first deconfinement of the cell.
- HF has a specific behavior: its formation is decorrelated from the other species.
- The gases released by the cell are mainly composed of flammable volatile solvents.

ARTICLE INFO

Keywords:

Li-ion battery
Abuse test
Overcharge
Vent gas analyses
Electrolyte
Flammability

ABSTRACT

As hazardous situations can occur during the life of a Li-ion battery, it is of great importance to understand its behavior under abusive conditions (mechanical, thermal or electrical). In particular, the study of overcharge, which consists of forcing a current through the cell, can be very helpful in improving battery safety. Very few studies in the literature have focused on the chemical reaction mechanism responsible for failure during overcharge. This is, however, of great interest because a Li-ion battery can produce reactions in a sealed container and is thus a highly reactive system. Here, experimental approaches are employed to understand the reaction mechanisms that occur during overcharge testing. Experiments consist of studying the overcharge kinetics of a commercial battery at an initial state of charge of 100%. The battery is maintained in a known volume and gaseous samples are withdrawn both at the end of the test and continuously during the test. The main gaseous species are then identified and quantified by gas phase chromatography coupled with mass spectrometry and FTIR spectroscopy. This experimental study is completed by a numerical investigation to determine the combustion parameters of the exhaust gases using a detailed reaction mechanism associated with a numerical code.

1. Introduction

Many devices involve Li-ion Batteries (cell phones, laptops, electric vehicles or airplanes) for their weight/power advantages. As hazardous situations can occur during the life of the battery, it is of great importance to understand its behavior under abusive conditions, whether mechanical (cross/deformation/penetration), thermal (external heating) or electrical (internal short circuit/external short circuit/overcharge/overdischarge). The literature concerning abuse tests on Li-ion batteries is extensive because these tests are aimed at improving battery safety. Moreover, there are a large number of possible tests as well as possible cell compositions and geometries.

In particular, the study of an abnormal electric situation such as

overcharge, which consists of forcing a current through the cell, can be very helpful in improving battery safety. In real life, overcharge can be caused when the cell voltage is abnormally increased by the charge control system, by a defective charger or when the wrong charger is used. The Li-ion battery can thus produce reactions in a sealed container and can be considered as a highly reactive system. This is an uncommon event, but when it occurs the consequences can be very severe [1] such as toxic and/or corrosive damage to the device and to persons, a risk of flammability or hot spot.

As Li-ion cells with carbonate-based electrolytes are widely marketed, the physical hazards are relatively well known. The chemical and health hazards are less well-known, however, and only a few studies have aimed at establishing correlations between cell response during an

* Corresponding author. ICARE – Institut de Combustion Aérodynamique Réactivité Environnement, UPR3021 CNRS-INSIS, Université d'Orléans – Collegium Sciences et Techniques, 1C, avenue de la Recherche Scientifique, CS 50060, 45071 Orleans Cedex 2, France.

E-mail addresses: yann.fernandes@cea.fr (Y. Fernandes), alain.bry@cea.fr (A. Bry), stephanie.de.persis@cnrs-orleans.fr (S. de Persis).

<https://doi.org/10.1016/j.jpowsour.2018.03.034>

Received 18 January 2018; Received in revised form 3 March 2018; Accepted 13 March 2018

Available online 11 April 2018

0378-7753/ © 2018 Elsevier B.V. All rights reserved.

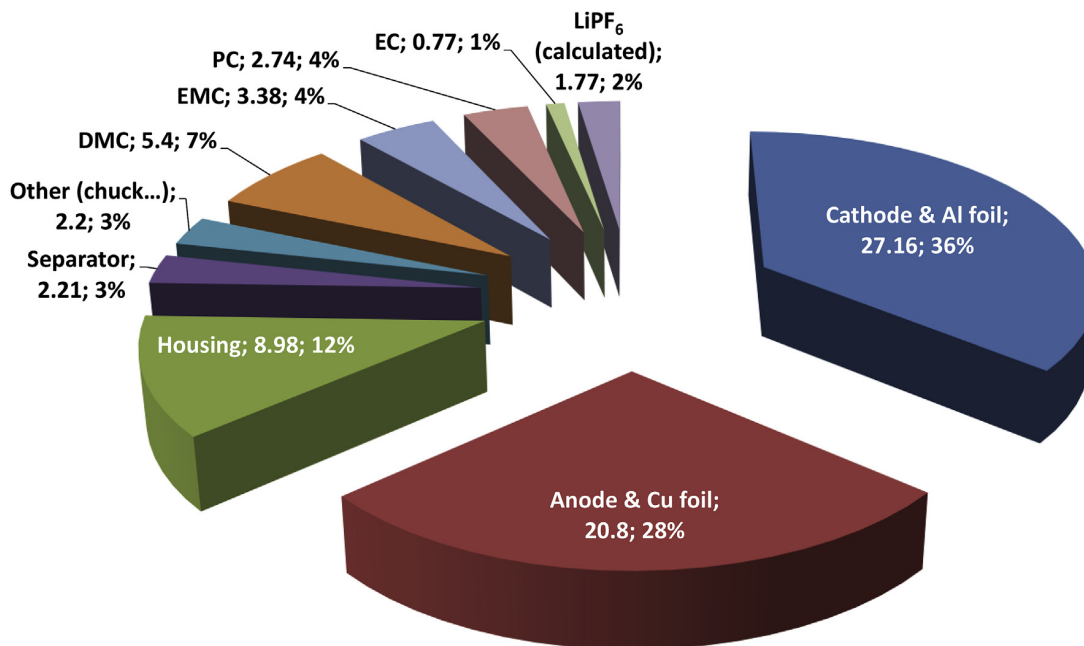


Fig. 1. Cell composition (elements; mass in g; mass ratio in %). The mass of the complete cell before disassembly is 75.41g.

abuse event and gas exhaust. The review of the available literature (see next section) shows that, whereas the behavior of cells with carbonate-based electrolytes is relatively well documented in the case of thermal abuse, few studies deal with overcharge abuse tests. Hence there is a need to gain more insight into the reaction mechanisms that occur during overcharge abuse tests. Besides, from a flammability hazard point of view, the gases released by the cell can be combustible, depending on the environment. There are two main reasons for the flammability/explosive hazard: i) the gas generation is large and sudden (venting) [2]; ii) the gas and flammable electrolyte solvent vapor released is a flammable or explosive mixture that can be easily ignited [3,4]. This hazard has thus to be taken into account. Consequently, there is a need to investigate the chemical reaction mechanism responsible for cell opening during overcharge. This is the aim of the present study.

In this paper, the overcharge abuse test of a 35 cm³ commercial Li_xFePO₄ LFP cell was studied. A new analytical setup and a specific procedure were established, making this study original and innovative. Gachot et al.(2014) [5] demonstrated that it is possible to identify gaseous released by a Li-ion battery by coupling Gas chromatography (GC) with Fourier Transform InfraRed (FTIR) and/or Mass Spectrometry (MS). In the present paper, not only the identification but also the quantification of each species was performed using GC/MS and FTIR. The battery was maintained in a closed chamber and the gaseous sample was withdrawn not only at the end of the test as is usually done, but also continuously during the test, enabling the main gaseous species to be continuously identified and quantified by FTIR and GC/MS. This study thus provides important new elements in the understanding of the reaction mechanisms, which still remain unclear, that occur during an overcharge abuse test. Finally, to complete the study from a flammability hazard point of view, the typical combustion parameters (fundamental flame velocities, adiabatic flame temperatures and heat release rates) of the exhaust gases were determined using a detailed reaction mechanism associated with a numerical code.

2. Experimental

2.1. Cell characteristics

A commercial cell, based on an LFP cathode, was tested. It is a cylindrical 26650 cell with an inner diameter of 26 mm and a length of 65 mm. The weight of the cell is 75g. According to the manufacturer's data, its nominal capacity is 2.5Ah and its nominal voltage is 3.6V. Current-limiting or temperature trip safety devices were not used in the cell. In order to carry out quantitative analyses, it is important to know the mass split of the cell components. As this information is kept confidential by the manufacturers, we conducted this analysis ourselves in collaboration with the LITEN laboratory of Grenoble. To characterize the cell components, a cell was completely discharged with a 1C-rate and then dismantled in a glove box providing an inert environment (H₂O and O₂ < 10ppmv).

The cell components (the anode, the cathode, the current collector foils, the separator and the housing material) were rinsed with acetonitrile and dried in a dessicator until stabilization of the weight. As expected, the studied cell has a cathode that belongs to the family of active material Li_xFePO₄ (LFP) and the anode belongs to the carbon family. Consequently, the comparison with literature results obtained with such cathodes can be envisaged. These materials were identified, after being rinsed with acetonitrile, by Scanning Electron Microscopy (SEM) and X-Ray Diffraction (XRD).

The separator foil was examined in inert atmosphere with thermal gravimetric analysis with a heat ramp of 10K.min⁻¹. An endothermic peak was observed at 150 °C corresponding to the fusion temperature of polypropylene. The thickness of the separator was 20 μm (measured with a micrometer). A FTIR spectroscopy analysis confirmed the nature of the separator.

A different methodology was used to quantify the volatile solvents, as the time between removing the separator and its immersion caused the evaporation of most of the solvents. Another cell was therefore dismantled in a polyethylene glove bag, the bag was then hermetically sealed and introduced in the glove box. The glove bag was connected to an FTIR analyzer, which quantified the volatile solvents until their total volatilization. The IR spectra (not shown here) were integrated and the solvent mass ratios of the electrolyte were determined. It was observed

Table 1

Summary of the available literature concerning abuse tests coupled with gas analyses. For each reference, the type of cathode, the solvent composition, the type of abuse, and the gases analyzed for carbon-based anodes are mentioned. Studies considering the same abuse test or a similar type of cathode are highlighted in red.

Reference	Type of Cathode	Solvents (Molar proportions)	Abuse test	Gas analysis
Kumai (1999) [16]	LCO	PC:EMC:DEC:DMC C (5:2:1:1)	Overcharge	CO ₂ -CO-CH ₄ -C ₂ H ₆ -C ₃ H ₈ -C ₃ H ₆
			Overdischarge	
Ohsaki (2005) [17]	LCO	EC:EMC	Overcharge	CO ₂ - CO - CH ₄ - C ₂ H ₄ - C ₂ H ₆ - H ₂
Kong (2005) [18]	LCO	EC:DEC (1.8:1)	Overcharge	CO ₂ - CO - CH ₄ - C ₂ H ₂ - C ₂ H ₄ - C ₂ H ₅ F - C ₂ H ₆ - C ₃ H ₆ - C ₃ H ₈
	LMO			
Doughty (2005) [6]	NCA	EC:EMC + additives (1:2)	Thermal (ARC)	CO ₂ - CO - CH ₄ - C ₂ H ₄ - C ₂ H ₅ F - C ₂ H ₆ - C ₃ H ₆ - C ₃ H ₈ - C ₄ species - H ₂
		EC:PC:EMC + additives (3:4.5:2)		
Abraham (2006) [7]	NCA	EC:EMC (1:2)	Thermal (ARC)	CO ₂ - CO - CH ₄ - C ₂ H ₄ - C ₂ H ₅ F - C ₂ H ₆ - C ₃ H ₆ - C ₃ H ₈ - H ₂ - solvent
Roth (2008) [8]	NCA	EC:EMC (1:2)	Thermal (ARC)	CO ₂ - CO - CH ₄ - C ₂ H ₄ - C ₂ H ₅ F - C ₂ H ₆ - C ₃ H ₆ - C ₃ H ₈ - C ₄ species - C ₅ H ₁₂ - H ₂
Li (2008) [22]	LCO-NMC	EMC:EC:PC (10:9:1)	Overdischarge	CO ₂ - CO - CH ₄ - C ₃ H ₆
Rivière [9](2011)	LMO	EC:DEC:DMC	Thermal (Tewarson calorimeter)	CO ₂ - CO - NO - SO ₂ - HCl - HF - THC
Somandepalli et al. (2014) [20]	LCO	N.D	Thermal on overcharged cells (Combustion Chamber)	CO ₂ - CO - CH ₄ - C ₂ H ₄ - C ₂ H ₆ - C ₃ H ₆ - C ₃ H ₈ - C ₄ H ₈ - C ₄ H ₁₀ - n C ₄ H ₁₀ - C ₄ H ₈ - C ₅ H ₁₂ - n C ₅ H ₁₂ - C ₆ H ₆ - C ₆ H ₁₄ - C ₇ H ₈ - C ₈ H ₁₀ - H ₂
Gachot (2014) [5]	N.D	N.D	N.D	CO ₂ - C ₂ H ₆ - C ₂ H ₅ F - C ₃ H ₆ O - C ₃ H ₈ - C ₃ H ₇ F - C ₄ H ₈ O ₂ - C ₄ H ₁₀ - C ₄ H ₁₀ - DEC
Golubkov (2014) [10]	LCO-NMC	DMC:EMC:EC (6:2:1)	Thermal (Heater reactor)	CO ₂ - CO - CH ₄ - C ₂ H ₄ - C ₂ H ₆ - H ₂
	NMC	DMC:EMC:EC:PC (7:1:1:1)		
	LFP	DMC:EMC:EC:PC (4:2:3:1)		
Larsson (2014) [11]	LFP	N.D	Thermal (Fire test chamber)	HF
Spinner (2015) [21]	LCO	DMC:EC:PC	Thermal on overcharged cells (Fire test chamber)	CO ₂ - CO - CH ₄ - SO ₂ - NO
Fu (2015) [12]	NMC	N.D	Thermal (Cone Calorimeter)	CO ₂ - CO
Yuan (2015) [19]	LFP	EC:DEC:DMC (1.8:1:1.4)	Overcharge	CO ₂ - CO - CH ₄ - C ₂ H ₄ - C ₂ H ₆
Golubkov (2015) [2]	NCA	EC:PC:DMC:EMC (4:2:3:1)		CO ₂ - CO - CH ₄ - C ₂ H ₄ - C ₂ H ₆ - H ₂
	LCO	DMC:EMC:EC:MPC (11: 1:4:0.25)	Thermal on overcharged cells (Heater reactor)	
Sun (2016) [13]	NCA	N.D	Thermal on overcharged cells	CO ₂ - CO - COS - C ₃ H ₄ O - C ₃ H ₂ N ₂ - C ₃ H ₅ N - C ₃ H ₆ O - C ₄ H ₈ O - C ₄ H ₁₁ N - C ₅ H ₈ - C ₅ H ₉ NO - C ₅ H ₆ - C ₁₀ H ₈ - SO ₂ - HF - PO _x
	LMO			
	LFP		Thermal (Fire test chamber)	
Zheng (2016) [23]	NCA	EC:DMC:EMC	Overdischarge	CO - CH ₄ - C ₂ H ₂ - C ₂ H ₄ - C ₂ H ₆ - C ₃ H ₈ - H ₂
Lammer (2017) [14]	NMC	N.D	Thermal (Heater reactor)	CO ₂ - CO - CH ₄ - C ₂ H ₂ - C ₂ H ₄ - C ₂ H ₆ - H ₂
Larsson (2017) [15]	LCO	N.D	Thermal (Fire test chamber)	HF - POF ₃
	LFP			
	NCA-LATP			

that the electrolyte is composed of LiPF_6 dissolved in dimethyl carbonate (DMC), ethyl methyl carbonate (EMC), ethylene carbonate (EC) and propylene carbonate (PC). The mole-ratios are 4:2.2:2.1:0.5. EC and PC were quantified by GC whereas DMC and EMC were quantified by FTIR. The concentration of the salt was assumed to be typical, i.e. 1 M in the solvent mixture. Fig. 1 shows the cell composition in terms of mass ratios (in %). The mass of the complete cell before disassembly was 75.41g.

2.2. Literature review

In order to compare our results to the available literature, two kinds of studies could be selected: those dealing with similar cells even if the abuse tests are different, and those dealing with similar abuse tests (overcharge) even if the cell composition is different. We finally selected only those that are coupled with gas analyses. Table 1 summarizes this literature review. For each case, the type of cathode, the solvent composition, the type of abuse, and the gases analyzed for carbon-based anodes are given. As shown in Table 1, among the abuse tests coupled with gas analyses, thermal tests are the best documented [5–15] whereas only a few studies concern overcharge tests [16–19]. Some other studies concern thermal tests on overcharged cells [2,13,20,21] or overdischarge [16,22,23].

Thermal tests are usually based on ARC (Accelerating Rate Calorimetry) that allows the determination of gas evolution from cells and electrolytes from room temperature up to high temperature (about 450 °C). The main vent gases often identified are CO_2 , CO, CH_4 , and C_2H_4 [5–15] as shown in Table 1. HF is also often mentioned [9,11,17,23]. Other subsequent products have also been detected such as H_2 [6–8,10,20], which is rarely identified despite its risk because it cannot be observed by FTIR. Our results can only be compared with those studies that deal with similar cell compositions, whatever the type of abuse test. This is the case of the studies carried out by Golubkov et al. [2,10] and by Larsson et al. [11]. The former are well documented while in the latter, only HF was identified. In Ref. [2], the authors studied thermal tests with 100% SOC charged cells with a capacity of 1.1Ah. These 18650 commercial cells weighing 38.8g were made with an LFP cathode and a 1 M LiPF_6 electrolyte with DMC/EMC/EC/PC (4:3:2:1). Before performing the thermal test at a rate of 2 °C.min⁻¹, the cell was charged to 100% SOC. After thermal runaway, CO_2 and H_2 were identified as well as CO, CH_4 , C_2H_4 and C_2H_6 in smaller amounts. HF was not measured. The first gas release was measured at 195 °C (first venting event) and the second one at 404 °C (second venting event) for three replicate measurements. The gas production, based on total pressure measurement, was about 50 mmol (1.2L) and found to be independent of the external thermal rate from 1.5 to 3.5 °C.min⁻¹. In Ref. [10], thermal tests were carried out with different states of charge (115% and 130% SOC) on cells whose characteristics were similar to the previous ones. The authors found that, after thermal runaway, the main gas exhaust was composed of CO_2 and H_2 , with smaller amounts of CO, CH_4 , C_2H_4 and C_2H_6 . In this second case, the first gas release was measured at 80 °C (first venting event) and the second one at 448 °C (second venting event). The gas production based on total pressure measurement was about 60 mmol (1.3L). The amount of gas exhausted when thermal runaway occurred for LFP was found to be relatively independent of the SOC from 0% to 130% SOC for an external thermal rate of 4 °C.min⁻¹ and the chemical nature of the identified species did not significantly change. Only the species proportions were modified with SOC change.

To the best of our knowledge and as shown in Table 1, there are only a few papers that deal with overcharge abuse tests. In 1999, Kumai et al. [16] described the gas analysis of a slightly overcharged cell (105% SOC) with a capacity of 1 Ah and no rupture of the casing. The cell used was a commercial 18650 cell with a LiCoO_2 cathode and a 1 M LiPF_6 electrolyte with a PC/EMC/DEC/DMC mixture. The main gases observed without cell opening and at 25 °C were volatile solvents: DMC,

EMC and the following gases: CO_2 , CH_4 , C_2H_6 and C_3H_8 for a small volume of 10.57 mL at room temperature. CO and H_2 could not be seen with the analysis device used.

In 2005, Ohsaki et al. [17] described gas analyses of an overcharged cell with a capacity of 0.65 Ah. The cell was a home-made prismatic cell with a LiCoO_2 cathode and a 1 M LiPF_6 electrolyte with an EC/EMC mixture. The main gases measured inside the cell were: CO_2 , H_2 , CO, CH_4 , C_2H_4 and C_2H_6 for a total volume of 22 mL. This volume and the chemical nature of the gaseous products did not change when the cell was placed in a thermo-regulated bath between 60 and 95 °C. The surface temperature of the prismatic cell remained low because of the shape of the cell or the thermo-regulated bath.

Kong et al. [18] described gas analyses of a 5V overcharged cell with a capacity of 1Ah without cell opening. The cell was a homemade 18650 cell with an LFP cathode and a 1 M LiPF_6 electrolyte with EC/DEC (1:1). Before overcharge tests, the authors conducted a normal cycling protocol and analyzed gases at the end of this protocol at room temperature. It was found that the nature of the gases did not change, only their amounts. The main gases were: CO_2 , C_2H_6 , C_2H_4 , CH_4 and $\text{C}_2\text{H}_5\text{F}$. Solvents, CO and H_2 could not be seen with the device used. The authors mentioned that similar gases were produced for two different cathodes (LCO and LMO) tested. The generation of gaseous species without cell opening thus seems to be independent of the cathode composition.

More recently, in 2015, Yuan et al. [19] described the overcharge of a 5.1V cell with a capacity of 2Ah with rupture of the casing. The cell used for gas analysis was a homemade cell, and thermocouples were inserted into the middle part of a wound jelly-roll to monitor their internal temperatures. The gas analysis was monitored at 170, 180 and 190% SOC (before rupture of the casing). The main gases were CO_2 and CO; H_2 could not be identified using this device.

2.3. Overcharge tests

In the present study, overcharge tests were carried out in a building with an explosion-proof room. As shown in Fig. 2, a specific setup was designed to ensure that the system remained gas-tight while enabling analysis of the vent gases. The abuse test consisted of charging the cell beyond its limit. The test was monitored by a video camera (film shown in supplementary file). The experimental conditions used in our study are summarized in Table 2 (cell CW). For comparison, the experimental conditions used by Refs. [16–19] are also given (note that these studies were already described in the previous section).

Supplementary video related to this article can be found at <http://dx.doi.org/10.1016/j.jpowsour.2018.03.034>.

In our case, the cell was maintained in a closed polypropylene test enclosure with a volume of 3.66L equipped with gas-tight passageways.

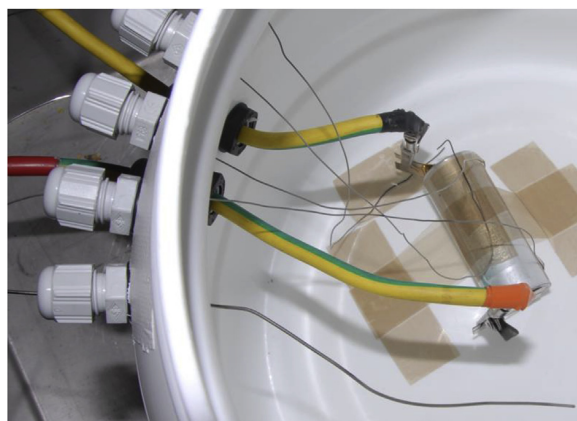


Fig. 2. Picture of the experimental device.

Table 2
 Comparison between experimental conditions of abuse overcharge tests available in the literature [16–19] and the present study.

	Kumai et al., 1999 [16]	Ohsaki et al., 2005 [17]	Kong et al., 2005 [18]	Yuan et al., 2015 [19]	Present study
Cell mass (g)	N.D	N.D	N.D	N.D	75.4
Capacity (Ah)	1	0.65	LCO: 1.1 LMO: 0.7 LFP: 1	2.0	2.5
Overcharge rate	880 cycles at 0.2C	1C	0.2C	1C	2C
Rupture of casing	No	No	No	Yes	Yes
Analysis time	1 point after 880 cycles at +5% of nominal capacity	5 points at different steps of the overcharge	1 point at 5.0V	3 points at different steps of the overcharge before rupture of casing	Continuous + 1 point after rupture of casing and stabilization of the thermo-electrical behavior of the cell
Maximum SOC (%)	105	N.D	N.D	200	135
Maximal external temperature (°C)	25	120	N.D	100 (238 internal)	145
Gaseous volume at SATP (mL)	10.6	24	N.D	N.D	1643.0

One of the effects of the overcharge test on a cell is to increase its temperature. This parameter is thus of great importance. To monitor the external temperature of the cell, the external plastic casing was removed and two K-type thermocouples secured at each electrode with Kapton tape were positioned on the cell surface.

Two metallic tabs were welded on each pole of the cell in order to ensure good electric contact during the overcharge abuse tests. Before the test, the cell was fully charged, 100% SOC, until reaching the nominal voltage (3.6V). Tests were conducted in ambient atmosphere conditions, i.e. in ambient air (20–25 °C) and at atmospheric pressure. The overcharge was applied during 2 h with a voltage of 7.2V and a current of 5A (corresponding to 2C-rate, meaning that in 30 min the SOC was increased by a factor of 100%).

Cell voltage, current and temperature were measured during the test period at a sample rate of 10 Hz with a data logger Yokogawa.

2.4. Description of the analytical tools

To analyze the exhaust gases, the cell was placed in an air-tight chamber. All the species exhausted from the cell after rupture of the casing were quantified using an innovative analytical procedure: sampling inside the chamber was done not only at the end of the abuse test, as is routinely the case, but also continuously during the overcharge test. This new procedure is detailed below. In both cases, the analytical tools used were based on FTIR spectroscopy and micro-gas phase chromatography with a TCD (Thermal Conductivity Detector) coupled with MS. Details are given in [Table A in the supplementary file](#).

2.4.1. Analytical procedure performed at the end of the abuse test

As mentioned above, overcharge tests were carried out in a closed propylene test chamber equipped with gas-tight passageways. Before each test, the tightness was checked by injecting a known volume of air, measured by volumetric counters. One of the gas-tight passageways was connected to a 300 mL sample bottle equipped with pressure sensors piloted by electro-pneumatic remotely actuable valves. Another gas-tight passageway was connected to a volatile organic compound monitor with a MiniRAE3000 PhotoIonization Detector (PID) allowing precise detection of the time at which the first rupture of the casing took place. At the end of the test, 600 mL of gases were sampled from the test chamber in two vacuum bottles thanks to the remotely actuable valves. The proportions of species in the bottles were assumed to be the same as in the test chamber.

For the separation, identification and quantification of the gaseous products withdrawn after the abuse test, the first bottle was analyzed with a VARIAN CP-4900 Micro GC. Chromatographic separation was done on two MS5A and one PLOTQ column. Helium was used as the micro GC carrier gas for one MS5A and the PLOTQ column, while argon

was used for the other MS5A.

Each column was equipped with a Thermal Conductivity Detector (TCD) which was used to detect and quantify permanent species. The micro-GC was calibrated for N₂, CH₄ and H₂.

The micro-GC quantification was realized by exploiting the linear response of the TCD detector for every species on each column. To complete the identification performed with the micro GC VARIAN, other analyses were performed using a SRA INSTRUMENTS micro GC connected to an AGILENT TECHNOLOGIES mass spectrometer. The mass range was set at 5–140 amu (atomic mass unit) and data acquisition was processed with SOPRANE and MSD COUPLAGE SRA Data Analysis software. Compounds were identified and the corresponding structural formulae assigned using the National Institutes of Standards (NIST) library for mass spectra, enabling the majority of products to be identified. H₂, CH₄, CH₃OH, C₂H₅OH were identified using reference chromatographic retention time and standard mass spectra obtained after injection of the corresponding species. For the following species: C₂H₄, C₂H₅F, CH₃OCH₃, CH₃OCHO, CH₃F, C₂H₆, and C₃H₆, experimental spectra were identified by comparison with those of the NIST database. Finally, only PF₃ was identified by using the probability of the NIST database (probability of 74%). The few remaining ones did not have a strong enough signal to be identified.

The second bottle was used to quantify CO and CO₂. For this purpose, an FTIR Bruker Equinox 55 spectrometer was used. IR spectra were recorded with a thermal detector DTGS (Deuterated TriGlycerine Sulfate) in the 370–5000 cm⁻¹ range with 1 cm⁻¹ resolution. Quantification was estimated thanks to calibration carried out with a standard reference gas cylinder of CO and CO₂ in the same pressure conditions as in the abuse test analysis.

2.4.2. Analytical procedure performed during the abuse test

Complementary tests were conducted with continuous analysis during the test to complete the analysis at the end of the test by adding the quantification of the solvent vapors. In addition, continuous analysis makes it possible to record the concentration profile of the gas exhausted from the cell during the test. The air-tight test chamber has a volume of 10.4L and is open to the ambient air in the laboratory thanks to an automatic one-way valve which allows laboratory air to enter the chamber but prevents it escaping from the chamber. This air input compensates the continuous air flow sucked in by the analyzers in order to maintain atmospheric pressure inside the chamber.

A multi-gas analyzer Environment SA MIR 9000 was used. It is equipped with an FTIR GASMET analyzer with a cell of 2 m optical path length and a cryogenic N₂ cooled MCT (mercury cadmium telluride) detector. To avoid condensation of less volatile compounds, the PTFE tubing and the cell were heated respectively to 120 °C and 180 °C. The sample was passed through heated filters to retain particles before

analysis. The spectral resolution was 8 cm^{-1} , the acquisition rate 0.17 Hz , and the spectral range $900\text{--}4200\text{ cm}^{-1}$. FTIR acquisition was done continuously through the system. All the air flow sucked in from the test chamber passes through the infrared cell.

The quantification is expressed by the software Calcmet from the calibration curves of each species studied. These curves were realized from FTIR spectra obtained at different concentrations present in the database of the software. For the EMC electrolyte solvent, the calibration curve was realized experimentally from mixtures of small known quantities of pure solvent and air zero.

In view of the large number of species emitted simultaneously, a spectral optimization process was performed by the software Calcmet from algorithms in order to obtain reliable results.

A 300 mL sample of chamber gas was collected at a precise point in the test to compare the continuous FTIR analysis over a small period of time with usual laboratory analyses and thus complete the analysis at this point with species that cannot be observed by FTIR. The laboratory

analyses were GC and FTIR.

3. Results and discussion

3.1. Thermo-electric results of the overcharge test

The overcharge tests were repeated nine times: the electrical, mechanical and thermal behaviors of the cell were reproducible in seven tests among the nine. During the seven reproducible overcharge tests, venting and thermal runaway were observed without explosion. During the other two, the cell surface temperature rose respectively to $300\text{ }^{\circ}\text{C}$ and $350\text{ }^{\circ}\text{C}$, possibly caused by a strong internal short circuit, leading to an explosion that precluded gas analysis.

Fig. 3 shows a reproducible result from an overcharge test of the cell, in which voltage (in V) and current (in A) (left-hand side) and temperature (in $^{\circ}\text{C}$) (right-hand side) are plotted as a function of time (in s). Fig. 3a shows the thermo-electric behavior of the cell in the time

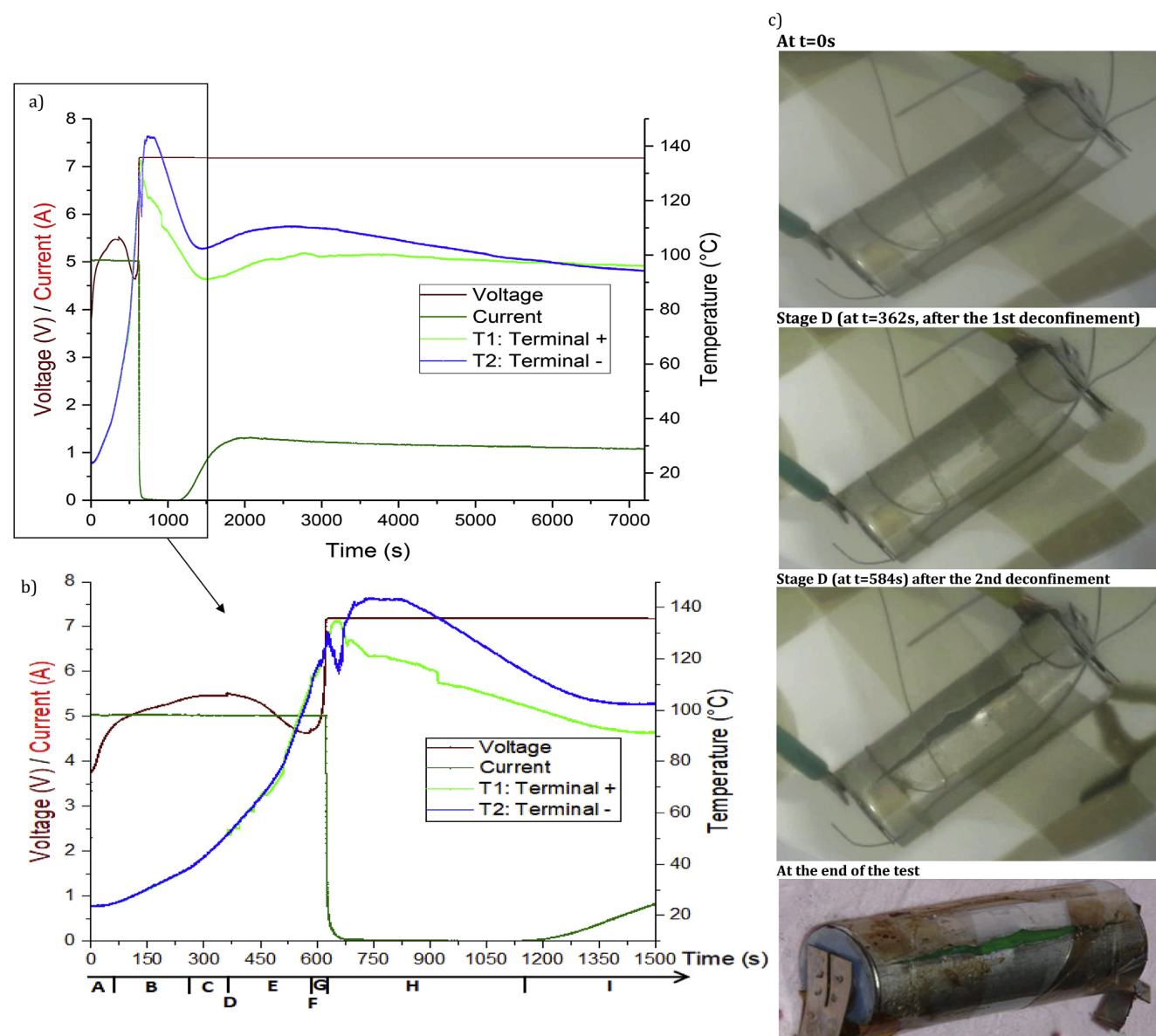


Fig. 3. Typical evolution of voltage (in V) and current (in A) [left-hand side] as well as temperature (in $^{\circ}\text{C}$) [right-hand side] as a function of time (in s): a) from 0 to 7000 s; b) from 0 to 1500 s; during an overcharge (2C) test of the cell together with c) pictures of the cell at various stages of the overcharge test: at $t = 0\text{ s}$, at $t = 362\text{ s}$ after the 1st deconfinement (stage D), at $t = 584\text{ s}$ after the 2nd deconfinement (stage F) at the end of the test.

range 0 to 7000s and Fig. 3b shows a zoom on the range 0 to 1500s. As shown in Fig. 3b, there are 9 stages (A to I):

- A) From 0 to 60s: The voltage rises from 3.4 to 4.8V at 1.4 V min^{-1} and the external surface temperature is equal to room temperature (25°C).
- B) From 60 to 260s: The voltage increase (after 5V) is slower than in step A (i.e. during the first minute). The external surface temperature increases at a rate of about 4°C.min^{-1} .
- C) From 260 to 362s: The voltage reaches a plateau at 5.5V at 280s. The external surface temperature increases more rapidly at a rate of about $7.5^\circ\text{C.min}^{-1}$.
- D) At 362s: The VOC monitor detects the presence of organic compounds. Liquid and a slight amount of gas are observed to escape from the casing near the negative electrode. The internal pressure of the cell reaches the rupture point of the casing. The SOC is 120%.
- E) From 362 to 584s: The voltage of the cell decreases slowly from 5.5V to 4.6V. The surface temperature of the cell increases again but at a higher rate of about $10.6^\circ\text{C.min}^{-1}$.
- F) At 584s: The metallic casing cracks all along the cell and a second gas release is observed. The surface temperature of the cell reaches 110°C .
- G) From 584 to 625s: After the second cell opening, smoke escapes from this crack. Just after the beginning of the smoke, the voltage increases rapidly and the surface temperature also increases at a rate of about $22.4^\circ\text{C.min}^{-1}$.
- H) From 625 to 1150s: At 625s, the current inside the cell terminates (0A) and the voltage reaches the maximum value of the generator (7.2V). At this time, the surface temperature is about 125°C and the state of charge is 135%. This is probably the onset of the melting of the separator, closing the porosity around 155°C which explains the termination of the electric current. Then, the surface temperature reaches a maximum value after the drop in the electric current (144°C on the negative side) and decreases slowly after.
- I) From 1150 to 7200s: A small residual electric current is observed with a temperature stabilized around 100°C .

Fig. 3c shows pictures of the cell at various stages of the overcharge test, highlighted in Fig. 3b: at $t = 0\text{s}$, 362s after the 1st deconfinement, 584s after the 2nd deconfinement and at the end of the test.

3.2. Exhaust gas analysis

3.2.1. Identification and quantification performed at the end of the abuse test

Vent gases were analyzed after the sampling at the end of the abuse test. The results were obtained from three reproducible overcharge tests on the basis of temperature and electric records. The gas emissions were quantified at a Standard Ambient Temperature and Pressure (SATP conditions, i.e. $T = 298\text{K}$ and $P = 1\text{atm}$). The quantities and concentrations of each sampled gas were similar in the three tests with a small standard deviation. Results are shown in Fig. 4 in terms of volume expressed (in mL). The mean value of the total volume exhausted by the cell at the end of the test (except solvent and HF vapor) was $645.8 \pm 37.1 \text{ mL}$. As shown in Fig. 4, altogether, 14 chemical species were identified by $\mu\text{-GC}$ analyses. Except for electrolyte solvents, the identified gases represent 99.7% of the total sampled gas supplied by the cell. Unidentified gas traces represent only 0.3%. The main species, i.e. those with the highest concentrations, were: CO_2 which accounted for about 47% of the sampled gas, H_2 and C_2H_4 with respectively 23% and 10%. CO represented 4.9% and $\text{C}_2\text{H}_5\text{F}$ 4.6%. The O_2/N_2 ratio measured after the abuse test was the same as that of ambient air. The cell did not exhaust either of these two gases in a measurable quantity. To complete the quantification of these minor species with the solvent vapors, special tests were conducted with in-situ continuous analyses in order to avoid condensation problems.

3.2.2. Identification and quantification performed during the abuse test

The results shown here were obtained using two reproducible abuse tests performed with continuous chemical analyses. These tests showed a typical thermoelectric behavior (similar to the result shown in Fig. 3) and a similar timing of the cell damage of an overcharge abuse Li-ion cell. As soon as the cell was no longer air-tight, the gas production was monitored. The exhaust gas concentrations were measured in real time. Fig. 5 gives the concentration evolution (in ppmv) with time (in s) of DMC, EMC, C_2H_4 (ethylene), CO_2 (carbon dioxide), CH_4 (methane), CO (carbon monoxide), CH_3OCH_3 (dimethyl ether), CH_3OCHO (methyl formate) and HF (hydrogen fluoride acid) as well as the temperature (in $^\circ\text{C}$). Fig. 5a and b show CO_2 , DMC, EMC and C_2H_4 concentrations in ppmv as a function of time (in s) as well as the evolution of temperature. Fig. 5c and d show CO , CH_3OCH_3 , CH_3OCHO , HF and CH_4 concentrations in ppmv as a function of time (in s). Concentrations, in ppmv, are plotted versus time, from 0 to 22500s in Fig. 5a and c. Concentrations, in ppmv, together with temperature (in $^\circ\text{C}$) are plotted versus time from 0 to 2400s in Fig. 5b and d.

From Fig. 5b and d, eleven steps can be distinguished in the off-gas released by the cell. These steps can be correlated with the thermoelectric results shown in Fig. 3b.

- 1) From 0 to 362s (corresponding to steps A to C in Fig. 3b): The cell does not exhaust any gaseous species.
- 2) At 362s and as mentioned previously in section 3.1. (step D in Fig. 3b), a small gaseous production is observed. This occurs at a surface temperature of 53°C and for a SOC of 120%. The detected molecules are: DMC, EMC, CH_4 , CO , CH_3OCHO , CH_3OCH_3 and CO_2 . Note that dihydrogen H_2 cannot be observed by FTIR.
- 3) From 362 to 584s (step E in Fig. 3b), the comparison between volume concentrations of the gaseous species gives the following order of magnitude: $\text{DMC} > \text{CO}_2 > \text{CO} > \text{EMC} > \text{CH}_4$

At low temperature, this first gas release represents about 0.7% of the total gas exhaust.

- 4) At 584s (step F in Fig. 3b): A large crack in the cell metallic casing is observed.
- 5) From 584 to 600s (step G in Fig. 3b), the gas release rate increases. The concentrations of DMC, EMC, CO_2 , CO and CH_4 also increase. The cell is cracked and the internal pressure equilibrates with atmospheric pressure.
- 6) At 600s (step G in Fig. 3b), the surface temperature of the cell reaches 116°C and the release of new chemical species such as CH_3OCH_3 , CH_3OCHO and C_2H_4 is observed.
- 7) From 600 to 840s (steps G and H in Fig. 3b), the surface temperature of the cell reaches the maximum value of 144°C but no electric current remains inside the cell. The concentration of all the species increases. At 840s, the comparison between volume concentrations of the gaseous species gives the following order of magnitude: $\text{DMC} > \text{CO}_2 > \text{C}_2\text{H}_4$, $\text{EMC} > \text{CO} > \text{CH}_3\text{OCH}_3 > \text{CH}_3\text{OCHO} > \text{CH}_4$.
- 8) From 840 to 900s (step H in Fig. 3b), the temperature decreases to 140°C . The cell starts to cool. The maximum concentration peak of the gaseous species CH_3OCH_3 , CH_3OCHO , CH_4 , CO , CO_2 is reached at 900s. A new chemical species, HF, is observed.
- 9) From 900 to 1500s (steps H and I in Fig. 3b), only DMC, EMC and HF concentrations continue to increase. The temperature decreases until 1500s, when the maximum DMC concentration is reached.
- 10) From 1500 to 2500s (step I in Fig. 3b), the temperature increases. At 2500s, the maximum EMC concentration is reached and then EMC concentration begins to decrease. HF is the only species whose concentration increases.
- 11) After 2500s, the temperature begins to decrease slowly and then reaches a plateau at about 95°C . Here again, HF is the only species whose concentration increases.

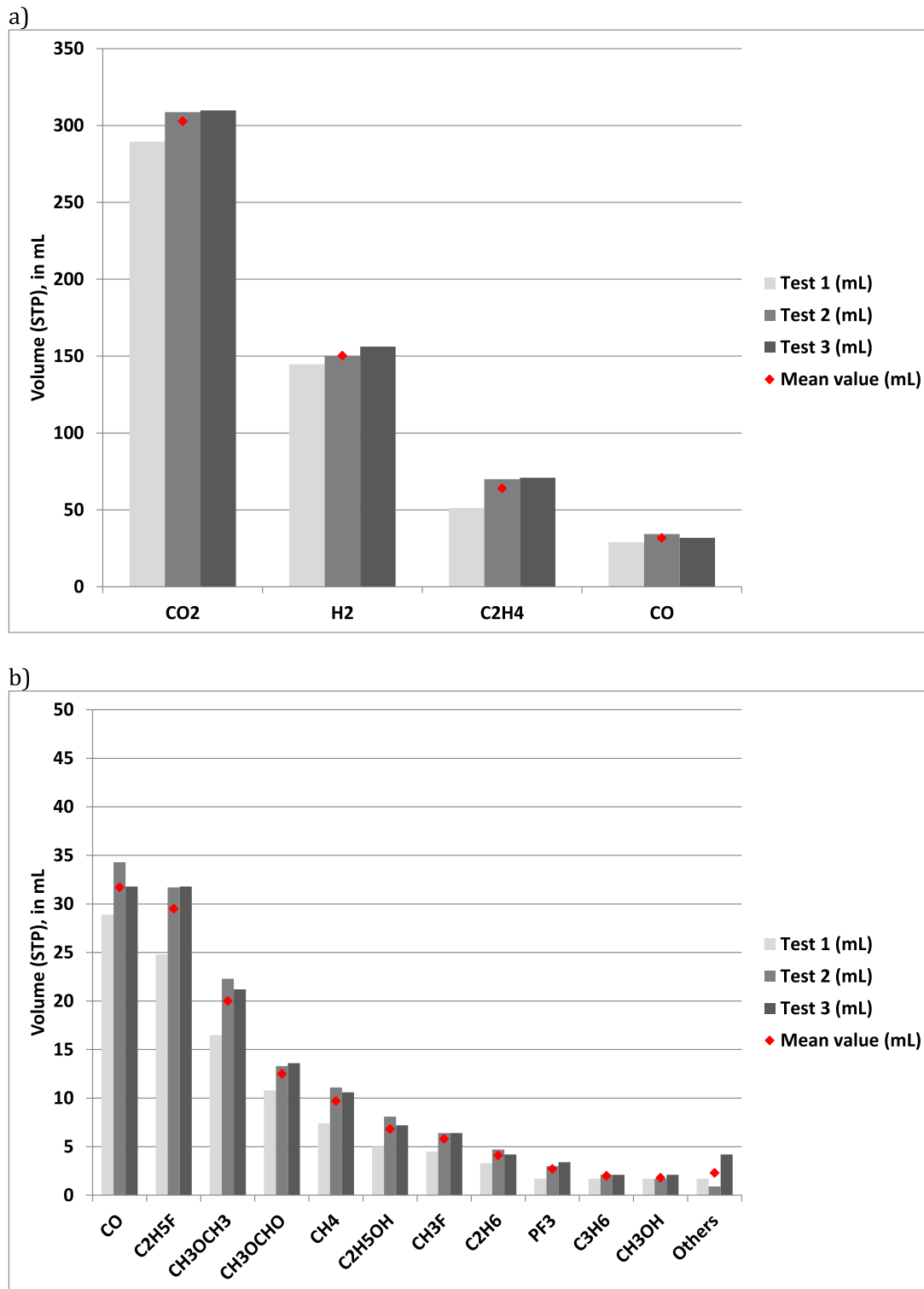


Fig. 4. Chemical composition of the vent gases in terms of volume (in mL) measured at the end of the abuse test: a) major species: CO₂, H₂, C₂H₄ and CO and b) minor species: C₂H₅F, CH₃OCH₃, CH₃OCHO, CH₄, C₂H₅OH, CH₃F, C₂H₆, PF₃, C₃H₆, CH₃OH, others.

The time-integration of the species concentrations was possible for DMC, EMC, CO, C₂H₄, CH₃OCH₃, CH₄, CH₃OCO, and HF. For CO₂, however, integration was not very precise because this gas is an atmospheric component.

As mentioned previously, a 300 mL sample of the chamber gas was

collected at 1104s in order to compare continuous FTIR analyses, over a small period of time, with the usual GC and FTIR analyses. DMC, EMC and HF were time-integrated. These results were added to the gas analysis performed at the end of the test and are shown in Fig. 6 in terms of mole fraction. The total volume of the measured vent gases in

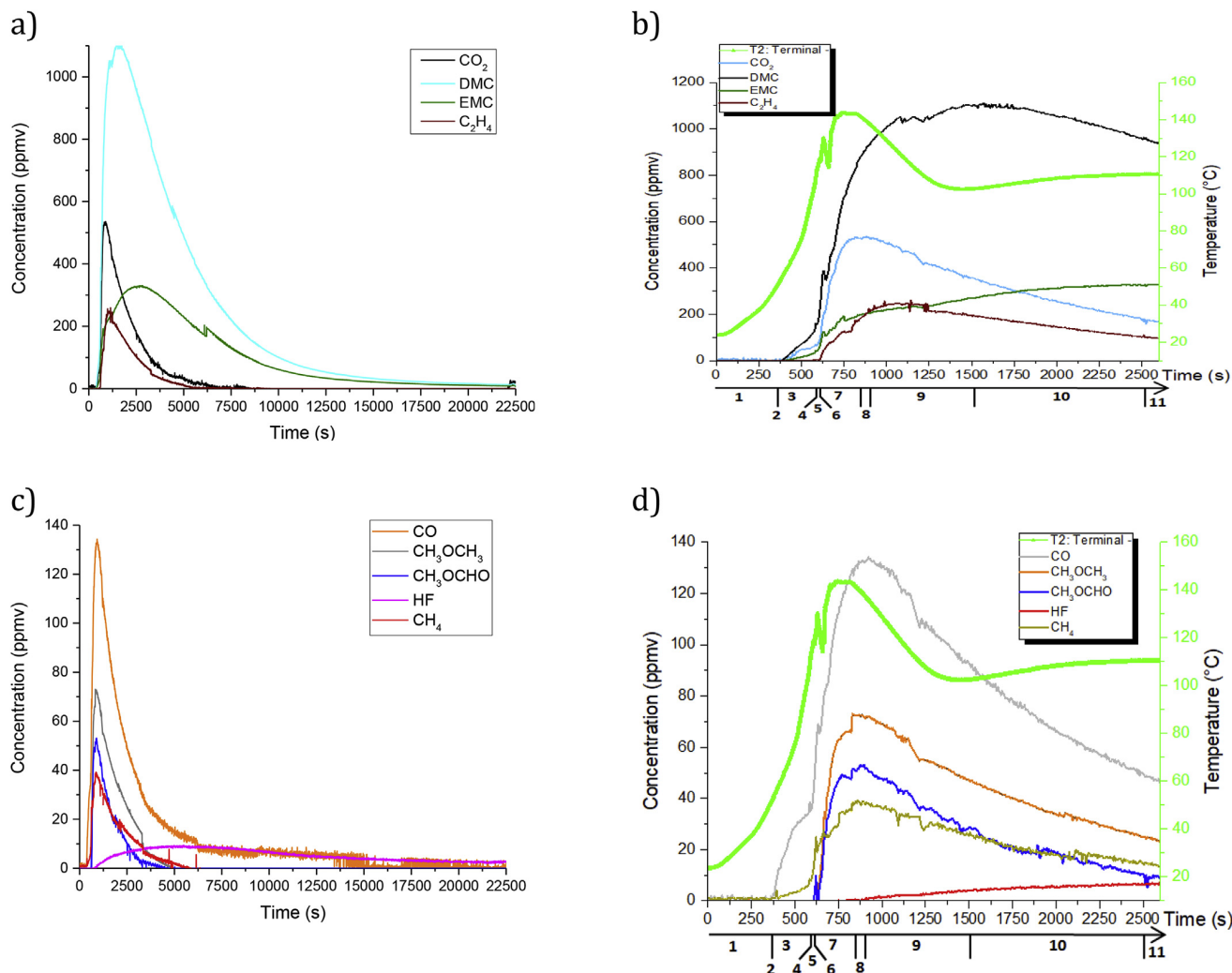


Fig. 5. Exhaust gas concentrations in ppmv as a function of time (in s): a) CO₂, DMC, EMC and C₂H₄ in the range 0 to 22500s; b) CO₂, DMC, EMC and C₂H₄ concentrations in the range 0 to 2500s; c) CO, CH₃OCH₃, CH₃OCHO, HF and CH₄ concentrations in the range 0 to 22500s; d) CO, CH₃OCH₃, CH₃OCHO, HF and CH₄ concentrations in the range 0 to 2500s.

STP conditions was 1643 mL. The HF results were considered to be the minimum as its production appears to continue after the FTIR analysis has stopped.

3.3. Overcharge tests: mass balance

Before and after each test, the cells were weighed. For the 7 reproducible tests, the mean mass loss was 6.5 ± 0.4 g, i.e. about 9% of the initial cell mass. Thanks to the analysis performed after the overcharge and during the tests it is possible to calculate the mass loss with the perfect gas law. The gas mass represents 0.85g without solvents and HF contributions. It is about 13% of the mass loss of the cell. The volatile solvent part of the total mass loss of the cell is 3.77g. This represents about 58% of the mass loss of the cell and 43% of the mass loss of the initial volatile solvent of the electrolyte. The rest of the volatile solvent was decomposed into gases or was trapped in the cell by the bobbin. At the end of the tests when solvents are not detected by the continuous FTIR, there is a remaining brown liquid on the chamber walls. The residual mass loss of 1.88g could be attributed to non-volatile solvents pushed out of the cell, hydrolyzed LiPF₆ salts, degradation solids [24] and HF generation. Note that it was not possible to investigate the remaining liquid for the following reasons: i) the liquid

is projected on the reactor walls during the test, making it very difficult to collect; ii) despite the tests carried out, we were unable to establish a reproducible procedure.

3.4. Discussion

As described previously in Fig. 6, there are 3 important steps for the gas released during the overcharge test.

The first one occurs with a small off-gas release by the cell with the following gaseous composition: DMC, EMC, CH₄, CO and CO₂ (see stages 1–3 in Fig. 6b). At this point, the SOC is about 120%. This result is in good agreement with the studies [16–18] described previously, except for C₃H₈ and C₂H₆ that were identified respectively by Refs. [16] and [18] and that we did not identify or quantify in similar amounts. This difference could be attributed to the solvent composition which is different in our case (see Table 2). The volume of the vent gases observed by Ref. [17] is very similar to the one measured in the present work for low surface temperature (~100 °C). An electrochemical origin is probably the best explanation for this first small gas exhaust, since the internal increase in temperature until the second step as well as the voltage higher than 5V could contribute to electrolyzing the solvents [25]. This first gas release is the smallest one and probably corresponds

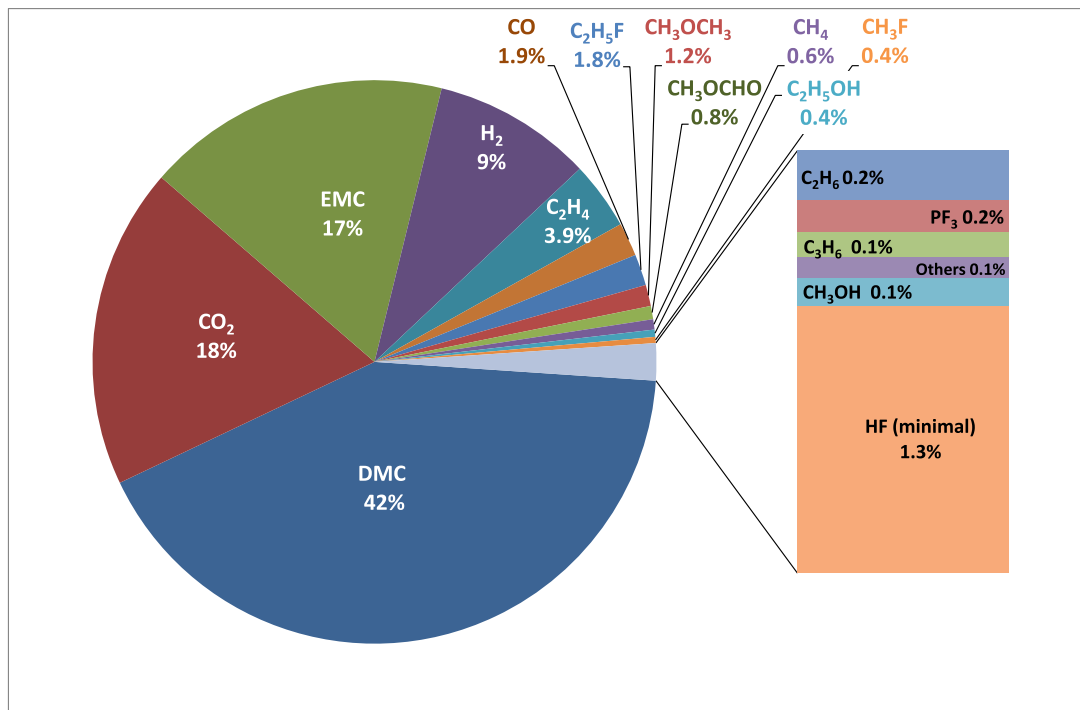


Fig. 6. Global chemical composition of the vent gases in terms of mole fractions in %. The total volume of the vent gases is 1643 mL in STP conditions.

to the filling of the internal volume of the cell, before reaching cell rupture. This first gas release is anaerobic with increasing pressure inside the battery.

The second important step is when a large opening of the cell casing is observed for a cell surface temperature above 110 °C and the termination of the electric current (step 4 to 7). The ionic current shifts to zero very quickly at SOC 130% because it is the beginning of the shutdown of the separator [26]. The cell then becomes capacitor-like. New gases such as CH₃OCH₃, CH₃OCHO and C₂H₄ appear and a large amount of gas is exhausted. The internal temperature rise above the surface temperature of 144 °C is probably the reason for this second, much larger, gas release. Our results are in good agreement with the study by Somandepalli et al. [20] who identified similar gases: CO₂, H₂, CO, CH₄, C₂H₄, C₂H₆ except C₃H₈, for a total volume of 6L. Note that the type of cathode was different from ours and the solvent proportions were not determined. This second gas release occurs under atmospheric pressure as the cell is open. Nevertheless, the gases are formed inside the cell and are carried out of the cell through solvent evaporation. As the gas composition is similar to that observed during the first gas release, one can conclude that the velocity of the gas release is such that air cannot enter the battery, implying that the gases are, once again, formed in anaerobic conditions.

The third important step is when the cell starts to cool (i.e. steps 8 to 10 in Fig. 6b and d). The concentrations of CH₃OCH₃, CH₃OCHO, CH₄, CO and CO₂ decrease and HF vapors appear. At the end of this step, only the HF concentration increases, whereas the concentration of the other gases decreases. The HF formation mechanism appears to be decoupled from the other reaction mechanisms as HF appears when all the other gases start to decrease. At this point, off-gas is no longer released by the cell. The HF formation mechanism could be due to water from chamber air, that can penetrate inside the cell and thus hydrolyze the LiPF₆ salt dissolved in the remaining non-volatile solvents. The comparison with a similar abuse test reported in the literature (see Table 2) shows that, despite the different chemical composition of the cells, the main species present in the off-gas release are similar. The proportions, however, are different. Other differences concern the

measured temperature. We obtained a similar order of magnitude of external temperatures as [19] (about 100 °C) and [17] (about 120 °C). Note that the internal temperature can be much higher than the external temperature in overcharge tests [19,27]. Nevertheless, external temperature seems to be a key parameter that plays an important role in the off-gas composition. The comparison with available data performed with a similar type of cathode shows that the external temperatures reached by our cell are lower than those observed in Ref. [2]. This is probably due to the fact that in Ref. [2], the cell was thermally insulated. Moreover, it is important to emphasize that the temperature gradient is different in the two cases: in our case, i.e. in the case of an overcharge abuse test, the temperature is higher inside the cell and in the case of thermal abuse tests, the external temperature is higher than the internal temperature. Moreover, in the case of overcharge, there is a hot point inside the cell, whereas in the case of thermal abuse tests, the cell is heated uniformly. This difference in the temperature gradient could also explain the amounts of gases. The gradient is much higher in our case than in Ref. [2], although the cells have a comparable mass. Finally, it is important to note that the main species identified by Refs. [19] and [2,10] in the case of thermal abuse on overcharged LFP cells were identical to the species identified and quantified in the present study.

In addition, the volume of exhaust gases differs between the various studies. Kumai et al. [16] mentioned a volume of 10.57 mL whereas Oshaki et al. [17] found a volume of 24 mL. These values are lower than ours but in the tests performed by these authors, the cell did not reach total deconfinement. On the whole, we found similar results to those reported by overcharge test studies, even when different types of cathode were used.

From these results, it was possible to outline new elements in the reaction mechanisms: i) the origin of the larger off-gas release appears to be thermal rather than electrochemical; ii) HF has a specific behaviour and its formation seems to be decorrelated from the other species.

In order to gain greater insight into the C-H-O reaction mechanisms, we checked whether the detailed reaction mechanisms available in the literature include the species that were identified and quantified in the

Table 3

DMC sub-mechanism composed of 23 reactions as described in Sun et al. [28]. Molecules identified and quantified are written in bold and italic. Radicals are underlined>. Note that CH_3OCHO (methyl formate), CH_2O (formaldehyde), $\text{CH}_3\text{OC}(=\text{O})\text{OCH}$ (methyl oxoethanoate), $\text{CH}_3\text{O}_2\text{H}$ (methyl peroxide) and H_2O_2 (hydrogen peroxide) were not detected. This could be due to the very fast reactivity of these species, their presence in very small amounts, or limitations of the analytical device.

R1:	$\text{DMC} \rightleftharpoons \text{CH}_3\text{OCH}_3 + \text{CO}_2$
R2:	$\text{DMC} \rightleftharpoons \text{CH}_3\text{OC}(=\text{O})\text{O} + \text{CH}_3$
R3:	$\text{DMC} \rightleftharpoons \text{CH}_3\text{OCHO} + \text{CH}_2\text{O}$
R4:	$\text{DMC} \rightleftharpoons \text{CH}_3\text{OC}(=\text{O})\text{OCH} + \text{H}_2$
R5:	$\text{DMC} \rightleftharpoons \text{CH}_3\text{OC}(=\text{O})\text{CH}_2 + \text{H}$
R6:	$\text{DMC} \rightleftharpoons \text{CH}_3\text{OCO} + \text{CH}_3\text{O}$
R7:	$\text{DMC} + \text{H} \rightleftharpoons \text{CH}_3\text{OC}(=\text{O})\text{CH}_2 + \text{H}_2$
R8:	$\text{DMC} + \text{O} \rightleftharpoons \text{CH}_3\text{OC}(=\text{O})\text{CH}_2 + \text{OH}$
R9:	$\text{DMC} + \text{O}_2 \rightleftharpoons \text{CH}_3\text{OC}(=\text{O})\text{CH}_2 + \text{HO}_2$
R10:	$\text{DMC} + \text{OH} \rightleftharpoons \text{CH}_3\text{OC}(=\text{O})\text{CH}_2 + \text{H}_2\text{O}$
R11:	$\text{DMC} + \text{CH}_3 \rightleftharpoons \text{CH}_3\text{OC}(=\text{O})\text{CH}_2 + \text{CH}_4$
R12:	$\text{DMC} + \text{HO}_2 \rightleftharpoons \text{CH}_3\text{OC}(=\text{O})\text{CH}_2 + \text{H}_2\text{O}_2$
R13:	$\text{DMC} + \text{CH}_3\text{O}_2 \rightleftharpoons \text{CH}_3\text{OC}(=\text{O})\text{CH}_2 + \text{CH}_3\text{O}_2\text{H}$
R14:	$\text{DMC} + \text{CH}_3\text{O} \rightleftharpoons \text{CH}_3\text{OC}(=\text{O})\text{CH}_2 + \text{CH}_3\text{OH}$
R15:	$\text{DMC} + \text{C}_2\text{H}_3 \rightleftharpoons \text{CH}_3\text{OC}(=\text{O})\text{CH}_2 + \text{C}_2\text{H}_4$
R16:	$\text{DMC} + \text{C}_2\text{H}_5 \rightleftharpoons \text{CH}_3\text{OC}(=\text{O})\text{CH}_2 + \text{C}_2\text{H}_6$
R17:	$\text{DMC} + \text{HCO} \rightleftharpoons \text{CH}_3\text{OC}(=\text{O})\text{CH}_2 + \text{CH}_2\text{O}$
R18:	$\text{DMC} + \text{CH}_3\text{OCO} \rightleftharpoons \text{CH}_3\text{OC}(=\text{O})\text{CH}_2 + \text{CH}_3\text{OC}(=\text{O})\text{H}$
R19:	$\text{CH}_3\text{OC}(=\text{O})\text{CH}_2 \rightleftharpoons \text{CH}_3\text{OCO} + \text{CH}_2\text{O}$
R20:	$\text{CH}_3\text{OC}(=\text{O})\text{O} \rightleftharpoons \text{CH}_3\text{O} + \text{CO}_2$
R21:	$\text{CH}_3\text{OCO} \rightleftharpoons \text{CH}_3 + \text{CO}_2$
R22:	$\text{CH}_3\text{OCO} \rightleftharpoons \text{CH}_3\text{O} + \text{CO}$
R23:	$\text{CH}_3\text{OC}(=\text{O})\text{CH}_2 + \text{CH}_3 \rightarrow \text{CH}_3\text{OC}(=\text{O})\text{O} + \text{C}_2\text{H}_5$

present study or not. Among the reaction mechanisms reported in the literature, only the pyrolysis/combustion of DMC was described. In particular, the sub-mechanism of Sun et al. [28] describes the pyrolysis of DMC; it includes 23 reactions, as listed in Table 3. It is important to note that among the species listed in this sub-mechanism, nearly all the molecules were identified and quantified. Radicals could not be detected. O_2 and H_2O are not present in the cell before its deconfinement. This shows that the origin of the off-gas can be attributed mainly to this volatile solvent. Nevertheless, some additional studies, dedicated in particular to the thermal degradation of carbonate solvents, would be required to assess the origin of the gases released by the cell.

4. Numerical combustion study of the vent gases

In the previous section, it was shown that the abuse by overcharge of the Li-ion battery released electrolyte solvents (DMC and EMC) together with partially reacted gases such as CO and H_2 . In this section, the thermochemical and combustion properties of the gases released by the cell are studied in order to determine if they can ignite and burn or not. For that purpose, a numerical study of the combustion of the vent gases was carried out. The composition of the initial gas mixture was determined from Fig. 6 considering only C-H-O species. As, to our knowledge, there is no reaction mechanism including EMC in the existing literature, we assume that the solvent vapors in the vent gases are only composed of DMC. The mixtures studied in this part are thus composed of 64% of DMC, 19.8% of CO_2 , 9.8% of H_2 , 4.2% of C_2H_4 and

Table 4

Composition of the initial mixture (reference case: DMC, in lean, stoichiometric and rich conditions and vent gases).

		$\text{C}_3\text{H}_6\text{O}_3$	O_2	N_2	CO_2	H_2	C_2H_4	CO
$\phi_{\text{DMC}} = 0.5$	DMC	0.0338	0.2030	0.7632				
	Vent gases	0.0319	0.1996	0.7505	0.0099	0.0049	0.0021	0.0011
$\phi_{\text{DMC}} = 1$	DMC	0.0654	0.1963	0.7382				
	Vent gases	0.0608	0.1901	0.7148	0.0188	0.0093	0.0040	0.0021
$\phi_{\text{DMC}} = 2$	DMC	0.1229	0.1843	0.6929				
	Vent gases	0.1111	0.1736	0.6528	0.0344	0.0170	0.0073	0.0039

Table 5

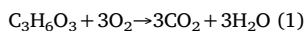
Adiabatic flame temperatures for the reference case (DMC) and the vent gas case in lean, stoichiometric and rich conditions. Initial temperature T_0 (K) ranges from 300 to 600 K.

T_0 (K)	T_{ad} (K) of vent gases			T_{ad} (K) of DMC		
	$\phi_{\text{DMC}} = 0.5$	$\phi_{\text{DMC}} = 1$	$\phi_{\text{DMC}} = 2$	$\phi_{\text{DMC}} = 0.5$	$\phi_{\text{DMC}} = 1$	$\phi_{\text{DMC}} = 2$
300	1561	2176	1527	1599	2185	1518
400	1638	2227	1596	1668	2233	1596
500	1717	2276	1671	1742	2280	1676
600	1798	2323	1749	1820	2326	1757

2.2% of CO. In order to describe the combustion chemistry with a detailed reaction mechanism, calculations were performed with the Chemical Workbench Code [29] and CHEMKIN-II [30]. Among the existing reaction mechanisms that are available in the literature to describe the combustion of DMC, i.e. Glaude et al. [31], Hu et al. [32], Sun et al. [28], we chose the latter as it was shown by the authors that it is better at estimating parameters both in combustion (laminar pre-mixed flame, ignition delays, opposed flow diffusion flame, laminar flame speeds, ignition delay time) and pyrolysis (laminar flow reactors) conditions. The Sun mechanism is composed of 257 species and 1563 reactions. It is associated with thermochemical properties and transport properties.

As suggested in Ref. [33], in order to determine how energetically the vent gases can burn, the following thermochemical and combustion parameters were computed: i) adiabatic flame temperature, i.e. the theoretical flame temperature reached by a mixture in adiabatic and isobaric conditions; ii) laminar flame speed, i.e. the velocity of a steady one-dimensional adiabatic free flame propagating in the doubly infinite domain. It is a fundamental parameter of any combustible mixture that depends on the stoichiometric ratio, pressure and temperature; iii) heat release rates, that correspond to the rates at which heat is released by a flame.

Results obtained with the vent gases were systematically compared with those obtained in the case of pure DMC in order to establish whether the amount of CO_2 is sufficient to prevent combustion of the vent gases. For thermochemical and laminar flame speed calculations, three mixtures were considered, corresponding to three different DMC equivalence ratios, ϕ_{DMC} . In the case of the combustion of DMC, $\text{C}_3\text{H}_6\text{O}_3$:



The equivalence ratio, ϕ_{DMC} is given by equation (1):

$$\phi_{\text{DMC}} = \frac{(x_{\text{DMC}}/x_{\text{O}_2})_m}{(x_{\text{DMC}}/x_{\text{O}_2})_{st}} = 3 \left(\frac{x_{\text{DMC}}}{x_{\text{O}_2}} \right)_m \quad (1)$$

In reaction (1), the equivalence ratio ϕ_{DMC} is 1, which corresponds to a stoichiometric combustion. When the fuel is the limiting reagent, the combustion is lean ($\phi_{\text{DMC}} < 1$) and when there is an excess of fuel, the combustion is rich ($\phi_{\text{DMC}} > 1$). Three equivalence ratios were selected (as in Sun et al. [28]): $\phi_{\text{DMC}} = 0.5, 1$ and 2 , which are close to the High and Low Flammability Limits of DMC (INIST). The corresponding

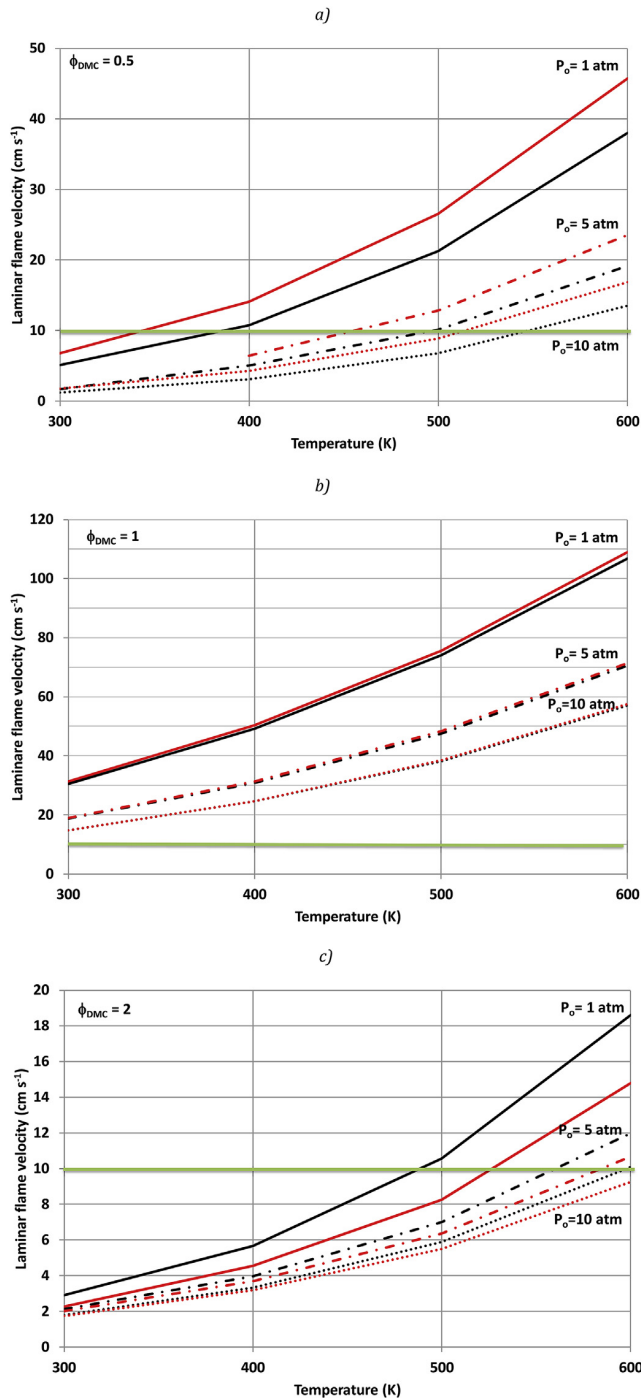


Fig. 7. Laminar flame velocities computed with CWB together with Sun mechanism for DMC/air flames (in red) and vent gases/air flames (in black) for a) lean conditions ($\phi_{DMC} = 0.5$); b) stoichiometric conditions ($\phi_{DMC} = 1$); and c) rich conditions ($\phi_{DMC} = 2$); as a function of initial temperature (from $T_0 = 300$ to 600K) and for $P_0 = 1$ atm (solid lines), 5 (dot-dashed lines) and 10atm (dotted lines). The green line shows the lower limit of laminar flame velocity (10 cm.s^{-1}). (For interpretation of the references to colour in this figure legend, the reader is referred to the Web version of this article.)

values of the mole fractions of the mixture composed of DMC, O₂ and N₂ are given in Table 4. For combustion of the vent gases, three cases were also considered, lean, stoichiometric and rich conditions related to DMC. The corresponding composition of the mixture is also given in

Table 6

Conditions (in orange) for which laminar flame speed is greater than 10 cm/s in the simulations performed in this work.

DMC/Vent gases		T ₀ (K)			
P ₀ (atm)	ϕ_{DMC}	300	400	500	600
1	0.5	Green	Orange	Orange	Orange
	1	Green	Orange	Orange	Orange
	2	Green	Orange	Orange	Orange
5	0.5	Green	Orange	Orange	Orange
	1	Green	Orange	Orange	Orange
	2	Green	Orange	Orange	Orange
10	0.5	Green	Orange	Orange	Orange
	1	Green	Orange	Orange	Orange
	2	Green	Orange	Orange	Orange

Legend: $S_L^\circ > 10 \text{ cm.s}^{-1}$ (Orange), $S_L^\circ < 10 \text{ cm.s}^{-1}$ (Green)

Table 4. In each case, the equivalence ratio of DMC is respected as well as the composition of the vent gases.

Calculations of adiabatic flame temperatures and laminar flame speeds were carried out for a temperature range of 300 to 600K and for 3 conditions of initial pressure: 1, 5 and 10 atm. This temperature range corresponds to the supposed temperature range during the overcharge test. The pressure range corresponds to a possible battery application environment, as overpressure can occur when gas emissions take place in a confined environment. Results for adiabatic flame temperatures (T_{ad}) are given in Table 5. In Table 5, initial pressure is not mentioned because from 300 to 600K, pressure has no influence on the adiabatic flame temperature since the dissociation of the gas phase does not change. As expected, whatever the case, the adiabatic temperature increases when the initial temperature increases. Whatever the initial temperature, the adiabatic temperature reached in the case of pure DMC is slightly higher than in the case of the vent gases. The adiabatic temperature is obtained with no heat loss and is thus a theoretical value. From this result, as mentioned in Harris et al. [33], it can be deduced that the higher the adiabatic temperature, the faster the heat release rate will be. Laminar flame speed is a fundamental combustion parameter. If the laminar flame speed is too low, the flame will extinguish. The lowest limit is around 5–10 cm.s⁻¹. Fig. 7 shows the laminar flame speeds computed with CWB together with the Sun mechanism for the previous conditions ($T_0 = 300$ to 600K, $P_0 = 1, 5$ or 10 atm, $\phi_{DMC} = 0.5, 1$ and 2.0). The case of vent gases/air flames is compared with DMC/air flames. Fig. 7 shows that in lean conditions, whatever the initial pressure, the laminar flame velocities of DMC/air flames are greater than those of vent gases/air flames. The reverse is observed in rich conditions. Similar laminar flame velocities are observed for stoichiometric conditions. Table 6 summarizes the conditions for which the laminar flame speed is greater than 10 cm.s⁻¹. In stoichiometric conditions, laminar flame velocities are greater than 10 cm.s⁻¹ in all cases. In lean mixtures, the conditions for which laminar flame speeds are greater than 10 cm.s⁻¹ are $T_0 > 400$ K for $P_0 = 1$ atm; $T_0 > 500$ K for $P_0 = 5$ atm and $T_0 > 550$ K for $P_0 = 10$ atm, and in rich conditions: $T_0 > 500$ K for $P_0 = 1$ atm; $T_0 > 600$ K for $P_0 = 5$ atm. Considering that the release of the gas occurs under atmospheric pressure, this implies that if a flame ignites, it can propagate.

Finally, the heat release rate (HRR) was computed. As argued by Ref. [33], it is a useful parameter to assess whether a flame in one cell will ignite a neighboring cell or not. As previously shown by these authors, HRR in cal.cm⁻³.s⁻¹ was estimated in the case of the diffusion flame stabilized by Glaude et al. [31]. A diffusion flame can simulate the ejection of gases from a cell as the flammable mixture encounters oxidizer (air). Calculations were carried out with the OPPDIF [34] code from CHEMKIN-II [30] together with the reaction mechanism of Glaude et al. [31] (for comparison with the results of Harris et al. [33]), in the following conditions:

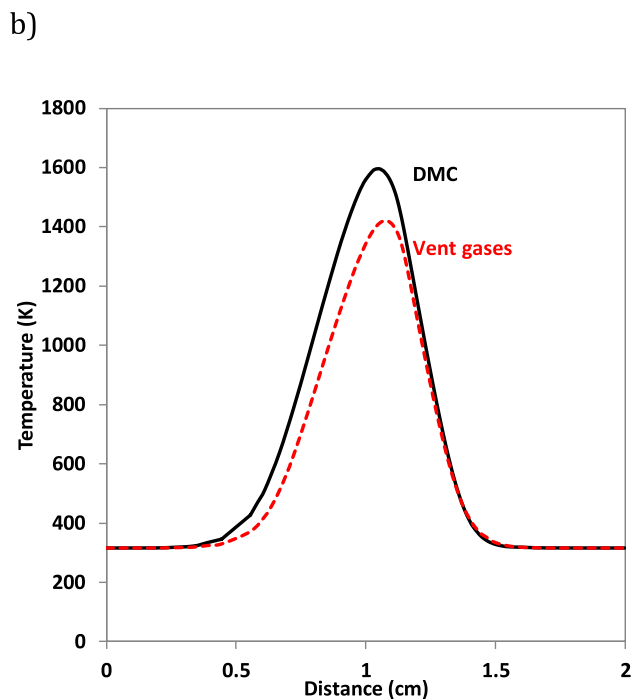
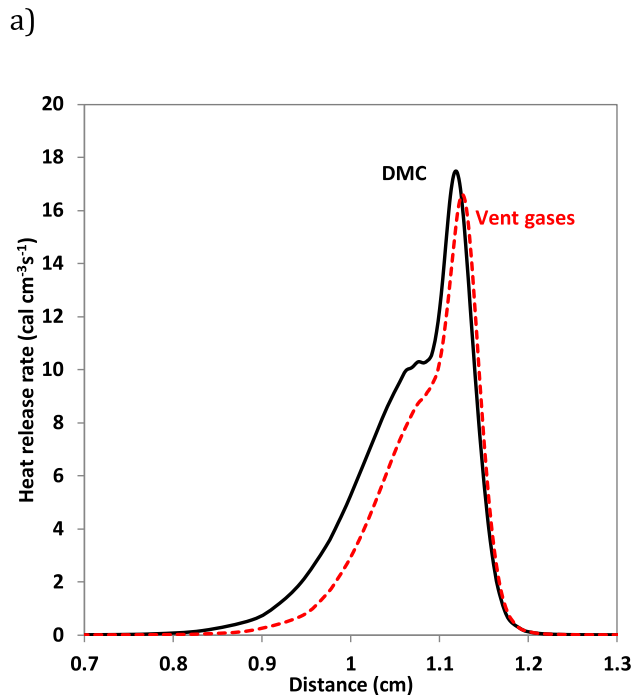


Fig. 8. a) Heat release (in $\text{cal}\cdot\text{cm}^{-3}\cdot\text{s}^{-1}$) and b) Temperature (in K); profiles across the counterflow diffusion DMC/air flame (black solid line) and vent gases/air flame (red dashed line). Calculations performed in conditions described in Ref. [31] with OPPDIF [34] from CHEMKIN-II [30] together with the Glaude et al. mechanism [31]. (For interpretation of the references to colour in this figure legend, the reader is referred to the Web version of this article.)

- inlet velocity for both fuel and oxidizer of $10\text{ cm}\cdot\text{s}^{-1}$ and inlet temperature of 315K;
- inlet fuel mixture composed of 8% fuel and 92% N_2 ;
- inlet oxidizer mixture composed of 39% O_2 and 61% N_2 ;
- a distance of 2 cm from the inlets.

In the calculations, the mixture-average option coupled with the Soret effect were used and the energy equation was solved. Fig. 8 shows the predicted heat release rate profiles together with the predicted temperature profiles for the DMC and the vent gas flames. The HRR calculated in the DMC flame and in the vent gas flame are similar (the maximum HRR is about $17.5\text{ cal}\cdot\text{s}^{-1}\cdot\text{cm}^{-3}$ in the DMC flame and $16.6\text{ cal}\cdot\text{s}^{-1}\cdot\text{cm}^{-3}$ in the vent gas flame) whereas the temperature profiles are different, slower in the case of the vent gases (the maximum temperature is respectively about 1600K in the DMC flame and 1420K in the vent gas flame). These results are in good agreement with the previous study by Harris et al. [33] and show that HRR, as concluded by these authors, is more useful for comparing the ability of a solvent to ignite neighboring cells. The results presented here show that the gases released during overcharge, despite the presence of carbon dioxide, have the same HRR as a DMC flame. As mentioned by Harris et al. [33], even if carbonate solvents such as DMC have lower HRR than analogous hydrocarbons, heat release by a DMC flame can be sufficient to ignite neighbouring cells. In our case, we showed that the amount of CO_2 in the vent gases is thus not sufficient to prevent flammability and is probably counterbalanced by the presence of flammable gases such as H_2 . The vent gases are able to ignite and release heat that could ignite a neighboring cell. As pointed out by Harris et al. [33], a fundamental combustion study is required to study the flammability of the vent gases. The present study is a numerical study and it would be necessary to increase the experimental and numerical databases relative to the electrolyte mixtures.

5. Conclusion

In the present study, overcharge tests on commercial Li-ion batteries were performed. Among the nine overcharge tests, seven had a typical thermoelectrical behavior, enabling the coupling with gas-phase analyses. A new and innovative setup was designed to analyse off-gas release by the cell during the test and at the end of the test. The gases released by the cell during the overcharge tests were then identified and quantified and the formation kinetics of the different species was determined. The mass balance was established and the formation of gases released by the cell during the overcharge test was elucidated. The following conclusions, some of which have not been previously reported in the literature, can be drawn from the observations in the experimental and numerical studies presented in the present paper:

1. Some species are produced after the first deconfinement of the cell.
2. HF has a specific behavior and its formation seems to be decoupled from the other species.
3. The main gas release occurs when the current is zero.
4. The gas phase released by the cell is mainly composed of flammable volatile solvents, which are responsible for flammability hazards in Li-ion batteries.
5. The similarity in the vent gas composition obtained either in overcharge abuse tests or in thermal abuse tests on an overcharged cell indicates that oxidoreduction reactions seem to be poorly responsible for the main off-gas release by the cell whereas temperature is the key parameter.

These findings are highly dependent, on the one hand, on the nature of the cathode material family because it determines the thermal runaway [2,10], and, on the other hand, on the electrolyte solvents because they contain volatile solvents that are important in determining the quantity, content and emissions of gases released by the cell. This study showed that volatile solvents are very sensitive to thermal runaway and are responsible for off-gas release. To prevent these problems, various solutions could be considered during the cell manufacturing process: either avoiding cell opening or limiting thermal runaway, or both. To avoid cell opening, non-volatile solvents should be used or internal pressure could be measured and a cut-off system provided to stop the

current in the event of a drastic increase in internal pressure. To limit thermal runaway, cooling of the cell should be performed.

The perspectives opened by this work concern both experimental and numerical procedures. In particular, a new experimental setup aimed at studying the thermal degradation of carbonate solvents, studied for various durations and for different initial temperatures, correlated to kinetic simulations will be carried out in order to investigate the reaction mechanisms.

Acknowledgements

The authors thank the “Conseil Régional du Centre Val de Loire”, France, which contributed to the financial support of this work. They also wish to thank the LITEN Laboratory, from CEA, in Grenoble for its help in cell characterizations.

Appendix A. Supplementary data

Supplementary data related to this article can be found at <http://dx.doi.org/10.1016/j.jpowsour.2018.03.034>.

References

[1] C. Hendricks, N. Williard, S. Mathew, M. Pecht, A failure modes, mechanisms, and effects analysis (FMMEA) of lithium-ion batteries, *J. Power Sources* 297 (2015) 113–120.

[2] A.W. Golubkov, S. Scheikl, R. Planteu, G. Voitic, H. Wiltsche, C. Stangl, G. Fauler, A. Thaler, V. Hacker, Thermal runaway of commercial 18650 Li-ion batteries with LFP and NCA cathodes – impact of state of charge and overcharge, *RSC Adv.* 5 (2015) 57171.

[3] G.G. Eshetu, J.-P. Bertrand, A. Lecoq, S. Grugeon, S. Laruelle, M. Armand, G. Marlair, Fire behavior of carbonates-based electrolytes used in Li-ion rechargeable batteries with a focus on the role of the LiPF₆ and LiFSI salt, *J. Power Sources* 269 (2014) 804–811.

[4] S. Hess, M. Wohlfahrt-Mehrens, M. Wachtler, Flammability of Li-Ion battery electrolytes: flash point and self-extinguishing time measurements, *J. Electrochem. Soc.* 162 (2015) A3084–A3097.

[5] G. Gachot, P. Ribière, D. Mathiron, S. Grugeon, M. Armand, J.-B. Leriche, S. Pilard, S. Laruelle, Gas chromatography/mass spectrometry as a suitable tool for the Li-ion battery electrolyte degradation mechanisms study, *Anal. Chem.* 83 (2011) 478–485.

[6] D.H. Doughty, E.P. Roth, C.C. Crafts, G. Nagasubramanian, G. Henriksen, K. Amine, Effects on additives on thermal stability of Li ion cells, *J. Power Sources* 146 (2005) 116–120.

[7] D.P. Abraham, E.P. Roth, R. Kostecky, S. MacLaren, D.H. Doughty, Diagnostic examination of thermally abused high-power lithium-ion cells, *J. Power Sources* 161 (2006) 648–657.

[8] E.P. Roth, Abuse response of 18650 Li-ion Cells with different cathodes using EC: EMC/LiPF₆ and EC: PC:DMC/LiPF₆ electrolytes, *ECS Transactions* 11 (2008) 19–41.

[9] P. Ribière, S. Grugeon, M. Morcrette, S. Boyanov, S. Laruelle, G. Marlair, Investigation on the fire-induced hazards of Li-ion battery cells by fire calorimetry, *Energy Environ. Sci.* 5 (2011) 5271–5280.

[10] A.W. Golubkov, D. Fuchs, J. Wagner, H. Wiltsche, C. Stangl, G. Fauler, G. Voitic, A. Thaler, V. Hacker, Thermal-runaway experiments on consumer Li-ion batteries with metal-oxide and olivin-type cathodes, *RSC Adv.* 4 (2014) 3633–3642.

[11] F. Larsson, P. Andersson, P. Blomqvist, A. Lorén, B.-E. Mellander, Characteristics of

lithium-ion batteries during fire test, *J. Power Sources* 271 (2014) 414–420.

[12] Y. Fu, S. Lu, K. Li, C. Liu, X. Cheng, H. Zhang, An experimental study on burning behaviors of 18650 lithium ion batteries using a cone calorimeter, *J. Power Sources* 273 (2015) 216–222.

[13] J. Sun, J. Li, T. Zhou, K. Yang, S. Wei, N. Tang, N. Dang, H. Li, X. Qiu, L. Chen, Toxicity, a serious concern of thermal runaway from commercial Li-ion battery, *Nano Energy* 27 (2016) 313–319.

[14] M. Lammer, A. Königseder, V. Hacker, Holistic methodology for characterisation of the thermally induced failure of commercially available 18650 lithium ion cells, *RSC Adv.* 7 (2017) 24425–24429.

[15] F. Larsson, P. Andersson, P. Blomqvist, B.-E. Mellander, Toxic fluoride gas emissions from lithium-ion battery fires, *Nature* 7 (2017) 10018.

[16] K. Kumai, H. Miyashiro, Y. Kobayashi, K. Takei, R. Ishikawa, Gas generation mechanism due to electrolyte decomposition in commercial lithium-ion cell, *J. Power Sources* 81–82 (1999) 715–719.

[17] T. Ohsaki, T. Kishi, T. Kuboki, N. Takami, N. Shimura, Y. Sato, M. Sekino, A. Satoh, Overcharge reaction of lithium-ion batteries, *J. Power Sources* 146 (2005) 97–100.

[18] W. Kong, H. Li, X. Huang, L. Chen, Gas evolution behaviors for several cathode materials in lithium-ion batteries, *J. Power Sources* 142 (2005) 285–291.

[19] Q.F. Yuan, F. Zhao, W. Wang, Y. Zhao, Z. Liang, D. Yan, Overcharge failure investigation of lithium-ion batteries, *Electrochim. Acta* 178 (2015) 682–688.

[20] V. Somandepalli, K. Marr, Q. Horn, Quantification of combustion hazards of thermal runaway failures in lithium-ion batteries, *SAE Int. J. Alt. Power* 3 (1) (2014) 98–104 <https://doi.org/10.4271/2014-01-1857>.

[21] N.S. Spinner, C.R. Field, M.H. Hammond, B.A. Williams, K.M. Myers, A.L. Lubrano, S.L. Rose-Pehrsson, S.G. Tuttle, Physical and chemical analysis of lithium-ion battery cell-to-cell failure events inside custom fire chamber, *J. Power Sources* 279 (2015) 713–721.

[22] H.-F. Li, J.-K. Gao, S.-L. Zhang, Effect of overdischarge on swelling and recharge performance of lithium ion cells, *Chin. J. Chem.* 26 (2008) 1585–1588.

[23] Y. Zheng, K. Qian, D. Luo, Y. Li, Q. Lu, B. Li, Y.-B. He, X. Wang, J. Li, F. Kang, Influence of over-discharge on the lifetime and performance of LiFePO₄/graphite batteries, *RSC Adv.* 6 (2016) 30474–30483.

[24] G. Gachot, P. Ribière, D. Mathiron, S. Grugeon, M. Armand, J.-B. Leriche, S. Pilard, S. Laruelle, Gas chromatography/mass spectrometry as a suitable tool for the Li-ion battery electrolyte degradation mechanisms study, *Anal. Chem.* 83 (2011) 478–485.

[25] K. Kanamura, Anodic oxidation of nonaqueous electrolytes on cathode materials and current collectors for rechargeable lithium batteries, *J. Power Sources* 81–82 (1999) 123–129.

[26] E.P. Roth, D.H. Doughty, D.L. Pile, Effects of separator breakdown on abuse response of 18650 Li-ion cells, *J. Power Sources* 174 (2007) 579–583.

[27] R.A. Leising, M.J. Palazzo, E.S. Takeuchi, K.J. Takeuchi, A study of the overcharge reaction of lithium-ion batteries, *J. Power Sources* 97–98 (2001) 681–683.

[28] W. Sun, B. Yang, N. Hansen, C.K. Westbrook, F. Zhang, G. Wang, K. Moshhammer, C.K. Law, An experimental and kinetic modeling study on dimethyl carbonate (DMC) pyrolysis and combustion, *Combust. Flame* 164 (2016) 224–238.

[29] Kintech Laboratory, Chemical Workbench, <http://www.kintechlab.com/products/chemical-workbench/> [accessed 17.12.01].

[30] R.J. Kee, F.M. Rupley, J.A. Miller, CHEMKIN-II: a Fortran Chemical Kinetics Package for the Analysis of Gas-Phase Chemical Kinetics, Sandia National Laboratories, 1989.

[31] P.A. Glaude, W.J. Pitz, M.J. Thomson, Chemical kinetic modeling of dimethyl carbonate in an opposed-flow diffusion flame, *24 Proc. Combust. Inst* 30 (2005) 1111–1118.

[32] E. Hu, Y. Chen, Z. Zhang, L. Pan, Q. Li, Y. Cheng, Z. Huang, Experimental and kinetic study on ignition delay times of dimethyl carbonate at high temperature, *Fuel* 140 (2015) 626–632.

[33] S.J. Harris, A. Timmons, W.J. Pitz, A combustion chemistry analysis of carbonate solvents used in Li-ion batteries, *J. Power Sources* 193 (2009) 855–858.

[34] E. Lutz, R.J. Kee, J.F. Grear, F.M. Rupley, OPPDF: Ortran Program for Computing Opposed-flow Diffusion Flames, Sandia National Laboratories, 1997.



Thermal-runaway experiments on consumer Li-ion batteries with metal-oxide and olivin-type cathodes

Andrey W. Golubkov,^{*a} David Fuchs,^a Julian Wagner,^b Helmar Wiltsche,^c Christoph Stangl,^d Gisela Fauler,^d Gernot Voitc,^e Alexander Thaler^a and Viktor Hacker^e

Cite this: *RSC Adv.*, 2014, 4, 3633

Received 11th October 2013
Accepted 26th November 2013

DOI: 10.1039/c3ra45748f

www.rsc.org/advances

Li-ion batteries play an ever-increasing role in our daily life. Therefore, it is important to understand the potential risks involved with these devices. In this work we demonstrate the thermal runaway characteristics of three types of commercially available Li-ion batteries with the format 18650. The Li-ion batteries were deliberately driven into thermal runaway by overheating under controlled conditions. Cell temperatures up to 850 °C and a gas release of up to 0.27 mol were measured. The main gas components were quantified with gas-chromatography. The safety of Li-ion batteries is determined by their composition, size, energy content, design and quality. This work investigated the influence of different cathode-material chemistry on the safety of commercial graphite-based 18650 cells. The active cathode materials of the three tested cell types were (a) LiFePO₄, (b) Li(Ni_{0.45}Mn_{0.45}Co_{0.10})O₂ and (c) a blend of LiCoO₂ and Li(Ni_{0.50}Mn_{0.25}Co_{0.25})O₂.

1 Introduction

Li-ion batteries have been commercially available since 1991.¹ As of 2013, Li-ion batteries are in wide use for portable electronics, such as cell phones and notebook computers. They are also gaining traction as a power source in electrified vehicles. Li-ion batteries have a high specific energy and favourable ageing characteristics compared to NiMH and lead acid batteries. However, there are concerns regarding the safety of Li-ion batteries. Abuse conditions such as overcharge, over-discharge and internal short-circuits can lead to battery temperatures far beyond the manufacturer ratings. At a critical temperature, a chain of exothermic reactions can be triggered. The reactions lead to a further temperature increase, which in turn accelerates the reaction kinetics. This catastrophic self-accelerated degradation of the Li-ion battery is called thermal runaway.²

During thermal runaway, temperatures as high as 900 °C can be reached,³ and the battery can release a significant amount of burnable and (if inhaled in high concentrations) toxic gas.⁴ To

quantify possible hazards of exothermic Li-ion battery over-temperature reactions, tests with complete batteries should be performed. Such experiments were undertaken with commercial Li-ion batteries produced for consumer electronics³⁻¹¹ and with Li-ion batteries fabricated in the laboratory.¹²⁻¹⁶

This work investigated the thermal stability of three types of commercially available Li-ion batteries for consumer electronics. Particular attention was given to (1) the dynamics of the thermal responses of the cells, (2) the maximum temperatures reached, (3) the amount of gases produced and (4) to the production rates of the gases. To further assess the hazard potential of the released gases, samples were taken and analysed with a gas chromatography system.

2 Experimental

2.1 Brief description of the test rig

To carry out unrestricted thermal-runaway experiments, a custom-designed test stand was built (Fig. 1). The main component of the test rig is a heatable reactor with electric feedthroughs for the temperature measurement and the inner sample heating. The reactor has gas feedthroughs that connect it to an inert gas flask, to a gas sampling station and to a cold trap with an attached vacuum pump. The pressure inside the reactor is recorded by a pressure transmitter. The whole structure is hosted inside a fume hood to prevent any escaping of gases and electrolyte vapours.

A removable sample holder is placed inside the reactor. The sample holder consists of a metal structure, which houses a

^aVIRTUAL VEHICLE Research Center, Inffeldgasse 21a, 8010 Graz, Austria. E-mail: andrey.golubkov@alumni.tugraz.at; Fax: +43-316-873-9002; Tel: +43-316-873-9639

^bGraz Centre for Electron Microscopy, Steyrergasse 17, 8010 Graz, Austria

^cInstitute of Analytical Chemistry and Food Chemistry, Graz University of Technology, Stremayrgasse 9/III, 8010 Graz, Austria

^dVarta Micro Innovation GmbH, Stremayrgasse 9, 8010 Graz, Austria

^eInstitute of Chemical Engineering and Environmental Technology, Graz University of Technology, Inffeldgasse 25C/II, 8010 Graz, Austria



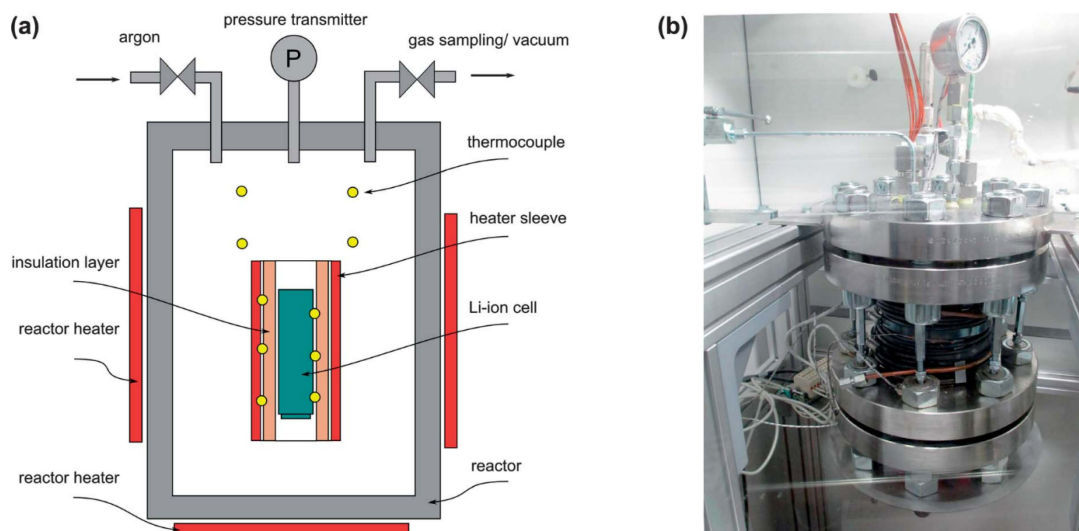


Fig. 1 (a) The reactor and its principal elements. (b) The reactor is the main component of the test stand.

heating sleeve and the thermocouples. A Li-ion battery with the dimensions 18650 (cylindrical geometry with $d = 18$ mm and $l = 65$ mm) can be fitted into the centre of the heating sleeve. The inside wall of the heating sleeve is thermally insulated. The role of the thermal insulation layer is to provide the thermal connection between the heating sleeve and the sample. Due to the low thermal conductivity of the insulation layer, a thermal runaway reaction can proceed in adiabatic-like conditions. Ten thermocouples measure the temperature at different positions inside the reactor: three thermocouples are directly attached to the sample housing, three thermocouples are attached to the heating sleeve and four thermocouples measure the gas temperature inside the reactor.

2.2 Testing method

Initially, the sample battery is CC/CV charged to the respective cut-off voltage. Then, the plastic envelope is removed from the cell and the cell mass and cell voltage are recorded. Three thermocouples are welded to the cell housing, and the whole package is inserted into the heating sleeve of the sample holder. The sample holder is placed inside the reactor. The reactor is evacuated and flushed with argon gas twice. The heaters are set to constant power, and the pressure and temperature signals are recorded. In order to trace fast temperature and pressure changes, each signal is recorded with a high sampling rate of 5000 samples per second.

When a critical temperature is reached, the cell goes into rapid thermal runaway: it produces gas and heat. During the thermal runaway, the temperature of the cell increases by several hundred degree Celsius in a few seconds. After the thermal-runaway event, the cell cools down slowly. Gas samples are taken and analysed with the gas chromatograph. In the next step, the vacuum pump is switched on, and the cooling trap is filled with liquid nitrogen. The gas is carefully released through

the cooling trap and the vacuum-pump into the fume hood. The reactor and the gas tubes between the reactor and the cooling trap are heated above 130 °C to avoid gas condensation.

By following this procedure, most liquid residue in the reactor is passed from the reactor to the cooling trap. The liquid residue can be easily removed from the cooling trap before the next experiment run.

2.3 Gas analysis

The compositions of the sampled gases were analysed using a gas chromatograph (GC, Agilent Technologies 3000 Micro GC, two columns, Mol Sieve and PLOTU). A thermal conductivity detector (TCD) was used to detect permanent gases. The GC was calibrated for H_2 , O_2 , N_2 , CO , CO_2 , CH_4 , C_2H_2 , C_2H_4 and C_2H_6 . Ar and He were used as carrier gases.

Note, that the current test set-up cannot detect HF, which can be a major source of toxicity of gas released by Li-ion batteries during thermal runaway.⁴

2.4 Cell-components identification

In order to identify the components of each cell species, several cells were disassembled: the cells were discharged to 2.0 V, and the cell casings were then carefully removed without causing short circuits. The exposed jelly rolls were subject to several tests.

For electrolyte identification, the jelly rolls were immersed in flasks with CH_2Cl_2 solution immediately after casing removal. The solutions were then analysed using a gas-chromatography-mass spectrometry system (GC-MS: Agilent 7890 & MS 5975MSD) with the ChemStation software and the NIST spectrum library. To analyse the solid materials of the cells, the extracted jelly rolls were separated into the anode, cathode and separator layers. After drying in a chemical fume hood, anode



and cathode-foil samples were taken for identification of the electrochemically active materials. Microwave-assisted sample digestion followed by inductively coupled plasma optical emission spectrometry (ICP-OES, Ciro Vision EOP, Spectro, Germany) was used to obtain the gross atomic compositions of the cathode active masses. A scanning-electron microscope with energy-dispersive X-ray spectroscopy (SEM/EDX: Zeiss Ultra55 & EDAX Pegasus EDX) was used to confirm the ICP-OES results for the compositions of the cathodes and to validate the anode materials.

For the mass-split calculation, the following procedure was followed for each cell type: positive and negative electrode samples were extracted from the jelly roll. The samples were rinsed with diethyl carbonate (DEC) and then dried again, in order to remove the remaining electrolyte residues from the active materials. The samples were weighed, and the geometries of the electrode foils were recorded, so that the mass split could be calculated. The amount of electrolyte was estimated as the mass difference between the initial cell mass and the calculated dry mass for each cell. The thickness of the active material layers on the electrode substrates was extracted from SEM images. The thicknesses of the aluminium and copper substrates were calculated from the measured area density. The thickness of the separator foils was measured with a micrometer.

2.5 Li-ion cells

18650 consumer cells with three types of chemistry were purchased for the experiments. The cells were produced by three well-known companies. For simplicity, the samples will be referred to as LFP, NMC and LCO/NMC cells, in order to reflect their respective cathode material. Despite the simple naming scheme, please note that the cells do not differ in the types of their cathode material alone. Naturally, they also have different layer geometries (Table 2) and different ratios of their component masses (Fig. 2), and there are differences in the composition of the active masses as well (Table 1).

- The LCO/NMC cell had a blended cathode with two types of electrochemically active particles LiCoO_2 and

$\text{Li}(\text{Ni}_{0.50}\text{Mn}_{0.25}\text{Co}_{0.25})\text{O}_2$. A clean cut through the sample was done with a focused ion beam (FIB). Subsequently, EDX measurements of the bulk materials of individual cathode particles were performed. The ratio of LCO and NMC layered oxide particles was estimated by comparing the SEM-EDX and ICP-OES results. The resulting ratio of LCO and NMC was $\text{LCO} : \text{NMC} = (66 : 34)$ with 5% uncertainty. The cells with LCO/NMC blended cathodes are a compromise to achieve high rate capability of LCO material and to maintain acceptable safety and high capacity of the NMC material.¹⁷ The average voltage of this cell was ~ 3.8 V.

- The NMC cell had a $\text{Li}(\text{Ni}_{0.45}\text{Mn}_{0.45}\text{Co}_{0.10})\text{O}_2$ layered oxide cathode. The properties of the NMC mixed oxide cathodes depended on the ratios of nickel, manganese and cobalt material. In general, NMC cells have an average voltage of ~ 3.8 V and high specific capacity.¹⁸

- The LFP cell had a LiFePO_4 cathode with olivine structure. This cathode type is known for featuring good safety characteristics. Commercial LiFePO_4 cathode material for high power Li-ion batteries consists of carbon-coated LiFePO_4 nano-scale particles. The cathode material is readily available and non-hazardous. Commercially available LFP cells have a lower operating voltage (~ 3.3 V) than cells with LCO and NMC cathodes.¹⁸

The active anode materials consisted only of carbonaceous material for all cells, as verified by SEM/EDX. The exact types of graphite materials could not be identified.

2.6 Electrical characterisation

An electrical characterisation of the cells was done with a BaSyTec CTS cell test system. In the first step, the cells were discharged to their respective minimum voltage. In the second step, the cells were charged using a pulse-pause protocol, until the voltage of the cells stayed above their respective maximum voltage during a pause. The current pulses were set to 100 mA and 30 s. The duration of the pauses was set to 50 s. The open-circuit voltage (OCV) at the end of each pause and the charge capacity were recorded (Fig. 3). For the NMC cell, the cell

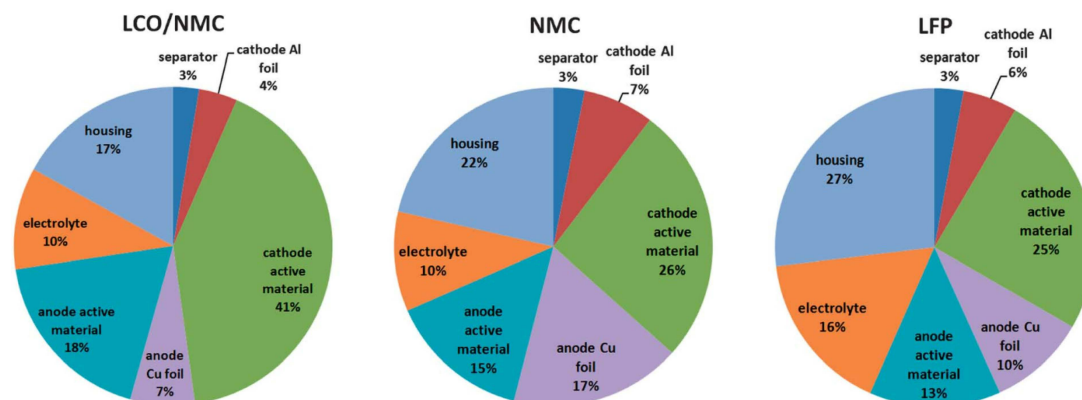


Fig. 2 Mass split (m%) of the main components of the three cell species.



Table 1 Overview of the three cells species used in the experiments. All ratios in this table are given as mol ratios. The electrolyte solvents are dimethyl carbonate (DMC), ethyl methyl carbonate (EMC), ethylene carbonate (EC) and propylene carbonate (PC)

		LCO/NMC	NMC	LFP
Cell mass	g	44.3	43.0	38.8
Capacity	A h	2.6	1.5	1.1
Minimum voltage	V	3.0	3.0	2.5
Maximum voltage	V	4.2	4.1	3.5
Electrolyte solvents		DMC : EMC : EC (6 : 2 : 1)	DMC : EMC : EC : PC (7 : 1 : 1 : 1)	DMC : EMC : EC : PC (4 : 2 : 3 : 1)
Cathode material		LiCoO ₂ : Li (Ni _{0.50} Mn _{0.25} Co _{0.25})O ₂ (2 : 1)	Li(Ni _{0.45} Mn _{0.45} Co _{0.10})O ₂	LiFePO ₄
Anode material		Graphite	Graphite	Graphite

manufacturer did not provide the voltage ratings. For safety reasons, 4.1 V was selected as the maximum voltage.

3 Results and discussion

3.1 Typical course of a thermal runaway experiment

In order to illustrate the events during the heat-up process and the thermal runaway itself, one experiment with a NMC cell is described here in detail:

The NMC sample cell was prepared as described above. At the start of the test, the cell heater sleeve was set to constant heating power. The sample was slowly heated, starting at 25 °C, with a heat-rate of ~2 °C min⁻¹. After reaching 220 °C, the cell went into rapid thermal runaway. The cell temperature rose from 220 °C to 687 °C in a few seconds. When the exothermic reaction ended, the cell cooled down slowly (Fig. 4a).

The amount of gas produced inside the pressure vessel was calculated by applying the ideal gas law:

$$n = \frac{pV}{R\theta_{\text{gas}}} - n_0 \quad (1)$$

where p is the recorded pressure in the reactor, $V = 0.0027 \text{ m}^3$ is the reactor volume, R is the gas constant, θ_{gas} is the recorded gas temperature in the reactor (in K), and n_0 is the initial amount of gas in the reactor at the start of the experiment.

At 160 °C, the safety vent device of the battery housing opened, and 0.02 mol of gas were released by the cell. The cell cooled down by 10 °C during the release process because of the

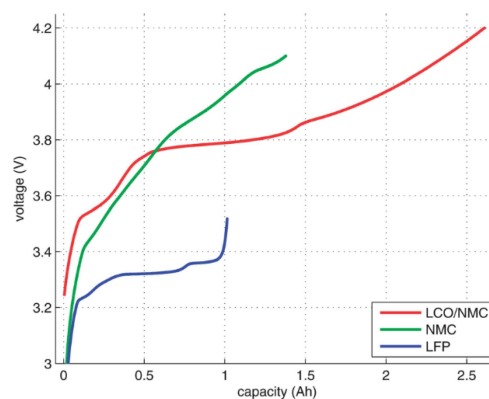


Fig. 3 OCV profiles of the three cell species.

Joule–Thomson effect. The vent opening was then probably clogged until, at 230 °C, concurrent with the rapid thermal runaway, the cell vented for a second time. The second venting was the major venting: an additional 0.15 mol of vent gas were produced (Fig. 4b).

Note that the amount of gas in the reactor decreased shortly after venting. This effect can be explained by the condensation of gas at the reactor walls. Since the reactor walls had a lower temperature (~150 °C) than the cell in full thermal runaway (up to 687 °C), the walls could act as a gas sink.

Table 2 Mass (m), area (A), thickness (d) and volume (V) of the main components of the three cell species. The geometrical volume of a standard 18650 cell is 16.5 cm^3

	LCO/NMC				NMC				LFP			
	m (g)	A (cm ²)	d (μm)	V (cm ³)	m (g)	A (cm ²)	d (μm)	V (cm ³)	m (g)	A (cm ²)	d (μm)	V (cm ³)
Separator	1.2	942	19	1.8	1.4	944	23	2.2	1.2	940	20	1.9
Cathode Al foil	1.7	403	16	0.6	3.1	389	30	1.1	2.1	396	19	0.7
Cathode active material	18.3	715	91	6.5	11.3	654	67	4.4	9.7	793	70	5.5
Anode Cu foil	2.9	402	8	0.3	7.5	418	20	0.8	3.9	396	17	0.7
Anode active material	8.1	739	81	6.0	6.2	695	60	4.2	5.2	793	50	4.0
Electrolyte	4.6				4.4				6.4			
Housing	7.5				9.2				10.5			
Sum	44.3			15.2	43.1			12.7	39.0			12.8



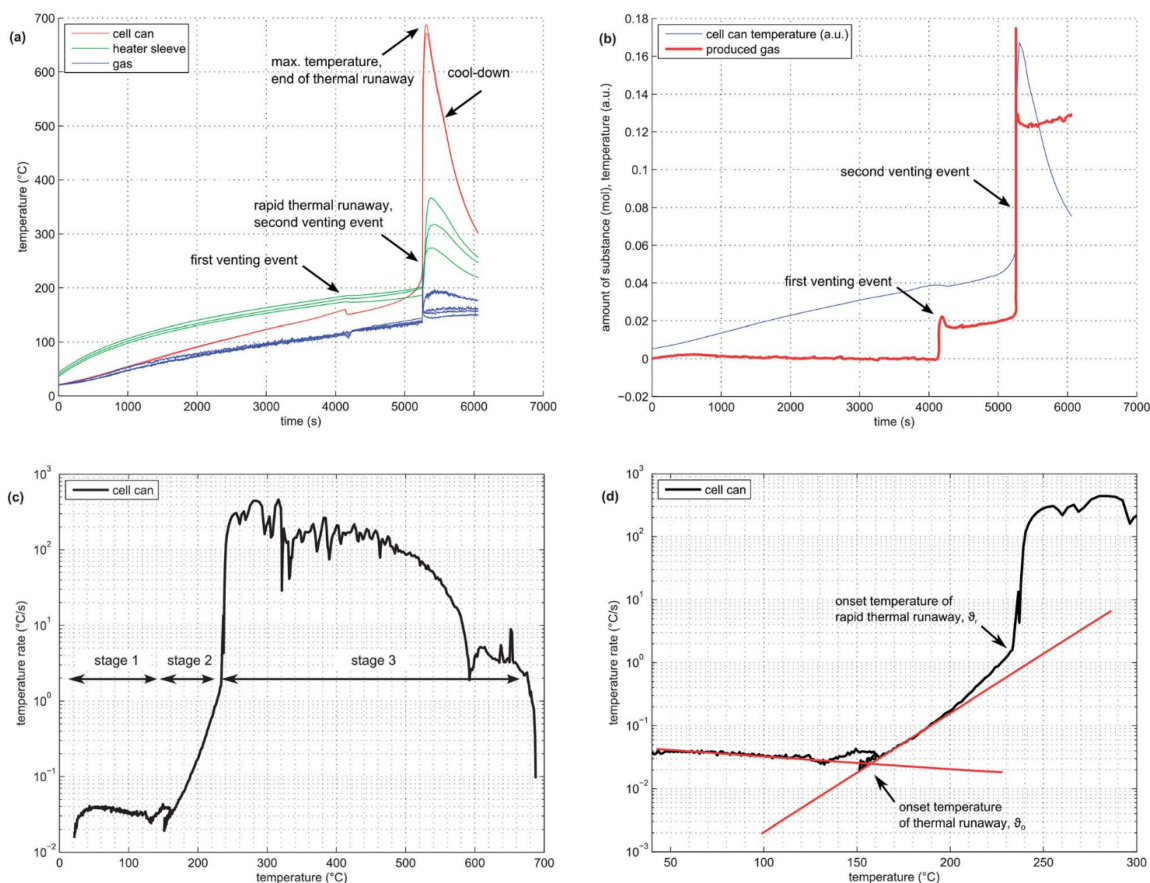


Fig. 4 (a) Temperature *versus* time plot of all temperature sensors in the pressure vessel. The whole duration of the experiment is shown. (b) Amount of produced gas *versus* time plot. Cell temperature is shown in arbitrary units. (c) Temperature rate of the cell *versus* cell temperature. Overview of a whole experiment duration. (d) Temperature rate of the cell *versus* cell temperature. The straight lines are fitted to the heat-up stage and to the quasi-exponential stage. The intersection of the two lines marks the onset point θ_o of the thermal runaway reaction. A sharp increase in the temperature rate marks the onset of the rapid thermal runaway θ_r .

In order to visualise subtle changes in thermal behaviour of the cell during the experiment, rate diagrams are utilized. Contrary to a common temperature *versus* time diagram (θ vs. t), the temperature rate is plotted *versus* temperature ($d\theta/dt$ vs. θ) in a rate diagram. This type of diagram is often used to visualise accelerating rate calorimetry (ARC) results as well. Three distinct experiment stages can be seen in the rate diagram for the NMC cell (Fig. 4c):

(1) Heat-up stage ($\theta < \theta_o$): In the temperature range from room temperature to θ_o at ~ 170 °C, the cell generated no heat. The heater sleeve was the only heat source in this phase. The negative peak at 130 °C is associated with endothermic separator melting. (It is analogous to a negative endothermic peak in a differential scanning calorimetry (DSC) diagram during the phase change of a sample). The temperature θ_o at which a cell starts to generate heat is commonly called the onset temperature of the thermal runaway.

(2) Quasi-exponential heating stage ($\theta_o < \theta < \theta_r$): At temperatures higher than θ_o , the battery became a heat source.

Between 170 °C and 220 °C, the temperature rate increase followed a nearly straight line in the logarithmic plot (Fig. 4d). At 220 °C, a sharp increase in temperature rate marked the end of the quasi-exponential heating stage.

(3) Rapid thermal runaway stage ($\theta_r < \theta < \theta_m$): At 220 °C, θ/dt increased sharply and initiated the rapid thermal runaway. The transition to thermal runaway was accompanied by a venting event. The thermal runaway ended when all reactants had been consumed. At this point, the maximum temperature $\theta_m = 687$ °C was reached.

It is difficult to pinpoint the exact transition between stage 1 and 2. Several endothermic events often occurred near the onset temperature θ_o ; the separator melt temperature was 130 °C, the cell safety vent usually opened at 160 °C and some material was released from the cell, causing a slight cool-down due to the Joule–Thomson effect. Thus, the exact value of θ_o can be obscured by the intermediate cell cool-down.

To keep it simple, θ_o was defined as the point at which the heating-rate curve switches from constant to quasi-exponential



rising. One line is fitted to the heat-up part and one line to the quasi-exponential part of the rate curve in the logarithmic rate plot. The onset temperature θ_o can be further defined as the temperature at which the two lines cross (Fig. 4d).

3.2 Thermal-runaway experiments

At least 3 thermal-runaway experiments were conducted with each of the three cell species. A temperature profile overview of all experiments is shown in Fig. 5a. Each species had its unique thermal-runaway characteristics. The high capacity, cobalt rich LCO/NMC cells reached the highest θ_m at $(853 \pm 24)^\circ\text{C}$ during thermal runaway. The cobalt poor NMC cells had a lower θ_m of $(678 \pm 13)^\circ\text{C}$. The LFP cells showed a less pronounced thermal runaway and reached a moderate θ_m of $(404 \pm 23)^\circ\text{C}$. The temperature curves showed small variations from sample to sample. It is likely that the variations were caused by different burst times of the rupture plates, which, together with subtle effects of venting, Joule–Thomson cool-down and clogging of the vent openings, influence the thermal-runaway reaction-pathways.

For the sake of completeness, two additional LFP experiments with different heater-sleeve heating-rates (1.5 and $3.5^\circ\text{C min}^{-1}$) were also included in the analysis (Fig. 5a). The thermal runaway characteristics of the LFP cell (θ_r , θ_m and n) did not depend on the heater-sleeve heating rate in the given heat-rate range. The two additional experiments contributed to the mean values in table 3 and Fig. 6

For clarity, only one representative curve for each cell species is shown in the following graphs.

Each cell species had distinctive kinetic thermal-runaway characteristics (Table 3 and Fig. 5b). Of the three specimen, the LCO/NMC cell showed the lowest θ_o and θ_r , hence the LCO/NMC cell was the cell most vulnerable to over-heating conditions. For the NMC cell, θ_o and θ_r were shifted to higher temperatures. Transition temperatures of the LFP specimen were noticeably higher than those of both metal/oxide cells (LCO/NMC and NMC). The LFP cell was able to

Table 3 Characteristic temperatures and venting parameters in the thermal-runaway experiments. Here, θ_o is the onset temperature, θ_r is the transition temperature into rapid thermal runaway, θ_m is the maximum recorded temperature, n is the total amount of gas produced as measured in the reactor at a reactor temperature of 150°C , and Δt is the typical venting duration

		LCO/NMC	NMC	LFP
θ_o	$^\circ\text{C}$	149 ± 2	168 ± 1	195 ± 8
θ_r	$^\circ\text{C}$	208 ± 2	223 ± 3	—
θ_m	$^\circ\text{C}$	853 ± 24	678 ± 13	404 ± 23
n	mmol	265 ± 44	149 ± 24	50 ± 4
Δt	s	0.8	0.2	30.0

withstand the highest temperature before going into thermal runaway.

Both metal oxide cells showed the three stages described above (heat-up, quasi exponential heating, rapid thermal runaway). In contrast, the thermal runaway profile of the LFP cell lacked a distinct quasi-exponential stage. For the LFP cell, it was difficult to find a clear distinction between θ_o and θ_r . Therefore, θ_r is not given for the LFP species.

During the thermal runaway, the cells produced a significant amount of gas (Table 3). The amount of gas strongly depended on the cell type. The highest amount of gas was released by the LCO/NMC cell, followed by the NMC cell. The LFP cell yielded the least amount of gas.

Two successive gas production events were evident in all experiments (Fig. 7):

1 In the first venting event, prior to rapid thermal runaway, the burst plate of the battery opened, and ~ 20 mmol were released by all three cell types.

2 In the second venting event, at the start of rapid thermal runaway, both metal-oxide cells released a high amount of additional gas at a high rate (Fig. 8). In contrast, the LFP cell released only a small amount of additional gas at a low production rate. In the case of the metal-oxide cells the gas was released in very short time. The NMC cell produced the main

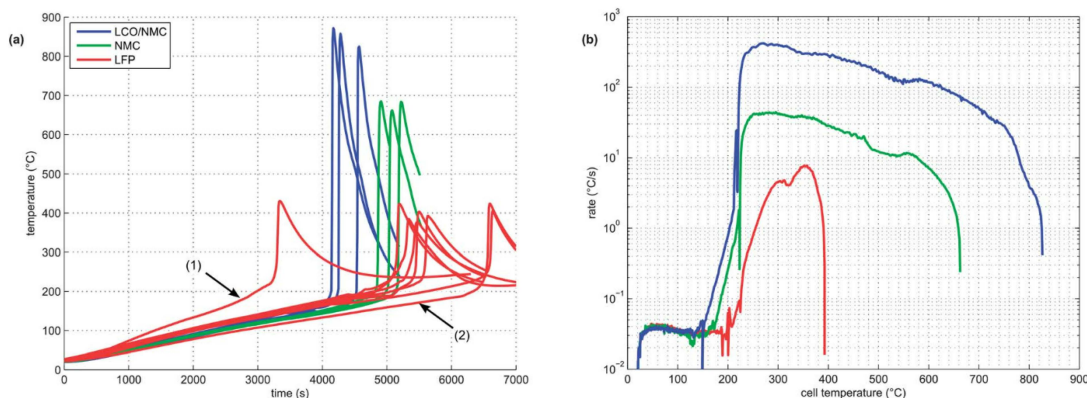


Fig. 5 (a) Overview of the time–temperature profiles for the cells tested. Data for the whole experiment durations and for the whole experiment sets is shown. For the sake of completeness, one LFP test with a higher (1) and one with a lower (2) heating rate of the heater sleeve are included. (b) Temperature rates from three representative experiments.



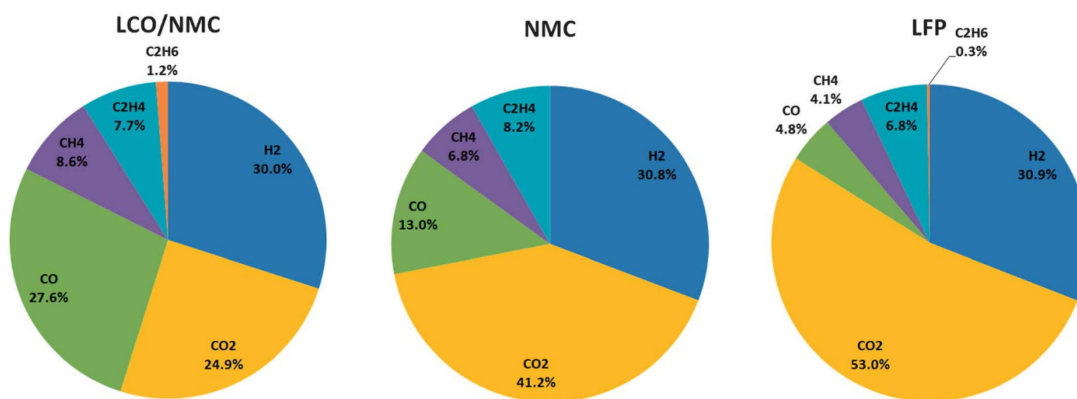


Fig. 6 Detected components of the produced gases (mol%).

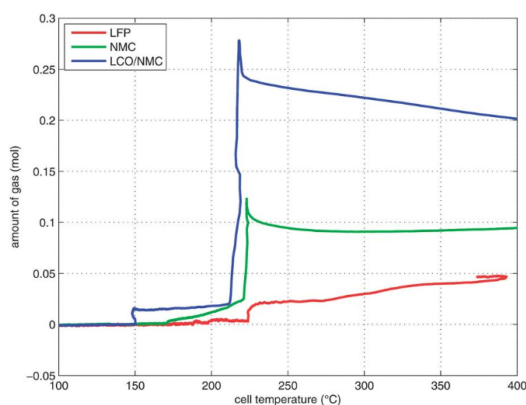


Fig. 7 Temperature-vent gas profiles. Note that the x-axis is limited to the relevant temperature range.

amount of gas in just 0.2 s, and the LCO/NMC in 0.8 s. After release, the hot gas was not in thermal equilibrium with the cooler walls of the reactor, and therefore the amount of gas

decreased, as the released gas came into contact with the walls and condensed. In contrast, the gas production duration of the second venting for the LFP cell was ~ 30 s. Because of the gradual release, the gases of the LFP cell were in better temperature equilibrium with the reactor walls and the gas condensation effect was not noticeable.

3.3 Gas analysis

At least one gas analysis was performed for each cell species. Each cell type showed a unique gas composition footprint (Fig. 6). The main components were H_2 and CO_2 . Both metal-oxide cells produced a significant amount of CO. Additionally, smaller fractions of CH_4 , C_2H_4 , and C_2H_6 were identified. As mentioned before, HF was not measured.

Most components of the gases are flammable. The gases can be toxic due to the presence of CO.

3.4 Gas producing reactions

During the thermal runaway gases are released by thermally and electrochemically driven reactions of the electrode active

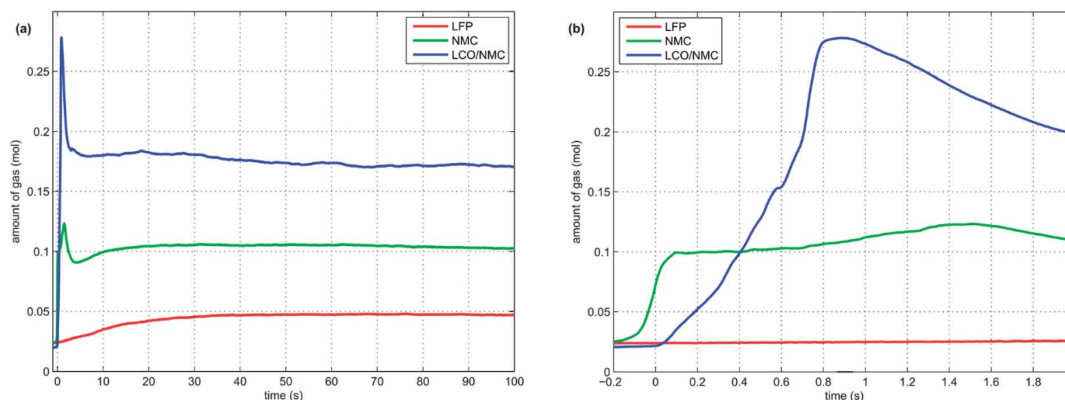
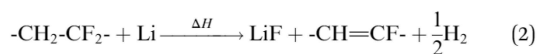


Fig. 8 Time-vent gas profiles. Note: to make the curves comparable, each curve was moved on the time axis, so that the second venting event starts at time zero. (a) The first 100 seconds and (b) the first 2 seconds of the second venting event are shown.

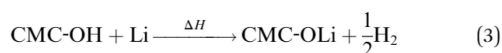


materials, the intercalated lithium, the binder, the solid electrolyte interface (SEI), the electrolyte and the separator.

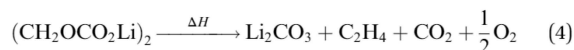
Evolution of H₂. One possible source of hydrogen is the reaction of the binder with Li⁰. Common binder materials are polyvinylidene fluoride (PVdF) and carboxymethyl cellulose (CMC).¹⁹ At temperatures above 230 °C graphite particles of the anode defoliate and Li is exposed to the surrounding electrolyte and binder.²⁰ Above 260 °C PVdF may react with Li at the anode and release H₂.²¹



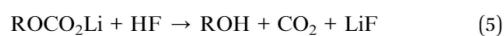
A similar reaction of CMC and Li may take place above 250 °C:²²



Evolution of CO₂. Many SEI and electrolyte mechanisms can lead to carbon dioxide generation. The SEI can decompose in thermally driven reactions,^{23,24}



or by reactions with traces of water or HF^{25,26,26-29}

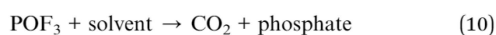
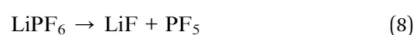


Li₂CO₃ may be present in the cathode³⁰ and/or can be produced by two-electron reduction of EC at the anode.³¹ Li₂CO₃ reacts with traces of HF with CO₂ evolution:^{24,30}

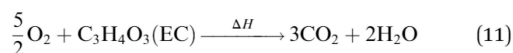


EC solvent reduction through SEI (re)formation at the carbon surface of the anode can release CO₂.^{32,33} Above 263 °C pure EC can thermally decompose and produce CO₂.³⁴ Linear carbonate solvents can decompose with CO₂ release in the presence of CH₃OLi.³¹

In the presence of impurities LiPF₆ may react to POF₃ that in turn reacts with the electrolyte in a decarboxylation reaction with CO₂ release:^{31,35-38}



In the presence of oxygen, combustion of the carbonate based electrolyte solvents takes place,^{28,34,39} e.g.



A plausible source of oxygen is the structural breakdown of delithiated metal oxide cathodes of the LCO/NMC and NMC cell.⁴⁰ It was shown, that CO₂ is mainly produced on the cathode side of an overcharged LCO cell.⁴¹ Therefore the electrolyte

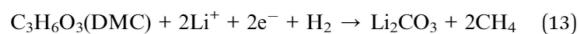
oxidation with O₂ freed from the cathode may be the dominant CO₂ producing reaction for the LCO/NMC and NMC cell. The cathode material of the LFP cell is thermally more stable and does not release oxygen.⁴²

Evolution of CO. One possible mechanism of carbon monoxide is the reduction of CO₂ with intercalated Li at the anode:^{26,43,44}

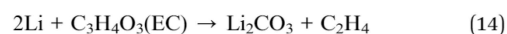


On the other hand, as shown in the case of an overcharged LCO cell, the main contribution of CO gas may come from the cathode side and not from the anode side.⁴¹ We suggest, that another source of CO may be incomplete combustion of carbon containing material with a limited amount of O₂ that is freed from the cathode.

Evolution of CH₄. In the presence of H₂ methane can be produced by reduction of the electrolyte to lithium carbonate⁴⁵⁻⁴⁷ e.g.



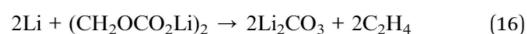
Evolution of C₂H₄. Ethylene can be produced by the reduction of EC at the lithiated anode^{31,39,47}



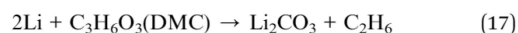
and^{24,48,49}



or by SEI decomposition²³



Evolution of C₂H₆. In an analogous reaction ethane can be produced by the reduction of DMC at the lithiated anode:^{31,39,48}



4 Conclusion and outlook

Three types of consumer Li-ion batteries with the format 18650 with different cathode materials were evaluated in thermal runaway tests. The cells were brought into thermal runaway by external heating. All tests were performed in a pressure-tight reactor in an argon atmosphere. In agreement with literature,⁵ the cell containing LFP showed the best safety characteristics. The LFP cell had the highest onset temperature (~195 °C), the smallest temperature increase during the thermal runaway (~210 °C), the lowest amount of produced gas (~50 mmol) and the lowest percentage of toxic CO in the gas (~4%). Unfortunately, it was also the cell with the lowest working voltage (3.3 V) and the lowest energy content (3.5 W h).

Batteries with higher energy content (5.7 W h and 9.9 W h) performed worse in safety tests. The onset temperature shifted



Paper

down to ~ 170 °C and ~ 150 °C, the temperature increase during thermal runaway rose to ~ 500 °C and ~ 700 °C, the amount of gas released was ~ 150 mmol and ~ 270 mmol, and significant percentages of CO (13% and 28%) were found for the NMC and LCO cells, respectively.

All cells released high amounts of H₂ and hydrocarbons. These gases are highly flammable. Even though the gas could not burn in the inert atmosphere inside the reactor, the surface of the high-energy cells reached temperatures of up to 850 °C during the experiments.

Modern devices are equipped with battery temperature and voltage monitoring. If a state beyond specification is detected, the devices shut down automatically to prevent battery abuse.¹⁸ If system shut-down can not prevent a thermal runaway in all cases, data in this work may be a valuable source for the specification of a robust energy-storage system which can withstand conceivable abuse events.

To reduce possible damage from thermal-runaway events in consumer devices, we suggest the following design optimization targets: (1) increase the temperature endurance and heat absorption capability of used materials; (2) minimize heat propagation to neighbouring burnable elements; (3) minimize gas ignition probability (e.g. mechanical separation of electric components from the gas release position).

This work has shown that the kinetics of the thermal-runaway process strongly depend on the energy content of the Li-ion battery. Future work will focus on the thermal runaway triggered by over-heating at different states of charge (SOC) and the thermal runaway caused by overcharge. Emphasis will be given to assessment of HF gas evolution, to gas analysis with GC-MS, and to the analysis of the liquid residues that are collected in the cooling trap.

Acknowledgements

The present work was conducted in the K2 project “New Component Simulation Models for HEVs” in the task “Li-Ion Battery Safety in Automotive Environment (LISAE)”. The authors would like to acknowledge the financial support of the “COMET K2 – Competence Centres for Excellent Technologies Programme” of the Austrian Federal Ministry for Transport, Innovation and Technology (BMVIT), the Austrian Federal Ministry of Economy, Family and Youth (BMWFJ), the Austrian Research Promotion Agency (FFG), the Province of Styria and the Styrian Business Promotion Agency (SFG). We would furthermore like to express our thanks to our supporting scientific project partners, namely Graz Centre for Electron Microscopy, Varta Micro Innovation GmbH and the Graz University of Technology. This work was made possible by the principal industrial project partners BASF SE and MAGNA STEYR Battery Systems GmbH & Co OG.

References

- 1 T. Nagaura and K. Tozawa, *Prog. Batteries Sol. Cells*, 1990, **9**, 209.
- 2 J. Wen, Y. Yu and C. Chen, *Mater. Express*, 2012, **2**, 197–212.

- 3 C.-Y. Jhu, Y.-W. Wang, C.-M. Shu, J.-C. Chang and H.-C. Wu, *J. Hazard. Mater.*, 2011, **192**, 99–107.
- 4 P. Ribière, S. Grugeon, M. Morcrette, S. Boyanov, S. Laruelle and G. Marlair, *Energy Environ. Sci.*, 2012, **5**, 5271.
- 5 D. Doughty and E. P. Roth, *Electrochem. Soc. Interface*, 2012, **21**, 37–44.
- 6 C.-Y. Jhu, Y.-W. Wang, C.-Y. Wen and C.-M. Shu, *Appl. Energy*, 2012, **100**, 127–131.
- 7 S.-I. Tobishima and J.-I. Yamaki, *J. Power Sources*, 1999, **81–82**, 882–886.
- 8 D. Belov and M.-H. Yang, *Solid State Ionics*, 2008, **179**, 1816–1821.
- 9 H. Maleki, G. Deng, A. Anani and J. Howard, *J. Electrochem. Soc.*, 1999, **146**, 3224.
- 10 C.-Y. Jhu, Y.-W. Wang, C.-Y. Wen, C.-C. Chiang and C.-M. Shu, *J. Therm. Anal. Calorim.*, 2011, **106**, 159–163.
- 11 C.-Y. Wen, C.-Y. Jhu, Y.-W. Wang, C.-C. Chiang and C.-M. Shu, *J. Therm. Anal. Calorim.*, 2012, **109**, 1297–1302.
- 12 E. P. Roth and C. J. Orendorff, *Electrochem. Soc. Interface*, 2012, **21**, 45–49.
- 13 D. Abraham, E. P. Roth, R. Kostecki, K. McCarthy, S. MacLaren and D. Doughty, *J. Power Sources*, 2006, **161**, 648–657.
- 14 Z. Chen, Y. Qin, Y. Ren, W. Lu, C. Orendorff, E. P. Roth and K. Amine, *Energy Environ. Sci.*, 2011, **4**, 4023.
- 15 D. H. Doughty, E. P. Roth, C. C. Crafts, G. Nagasubramanian, G. Henriksen and K. Amine, *J. Power Sources*, 2005, **146**, 116–120.
- 16 G. Nagasubramanian and C. J. Orendorff, *J. Power Sources*, 2011, **196**, 8604–8609.
- 17 K.-S. Lee, S.-T. Myung, D.-W. Kim and Y.-K. Sun, *J. Power Sources*, 2011, **196**, 6974–6977.
- 18 Z. J. Zhang and P. Ramadass, *Encyclopedia of Sustainability Science and Technology*, Springer, New York, 2012.
- 19 J.-H. Lee, U. Paik, V. a. Hackley and Y.-M. Choi, *J. Electrochem. Soc.*, 2005, **152**, A1763.
- 20 O. Haik, S. Ganin, G. Gershinshy, E. Zinigrad, B. Markovsky, D. Aurbach and I. Halalay, *J. Electrochem. Soc.*, 2011, **158**, A913.
- 21 A. D. Pasquier, *J. Electrochem. Soc.*, 1998, **145**, 472.
- 22 W. Haiyan, A. Tang and W. Kelong, *Chin. J. Chem.*, 2011, **29**, 27–32.
- 23 M. N. Richard and J. Dahn, *J. Electrochem. Soc.*, 1999, **146**, 2068.
- 24 M. Onuki, S. Kinoshita, Y. Sakata, M. Yanagidate, Y. Otake, M. Ue and M. Deguchi, *J. Electrochem. Soc.*, 2008, **155**, A794.
- 25 J.-S. Hong, H. Maleki, S. A. Hallaj, L. Redey and J. R. Selman, *J. Electrochem. Soc.*, 1998, **145**, 1489.
- 26 D. Aurbach, A. Zaban, Y. Gofer, Y. E. Ely, I. Weissman, O. Chusid and O. Abramson, *J. Power Sources*, 1995, **54**, 76–84.
- 27 D. Aurbach, *J. Electrochem. Soc.*, 1995, **142**, 2882.
- 28 W. Kong, H. Li, X. Huang and L. Chen, *J. Power Sources*, 2005, **142**, 285–291.
- 29 D. Aurbach, *J. Electrochem. Soc.*, 1991, **138**, 3529.



- 30 C. Doh, D. Kim, J. Lee, D. Lee, B. Jin, H. Kim, S. Moon, Y. Hwang and A. Veluchamy, *Bull. Korean Chem. Soc.*, 2009, **30**, 783.
- 31 G. Gachot, P. Ribière, D. Mathiron, S. Grugeon, M. Armand, J.-B. Leriche, S. Pilard and S. Laruelle, *Anal. Chem.*, 2011, **83**, 478–485.
- 32 C. Yang, Y. Wang and C. Wan, *J. Power Sources*, 1998, **72**, 66–70.
- 33 S. Mori, H. Asahina, H. Suzuki, A. Yonei and K. Yokoto, *J. Power Sources*, 1997, **68**, 59–64.
- 34 G. G. Botte and T. J. Bauer, *J. Power Sources*, 2003, **119–121**, 815–820.
- 35 A. Hammami, N. Raymond and M. Armand, *Nature*, 2003, **424**, 635–636.
- 36 C. L. Champion, W. Li and B. L. Lucht, *J. Electrochem. Soc.*, 2005, **152**, A2327.
- 37 C. L. Champion, W. Li, W. B. Euler, B. L. Lucht, B. Ravdel, J. F. DiCarlo, R. Gitzendanner and K. M. Abraham, *Electrochem. Solid-State Lett.*, 2004, **7**, A194.
- 38 T. Kawamura, A. Kimura, M. Egashira, S. Okada and J.-I. Yamaki, *J. Power Sources*, 2002, **104**, 260–264.
- 39 R. Spotnitz and J. Franklin, *J. Power Sources*, 2003, **113**, 81–100.
- 40 I. Belharouak, W. Lu, D. Vissers and K. Amine, *Electrochem. Commun.*, 2006, **8**, 329–335.
- 41 T. Ohsaki, T. Kishi, T. Kuboki, N. Takami, N. Shimura, Y. Sato, M. Sekino and A. Satoh, *J. Power Sources*, 2005, **146**, 97–100.
- 42 A. K. Padhi, *J. Electrochem. Soc.*, 1997, **144**, 1188.
- 43 A. D. Pasquier, F. Disma and T. Bowmer, *J. Electrochem. Soc.*, 1998, **145**, 472.
- 44 S. E. Sloop, J. B. Kerr and K. Kinoshita, *J. Power Sources*, 2003, **119–121**, 330–337.
- 45 K. Kumai, *J. Power Sources*, 1999, **81–82**, 715–719.
- 46 J.-S. Shin, C.-H. Han, U.-H. Jung, S.-I. Lee, H.-J. Kim and K. Kim, *J. Power Sources*, 2002, **109**, 47–52.
- 47 H. Yoshida, T. Fukunaga, T. Hazama, M. Terasaki, M. Mizutani and M. Yamachi, *J. Power Sources*, 1997, **68**, 311–315.
- 48 G. Gachot, S. Grugeon, G. G. Eshetu, D. Mathiron, P. Ribière, M. Armand and S. Laruelle, *Electrochim. Acta*, 2012, **83**, 402–409.
- 49 D. Aurbach, A. Zaban, Y. Ein-Eli, I. Weissman, O. Chusid, B. Markovsky, M. Levi, E. Levi, A. Schechter and E. Granot, *J. Power Sources*, 1997, **68**, 91–98.





Cite this: *RSC Adv.*, 2015, 5, 57171

Thermal runaway of commercial 18650 Li-ion batteries with LFP and NCA cathodes – impact of state of charge and overcharge

Andrey W. Golubkov,^{*a} Sebastian Scheikl,^a René Planteu,^a Gernot Voitic,^b Helmar Wiltsche,^c Christoph Stangl,^d Gisela Fauler,^d Alexander Thaler^a and Viktor Hacker^b

Thermal runaway characteristics of two types of commercially available 18650 cells, based on Li_xFePO_4 and $\text{Li}_x(\text{Ni}_{0.80}\text{Co}_{0.15}\text{Al}_{0.05})\text{O}_2$ were investigated in detail. The cells were preconditioned to state of charge (SOC) values in the range of 0% to 143%; this ensured that the working SOC window as well as overcharge conditions were covered in the experiments. Subsequently a series of temperature-ramp tests was performed with the preconditioned cells. Charged cells went into a thermal runaway, when heated above a critical temperature. The following thermal runaway parameters are provided for each experiment with the two cell types: temperature of a first detected exothermic reaction, maximum cell temperature, amount of produced ventgas and the composition of the ventgas. The dependence of those parameters with respect to the SOC is presented and a model of the major reactions during the thermal runaway is made.

Received 2nd April 2015
Accepted 22nd June 2015

DOI: 10.1039/c5ra05897j

www.rsc.org/advances

1 Introduction

Li-ion batteries^{1,2} excel in energy density and cycle life. Unfortunately those benefits come with a price: when Li-ion batteries are mistreated with high over-temperature or strong overcharge, they can transit into a so-called thermal runaway. During the thermal runaway, the battery temperature increases due to exothermic reactions. In turn, the increased temperature accelerates those degradation reactions and the system destabilizes. At the end of the thermal runaway, battery temperatures higher than 1000 °C can be reached and high amounts of burnable and harmful gases can be released.

Because Li-ion batteries are widely used, the possible hazards of Li-ion batteries are a key issue for automotive, aerospace and consumer electronics industries. The safety characteristics of Li-ion battery systems depend (a) on the used cell type (geometry, materials), (b) on the initial conditions before misuse (state of charge, ageing effects), (c) on the type of misuse (over-temperature, over-charge) and (d) on

external measures (built-in safety devices, forced cooling, confinement).^{3–5}

In the past, accelerated rate calorimetry (ARC) tests with limited maximum temperature^{6–12} and without limitation¹³ as well as fire experiments and mechanical abuse^{14–17} with complete Li-ion cells were done. Recently over-temperature and over-charge tests with large format cells (which may be used for automotive applications) were published.^{18–20} It is known that the severity of the thermal runaway event in over-temperature experiments increases with increasing SOC.^{4,21–27} It is also known, that a thermal runaway can be triggered by strong overcharge beyond safe voltage limits of the cell.^{28–34} Even if the overcharge condition does not trigger a thermal runaway, safety may be compromised by Li-plating on the anode.³⁵

In our previous publication³⁶ the safety characteristics of three different commercial Li-ion batteries charged to 100% SOC were investigated. It was demonstrated, that cells with cathodes based on iron-phosphate as well as on metal-oxide material exhibit a thermal runaway in thermal-ramp experiments. The severity of the thermal runaway showed a strong dependence on the material composition of the cells.

In this publication two cell types are introduced and the mass inventory of the cells is calculated based on tear down results. The thermal runaway testing method is explained and the outcomes of experiments with discharged, partially charged, fully charged and over-charged cells are presented. Possible chemical reactions are listed and quantitative calculations of ventgas generation are made for two cases.

^aKompetenzzentrum – Das Virtuelle Fahrzeug Forschungsgesellschaft mbH, Inffeldgasse 21a, A-8010 Graz, Austria. E-mail: andrej.golubkov@alumni.tugraz.at

^bInstitute of Chemical Engineering and Environmental Technology, Graz University of Technology, Inffeldgasse 25/C/II, 8010 Graz, Austria

^cInstitute of Analytical Chemistry and Food Chemistry, Graz University of Technology, Stremayrgasse 9/III, 8010 Graz, Austria

^dVarta Micro Innovation GmbH, Stremayrgasse 9, 8010 Graz, Austria



2 Samples

The two types of commercially available Li-ion batteries, with the geometrical format 18650, were purchased from two well known manufacturers. The first cell, rated to a nominal capacity of $C^{\text{nom}} = 1.1 \text{ A h}$ is based on a Li_xFePO_4 (LFP) cathode. The LFP material is considered as relatively safe. Unfortunately commercial LFP-based cells have lower capacity and nominal voltage compared to metal-oxide based cells. According to the datasheet the LFP cell is designed for a maximum discharge current of 30 A and has a cycle life of >1000 full discharge cycles.

The second cell has a much higher nominal capacity $C^{\text{nom}} = 3.35 \text{ A h}$ and is based on a $\text{Li}_x(\text{Ni}_{0.80}\text{Co}_{0.15}\text{Al}_{0.05})\text{O}_2$ (NCA) cathode. To our knowledge, this mass produced cell has the highest energy density which is commercially available as of 2013. It is specified to a maximum discharge current of 6.7 A h and its cycle life is >300 cycles.

In the following, the two cell types will be denoted as LFP and NCA for easy reading.

2.1 Cell composition, methods

For the interpretation of the misuse experiment results it is beneficial to know the mass split of the cell components. Unfortunately information regarding detailed cell composition is kept confidential by the manufacturers. We had to make a tear down and an analysis of the cell components for both cell species by ourselves. The following parameters were measured directly using the same methods and equipment as in ref. 36:

- Mass of the anode and cathode coating, the electrolyte, the current collector foils, the separator and the housing material.
- The solvent mass-ratios of the electrolyte. Detected solvents were dimethyl carbonate (DMC), ethyl methyl carbonate (EMC), ethylene carbonate (EC), propylene carbonate (PC) and methyl phenyl carbonate (MPC).
- The mole-ratios of the different transition metals and phosphor in the cathode coating.

Additionally, separator foils were examined with differential scanning calorimetry coupled with thermal gravimetric analysis (DSC-TGA, NETZSCH STA 449 C). Separator samples were rinsed with diethyl carbonate and dried in a desiccator for 12 hours. During the test the DSC-TGA was flushed with and the heat ramp was set to 10 K min^{-1} .

2.2 Cell composition, results and discussion

It is not in the scope of this work to compile an exhaustive material inventory of the two commercial cell types. Nevertheless, to obtain some insight into chemical reactions taking place during cell misuse, it is helpful to make at least rough estimations for cell components that were not accessible to direct measurements (Table 1). Estimations for the amount and composition of active material, particle coating, binder, carbon black and the SEI in the electrode coatings as well as for the amount of salt, additives and soluble SEI in the electrolyte were discussed with our project partners. Effects of cell formation were considered. The compositions of the separators were estimated from DSC measurements.

2.2.1 Binder and conducting agent. The mass ratio of binder material and conducting agents in the electrode coatings was not measured. We assume that sodium carboxymethylcellulose (CMC) with a degree of carboxymethyl substitution (DS) of 0.7 is used as the anode binder³⁷ and polyvinylidene fluoride (PVDF) is used as the cathode binder.³⁸ CMC is a cost effective binder material in the anode, but can not be used in the cathode. We suppose that 5% of anode coating and 2.5% (NCA) or 5% (LFP) of cathode coating is binder material.

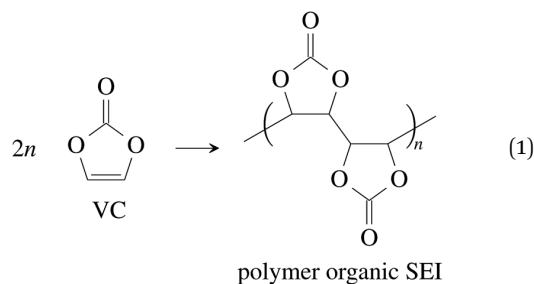
Additionally a conducting agent is needed to improve the electrical conductivity between the cathode particles and cathode substrate-foil. We suppose that 2.5% (NCA) or 5% (LFP) of cathode coating consists of carbon black. We justify the increased amount of binder and conducting agent of the LFP cell with its higher power capability.

2.2.2 LFP particle coating. The active cathode material of the LFP cell consists of Li_xFePO_4 . The Li_xFePO_4 particles need to be nano structured and carbon coated to achieve good diffusion of Li-ions and good inter-particle electrical conductivity.³⁹ It is hard to tell which amount of carbon coating was actually used in the tested commercial battery. Optimum values of carbon coating found in the literature vary from 1.5% to 15%.⁴⁰ We assume that 10% of the LFP cathode consists of carbon coating. Please note, that this might be the upper estimate. One of the reviewers suggested, that the carbon coating of a commercial battery is probably in the range of 1% to 2%.

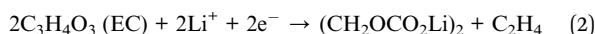
2.2.3 Electrolyte and SEI. The amount of salt in the electrolyte could not be measured as well, it is supposed that both cells use the traditional salt LiPF_6 with a concentration of 1.1 mol L^{-1} . The density of the electrolytes is estimated with 1.21 kg L^{-1} .

Vinylene carbonate (VC) is a common solid electrolyte interface (SEI) improving additive.⁴¹ We assume that 2% of VC was added to the electrolyte.⁴² During initial charging VC and EC undergo reduction reactions and form the SEI at the surface of the graphite particles of the anode. A fully developed SEI prevents further reduction of the electrolyte solvents.⁴³ The SEI composition and formation reactions can be complicated^{41,44,45} and lie beyond the scope of this work. Instead, for further calculations, we treat the SEI as being made of only four components:

- (1) The polymerization product of VC^{41,46}



- (2) The organic Li-carbonate from EC reduction⁴⁷⁻⁴⁹



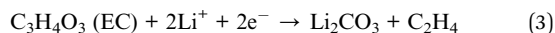
Open Access Article. Published on 22 June 2015. Downloaded on 3/4/2022 3:40:11 PM.
 This article is licensed under a Creative Commons Attribution 3.0 Unported Licence.



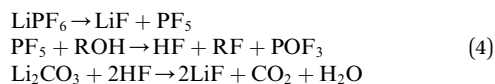
Table 1 Mass split of the discharged NCA and LFP cell. Please note, that the mass ratios for the binder, carbon black, the SEI and the salt were not measured; instead rough estimates are given. The chemical formulas for the SEI are taken from literature. The composition of the separator is deduced from DSC-TGA scans. For known or estimated materials the molar mass M and the amount of material n in the cell is given. For polymers M and n of the monomers is given. In the case of CMC the average number of atoms per monomer is used. The Li fractions in the molecular formulas of the electrodes were calculated for discharged cells with consideration of the irreversible capacity loss n_{Li}^{irr} and the residual capacity n_{Li}^{res} . In addition, the maximum theoretical capacity of intercalated Li in the electrodes was calculated using Faraday's laws of electrolysis

Component	NCA cell					LFP cell						
	Mass ratio	Mass (g)	Formula	M ($g\ mol^{-1}$)	n (mmol)	Li-capacity (A h)	Mass ratio	Mass (g)	Formula	M ($g\ mol^{-1}$)	n (mmol)	Li-capacity (A h)
Cathode coating:												
Active material	95.0%	17.04	$Li_{0.925}(Ni_{0.80}Co_{0.15}Al_{0.05})O_2$	95.6	178.2	4.78	80.0%	7.73	$Li_{0.882}FePO_4$	156.9	49.2	1.32
Particle coating	—	—	—	—	—	—	10.0%	0.97	C	12.0	80.5	—
Carbon black	2.5%	0.45	C	12.0	37.4	—	5.0%	0.48	C	12.0	40.2	—
Binder (PVDF)	2.5%	0.45	$(C_2H_2F_2)_n$	64.0	7.0	—	5.0%	0.48	$(C_2H_2F_2)_n$	64.0	7.5	—
Sum	100%	17.93	—	—	—	—	100%	9.66	—	—	—	—
Anode coating:												
Graphite	93.5%	10.92	$Li_{0.008}C_6$	72.1	151.5	4.06	93.5%	4.84	$Li_{0.006}C_6$	72.1	67.2	1.80
Binder (CMC)	5.0%	0.58	$(C_{7.4}H_{10.7}O_{6.4})_n$	202.1	2.9	—	5.0%	0.26	$(C_{7.4}H_{10.7}O_{6.4})_n$	202.1	1.3	—
SEI, lithium fluoride	0.4%	0.04	LiF	25.9	1.7	—	0.4%	0.02	LiF	25.9	0.8	—
SEI, lithium carbonate	1.1%	0.13	Li_2CO_3	73.9	1.7	—	1.1%	0.06	Li_2CO_3	73.9	0.8	—
Sum	100.0%	11.67	—	—	—	—	100.0%	5.18	—	—	—	—
Separator:												
PP	—	—	—	—	—	—	66%	0.76	$(C_3H_6)_n$	42.1	18.0	—
PE	—	—	—	—	—	—	34%	0.39	$(C_3H_4)_n$	28.1	13.9	—
UHMWPE	100%	0.70	$(C_2H_4)_n$	28.1	25.0	—	—	—	—	—	—	—
Sum	100%	0.70	—	—	—	—	100%	1.15	—	—	—	—
Electrolyte:												
SEI, polymer organic	2.0%	0.09	$(C_6H_4O_6)_n$	86.1	1.0	—	2.0%	0.13	$(C_6H_4O_6)_n$	172.1	0.7	—
SEI, organic	12.7%	0.56	$(CH_2OCO_2Li)_2$	162.0	3.5	—	3.9%	0.25	$(CH_2OCO_2Li)_2$	162.0	1.5	—
EC	17.1%	0.75	$C_3H_4O_3$	88.1	8.5	—	24.8%	1.59	$C_3H_4O_3$	88.1	18.1	—
DMC	49.7%	2.19	$C_3H_6O_3$	90.1	24.3	—	33.0%	2.12	$C_3H_6O_3$	90.1	23.5	—
EMC	5.3%	0.23	$C_4H_8O_3$	104.1	2.2	—	16.5%	1.06	$C_4H_8O_3$	104.1	10.2	—
PC	—	—	—	—	—	—	8.3%	0.53	$C_4H_6O_3$	102.1	5.2	—
MPC	2.7%	0.12	$C_8H_8O_3$	196.1	0.6	—	—	—	—	—	—	—
Salt	10.6%	0.46	LiPF ₆	151.9	3.1	—	11.5%	0.74	LiPF ₆	151.9	4.9	—
Sum	100.0%	4.41	—	—	—	—	100.0%	6.41	—	—	—	—
Inactive components:												
Housing (metal can)	—	5.71	—	—	—	—	—	10.45	—	—	—	—
Cathode Al foil	—	1.20	—	—	—	—	—	2.14	—	—	—	—
Anode Cu foil	—	2.72	—	—	—	—	—	3.86	—	—	—	—
Other components	—	1.05	—	—	—	—	—	—	—	—	—	—
Sum	—	10.69	—	—	—	—	—	16.46	—	—	—	—
Total sum	—	45.40	—	—	—	—	—	38.87	—	—	—	—

(3) The inorganic Li-carbonate Li_2CO_3 from EC reduction⁵⁰⁻⁵²



(4) And LiF which can be produced from decomposition of the salt and the Li-carbonate⁵³



We assume that all VC (2% of electrolyte) goes into polymerization (1) and that the additional SEI components $(\text{CH}_2\text{OCO}_2\text{Li})_2$: Li_2CO_3 : LiF are in the ratio 1/2 : 1/4 : 1/4.⁴⁴ The components of the SEI are listed (Table 1) as a part of either anode or electrolyte depending on their solubility in the electrolyte solvent.⁵⁴ To calculate the actual amounts of lithium containing SEI we need to take the irreversible capacity loss into account.

2.2.4 Irreversible capacity loss. We think that the most economical anode material for both manufacturers is surface treated natural graphite. During cell assembly the graphite is in delithiated state and the cathode is in fully lithiated state. At the first charging (cell formation) an amount of lithium $n_{\text{Li}}^{\text{irr}}$ that is equivalent to ~8% of the maximum anode-Li-capacity is trapped.² The associated charge C^{irr} is called irreversible capacity loss:

$$n_{\text{Li}}^{\text{irr}} = 0.08n_{\text{C}_6}^{\text{a}} \quad (5)$$

$$C^{\text{irr}} = Fn_{\text{Li}}^{\text{irr}} \quad (6)$$

here F is the Faraday constant and $n_{\text{C}_6}^{\text{a}}$ is the amount of graphite units C_6 in the anode (in mol). We assumed that all trapped lithium is integrated and immobilized in the SEI according to the chemical reactions (2)-(4). The calculated values for the NCA and LFP cell are $n_{\text{Li}}^{\text{irr}}(\text{NCA}) = 12.1$ mmol and $n_{\text{Li}}^{\text{irr}}(\text{LFP}) = 5.4$ mmol respectively. As a consequence, after formation, the cathode can never again be fully lithiated. Even when the cell is fully discharged, $n_{\text{Li}}^{\text{irr}}$ is missing, and the amount of Li per stoichiometric formula in the cathode is <1 .

The effect of the missing lithium $n_{\text{Li}}^{\text{irr}}$ (proportional to C^{irr}) in the cathode is taken into account in further stoichiometric calculations.

2.2.5 Residual capacity. Commercial Li-ion cells must not be discharged beyond their rated minimal operation voltage ($V_{\text{min}}(\text{NCA}) = 2.5$ V and $V_{\text{min}}(\text{LFP}) = 2.0$ V) during normal cycling. If cells are discharged to voltages lower than V_{min} dissolution of the copper foil may occur,⁵⁵ because the anode potential may reach the oxidation potential⁵⁶ of Cu. Anodes of cells that are discharged to V_{min} are not fully delithiated, instead a small amount of Li stays in the anodes and acts as a safety margin to keep the anode potentials below the copper dissolution potential. We assume that the residual capacity C^{res} (which is proportional to the amount of residual Li $n_{\text{Li}}^{\text{res}}$) equals to 1% of the nominal cell capacity:

$$C^{\text{res}} = 0.01C^{\text{nom}} \quad (7)$$

$$n_{\text{Li}}^{\text{res}} = 1/FC^{\text{res}} \quad (8)$$

The amount of residual lithium is considered in further calculation of the lithiation states of both electrodes.

2.3 Available capacities in the electrodes

With identified amount of active cathode material $n_{\text{cat}}^{\text{a}}$ and with known C^{irr} and C^{res} the theoretically usable capacity of the cathode after cell formation can be calculated

$$C_{\text{cat}}^{\text{u}} = Fn_{\text{cat}}^{\text{a}} - C^{\text{irr}} - C^{\text{res}} \quad (9)$$

and compared to the nominal capacity as given in the data sheet.

In the case of LFP cell $C_{\text{cat}}^{\text{u}} = 1.16$ A h. In theory, LFP material can be fully delithiated, and $C_{\text{cat}}^{\text{u}}$ should be equal to C^{nom} . In our work, the calculated $C_{\text{cat}}^{\text{u}}$ exceeded C^{nom} . According to the data sheet the LFP cell is rated to $C^{\text{nom}} = 1.1$ A h and the measured capacities in the allowed voltage range were even smaller (Fig. 1). The discrepancy may be caused by incomplete utilization of the LFP material of a real cell or by ageing effects of the cathode.

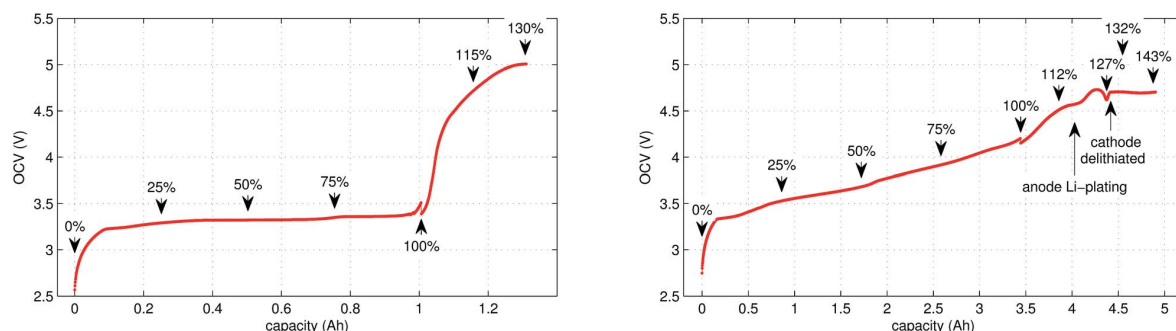


Fig. 1 OCV characteristics of the (left) LFP and (right) NCA cells. Measured values in the allowed voltage range and additionally in the overcharge region are given. SOC points, at which temperature-ramp experiments were done, are marked. Rough estimates, where Li-plating and complete cathode delithiation may occur, are indicated for the NCA cell. The discontinuities at 100% are caused by relaxations during the time-gaps between cycling and the overcharge experiments.



It is noteworthy that the available capacity of the LFP anode

$$C_{\text{and}}^{\text{u}} = F n_{\text{C}_6}^{\text{a}} \quad (10)$$

exceeds the $C_{\text{cat}}^{\text{u}}$ by 50%. In other words, the anode of the LFP cell is overbalanced. This makes sense for a high power cell, as it allows high charging currents with reduced risk of Li-plating.

In contrast to LFP, the NCA cathodes should not be fully delithiated during normal operation. Correspondingly, the theoretically available capacity of the NCA cell of 4.42 A h was higher than the nominal capacity 3.35 A h. The calculated capacity of the active material in the anode was 4.06 A h. That means the NCA anode was slightly overbalanced by 21%.

2.3.1 Separator. The composition of the separator materials was deduced from DSC-TGA measurements. The separator of the LFP cells showed endothermic (melting) peaks at 132 °C and 159 °C which are typical for a 3-layered laminate with a polyethylene (PE) core between two polypropylene (PP) skin layers (PP/PE/PP). We assume that the LFP separator consists of 2/3PP and 1/3PE.

The separator of the NCA cell showed only one indistinct endothermic peak at ~130 °C. We assume that the NCA separator consists of ultra-high molecular weight polyethylene (UHMWPE) membrane.^{57,58}

3 Experimental

In this work a total of 23 thermal ramp experiments with the two cell types were done at different SOC. Each experiment consisted of the following steps; the cell underwent a open circuit voltage (OCV) check, was charged to the selected SOC and inserted into the sample holder. The sample holder was attached inside a sealed reactor and the thermal ramp experiment was started (the test-rig and thermal ramp method is described in ref. 36). After the thermal ramp experiment gas samples were taken and analysed.

3.1 Initial OCV check

We applied the same OCV measurement procedure as in ref. 36. Each sample was fully discharged to 0% SOC (2.5 V) and then fully charged to 100% SOC (LFP: 3.5 V, NCA: 4.2 V). The health status of the cells was checked by comparing the measured capacities with the nominal capacity from the manufacturer. Typical OCV profiles are given in Fig. 1. BaSyTec CTS cell test system and Heiden Power DC-source-load were used for battery cycling.

3.2 Sample preparation

After the OCV check the insulation foil was stripped from the cell and the sample was weighed. Three K-type thermocouples were spot-welded to the cell housing. Then the sample was wrapped in a thermal insulation layer and inserted into the heating sleeve of the sample holder. Finally, the sample holder was installed inside the reactor, the electrical connections were made and the reactor was sealed.

3.3 SOC set-point

The cell was brought to the desired SOC by charging or discharging, starting from 100% SOC. The coulomb counting method was used for SOC calculation and the charge/discharge was stopped when the required SOC was reached. For experiments with SOC < 100% the cell was discharged outside of the reactor. For SOC > 100% the cell was overcharged inside the reactor, for safety reasons. In order to prevent cell heating, the overcharge current was set to very low values. The SOC set-points of all experiments are marked in Fig. 1.

3.4 Thermal-ramp experiment

The sealed reactor was evacuated and flushed with inert gas. The heaters were turned on. The sample inside the reactor was heated slowly with a rate of 2 °C min⁻¹ (NCA) or 4 °C min⁻¹ (LFP). Cell temperatures, gas temperatures and the pressure in the sealed reactor were recorded. At some point the cell transitioned into thermal runaway and ventgas was released in the reactor. The amount of gas inside the reactor $n_{\text{sum}}^{\text{ideal}}$ was calculated using the ideal gas law

$$n_{\text{sum}}^{\text{ideal}} = \frac{pV}{R\theta_{\text{gas}}} - n_0 \quad (11)$$

Here p denotes the pressure in the reactor, $V = 0.0027 \text{ m}^3$ is the reactor volume, R is the gas constant, θ_{gas} is the gas temperature in the reactor (in K) and n_0 is the initial amount of gas in the reactor at the start of the experiment.

The eqn (11) is only valid, when θ_{gas} is equal to the mean gas temperature in the reactor. During the thermal runaway a violent cell venting may take place and hot gases are released into the pressure vessel. In the first seconds after venting, when the gas temperature inside the reactor is not homogeneous, $n_{\text{sum}}^{\text{ideal}}$ may be over or underestimated. Thus, given $n_{\text{sum}}^{\text{ideal}}$ values were calculated when the gas temperature was in equilibrium.

3.5 Ventgas analysis

Gas samples were taken after the thermal runaway reaction. If no thermal runaway occurred, then the gas samples were taken after the cell temperature exceeded 250 °C. The gas was analysed with a gas chromatograph system (GC, Agilent Technologies 3000 Micro GC, two columns, Mol Sieve and PLOTU). A thermal conductivity detector (TCD) was used to detect permanent gases. The GC was calibrated for H₂, O₂, N₂, CO, CO₂, CH₄, C₂H₂, C₂H₄ and C₂H₆. The GC used Ar and He as carrier gases.

3.6 Role of the inert gas

Before each experiment, the reactor was filled with inert gas to prevent reactions of the vent-gas with the reactor atmosphere. We used either N₂ or Ar as inert gas. Both gases have advantages and disadvantages.

- Advantages of using Ar as inert gas: in this case N₂ is not present in the reactor. There are no reactions which can produce N₂ during thermal runaway. The only possible source



of N₂ in a ventgas sample is leakage from ambient air. Therefore, the presence of N₂ (accompanied by O₂) in the GC results indicates gas leakage. The amount of Ar in the samples could not be quantified, because it was used as a carrier gas in the GC setup.

• Advantages of using N₂ as inert gas: in this case N₂ fulfils two functions. It serves as inert gas and also as an internal standard. Since the amount of N₂ in the reactor is known ($V_{N_2} = 0.0027 \text{ m}^3$), absolute amounts of other detected gas components can be derived from their relative GC results r_i^{GC}

$$n_i^{GC} = \frac{n_{N_2}}{r_{N_2}^{GC}} r_i^{GC} \quad (12)$$

The absolute amount of vent-gas n_{sum}^{GC} can be calculated from the GC results.

$$n_{sum}^{GC} = \sum_{i \neq N_2} n_i^{GC} \quad (13)$$

The amount of ventgas calculated with the ideal gas eqn (11) can be compared with the total amount of gas from GC results (13). If $n_{sum}^{ideal} = n_{sum}^{GC}$ than it is likely, that all formed gases were detected by the GC.

However, there is also one strong disadvantage of using N₂. If leaks from ambient air occur, leaked N₂ falsifies the internal standard. Therefore, for the most experiments we used Ar as inert gas in the reactor and detected N₂ indicated gas leaks.

Only in the last three experiments, after enough experience was gained, we were confident to use N₂ as the inert gas.

4 Results

We did 23 thermal-ramp experiments with NCA and LFP cells set to different SOC. The results are summarized in Tables 2 and 3. Typical experiment runs are shown in Fig. 2 and 4. The dependence of the thermal runaway parameters on the SOC is visualised in Fig. 3 and 5.

4.1 NCA cells

We tested the thermal stabilities of discharged as well as partially charged, fully charged and over charged NCA cells.

Discharged NCA cells (Experiment 1–5) showed no pronounced thermal runaway characteristics. Only small unremarkable exothermic peaks were observed between 150 °C and 300 °C. The amount of gas depended on the timespan which the cells spend at increased temperature: after the initial burst plate opening of the cell housing the vent-gas was released from the cell into the reactor with a uniform rate. There was no sudden gas liberation and no violent chemical reaction. CO₂ was the major identified component of the vent-gas. Interestingly, the mass loss of the discharged cells of 4.4 g equalled to the mass of electrolyte in the cells (Table 1).

In Experiment 1 we used N₂ as internal standard. The GC detected $n_{sum}^{GC} = 23.2 \text{ mmol}$ of produced gas (Table 3). In

Table 2 Results of thermal ramp experiments with NCA and LFP cells. Here SOC is the state of charge, θ_o is the onset temperature, θ_m is the maximum cell temperature during the experiment, Δm is the mass loss of the cell, n_{sum}^{ideal} is the measured amount of produced vent-gas (11) and the chemical components are those species that were detected by the GC system. Missing values could not be measured or detected. The ratios of the detected gases are given in mol%

No.	Cell	SOC (%)	θ_R (°C)	θ_m (°C)	Δm (g)	n_{sum}^{ideal} (mmol)	H ₂ (%)	CO ₂ (%)	CO (%)	CH ₄ (%)	C ₂ H ₄ (%)	C ₂ H ₆ (%)
1	NCA	0	—	302	—	65	1.7	94.6	1.6	1.6	0.3	—
2	NCA	0	160	316	4.4	52	1.8	94.7	1.9	1.2	0.4	—
3	NCA	0	160	315	4.5	55	1.2	96	1.5	1.1	0.2	—
4	NCA	0	161	214	4.4	39	0.9	96.2	1.1	1.4	0.3	—
5	NCA	0	150	243	4.4	59	0.8	96.6	1	1.3	0.3	—
6	NCA	25	150	739	5.9	67	15.5	62.7	5.5	8.7	7.5	—
7	NCA	50	140	970	8.5	157	17.5	33.8	39.9	5.2	3.2	0.4
8	NCA	75	140	955	—	217	24.2	20.8	43.7	7.5	3.3	0.5
9	NCA	100	144	904	—	273	22.6	19.7	48.9	6.6	2.4	—
10	NCA	100	138	896	20.5	314	26.1	17.5	44	8.9	2.7	0.9
11	NCA	100	136	933	20.9	244	28.5	22.7	41.5	5.9	1.3	0.3
12	NCA	112	144	—	19.2	252	25.1	18.8	48.1	5.9	2.1	—
13	NCA	120	80	929	—	281	23.5	20.8	48.7	5.4	1.6	—
14	NCA	127	80	983	—	317	28.8	16.2	46.6	6.4	1.3	0.3
15	NCA	132	80	943	17	262	25.8	18.9	49.2	4.7	1.4	—
16	NCA	143	65	1075	20.1	303	26.2	22	43.4	6.9	1.5	—
17	LFP	0	—	251	6.1	55	2.7	93.5	1.8	0.7	0.7	0.7
18	LFP	25	195	231	6.1	31	7.1	85.3	3.1	1.2	3.1	0.2
19	LFP	50	130	283	6.1	32	20.8	66.2	4.8	1.6	6.6	—
20	LFP	75	149	362	6.3	41	21.8	62.6	6.4	1.9	6.3	1
21	LFP	100	140	440	7.1	32	29.4	48.3	9.1	5.4	7.2	0.5
22	LFP	115	155	395	6.2	61	34	52.2	6.4	2.6	4.7	0.1
23	LFP	130	80	448	—	58	30.1	55.8	7.7	6.4	—	—



Table 3 Thermal runaway parameters of experiments with NCA cells. Experiments with N_2 as internal standard were selected and the amounts of measured gases are given in absolute units (12). The amount of vent-gas n_{sum}^{ideal} and n_{sum}^{GC} was calculated with ideal gas eqn (11) and with results of the GC (13) respectively

No.	SOC (%)	n_{sum}^{ideal} (mmol)	n_{sum}^{GC} (mmol)	H_2 (mmol)	CO_2 (mmol)	CO (mmol)	CH_4 (mmol)	C_2H_4 (mmol)
1	0	65.4	23.2	0.4	21.9	0.4	0.4	0.1
13	120	281.3	279.1	65.5	57.9	136	15.1	4.6
14	127	317	317.1	91.6	51.6	148.6	20.2	4.1

contrast, the amount of ventgas inside the reactor (11) was much higher $n_{sum}^{ideal} = 65.4$ mmol. We conclude that the GC could not identify the missing 42.2 mmol of gas, because its setup was optimized for a limited set of permanent gases.

The cells with $SOC \geq 25\%$ displayed an unmistakable thermal runaway behaviour. When (partially) charged NCA cells were heated beyond a critical temperature, self accelerating exothermic reactions started and the cell temperatures suddenly increased up to maximum values in the range of 739 °C and 1075 °C.

The onsets of the exothermic reactions were obtained from the rate plot: the temperature, where a first clear deviation towards increased temperature rate was detected, was defined as the onset temperature θ_o . For NCA cells with $SOC \leq 100\%$ θ_o was in the range between 136 °C and 160 °C. Overcharged NCA cells ($SOC > 100\%$) showed much lower onset temperatures

between 65 °C and 80 °C. It is an important finding, that over-charged NCA cells can proceed straight into thermal runaway when heated above 65 °C.

The thermal runaway reactions were accompanied by abrupt vent-gas releases. Cells with higher SOC produced more vent-gas. Up to 317 mmol of gas were recorded. The gas composition depended on the SOC as well: the fractions of CO_2 decreased and the fractions of CO and H_2 increased with rising SOC. A clear trend for other detected gases (CH_4 , C_2H_4 and C_2H_6) was not observed.

We used N_2 as inert gas in the Experiments 13 and 14 (over-charged NCA) in the same way as in Experiment 1. The calculated amounts of gas n_{sum}^{ideal} and n_{sum}^{GC} were in good agreement, indicating that all produced gases were detected by the GC. In other words, it is likely that the quantitative GC results (Table 3) represent the major vent-gas components for over-charged cells and that only smaller amounts of gas may be missing.

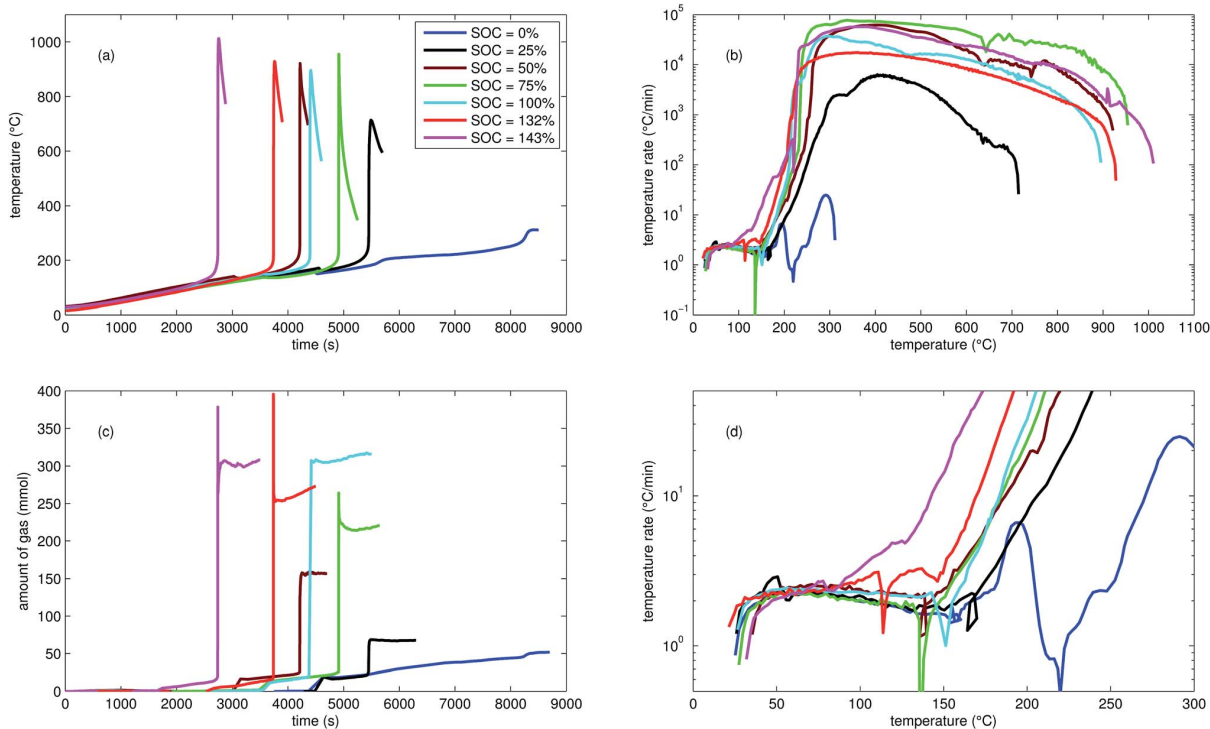


Fig. 2 Typical thermal ramp experiments with NCA cells. (a) Cell temperature profiles. (c) Amount of produced vent-gas. The overshoot peaks are artefacts of the calculation (11) caused by inhomogeneous gas temperature. (b) Cell temperature rate $d\theta/dt$ vs. cell temperature θ , full temperature range. (d) Close up view of the cell temperature rate.



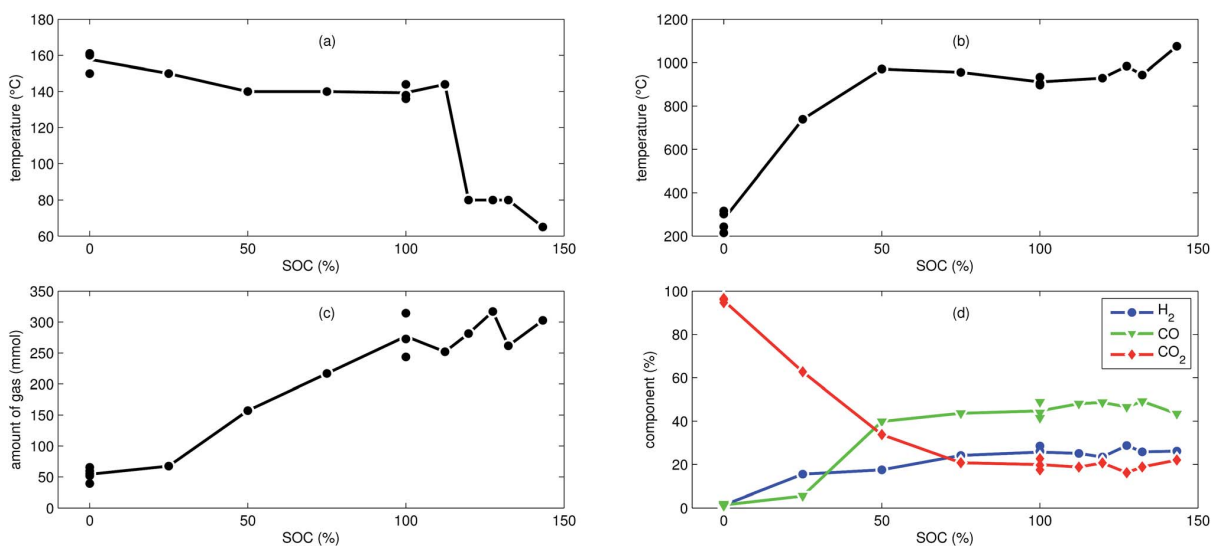


Fig. 3 Characteristic thermal runaway parameters from all NCA experiments. (a) Onset cell temperature θ_o . (b) Maximum cell temperature θ_m . (c) Amount of produced gas n_{sum}^{ideal} . (d) Main detected gas components r_i^{GC} .

4.2 LFP cells

In addition to the experiments with NCA cells, we did 7 thermal-ramp experiments with LFP cells at different SOC (Table 2).

The discharged LFP cell (Experiment 17) showed a behaviour similar to discharged NCA cells. Exothermic reactions could not be detected. After the initial burst plate opening of the cell housing, the amount of gas increased evenly over time as the cell

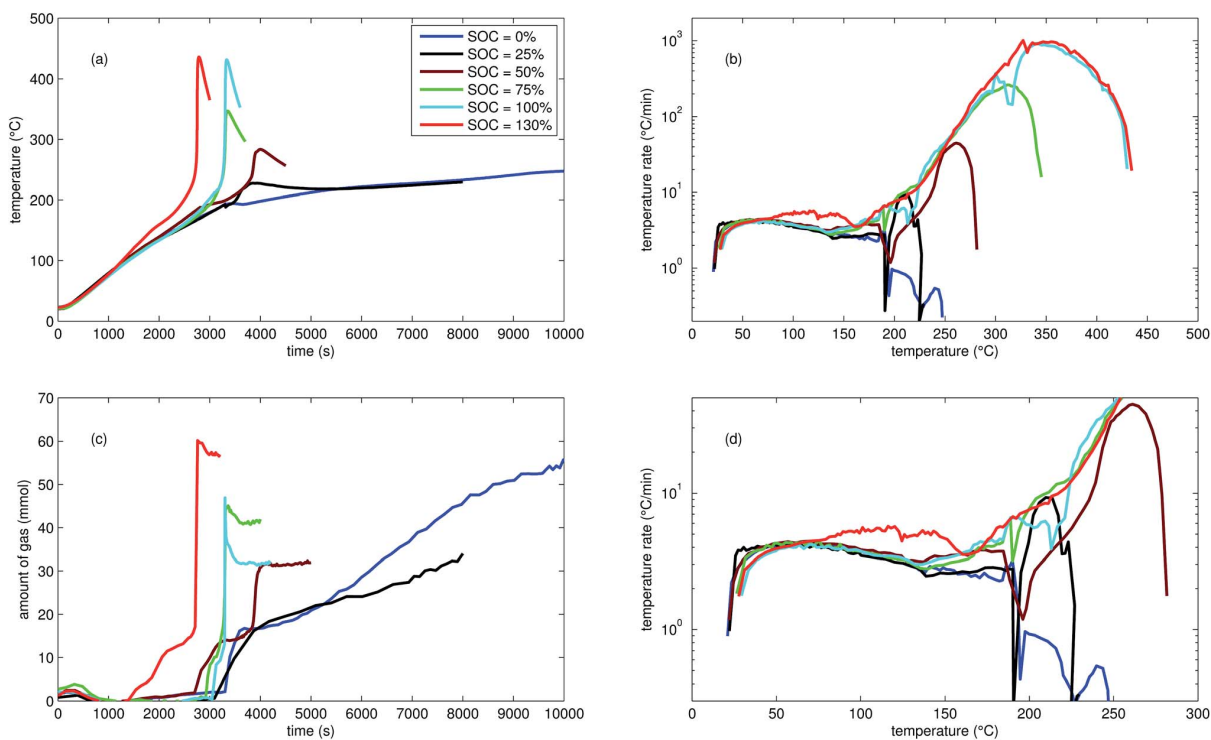


Fig. 4 Typical experiments with LFP cells: (a) cell temperature profiles. (c) Amount of produced vent-gas. (b) Cell temperature rate $d\theta/dt$ vs. cell temperature θ , full temperature range. (d) Close up view of the cell temperature rate.



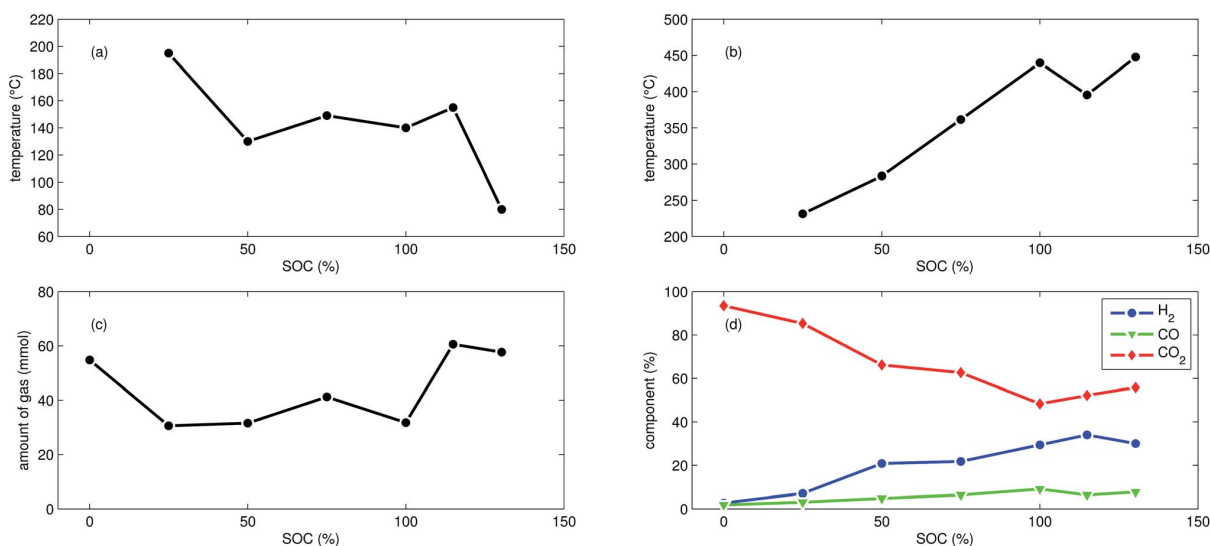


Fig. 5 Summary of all experiments with LFP cells at different SOC: (a) onset cell temperature θ_o . (b) Maximum cell temperature θ_m . (c) Amount of produced gas n_{sum}^{ideal} . (d) Main detected gas components r_i^{GC} .

was heated. For the discharged cell, the GC registered essentially only CO_2 . We suspect that the GC could not detect all gas components that were produced by the discharged cell: similar to Experiment 1 with a discharged NCA cell, significant amounts of gas may be missing in the GC results, simply because the used GC equipment was not capable of detecting them.

First mild exothermic reactions were seen for a cell that was charged to 25% SOC. The reactions were not strong enough to evolve into a distinct thermal runaway. Vent gas was produced continuously with time, likewise to the experiments with discharged cells.

LFP cells charged to $SOC \geq 50\%$ showed pronounced thermal runaway reactions. Increasing SOC caused increasing maximum temperatures during thermal runaway. The maximum temperatures θ_m ranged from 283 °C to 448 °C.

The onset temperature θ_o was ~ 140 °C for cells between 50% SOC and 100% SOC. The cell overcharged to 130% SOC showed an exothermic reaction already at 80 °C. In contrast to overcharged NCA cells, the initial exothermic reaction of the overcharged LFP cell could not sustain a full thermal runaway. The overcharged LFP cell proceeded into thermal runaway only after it was heated by the heating sleeve beyond 140 °C.

The amount of gas n_{sum}^{ideal} ranged between 31 mmol and 61 mmol and showed no clear dependence on the SOC. With increasing SOC the relative composition of the detected gases changed to lower CO_2 and higher H_2 fractions. The fractions of CO (max. 9.1%) were lower than for NCA cells.

The mass loss of the LFP cells ranged from 6.1 g to 7.1 g and is comparable to the amount of electrolyte (6.5 g) in these cells.

5 Discussion

It is tempting to pinpoint the main contributors of heat and gas release during the thermal runaway reactions. Can the amount

of produced gas and its components be explained with a set of chemical equations?

Material n_j^a that is available for the reaction system is listed in Table 1. In addition lithium $n_{O_2}^a$ and oxygen n_{Li}^a may be released in heated cells. Part of the material is consumed (by becoming a reactant n_j^r of the reaction system).

$$0 \leq n_j^r \leq n_j^a \quad (14)$$

The reaction products may consist of gases, fluids and solids. A measurable subset of the resulting gaseous products n_i^{GC} and the sum of ventgas n_{sum}^{ideal} is given in Table 3. The challenge is to find the right set A of equations and to find the utilisation number b for each equation (how often is each equation applied) so that the calculated amounts of products n_i^p match the measured values:

$$\text{minimize } (n_i^{GC} - n_i^p) > 0 \quad (15)$$

and

$$\text{minimize } \left(n_{sum}^{ideal} - \sum_{i=\text{gaseous}} n_i^p \right) > 0 \quad (16)$$

In other words, the difference of calculated and measured amounts of products is defined as the cost function and the system is restricted by the amounts of reactants and products. The algorithm should minimise the cost function and respect the restrictions.

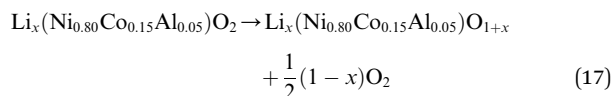
The mathematical problem was solved using the LIPSOL linear programming toolbox in Matlab. The set of chemical equations and two explicit calculations (discharged NCA cell, Experiment 1 and over-charged NCA cell, Experiment 13) are disclosed in the next subsections:



5.1 Oxygen release from cathode material

At elevated temperatures cathode materials of Li-ion batteries can release oxygen. It is believed, that the exothermic reaction of oxygen with electrolyte is the main contributor to the extent of the thermal runaway effect.⁴ The amount of released oxygen depends on the lithiation state of the cathode.

In ref. 59–62 it is shown, that delithiated $\text{Li}_x(\text{Ni}_{0.80}\text{Co}_{0.15}\text{Al}_{0.05})\text{O}_2$ cathode material undergoes complex phase transitions accompanied by formation of O_2 in the temperature range from 175 °C to 600 °C. In a simplified scheme, heated NCA transits from layered to rock salt structure with O_2 release, depending on the lithiation state:



The lithiation state x can be calculated using

$$x = 1 - \frac{n_{\text{Li}}^{\text{irr}} + n_{\text{Li}}^{\text{res}} + 1/F \text{SOC} C^{\text{nom}}}{n_{\text{NCA}}^{\text{a}}} \quad (18)$$

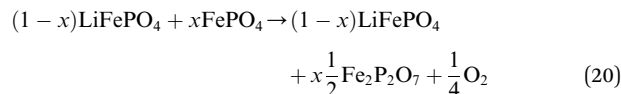
The amount of liberated O_2 is

$$n_{\text{O}_2}^{\text{a}} = \frac{1-x}{2} n_{\text{NCA}}^{\text{a}} \quad (19)$$

This calculation gives $n_{\text{O}_2}^{\text{a}}$ (SOC = 100%) = 69.2 mmol for a fully charged NCA cell and $n_{\text{O}_2}^{\text{a}}$ (SOC = 0%) = 6.7 mmol for a fully discharged NCA cell.

LFP cathodes have better thermal stability than layered metal oxide cathodes such as $\text{Li}_x(\text{Ni}_{0.80}\text{Co}_{0.15}\text{Al}_{0.05})\text{O}_2$, because of the strong covalent bonds of the phosphate groups of Li_xFePO_4 .⁶³ Nevertheless a phase transition with O_2 release of heated FePO_4 can be detected by XRD experiments.^{64,65} If assumed that the

partly lithiated LFP cathode in a Li-ion battery consists of a mix of lithiated (LiFePO_4) and delithiated (FePO_4) particles⁶⁶ then the oxygen release of a partially charged cathode is given by:



The absolute amount of O_2 from the LFP cell can be calculated with equations similar to (18) and (19).

Both cathodes materials NCA and LFP can contribute O_2 (Fig. 6) which in turn can take part in further exothermic degradation reactions. The amount of O_2 is higher for delithiated cathodes (battery is charged). Note, that because of the irreversible capacity loss during formation of actual cells, the cathode can not be fully lithiated by discharge of the cell: even at 0% SOC (battery is discharged) the lithiation factor $x < 1$ and a small amount of O_2 may be released.

5.2 Exposure of lithium by the anode

On the anode side graphite particles can defoliate and expose intercalated Li at temperatures above 230 °C.^{67,68} The amount of released Li depends on SOC of the battery:

$$n_{\text{Li}}^{\text{a}} = 1/F \text{SOC} C^{\text{nom}} + n_{\text{Li}}^{\text{res}} \quad (21)$$

The NCA cell can release n_{Li}^{a} (SOC = 100%) = 126.2 mmol in the fully charged state and n_{Li}^{a} (SOC = 0%) = 1.24 mmol in discharged state.

5.3 Typical chemical reactions

In this section we compile a list of probable degradation reactions which may take place during thermal runaway. The most significant chemical reactions may be reactions with O_2 and Li: partially delithiated cathodes release O_2 and partially lithiated anodes release Li at elevated temperatures (17), (20) and (21). Both released materials are highly reactive and promote a number of reactions that are summarized in a previous publication.³⁶ Additionally, following reactions are considered:

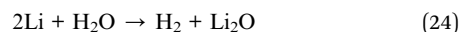
Combustion of the carbon black (conducting additive) or anode graphite



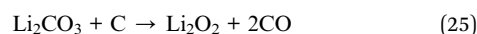
the water-gas shift reaction



oxidation of exposed Li with water



endothermic decomposition of liquid lithium carbonate (at high temperatures, $\theta_{\text{melt}} = 720$ °C) with carbon black⁶⁹



hydrolysis of the hexafluorophosphate salt^{70,71}

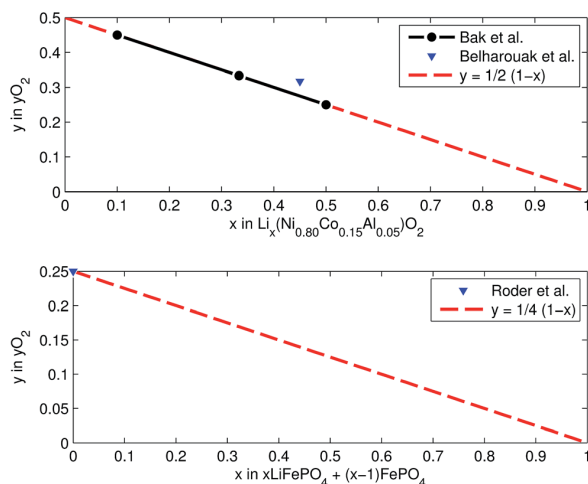
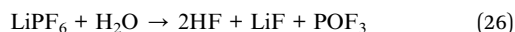


Fig. 6 Oxygen release at different lithiation states: (a) NCA powder upon heating up to 600 °C (from ref. 59 and 61) and (b) LFP powder in electrolyte upon heating to 350 °C (from ref. 64).

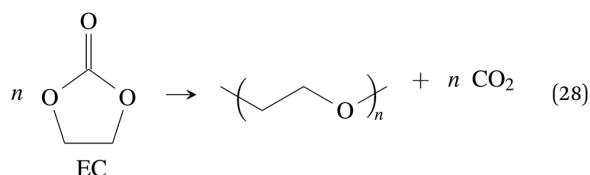




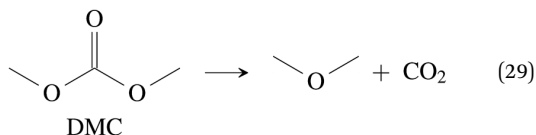
5.4 Alternative CO₂ producing reactions

CO₂ was the main gaseous product that was identified in the ventgas of discharged cells. Little O₂ is available in cells at 0% SOC and it is questionable if combustion alone can account for all CO₂. Therefore effort was made to find further alternative reactions with CO₂ evolution without oxygen involvement. Following reactions were found in the literature:

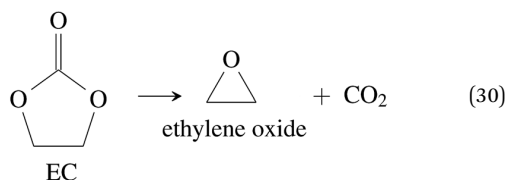
Ring-opening and polymerisation of EC and PC⁷²⁻⁷⁴ e.g.:



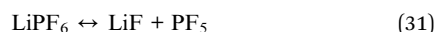
thermal decomposition of the carbonate esters^{50,75,76} e.g.:



or



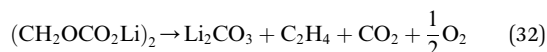
Gnanaraj *et al.* notes⁷⁵ that the electrolyte salt decomposes



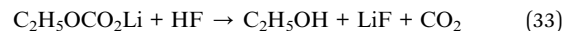
and the resulting strong Lewis base PF₅ lowers the onset-temperatures of solvent decomposition reactions by acid-base catalysis. The onset temperature for DEC and DMC decomposition lies at 170 °C (ref. 75) and 190 °C (ref. 77) respectively. This values are well below the maximal temperatures reached in our thermal-ramp experiments. Electrolyte decomposition with CO₂ release was also observed in other research.^{5,78}

The maximum amount of CO₂ generated from purely thermal decomposition of the electrolyte solvents (28)–(30) is only limited by the amount of available electrolyte.

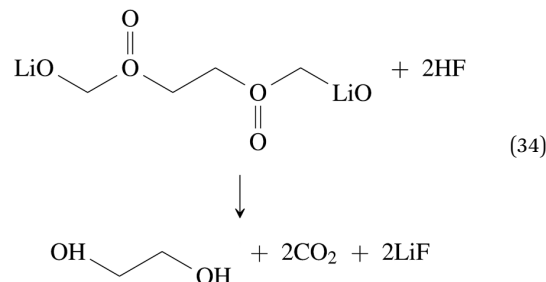
Further CO₂ may be produced from the SEI degradation: The organic SEI produced by EC reduction (2) can decompose in thermally driven reactions,⁷⁹



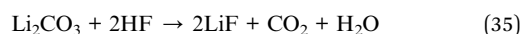
or react with HF analogous to⁸⁰



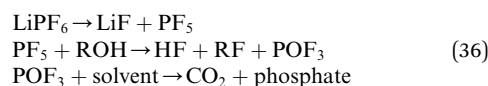
with the proposed scheme



Inorganic SEI can react with HF as well.^{48,53}



In the presence of impurities such as trace water LiPF₆ may react to POF₃ that in turn reacts with the electrolyte in a decarboxylation reaction with CO₂ release:^{50,77,81-83}



What is the most significant CO₂ production mechanisms in oxygen depleted environment? In the case of the NCA cell (Table 1) decomposition of all electrolyte solvent (28)–(30) may translate to 35.0 mmol CO₂. The amount of SEI is lower than the amount of electrolyte solvents and therefore only 8.7 mmol of CO₂ can be produced with eqn (34) and (35). The reactions involving HF (33)–(36) may be further suppressed by the limited amount of trace ROH and LiPF₆.

5.5 Gas release of a discharged NCA cell

In the Experiment 1 a discharged NCA cell was subject to a thermal-ramp test and absolute amounts of produced gas

Table 4 Model reaction system for the Experiment 1 (discharged NCA cell)

Reaction 1	Utilization <i>b</i> ₁ (mmol)
DMC _{liq} → DMC _{gas}	11.6
EC _{liq} → EC _{gas}	8.5
MPC _{liq} → MPC _{gas}	0.6
(CH ₂ OCO ₂ Li) ₂ → Li ₂ CO ₃ + C ₂ H ₄ + CO ₂ + 0.5O ₂	0.1
CMC + 3.175O ₂ → 7.4CO + 5.35H ₂ O	1
PVDF + Li → (CH=CF) + 0.5H ₂ + LiF	0.9
0.5O ₂ + H ₂ → H ₂ O	7
CO + H ₂ O → CO ₂ + H ₂	7.2
DMC → CO ₂ + CH ₃ OCH ₃	12.5
EMC → CO ₂ + CH ₃ OC ₂ H ₅	2.2
DMC + 2Li + H ₂ → Li ₂ CO ₃ + 2CH ₄	0.2



Table 5 Initially available material in the cell as well as material that is consumed as a reactant according to the proposed reaction system in Table 4 for the Experiment 1 (discharged NCA cell)

Compound <i>j</i>	Availability n_j^a (mmol)	Consumption n_j^c (mmol)
PE	25	0
O ₂	6.7	6.7
C	946.4	0
CMC	2.9	1
PVDF	7	0.9
DMC _{liq}	24.3	24.3
EMC _{liq}	2.2	2.2
EC _{liq}	8.5	8.5
MPC _{liq}	0.6	0.6
LiPF ₆	3.1	0
(CH ₂ OCO ₂ Li) ₂	3.5	0.1
C ₆ H ₄ O ₆	1	0
Li	1.3	1.3
Li ₂ CO ₃	1.7	0
LiF	1.7	0

components were measured (Table 3). Gas analysis with GC gave 23.2 mmol of CO₂ and small amounts of H₂, CO and hydrocarbons. The overall amount of produced gas n_{sum}^{ideal} inside the heated reactor was 65.4 mmol. This means that the GC system was unable to detect 42.2 mmol of unknown gas components.

What is the source of CO₂ and what is the nature of the not identified gas components? The cathode material of a discharged cell is not fully lithiated and may release a small amount of O₂ (19). The released O₂ can participate in a combustion reaction, but the amount of released O₂ is not sufficient to produce all measured CO₂ ($n_{O_2}^a = 6.7$ mmol vs. $n_{CO_2}^{GC} = 21.9$ mmol). We needed to consider alternative reactions in order to account for the measured amounts of gases.

Table 6 Produced material in the Experiment 1 (discharged NCA cell): calculated values of the model reaction system according to Table 4, values quantified by the GC system and the overall measured amount of produced gas inside the reactor

Compound <i>i</i>	Calculated n_i^b (mmol)	From GC n_i^{GC} (mmol)	n_{sum}^{ideal} (mmol)
O ₂	0	0.1	—
—[CH=CF]—	0.9	—	—
Li ₂ CO ₃	0.3	—	—
DMC _{gas}	11.6	—	—
EC _{gas}	8.5	—	—
MPC _{gas}	0.6	—	—
CH ₃ OCH ₃	12.5	—	—
CH ₃ OC ₂ H ₅	2.2	—	—
H ₂ O	5.3	—	—
CO	0.4	0.4	—
CO ₂	21.9	21.9	—
H ₂	0.4	0.4	—
CH ₄	0.4	0.4	—
C ₂ H ₂	0.1	0.1	—
Sum of gaseous products	63.9	23.2	65.4

Table 4 was calculated with the linear optimisation algorithm. It gives one possible set of reactions to reproduce the measured value of CO₂ and the overall amount of produced gas in the reactor. Because of the elevated temperature all liquid solvents present inside the Li-ion cell either decompose or evaporate (Table 5). The calculation gives rise to new gaseous components and the amount of those components can be compared to the actual measurements (Table 6).

In this mathematical solution, the missing 42.2 mmol of gas consist mainly of solvent decomposition products (CH₃OCH₃, CH₃OC₂H₅) and remaining solvents as well as water in gaseous state. Such gases can not be found by the GC system due to following reasons: (a) the sampler of the GC runs at room temperature and therefore the solvents condense and are not

Table 7 Model reaction system for the Experiment 13 (over-charged NCA cell)

Reaction <i>l</i>	Utilization b_l (mmol)
DMC + 1.5O ₂ → 3CO + 3H ₂ O	10.4
DMC → C ₂ H ₄ + CO ₂ + H ₂ O	1.1
EC + O ₂ → 3CO + 2H ₂ O	8.5
MPC _{liq} + 4.5O ₂ → 8CO + 4H ₂ O	0.6
C + 0.5O ₂ → CO	60.9
CO + 0.5O ₂ → CO ₂	12.3
(CH ₂ OCO ₂ Li) ₂ + 2Li → 2Li ₂ CO ₃ + C ₂ H ₄	3.5
C ₆ H ₄ O ₆ + 2O ₂ → 6CO + 2H ₂ O	1
CMC + 3.175O ₂ → 7.4CO + 5.35H ₂ O	2.9
PVDF + O ₂ → 2CO + 2HF	7
CO + H ₂ O → CO ₂ + H ₂	15.5
2Li + H ₂ O → H ₂ + Li ₂ O	57.5
DMC → CO ₂ + CH ₃ OCH ₃	5.3
EMC → CO ₂ + CH ₃ OC ₂ H ₅	2.2
DMC + 2Li + H ₂ → Li ₂ CO ₃ + 2CH ₄	7.5
Li ₂ CO ₃ → Li ₂ O + CO ₂	3.1
Li ₂ CO ₃ + 2HF → 2LiF + CO ₂ + H ₂ O	13.1
LiPF ₆ + H ₂ O → 2HF + LiF + POF ₃	3.1
POF ₃ + 2H ₂ O → POF(OH) ₂ + 2HF	3.1

Table 8 Initially available material in the cell as well as material that is consumed as a reactant according to the proposed reaction system in Table 7 for the Experiment 13 (over-charged NCA cell)

Compound <i>j</i>	Availability n_j^a (mmol)	Consumption n_j^c (mmol)
PE	25	0
O ₂	81.6	81.6
C	946.4	60.9
CMC	2.9	2.9
PVDF	7	7
DMC _{liq}	24.3	24.3
EMC _{liq}	2.2	2.2
EC _{liq}	8.5	8.5
MPC _{liq}	0.6	0.6
LiPF ₆	3.1	3.1
(CH ₂ OCO ₂ Li) ₂	3.5	3.5
C ₆ H ₄ O ₆	1	1
Li	151	137
Li ₂ CO ₃	1.7	1.7
LiF	1.7	0



Table 9 Produced material in the Experiment 13 (over-charged NCA cell): calculated values of the model reaction system according to Table 7, values quantified by the GC system and the overall measured amount of produced gas inside the reactor

Compound <i>i</i>	Calculated n_i^p (mmol)	From GC n_i^{GC} (mmol)	n_{sum}^{ideal} (mmol)
LiF	29.3	—	—
POF(OH) ₂	3.1	—	—
Li ₂ O	60.6	—	—
CH ₃ OCH ₃	5.3	—	—
CH ₃ OC ₂ H ₅	2.2	—	—
CO	136	136	—
CO ₂	52.6	57.9	—
H ₂	65.5	65.5	—
CH ₄	15.1	15.1	—
C ₂ H ₄	4.6	4.6	—
Sum of gaseous products	281.3	279.1	281.3

injected into the GC column and (b) the present GC setup is not designed to identify and quantify any components other than H₂, O₂, N₂, CO, CO₂, CH₄, C₂H₂, C₂H₄ and C₂H₆.

5.6 Gas release of a charged NCA cell

The situation changes when the cells in thermal ramp experiments are charged. High amounts of oxygen and lithium become available and the cells go into distinct thermal runaway. In the Experiment 13 (Table 3) an overcharged NCA cell was tested and the vent-gases were quantified by the GC system using an internal N₂ standard.

The cell in Experiment 13 was overcharged to a capacity of 4.03 A h (120% SOC). The lithiation factor of the cathode was $x_{Li}^{cat} = 0.08$ and the calculated oxygen release (17) was $n_{O_2}^a = 81.6$ mmol. The lithiation factor of the anode was $x_{Li}^{and} = 1.00$ and the amount of intercalated Li on the anode side equalled $n_{Li}^a = 151$ mmol. In other words, the anode was fully lithiated to the maximum theoretical Li capacity. The cell produced 281.3 mmol of ventgas during thermal runaway and high amounts of CO, H₂, CO₂ were detected.

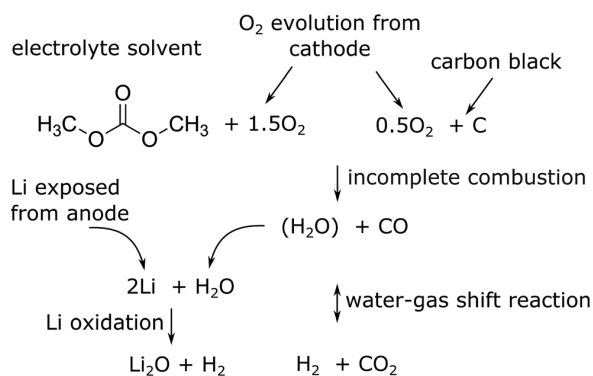


Fig. 7 Proposed main reaction system for a thermal runaway of a (partially) charged or over-charged Li-ion battery.

To find one of the possible solutions explaining the measured gas composition the equations in Table 7 were used. In this exemplary mathematical solution all electrolyte solvents, organic SEI, lithium carbonate and the released O₂ were consumed (Table 8). The major products in the calculation were the gases as measured by the GC as well as the solids LiF and Li₂O. The overall amount of measured gas n_{sum}^{ideal} and the amounts of the individual gas components n_i^{GC} could be reproduced by the calculation (Table 9). The quantity of LiF and Li₂O was not measured and therefore not verified by the experiments.

The major reactions which were responsible for the gas and heat production during thermal runaway are summarized in a simplified picture (Fig. 7). In this scheme the released oxygen triggers a chain of exothermic reactions. Because of O₂ insufficiency incomplete combustion of organic material takes place. The resulting H₂O reacts with the exposed Li with H₂ production. Simultaneously H₂ and CO₂ are produced with the water-gas shift reaction. In the end the main gases are CO, CO₂ and H₂.

Although the calculation shows good agreement of measured and computed amounts of gas it has some flaws: (a) the full amount of CO₂ could not be reproduced (b) it is not considered, that the separator material must decompose and add additional gas volume at temperatures >900 °C and (c) in reality the reactants are not distributed homogeneously when the reactions take place, instead material is violently expelled from the cell into the reactor during thermal runaway. Further work is needed to take those effects into account.

6 Conclusions and outlook

We measured the thermal runaway characteristics of commercial Li-ion cells in destructive thermal ramp experiments in inert atmosphere. Our samples were 23 NCA and LFP based Li-ion batteries with the geometrical format 18650 charged to different SOC. The main findings of this work are:

(1) The cell material and cell design (e.g. high energy density vs. high power density) have a high influence on the maximum cell temperature and on the released gases in thermal runaway conditions (Table 10). Charged NCA cells showed a drastic thermal runaway behaviour. NCA cells could reach maximum temperatures of 1075 °C and they released up to 317 mmol of gas (equal to 7.1 L at standard conditions). Charged LFP cells exhibited a less pronounced thermal runaway: maximum cell temperatures as high as 448 °C were observed and the LFP cells released up to 61 mmol of gas.

(2) Discharged cells showed no thermal runaway upon heating up to ~250 °C. Both cell types needed to be at least partially charged in order to go into thermal runaway.

(3) The severity of the thermal runaway increased with increasing SOC.

(4) The thermal runaway reactions produced high amounts of CO, H₂ and CO₂ thus making the gas flammable and potentially toxic. The gas composition depended on the cell type and SOC. NCA cells produced more CO and H₂ than LFP



Table 10 Comparison of the two tested cell types. Cell specifications and averaged experimental results

		LFP	NCA
Voltage (50% SOC)	V	3.32	3.68
Nominal capacity	A h	1.1	3.35
Cell mass	g	38.87	45.40
Max continuous discharge	A	30	6.7
Cycle life		>1000	>300
Min. SOC for a pronounced thermal runaway	%	50	25
Onset temperature θ_o (100% SOC)	°C	140	139
Max. temperature θ_m (100% SOC)	°C	440	911
Produced gas n_{sum}^{ideal} (100% SOC)	mmol	32	277
Detected CO ₂ (100% SOC)	%	48.3	20.0
Detected CO (100% SOC)	%	9.1	44.8
Detected H ₂ (100% SOC)	%	29.4	25.7
Impact of overcharge		Weak	Strong

cells. Discharged cells generated mainly CO₂. Increased SOC led to increased amounts of CO and H₂.

(5) The SOC and the cell type had less effect on the onset temperature, as long as no Li plating occurred. Overcharge may cause metallic Li deposition on the anode which compromises the thermal stability. The onset temperature of overcharged cells decreased dramatically from 140 °C to values as low as 65 °C!

(6) In three experiments, the absolute amounts of gases from NCA cells were quantified. It is shown, that it is theoretically possible to explain the absolute amounts of the measured gases with a set of chemical degradation reactions and with known amounts of initial material in the cell.

(7) We think that the main reactions in charged cells are combustion of carbonous material and Li oxidation. Both are strong exothermic reactions which contribute to the energy release during the thermal runaway of a Li-ion battery. The amounts of O₂ and Li available to degradation reactions depend on the SOC as well as on the amount and type of active cathode and anode material. Higher SOC increases the O₂ release of the cathode and the amount of intercalated Li in the anode. In over-charged cells these amounts increase further and deposition of highly reactive metallic Li may occur on the anode.

(8) It is proposed that both, the cathode and anode side participate in the reaction system. Therefore experiments with only one electrode may not cover the full picture.

Many open questions concerning the safety of Li-ion batteries remain. The industry needs scaling rules to evaluate the safety of large battery systems with hundreds of cells based on results of misuse experiments with individual cells. Many test results exist for small 18650 cells but we think that more effort must be made to understand the thermal runaway behaviour of large cells with capacities as high as 60 A h. It is yet to prove, if specific amount of gas and heat are the same for small and large cells. The risks of fire and toxicity (including HF) of vent gas must be quantified for real life applications

including misuse of battery packs for electric vehicles, airliners and for home storage of solar energy.

Our future work in the next three years will include (a) additional testing of 18650 cells in an improved test rig, (b) experiments with large automotive Li-ion cells in a new large test rig, (c) bottom up thermodynamic calculations of the chemical reaction systems and (d) top down FEM simulation of failure propagation and the reaction kinetics in large battery packs.

Nomenclature

Δm	Mass loss of the cell, caused by temperature ramp experiment (g)
θ	Cell temperature (°C)
θ_m	Maximum cell temperature during the temperature ramp experiment (°C)
θ_o	Onset temperature of the thermal runaway (°C)
θ_{gas}	Gas temperature inside the reactor (K)
C^{irr}	Charge associated with n_{Li}^{irr} (A h)
C^{nom}	Typical cell capacity as specified in the datasheet (A h)
C^{res}	Charge associated with n_{Li}^{res} (A h)
C_{and}^{u}	Theoretically usable capacity of the anode (A h)
C_{cat}^{u}	Theoretically usable capacity of the cathode (A h)
F	Faraday constant ($F = 96\,485\text{ A s mol}^{-1}$)
n_i^a	Amount of substance i in a pristine cell, at the start of a thermal ramp experiment (mol)
n_i^p	Theoretically calculated amount of product i , which is produced by chemical reactions during the thermal runaway (mol)
n_j^a	Amount of material j in the cell, that is available for chemical reactions during the thermal runaway (mol)
n_{cat}^a	Amount of either LFP or NCA units in the cathode
n_i^{GC}	Absolute amount of gas component i in the reactor, calculated from GC results (mol)
n_{sum}^{GC}	Amount of gas produced by a cell during a temperature ramp experiment, calculated from GC results (mol)
n_{sum}^{ideal}	Amount of gas produced by a cell during a temperature ramp experiment, calculated with the ideal gas law (mol)
n_{Li}^{irr}	Amount of irreversibly trapped Li in the anode caused by initial cell formation (mol)
n_{Li}^{res}	Amount of residual Li in the anode of a cell which is discharged to V_{min} (mol)
n_j^r	Theoretically calculated amount of reagent j in the cell, which is consumed by chemical reactions during the thermal runaway (mol)
n_o	Initial amount of gas in the reactor at the start of the experiment (mol)
n_{N_2}	Actual amount of N ₂ in the reactor (mol)
P	Gas pressure in the reactor (Pa)
R	Gas constant ($R = 8.314\text{ J mol}^{-1}\text{ K}^{-1}$)
r_i^{GC}	Result of GC measurement: fraction of gas component i in the GC sample (mol%)
T	Time (s)
V	Volume of the reactor (m ³)
V_{min}	Minimum cell voltage as specified in the datasheet (V)
x	Lithiation factor of the anode or cathode



Acknowledgements

VIRTUAL VEHICLE Research Center is funded within the COMET Competence Centers for Excellent Technologies programme by the Austrian Federal Ministry for Transport, Innovation and Technology (BMVIT), the Federal Ministry of Science, Research and Economy (BMWFV), the Austrian Research Promotion Agency (FFG), the province of Styria and the Styrian Business Promotion Agency (SFG). The COMET programme is administrated by FFG. We would furthermore like to express our thanks to our supporting scientific project partners, namely "Varta Micro Innovation GmbH" and to the Graz University of Technology. The work was made possible by the principal industrial project partners "BASF SE" and by "MAGNA STEYR Battery Systems GmbH & Co OG".

References

- 1 K. Xu, *Chem. Rev.*, 2004, **104**, 4303–4417.
- 2 Z. J. Zhang and P. Ramadass, in *Encycl. Sustain. Sci. Technol.*, Springer New York, New York, NY, 2012, pp. 319–356.
- 3 J. Wen, Y. Yu and C. Chen, *Mater. Express*, 2012, **2**, 197–212.
- 4 D. Doughty and E. P. Roth, *Electrochem. Soc. Interface*, 2012, **21**, 37–44.
- 5 E. P. Roth and C. J. Orendorff, *Electrochem. Soc. Interface*, 2012, **21**, 45–49.
- 6 D. Abraham, E. P. Roth, R. Kostecki, K. McCarthy, S. MacLaren and D. Doughty, *J. Power Sources*, 2006, **161**, 648–657.
- 7 Z. Chen, Y. Qin, Y. Ren, W. Lu, C. Orendorff, E. P. Roth and K. Amine, *Energy Environ. Sci.*, 2011, **4**, 4023.
- 8 G. Nagasubramanian and C. J. Orendorff, *J. Power Sources*, 2011, **196**, 8604–8609.
- 9 H. Maleki, G. Deng, A. Anani and J. Howard, *J. Electrochem. Soc.*, 1999, **146**, 3224.
- 10 P. Ping, Q. Wang, P. Huang, J. Sun and C. Chen, *Appl. Energy*, 2014, **129**, 261–273.
- 11 P. Röder, B. Stiaszny, J. C. Ziegler, N. Baba, P. Lagaly and H.-D. Wiemhöfer, *J. Power Sources*, 2014, **268**, 315–325.
- 12 M. Fleischhammer, T. Waldmann, G. Bisle, B.-I. Hogg and M. Wohlfahrt-Mehrens, *J. Power Sources*, 2015, **274**, 432–439.
- 13 D. H. Doughty, E. P. Roth, C. C. Crafts, G. Nagasubramanian, G. Henriksen and K. Amine, *J. Power Sources*, 2005, **146**, 116–120.
- 14 J. Lamb and C. J. Orendorff, *J. Power Sources*, 2014, **247**, 189–196.
- 15 G. Trattning and W. Leitgeb, in *Automot. Batter. Technol.*, Springer, 2014, pp. 19–37.
- 16 X. Liu, S. I. Stolarov, M. Denlinger, A. Masias and K. Snyder, *J. Power Sources*, 2015, **280**, 516–525.
- 17 P. Ping, Q. Wang, P. Huang, K. Li, J. Sun, D. Kong and C. Chen, *J. Power Sources*, 2015, **285**, 80–89.
- 18 X. Feng, M. Fang, X. He, M. Ouyang, L. Lu, H. Wang and M. Zhang, *J. Power Sources*, 2014, **255**, 294–301.
- 19 F. Larsson and B.-E. Mellander, *J. Electrochem. Soc.*, 2014, **161**, A1611–A1617.
- 20 P. Huang, Q. Wang, K. Li, P. Ping and J. Sun, *Sci. Rep.*, 2015, **5**, 7788.
- 21 H. Wang, A. Tang and K. Wang, *Chin. J. Chem.*, 2011, **29**, 27–32.
- 22 C.-Y. Wen, C.-Y. Jhu, Y.-W. Wang, C.-C. Chiang and C.-M. Shu, *J. Therm. Anal. Calorim.*, 2012, **109**, 1297–1302.
- 23 T.-Y. Lu, C.-C. Chiang, S.-H. Wu, K.-C. Chen, S.-J. Lin, C.-Y. Wen and C.-M. Shu, *J. Therm. Anal. Calorim.*, 2013, **114**, 1083–1088.
- 24 C.-Y. Jhu, Y.-W. Wang, C.-M. Shu, J.-C. Chang and H.-C. Wu, *J. Hazard. Mater.*, 2011, **192**, 99–107.
- 25 C.-Y. Jhu, Y.-W. Wang, C.-Y. Wen, C.-C. Chiang and C.-M. Shu, *J. Therm. Anal. Calorim.*, 2011, **106**, 159–163.
- 26 H. Ishikawa, O. Mendoza, Y. Sone and M. Umeda, *J. Power Sources*, 2012, **198**, 236–242.
- 27 E. P. Roth and D. H. Doughty, *J. Power Sources*, 2004, **128**, 308–318.
- 28 S.-i. Tobishima and J.-i. Yamaki, *A consideration of lithium cell safety*, 1999.
- 29 D. Belov and M.-H. Yang, *Solid State Ionics*, 2008, **179**, 1816–1821.
- 30 Y. Zeng, K. Wu, D. Wang, Z. Wang and L. Chen, *J. Power Sources*, 2006, **160**, 1302–1307.
- 31 T. Ohsaki, T. Kishi, T. Kuboki, N. Takami, N. Shimura, Y. Sato, M. Sekino and A. Satoh, *J. Power Sources*, 2005, **146**, 97–100.
- 32 J. Jeevarajan, in *Lithium-Ion Batter. Adv. Appl.*, Elsevier, 2014, pp. 387–407.
- 33 C. Orendorff, *Electrochem. Soc. Interface*, 2012, **21**, 61–65.
- 34 R. a. Leising, M. J. Palazzo, E. S. Takeuchi and K. J. Takeuchi, *J. Electrochem. Soc.*, 2001, **148**, A838.
- 35 Z. Li, J. Huang, B. Yann Liaw, V. Metzler and J. Zhang, *J. Power Sources*, 2014, **254**, 168–182.
- 36 A. W. Golubkov, D. Fuchs, J. Wagner, H. Wiltse, C. Stangl, G. Fauler, G. Voitic, A. Thaler and V. Hacker, *RSC Adv.*, 2014, **4**, 3633.
- 37 J.-H. Lee, U. Paik, V. a. Hackley and Y.-M. Choi, *J. Electrochem. Soc.*, 2005, **152**, A1763.
- 38 S.-L. Chou, Y. Pan, J.-Z. Wang, H.-K. Liu and S.-X. Dou, *Phys. Chem. Chem. Phys.*, 2014, **16**, 20347–20359.
- 39 Z. Chen and J. R. Dahn, *Reducing Carbon in LiFePO₄/C Composite Electrodes to Maximize Specific Energy, Volumetric Energy, and Tap Density*, 2002.
- 40 J. Wang and X. Sun, *Energy Environ. Sci.*, 2012, **5**, 5163.
- 41 H. Ota, Y. Sakata, A. Inoue and S. Yamaguchi, *J. Electrochem. Soc.*, 2004, **151**, A1659.
- 42 J. C. Burns, R. Petibon, K. J. Nelson, N. N. Sinha, A. Kassam, B. M. Way and J. R. Dahn, *J. Electrochem. Soc.*, 2013, **160**, A1668–A1674.
- 43 S. Zhang, *J. Power Sources*, 2006, **162**, 1379–1394.
- 44 E. Peled, D. Golodnitsky, A. Ulus and V. Yufit, *Electrochim. Acta*, 2004, 391–395.
- 45 K. Ushirogata, K. Sodeyama, Y. Okuno and Y. Tateyama, *J. Am. Chem. Soc.*, 2013, **135**, 11967–11974.
- 46 L. El Ouatani, R. Dedyvere, C. Siret, P. Biensan, S. Reynaud, P. Iratcabal and D. Gonbeau, *J. Electrochem. Soc.*, 2009, **156**, A103.



- 47 G. Gachot, S. Grugeon, G. G. Eshetu, D. Mathiron, P. Ribière, M. Armand and S. Laruelle, *Electrochim. Acta*, 2012, **83**, 402–409.
- 48 M. Onuki, S. Kinoshita, Y. Sakata, M. Yanagidate, Y. Otake, M. Ue and M. Deguchi, *J. Electrochem. Soc.*, 2008, **155**, A794.
- 49 D. Aurbach, A. Zaban, Y. Ein-Eli, I. Weissman, O. Chusid, B. Markovsky, M. Levi, E. Levi, A. Schechter and E. Granot, *J. Power Sources*, 1997, **68**, 91–98.
- 50 G. Gachot, P. Ribière, D. Mathiron, S. Grugeon, M. Armand, J. B. Leriche, S. Pilard and S. Laruelle, *Anal. Chem.*, 2011, **83**, 478–485.
- 51 R. Spotnitz and J. Franklin, *J. Power Sources*, 2003, **113**, 81–100.
- 52 H. Yoshida, T. Fukunaga, T. Hazama, M. Terasaki, M. Mizutani and M. Yamachi, *J. Power Sources*, 1997, **68**, 311–315.
- 53 C. Doh, D. Kim, J. Lee, D. Lee, B. Jin, H. Kim, S. Moon, Y. Hwang and A. Veluchamy, *Bull. Korean Chem. Soc.*, 2009, **30**, 783.
- 54 K. Tasaki and S. J. Harris, *J. Phys. Chem. C*, 2010, **114**, 8076–8083.
- 55 H. Maleki and J. Howard, *J. Power Sources*, 2006, **160**, 1395–1402.
- 56 H. He, Y. Liu, Q. Liu, Z. Li, F. Xu, C. Dun, Y. Ren, M.-x. Wang and J. Xie, *J. Electrochem. Soc.*, 2013, **160**, A793–A804.
- 57 X. Huang, *J. Solid State Electrochem.*, 2010, **15**, 649–662.
- 58 C. T. Love, *J. Power Sources*, 2011, **196**, 2905–2912.
- 59 S.-m. Bak, K.-w. Nam, W. Chang, X. Yu, E. Hu, S. Hwang, E. A. Stach, K.-B. Kim, K. Y. Chung and X.-Q. Yang, *Chem. Mater.*, 2013, **25**, 337–351.
- 60 K.-W. Nam, S.-M. Bak, E. Hu, X. Yu, Y. Zhou, X. Wang, L. Wu, Y. Zhu, K.-Y. Chung and X.-Q. Yang, *Adv. Funct. Mater.*, 2013, **23**, 1047–1063.
- 61 I. Belharouak, W. Lu, D. Vissers and K. Amine, *Electrochem. Commun.*, 2006, **8**, 329–335.
- 62 H. J. Bang, H. Joachin, H. Yang, K. Amine and J. Prakash, *J. Electrochem. Soc.*, 2006, **153**, A731.
- 63 Z. Li, D. Zhang and F. Yang, *J. Mater. Sci.*, 2009, **44**, 2435–2443.
- 64 P. Röder, N. Baba, K. Friedrich and H.-D. Wiemhöfer, *J. Power Sources*, 2013, **236**, 151–157.
- 65 J. Kim, K.-Y. Park, I. Park, J.-K. Yoo, J. Hong and K. Kang, *J. Mater. Chem.*, 2012, **22**, 11964.
- 66 W.-J. Zhang, *J. Power Sources*, 2011, **196**, 2962–2970.
- 67 O. Haik, S. Ganin, G. Gershtinsky, E. Zinigrad, B. Markovsky, D. Aurbach and I. Halalay, *J. Electrochem. Soc.*, 2011, **158**, A913.
- 68 Y. He, Z. Tang, Q. Song, H. Xie, Q. Xu, Y. Liu and G. Ling, *Thermochim. Acta*, 2008, **480**, 15–21.
- 69 J.-w. Kim and H.-g. Lee, *Metall. Mater. Trans. B*, 2001, **32**, 17–24.
- 70 R. Yazami and A. Martinet, in *Fluorinated Mater, Energy Conversion*, Elsevier Science, 1st edn, 2005, ch. Fluorinate, pp. 173–194.
- 71 L. Terborg, S. Weber, F. Blaske, S. Passerini, M. Winter, U. Karst and S. Nowak, *J. Power Sources*, 2013, **242**, 832–837.
- 72 L. Vogdanis and W. Heitz, *Makromol. Chem., Rapid Commun.*, 1986, **7**, 543–547.
- 73 L. Vogdanis, B. Martens, H. Uchtmann, F. Hensel and W. Heitz, *Makromol. Chem., Rapid Commun.*, 1990, **191**, 465–472.
- 74 S. E. Sloop, J. B. Kerr and K. Kinoshita, *J. Power Sources*, 2003, **119–121**, 330–337.
- 75 J. S. Gnanaraj, E. Zinigrad, L. Asraf, H. E. Gottlieb, M. Sprecher, M. Schmidt, W. Geissler and D. Aurbach, *J. Electrochem. Soc.*, 2003, **150**, A1533.
- 76 G. Gachot, S. Grugeon, I. Jimenez-Gordon, G. G. Eshetu, S. Boyanov, A. Lecocq, G. Marlair, S. Pilard and S. Laruelle, *Anal. Methods*, 2014, **6**, 6120.
- 77 T. Kawamura, A. Kimura, M. Egashira, S. Okada and J.-I. Yamaki, *J. Power Sources*, 2002, **104**, 260–264.
- 78 G. G. Botte and T. J. Bauer, *J. Power Sources*, 2003, **119–121**, 815–820.
- 79 M. N. Richard and J. Dahn, *J. Electrochem. Soc.*, 1999, **146**, 2068.
- 80 W. Kong, H. Li, X. Huang and L. Chen, *J. Power Sources*, 2005, **142**, 285–291.
- 81 A. Hammami, N. Raymond and M. Armand, *Nature*, 2003, **424**, 635–636.
- 82 C. L. Champion, W. Li and B. L. Lucht, *J. Electrochem. Soc.*, 2005, **152**, A2327.
- 83 C. L. Champion, W. Li, W. B. Euler, B. L. Lucht, B. Ravdel, J. F. DiCarlo, R. Gitzendanner and K. M. Abraham, *Electrochem. Solid-State Lett.*, 2004, **7**, A194.





Cite this: *RSC Adv.*, 2017, 7, 24425

Holistic methodology for characterisation of the thermally induced failure of commercially available 18650 lithium ion cells

Michael Lammer, * Alexander Königseder and Viktor Hacker

An innovative approach to holistic analysis of thermally induced battery failure has been developed. A purpose-built test rig with high reproducibility within the specific setup produces reliable experimental data. Thermal ramp experiments at a defined state of charge are conducted on three types of commercial lithium ion batteries of the 18650 format. Thermally induced cell break-down is detected by temperature measurement on the cell surface. These failure scenarios comprise the venting of gas and particles and the exothermic process of thermal runaway. The tests showed heat emissions of up to 31 kJ during the final phase, with the battery surface reaching up to 877 °C. The release of gas is continuously logged and analysed by micro-GC. The main components are flammable and, due to the high concentration of CO of up to 61.4%, highly toxic. The maximum total gas emission during the deflagration of the cell was 5495 cm³.

Received 3rd March 2017
Accepted 27th April 2017

DOI: 10.1039/c7ra02635h
rsc.li/rsc-advances

1 Introduction

Lithium ion batteries are employed in a wide field of applications. From portable electronic devices and e-mobility up to stationary storage systems, this technology is used due to its reliability and high power density for energy storage by numerous charge/discharge cycles. However, high power density also imposes increased danger in case of failure. Public opinion on and general acceptance of this energy storage technology is directly related to safety and risks during operation. Catastrophic battery malfunction also heavily affects the attitude towards the final products powered by these cells, turning battery monitoring in combination with risk assessment to a key competence area for safe operation.

As batteries contain fuel and oxidiser within one sealed compartment, understanding fire hazards is of great importance.^{1,2} Organic electrolytes and temperature sensitive electrode materials require elaborated heat management systems in battery packs.^{3,4} Under operating conditions Joule heat is generated within the cell.^{5,6} This heat has to be dispersed by the cell in order to maintain its temperature. Excess heat from internal short circuits or external influence eventually leads to critical conditions.^{7–10} Evaporation of electrolyte and gas formation from thermally induced decomposition pressurise the battery. Though pressure relief from integrated safety vents may prevent cell rupture, the emission of flammable vapour and gas still poses a safety risk.^{3,11} Full scale exothermic degradation of

the battery components releases reactive substances like oxygen, carbon monoxide and previously intercalated lithium.^{12–14} The emission of heat poses an obvious threat to cells nearby, thus endangering the whole battery pack and system.

Calorimetric assessment of battery components and complete cells has been performed recently by several groups.^{4,15–20} This method is widely used for characterisation of thermally induced reactions of unstable substances, making it useful for this kind of investigation of batteries. Using adiabatic calorimetry allows the prediction of thermal hazards in large scale applications.⁴ As lithium ion cells are complex systems, calorimetric analysis on them is a challenging task. Specialised or custom made equipment is used for characterisation of the thermal response.^{15,17,19} Cone calorimeters are employed for characterising the burning characteristics, *i.e.* the thermal degradation and heat release under air atmosphere.^{7,20} These tests are commonly performed on the basis of single cells or small battery packs, but also fire tests on vehicle scale are performed.^{21,22}

Previously conducted studies on thermal ramp tests provided the framework for the new and improved test setup presented within this paper. Measuring the pressure increase in the test container has been used for determination of the amount of vent gas. Withdrawing gas samples after the thermal ramp test gave a cumulative overview of the released gases.^{14,23–25}

This work focuses on determination of thermal degradation of small cylindrical cells (18650 format) using a custom made test rig for holistic experiments. Heat is provided by an electric resistance furnace. The response to the external heat influx is determined by evaluation of the heat consumed and released during critical events like venting and exothermic failure. The

Institute of Chemical Engineering and Environmental Technology, University of Technology Graz, Inffeldgasse 25/C/II, 8010 Graz, Austria. E-mail: michael.lammer@tugraz.at; Tel: +43 316 873 8795



quasi-adiabatic nature of these events allows the calorimetric quantification of the heat of reaction.³ The identification of critical self-heating rates indicates the transition into degradative processes and thermal runaway. A system for reproducible and accurate gas sampling at ambient pressure allows for analysis and quantification of the vent gas at certain points of interest. Using this improved technique, the gas emission is investigated in a temporally resolved way. Valuable insights into the degradation of battery components and safety issues such as toxicity and pressure evolution are gained by this test method.

2 Experimental

2.1 Anatomy of the thermal ramp test

Three types of commercial, state of the art 18650 Li-ion cells are charged to 100% state of charge according to the manufacturer's data sheet using a CC/CV charging routine. After removing the plastic sheet the cell's mass is determined. Three thermocouples are secured on the cell surface by a sheet of glass fibre cloth. The gas sampling device is prepared by flushing the sample vials and syringe pump with argon. The tubular reactor itself is also flushed with inert gas to prevent reactions with ambient gases. Additional thermocouples are located on the sample holder and reactor wall. A schematic overview of the test rig is depicted in Fig. 1.

The furnace is preheated to 80 °C, then slow and continuous heating (thermal ramp 0.5 °C min⁻¹) is performed for the duration of the experiment *i.e.* until the deflagration of the cell.

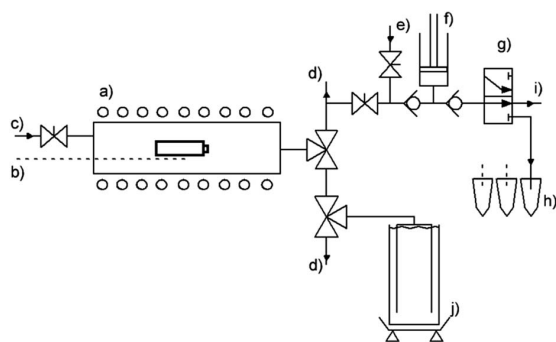


Fig. 1 Schematic of the test rig consisting of electric resistance furnace containing the cell under test (a), thermocouples (b), inert gas inlet (c), off gas releases (d), purge gas inlet (e), syringe pump (f), automated multi-port valve (g), sample vials for GC-analysis (h), purge port (i) and fluid displacement tubes including scales (j).

Elevated temperature initiates degradation reactions and phase transitions, leading to the pressure build-up within the battery can. Upon reaching a certain temperature, the first venting incident occurs. During this event, the built-in safety rupture disk releases excess pressure from the cell. Gas samples are withdrawn at this point automatically by a syringe pump. These samples are consecutively fed into argon filled GC-vials for the *ex situ* analysis via GC (Agilent micro-GC 3000A). Further heating leads to the decomposition of the electrode material and eventually to thermal runaway. This exothermic event is characterised by large emission of gas and particles and a sharp increase of the cell temperature to over 870 °C. The characteristic events are detected by changes of the cell's temperature heating rate. The amount of vent-gas is quantified by displacement of water from corresponding vessels. The displaced liquid is continuously quantified by weighing and the amount of gaseous emission is calculated.

2.2 Test procedure

The cells used in this work are of comparable nominal capacity and cell chemistry (Table 1). The cells are suitable for high power and high energy applications, making them favourable for e-mobility applications. All experiments were conducted with fully charged cells (State of Charge, SoC = 100%). The cells were conditioned on a BaSyTec Battery Test System (BaSyTec GmbH). The electrode material (lithium nickel cobalt aluminium oxide – NCA) is not thermally stable and releases oxygen at elevated temperatures, thus promoting degenerative reactions.^{18,26} There are no manufacturer data available on anode composition, electrolyte and additives. According to an investigation by Spotnitz and Franklin,¹² the main contribution towards thermal runaway is made by the positive electrode and electrolyte decomposition. The carbonic anodes mainly release intercalated lithium during thermal degradation. The lithium consequently reacts with the organic solvent or fluorinated binder forming hydrocarbons and Li₂CO₃ or LiF respectively. The thermal impact of these negative electrode degradation reactions is largely negligible.

2.3 Evaluation of the thermal events

All cells show approximately similar characteristics during the thermal ramp test (Fig. 2). At temperatures above 120 °C, the degradation of electrolyte and separator produces gaseous products and the critical cell pressure is reached. The safety rupture disk implemented within the positive terminal releases the pressurised gas. The resulting Joule–Thomson cooling initiates a drop in cell temperature. The external heating

Table 1 Basic characteristics of the cells used within this work

Device	Cathode material	Nominal capacity/mA h	Cell mass/g	Maximum discharge current/mA
ICR18650-32A	LiNi _{0.8} Co _{0.15} Al _{0.05} O ₂	3200	48.62 ± 0.03	6400
INR18650-35E	LiNi _{0.8} Co _{0.15} Al _{0.05} O ₂	3500	47.68 ± 0.03	8000
INR18650MJ1	LiNi _{0.8} Co _{0.15} Al _{0.05} O ₂	3500	46.35 ± 0.09	10 000



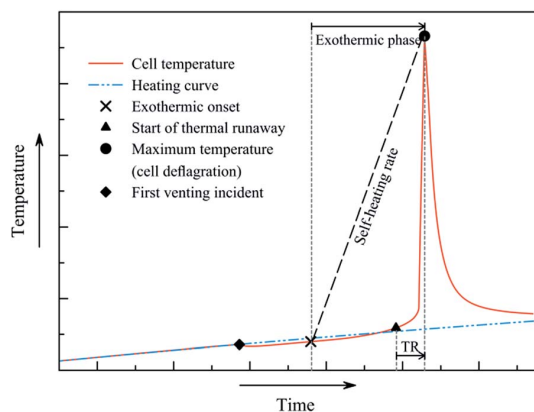


Fig. 2 Schematic of the temperature development and the characteristic points and sections. The respective heat is calculated from the temperature difference between cell (measurement) and heating curve (parabolic fit).

initiates the following processes and consequently the thermal runaway. The event of thermal runaway is defined at a heating rate of $2\text{ }^{\circ}\text{C min}^{-1}$ or more. As the can is open at this point, gas is released continuously. The final phase of the thermal runaway (TR) – the deflagration of the cell – is observable as the temperature increases sharply to over $800\text{ }^{\circ}\text{C}$.

The characteristic events occur at quasi-adiabatic conditions,^{3,4} thus allowing the calculation of the respective amount of produced heat. The relative temperatures during cooling and self-heating were determined by relating the cell temperatures to the heating ramp (Fig. 2). A negative relative temperature *i.e.* a cooling process corresponded to energy taken up by the event. The occurrence of positive relative temperature *i.e.* a self-heating process was related to the emission of heat from the battery. Cell deflagration is associated with intense heat release. Beyond this event, the cell is cooling down due to the temperature gradient.

By analysing the rate plot (dT/dt vs. T) the characteristic points are identified (Fig. 3). Initiation of the exothermic phase (exothermic onset – T_{onset}) is determined as the point of inflexion in the rate curve at around $135\text{ }^{\circ}\text{C}$. This is associated to the increasing self-heating rate opposed to the decreasing heating of the external heat source. The self-heating rate is considered safety relevant^{1,27} and is averaged over the progress of the total exothermic phase.

2.4 Determination of the vent gas composition and amount

The released gas (vent gas) displaces water from a system of communicating vessels. Continuous weighing of the displaced fluid was performed to quantify the amount of vent gas. Picking gas samples at characteristic points (Fig. 2) is performed automatically. Characterisation of the samples is performed by use of an Agilent micro-GC 3000A. Gas emissions were quantified at standard ambient temperature and pressure (SATP conditions). Whereas the first venting mainly releases CO_2 as non-condensing emission, later venting at higher temperature emits a wide variety of gaseous products.

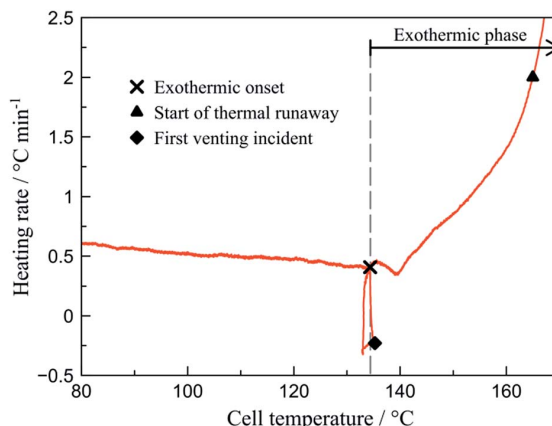


Fig. 3 Rate plot (ICR18650-32A) used for the determination of the characteristic events. The rate increase at around $135\text{ }^{\circ}\text{C}$ signifies the exothermic onset, the steep drop at $130\text{ }^{\circ}\text{C}$ is related to the first venting incident, thermal runaway ($>2\text{ }^{\circ}\text{C min}^{-1}$) starts at $165\text{ }^{\circ}\text{C}$. Cell deflagration is not depicted.

3 Results and discussion

None of the oxygen released from the active material could be determined directly by GC. Supposedly the oxygen reacts directly within the battery forming secondary products detectable by gas chromatography.

The heat consumed during the first venting offers insight into battery safety. By releasing gas from the previously sealed can, the cell temperature drops up to $4\text{ }^{\circ}\text{C}$ (first venting incident – Fig. 2). This might prevent thermal runaway in case of internal failure.²⁸ The maximum energy consumption was observed at INR18650-35E. The gas emission at this event consisted mainly of CO_2 from thermal degradation of the SEI layer and consecutive conversion of the electrolyte component ethylene carbonate on contact with the electrode.^{24,29} This fact is associated to the increased oxygen release^{18,24-26} from the cathode material in its partly lithiated state. By the thermally promoted transitions from a layered system to a particulate rock-salt system oxygen is made available for further

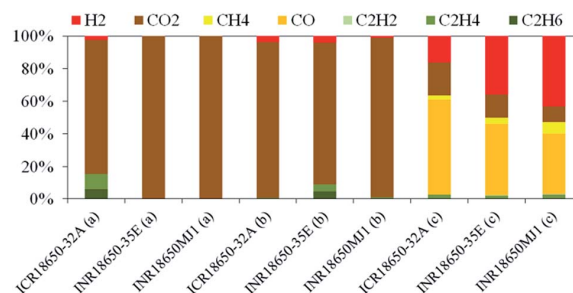


Fig. 4 Average relative amounts of quantified gaseous species for each of the tested cells; (a) represents the gas mixture released during the first venting incident, (b) is related to the thermal runaway and (c) shows the gaseous deflagration products.



Table 2 Average gaseous emission at the three characteristic events (first venting, thermal runaway and cell deflagration) for each of the tested cells. The number of tests conducted varied ($n = 2$ to $n = 4$) for each of the cell types

Event	Device	Emission/mmol	Emission/cm ³	H ₂ /%	CO ₂ /%	CH ₄ /%	CO/%	C ₂ H ₂ /%	C ₂ H ₄ /%	C ₂ H ₆ /%
1 st venting	ICR18650-32A	3.69	90.30	2.43	82.19	0.00	0.00	0.00	9.32	6.06
	INR18650-35E	6.20	151.70	0.00	100.00	0.00	0.00	0.00	0.00	0.00
	INR18650MJ1	1.64	40.10	0.00	100.00	0.00	0.00	0.00	0.00	0.00
Thermal runaway	ICR18650-32A	0.22	5.40	3.71	95.56	0.00	0.00	0.00	0.74	0.00
	INR18650-35E	0.00	0.00	3.87	87.24	0.00	0.00	0.00	4.20	4.70
	INR18650MJ1	0.24	5.80	0.87	98.06	0.00	0.00	0.00	1.07	0.00
Deflagration	ICR18650-32A	125.84	3078.80	15.94	20.40	2.50	58.41	0.22	2.44	0.09
	INR18650-35E	224.60	5494.90	35.68	14.50	3.66	44.00	0.14	1.95	0.06
	INR18650MJ1	215.03	5260.90	43.15	9.76	6.97	37.22	0.16	2.69	0.06

Table 3 Overview of the thermal results of the performed thermal ramp experiments ($n = 6$). Q_{vent} indicates the heat consumed by Joule–Thomson cooling; Q_{TR} corresponds to the heat released over the process of thermal runaway; T_{max} shows the temperature during cell deflagration; T_{onset} is the cell temperature present at the beginning of exothermic reactions; T_{TR} corresponds to the cell temperature at a self-heating rate of 2 °C min⁻¹; rate shows the mean self-heating rate over the total duration of the exothermic phase

Cell	Q_{vent}/J	Q_{TR}/J	$T_{\text{max}}/^\circ\text{C}$	$T_{\text{onset}}/^\circ\text{C}$	$T_{\text{TR}}/^\circ\text{C}$	Rate/ $^\circ\text{C min}^{-1}$	Duration/min
ICR18650-32A	-69.75 ± 6.56	29 488.70 ± 1760.94	744.80 ± 57.56	96.79 ± 2.13	167.13 ± 2.42	4.96 ± 0.44	130.78 ± 3.35
INR18650-35E	-135.83 ± 26.99	23 681.63 ± 2737.52	631.29 ± 85.85	107.22 ± 5.56	158.00 ± 1.26	5.19 ± 1.20	105.18 ± 12.63
INR18650MJ1	-68.85 ± 9.34	17 319.47 ± 2256.38	496.05 ± 71.52	107.21 ± 2.75	151.32 ± 3.04	5.29 ± 1.09	74.06 ± 7.07

degradation reactions.^{26,30} These include the exothermic reaction with carbonaceous species, releasing CO and CO₂ at high temperatures.

ICR18650-32A also released C₂H₆, C₂H₄ and H₂ in significant concentrations. The hydrocarbons may derive from the decomposition of the SEI.^{3,21,31} Hydrogen is the product of the reduction of water deriving from combustion reactions by CO or free lithium. The average vent gas composition is shown in Fig. 4 and Table 2 respectively. The vent gas composition at this stage was similar in all the tested batteries. Up to 5495 cm³ (INR18650-35E) of gas were released from the batteries. A maximum proportion of CO of 48% (ICR18650-32A) and H₂ of 43% (INR18650MJ1) were measured in the vent gas during thermal runaway. Main source of CO is the reaction of carbonaceous material with oxygen released from the cathode material.

Table 3 summarises the amounts of heat consumed and released during the thermal ramp experiments as well as corresponding exothermic onset and the temperature of the beginning of the thermal runaway. Thermal characterisation was performed during all of the experiments, thus allowing precise statistical evaluation. The heat release and self-heating rate for all cells was similar. ICR18650-32A reached the highest maximum temperature due to its high exothermic heat output. INR18650MJ1 showed the lowest maximum temperature – 59% of exothermic heat compared to ICR18650-32A. The strongest Joule–Thomson cooling was observed on INR18650-35E – nearly 150% of endothermic energy compared to the other cells under test. Compared to INR18650MJ1, ICR18650-32A takes 43% longer (additional 57 min) to undergo deflagration after the initiation of exothermic events. The heating rate over the exothermic phase is comparable; the length of this phase varies. As indicated by gas analysis, most of the

degradative processes occur within this phase, emphasising the safety relevance of this period.

4 Conclusion and outlook

The holistic approach for the thermal ramp experiments proved to generate reproducible results and to be effective in use. Continuous measurements of the cell temperature have been a simple yet effective way of determining and interpreting the main events of the thermal ramp experiment. Displacement of liquid water by the vent gas emission during the thermal runaway offered a reliable way of measuring the gas release without pressurisation of the reactor. Operating the system at ambient pressure allows precise gas sampling at certain points of interest, thus providing temporally resolved emission characterisation. By calculating the rate of temperature change, the onset of the exothermic reactions and the beginning of the thermal runaway, defined by a temperature change above 2 °C min⁻¹, had been detected and statistically certified. Characterisation of the heat dissipated during the first venting incident and the thermal runaway combined with the analysis of gases released at these events allowed for further insight and safety considerations. The intense heat release poses a direct threat to people and equipment working with the device. The emission of large quantities of flammable gases, mainly H₂ and CO, intensifies the hazard of fire under these conditions.

The amount of gas reached a maximum of 5494.90 cm³ for the cell INR18650-35E. Even though the cathode material and the nominal capacity of the cells are similar, the results vary drastically. The cell type with the lowest nominal capacity (ICR18650-32A; 3200 mA h) produces the highest heat emission of approx. 30 kJ at the lowest onset temperature of approx. 97 °C, signifying a very volatile system reaching a maximum



temperature of approx. 745 °C. On the other hand it showed a protracted exothermic phase lasting 130 min, offering time for intervention in case of malfunction. This signifies the superiority of INR18650-35E, which exhibits a higher onset temperature at approx. 107 °C and a lower maximum temperature of 631 °C. Furthermore, it dissipated additional 50% of heat during venting. This total dissipation of approx. -136 J increases the possibility of terminating detrimental reactions resulting from self-heating. INR18650MJ1 offered a comparable exothermic onset and thermal runaway temperature but inferior Joule-Thomson cooling of -69 J. The heat emission during thermal runaway (approx. 17.5 kJ) and the maximum temperature were the lowest determined in this study. Lower heat emission reduces the hazards within a confined battery pack, exposing neighbouring cells to less heat in case of catastrophic malfunction. This diminishes the risk of a thermally induced battery failure propagating through the system.

Acknowledgements

The financial support of the project ISALIB by the Austrian Ministry of Transport, Innovation and Technology (BMVIT) and The Austrian Research Promotion Agency (FFG) through the program "Mobilität der Zukunft" (2014–2017) and the co-operation of our project partners Kompetenzzentrum – Das virtuelle Fahrzeug, Graz and Samsung SDI, Graz is gratefully acknowledged.

References

- 1 D. H. Doughty and A. A. Pesaran, *Vehicle Battery Safety Roadmap Guidance*, National Renewable Energy Laboratory, 2012.
- 2 T. H. Dubaniewicz and J. P. DuCarme, *IEEE Trans. Ind. Appl.*, 2013, **49**, 2451–2460.
- 3 Q. Wang, P. Ping, X. Zhao, G. Chu, J. Sun and C. Chen, *J. Power Sources*, 2012, **208**, 210–224.
- 4 C. Y. Jhu, Y. W. Wang, C. Y. Wen and C. M. Shu, *Appl. Energy*, 2012, **100**, 127–131.
- 5 T. Waldmann, S. Gorse, T. Samtleben, G. Schneider, V. Knoblauch and M. Wohlfahrt-Mehrens, *J. Electrochem. Soc.*, 2014, **161**, A1742–A1747.
- 6 M. Ecker, N. Nieto, S. Käbitz, J. Schmalstieg, H. Blanke, A. Warnecke and D. U. Sauer, *J. Power Sources*, 2014, **248**, 839–851.
- 7 Y. Fu, S. Lu, K. Li, C. Liu, X. Cheng and H. Zhang, *J. Power Sources*, 2015, **273**, 216–222.
- 8 T. D. Hatchard, D. D. MacNeil, D. A. Stevens, L. Christensen and J. R. Dahn, *Electrochem. Solid-State Lett.*, 2000, **3**, 305–308.
- 9 P. Ping, Q. Wang, P. Huang, K. Li, J. Sun, D. Kong and C. Chen, *J. Power Sources*, 2015, **285**, 80–89.
- 10 T. M. Bandhauer, S. Garimella and T. F. Fuller, *J. Electrochem. Soc.*, 2011, **158**, R1.
- 11 P. Keil and A. Jossen, in *EVS28 International Electric Vehicle Symposium and Exhibition*, 2015, pp. 1–11.
- 12 R. Spotnitz and J. Franklin, *J. Power Sources*, 2003, **113**, 81–100.
- 13 C. R. Birkl, M. R. Roberts, E. Mcturk, P. G. Bruce and D. A. Howey, *J. Power Sources*, 2016, **341**, 1–35.
- 14 D. Doughty and E. P. Roth, *Electrochem. Soc. Interface*, 2012, 37–44.
- 15 X. Liu, S. I. Stolarov, M. Denlinger, A. Masias and K. Snyder, *J. Power Sources*, 2015, **280**, 516–525.
- 16 E. Schuster, C. Ziebert, A. Melcher, M. Rohde and H. J. Seifert, *J. Power Sources*, 2015, **286**, 580–589.
- 17 X. Feng, M. Fang, X. He, M. Ouyang, L. Lu, H. Wang and M. Zhang, *J. Power Sources*, 2014, **255**, 294–301.
- 18 S. K. Martha, O. Haik, E. Zinigrad, I. Exnar, T. Drezen, J. H. Miners and D. Aurbach, *J. Electrochem. Soc.*, 2011, **158**, A1115.
- 19 G. Nagasubramanian and K. Fenton, *Electrochim. Acta*, 2013, **101**, 3–10.
- 20 F. Larsson, P. Andersson, P. Blomqvist, A. Lorén and B.-E. Mellander, *J. Power Sources*, 2014, **271**, 414–420.
- 21 N. S. Spinner, C. R. Field, M. H. Hammond, B. A. Williams, K. M. Myers, A. L. Lubrano, S. L. Rose-Pehrsson and S. G. Tuttle, *J. Power Sources*, 2015, **279**, 713–721.
- 22 A. Lecocq, M. Bertana, B. Truchot and G. Marlair, in *2. International Conference on Fires in Vehicles*, 2014.
- 23 A. W. Golubkov, D. Fuchs, J. Wagner, H. Wiltsche, C. Stangl, G. Fauler, G. Voitic, A. Thaler and V. Hacker, *RSC Adv.*, 2014, **4**, 3633–3642.
- 24 A. W. Golubkov, S. Scheikl, R. Planteu, G. Voitic, H. Wiltsche, C. Stangl, G. Fauler, A. Thaler and V. Hacker, *RSC Adv.*, 2015, **5**, 57171–57186.
- 25 F. Larsson and B.-E. Mellander, *J. Electrochem. Soc.*, 2014, **161**, A1611–A1617.
- 26 Y. Huang, Y.-C. Lin, D. M. Jenkins, N. A. Chernova, Y. Chung, B. Radhakrishnan, I.-H. Chu, J. Fang, Q. Wang, F. Omenya, S. P. Ong and M. S. Whittingham, *ACS Appl. Mater. Interfaces*, 2016, **8**, 7013–7021.
- 27 M. Börner, A. Friesen, M. Grütze, Y. P. Stenzel, G. Brunklaus, J. Haetge, S. Nowak, F. M. Schappacher and M. Winter, *J. Power Sources*, 2017, **342**, 382–392.
- 28 P. G. Balakrishnan, R. Ramesh and T. Prem Kumar, *J. Power Sources*, 2006, **155**, 401–414.
- 29 J. L. Tebbe, T. F. Fuerst and C. B. Musgrave, *ACS Appl. Mater. Interfaces*, 2016, 26664–26674.
- 30 E. Hu, S.-M. Bak, J. Liu, X. Yu, Y. Zhou, S. N. Ehrlich, X.-Q. Yang and K.-W. Nam, *Chem. Mater.*, 2014, **26**, 1108–1118.
- 31 M. N. Richard and J. R. Dahn, *J. Electrochem. Soc.*, 1999, **146**, 2068–2077.





Contents lists available at ScienceDirect

Journal of Power Sources

journal homepage: www.elsevier.com/locate/jpowsour



Characteristics of lithium-ion batteries during fire tests



Fredrik Larsson^{a, b, *}, Petra Andersson^a, Per Blomqvist^a, Anders Lorén^a,
Bengt-Erik Mellander^b

^a SP Technical Research Institute of Sweden, Brinellgatan 4, SE-501 15 Borås, Sweden

^b Department of Applied Physics, Chalmers University of Technology, SE-412 96 Göteborg, Sweden

HIGHLIGHTS

- Fire tests on commercial lithium–iron phosphate cells and laptop battery packs.
- Heat release rate (HRR) measured, higher state of charge (SOC) gives higher HRR peaks.
- Toxic emissions of HF and POF₃ (not detected) quantitatively measured.
- Higher total HF emission for lower SOC values.

ARTICLE INFO

Article history:

Received 24 June 2014

Received in revised form

5 August 2014

Accepted 8 August 2014

Available online 15 August 2014

Keywords:

Lithium ion

Battery

Hydrogen fluoride

Phosphorous oxyfluoride

Heat release rate

Fire

ABSTRACT

Commercial lithium-ion battery cells are exposed to a controlled propane fire in order to evaluate heat release rate (HRR), emission of toxic gases as well as cell temperature and voltage under this type of abuse. The study includes six abuse tests on cells having lithium–iron phosphate (LFP) cathodes and, as a comparison, one test on conventional laptop battery packs with cobalt based cathode. The influence of different state of charge (SOC) is investigated and a limited study of the effect of water mist application is also performed. The total heat release (THR) per battery energy capacity are determined to be 28–75 kJ Wh⁻¹ and the maximum HRR values to 110–490 W Wh⁻¹. Hydrogen fluoride (HF) is found in the released gases for all tests but no traceable amounts of phosphorous oxyfluoride (POF₃) or phosphorus pentafluoride (PF₅) are detected. An extrapolation of expected HF emissions for a typical automotive 10 kWh battery pack exposed to fire gives a release of 400–1200 g HF. If released in a confined environment such emissions of HF may result in unacceptable exposure levels.

© 2014 Elsevier B.V. All rights reserved.

1. Introduction

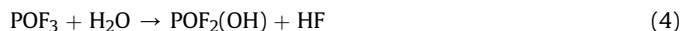
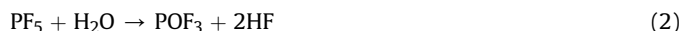
Lithium-ion batteries are widely used since they offer great benefits compared to many other battery technologies. Advantages such as high energy and power density, long life time and the possibility of fast charging make them attractive for consumer products and electrified vehicles. Nevertheless Li-ion batteries contain reactive and flammable materials, therefore safety issues are a concern and a number of incidents involving Li-ion batteries have been reported over the last couple of years [1–4]. Overheating of the batteries may result in exothermal reactions and lead to a thermal runaway with excessive amounts of heat, gas emissions,

fire and potentially explosion/rapid disassembling [1,5–6]. Even in case there is no thermal runaway, a heated battery can still vent flammable and toxic gases. Examples of toxic gases that may originate from such events are hydrogen fluoride, HF, and phosphorous oxyfluoride, POF₃. The toxicity of HF is quite well known [7] since it is formed during several chemical decomposition processes and fires but the toxicity of the POF₃ is currently unknown. Actually, the toxicity of POF₃ might act with other poisoning mechanisms than just by formation of three equivalents of HF. Therefore, critical limits of exposure might be lower for POF₃ than for HF as in the chlorine analog POCl₃/HCl [8]. The origin of the fluorine compounds is primarily the battery electrolyte but emissions can also come from the binder (e.g. PVdF) of the active electrode materials. The electrolyte usually contains flammable organic solvents some of which are volatile at modest temperatures (below 100 °C) and the commonly used Li-salt, lithium hexafluorophosphate, LiPF₆, has a limited thermal stability upon

* Corresponding author. Department of Applied Physics, Chalmers University of Technology, SE-412 96 Göteborg, Sweden. Tel.: +46 10 5165928; fax: +46 33 125038.

E-mail addresses: fredrik.larsson@sp.se, vegan@chalmers.se (F. Larsson).

heating. The decomposition of LiPF_6 can be described, according to Yang et al. [9] and Kawamura et al. [10], by:



When LiPF_6 is heated in a dry and inert atmosphere it decomposes to lithium fluoride, LiF , which is a solid compound at temperatures below 845°C and phosphorus pentafluoride, PF_5 , which is a gas and a strong Lewis acid, see Eq. (1). In the presence of water/moisture PF_5 produces POF_3 , and HF (Eq. (2)). LiPF_6 can also react directly with water/moisture to form LiF , POF_3 and HF according to Eq. (3). In fact, LiPF_6 is highly susceptible to hydrolysis by even trace amounts of moisture [11]. Furthermore, Kawamura et al. [10] suggested that POF_3 could react with water and form $\text{POF}_2(\text{OH})$ and HF according to Eq. (4).

The decomposition of electrolytes containing LiPF_6 forming HF is complex and has mainly been studied at ambient temperature and during heating (but not in situations where there is a fire) [12–19]. Besides emissions containing fluorine and vaporized solvents, a Li-ion cell can also emit other gases, e.g. H_2 , CO , CO_2 , CH_4 , C_2H_6 and C_2H_4 [20–22]. Gases can actually be emitted from batteries under several types of abuse conditions such as overheating, overcharge [23], short circuit, fires etc. A few studies are published on heat release rate (HRR) and emissions of toxic gases from Li-ion batteries in fire conditions. Ribière et al. [24] used a Tewarson fire calorimeter to study the HRR and toxic gases from commercial 2.9 Wh pouch cells with LiMn_2O_4 (LMO) cathode and graphite anode and found e.g. that the total HF release was higher for lower state of charge (SOC) values. Eshetu et al. [25] studied fire properties and toxicity for commonly used Li-ion battery electrolytes but without Li-salt and thus without the possibility to produce HF .

This paper presents results from fire tests of commercially available Li-ion battery cells. Parameters such as heat release rate, cell voltage and surface temperature are measured as well as HF and POF_3 emissions. The influence of application of water is examined to a limited extent by introducing water mist into the flames.

2. Experimental

The tests were conducted using the measurement and gas collection system of a Single Burning Item (SBI) apparatus, that is normally used for classification of building materials according to the European Classification scheme EN13823 [26]. The experimental setup is shown in Fig 1. The cells/batteries were placed on a wire grating (large gratings about $4\text{ cm} \times 10\text{ cm}$) as seen in Fig 2. A propane burner was placed underneath the cells/batteries and was ignited two minutes after the start of the test. The HRR of the burner alone was approximately 15 kW. Abuse tests were performed on 7 Ah EiG LFP pouch cells, 3.2 Ah K2 LFP cylindrical cells, and on 16.8 Ah Lenovo laptop battery packs, see Table 1.

Test 1–5 used commercially available pouch cells with lithium–iron phosphate (LFP), LiFePO_4 , cathode and carbon based anode. Each test consisted of five cells that were mechanically fastened together with steel wire (0.8 mm diameter). The terminal tabs of the cells were cut for all cells but the mid one (the third cell), for which the cell voltage was measured. On both sides of the third cell type K thermocouples were centrally attached measuring the cell surface temperature. Temperature values presented in this

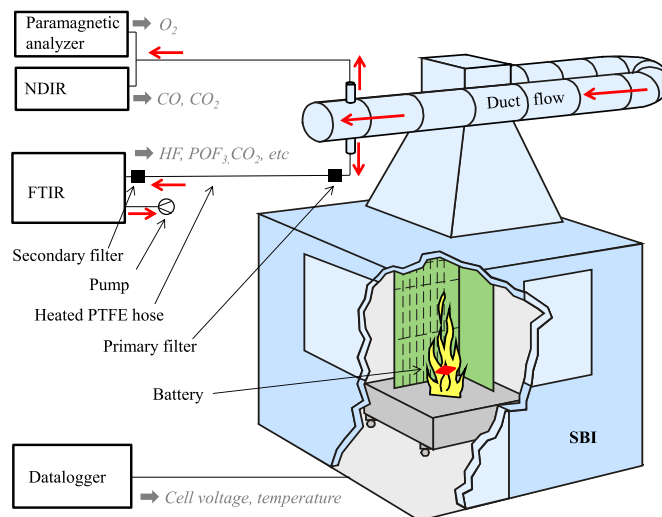


Fig. 1. Schematic illustration over experimental setup.

paper are the average of these thermocouple readings. The temperature and cell voltage was measured with a sample rate of 1 Hz using a data logger, Pico Technology ADC-24. In test 3, water mist was manually applied as a spray into the flames above the battery to study any influence from additional water on the composition of the gas emissions. In test 6, nine K2 26650-cells, i.e. cylindrical cells 26 mm in diameter and 65 mm long, were placed standing up next to each other inside a box. The box had side walls made of non-combustible silica board and steel net at the bottom and top. It was used as a safety precaution to avoid possible projectiles. In test 7, two identical laptop battery packs were used and placed inside a steel net and fastened on the wire grating.

The cells in test 1–6 were set to the selected SOC-level, according to Table 1, by a charge/discharge procedure using an ordinary laboratory power aggregate and a Digatron battery test equipment. The two laptop battery packs in test 7 were fully charged using a laptop computer. All batteries were unused but had different calendar aging. The EiG cells were approximate 2–3 years old, the K2 cells were approximate 1–2 years old and the laptop battery pack was less than 6 months old.

The laptop battery packs in test 7 differ from the other test objects. First, they consist of not only the cells but also electrical connectors, plastic housing and electronic circuits. Secondly, they



Fig. 2. The 5-cells pack of EiG cells placed on a wire grating.

Table 1
 Test objects.

Test no.	Battery type	No. of cells	Nominal capacity (Ah)	Weight (g)	Test condition
1	EiG ePLB-F007A	5	35	1227.9	100% SOC
2	EiG ePLB-F007A	5	35	1229.7	100% SOC
3	EiG ePLB-F007A	5	35	1229.3	100% SOC + water mist
4	EiG ePLB-F007A	5	35	1228.6	0% SOC
5	EiG ePLB-F007A	5	35	1227.6	50% SOC
6	K2 LFP26650EV	9	28.8	734.8	100% SOC
7	Lenovo laptop battery packs	12 ^a	33.6	639.0	100% SOC

^a Two laptop battery packs were used at the same time, each with 6 cells.

have cobalt based cell chemistry with a higher cell voltage, 3.7 V vs 3.2 V for the LFP-cells. Thirdly, in each battery pack, 3 cells are electrically connected in series increasing the voltage to 11.1 V.

All tests were video recorded. The tests were performed during two days and in the beginning of each day a blank test was conducted in order to be able to subtract the burner influence on the HRR values and to make a blank for the gas analysis. The burner was active for a varying duration in the different tests, between 17 and 32 min, i.e. as long as a heat release contribution from the battery was still present. The fire emissions from the test object were collected in a ventilation duct. In test 1–2 a duct flow of $0.6 \text{ m}^3 \text{ s}^{-1}$ was used but in order to increase emission concentrations in the ventilation the duct flow was decreased to $0.4 \text{ m}^3 \text{ s}^{-1}$ in test 3–7.

A Servomex 4100 Gas purity analyser was used to measure the oxygen content of the flow by a paramagnetic analyzer and CO and CO₂ were determined by a non-dispersive infrared (NDIR) sensor. The HRR was calculated using the method of oxygen consumption and was corrected for CO₂ [26]. A part of the flow in the ventilation duct was extracted for on-line FTIR analysis. This sub-flow was extracted through an 8.5 m sampling PTFE hose, heated to 180 °C, using a pump (3.5 L min^{-1}) located after the FTIR measurement cell. The sampled gas is passed through a primary filter (M&C ceramic filter, heated to 180 °C) before the heated hose and thought a second filter (M&C sintered steel filter, heated to 180 °C) before the FTIR. After each test the primary filter was chemically analyzed for fluoride content since it is known that HF may be partly adsorbed by this type of filter [27]. The fluoride adsorbed by the filter was determined by method B.1 (b) of the SS-ISO 19702:2006 Annex B standard, where the filter is leached in water in an ultrasonic bath for at least 10 min. Thereafter the fluoride content in the water is measured by ion chromatography with a conductive detector. The amount of HF is calculated by assuming that all fluoride ions present in the filter derives from HF. The concentration of the emitted gas was measured by Fourier transform infrared spectroscopy (FTIR) using a Thermo Scientific Antaris IGS analyzer (Nicolet) with a gas cell. The spectral resolution of the FTIR was 0.5 cm^{-1} . The gas cell was of 0.2 L, had a path length of 2.0 m, a cell pressure of 86.7 kPa was maintained and the cell was heated to 180 °C. Each spectrum used 10 scans which gave a new spectrum every 12 s. There is a natural time delay between the gas measurement of the SBI and the FTIR in the measurement setup. The HRR and FTIR results presented in this paper were therefore time synchronized by overlaying of CO₂ measurements from the FTIR and the NDIR.

FTIR is a suitable technique to measure the concentrations of HF and POF₃ in the emitted fire gases. The FTIR was calibrated for a number of compounds, e.g. HF, when delivered from the supplier. However, it was found that the HF calibration was not accurate enough so it was recalibrated, see Andersson et al. [28] for a detailed description of the calibration procedure. The FTIR was also calibrated for POF₃. PF₅ could only be qualitatively determined by its spectral signature [28] but no traces of PF₅ could be found in the

Table 2
 The spectral bands used for HF and POF₃.

Spectral bands (cm ⁻¹)	Type of band
<i>HF</i>	
4203–4202	HF R-branch stretching mode [29]
4175–4172	HF R-branch stretching mode [29]
<i>POF₃</i>	
1418–1413	P–O stretching mode [9]
874–868	P–F symmetric stretching mode [9]

fire tests probably due to that the PF₅ is highly reactive. The detection limits were 2 ppm for HF and 6 ppm for POF₃. The spectral bands used for Classical Least Square (CLS) type quantification of HF and POF₃ are stated in Table 2.

3. Results and discussion

The HRR results for the EiG battery cells with 0%, 50% and 100% SOC are shown in Fig. 3. High SOC values give high HRR peaks and the temperature and voltage measurements in Fig. 4 confirm that cells with high SOC value give a more reactive response, with rapid temperature increase and earlier voltage breakdown. Studies using other techniques confirm our results that battery cells with higher SOC are more thermally reactive, using e.g.; fire calorimeter [24], accelerating-rate calorimetry (ARC) [5] and VSP2 adiabatic calorimeter [30]. The HRR from the nine K2 cells in test 6 and the two complete laptop battery packs in test 7 can be seen in Fig. 5. The laptop pack includes the plastic box and have Li-ion cells with the more reactive cobalt based cathode, while the K2 cells (as well as the EiG cells) have LFP cathodes which are known to be significantly more stable [5,31–34]. The higher HRR values for the laptop cells are thus expected.

Outbursts from fully charged cells (100% SOC) of EiG, K2 and laptop packs were visually observed, see Fig. 6 for a typical example. The outbursts originate from ignition of the rapid gas release from a cell upon opening due to excessive cell pressure and correspond to the sharp spikes in the HRR curves, see Figs. 3 and 5. In most cases, one HRR-spike could be detected for each individual cell. For EiG cells with 50% and 0% SOC no spikes were observed in the HRR curves, instead two broad maxima were found. The orientation of the cells on the wire grating varied due the different packaging types (pouch, cylindrical, complete battery pack) which might have influenced the results. However, tests 1–5 used the same cell type and setup. The results of tests 6–7 can be seen as examples of possible events for these types of cells.

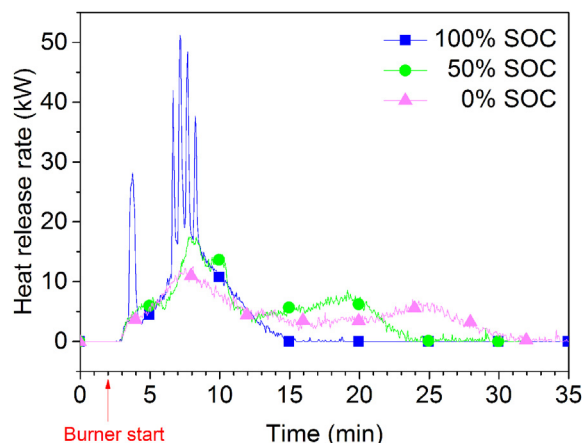


Fig. 3. Heat release rate for EiG cells with 0%, 50% and 100% SOC.

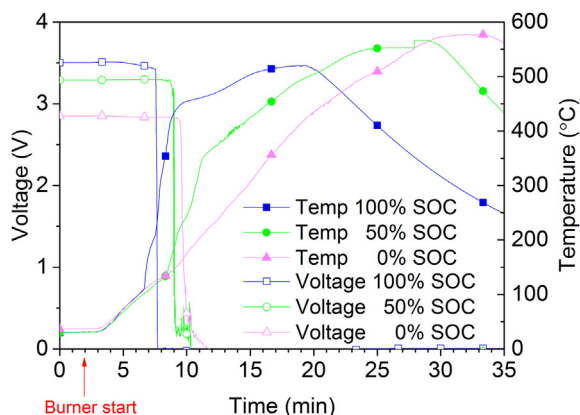


Fig. 4. Mid cell temperature and voltage for EIG with 0%, 50% and 100% SOC.

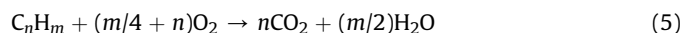


Fig. 6. Outbursts from EIG 100% SOC (test 1).

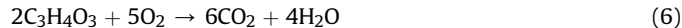
The fire test on EIG cells with 100% SOC was repeated two times (tests 1–2) without water mist application and one time (test 3) with water mist applied approximately 6.5 min after burner start. Fig. 7 shows HRR, HF emission rate, voltage and temperature for the mid cell, in test 2. Rapidly propagating flames released from the battery cells were visually observed five times during the test and denoted outbursts, marked in Fig. 7, and coincided with the five spikes in the HRR curve. The hydrogen fluoride concentration showed a rapid increase at the end of the HRR peak and the HF maximum plateau was reached just after the HRR spikes. The delay between HF production and HRR is not due to gas transport time since it is compensated by CO₂ synchronization, the reason is due to delay times in the sampling system. As expected, the temperature of the mid cell showed a steep increase connected to the HRR peaks, the outbursts and the voltage breakdown. The maximum temperature reached in this measurement was 521 °C. Test 1 and test 2 show similar values and behavior, the variation between the tests is due to the nature of the fire characteristics.

Fig. 8 shows test 3 where 100% SOC EIG cells were tested with water mist application. Most of the results of the tests with and without water mist are similar, but the maximum HF concentration recorded at the time of applying the water mist into the flames is approximately twice as high as that in tests 1–2. However, the total amount of measured HF from FTIR and absorbed by the primary filter is of the same order for all tests 1–3. The water mist was certainly not the only source of water in this experiment, in addition to water existing in the atmosphere water is produced by the

combustion process. In the general case of combustion of hydrocarbons water is produced:



and in the oxidation of ethylene carbonate (EC), C₃H₄O₃, a commonly used Li-ion solvent, water is thus produced according to:



When propane, C₃H₈, is combusted, 1 mol of propane produces 4 mol of water according to Eq. (5). In test 1–3 the 15 kW propane burner was active during 17 min and given the heat of combustion of propane, 2044 kJ mol⁻¹, the amount of water produced from the burner can be calculated to be approximately 550 g.

The water concentration in the exhaust duct was measured by the FTIR, see Fig. 9 for the results of test 1–3. The water concentration shown for test 3 is scaled (factor 0.4/0.6) due to the lower duct flow in order to allow a comparison with the measured values of test 1–2. The outbursts result in an increased water concentration and the effects on the measured water concentration from the applied water mist is also clearly seen. Calculated from the measured data, the mass of the added water mist was around 400 g

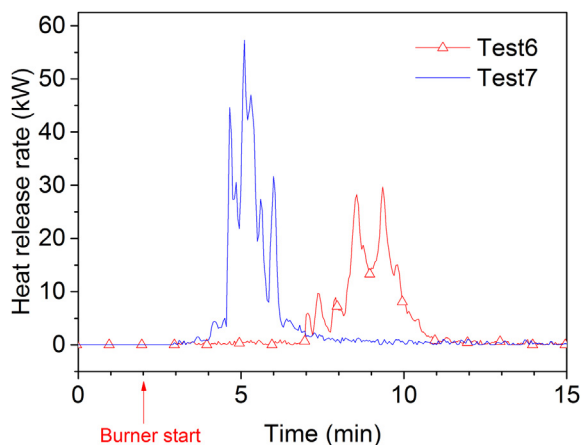


Fig. 5. Heat release rate for K2 cells (test 6) and laptop battery packs (test 7).

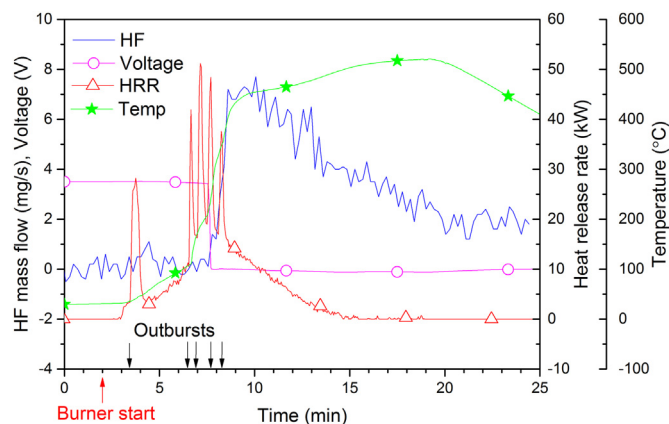


Fig. 7. Results for EIG 100% SOC (test 2).

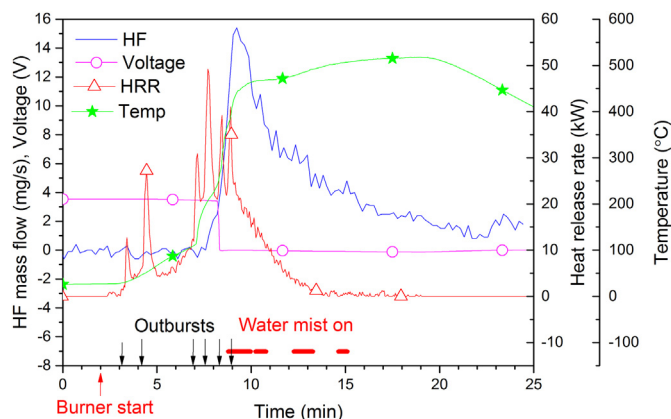


Fig. 8. Results for EiG 100% SOC with water mist (test 3).

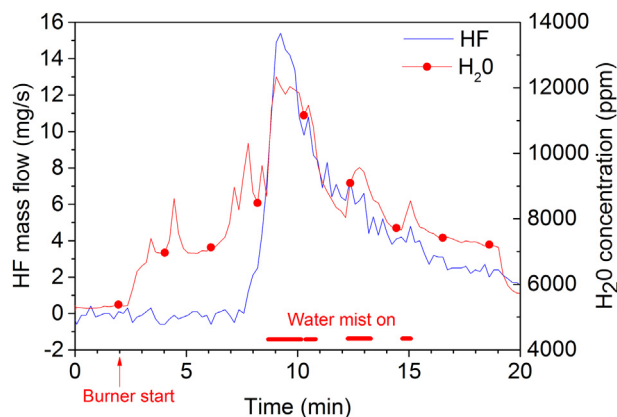


Fig. 10. HF mass flow and water concentration for test 3.

while around 350 g water was released due to the combustion of battery materials. The water in the duct flow from ambient air was around 1500 g for test 3 and 2300 g in test 1–2 (due to higher duct flow rate). The time of the water mist application was relatively short and the water mist was applied in the reaction zone, thus the impact from this source of water was potentially high which is also seen in Fig. 9. The amounts of water from ambient air were large but the impact should have been low since only part of the air flow passed the reaction zone above the battery and no effect on the HF concentration was observed due to the higher ambient water content in the duct flow in test 1–2 compared to test 3. Fig. 10 shows the correlation between HF production and water concentration for test 3. No HF production directly associated with the outbursts can be seen but the application of water mist seems to influence the HF production. However, the added water mist only temporarily increased the emission of HF but did not change the total amount of HF produced. Anyhow, only one test with water mist application was performed and the correlation between the water mist application and the increased HF peak production could possibly depend on other factors than the additional water introduced by the water mist.

Fig. 11 shows the measured production rate of HF for all EiG tests. For 0–50% SOC the peaks are broadened compared to the peaks for the 100% SOC cells and the total amount of measured HF is about double that of the 100% SOC cells. Detailed results from all the tests can be found in Table 3. Total yields in mg g^{-1} are calculated as total amount of HF divided per weight loss of the batteries.

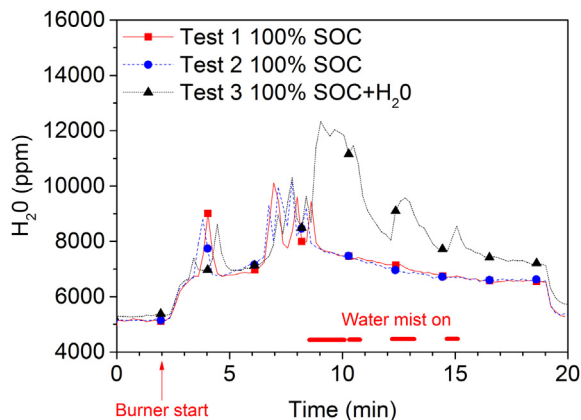


Fig. 9. Water concentrations measured in test 1–3. The increased water level in test 3 due to water mist application is clearly seen.

In test 7 the weight loss also included the burning of pack materials, e.g. plastic housing. Total yields in mg Wh^{-1} are calculated as total amount HF in mg divided by total energy capacity, Wh, of the batteries for each test. Whichever of these yield values that are used, the EiG cells with 0% or 50% SOC showed the highest HF values. The measured data indicate a relationship between SOC and the total released HF emissions, with increased total amounts of HF emission for lower SOC. Ribière et al. [24] found somewhat similar results by studying single cells with 100%, 50% and 0% SOC, showing an increasing total amount of HF emissions for decreasing SOC value. The reason for this is unknown and an investigation of the relationship would require further studies. The HF concentrations measured were in all cases well above the detection limit but no significant amounts of POF_3 could be detected in any of the tests. FTIR measurements on samples of similar electrolytes with LiPF_6 in a cone calorimeter have shown the production of POF_3 to be in the order of 1/20 of the HF production [28]. The detection limit of POF_3 in the FTIR measurements is 3 times higher than for HF, thus there could have been POF_3 present during the measurements which has not been detectable.

The HRR values presented in this paper are calculated using the oxygen consumption method. This technique is well accepted and used in fire calorimetry measurements. For the case of battery fires, the technique might however have some limitations since it will not account for energy liberated by Joule heating through electrical

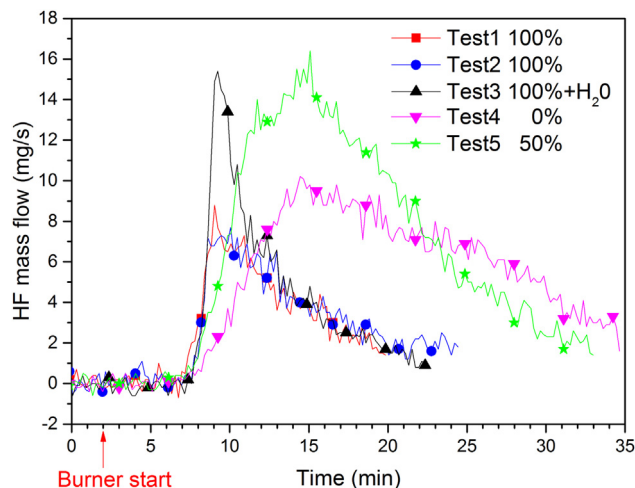


Fig. 11. HF mass flow for EiG cells with different SOC (indicated by % in figure legend) in tests 1–5.

Table 3
 Detailed results of heat release rate, energy release, hydrogen fluoride emissions for test 1–7.

Test no.	Weight loss (g)	Max heat release (kW)	Total heat release (kJ)	Hydrogen fluoride					
				Max production rate (g s ⁻¹)	Total amounts from FTIR (g)	Total amounts from filter (g)	Total amounts (g)	Total yields (mg g ⁻¹)	Total yields (mg Wh ⁻¹)
1	346	55	7731	0.0088	3.2	1.7	4.9	14	44
2	342	51	7526	0.0077	3.9	2.4	6.3	18	56
3	341	49	8095	0.0154	4.2	1.5	5.7	17	51
4	353	13	8314	0.0102	9.7	1.6	11.3	32	100
5	354	17	8452	0.0164	12.0	1.9	13.9	39	120
6	145	29	2766	0.0029	1.2	1.0	2.2	15	24
7	258	57	3470	0.0011	Not detected	1.9	1.9	7.3	15

discharge, e.g. internal short circuits in a cell due to melted separator. Ribière et al. [24] estimates the error to be max 10% and thereby claim the oxygen consumption method to be usable. Besides the issue with Joule heating, the Li-ion battery can release its own oxygen [5]. The oxygen release varies with different Li-ion cell chemistries, and is typically lowest for LFP. In this test method a large amount of air is passed in the duct flow and the effect of released oxygen is regarded as negligible.

In order to simplify an estimation of the heat and gas emission hazards for this type of lithium-ion batteries the values have been normalized to the energy capacity of the batteries. Table 4 shows such values from our study as well as calculated values using data from Ribière et al. [24]. Again, note that the values for the laptop battery pack also accounts for the plastic housing. The EiG cells have about the double total heat release, 67–75 kJ Wh⁻¹, compared to the other batteries in Table 4. Also, the influence of SOC levels is small compared to the differences between the battery types. The maximum HRR per Wh calculated from our experimental data, 110–490 W Wh⁻¹, is, however, lower than the values reported by Ribière et al. [24], 300–1900 W Wh⁻¹, who used a different test procedure. Normalized values for the total HF release vary in our study between 15 and 124 mg Wh⁻¹, a wider range than that found by Ribière et al. [24].

In general, the measured values of the amount of HF produced in fire tests are comparatively high and could pose a serious hazard if released in an enclosed environment. For example, the 7 Ah EiG battery cell can typically be used in a plug-in electric vehicle (PHEV) and a 10 kWh battery pack of a PHEV could consist of 448 such cells (a battery system of 112 cells in series and 4 cells in parallel; cell voltage 3.2 V nominal, pack voltage 358.4 V nominal). If we extrapolate our results for the 5-cell packs by multiplying by a factor of 448/5 = 89.6, it may represent a scenario of a complete fire of a PHEV battery pack. The extrapolation gives 400–1200 g HF depending on the state of charge for the EiG cells where high SOC gives lower HF. Even though the extrapolation is extensive and therefore can be questionable the result is in the same order of magnitude as that reported by Lecocq et al. [35] who conducted

Table 4
 Total heat release, maximum HRR value and total HF release, normalized values for energy capacity.

Battery	Nominal energy capacity (Wh)	Normalized total heat release (kJ Wh ⁻¹)	Normalized maximum HRR (W Wh ⁻¹)	Normalized total HF release (mg Wh ⁻¹)
Five EiG cells	112	67–75	110–490	44–124
Nine K2 cells	92	30	310	24
Two laptop battery packs	124	28	460	15
Single cell, calculated from Ribière et al. [24]	11	28–35	300–1900	37–69

complete vehicle fire tests including HF measurements of two electric vehicles (EV) with fully charged batteries (100% SOC) and on two similar gasoline powered combustion engine passenger cars (none-EV). Lecocq et al. [35] measured significant HF emissions from all four vehicles, both EV and similar none-EV, and suspected that the HF emissions from all vehicles could in part originate from air conditioner system. Using the values in Lecocq et al. [35], and calculating the difference in total HF release between the EV and the similar none-EV an estimate of the contribution to the HF release from the Li-ion battery can be found to be 919 g for a 16.5 kWh Li-ion battery and 657 g for a 23.5 kWh Li-ion battery. Scaling these values for a 10 kWh battery results in 280–557 g of released HF.

If we assume that all the emitted HF is released within a closed passenger compartment of 5 m³ of an electrified vehicle we obtain HF concentrations between 80 and 240 g m⁻³. NOISH (The National Institute for Occupational Safety and Health) in USA stated the IDLH (Immediately Dangerous To Life or Health) value for HF to 30 ppm corresponding to a concentration of HF in air of 0.025 g m⁻³ [7]. Our values which are similar to those of Lecocq et al. [35] exceed the IDLH by about four orders of magnitude. The reported HF values from Ribière et al. [24] also by far exceed the IDLH value. However, the experimental data reported here comes from a limited study and the calculation assumes a somewhat extreme theoretical situation which differs from real fire situations, i.e. all HF is emitted and trapped in the compartment and that the passenger stays in the compartment. Anyhow, even if the emission occurs in a much larger volume, e.g. in a garage, the HF levels can still be very high. The reported HF values thus indicate that a critical situation might occur in the case of a thermal event in a Li-ion battery pack. Although we could not directly detect the presence of POF₃, it may also be present in considerable amounts since indications are that HF and POF₃ is produced with a ratio of about 1:20 [28].

4. Conclusions

The tests show that lithium-ion battery cells exposed to fire are significantly more reactive at 100% SOC than at lower SOC values and energetic outbursts were observed. The HRR peak values thus varied in a rather wide range, between 13 and 57 kW for batteries with approximately 100 Wh energy capacity. The normalized total heat release per energy capacity was 28–75 kJ Wh⁻¹ and the normalized maximum HRR values were 110–490 W Wh⁻¹.

The amount of HF released varied between 15 and 124 mg Wh⁻¹. Lower SOC values gave higher amounts of HF. Extrapolation of data shows that the potential HF release from a 10 kWh PHEV battery is in the range 400–1200 g HF. If this amount of HF would be released inside a passenger compartment of 5 m³ the HF concentration would be 80–240 g m⁻³, that is magnitudes higher than acceptable short time exposure levels. Besides HF, there may also be significant emissions of POF₃, a compound which might be more toxic than HF.

Although these estimates are based on an extrapolation and can be regarded as a hypothetical case it highlights the risks associated with toxic emissions at battery fires and the need to find replacements for the fluorine content in the Li-salt and binder used in Li-ion battery cells. The influence of additional water in form of water mist seemed to increase the HF emissions momentarily, however the total HF release was the same. Further studies of the relationship between water and HF emissions in fires are needed in order to thoroughly evaluate potential risks related to the use of water as firefighting medium in electric vehicle fires.

Acknowledgments

The authors gratefully acknowledge the Swedish Energy Agency and the FFI-program as well as the Swedish Fire Research Board for financial support. Several persons at SP Fire Technology are acknowledged for their contribution to this work, including Lars Pettersson and Magnus Samuelsson.

References

- [1] Z.J. Zhang, P. Ramadass, W. Fang, in: G. Pistoia (Ed.), *Lithium-ion Batteries Advances and Applications*, Elsevier, Amsterdam, 2014, pp. 409–435.
- [2] Q. Wang, P. Ping, X. Zhao, G. Chu, J. Sun, C. Chen, *J. Power Sources* 208 (2012) 210–214.
- [3] D. Lisbona, T. Snee, *Process Saf. Environ. Prot.* 89 (2011) 434–442.
- [4] <http://edition.cnn.com/2014/01/14/travel/787-dreamliner/>, 2014-05-13.
- [5] D. Doughty, E.P. Roth, *Electrochem. Soc. Interface* (Summer 2012) 37–44.
- [6] F. Larsson, P. Andersson, B.-E. Mellander, in: B. Sandén, P. Wallgren (Eds.), *Systems Perspectives on Electromobility*, Chalmers University of Technology, Göteborg, 2014, ISBN 978-91-980973-9-9, pp. 33–44.
- [7] Documentation for Immediately Dangerous to Life or Health Concentrations (IDLHs) for Hydrogen Fluoride (as F), The National Institute for Occupational Safety and Health (NIOSH), USA, May 1994. <http://www.cdc.gov/niosh/idlh/7664393.html>.
- [8] Middelman, *Hygieniska gränsvärden AFS 2011:18, Hygieniska gränsvärden Arbetsmiljöverkets föreskrifter och allmänna råd om hygieniska gränsvärden*, Swedish Work Environment Authority, Sweden, 2011, ISBN 978-91-7930-559-8, ISSN:1650-3163.
- [9] H. Yang, G.V. Zhuang, P.N. Ross Jr., *J. Power Sources* 161 (2006) 573–579.
- [10] T. Kawamura, S. Okada, J.-i. Yamaki, *J. Power Sources* 156 (2006) 547–554.
- [11] Q.-S. Wang, J.-H. Sun, G.-Q. Chu, X.-L. Yao, C.H. Chen, *J. Therm. Anal. Calorim.* 89 (1) (2007) 245–250.
- [12] C.G. Barlow, *Electrochem. Solid-State Lett.* 2 (8) (1999) 362–364.
- [13] S.E. Sloop, J.B. Kerr, K. Kinoshita, *J. Power Sources* 119–121 (2003) 330–337.
- [14] C.L. Campion, W. Li, W.B. Euler, B.L. Lucht, B. Ravdel, J.F. DiCarlo, R. Gitzendanner, K.M. Abraham, *Electrochem. Solid-State Lett.* 7 (7) (2004) A194–A197.
- [15] C.L. Campion, W. Li, B.L. Lucht, *J. Electrochem. Soc.* 152 (12) (2005) A2327–A2334.
- [16] S.F. Lux, I.T. Lucas, E. Pollak, S. Passerini, M. Winter, R. Kostecki, *Electrochem. Commun.* 14 (2012) 47–50.
- [17] H. Yang, X.-D. Shen, *J. Power Sources* 167 (2007) 515–519.
- [18] M.D.S. Lekgoathi, B.M. Vilakazi, J.B. Wagener, J.P. Le Roux, D. Moolman, *J. Fluor. Chem.* 149 (2013) 53–56.
- [19] Hammami, N. Raymond, M. Armand, *Nature* 424 (2003) 635–636.
- [20] T. Ohsaki, T. Kishi, T. Kuboki, N. Takami, N. Shimura, Y. Sato, M. Sekino, A. Satoh, *J. Power Sources* 146 (2005) 97–100.
- [21] E.P. Roth, C.J. Orendorff, *Electrochem. Soc. Interface* (Summer 2012) 45–49.
- [22] D.P. Abraham, E.P. Roth, R. Kostecki, K. McCarthy, S. MacLaren, D.H. Doughty, *J. Power Sources* 161 (2006) 648–657.
- [23] M.D. Chatelain, T.E. Adams, *Proc. Power Sources Conf.* 42 (2006) 87–89.
- [24] P. Ribière, S. Grugeon, M. Morcrette, S. Boyanov, S. Laruelle, G. Marlair, *Energy Environ. Sci.* 5 (2012) 5271–5280.
- [25] G.G. Eshetu, S. Grugeon, S. Laruelle, S. Boyanov, A. Lecocq, J.-P. Bertrand, G. Marlair, *Phys. Chem. Chem. Phys.* 15 (2013) 9145–9155.
- [26] EN 13823:2010, Reaction to Fire Tests for Building Products – Building Products Excluding Floorings Exposed to the Thermal Attack by a Single Burning Item, European Committee for Standardization, Brussels, 2010.
- [27] ISO 19702:2006, Toxicity Testing of Fire Effluents – Guidance for Analysis of Gases and Vapours in Fire Effluents Using FTIR Gas Analysis, International Organization for Standardization, Geneva, 2006.
- [28] P. Andersson, P. Blomqvist, A. Lorén, F. Larsson, *Investigation of Fire Emissions from Li-ion Batteries*, SP Report 2013:5, SP Technical Research Institute of Sweden, Borås, Sweden, 2013, ISBN 978-91-87461-00-2.
- [29] J.M. Hollas, *Modern Spectroscopy*, third ed., John Wiley & Sons, Chichester, 1996.
- [30] C.-Y. Jhu, Y.-W. Wang, C.-M. Shu, J.-C. Chang, H.-C. Wu, *J. Hazard. Mater.* 192 (2011) 99–107.
- [31] H. Joachin, T.D. Kaun, K. Zaghbi, J. Prakash, *J. Electrochem. Soc.* 156 (6) (2009) A401–A406.
- [32] G. Chen, T.J. Richardson, *J. Electrochem. Soc.* 156 (9) (2009) A756–A762.
- [33] G. Chen, T.J. Richardson, *J. Power Sources* 195 (2010) 1221–1224.
- [34] K. Zaghbi, J. Dubé, A. Dallaire, K. Galoustov, A. Guerfi, M. Ramanathan, A. Benmayza, J. Prakash, A. Mauger, C.M. Julien, *J. Power Sources* 219 (2012) 36–44.
- [35] Lecocq, M. Bertana, B. Truchot, G. Marlair, in: P. Andersson, B. Sundström (Eds.), *Conference Proceedings of Fires in Vehicles (FIVE) 2012*, SP Technical Research Institute of Sweden, Borås, Sweden, 2012, pp. 183–193.



Naval Research Laboratory

Washington, DC 20375-5320

NRL/FR/6104--14-10,262

Lithium Battery Fire Tests and Mitigation

FREDERICK W. WILLIAMS

*Senior Scientific Staff Office
Chemistry Division*

GERARD G. BACK

*Hughes Associates
Baltimore, Maryland*

August 25, 2014

Approved for public release; distribution is unlimited.

REPORT DOCUMENTATION PAGE			<i>Form Approved</i> <i>OMB No. 0704-0188</i>		
Public reporting burden for this collection of information is estimated to average 1 hour per response, including the time for reviewing instructions, searching existing data sources, gathering and maintaining the data needed, and completing and reviewing this collection of information. Send comments regarding this burden estimate or any other aspect of this collection of information, including suggestions for reducing this burden to Department of Defense, Washington Headquarters Services, Directorate for Information Operations and Reports (0704-0188), 1215 Jefferson Davis Highway, Suite 1204, Arlington, VA 22202-4302. Respondents should be aware that notwithstanding any other provision of law, no person shall be subject to any penalty for failing to comply with a collection of information if it does not display a currently valid OMB control number. PLEASE DO NOT RETURN YOUR FORM TO THE ABOVE ADDRESS.					
1. REPORT DATE (DD-MM-YYYY) 25-08-2014		2. REPORT TYPE Formal Report		3. DATES COVERED (From - To) September 2013 – December 2013	
4. TITLE AND SUBTITLE Lithium Battery Fire Tests and Mitigation			5a. CONTRACT NUMBER		
			5b. GRANT NUMBER		
			5c. PROGRAM ELEMENT NUMBER		
6. AUTHOR(S) Frederick W. Williams and Gerard G. Back*			5d. PROJECT NUMBER		
			5e. TASK NUMBER		
			5f. WORK UNIT NUMBER 61-8513-K-3-5		
7. PERFORMING ORGANIZATION NAME(S) AND ADDRESS(ES) Naval Research Laboratory 4555 Overlook Avenue, SW Washington, DC 20375-5320			8. PERFORMING ORGANIZATION REPORT NUMBER NRL/FR/6104--14-10,262		
9. SPONSORING / MONITORING AGENCY NAME(S) AND ADDRESS(ES) Office of Naval Research One Liberty Center 875 North Randolph Street Suite 1425 Arlington, VA 22203-1995			10. SPONSOR / MONITOR'S ACRONYM(S) ONR		
			11. SPONSOR / MONITOR'S REPORT NUMBER(S)		
12. DISTRIBUTION / AVAILABILITY STATEMENT Approved for public release; distribution is unlimited.					
13. SUPPLEMENTARY NOTES *Hughes Associates, 3610 Commerce Drive, Suite 817, Baltimore, MD 21227					
14. ABSTRACT More than 100 lithium battery casualty tests were conducted to characterize the conditions produced during a range of both unmitigated and mitigated casualties. Both primary and secondary batteries were tested. This report summarizes the data and findings from these tests, including methods of mitigating thermal runaway of these cells under casualty conditions.					
15. SUBJECT TERMS Lithium batteries Failure Heat propagation Mitigation					
16. SECURITY CLASSIFICATION OF:			17. LIMITATION OF ABSTRACT Unclassified Unlimited	18. NUMBER OF PAGES 68	19a. NAME OF RESPONSIBLE PERSON Frederick W. Williams
a. REPORT Unclassified Unlimited	b. ABSTRACT Unclassified Unlimited	c. THIS PAGE Unclassified Unlimited			19b. TELEPHONE NUMBER (include area code) 202-767-2476

This page
intentionally
left blank

CONTENTS

ACRONYMS.....	v
EXECUTIVE SUMMARY	E-1
1 INTRODUCTION	1
2 DEFINITIONS	1
3 BATTERY TUTORIAL.....	2
3.1 General	2
3.2 Chemistries.....	3
3.3 Cell Construction/Configuration	5
3.4 Battery Packs.....	6
4 BATTERY CASUALTY CHARACTERIZATION TESTS — OVERVIEW	7
5 COMMERCIALLY AVAILABLE BATTERY/CELL DESCRIPTIONS	8
6 REACTION DESCRIPTIONS (SINGLE CELL).....	10
6.1 Initiating Events	10
6.2 General Types of Casualties.....	10
6.3 Observed Cell Casualties.....	11
6.4 SOC Effects on Reaction Types (Li-Ion Only)	15
7 REACTION PRODUCTS TESTING AND RESULTS (SINGLE CELL).....	18
7.1 Reaction Products Test Description	18
7.2 Reaction Products for Cells at 100% SOC.....	18
7.3 SOC Effects on Reaction Products.....	23
7.4 Reaction Products at Low Oxygen Levels	23
7.5 Acid Gas Production	23
7.6 Gas Volume Production	23
8 HEAT RELEASE RATE TESTS AND RESULTS (SINGLE CELL).....	24
8.1 Heat Release Rate Test Description	24
8.2 Heat Release Rate Test Results	25
9 HEAT RELEASE RATE TESTS AND RESULTS (GROUPS OF CELLS).....	27
9.1 Burning Characteristics of Commercially Available Battery Packs/Modules	27
9.2 SOC Effects on Combustion Energy Released	32
9.3 Combustion Energy as a Function of Electrical Energy.....	33
9.4 HRRs of Bulk Storage Configurations.....	34
10 SAFE STORAGE AND CASUALTY MITIGATION OF MULTICELL LITHIUM BATTERIES.....	35
10.1 Battery Storage Locker (BSL) Development History	35

10.2	Detection System Development History	37
10.3	Suppression System Development History	37
10.4	Mitigation Test Results	39
10.5	Suppression Summary	44
11	UNMITIGATED BATTERY PACK REACTIONS INSIDE A PRESSURE VESSEL.....	44
11.1	BSL Worst-Case Thermal Conditions.....	45
11.2	Gas Production	49
12	BATTERY CASUALTY CLASSIFICATION	49
13	SUMMARY.....	50
	REFERENCES	52
	APPENDIX — Video Clips from Lithium Single Cell and Multicell Battery Casualties.....	53

ACRONYMS

Ah	Ampere Hours
BCS	Battery Charging Station
BCCT	Battery Casualty Characterization Tests
BLEVE	Boiling Liquid Expanding Vapor Explosion
BSC	Battery Stowage Compartment
BSL	Battery Storage Locker
C	Celsius
CAS	Chemical Abstract Service
CBD	Chesapeake Bay Detachment
COTS	Commercial Off The Shelf
F	Fahrenheit
ft	Feet
FTIR	Fourier Transform Infrared Spectroscopy
GC-MS/IR	Gas Chromatography–Mass Spectroscopy/Infrared
HMS	Hazard Mitigation Suite
HMT	Hazard Mitigation Test
HRR	Heat Release Rate
HSD	Heat Sensing Device
kW	Kilowatts
kWh	Kilowatt Hours
LBCMS	Lithium Battery Casualty Mitigation System for Lithium Battery Fires
LEL	Lower Explosive Limit
MCE	Maximum Credible Event
MW	Megawatts
NRL	Naval Research Laboratory
PHA	Preliminary Hazard Analysis
PHRR	Peak Heat Release Rate
SHA	System Hazard Analysis
SOC	State of Charge
VOC	Volatile Organic Compound

This page
intentionally
left blank

EXECUTIVE SUMMARY

Lithium batteries can pose a significant hazard during an acute casualty. Potential causes of such casualties include an electrical or mechanical short, overcharging the battery, exposure to excess heat, physical abuse, or spontaneous failure due to a latent defect. During this reaction, the battery may violently vent or rupture, releasing combustible, toxic, and/or acidic vapors and aerosols, and/or incandescent metal particles or carbon. These may result in a major fire or explosion and release of large quantities of toxic and acidic gases. More than 100 battery casualty and mitigation tests were conducted from 2009 to 2012 by the Naval Research Laboratory (NRL) aboard the research test ship ex-USS *Shadwell*. This report summarizes the results of these tests based on specific battery chemistries.

Primary and secondary lithium batteries with a range of chemistries, form factors, and capacities were tested. Lithium batteries may be made up of layers of anode (copper foil coated with a specialty carbon) and cathode (typically aluminum foil coated with a lithiated metal oxide or phosphate) separated by a microporous polyolefin film referred to as a separator. An electrolyte composed of an organic solvent and dissolved lithium salt provides the medium for lithium ion transport. A cell is constructed by stacking alternating layers of electrodes (typical for high-rate capability prismatic cells), or by winding long strips of electrodes into a “jelly roll” configuration (typical for cylindrical cells).

The lithium battery chemistries currently used throughout the industry produce cell voltages ranging from 3.2 to 4.2 V. The capacity of the cell (measured in ampere-hours) varies widely and is a function of the number of layers of electrodes in a prismatic cell or the length of the strip in a cylindrical cell. The commercial industry combines a large number of cells wired together in series and in parallel to produce battery packs and modules with a desired voltage and capacity. These packs can contain hundreds of cells.

NRL battery casualty tests were conducted on individual cells and on a variety of battery packs. The cell chemistries studied are Li/LiCoO₂, Li/Li_{0.5}CoO₂, Li/SOCl₂, Li/LiFePO₄, Li/CF_x, Li/MnO₂, Li/SO₂Cl₂-SOCl₂, and Li/NiCoAlO₄. All tests reported here were conducted on commercially available battery cells.

Based on the tests conducted, single cell reactions can be described using six terms: vent, smoker, flare, burner, explosive, and fireball. Smaller, lower capacity solid cathode cells typically vent and/or smoke and medium to higher capacity cells (specifically the oxyhalides) either ignite and burn or explode. Intuitively, one expects the type of reaction to be a function of the amount of energy contained in the cell at the time of the event. Therefore, the type of reaction should be a function of both the battery capacity and the state of charge (SOC) at the time of the event. Based on a very limited data set (not statistically valid), it appears that the threshold between a venting and a flaming reaction lies in the 10 to 20 watt-hour range. Battery pack configurations can significantly alter these single cell results.

The reaction products measured when a cell vents (without ignition) are electrolyte constituents, such as carbonates or oxyhalides. These are organic solvent gases and aerosols with flammable constituents and the potential to ignite. In some instances, the carbonates break down upon release to produce high levels of CO₂, CO, and a range of hydrocarbons. When a cell burns in a casualty, the electrolyte burns fairly efficiently, producing primarily CO₂ as the by-product. Acid gas can also be produced and is directly related to cell chemistry (and appears to be related to cell capacity): cells that

contain sulfur (e.g., Li/SOCl₂) produce sulfuric acid, cells that contain fluorine (e.g., LiPF₆) produce hydrofluoric acid, and cells that contain chlorine (e.g., Li/SOCl₂) produce hydrochloric acid. There is not enough data to develop a quantitative relationship between cell energy and acid gas production, but for a given cell chemistry, the amount of acid gas produced is expected to be directly proportional to the cell energy.

The mean heat release rate (HRR) for the small commercial cells (such as the AA size) is typically on the order of 10 kW. The larger commercial cells can produce mean heat release rates approaching 100 kW. The more reactive cell chemistries (i.e., Li/SOCl₂ and Li/SO₂Cl₂-SOCl₂) produce violent/explosive type reactions approaching 500 kW.

Tests conducted with multiple-cell packs demonstrate that single cell data for a specific cell type may not be indicative of the reactions of battery packs made up of those same cells: single cell tests and battery pack tests yielded different types of reactions. Specifically, except for the iron phosphate cells, all the packs/modules produced burning reactions, while many of the single cells only vented and never caught fire. This difference was attributed to the greater amount of electrical energy contained in a pack that could contribute to the severity of the reaction and provide an ignition source. In addition, during almost every unmitigated pack/module test, all the cells reacted and the casing materials were completely consumed.

The heat release rate of the multicell packs was a function of the propagation rate from cell to cell within the battery pack and the contribution of the battery pack casing material. The propagation rate from cell to cell ranged from seconds to minutes depending of the type of cell and the battery pack configuration. Some of the smaller packs were consumed in a few minutes while some of the larger packs reacted/burned for over an hour.

Combustion energy of a battery pack was shown to be proportional to the electrical energy contained in the pack after adjusting for the contribution of the packaging material. Some battery packs have metal casings that provide little if any contribution to the fire, whereas some packs have thick hard plastic casings that provide a significant contribution to the fire. After adjusting the combustion energies to account for the case material, the combustion energy is typically about six times the electrical energy potential of the battery.

With respect to suppression, the results from these tests demonstrate that it is virtually impossible to stop a reaction within a lithium cell once it has begun. Consequently, the objective of a fire suppression system should be to thermally manage the conditions in the space and try to cool adjacent cells in an attempt to slow or prevent cell-to-cell propagation. Suppression of the packaging material is also desired. Water appears to be the best suppression agent.

The ability of a suppression system to prevent secondary cell reactions within a complex battery pack is, in part, a function of the openness of the battery pack housing. If the battery housing is fairly open, a fast acting suppression system may be able to reduce the exposures to the adjacent cells within the housing to below the critical temperature value (below the level at which adjacent cells react). The best way to achieve this objective is to rapidly submerge the battery pack in water. The severity of the initial reaction, the proximity of the adjacent cells, and the vulnerability of adjacent cells are variables associated with achieving this performance objective. If the cells are contained within a closed housing (air tight, water tight, or even just a fairly tight enclosure), the suppression system will not be able to contain the reaction to the initial cell, and in most scenarios, all the cells within the pack will react, even if submerged under water. Battery pack submersion does prevent the spread to other packs.

A water spray/sprinkler system (versus a flooding system) has the ability to thermally manage the conditions around the pack of origin, but is unlikely to be effective in preventing the complete consumption/reaction of that initial pack. In some instances, passive thermal barriers between battery packs combined with the thermal management provided by a water spray/sprinkler system is the best approach to mitigate the overall hazard/risk. Two such configurations of a mitigation suite, called the Lithium Battery Casualty Mitigation System, were developed and tested.

There are currently no established criteria for classifying the hazards associated with a lithium battery casualty. Although the data presented here and historical data show that lithium batteries have the potential to ignite and cause a fire, the primary hazard associated with a battery casualty appears to be the gases produced during the reaction. These gases have been determined to be toxic and/or flammable. The concentration of toxic and/or flammable gases produced is a function of the battery chemistry, the number of cells involved in the reaction, the type of reaction (i.e., burning or venting), and the size of the compartment in which the reaction occurs. Since copious amounts of gases are produced during the reaction of larger batteries and battery packs, it must be assumed that any battery casualty will render the storage compartment untenable for unprotected personnel (personnel not wearing a breathing apparatus). During a venting scenario, the resulting mixture could be in the flammable range. A delayed ignition of these gases could produce a large fireball and overpressures that could produce structural damage and additional battery casualties. The consequences from such a scenario could be catastrophic.

The results presented here provide a general understanding of the hazards associated with lithium batteries and approaches to minimize the risk. The reaction characteristics and lessons learned provide a starting point for the development of a database that can be used both to conduct analytical assessments of lithium battery hazards and to develop battery packs for future applications.

This page
intentionally
left blank

LITHIUM BATTERY FIRE TESTS AND MITIGATION

1 INTRODUCTION

Lithium batteries can pose a significant hazard during an acute casualty. Potential causes for such casualties include an electrical or mechanical short, overcharging the battery, exposure to excess heat, physical abuse, or spontaneous failure due to latent defect. During this reaction, the battery may violently vent or rupture, releasing combustible, toxic, and/or acidic vapors and aerosols, and/or incandescent metal particles or carbon. These may result in a major fire or explosion and release of large quantities of toxic and acidic gases.

The Naval Research Laboratory (NRL) recently participated in several major research programs initiated to characterize and mitigate lithium battery fire hazards. The overall goal is to be able to safely handle, store, and charge this class of energy sources. More than 100 battery casualty tests were conducted between 2009 and 2012 to characterize the conditions produced during a range of both unmitigated and mitigated casualties, and to evaluate different containment and suppression systems. This report summarizes the results of these tests. The discussion is divided into data for single cells and data for groupings of cells that comprise what is termed a battery pack. Video clips of some of the tests are presented in the Appendix (on enclosed DVD).

2 DEFINITIONS

The following definitions apply to this report:

Battery: A power source designed to meet the specific needs of an application (voltage, current, power output/duration), containing one or more cells.

Battery pack: A group of cells permanently wired together.

Capacity: The quantity of electrical charge delivered by a battery under specific conditions. It is usually expressed in ampere-hours (Ah).

Casing: The outer shell of a cell or a battery.

Casualty: A scenario consisting of one or more cell reactions leading to a cell failure.

Cell: The smallest individual constituent energy storage unit of a battery.

Electrolyte: Any substance containing free ions that make the substance electrically (ionically) conductive. Most of the electrolytes assessed in this report are liquid and are mixtures of covalent organic and inorganic solvents containing dissolved ionic lithium salts. Where the electrolytes are not organic esters/carbonate mixtures, they are inorganic oxyhalides, usually with sulfur components.

Hazard: An existing or potential condition that can result in a mishap.

Housing: A structure that surrounds the battery pack that is an integral part of the battery. The battery casing and battery housing may be synonymous terms.

Large form cell: A single cell larger in form than two “D” size cells.

Lithium battery: For the purpose of this report, lithium batteries include all cells or batteries in which lithium metal, any lithium alloy, or any form of lithium in a supporting matrix serves as the active anodic component.

Lithium-ion battery: Lithium-ion batteries are comprised of cells that use lithium intercalation compounds as the positive and negative electrodes. As the battery is cycled, lithium ions (Li+) exchange between the positive and negative electrodes. Lithium-ion batteries are a subset of “lithium battery.”

Primary battery: A battery designed to be discharged only once, i.e., not designed to be recharged; also called a nonrechargeable battery.

Reaction: A cell-level event resulting from one of the following: electrical abuse (shorting or overcharging), thermal abuse, or physical damage.

Secondary battery: A battery in which the electrochemical reaction is thermodynamically reversible and is designed to be recharged in use. Common secondary batteries include the lead-acid, nickel-cadmium, and lithium-ion batteries common to many consumer products. A secondary battery may also be referred to as a rechargeable battery.

Thermal runaway: An internal reaction within a cell or battery that generates enough heat to cause the cell to fail in one or more of the following modes: vent aerosols or smoke, jet incandescent particles, jet fire, explode, or ignite/catch fire. The intrinsic nature of thermal runaway is thermal acceleration of nearby cells to form a cascading event.

3 BATTERY TUTORIAL

3.1 General

Lithium batteries are a family of cells that consist of a lithium anode (negative terminal) and a variety of different types of cathodes (positive terminal) and electrolytes [1]. Lithium batteries are grouped into two general categories: primary and secondary batteries. Primary lithium batteries are comprised of single-use cells containing metallic lithium anodes and cannot be recharged. Secondary lithium-ion batteries are comprised of rechargeable cells containing an intercalated lithium compound for the anode and cathode. In this report, nonrechargeable (primary) lithium batteries are referred to as “lithium primary” batteries (often referred to as simply “lithium” batteries in the battery industry), and rechargeable (secondary) lithium batteries are “lithium-ion” or “Li-ion” batteries.

Lithium primary batteries can be classified into several categories based on the type of electrolyte (or solvent) and cathode material used. These classifications include soluble-cathode cells, solid-electrolyte cells, and solid-cathode cells.

Soluble-cathode cells use liquid or gaseous cathode materials, such as sulfur dioxide (SO₂) or thionyl chloride (SOCl₂), that dissolve in the electrolyte or are the electrolyte solvent. These soluble cathode lithium cells are used for low to high discharge rate applications. The high-rate designs, using large electrode surface areas, are noted for their high power density and are capable of delivering the highest current densities of any active primary cell.

Solid-electrolyte cells are noted for their extremely long storage life, in excess of 20 years, but are capable of only low-rate discharge in the microampere range. They are used in applications such as

memory backup, cardiac pacemakers, and similar equipment where current requirements are low but long life is critical. This battery type was not evaluated in the programs reported here.

Solid-cathode cells are the most commonly used type of lithium primary cell. They are designed, generally, for low- to medium-rate applications such as memory backup, security devices, portable electronic equipment, photographic equipment, watches, calculators, and small lights. Although a number of different solid-cathode lithium batteries have been developed, the lithium/manganese dioxide (Li/MnO₂) battery was one of the first to be used commercially and is still the most popular. It is relatively inexpensive, has excellent shelf life, has good high-rate and low-temperature performance, and is available in coin and cylindrical cells. The lithium/carbon monofluoride (Li(CF)_n) battery is another of the early solid-cathode batteries and is attractive because of its high theoretical capacity and flat discharge characteristics. It is also manufactured in coin, cylindrical, and prismatic configurations. The higher cost of polycarbon monofluoride has affected the commercial potential of this system but it is finding use in biomedical, military, and space applications. The construction of these primary cells is similar to that of the secondary (lithium-ion) cells described next.

Secondary/lithium-ion batteries are used across a range of portable applications ranging from consumer electronics to medical technology to military systems. They are characterized by medium to high energy density and are being developed in a variety of chemistries. In a lithium-ion cell, layers of anode (copper foil coated with a specialty carbon) and cathode (typically aluminum foil coated with a lithiated metal oxide or phosphate) are separated by a microporous polyolefin film referred to as a separator. An electrolyte composed of an organic solvent and dissolved lithium salt provides the medium for lithium ion transport. A cell can be constructed by stacking alternating layers of electrodes (typical for high-rate capability prismatic cells), or by winding long strips of electrodes into a “jelly roll” configuration (typical for cylindrical cells). Lithium ions move from the anode to the cathode during discharge and are intercalated into the cathode (i.e., inserted into voids in the crystallographic structure). The ions reverse direction during charging, as shown in Fig. 1.

3.2 Chemistries

The most common type of lithium-ion cell contains an intercalated lithium (lithium alloy) anode and lithiated cobalt dioxide as cathode. These batteries are inexpensive and have medium to high energy densities, but can self-discharge (begin a thermal runaway reaction) at temperatures in the 60 °C range. Since lithium ions are intercalated into host materials during charge or discharge, there is no free lithium metal within a lithium-ion cell. Consequently, if a cell ignites due to external flame impingement or due to an internal short, “metal fire” (e.g., lithium, sodium, or magnesium) suppression equipment and techniques are neither appropriate nor cost effective for controlling the fire.

Other chemistries, principally primary chemistries, that are being actively pursued/developed by the battery industry include thionyl chloride, sulfuranyl chloride, sulfur dioxide, carbon monofluoride, and manganese dioxide. These cells have the highest energy densities (about twice that of Li-ion cells) but are more expensive based on total deliverable energy and useable life. The solid-electrode group of batteries is comprised of “specialty” type cells used primarily in the medical profession. These cells include silver, copper, iron, and lead (oxides and sulfides) chemistries. These cells are highly reliable, very expensive, and have limited current capacities. The automotive industry is aggressively pursuing higher energy density chemistries that may eventually be adopted for the commodity type usages.

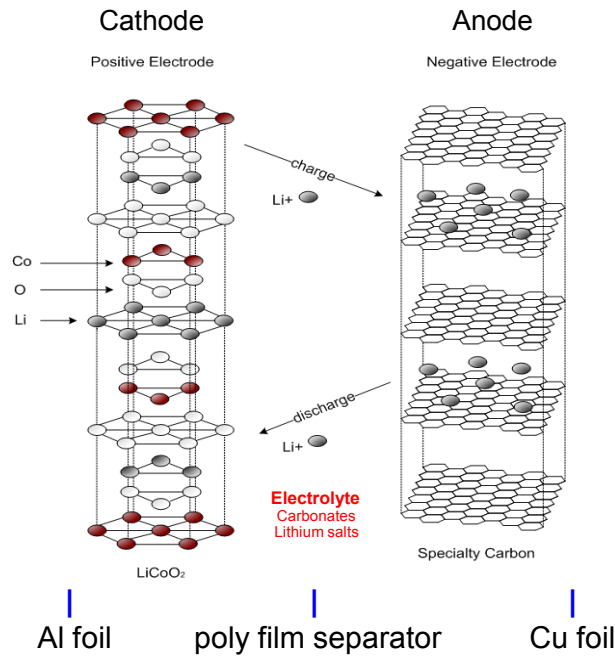


Fig. 1 — Generalized Li-ion cell components/configuration

The electrolyte in a lithium-ion cell is typically a mixture of a lithium salt dissolved in organic carbonates such as ethylene carbonate or diethyl carbonate. The compounds vary depending upon desired cell properties. For example, a cell designed for low-temperature applications will likely contain a lower viscosity electrolyte than one optimized for room temperature applications.

The flammability characteristics of common carbonates used in lithium cell electrolytes in a neat state are provided in Table 1. These characteristics apply only to liquefied carbonates. During a cell venting scenario, when the electrolyte may be released as an aerosol with partial decomposition to lower molecular weight species, both the flash point and the auto-ignition temperature may be lower.

The lithium-ion electrolyte solution contains solvated lithium ions, which are provided by lithium salts, most commonly lithium hexafluorophosphate (LiPF_6). At elevated temperatures, LiPF_6 decomposes to release hydrofluoric acid (HF) during a battery casualty if the resulting materials are exposed to moisture. The higher energy density primary cells also produce acid gases (sulfuric and hydrochloric) during high-temperature reaction processes if exposed to moisture in the air.

Table 1 — Flammability Characteristics of Typical Electrolyte Compounds

Compound	CAS Registry Number	Molecular Formula	Flash Point	Boiling Point	Auto-Ignition Temperature	Heat of Combustion
Diethyl Carbonate (DEC)	105-58-8	C ₅ H ₁₀ O ₃	25°C 77°F	126°C 259°F	445°C 833°F	-20.9 kJ/ml -5.0 kcal/ml
Dimethyl Carbonate (DMC)	616-38-6	C ₃ H ₆ O ₃	18°C 64°F	91°C 195°F	458°C 856°F	-15.9 kJ/ml -3.8 kcal/ml
Ethylene Carbonate (EC)	96-49-1	C ₃ H ₄ O ₃	145°C 293°F	248°C 478°F	465°C 869°F	-17.2 kJ/ml -4.1 kcal/ml
Ethyl Methyl Carbonate (EMC)	623-53-0	C ₄ H ₈ O ₃	25°C 77°F	107°C 225°F	440°C 824°F	-19.2 kJ/ml -4.6 kcal/ml
Propylene Carbonate (PC)	108-32-7	C ₄ H ₆ O ₃	135°C 275°F	242°C 468°F	455°C 851°F	-20.1 kJ/ml -4.8 kcal/ml
Tetrahydrofuran (THF)	109-99-9	C ₄ H ₈ O	-14°C 6°F	65°C 149°F	321°C 610°F	-31.2 kJ/ml -7.5 kcal/ml
Dimethylether	115-10-6	C ₂ H ₆ O	-41°C -42°F	-23.7°C 11°F	350°C 662°F	-51.3 kJ/ml -12.3 kcal/ml
1,3-Dioxolane	646-06-0	C ₃ H ₆ O ₂	2°C 35°F	75°C 167°F	?	-24.4 kJ/ml -5.8 kcal/ml
1,2-Dimethoxyethane (Ethylene Glycol)	110-11-4	C ₄ H ₁₀ O ₂	104°C 232°F	83°C 197.5°F	400°C 752°F	-21.3 kJ/ml -5.1 kcal/ml
Acetonitrile (Methyl Cyanide)	75-05-8	CH ₃ CN	6°C 42°F	81.6°C 179°F	524°C 975°F	-23.9 kJ/ml -5.7 kcal/ml
Thionyl Chloride	7719-09-7	SOCl ₂	?	78.8°C 174°F	?	?

Source: <http://webbook.nist.gov/chemistry/>

3.3 Cell Construction/Configuration

There are three basic lithium battery cell designs: coin shaped, cylindrical, and prismatic (Fig. 2). Coin shaped cells (sometimes referred to as button cells) are low-current cells used in watches, calculators, and remote keyless entry systems for cars, to name a few examples. They are available in many sizes and capacities, with a common variety being the 3 V manganese variety. Cylindrical cells incorporate the same design parameters that have been the standard for alkaline cells for years (A, AA, AAA, C, and D cells) with the option of spiral or bobbin internal construction. Prismatic cells include standard 9 V battery designs. A prismatic variety referred to as “pouch” cells are typically used in laptop computers.

Cell construction is a major variable affecting the severity of a battery mishap. The severity of a reaction is in part related to the buildup and release of pressure from inside the cell. Some cells have pressure relief vents and these typically produce less severe reactions than unvented cells that contain the pressure.



Fig. 2 — Typical cell designs. Top row: prismatic, cylindrical. Middle row: pouch (prismatic). Bottom row: coin.

3.4 Battery Packs

A lithium battery pack is made from two or more individual cells packaged together. The cells are connected/wired together to achieve a desired voltage and capacity. Connecting cells in parallel increases pack ampere-hour and discharge capacity, while connecting cells in series increases pack voltage. The cylindrical cell form factor 18650 is the “workhorse” of the lithium-ion battery industry and is used in a majority of commercially available battery packs. The “18” refers to the diameter of the cell and the “65” refers to the length of the cell, both in millimeters. Examples of battery packs produced with cylindrical cells are shown in Fig. 3.

In large format battery packs, cells may be connected together in series and/or in parallel to form battery modules, which may then be connected in series and/or in parallel to make larger battery packs to meet desired voltage and capacity requirements. Modules are used to facilitate different configurations and easy replacement of faulty portions of large battery packs (a module is a Lowest Replaceable Unit, LRU). Large format battery pack architecture can be significantly more complex than small consumer electronics battery packs which typically contain series connected elements consisting of two or more parallel connected cells. Many larger battery packs have built-in circuitry used to monitor charging and control the discharge cycle of the battery (i.e., shut down the battery when the charge level drops below a specified value). These large battery packs are used in the automotive industry.



Fig. 3 — Example battery packs

4 BATTERY CASUALTY CHARACTERIZATION TESTS — OVERVIEW

For U.S. Navy applications, the Navy requires that all lithium batteries are reviewed and formally approved in the context of each application. The Navy has adopted requirements and protocols for certifying lithium batteries that include Preliminary Hazard Analysis (PHA), Battery Casualty Characterization Tests (BCCT), Hazard Mitigation Tests (HMT), and a final System Hazard Analysis (SHA).

The BCCTs are typically conducted in two phases: single cell tests and all-up battery pack tests. The rationale is to quantify the reaction on a smaller, manageable scale, then increase the size and severity once the magnitude of the reaction has been bounded. A summary of the types of tests and associated parameters that make up the BCCT is provided below.

Battery casualty initiation: A key parameter of the BCCT is the method used to initiate the battery casualty. The method(s) used during the BCCT is typically determined in the PHA. For example, the most likely and most severe scenario for a lithium-ion battery results from being overcharged. Other potential initiating events include an internal manufacturer's defect, physical damage, and an external heat source.

Reaction products analysis: Tests are conducted to characterize the products released during the cell/battery casualty. A comprehensive approach is required that includes an initial qualitative study to assess the nature of the expected chemical species and relative concentration ranges. Ultimately, the products are assessed in terms of acidity, corrosiveness, toxicity, and aerosol particle composition. Real-time analysis is done via electrochemical sensors and optical methods (in situ Fourier transform infrared spectroscopy, FTIR). Samples are also collected using gas sampling canisters, sorbent tubes, and impingers. These grab samples are analyzed using a gas chromatography–mass spectrometry/infrared (GC-MS/IR) technique.

Heat release rate (HRR): The heat release rate is determined for each type/model of cell and battery. The HRR may determine whether there will be a cascading effect in a casualty. A hood calorimeter is used to make these measurements through an assessment of combustion products. This may also be done in an apparatus that allows the measurement of oxygen consumption during the casualty. When

measuring the HRR for a specific battery, in most cases there is an acceleration of the HRR, termed the peak heat release rate, PHRR.

Thermal exposures: The thermal exposure produced during the casualty (near field) is measured using both radiometers and calorimeters. These measurements provide information on exposures to items intimate with the casualty and provide an indication of the likelihood of a cascading event (reactions of adjacent batteries). “Mock collateral casualty exposure items” may be used in addition to radiometers and calorimeters to determine significant heating of local items to a casualty event.

Smoke generation: The amount of smoke/aerosols produced during the casualty is determined using an optical density meter. The measurement is typically made in the stack (hood exhaust ductwork) just below the gas sampling probe and in the test compartment.

Pressure transients: Pressure transients are recorded during these tests (both near field and far field). The pressure release may be a moderate and sustained pressure rise from low-order combustion to deflagration of battery components internal to the cell(s). The pressure release may also be sudden and abrupt stemming from a sudden failure of pressure containment of battery cell cases or battery pressure containment vessels.

Fragmentation of the cell and/or battery casing: Debris may be ejected from the article under test at high velocities. The location of flying debris (a debris map) is documented after each test. This debris may include small to large portions of the cell and/or battery casings, battery enclosures, or pressure vessel housings. Video recorded during each test is analyzed (frame by frame) to assess whether the debris is burning/flaming while it is ejected. Alternate measurement techniques include witness plates to capture the debris thrown or impact sensors. Burning incandescent debris provides a secondary ignition source that can result in fire spread and/or other battery casualties.

5 COMMERCIALY AVAILABLE BATTERY/CELL DESCRIPTIONS

The battery cells that were tested during these programs are described in Tables 2 through 5. All are commercially available cells. A number of these cells were assessed for heat release rate only in a battery pack configuration, not individually.

Table 2 — A/AA and Pouch-size Commercially Available Cells Tested

Cell Manufacturer	A	B-1	B-2	C-1	D-1	E
Type	Secondary	Secondary	Primary	Secondary	Secondary	Secondary
Form Factor	Pouch cell	AA Cell	AA Cell	18650	18650	18650
Chemistry	Li/LiCoO ₂	Li/Li _{0.5} CoO ₂	Li/SOCl ₂	Li/LiFePO ₄	Li/LiFePO ₄	Li/Li _{0.5} CoO ₂
Voltage	3.7 V	3.7 V	3.6 V	3.3 V	3.2 V	3.7 V
Capacity	3.3 Ah	0.16 Ah	2.0 Ah	1.1 Ah	1.5 Ah	2.2 Ah
Energy	12.2 Wh	0.6 Wh	7.2 Wh	3.6 Wh	4.8 Wh	8.1 Wh
Mass	95 g	19 g	18 g	39 g	46 g	48 g

Table 3 — C-size Commercially Available Cells Tested

Cell Manufacturer	F	H-1	D-2	C-2
Type	Secondary	Primary	Secondary	Secondary
Form Factor	C Cell	5/4 C Cell	5/4 C Cell	5/4 C Cell
Chemistry	Li/CF _x	Li/MnO ₂	Li/LiFePO ₄	Li/LiFePO ₄
Voltage	3.0 V	3.3 V	3.2 V	3.3 V
Capacity	5.0 Ah	6.1 Ah	3.2 Ah	1.1 Ah
Energy	15.0 Wh	20.1 Wh	10.3 Wh	3.6 Wh
Mass	42 g	71 g	82 g	70 g

Table 4 — D-size Commercially Available Cells Tested

Cell Manufacturer	K	G	H-2	B-3	B-4
Type	Primary	Primary	Primary	Primary	Primary
Form Factor	DD Cell	D Cell	D Cell	D Cell	D Cell
Chemistry	Li/CF _x	Li/SOCl ₂	Li/MnO ₂	Li/SOCl ₂	Li/SO ₂ Cl ₂ -SOCl ₂
Voltage	3.6 V	3.6 V	3.3 V	3.6 V	3.9 V
Capacity	40.0 Ah	19.0 Ah	11.1 Ah	19.0 Ah	16.5 Ah
Energy	144.0 Wh	68.4 Wh	37.0 Wh	68.4 Wh	64.4 Wh
Mass	320 g	100 g	115 g	93 g	100 g

Table 5 — Large Form and Pouch Commercially Available Single Cells Tested

Cell Manufacturer	I-1	I-2	J	I-3
Type	Secondary	Secondary	Secondary	Secondary
Chemistry (Cathode)	Lithium Nickel Cobalt Aluminum Oxide	Lithium Nickel Cobalt Aluminum Oxide	Lithium Polymer Format Lithium Cobalt Oxide	Lithium Nickel Cobalt Aluminum Oxide
Voltage	3.6 V	3.6 V	4.2 V	3.6 V
Capacity	4.0 Ah	33.0 Ah	53.0 Ah	52.0 Ah
Energy	14.4 Wh	118.8 Wh	222.6 Wh	187.2 Wh
Mass	340 g	940 g	1200 g	1000 g

6 REACTION DESCRIPTIONS (SINGLE CELL)

6.1 Initiating Events

The primary failure mode of a lithium battery is associated with a flaw or damage to the thin porous electrical insulation layer that separates the anode and the cathode (the separator). This is typically a microporous polyolefin layer 15 to 40 micrometers in thickness for the Li-ion cells and a glass or ceramic paper for oxyhalide cells. A flaw/damage to the separator can result in an internal short circuit that produces enough heat to vaporize the electrolyte and result in a boiling liquid expanding vapor explosion (BLEVE) type reaction. The separator can fail due to internal defects (production issues), physical damage (handling issues), exposure to high temperature (fire), and in the case of secondary cells, overcharging resulting in bridging of the separators. Once an internal short develops, a sudden release of stored energy can occur that may result in thermal runaway. This event can cascade to adjacent cells and throughout an entire battery pack and destroy the device the battery is serving. Fires involving lithium batteries can initiate within the product, which means that in storage, a fire can initiate deep within a battery pack or piece of equipment, beyond the influence of conventional fire protection systems.

The potential for manufacturers' defects was emphasized during the 1st Battery Safety Conference conducted November 2011 in Boston. In the presentation "Advances in System Design, Integration and Testing for Safety and Reliability," keynote speaker Dr. Brian Barnett (of TIAX LLC, a technology advancement company) presented the conclusions of an extensive study that found the probability of a manufacturer's defect is 10^{-6} . This failure rate is not bad when compared to other baseline probabilities such as electrical equipment failure (10^{-4}) and human error (10^{-2} to 10^{-3}). However, 10^{-6} is large when considering the number of cells produced per year (10^{10}) and increasing each year through wider use of these popular energy sources. This translates into the possibility of thousands of defects/failures per year.

6.2 General Types of Casualties

The experimental data suggest that the severity of a casualty reaction is a function of a number of parameters including battery size, chemistry, construction, and the charge level of the battery. In almost every battery casualty test conducted to date, the same hazardous components have been observed: flammable by-products (aerosols, vapors, and liquids), toxic gases, and flying debris (some burning), and in some instances, sustained burning of the electrolyte and casing material. The following sections provide a general terminology for describing cell level reactions.

During a runaway reaction within a cell, a significant amount of gas is produced that causes an increase in pressure within the cell housing. The mechanism of release of this pressure is dependent on the rate of the reaction and the configuration of the cell housing. For example, at a low state of charge (SOC), the event may consist of a small amount of liquid/aerosol sprayed through the overpressure vents (if available) or through a seam in the battery housing. The vented products are typically flammable and can be ignited if exposed to a flame.

At a high SOC (fully charged batteries), the venting is much more forceful and typically involves a much larger volume of liquid/aerosol. The flammable electrolyte liquid/aerosol can be ignited, forming small torch-like flames at the vent locations. During some instances, the electrolyte and battery contents may ignite with sustained burning, producing a moderate size, nonviolent fire.

In some cases, there can be a stronger, sometimes substantial, pressure pulse associated with this electrolyte release. Depending on the battery construction, flaming debris can be expelled (sprayed or thrown from the battery). Occasionally, the pressure release ports fail to operate correctly (or the battery is not equipped with vent ports), causing a buildup of pressure inside the cell casing until the casing fails.

When this occurs, the cell explodes, expelling the contents throughout the test chamber, producing a measurable pressure pulse. These explosive type reactions can vary from firecracker type bangs to as loud as shotgun blasts or greater. As with the slower venting scenarios, if the contents are flammable, the aerosol emitted can be ignited. Since the entire electrolyte content of the battery is released at once in these explosive type reactions, a substantial fireball occurs if the products are ignited. The ejected burning or incandescent material may start nearby fires or ignite the vapors being vented from the cell/battery. In these studies, the lithium-ion and solid cathode lithium cells use a flammable electrolyte.

In summary, single cell reactions can be described using the following six terms: vent, smoker, flare, burner, explosive, and fireball. Figure 4 shows photographs of all these scenarios except venting. Video clips are presented in the Appendix.

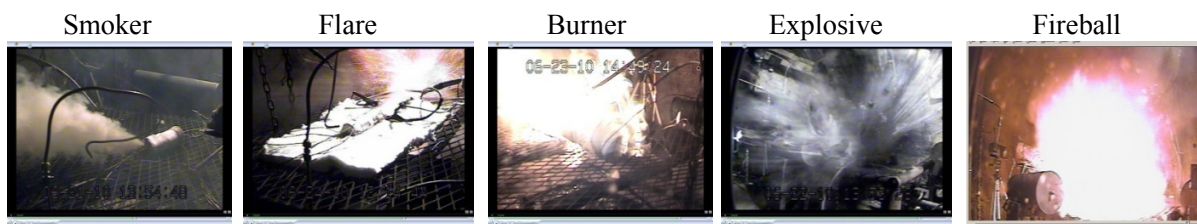


Fig. 4 — Single cell reaction classifications

6.3 Observed Cell Casualties

The reactions observed in the commercially available cells are described in Tables 6 through 9. In general, the smaller, lower capacity solid-cathode cells typically vented and/or smoked and the medium to higher capacity cells (specifically the oxyhalides) either ignited and burned or exploded.

Intuitively, one expects the type of reaction to be a function of the amount of energy contained in the cell at the time of the event. If this is the case, the type of reaction should be a function of both the battery capacity and the state of charge at the time of the event. Based on a very limited data set (i.e., not a statistically valid set of data), it appears that the threshold between a venting and a flaming reaction lies in the 10 to 20 Wh range. Battery pack configurations can significantly alter these single cell results.

Table 6 — A/AA/Pouch-size Commercially Available Cell Reaction Descriptions





Cell Manufacturer	A	B-1	C-1	E
Type	Secondary	Secondary	Secondary	Secondary
Form Factor	Pouch cell	AA Cell	18650	18650
Chemistry	Li/CoO ₂	Li/Li _{0.5} CoO ₂	Li/FePO ₄	Li/Li _{0.5} CoO ₂
Voltage	3.7 V	3.7 V	3.3 V	3.7 V
Capacity	3.3 Ah	0.16 Ah	1.1 Ah	2.2 Ah
Energy	12.2 Wh	0.6 Wh	3.6 Wh	8.1 Wh
SOC	100%	100%	100%	100%
Initiator	Calrod heater	Calrod heater	Calrod heater	Calrod heater
Reaction Type	Moderate venting	Moderate venting	Moderate venting	Venting/small flames
Reaction Description	Moderate venting for 1:12, no flames	Moderate venting for 0:22 followed by nonviolent rupture	Moderate venting for 0:48 followed by violent rupture, no flames	Moderate venting with small flames, short duration event (0:15)
Reaction Photograph				

Table 7 — C-size Commercially Available Cell Reaction Descriptions




Cell Manufacturer	F	H-1	D-2
Type	Secondary	Primary	Secondary
Form Factor	C Cell	5/4 C Cell	5/4 C Cell
Chemistry	Li/CF _x	Li/MnO ₂	Li/LiFePO ₄
Voltage	3.0 V	3.3 V	3.2 V
Capacity	5.0 Ah	6.1 Ah	3.2 Ah
Energy	15.0 Wh	20.1 Wh	10.3 Wh
SOC	100%	100%	100%
Initiator	Calrod heater	Calrod heater	Calrod heater
Reaction Type	Moderate flaming	Flare with sparks	Vent/Smoker
Reaction Description	3:45 venting, rupture with sparks, 1:30 burning	0:18 Roman candle, 0:57 moderate burning	Moderate venting of about one minute
Reaction Photograph			

Table 8 — D-size Commercially Available Cell Reaction Descriptions


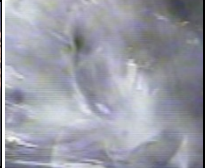
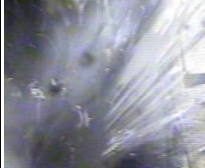





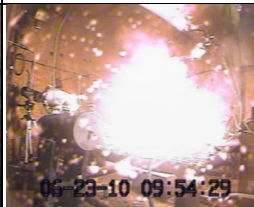
Cell Manufacturer	H-2	B-3	B-4	K	G
Type	Primary	Primary	Primary	Primary	Primary
Form Factor	D Cell	D Cell	D Cell	DD Cell	D Cell
Chemistry	Li/MnO ₂	Li/SOCl ₂	Li/SO ₂ Cl ₂	Li/CF _x	Li/SOCl ₂
Voltage	3.3 V	3.6 V	3.9 V	3.6 V	3.6 V
Capacity	11.1 Ah	19.0 Ah	16.5 Ah	40.0 Ah	19.0 Ah
Energy	37.0 Wh	68.4 Wh	64.4 Wh	144.0 Wh	68.4 Wh
SOC	100%	100%	100%	100%	100%
Initiator	Calrod heater	Calrod heater	Calrod heater	Calrod heater	Propane flame
Reaction Type	Flare	Explosion	Explosion	Vigorous flaming	Rupture
Reaction Description	Fast venting with flaming combustion, long duration event (1:00)	Explosion, small fireball, no residual burning	Explosion, small fireball, no residual burning	Violent rupture with vigorous burning	Cell ruptured sometime during test (unnoticeable)
Reaction Photograph					

Table 9 — Large Form and Pouch Cell Reaction Descriptions

Manufacturer	I-1	I-2	J	I-3
Type	Secondary	Secondary	Secondary	Secondary
Chemistry	Lithium Nickel Cobalt Aluminum Oxide	Lithium Nickel Cobalt Aluminum Oxide	Lithium Polymer Format Lithium Cobalt Oxide	Lithium Nickel Cobalt Aluminum Oxide
Voltage Capacity Energy	~4 V ~5 Ah ~20 Wh	~4 V ~32 Ah ~128 Wh	~4 V ~53 Ah ~200 Wh	~4 V ~52 Ah ~208 Wh
SOC	100%	100%	100%	100%
Initiator	Calrod heater	Calrod heater	Calrod heater	Calrod heater
Reaction Type	Vent/Smoker	Smoker/flare	Fireball	Fireball
Reaction Description	Moderate venting for several minutes, no ignition/flames	Moderate venting that was ignited manually. Once ignited, flames jetted from end for several minutes.	Cell produced a 4–5 ft diameter fireball for about 30 seconds	Cell produced a 4–5 ft diameter fireball for about 30 seconds
Photograph				

6.4 SOC Effects on Reaction Types (Li-Ion Only)

A quasi-parametric assessment of the effects of SOC on cell level reactions was conducted on the large form and pouch cells. A detailed description of the reactions is provided in Table 10 and a summary in Table 11.

The lithium nickel cobalt aluminum oxide cells (~20 Wh, manufacturer I-1) produced significant amounts of smoke with very little flame and little if any HRR, regardless of SOC. These cells are classified as “vent/smokers.” The same chemistry but larger capacity cells (~128 Wh, manufacturer I-2) vented/smoked at a low SOC (20%) but caught fire and readily burned at a higher SOC (100% and overcharged). These cells are considered “flares/burners.” The lithium polymer format lithium cobalt oxide cells (~200 Wh, manufacturer J) burned slowly at a low SOC (20%) but produced fireballs at higher charge levels and are considered “burners” and “fireballs” depending on the SOC. The lithium nickel cobalt aluminum oxide cells (~200 Wh) exploded (hydraulic/pneumatic) at a low SOC (20%) but produced fireballs at higher charge levels and are considered “explosive” and “fireballs” depending on the SOC. All cells reacted more violently when initiated by deliberate overcharging.

As shown in Tables 10 and 11, the reaction severity tends to increase with the SOC of the battery. This is expected, since the higher the SOC, the more energy available in the cell to generate heat,

vaporize the electrolyte, and rupture the cell casing. As noted in Section 6.3, there appears to be a threshold between a venting and a flaming reaction in the 10 to 20 Wh range. Again, battery pack configurations can significantly alter these single cell results.

Although reaction severity increases with SOC, the HRR is not necessarily a function of the SOC. At lower SOC, there is less tendency for the cell to burn, thus less HRR; but if ignited at low SOC, the total HRR is about the same as at high SOC. This is shown in Section 8.2.

Table 10 — Large Form and Pouch Cell Reaction Descriptions for Various SOCs







Battery/ Cell Classification	20% SOC	100% SOC	Overcharged
<p>I-1</p> <p>Vent/ Smokers</p> <p>~14.4 Wh 340 g</p>	<p>Battery vented (slow)/no fire</p> <p>PHRR <5 kW Avg. HRR <5 kW Fire duration – NA</p> 	<p>Battery vented (moderate)/no fire (similar to previous test)</p> <p>PHRR <5 kW Avg. HRR <5 kW Fire duration – NA</p> 	<p>Battery jetted aerosol/smoke from one end for about 1 minute, no fire</p> <p>PHRR <5 kW Avg. HRR <5 kW Fire duration – NA</p> 
<p>I-2</p> <p>Burners/ Fireballs</p> <p>~120 Wh 940 g</p>	<p>Battery vented prolonged dense aerosol/no fire</p> <p>PHRR <5 kW Avg. HRR <5 kW Fire duration – NA</p> 	<p>Battery vented gases that were ignited by sparker followed by prolonged sustained burning</p> <p>PHRR <5 kW Avg. HRR <5 kW Fire duration – NA</p> 	<p>Battery produced a fireball (4–5 ft diameter) followed by sustained burning from both ends of the battery</p> <p>PHRR 120 kW Avg. HRR 50 kW Fire duration 40 sec</p> 

Table 10 (cont.) — Large Form and Pouch Cell Reaction Descriptions for Various SOCs



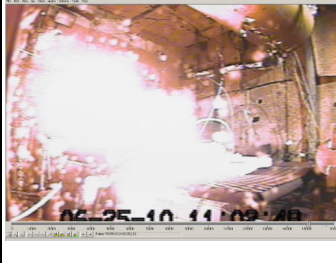

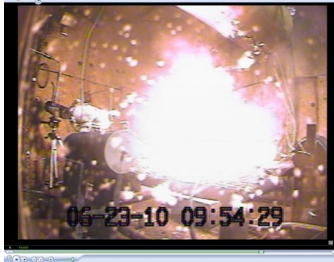
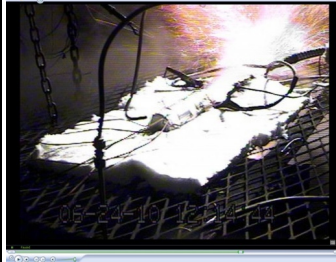
Battery/ Cell Classification	20% SOC	100% SOC	Overcharged
<p>J</p> <p>Burners/ Fireballs</p> <p>~222 Wh 1200 g</p>	<p>Battery vented and burned slowly</p> <p>PHRR 55 kW Avg. HRR 27 kW Fire duration 80 sec</p> 	<p>Battery reacted producing a fireball (4–5 ft diameter) followed by sustained burning (smaller size)</p> <p>PHRR 120 kW Avg. HRR 50 kW Fire duration 35 sec</p> 	<p>Battery jetted aerosol then instantaneously ignited, producing fireball greater than 5 ft diameter</p> <p>PHRR 135 kW Avg. HRR 65 kW Fire duration 10 sec</p> 
<p>I-3</p> <p>Explosive/ Fireballs</p> <p>~190 Wh 1000 g</p>	<p>Sudden violent rupture spreading debris throughout the chamber, no fire, limited smoke</p> <p>PHRR <5 kW Avg. HRR <5 kW Fire duration – NA</p> 	<p>Battery violently ruptured into a fireball (4–5 ft diameter) followed by sustained burning (smaller size)</p> <p>PHRR 92 kW Avg. HRR 45 kW Fire duration 22 sec</p> 	<p>End blew off of battery, flames jetted (~ 5 ft) from open end</p> <p>PHRR 98 kW Avg. HRR 50 kW Fire duration 25 sec</p> 

Table 11 — Summary of Large Form and Pouch Cell Reactions for Various SOC's

Cell	SOC	Reaction Description
I-1	20%	Minor off-gassing and contribution to heat release rate.
I-1	100%	Minor off-gassing and contribution to heat release rate.
I-2	20%	Minor off-gassing and contribution to heat release rate.
I-2	100%	Significant off-gassing and moderate contribution to heat release rate.
I-2	100%+	Major off-gassing and significant contribution to heat release rate, as cells jetted violently and exited the containment.
J	20%	Significant off-gassing and contribution to heat release rate. Surprisingly little damage to cell assemblies.
J	100%	Significant off-gassing and contribution to heat release rate. Surprisingly little damage to cell assemblies.
I-3	20%	Off-gassing and moderate contribution to heat release rate.
I-3	100%	Significant off-gassing and contribution to heat release rate. Battery left test table.
I-3	100%+	Major off-gassing and significant contribution to heat release rate, as cells jetted violently and exited the containment.

7 REACTION PRODUCTS TESTING AND RESULTS (SINGLE CELL)

7.1 Reaction Products Test Description

Reaction products were measured and documented using a range of standard analytical techniques. The reaction products tests were conducted in a 5 m³ (177 ft³) enclosure at the Naval Research Laboratory Chesapeake Bay Detachment test site located in Chesapeake Beach, Maryland. The casualty was typically initiated by heating the exterior of the cell using a cartridge heater (Calrod heater) fastened to the side of the cell. The products were assessed in terms of acidity, corrosiveness, and toxicity. Real-time analysis was done via electrochemical sensors and optical methods. Samples were also collected using gas sample canisters, sorbent tubes, and impingers. The collected samples were analyzed using gas chromatography–mass spectrometry/infrared (GC-MS/IR).

7.2 Reaction Products for Cells at 100% SOC

7.2.1 Reaction Products of Commercially Available Cells

The reaction products measured for the commercial cells are listed in Tables 12 through 14. When the cell vents (without ignition), the majority of the products released are aerosol electrolyte constituents (e.g., carbonates or oxyhalides). A significant amount of these organic solvent gases and aerosols have flammable constituents. This aerosol mixture was not further characterized in these tests, but a reaction products test chamber could be equipped with an oxygen analyzer and an explosive gas meter to measure the Lower Explosive Limit (LEL) of the gases within the chamber, and other equipment to measure aerosol concentrations (the flammability of aerosols are dependent on particle size and number density). In some venting scenarios, the carbonates break down upon release to produce high levels of carbon

dioxide (CO₂) and carbon monoxide (CO). When the cell burns during a casualty, the electrolyte burns fairly efficiently, producing primarily CO₂ as the by-product, as determined by in situ gas analyzers.

The production of acid gas is directly related to the cell chemistry (and appears to be related to cell capacity). Cells that contain sulfur produce sulfuric acid, cells that contain fluorine produce hydrofluoric acid, and cells that contain chlorine produce hydrochloric acid. There is not enough data to develop a quantitative relationship between cell energy and the amount of acid gas produced, but for a given cell chemistry, the amount of acid gas produced is expected to be directly proportional to the cell energy.

Table 12 — A/AA/Pouch-size Commercially Available Cell Reaction Products

Compounds	A Pouch cell 100% SOC	B-1 AA cell 100% SOC	C-1 18650 100% SOC	E 18650 100% SOC
	mg	mg	mg	mg
Butyrolactone				
Tetrahydrofuran			50	
Propene	175	24	5	
Benzene				
Hexafluoropropene				
Isoprene			10	
Methyl Carbonate			350	7
1,3 Butadiene	20			
Chlorobenzene			50	
1,2 Dimethoxyethane			10	
Isobutene	90			
Ethanol		33		
CO ₂	5500			3300
CO	825			675
SO ₂				37
Hydrochloric Acid				
Hydrofluoric Acid				
Propylene Carbonate				
1,2 Methoxyethane				
Dimethyl Carbonate	2200	825	1210	156
Ethylene Carbonate	2000		660	238
1,2 Dimethoxyethane	110			
Total (g)	10.9	0.9	2.3	4.4
Initial Mass of Cell (g)	95	19	39	48
Percentage (%)	12	5	6	9

Table 13 — C-size Commercially Available Cell Reaction Products

Compounds	F C Cell 100% SOC	H-1 5/4 C Cell 100% SOC	D-2 5/4 C Cell 100% SOC
	mg	mg	mg
Butyrolactone	305		
Tetrahydrofuran	10		
Propene	13		5
Benzene	11		
Hexafluoropropene	7		
Isoprene	11		31
Methyl Carbonate		12	305
1,3 Butadiene			
Chlorobenzene			
1,2 Dimethoxyethane			
Isobutene			
H ₂ SO ₄			88
CO ₂	20350	14301	12310
CO	1232	2695	1865
SO ₂	77	105	
Hydrochloric Acid			280
Hydrofluoric Acid	92		140
Propylene Carbonate		220	
1,2 Methoxyethane		1513	
Dimethyl Carbonate			75
Ethylene Carbonate			
1,2 Dimethoxyethane			
Carbonyl Sulfide			269*
Dimethyl Sulfide			406*
Ethyl Methyl Sulfide			113*
Total (g)	22.1	18.9	15.9
Initial Mass of Cell (g)	42	71	82
Percentage (%)	53	27	19

* Reaction produced moderate amounts of sulfide compounds

Table 14 — D/DD-size Commercially Available Cell Reaction Products

Compounds	H-2	B-3	B-4	K
	D Cell 100% SOC	D Cell 100% SOC	D Cell 100% SOC	DD Cell 100% SOC
	mg	mg	mg	mg
Butyrolactone				
Tetrahydrofuran	1752			
Propene	65			
Benzene	18	7	3	
Hexafluoropropene				
Isoprene				
Methyl Carbonate				15
1,3 Butadiene	13			
Chlorobenzene	27			
1,2 Dimethoxyethane	700			
Isobutene	27			
H ₂ SO ₄		1050	390	600
CO ₂	13750	26000	27500	
CO	2640	413	330	3465
SO ₂	105	4455	4125	4950
Hydrochloric Acid		2200	1403	440
Hydrofluoric Acid				1193
Propylene Carbonate	633			
1,2 Methoxyethane				
Dimethyl Carbonate				
Ethylene Carbonate				
1,2 Dimethoxyethane	3080			
Carbon Tetrachloride		26	21	
Total (g)	22.8	34.2	31.1	10.7
Initial Mass of Cell (g)	115	93	100	320
Percentage (%)	20	37	31	3

7.2.2 Reaction Products of Large Form and Pouch Lithium-Ion Cells

The reaction products measured for the large form and pouch lithium-ion cells are listed in Table 15. When the cell vents (no ignition), the majority of the products released are electrolyte constituents (i.e., carbonates). Therefore, a significant amount of the gas has flammable constituents. In some instances, the carbonates break down upon release to produce high levels of CO and CO₂, especially under thermal runaway conditions at higher state of charge. When the cell burns, the electrolyte burns fairly efficiently, producing primarily CO₂ and water as the by-products.

Large form oxyhalide catholyte (primary) cells were not tested in these studies. The larger quantities of oxyhalide catholyte in these cells would likely produce higher levels of sulfur- and chloride-based compounds during venting and cell failures.

Table 15 — Large Form and Pouch Cell Reaction Products

Compound	I-1	I-2	J	I-3
	100% SOC (mg)	100% SOC (mg)	100% SOC (mg)	100% SOC (mg)
1,3 Butadiene	7	95	125	
1,4 Dioxane	34		25	
Benzene		145	25	43
Bromomethane	50	90	125	
CO ₂	1265	8800	11825	13780
Chloromethane			48	37
Dimethyl Carbonate	1870	4125	4675	5225
Ethylbenzene		25	15	
Ethylene	94	495	1100	1100
Ethylene Carbonate	1018	1870	4235	4540
Hydrobromic Acid		6		
Hydrochloric Acid			60	60
Hydrofluoric Acid	99	55	630	550
Methane	550	2750	1375	1515
Methyl Butyrate	5500	18370	16225	
Methyl Fluoride	17	61	66	66
Phosphoric Acid	46		75	85
Propene	255	1000	1500	55
Styrene	37	65	10	
SO ₂			1100	
Tetrahydrofuran		34	10	
Toluene	36	65	10	
* Total (g)	11	38	43	27
Initial Mass of Cell (g)	340	940	1200	1000
Percentage (%)	3	4	4	3

* These totals do not include the CO₂ values above, which would dramatically increase these totals.

7.3 SOC Effects on Reaction Products

The SOC of the cell affects the type of reaction. Low SOC cells tend to vent pneumatically or hydraulically. At higher SOC, cells tend to ignite. When the cell vents (with no ignition), the majority of the products released are electrolyte constituents (e.g., carbonates) or partial thermal breakdown products, including hydrogen and methane. A significant amount of these reaction products are flammable. In some instances, the carbonates break down upon release to produce high levels of CO₂ and CO. When the cell burns, the electrolyte burns fairly efficiently, producing primarily CO₂ and water vapor as the by-products.

Acid gas production appears to be higher in the burning reactions, and consequently, tends to be higher for higher SOC lithium batteries. Higher SOC also results in greater energy dissipation and heating or potential for incandescent materials such as metal foils and carbonaceous compounds being ejected.

7.4 Reaction Products at Low Oxygen Levels

At lower oxygen concentration, cells are less likely to ignite; they tend to vent only, and the reaction products are as previously described for venting reactions. For example, the H-1 cell at 21% oxygen vented and burned. At 12% oxygen, the cell only vented and sparked but did not ignite.

7.5 Acid Gas Production

The acid gas production is directly related to the cell chemistry, as noted above. For lithium oxyhalide catholyte cells, the acid gas formation can overwhelm the available water in the local atmosphere, or the addition of water vapor will increase the acid formation under these conditions.

7.6 Gas Volume Production

The volume of gas produced by each cell was estimated using the ideal gas law and the steady-state pressure in the test chamber after each test. These chamber pressures and associated gas volumes are listed in Table 16. The term steady-state used in the table means that these were the conditions measured after the gas temperature in the chamber enclosure had cooled back to ambient conditions. In many cases, the chamber pressure spiked higher than the values listed in Table 16 due to expansion of the gases as the temperature increased in the chamber during the reaction. For some oxyhalide cell chemistries, the apparent gas volume expansion will not make sense until the reaction products that are gaseous at high temperature fall below their boiling point and liquefy or solidify. Examples are lithium sulfide, lithium chloride, and aluminum chloride.

Additional work is needed to use these characterizations and this characterization technique. The electrolyte percentage in lithium-ion cells, for instance, is typically within 3% of the cell mass. For cells that vary by an order of magnitude in mass (cell E versus cell I-1) in a fixed volume chamber at similar SOC, statistically the final pressure is the same.

Table 16 — Cell Level Gas Production Quantities

Cell	SOC	Steady-State Pressure (atm)	Steady-State Gas Volume (m ³)
A Pouch Cell	100%	1.00	Neg.
B-1 AA Cell	100%	1.00	Neg.
C-1 18650	100%	1.00	Neg.
E 18650	100%	1.05	0.017
F C Cell	100%	1.10	0.034
H-1 5/4 C Cell	100%	1.08	0.027
H-2 D Cell	100%	1.13	0.044
B-3 D Cell	100%	1.06	0.020
B-4 D Cell	100%	1.15	0.051
K DD Cell	100%	1.25	0.085
I-1 Large Form	100%	1.00	Neg.
I-2 Large Form	100%	1.05	0.017
J Pouch Cell	100%	ND	ND
I-3 Large Form	100%	1.5	0.170

ND = no data; Neg. = negligible effects

8 HEAT RELEASE RATE TESTS AND RESULTS (SINGLE CELL)

8.1 Heat Release Rate Test Description

Heat release rate and related parameters were characterized on the U.S. Navy test ship ex-USS *Shadwell* located in Mobile, Alabama [2]. The heat release rate of the cell casualty was determined using a hood calorimeter. Four other types of measurements were made during the HRR tests: unburned hydrocarbons, smoke production (obscuration), thermal exposures (radiant and total), and overpressures. The energy contained in the unburned hydrocarbons was added to the HRR measured by the hood. Smoke production was assessed using an optical density meter installed in the compartment. The thermal exposures were determined by mapping the radiant and total heat fluxes in close proximity to the cell. Infrared and radiometric imaging cameras were also used to quantify hot gas release that may impinge on nearby objects. The overpressures were measured both local to the cell and globally in the test compartment.

The tests were conducted under a 1 MW hood calorimeter. The hood calorimeter was instrumented for gas temperature, gas velocity (volumetric flow rate), and typical fire/combustion gas concentrations (CO, CO₂, and O₂). The water vapor constituent of the combustion process was removed with an ice-water cold trap. In addition, explosive gas concentrations (Lower Explosive Limit) and potentially toxic and flammable gases (e.g., SO₂ and volatile organic compounds, VOCs) were measured. The test compartment and area below the hood were instrumented for temperature (five thermocouple trees), pressure, and smoke obscuration (using three optical density meters). The area around the test specimen/battery was instrumented to measure any localized exposures produced by the battery casualty. A computerized data acquisition system was used to collect and record the measurements during the test at a rate of one scan per second (1 Hz).

8.2 Heat Release Rate Test Results

8.2.1 HRRs of Commercially Available Cells

In general, the heat release rates of the commercially available cells were too low to measure using the 1 MW hood calorimeter on the ex-USS *Shadwell*. In future assessments, the heat release rates of the small commercial cells will be measured using a recently installed smaller hood calorimeter with a range from 10 to 100 kW.

Although the HRRs of the smaller commercial cells could not be measured using the 1 MW hood calorimeter, an estimation of the heat energy content of these cells was made based on the temperatures measured in the test chamber during reaction products testing at CBD. Specifically, the energy released was estimated by multiplying the mass of the gas in the CBD test chamber, an average specific heat for the gas(es), and the increase in temperature that occurred in the chamber during reaction. The resulting energies are listed in Table 17. The mean HRRs were determined by dividing the total energy released, by the duration of the reaction (determined based on measurements and visual observations). These values are also shown in Table 17.

Table 17 — HRRs of Commercially Available Cells

Cell	SOC	Delta-T (°C)	Mean HRR (kW)	Duration (sec)	Energy Released (kJ)
A Pouch Cell	100%	Neg.	Neg.	Neg.	Neg.
B-1 AA Cell	100%	Neg.	Neg.	Neg.	Neg.
C-1 18650	100%	Neg.	Neg.	Neg.	Neg.
E 18650	100%	5	0.4	70	27.5
F C Cell	100%	50	3.0	90	275
K DD Cell	100%	30	5.5	30	165
H-1 5/4 C Cell	100%	36	3.3	60	200
H-2 D Cell	100%	131	6	120	720
B-3 D Cell	100%	85	> 470	< 1	470
B-4 D Cell	100%	60	> 330	< 1	330

Neg. = negligible

8.2.2 HRRs of Large Form and Pouch Cells

The HRR data for large form and pouch cells are provided in Table 18. The cells were tested at three SOC: 20%, 100%, and overcharged (listed in the table as 100%+). The cell/SOC combinations that show negligible HRRs produced venting reactions with little or no burning. These were measured using a special-purpose smaller hood and lower air flow interfaced to the 1 MW hood instrumentation. Special gas collection and air flow would be needed to achieve measureable HRRs and PHRRs for moderate size single cells of lithium primary (with organic) and lithium-ion cells.

Table 18 — HRRs of Large Form and Pouch Cells

Cell	SOC	Peak HRR (kW)	Mean HRR (kW)	Duration (sec)	Energy Released (MJ)
I-1	20%	Neg.	Neg.	-	-
I-1	100%	Neg.	Neg.	-	-
I-1	100%+	Neg.	Neg.	-	-
I-2	20%	Neg.	Neg.	-	-
I-2	100%	Neg.	Neg.	-	-
I-2	100%+	50	~15	40	600
I-3	20%	Neg.	Neg.	-	-
I-3	100%	45	~10	22	220
I-3	100%+	50	~15	25	375
J	20%	27	~10	80	800
J	100%	50	~25	35	875
J	100%+	50	~50	25	1250

Neg. = negligible; - = Could not be accurately determined

9 HEAT RELEASE RATE TESTS AND RESULTS (GROUPS OF CELLS)

9.1 Burning Characteristics of Commercially Available Battery Packs/Modules

The commercially available battery packs/modules that were tested are described in Table 19 and the burning characteristics are summarized in Table 20. The first notable observation during testing was that the packs/modules reacted differently compared to the single cell tests. Specifically, except for the iron phosphate cells (discussed below), all the packs/modules produced burning reactions, while many of the single cells just vented and never caught fire. In addition, during almost every unmitigated pack/module test, all the cells in the module reacted and the casing materials were completely consumed.

Table 19 — Commercially Available Battery Packs Tested

No. of Cells	10	10	24	63	32
Cell Type	D Cell	D Cell	18650	18650	5/4 C Cell
Manufacturer	H-2	Li-SO ₂ *	E	E	H-1
Type	Primary	Primary	Secondary	Secondary	Primary
Voltage	27 V	27 V	30 V	26 V	24 V
Capacity	11.1 Ah	15.0 Ah	7.2 Ah	21.0 Ah	24.4 Ah
Energy	300 Wh	405 Wh	207 Wh	540 Wh	586 Wh
No. of Cells	90	6	4	4	
Cell Type	Li/MnO ₂ *	Pouch	18650	26650	
Manufacturer		A	C-1	C-2	
Type	Primary	Secondary	Secondary	Secondary	
Voltage	24 V	22.2 V	13.2 V	13.2 V	
Capacity	30.0 Ah	3.85 Ah	1.1 Ah	2.3 Ah	
Energy	720 Wh	85.5 Wh	14.5 Wh	30.4 Wh	

* These cells were not tested as single cells

Table 20 — Commercially Available Battery Pack HRRs



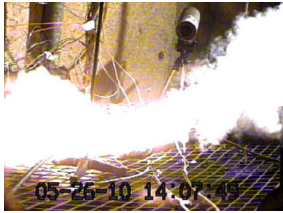
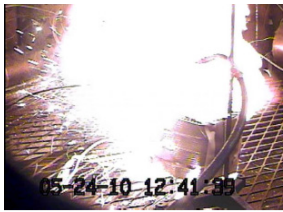





Pack/ Module Mfr. or Type	No. of Cells	Peak HRR (kW)	Mean HRR (kW)	Duration (sec)	Total Energy Released (MJ)	Fire Photograph
E	1 pack of 24	120	~35	60, 200	6.9	
	16 packs of 24	240	~150	560	85.0	
E	2 packs of 63	185	~60	100, 350	21.2	
H-1	1 pack of 32	135	~35	120, 320	11.4	
H-2	1 pack of 10	125	~50	250	13.2	
	2 packs of 10	115	~50	240, 540	25.5	
	3 packs of 10	165	~90	100, 350	32.5	
	10 packs of 10	inconclusive				
LiMnO₂	1 pack of 90	130	~60	120, 120	14.2	

Table 20 (cont.) — Commercially Available Battery Pack HRRs

Pack/ Module Mfr. or Type	No. of Cells	Peak HRR (kW)	Mean HRR (kW)	Duration (sec)	Total Energy Released (MJ)	Fire Photograph
Li-SO ₂	1 pack of 10	35	20	300	6.0	
C-1	1 pack of 4 18650 cells	<5	Neg.	100, 350	Neg.	
C-2	1 pack of 4 26650 cells	<5	Neg.	100, 350	Neg.	
A	1 pack of 6 pouch cells	10	~5	175	0.9	

Neg. = negligible

The pack/module burning characteristics presented in Table 20 are the most severe measured during testing (for that specific set of conditions). There were many instances when the same test was conducted multiple times and produced significantly different results each time. Specifically, the heat release rate histories showed dramatic differences (i.e., lower intensity, longer duration burns sometimes); however, the total thermal energy released was typically in good agreement across the repeated tests.

An example of HRR variation is provided in Fig. 5, which shows the heat release rate histories of two tests conducted with two 63-cell 18650 (manufacturer E) Li/Li_{0.5}CoO₂ battery packs/modules at 100% SOC. The left graph shows a lower intensity (105 kW PHRR), longer duration event and the right graph shows a higher intensity (190 kW PHRR), shorter duration event. The two tests were conducted with identical conditions. The propagation from one pack to the receptor pack can be seen to initiate in

the slight double spike midway through the event. This transition (two distinct HRR contributions) is more clearly seen for the 20% SOC event in Fig. 9.

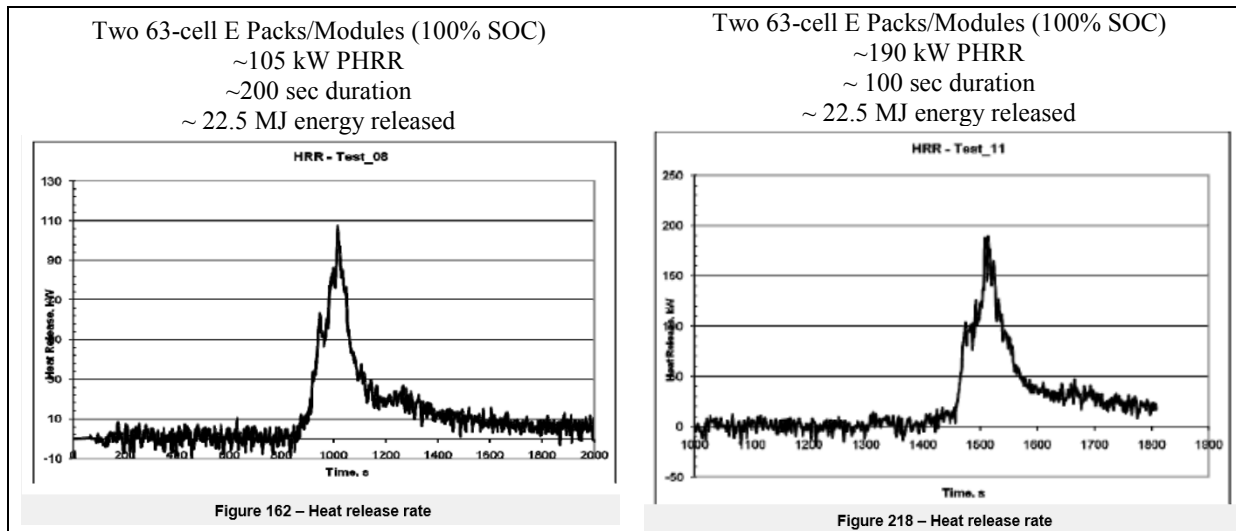


Fig. 5 — Example of variations in burning characteristics for identical tests

A typical single pack HHR plot is provided in Fig. 6. The plot shows a single spike representing the period during which all the cells within the pack vent and ignite. This period typically lasts 1 to 2 minutes, depending on the type and number of cells within the pack. After this rapid-growth-rate, high-intensity burning period, the reaction then decays to a small/steady fire that lasts 3 to 5 minutes as the combustible packaging, circuit boards, and wiring (insulation) is consumed.

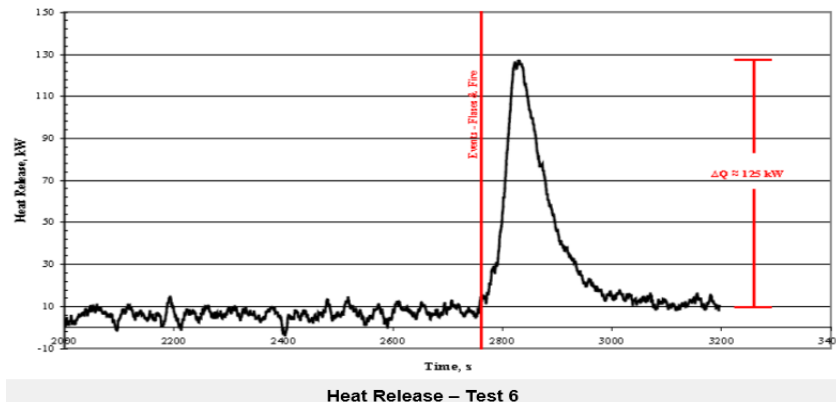


Fig. 6 — Typical HRR history for a single pack/module of lithium primary cells

For multiple packs/modules, the HRR history can have a single spike or multiple spikes, depending on how quickly the fire spreads to the adjacent pack (and the level of communication between packs). A typical multiple pack HRR plot with multiple spikes is shown in Fig. 7. The multiple spikes indicate the fire spreading to adjacent packs. The time between the spikes appears to be loosely related to the thermal inertia of the packaging. For example, the time between spikes is typically greater for the E and H-2 packs due to the thickness of the hard plastic battery case. Conversely, the time between spikes is shorter and typically less pronounced for thinner battery cases such as the shrink wrap used on the E battery packs/modules. In any case, after all the cells have reacted, the fire decays to a small/steady fire that lasts 3 to 5 minutes as the combustible packaging, circuit boards, and wiring (insulation) are consumed.

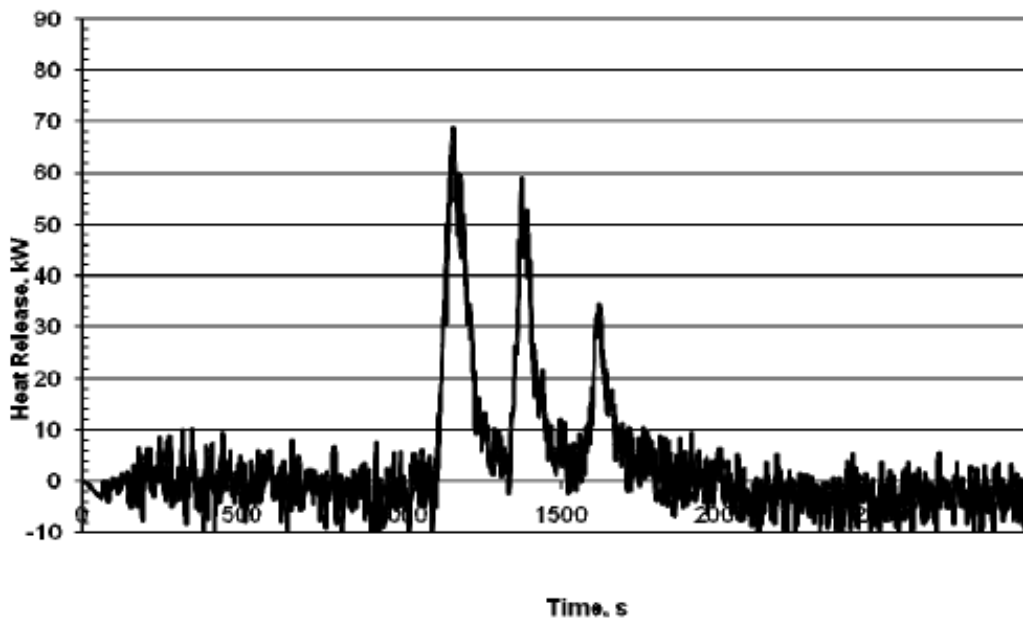


Fig. 7 — Typical HRR history for a group of packs/modules

As noted above, the phosphate-based lithium-ion packs/modules were the only ones tested that did not readily react to consume all the cells in the pack. Four tests were conducted with C-1 and C-2 battery packs (two 1100 mAh and two 2300 mAh). The results were similar for each of the four tests. In short, a single cell within each pack was heated until the cell achieved thermal runaway, but the reaction never spread to any of the adjacent cells. Figure 8 shows one of these packs being tested. Only one cell in the pack reacted.



Fig. 8 — Typical phosphate-based pack/module (C-1) under test

9.2 SOC Effects on Combustion Energy Released

Although the type of reaction, venting versus flaming, appears to be a function of SOC at the single cell level, the amount of combustion energy released during a burning reaction (the most common reaction at the pack/module level) appears to be constant regardless of SOC. An example of this is shown in Fig. 9. The left graph shows the HRR of two 63-cell E packs at 20% SOC and the right graph shows the HRR of two 63-cell E packs at 100% SOC. Although the peaks and the durations are different, the total combustion energy released during the two reactions is essentially identical (~22.5 MJ).

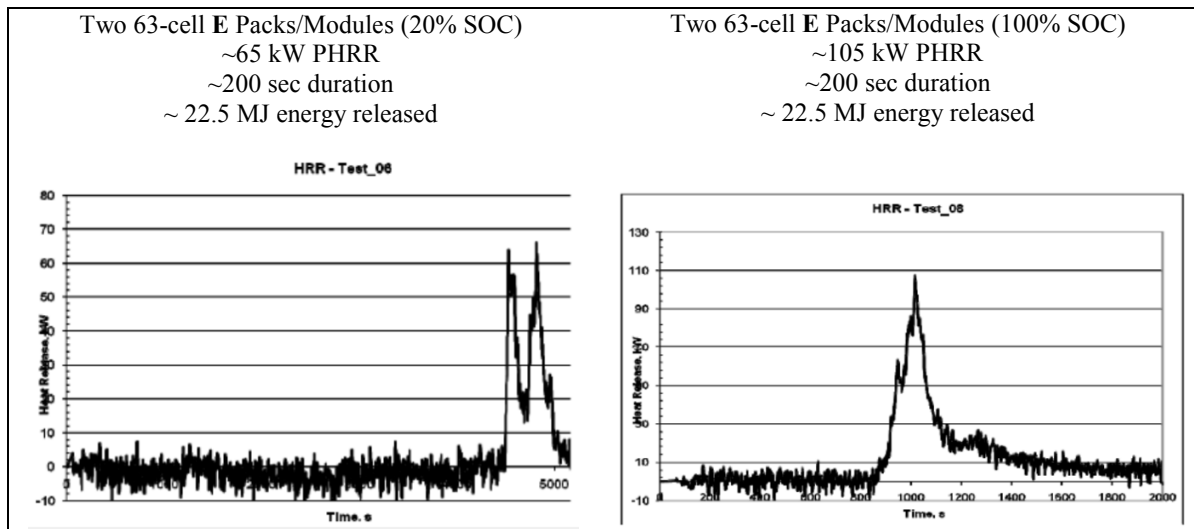


Fig. 9 — Example of two tests with equal amounts of energy released

9.3 Combustion Energy as a Function of Electrical Energy

Intuitively, one expects the combustion energy potential to be proportional to the electrical energy potential. The rationale is that the fuel load, i.e., the amount of combustibles (electrolyte and separator material), should be proportional to the electrical energy potential.

The published [1] electrical energy potential for each test configuration and the measured combustion energy released are shown in Table 21. The two right-hand columns show the ratio of the measured combustion energy to the published electrical energy.

At initial glance, there appears to be a fairly wide range in the ratios of combustion energy to electrical energy (5 to 12). However, the lithium-ion E battery packs have a hard plastic case with about 150 grams of plastic material. This plastic contributes about 30% of the total combustion energy for the pack. Similarly, the lithium manganese oxide H-2 battery packs have a hard plastic case with about 200 grams of plastic material. This plastic contributes about 40% of the total combustion energy for the pack.

After adjusting the combustion energies to account for the case material, there is fairly good agreement between the results of these tests, suggesting that the combustion energy is typically about six times the electrical energy potential of the battery.

Table 21 — Combustion Energy and Electrical Energy Comparison

Cell Type	No. of Cells	Combustion Energy Released (MJ)	Electrical Energy (Wh, MJ)	Ratio Comb./Elect.	Adjusted Ratio Comb./Elect.
E	1 pack of 24	6.9	207, 0.75	9.2	6.4
E	16 packs of 24 in a cardboard box	85.0	3312, 11.9	7.1	5.4
E	2 packs of 63	21.2	1080, 3.9	5.4	5.4
H-1	32	11.4	586, 2.1	5.4	5.4
H-2	1 pack of 10	13.2	300, 1.1	12	7.2
H-2	2 packs of 10	25.5	600, 2.2	11.6	6.9
H-2	3 packs of 10	32.5	900, 3.2	10.1	6.1
LiMnO ₂	1 pack	14.2	720, 2.6	5.4	5.4

9.4 HRRs of Bulk Storage Configurations

Two HRR tests were conducted in bulk packing configurations such as might be encountered in shipping and storage. The first test consisted of 16 packs of 24 cells each of E type cells packed in a cardboard shipping box. The second test consisted of six 10-cell boxes of F cells. Pre-test photos and the HRR histories measured during the two tests are shown in Figs. 10 and 11. The 16 packs of E cells were triggered by exposure to a propane flame, and the six boxes of F cells were initiated by heat tape wrapped around the boxes.

A comparison between these results and the smaller scale tests suggests that for these two configurations, the cells tended to react sequentially rather than simultaneously. The peak HRRs were similar to the smaller battery configurations but the duration of burning was longer. These two tests provide only limited data; a rapidly growing reaction with numerous cells reacting simultaneously is easily conceivable.



Fig. 10 — Bulk storage test, E type cells

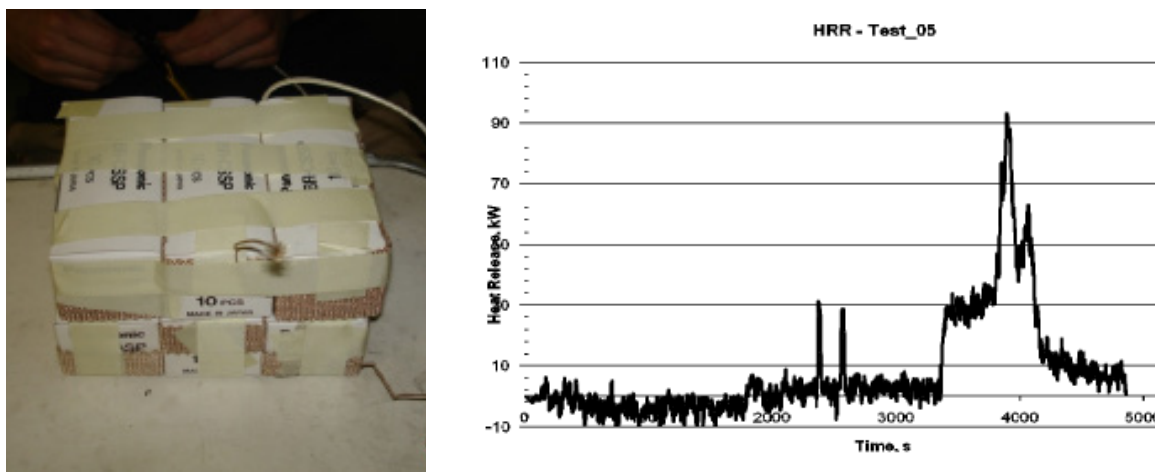


Fig. 11 — Bulk storage test, F type cells

10 SAFE STORAGE AND CASUALTY MITIGATION OF MULTICELL LITHIUM BATTERIES

One objective of the battery casualty test programs was to develop a facility to contain large lithium batteries and prevent a cascading casualty during storage and charging. The containment/mitigation structure developed is termed a Battery Storage Locker (BSL). In general terms, the BSL was designed to limit a casualty to the initial battery and to contain, to the maximum extent possible, the exposures (both thermal and products) produced by the event. The final mitigation system includes a pressure vessel housing to contain the gaseous products released during a casualty, a smoke detection system to notify personnel of the event, and a self-contained, closed head sprinkling system designed to suppress and ultimately extinguish a fire. The entire package is referred to as the Lithium Battery Casualty Mitigation System (LBCMS).

10.1 Battery Storage Locker (BSL) Development History

The initial approach was to develop a BSL similar to a commercial off-the-shelf (COTS) flammable liquid storage cabinet. Two series of tests were conducted to quantify the conditions produced in a prototype rectangular BSL and to assess/refine the design for the overall LBCMS. These conditions became the basis for the performance requirements for the system and components. Later, a cylindrical BSL was developed and tested (see Section 10.4.2).

The rectangular BSL design was based on a box-in-a-box concept. The inner box is the battery compartment. The battery compartment provides a passive barrier to contain the initial battery casualty and prevent direct exposures to and from adjacent battery packs. The battery compartment is also designed to contain the extinguishing agent (i.e., water) so that the battery can be completely submerged to aid in extinguishment and minimize cell-to-cell propagation within the battery. The battery compartment is equipped with a hinged lid (held closed by gravity, not secured) that is designed to vent the pressure and products of the initial battery casualty into the outer box. The outer box is a sealed unit that serves as a plenum to contain the reaction products.

The prototype BSL (Fig. 12) was constructed of 0.64 cm (0.25 in.) steel plate with dimensions of 46 cm × 46 cm × 1860 cm (18 in. × 18 in. × 73 in.). It contained three battery compartments and a plenum area located above and in front of each compartment. Each battery compartment was roughly 30 cm deep × 30 cm tall × 60 cm long (12 in. × 12 in. × 24 in.). The top of the BSL was also equipped with a hinged lid to provide access to the battery compartments. This lid was held shut using two latches located at the front of the BSL.

Each battery compartment was equipped with a closed head sprinkler to suppress and extinguish a casualty within the compartment. During development, a variety of detection technologies were installed in the plenum to aid in the downselect of the final technology.

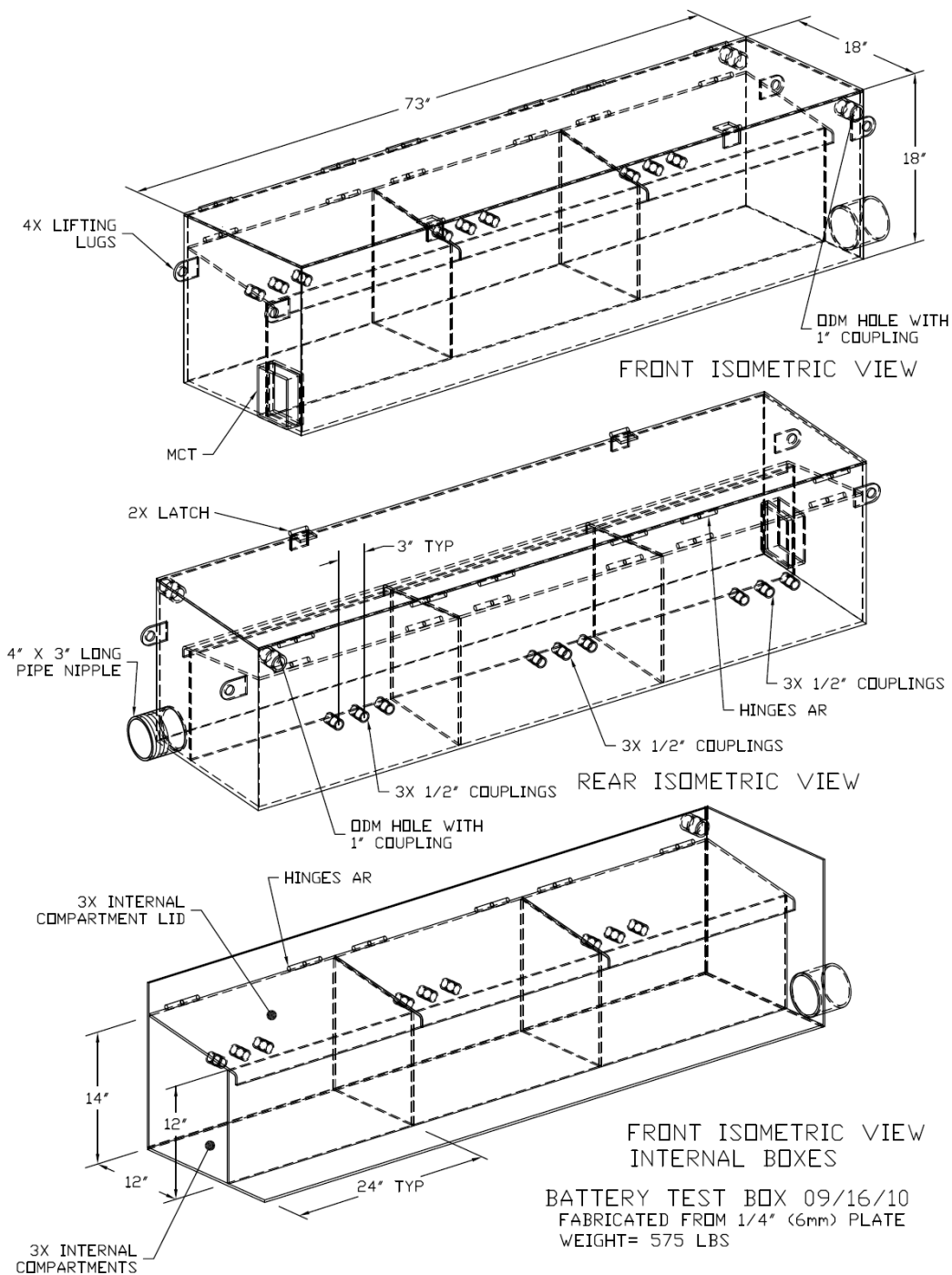


Fig. 12 — Prototype BSL schematic

10.2 Detection System Development History

During the development tests, the rectangular BSL was instrumented for both temperature and optical density so it could be determined if standard off-the-shelf heat and smoke detectors would be suitable for this application. In addition, two commercially available detectors were installed in the battery storage compartment: a heat sensing device (HSD) and an aspirated smoke detection system.

During the vast majority of the tests, there was no indication of the casualty outside the cell or pack prior to the event. Short-circuits or overcharge may produce sufficient local heating to be detected prior to the casualty if the battery pack is instrumented internally for temperature. A sudden increase or decrease in battery voltage may also indicate an ensuing battery casualty, but the voltage was not measured during these tests.

During the vast majority of the tests, the reaction of a single cell within the BSL produced effects that would be detectable using almost any of the available COTS technologies (i.e., heat and smoke). The battery compartment and the plenum space became obscure (80% to 100%) with smoke/aerosol particles during every casualty. COTS photoelectric type smoke detectors typically alarm when exposed to obscurations between 3% and 5%, making them a good option for this application. During many of the tests, there was a significant temperature increase (between 30 and 300 °C) in the battery compartment, indicating that temperature sensors would also work well in this application (i.e., inside the battery compartment to detect the battery casualty).

Ultimately, the results supported the selection of a photoelectric smoke detector for use as an early warning device to notify personnel.

10.3 Suppression System Development History

Table 22 provides an overview of the fire suppression systems considered and their anticipated capabilities for this application. Also included are a number of concerns associated with each technology/system.

Since a battery casualty typically cannot be detected prior to the first cell reaction (venting and/or fire), the suppression system for this application must be able to extinguish any fires in normal combustible materials, minimize the potential for secondary reactions (in adjacent cells and/or battery packs), and mitigate the hazards/exposures produced by the initial reaction (i.e., absorb the heat given off by the initial reaction, minimize the exposures to adjacent cells and batteries surfaces by cooling, and scrub some of the particles and compounds out of the vented gases).

Only water-based systems have the capabilities to meet these desired performance objectives. Gaseous agent systems have excellent fire extinguishing capabilities (they can extinguish most combustible materials in less than a minute of agent discharge) but have no cooling capabilities to help mitigate the hazard to adjacent cells or batteries.

The two systems that showed the most potential for this application were a water deluge (flooding) system and a sprinkling system. Additives such as foams would have been investigated if the “water only” systems could not meet the desired levels of performance. Ultimately, a closed head sprinkling system was selected for this application. The closed head sprinkling system has the advantage over other technologies of not needing a separate detection and activation system, making it the simplest, most cost effective, and easiest to maintain.

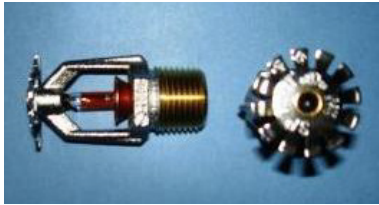
Table 22 — Suppression System Capabilities and Limitations

System	Capabilities	Limitations/Concerns
Seawater Flooding	Suppression, cooling, exposure protection	Shorting, collateral damage, electrolysis (hydrogen explosion)
Potable Water Flooding	Suppression, cooling, exposure protection	Shorting, collateral damage, electrolysis (hydrogen explosion)
Seawater Sprinkling	Cooling	Limited shorting collateral damage
Potable Water Sprinkling	Cooling	Limited shorting collateral damage
AFFF Sprinkling	Cooling	Limited shorting collateral damage
Medium Expansion or Compressed Air Foam	Suppression, cooling, exposure protection	Limited shorting collateral damage
High Expansion Foam	Suppression, cooling, exposure protection	Limited shorting collateral damage
Inert Gas	Suppression	No cooling
Halocarbons	Suppression	No cooling
Water Mist	Suppression, cooling	Limited shorting collateral damage
Powders/Aerosols	Suppression	No cooling
Aqueous Agents	Suppression, cooling	Limited shorting collateral damage

The suppression system chosen for the LBCMS consists of an individually thermally activated sprinkler (a closed head sprinkling system) installed above the center of each battery compartment. Standard Tyco pendent sprinkler heads (57 °C/135 °F) with k-factors of 80 lpm/bar^{1/2} (5.6 gpm/psi^{1/2}) were selected and tested for this application. Additional information on the sprinkler heads is provided in Table 23.

During the development and validation tests, the system was designed to fill the battery compartment with water in less than 20 seconds from activation. The system was secured (turned off) about 40 seconds after activation. This corresponds to twice the amount of water required to fill a single battery compartment.

Table 23 — Sprinkler Head Information

Manufacturer and Model	Tyco Pendent Sprinkler Head
K-Factor	80 lpm/bar ^{1/2} (5.6 gpm/psi ^{1/2})
Temperature Rating	57 °C (135 °F)
Response Time Index (RTI)	32 (m-s) ^{1/2} (58 (ft-s) ^{1/2})
Photograph	

10.4 Mitigation Test Results

10.4.1 Rectangular BSL Suppression Test Results

The capabilities of the suppression system installed in the rectangular BSL were assessed against two battery packs: 24 18650 type E cells and 10 D type H-2 cells. These batteries were selected because they produce a burning reaction that readily propagates to all the cells within the pack. Also, the individual cells are obstructed from direct water spray impingement from the sprinkler head due to packaging material. Table 24 describes these battery packs.

Table 24 — Battery Packs Tested in the Rectangular BSL

No. of Cells	24	10
Cell Type	18650	D Cell
Manufacturer	E	H-2
Type	Secondary	Primary
Voltage	30 V	27 V
Capacity	7.2 Ah	11.1 Ah
Energy	207 Wh	300 Wh

During the first series of scoping tests, only one suppression test (H-2 pack) was conducted. The results suggested that a single individually thermally activated sprinkler head was a viable option for the battery compartment fire suppression system. During the second test series, four additional fire suppression tests and two baseline tests without suppression were conducted to further quantify the capabilities of the system. The results of these tests are summarized in Table 25.

Table 25 — Rectangular BSL Suppression System Test Results

Battery Description	Max. Battery Comp. Temp. (°C)	Max. Adjac. Battery Comp. Temp. (°C)	Max. Plenum Temp. (°C)	Sprinkler Activ. Time (sec)	Exting. Time* (sec)	No. of Cells that Reacted
One E pack of 24 cells	250	80	115	**5–10	NA	24 of 24
One E pack of 24 cells	165	25	30	5–10	~20	6 of 24
Three E packs, total 72 cells	200	30	85	5–10	~30	24 of 72
One H-2 pack of 10 cells	250	125	200	**5–10	NA	10 of 10
One H-2 pack of 10 cells	125	25	75	5–10	~15	4 of 10
Three H-2 packs, total 30 cells	145	175	***325	5–10	~35	15 of 30

* These are estimates due to the difficulty in determining the actual extinguishment time

** For this test, the water was not allowed to flow

*** The flammable electrolyte gases were burning outside of the battery compartment in the plenum

As shown in Table 25, three tests were conducted with each battery type: a single battery pack baseline test without suppression, a single battery pack test with suppression, and a test with three battery packs taped together to assess the ability of the system to prevent pack-to-pack propagation.

During the baseline tests, the casualty rapidly propagated through the entire pack(s), consuming all the cells in less than 2 minutes. In both cases (E and H-2), the plastic case continued to burn for another 2 to 3 minutes.

When repeated with the suppression system operational, the system activated within 10 seconds and the reaction was stopped before all the cells in the pack were consumed and before the battery case ignited (i.e., the fire was extinguished about 10 seconds after the start of discharge). Only 25% of the E cells were consumed and 40% of the H-2 cells were consumed.

When the tests were repeated with the three-pack configurations, the system again activated within 10 seconds and the reactions were stopped before all the cells in the pack of origin were consumed, but the fire did spread into one of the adjacent packs. This fire spread to the adjacent pack was an anomaly of the test configuration. Specifically, the wires/Calrod used to heat the cells in the center pack ran through the center of one of the adjacent packs. This wire run provided a path for the hot gases that were being released from the pack of origin to ignite the adjacent pack. However, in both three-pack tests, only one or two cells in the adjacent pack reacted prior to the suppression/extinguishment of the entire group of batteries. In both cases, the fire was extinguished less than 30 seconds after the start of discharge. Only 33% of the E cells were consumed and 50% of the H-2 cells were consumed in the pack of origin during these multiple pack tests.

With respect to thermal management, the sprinkler rapidly suppressed and extinguished the fires and prevented the spread of fire to batteries stowed in adjacent battery compartments (based on the temperatures measured in the adjacent areas).

10.4.2 Pressurizable Cylindrical BSL Suppression Test Results

Some lithium battery packs produce significant overpressure during a casualty. These pressures could not be contained in the rectangular design BSL. A pressurizable cylindrical BSL with three battery compartments was designed to handle up to 50 psig pressures with a vent.

The original battery pack intended to be stowed in the LBCMS, consisting of thionyl and sulfonyl chloride lithium cells (B-2, B-3, and B-4), was shown to be too energetic during casualty events to be contained within a reasonably designed BSL. Accordingly, notional battery packs were constructed using less energetic cells. These notional battery packs (referred to as Pack #1, Pack #2, and Pack #3) provide the necessary energy and power for some applications. The battery packs tested are described in Table 26.

Table 26 — Battery Pack Configurations

Battery Pack Designation (% of volume)	Cell	Manufacturer	No. of Cells	Configuration
Bulk	C	F	30	Three 10-cell boxes
1 Pack	18650	E	10	1 pack of 10 cells
Pack A	Large form	I-3	9	3 packs of 3 cells
Pack #1 – 25%	5/4 C	H-1	112	14 sticks of 8 cells
Pack #1 – 50%	5/4 C	H-1	224	28 sticks of 8 cells
Pack #1 – Full	5/4 C	H-1	416	52 sticks of 8 cells
Pack #2 – Full	18650	E	441	7 modules of 63 cells
Pack #3 – 25%	C	F	120	12 sticks of 10 cells
Pack #3 – 50%	C	F	250	25 sticks of 10 cells
Pack #3 – Full	C	F	480	48 sticks of 10 cells

The full battery pack configurations are shown in Fig. 13. In all cases, the cells that make up the pack were placed in an open-ended aluminum cylinder (8.5 in. internal diameter) to simulate the casing of a commercial battery pack. With respect to cell configuration/orientation, Pack #1 and Pack #3 consisted of a group of closely nestled cells packed end to end (in “sticks”) that were physically held connected together in series by a layer of shrink wrap PVC tubing to simulate a nominal battery assembler’s packaging. These “sticks” were secured to each other mechanically. Pack #2 consisted of seven 63-cell modules secured to each other by hot-melt glue.

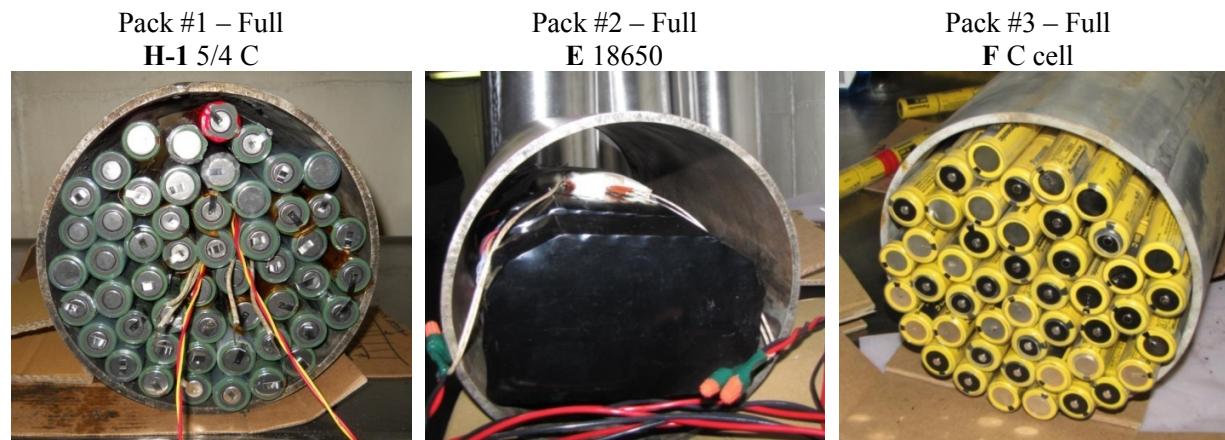


Fig. 13 — Typical battery stick and 63-cell module loading configurations

For testing, the open-ended aluminum cylinder was placed inside a cylindrical battery compartment and into the pressure vessel (Fig. 14). In most tests, the open ends of the aluminum cylinder were partially sealed to simulate the potential water flow obstructions of an actual battery pack (i.e., to reduce the flow rate of water into the center of the pack).



Fig. 14 — Pressurizable containment configuration

Two series of suppression tests were conducted in the pressurizable BSL to assess the capabilities of the overall LBCMS. The first series tested against the reduced scale/partial battery packs (up to 50% of an all-up battery pack; see Table 26). In the second series, the capabilities were validated against the full battery packs (Table 26). Results of the ten tests are summarized in Table 27.

Table 27 — Cylindrical BSL Suppression System Test Results

Battery Pack Description (Pack #)	Max. Battery Comp. Temp. (°C)	Max. Adjac. Battery Comp. Temp (°C)	Max. Plenum Temp. (°C)	Sprinkler Activ. Time (sec)	Exting. Time* (sec)	No. of Cells that Reacted
30 F Cells	170	30	37	~90	~100	3
10 E Cells	80	30	36	<30	<30	4
9 I-3 Cells	135	35	110	7	16	1
112 H-1 Cells (#1, 25%)	65	25	29	10	10	2
** 224 H-1 Cells (#1, 50%)	325	70	260	15	10	28
416 H-1 Cells (#1, Full)	175	35	135	15	25	4
7 × 63 E Cells (#2, Full)	95	35	65	9	~60	16
120 F Cells (#3, 25%)	160	25	43	45	45	6
** 250 F Cells (#3, 50%)	385	55	125	15	15	100
480 F Cells (#3, Full)	95	35	80	10	37	6

* These are estimates due to the difficulty in determining the actual extinguishment time.

** The discharge of water was intentionally delayed to further challenge the LBCMS.

Specific findings of the ten tests are summarized as follows:

- The BSL (and installed systems) met all LBCMS requirements to contain the casualty to a single battery and prevent products of combustion from escaping the LBCMS.
- The smoke detector (photoelectric) installed in the BSL alarmed early into the casualty during every test and could be heard outside the pressure vessel.
- Only the sprinkler in/above the battery compartment of origin activated during any of these tests.
- The sprinkler head typically activated early in the casualty and within a few seconds of water discharge, stopped the reaction/casualty (with only a few cells reacting).
- For fast growing casualties, the sprinkler head typically activated about 15 seconds into the event.
- The maximum temperatures measured in the battery compartment of origin for normal LBCMS operation (i.e., no delay in water discharge) ranged from 65 °C to 175 °C.

- The maximum temperatures measured in the plenum for normal LBCMS operation (i.e., no delay in water discharge) ranged from 29 °C to 135 °C and the maximum temperatures measured in adjacent battery compartments (also called pigeon holes) ranged from 25 °C to 35 °C.
- For normal LBCMS operation (i.e., no delay in water discharge), the maximum pressure produced in the BSL was less than 10 psi overpressure (pressure due to both the gas generated during the casualty and the water injected to suppress the casualty).
- The two primary hazardous gases produced during these battery casualties were CO₂ and CO. During these suppression tests, the amount (mass) of CO₂ produced ranged from 0.02 to 0.08 kg. The amount (mass) of CO produced ranged from 0.01 to 0.05 kg.

10.5 Suppression Summary

The ability of a suppression system to prevent secondary cell reactions within a complex battery pack is, in part, a function of the openness of the battery pack housing. If the cells are contained within a closed housing (air tight, water tight, or even just a fairly tight enclosure), the mitigation system will not be able to contain the reaction to the initial cell within a single battery, and in most scenarios, all of the cells within the pack will react, even if submersed under water.

If the battery housing is fairly open, a fast acting mitigation system may be able to reduce the exposures to the adjacent cells within the housing below the critical value (below the level at which adjacent cells react). The best way to achieve this objective is to rapidly submerge the battery pack in water. The severity of the initial reaction, the proximity of the adjacent cells, and the vulnerability of adjacent cells are variables associated with achieving this performance objective. A water spray system (versus a flooding system) has the ability to thermally manage the conditions around the pack of origin, but is unlikely to be effective in preventing the complete consumption/reaction of the initial pack.

The data in Table 27 are from tests in which the individual cells were loosely packed and thus water could surround and cool each cell. This prevented total destruction of the battery pack in the BSL.

11 UNMITIGATED BATTERY PACK REACTIONS INSIDE A PRESSURE VESSEL

Three tests were conducted to validate the capabilities of the LBCMS (using the cylindrical BSL) against a number of worst-case scenarios: unabated reaction of an entire battery pack within the BSL and pressure vessel. These tests were conducted with all-up battery packs (full 100% packs) and are summarized in Table 28.

Table 28 — Conditions Produced Inside a Pressure Vessel

	7 × 63 E Cells	416 H-1 Cells	480 F Cells
Casualty Duration (sec)	300	96	162
No. Cells Reacted	441	416	480
Reaction Rate (cells/sec)	1.3	4.3	3.0
Max. Temp. Battery Storage Compartment (°C)	600	880	1000+
Max. Temp. Plenum (°C)	400	310	435
Max. Temp. Adj. Battery Storage Compartment (°C)	80	80	100
Volume of Gases Produced (m ³)	5.6	9.4	9.3
Volume of CO ₂ Released (m ³)	5.1	6.1	6.1
Volume of CO Released (m ³)	0.5	3.3	3.2
Total Mass of CO ₂ Produced (kg)	6.4	10.9	9.4
Total Mass of CO Produced (kg)	0.73	3.8	3.4

11.1 BSL Worst-Case Thermal Conditions

The maximum temperatures measured in the center battery compartment of the LBCMS (the one containing the battery casualty) ranged from 600 °C to over 1000 °C. The maximum temperatures measured in the plenum ranged from 310 °C to 435 °C and the maximum temperatures measured in adjacent battery storage compartments ranged from 80 °C to 100 °C. Although some of the batteries in the adjacent battery storage compartments showed moderate thermal damage, none of the batteries stowed in the adjacent battery storage compartments reacted during any of these worst-case tests.

Figures 15 and 16 show the worst-case thermal conditions produced in the BSL during these tests, which occurred in the test conducted with 480 F cells. The reaction began about 61 minutes into the test. The battery compartment containing the casualty exceeded 1000 °C about 3 minutes into the casualty. The aluminum cylinder used to house the cells (surrogate battery case) was significantly damaged with only the bottom half remaining at the end of the test. The plenum temperature above the battery storage compartment reached 435 °C. The adjacent battery storage compartments remained below 100 °C for the entire test.

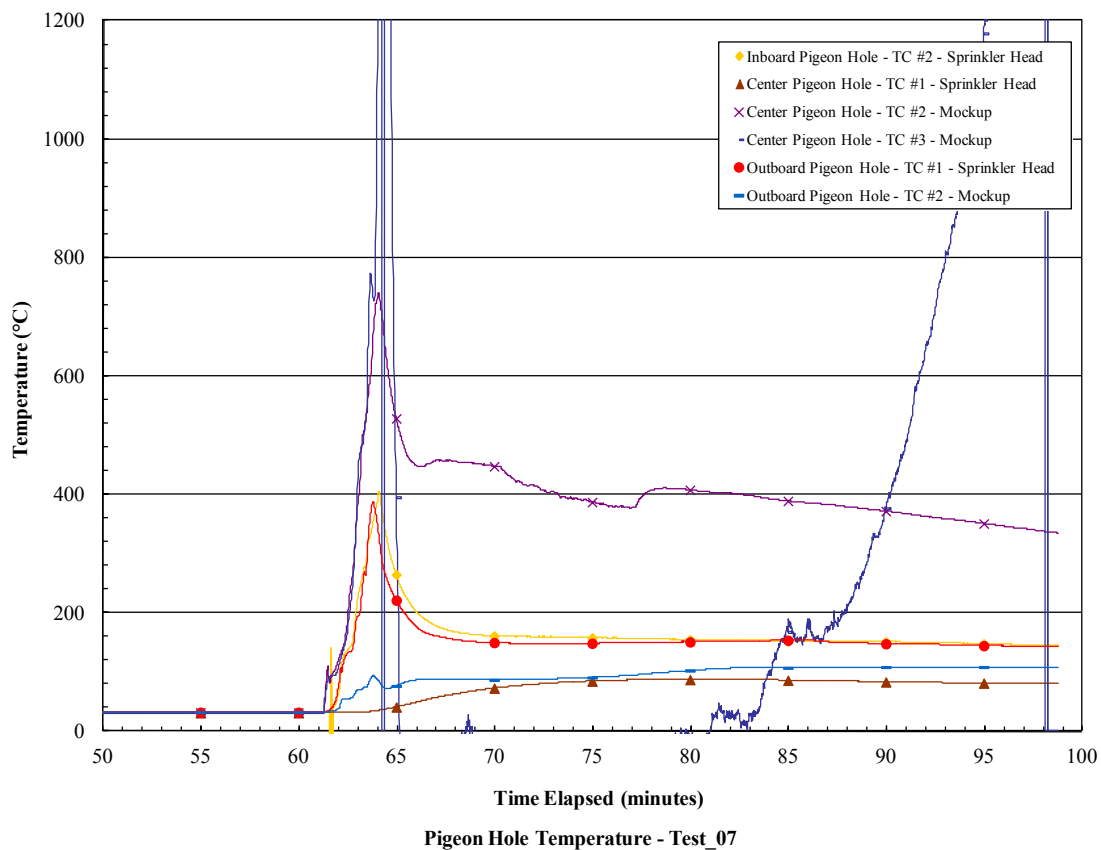


Fig. 15 — BSL worst-case thermal conditions in the compartment containing the battery (480 cells) (TC = thermocouple)

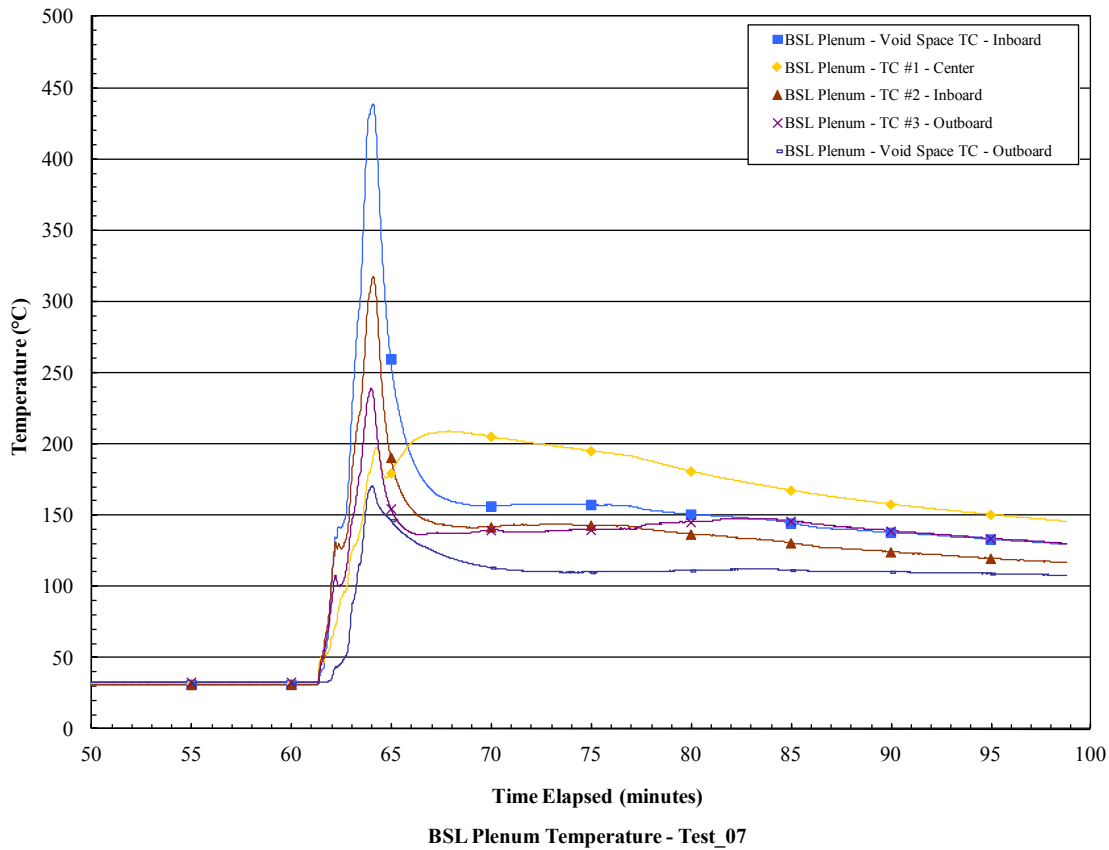








Fig. 16 — BSL worst-case thermal conditions in the plenum (480 cells) (TC = thermocouple)

The reactions of the battery pack significantly damaged the aluminum cylinder used to simulate a representative battery housing. Table 29 shows pre-test and post-test photographs of the battery packs and aluminum housings. As can be seen, some of the packs/cells released enough heat to completely destroy the housing.

The data collected during these tests provide valuable information on the reaction rates (cell-to-cell propagation) of a battery casualty in a confined space, involving a battery containing a large number of cells. The unabated cell-to-cell propagation rates (shown in Table 28) ranged from 1.3 to 4.3 cells per second. Surprisingly, the reactions continued inside the BSL even though there was no oxygen to support combustion of the vented products. It was assumed that the heat logged in the BSL prior to the complete consumption of oxygen was adequate to continue the reaction of the remaining cells in the pack. The reaction of these remaining cells still logged additional heat energy inside the BSL in the absence of combustion. Reactions of cells at low oxygen levels and the mechanism driving cell-to-cell propagation are topics that should be further investigated.

Table 29 — Damage Photographs

Battery	Pre-Test Photograph	Post-Test Photograph
<p>7 × 63 E Cells</p>	 A cylindrical battery assembly with several colored wires (red, yellow, black) connected to its top. The battery is mounted on a metal surface.	 The same cylindrical battery assembly after testing, showing significant damage and a grey, powdery substance covering the top and sides.
<p>416 H-1 LiMnO4 Cells</p>	 A cylindrical battery assembly with a green terminal cap and red wires, mounted on a metal surface.	 A hand wearing a blue glove is shown peeling away a layer of grey, powdery material from the top of the battery assembly.
<p>480 F Cells</p>	 A cylindrical battery assembly with yellow and red wires, mounted on a metal surface next to a green flange.	 The same cylindrical battery assembly after testing, showing significant damage and a grey, powdery substance covering the top and sides.

11.2 Gas Production

During these worst-case tests, the volume of combustion gases released/produced during the reaction inside the BSL ranged from 5.6 to 9.4 m³. About 65% of this gas was CO₂ and remaining was CO. On a mass basis, the amount of CO₂ produced ranged from 6.4 to 10.9 kg and the amount of CO produced ranged from 0.7 to 3.8 kg.

A significant quantity of unburned hydrocarbons was also produced but the amount could not be quantified with the instruments installed in the BSL and test compartment during these tests.

The cylindrical BSL was designed to vent the reaction gases when the pressure in the BSL reached 50 psi. Therefore, it was estimated that 85% of this gas vented outside the LCBMS.

12 BATTERY CASUALTY CLASSIFICATION

There are currently no established criteria for classifying the hazards associated with a lithium battery casualty. Table 30 provides a simplified approach to characterizing these events. A general description of these hazards follows.

Table 30 — Battery Hazard Classifications (Simplified Approach)

Hazard Parameter	Significant	Moderate	Insignificant
Explosion and Fragments	Will cause injury to unprotected personnel within the compartment of origin with compartment overpressures >1 PSIG or or release of any fragment with >15 ft/sec velocity or >20 ft-lb impact loading	Could cause injury to unprotected personnel in close proximity to the battery with compartment overpressures >0.25 PSIG or release of any fragment with >5 ft/sec velocity	Unlikely to cause injury (<0.05 PSIG overpressure) and no debris greater than 0.2 ft from battery
Fire/Thermal – HRR	PHRR > 100 kW for any duration	100 kW > PHRR >10 kW	PHRR < 10 kW
Fire – Fragments	Flaming fragments projected > 3 ft	Flaming fragments projected up to 3 ft	No flaming fragments
Aerosol Products	Loss of visibility within the compartment of origin and/or the production of explosive mixtures	Loss of visibility in close proximity to the battery (3 ft)	No loss of visibility
Gaseous Products (F)	Flammable concentrations within the compartment of origin	Flammable concentrations in close proximity to the battery	No flammable gases produced
Gaseous Products (T)	Toxic/hazardous concentrations within the compartment of origin for protected personnel	Toxic/hazardous concentrations in close proximity to the battery for unprotected personnel	No toxic/hazardous gases produced

PHRR = Peak Heat Release Rate

(F) = Flammable

(T) = Toxic

The same hazard parameters are typically produced during every reaction but to varying degrees: flammable by-products (aerosols, vapors, and liquids), toxic gases, flying debris (some burning), and sustained burning.

On a local scale, the exposures produced by the reaction are a function of the battery chemistry, the number of cells involved in the reaction, and the distance between the battery and the item of concern. On a global scale, the exposures produced by the reaction are a function of the battery chemistry, the number of cells involved in the reaction, and the size of the compartment in which the reaction occurs.

In the case of immediate ignition of gases as they discharge from a battery, the thermal exposures produced by the casualty are localized to a region around the reaction and significantly decrease with distance away from the battery/battery pack. Therefore, thermal exposures to equipment and personnel are only a concern in the region in close proximity to the battery (within a few feet of the battery). The main concern associated with these localized thermal conditions is the exposures to adjacent cells within the pack and adjacent batteries/battery packs within the storage device.

There is also a separate concern associated with nearby combustible materials. Based on limited data, it may be assumed that flaming debris from a battery casualty could cause ignition of combustible materials anywhere within the fragment zone/volume. Precautions should be taken to avoid or limit the storage of combustible materials near lithium batteries.

The primary hazard associated with a battery casualty appears to be the gases produced during the reaction. These gases have been determined to be toxic and in some cases flammable. The concentration of toxic and/or flammable gases is a function of the battery chemistry, the number of cells involved in the reaction, and the size of the compartment in which the reaction occurs. Due to the production of copious amounts of gases during the reaction of larger batteries and battery packs, it must be assumed that any battery casualty will render the storage compartment untenable for unprotected personnel (personnel not wearing a breathing apparatus).

Another significant concern is the production of a flammable mixture of gases (explosive mixture) within the storage compartment. If the resulting mixture is in the flammable range, the delayed ignition of the gases in the space can produce a large fireball and overpressures that could produce structural damage and additional battery casualties. In this scenario, the thermal exposure would be on a large scale, resulting in a hazard to personnel from thermal exposure, overpressures, and flying debris.

13 SUMMARY

The Naval Research Laboratory recently participated in, and completed, several major research programs initiated to characterize and mitigate lithium battery fire hazards for a number of applications. More than 100 battery casualty tests were conducted to characterize the conditions produced during a range of both unmitigated and mitigated casualties. This report summarizes the results of these tests.

The primary failure mode of a lithium battery is associated with a flaw or damage to the thin porous electrical insulation layer that separates the anode and the cathode (the separator). This is typically a microporous polyolefin layer in the Li-ion cells and a glass or ceramic paper in oxyhalide cells. Damage to the separator can result in an internal short circuit that produces enough heat to vaporize the electrolyte or in the case of a primary metallic lithium anode, melt and allow massive internal shorting and direct anode-catholyte reactions that result in a violent venting or explosive reaction. The separator can fail due to internal defects (production issues), physical damage (handling issues), exposure to high temperature (fire), and in the case of secondary cells, overcharging resulting in bridging of the separators. Once an internal short develops, a sudden release of stored energy occurs, commonly referred to as thermal

runaway. This event can cascade to adjacent cells and throughout an entire battery pack and ultimately destroy the device the battery is installed in and catastrophically impact the platform and personnel.

The requirements the U.S. Navy has adopted for the lithium battery safety program include a Preliminary Hazard Analysis, Battery Casualty Characterization Tests, Hazard Mitigation Tests, and a final Systems Hazard Analysis (SHA). There are two general types of tests conducted to characterize the battery casualty: reaction products testing and burning characteristics testing (heat release rate).

In the testing reported here, the reaction products were characterized for 19 different cells covering a range of chemistries, form factors, and capacities.

In general, when a cell casualty can be described as a venting reaction (no ignition), the majority of the products released are electrolyte constituents (i.e., carbonates or oxyhalides). These flammable gases and aerosols can accumulate and have the potential to produce an explosive atmosphere (explosion hazard). Explosive environments can be prevented by rapidly ventilating the space.

For the oxyhalides, the resulting dispersion generates an immediate risk to personnel from the acid gases (HCl, H₂SO₄, and HF). These products are also hazards to electronic equipment and have long-term effects on materials of construction.

For cell casualties that result in a burning reaction, the organic based electrolytes burn efficiently, producing CO₂ as the primary by-product, provided sufficient oxygen is available in the supporting atmosphere. Other products include CO and some amount of acid gases. Complete combustion is not assured, as the electrolyte and constituents are dense and may consume the limited oxygen in the cell, shifting the combustion products toward incomplete combustion with a large production of CO.

The acid gas production is directly related to the cell chemistry (and appears to be related to cell capacity and overall thermal effects), especially in the presence of high water vapor. Cells that contain sulfur produce sulfuric acid, cells that contain fluorine produce hydrofluoric acid, and cells that contain chlorine produce hydrochloric acid. It is proposed that for a given cell chemistry, the amount of acid gas produced should be directly proportional to the cell energy.

The heat release rates of the majority of the single cells were too low to measure using the 1 MW hood calorimeter on the ex-USS *Shadwell*. For future assessments, the heat release rates of the small commercial cells will be measured using a smaller hood calorimeter (10 to 100 kW). Ultimately, the HRRs of many of these cells were determined based on the results of tests on battery packs.

A wide range of battery pack configurations, groups of battery packs, and groups of battery modules were tested during these programs. There were significant differences in the types of reactions observed in the pack/module tests compared to the single cell tests. Specifically, except for the iron phosphate cells, almost all the packs/modules produced burning reactions, while many of the single cells only vented and never caught fire. In addition, during almost every unmitigated pack/module test, all the cells in the battery pack/module reacted and the casing materials were completely consumed.

The combustion energy potential was shown to be proportional to the electrical energy potential. The rationale is that the amount of combustibles (electrolyte and separator material) should be proportional to the electrical energy potential. However, the battery pack casing can provide a significant amount of fuel/energy to the fire. After adjusting the combustion energies to account for the case material, there is fairly good agreement between the results of the tests, suggesting that the combustion energy is typically about six times the electrical energy potential of the battery. The effect of a plastic case and packaging mass was found to be as high as 70% of the overall HRR with low thermal effect cells. Iron phosphate

based cells were combined and tested with ruggedized shipping containers and found to be fairly benign compared to other lithium batteries tested.

With respect to the fire hazard, the fire produced by the battery packs assessed during these programs was fairly energetic, but as a whole, should not be overmatching for a standard, properly attired fire response team. Most of the battery packs assessed during this program, with the exception of the large format battery packs, produced fires equivalent to the size of a large trashcan fire (20 to 50 kW). The large format battery packs contained an amount of energy equivalent to a gallon or two of JP-5 fuel (200 to 700 kW). In either case, suited-out responding personnel should be able to approach a battery casualty consisting of one of these and suppress/extinguish the fire through the application of copious amounts of water. However, for unmitigated bulk storage configurations, the fire has the potential to rapidly spread and can produce flashover conditions within the room.

Fire spread to adjacent batteries can be prevented by stowing the battery in a metal case and/or a segregated metal cabinet/locker. Fire insulation may also be required depending on the battery casualty characteristics, the thickness of the metal structure, and proximity to adjacent combustibles or batteries. Limitations of air and replenishment air will limit fire spread and may serve as a passive suppression system, although there is a possibility of back draft explosion as air is reintroduced to a hot room.

The precepts for the rapid control and suppression of a battery casualty were based on the development of a Battery Storage Locker similar to a commercial off-the-shelf flammable liquid storage cabinet. Tests were conducted to quantify the conditions produced in a prototype rectangular BSL and to assess/refine the design of an overall LBCMS. These conditions became the basis for the performance requirements for the system and components. The final design was a pressurizable cylindrical BSL. Two series of tests were conducted to validate the capabilities of the cylindrical BSL and the overall LBCMS.

Thirty-seven mitigation tests were conducted, all of which included some form of detection and 13 of which included active suppression.

The detection test results show that there are no universal precursors to a battery casualty that can be used for early warning detection for all types of batteries and systems. However, the results demonstrated that a smoke detector works well for detecting a casualty early into the event (i.e., after the first cell or group of cells have vented and/or caught fire).

The suppression system results show that water, or water-based agents, have good capabilities for managing the heat released during a battery casualty and have the potential to stop fire spread to adjacent batteries. The results demonstrate that cell-to-cell propagation within a large multicell pack can be stopped if the pack is rapidly submersed in water if the water can penetrate the battery pack. The final BSL design includes a sprinkler head installed inside each battery storage compartment. If battery packs (of the type studied) are colocated in adjacent storage areas, it is recommended they be protected from radiative and convective heat transfer.

REFERENCES

1. D. Linden and T. Reddy, *Handbook of Batteries*, 3rd ed. (McGraw-Hill, 2002).
2. F.W. Williams, X. Nguyen, J. Buchanan, J.P. Farley, J.L. Scheffey, J.T. Wong, H.V. Pham, and T.A. Toomey, "Ex-USS Shadwell (LSD-15): The Navy's Full Scale Damage Control RDT&E Facility," NRL Memorandum Report NRL/MR/6180--01-8576, August 24, 2001.

APPENDIX

**VIDEO CLIPS FROM LITHIUM SINGLE CELL AND
 MULTICELL BATTERY CASUALTIES**

Video clips (MP4 files) are on the enclosed DVD

A1 SINGLE CELL BATTERY CASUALTY VIDEO CLIPS

B-1 Cells Li/Li_{0.5}CoO₂ AA Size

File	Camera	Date	Start Time	SOC, %	Insult
146	Clip 8	11/3/2009	?	100	Heater
147	Clip 11	11/4/2009	?	100	Heater

B-2 Cells Li/SOCl₂ AA Size

File	Camera	Date	Start Time	SOC, %	Insult
123	5	8/20/2009	11:35:25	100	Propane

B-3 Cells Li/SOCl₂ D Size

File	Camera	Date	Start Time	SOC, %	Insult
151		4/15/2010	?	100	Heater
118		8/3/2010	12:47:20	100	Heater
119		10/13/2010	13:26:45	100	Heater

B-4 Cells Li/SO₂Cl₂-SOCl₂ D Size

File	Camera	Date	Start Time	SOC, %	Insult
157		4/16/2010	use all	100	Heater
120		8/6/2010	13:01:50	100	Heater

C-1 Cells LiFePO₄ 18650 Size

File	Camera	Date	Start Time	SOC, %	Insult
73	Exterior	1/4/2010	13:21:00	~40	Heater
74	Exterior	1/5/2010	10:15:15	100	Heater
75	Exterior	1/8/2010	14:21:30	discharged	Heater

D-2 Cell Li/LiFePO₄ 26650 Size

File	Camera	Date	Start Time	SOC, %	Insult
141*	Outside Chamber	7/19/2011	10:41:45	100	Heater

*Note: the banner on the video clip describes a 18650 form fit, when actually it is a 26650 form fit.

E Cell Li/Li_{0.5}CoO₂ 18650 Size

File	Camera	Date	Start Time	SOC, %	Insult
83	Exterior	8/2/2010	13:56:00	100	Heater

F Cells Li/CF_x C Size

File	Camera	Date	Start Time	SOC, %	Insult
142	Outside Chamber	4/12/2010	7:00	100	Heater
143	Outside Chamber	4/12/2010	3:40	100	Heater
163	Exterior	5/24/2010	10:31:00	100	Heater
86	Inside Box	8/2/2010	15:03:20	100	Heater
88	Outside Box	8/2/2010	15:03:16	100	Heater

H-1 Cell Li/MnO₂ 5/4 C Size

File	Camera	Date	Start Time	SOC, %	Insult
159	Outside Chamber	4/14/2010	?	100	Heater

H-2 Cell Li/MnO₂ D Size

File	Camera	Date	Start Time	SOC, %	Insult
158	Outside Chamber	4/12/2010	?	100	Heater

I-1 Cells LiNiCoAlO₄ Large Form Size

File	Camera	Date	Start Time	SOC, %	Insult
91	Exterior	6/21/2010	11:36:50	20	Heater
92*	Exterior	6/21/2010	11:40:00	20	Heater
96	Exterior	12/7/2012	9:19:10	100	Burner
94	Exterior	6/21/2010	13:54:38	100	Heater

*This is a continuation of file 91 same test later time

I-2 Cells LiNiCoAlO₄ Large Form Size

File	Camera	Date	Start Time	SOC, %	Insult
98	Exterior	12/6/2010	14:07:20	20	Burner
100	Exterior	6/22/2010	9:34:00	20	Heater
102	Exterior	6/22/2010	11:22:10	100	Heater
106	Exterior	6/24/2010	14:43:30	100+	Overcharge

I-3 Cells LiNiCoAlO₄ Large Form Size

File	Camera	Date	Start Time	SOC, %	Insult
108	Exterior	6/22/2010	13:53:25	20	Heater
109	Exterior	12/7/2010	12:26:50	100	Burner
112	Exterior	12/8/2010	13:28:28	100	Burner
110	Exterior	6/23/2010	9:54:20	100	Heater
113	2	6/24/2010	12:14:40	100+	Overcharge

J Cells LiCoO₂ Polymer Pouch Size

File	Camera	Date	Start Time	SOC, %	Insult
78	Exterior	12/8/2010	11:56:00	100	Burner
79	Exterior	6/23/2010	14:49:19	100	Heater
81	Exterior	6/25/2010	11:02:45	100+	Overcharge

Li/MnO₂ cell 18650 Size

File	Camera	Date	Start Time	SOC, %	Insult
162	Outside Chamber	6/17/2010	11:57:55	100	Heater

A2 MULTICELL LITHIUM BATTERY CASUALTY VIDEO CLIPS

Li/Li_{0.5}CoO₂ 18650 Size

File	Camera	Date	Start Time	SOC, %	Insult
125		5/26/2010	14:-07:47	20	Heater
126		5/27/2010	9:45:04	100	Heater
127*			9:45:35		
128		5/28/2010	11:53:21	100	Heater
129**			11:53:54		

*Continuation of the test shown in File 126

**Continuation of the test shown in File 128

Simulated #3 Battery Li/CF_x (480 cells) C Size

File	Camera	Date	Start Time	SOC, %	Insult
52*		9/22/2011	11:44:40	100	heater

*Pressure vessel with the relief valve set at 50 psi.

LiCoO₂ Polymer Pouch Size

File	Camera	Date	Start Time	SOC, %	Insult
61	Exterior	1/7/2010	13:51:50	100	Heater
63	Exterior	1/7/2010	16:42:10	100	Heater
11	Exterior	12/15/2010	14:27:48	100+	Overcharge
12	Infrared	12/15/2010	14:27:48	100+	Overcharge

Li/FePO₄ 18650 Size

File	Camera	Date	Start Time	SOC, %	Insult
58	Exterior	1/5/2010	13:24:00	100	Heater

Li/FePO₄ 26650 Size

File	Camera	Date	Start Time	SOC, %	Insult
57	Exterior	1/14/2010	11:21:00	100	Heater
54	Exterior	1/7/2010	15:43:30	100	Heater

Li/MnO₂ 5/4 C Size

File	Camera	Date	Start Time	SOC, %	Insult
68	2	8/4/2010	14:07:00	100	Heater
69	3	8/5/2010	9:55:15	100	Heater

LiNiCoAlO₄ Large Form Size

File	Camera	Date	Start Time	SOC, %	Insult
26	Passageway	12/16/2010	10:07:20	100+	Overcharge



Article

Toxic Gas Emissions from Damaged Lithium Ion Batteries—Analysis and Safety Enhancement Solution

Antonio Nedjalkov^{1,*}, Jan Meyer¹, Michael Köhring², Alexander Doering²,
Martin Angelmahr², Sebastian Dahle³, Andreas Sander⁴, Axel Fischer⁵ and
Wolfgang Schade^{1,2}

¹ Institute of Energy Research and Physical Technologies, Clausthal University of Technology, Am Stollen 19H, 38640 Goslar, Germany; jan.meyer@tu-clausthal.de (J.M.); wolfgang.schade@hhi.fraunhofer.de (W.S.)

² Department Fiber Optical Sensor Systems, Fraunhofer Heinrich Hertz Institute, Am Stollen 19H, 38640 Goslar, Germany; michael.koehring@hhi.fraunhofer.de (M.K.); alexander.doering@hhi.fraunhofer.de (A.D.); martin.angelmahr@hhi.fraunhofer.de (M.A.)

³ Institute of Energy Research and Physical Technologies, Clausthal University of Technology, Leibnizstrasse 4, 38678 Clausthal-Zellerfeld, Germany; s.dahle@pe.tu-clausthal.de

⁴ Knein Technische Textilien GmbH, Am Boscheler Berg 32a, 52134 Herzogenrath-Merkstein, Germany; andreas.sander@ktex-gmbh.de

⁵ CUTEC Institut GmbH, Leibnizstraße 21-23, 38678 Clausthal-Zellerfeld, Germany; axel.fischer@cutec.de

* Correspondence: antonio.nedjalkov@tu-clausthal.de; Tel.: +49-5321-3816-8408; Fax: +49-5321-3816-8401

Academic Editor: Andreas Jossen

Received: 7 December 2015; Accepted: 29 February 2016; Published: 7 March 2016

Abstract: Lithium ion batteries play an increasing role in everyday life, giving power to handheld devices or being used in stationary storage solutions. Especially for medium or large scale solutions, the latter application confines a huge amount of energy within a small volume; however, increasing the hazard potential far above the common level. Furthermore, as the safety hazards of lithium ion cells have been known for years, impressively shown by several burning cars or laptops, the need for a further enhancement of the safety of these systems is rising. This manuscript presents measurements of the gas emission from lithium ion batteries in case of a malfunction for different scenarios, showing a large variety of species with mostly toxic to highly toxic properties. The measurements were carried out using a combination of gas chromatography-mass spectrometry (GC-MS), quadrupole mass spectrometry (QMS), photoacoustic spectroscopy, and chemical analysis. It is shown that the inflammation of a cell can be overcome, also preventing a cascading effect to neighboring cells, but giving rise to worse toxic gas emission. Furthermore, a filtration concept is presented that decreases the concentration of the emitted components significantly and promises filtration below immediately dangerous to life or health (IDLH) equivalent levels.

Keywords: lithium ion; battery safety; thermal runaway; cell venting; health hazard; gas filtration

1. Introduction

Energy storage is one of the key topics of scientific and engineering research in order to provide a reliable concept for the power supply in the future. The technical requirements for storage technologies differ strongly depending on the specific application. While a short, and even ultra-short, storage of energy is needed for power grid stabilization, the growing market share of renewable energy sources constantly increases the need for 24 h energy storage solutions [1]. Conventional battery technologies, like lead-acid batteries, simply do not reach the requirements in terms of power and energy density to overcome this shortage in power storage demand [2,3]. The most promising technology to solve this problem for the next decades is lithium ion technology. With their advanced state of technology and the wide operation in consumer electronics, lithium ion batteries are the perfect candidate for

e-mobility, clean room, or critical infrastructure power solutions and even large scale stationary energy storage [4–6].

Nevertheless, safety issues become more and more important, because of the increasing energy content in storage devices. In recent years, several accidents have shown the hazard potential of lithium ion cells; primary safety hazards are the ignition of the cell and its toxic emission gases [7,8].

This work presents investigations on the gas emission from off-the-shelf, large-scale lithium ion batteries for different enclosure conditions in case of an internal failure and demonstrates the feasibility of a fire prevention setup, as well as a filtration of the hazardous components.

2. Experimental

2.1. Measurement Setup

Figure 1 shows the experimental setup used for the emission measurements; three different scenarios have been under test. For each scenario, the lithium ion cell was mounted at the bottom of a plastic barrel (120 L, polyethylene (PE)). Pouch cells consisting of a layered cathode crystal structure from a composite complex of nickel, manganese, and cobalt (NMC) with an electrical capacity of 40 Ah (LiTec Battery GmbH, Kamenz, Germany) were used. The cell's anode material is graphite. From the cell's material safety data sheet it is known that the electrolyte composition is based on ethyl methyl carbonate (EMC) and ethylene carbonate (EC) in unknown weight ratios using lithium hexafluorophosphate (LiPF_6) as the conducting salt. In order to provoke a reproducible and strong reaction similar to the event of an internal failure, the setup was equipped with a penetration test device (mass: 1.7 kg; height: 0.8 m; nail diameter: 3.8 mm), for a test similar to SAND2005-3123 [9]. Each cell under test was slightly overcharged to about 4.3 V in order to guarantee a thermal runaway after the nail penetration device was triggered. A pumping system with integrated temperature, pressure and flow sensors (DESAGA GS 212) was used to carry the emission gases to the analytics setup. The pumping system consisted of one suction regulator per measuring device, these are one for the activated charcoal tube, one for the silica gel tube and one for the wash-bottle with sodium hydroxide. Therefore, the suction regulators were operated in parallel in order to guarantee similar flow characteristics for each measuring device. The suction regulators' flow rates were set to around 1.5 L/min. The gas mixture was led by polytetrafluoroethylene (PTFE) tubing to the aforementioned analytics. The tubing for each measuring device was of similar length and chosen as short as possible (1–2 m); moreover it was not externally heated and at ambient temperature. Although this can lead to condensation of gas in the tubes, this effect can be neglected for a relative comparison between the three scenarios.

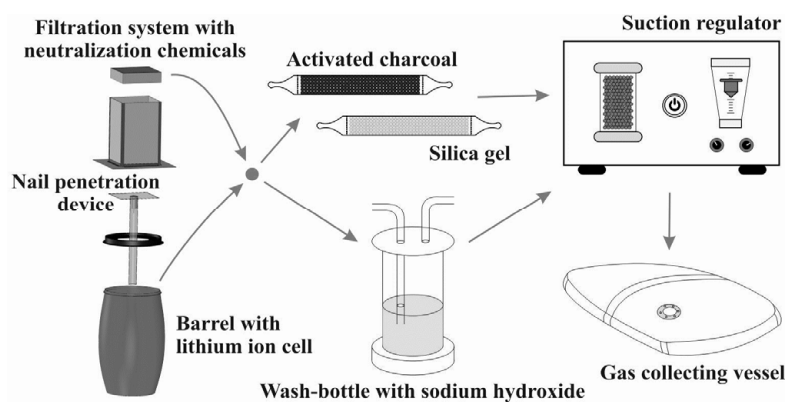


Figure 1. Schematic experimental setup for the determination of harmful battery gas substances. Polytetrafluoroethylene (PTFE) tubing was used to connect all components with a separate suction regulator for each tube.

The experimental scenarios can be described as follows:

- (1) Catching fire: a single bare lithium ion cell is mounted within the barrel. The barrel is shut partly by a cover, which prevents the barrel from explosion but retains most of the emission gases. PTFE tubing leads the gas mixture to the analytics.
- (2) Fire prevention: conducted as Experiment 1, the cell under test is, additionally, wrapped within a specially-developed textile composite structure which is gas permeable but prevents flying sparks (FlotreX S500, Knein Technische Textilien GmbH, Herzogenrath-Merkstein, Germany). This cover material is made out of three layers: a fiberglass mesh, a finely-pored pure glass fleece, and a knitted fabric made of stainless steel-reinforced para-aramid fibers. Video "Experimental Setup Scenario 2" in Supplementary Materials presenting this particular experimental setup is available in the online version.
- (3) Gas filtration: the experiment, as described under 2 is repeated using a tightly sealed barrel with a gas filtration unit mounted on top. The unit consists of five different stages: a particle filtration grid, three pellet layers of 18 dm³ activated charcoal, 9 dm³ potassium permanganate and 9 dm³ activated alumina, as well as a fine particle filter (CCP 610/210/510, SF 14, Viledon Freudenberg, Weinheim, Germany) (Figure 2). A gas bag is used to collect all gas emission behind the filtration; the PTFE tubing is inserted into this bag.

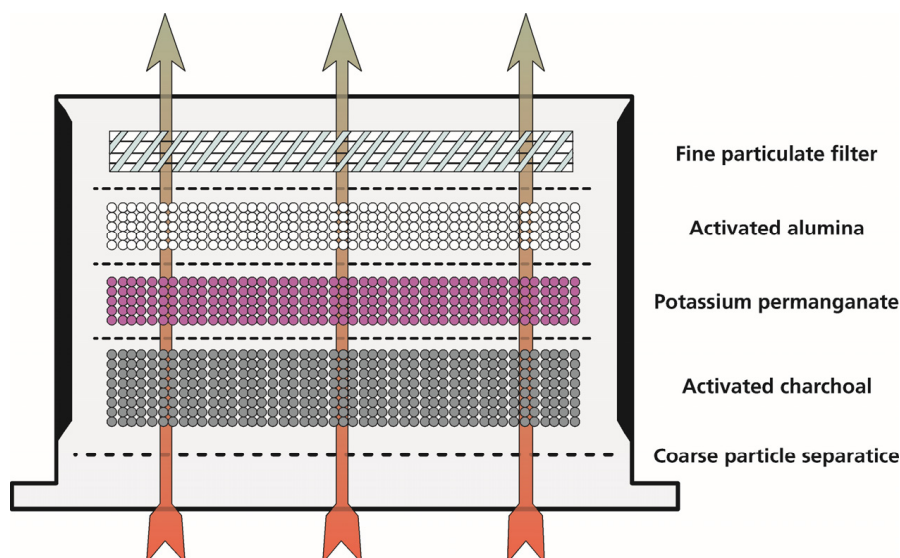


Figure 2. Schematic drawing of the filtration unit setup; five filtration stages are used. The size of the filtration unit is about 30 × 30 × 60 cm³.

2.2. Analytical Methods

First investigations on the emission gases from lithium ion cells and former works [10–12] showed, that a large variety of species were to be expected. As no state-of-the-art analysis system is known that is capable of a cross-sensitivity free detection of all expected emission components, different spectroscopic and chemical analysis techniques were combined. Gas chromatography-mass spectrometry (GC-MS) was used to detect larger molecules, mainly volatile organic compounds, starting from about four carbon atoms per molecule. Smaller components were determined via quadrupole mass spectrometry (QMS), starting from 1 u. In order to get insight in the time dependence of the reaction, an optical sensor based on quartz-enhanced photoacoustic spectroscopy (QEPAS) was used to detect CO, exemplarily. For its radical behavior, HF was determined chemically via ion chromatography (IC) and conductivity measurements. In order to suppress reactions with other species before its detection the HF was dissolved in wash bottles; see Section 2.2.3 for details. It is assumed that all detected fluoride ions result from dissociated HF.

2.2.1. Gas Chromatography-Mass Spectrometry

Gaseous samples for gas chromatographic analyses were collected using test tubes filled with activated charcoal (Aktivkohle Typ G, Dräger, Lübeck, Germany) and silica gel (Silica Typ G, Dräger), respectively. The sorbents were extracted with carbon disulfide for activated charcoal and methanol for silica gel. The screenings for organic compounds were carried out with a Shimadzu Europe GC-MS QP 5050 gas chromatograph (Duisburg, Germany). A Restek Rxi-5 Silms column was used (60 m, inner diameter: 0.25 mm, film 0.25 μm , Bellefonte, PA, USA).

2.2.2. Quadrupole Mass Spectrometry

A commercial gas analyzing system (MFM Analytical Systems, Multigas Analyzer MGA, Clausthal-Zellerfeld, Germany) is employed to determine the composition of the filtered gas. The MGA uses a quadrupole mass spectrometer together with the combination of a turbo molecular pump and a scroll pump. The internal gas inlet system consists of an ultra-high vacuum (UHV) leak valve, thus having no influence on the gas composition in contrast to other common setups, e.g., capillary tubes.

For the quantitative analysis of the mass spectra, background spectra prior to the gas dosage were subtracted from the measured data. Fragmentation intensities for all gas components have been taken from Stein [13] or own measurements. Due to a lack of references for some of the detected compounds, no correction for relative sensitivity factors was carried out.

2.2.3. HF Determination via Ion Chromatography

Gaseous samples for the fluoride determination were collected in wash bottles filled with 40 mL 0.1 M NaOH, each. Portion of the samples were transferred to a Metrohm 761 Compact IC ion chromatograph (Herisau, Switzerland). An ASUPP 4 column with a mixture of 1.8 mmol Na_2CO_3 /1.7 mmol NaHCO_3 was used as eluent. Detection was performed by conductivity measurement. The detection limit for HF is 0.7 ppm and the measurement was performed according to VDI guideline 2470.

2.2.4. Quartz-Enhanced Photoacoustic Spectroscopy

In order to gain additional information about the processes and its emissions, an optical sensing scheme was used. QEPAS exploits highly resonant micro tuning forks to detect the photoacoustically-induced sound wave emitted by the target gas mixture [14]. As this technique uses the optical absorption features of the target species for detection instead of measuring their mass, an additional set of information can be acquired to overcome uncertainties of the other detection methods (e.g., molecules with identical mass). Furthermore, QEPAS enables an online measurement, giving information about the temporal behavior of the signal. As one critical component of the presented measurements, CO was chosen as target gas; optical excitation is achieved using a fiber-coupled distributed feedback (DFB) diode laser near 1570 nm.

3. Results and Discussion

For each experiment an emerging gas amount of approximately 200 SL (5 SL/Ah) caused by the induced thermal runaway was observed. Figure 3 shows the retrieved data from GC-MS, QMS, and QEPAS for the measurements of Scenario 2. These graphs were chosen exemplarily, as the gas mixtures from Scenario 2 show far more variety and concentration of hazardous substances—155 in all. It can be seen that most substances appear in the GC-MS spectrum retrieved from the charcoal sample (Figure 3a), whereas far fewer components adsorb on silica (Figure 3b). In the QMS-spectrum, the expected composition of atmospheric air mixed with the species from the battery emission can be seen. Although the *in situ* measurement with the QEPAS-sensor was performed only for Scenario 2, it shows a good insight of the temporal behavior of the process, starting with the emission peak shortly

after the nail penetration and nearly exponentially decaying over time. Furthermore, it underlines the high CO content detected by QMS for Scenarios 2 and 3.

More detailed insight into the measurement results can be gained by a comparison of the three scenarios. Based on the quantity, dangerousness, and toxicity of the respective components, a selection of 11 crucial gas mixture constituents was chosen from the measurement data. In Table 1, the respective substances and their hazard potential [15] are listed, a diagram depicting the corresponding concentrations for all three scenarios is shown in Figure 4.

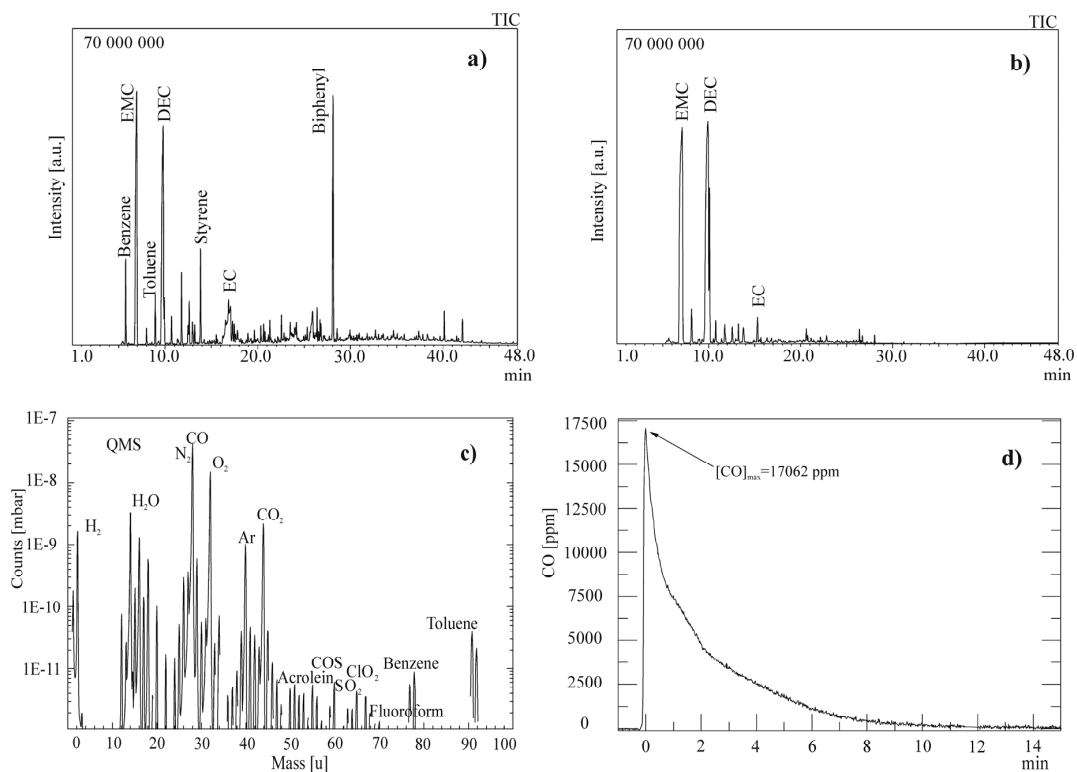


Figure 3. Results of the gas chromatography-mass spectrometry (GC-MS) analysis with (a) activated charcoal tube and (b) silica gel tube of (c) the quadrupole mass spectrometry (QMS) analysis and (d) the quartz-enhanced photoacoustic spectroscopy (QEPAS)-measurement for Scenario 2.

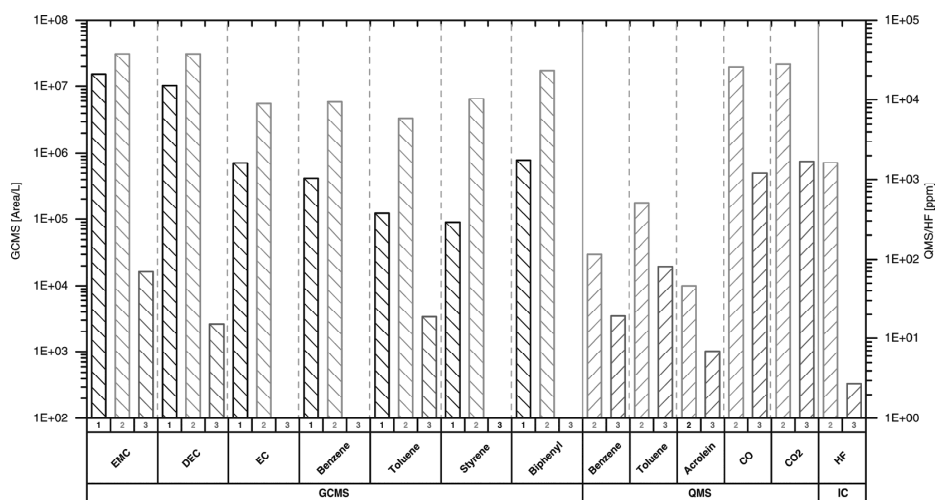


Figure 4. Results of the GC-MS, QMS investigations and HF detection for 11 determinant gas constituents for all three scenarios (1–3).

Table 1. Eleven crucial gas mixture constituents and their hazards. EMC: ethyl methyl carbonate; DEC: diethyl carbonate; EC: ethylene carbonate; CO: carbon monoxide; and COS: carbonyl sulfide.

Substance	Hazards According to EU Regulation (EG) Act 1272/2008
EMC	Eye irritation; flammable liquid; H226; H315; H319; H335; Skin irritation, specific target organ toxicity-single exposure.
DEC	Eye irritation; flammable liquid; H226; H315; H319; H335; skin irritation; specific target organ toxicity-single exposure.
EC	Eye irritation; H315; H319; H335; skin irritation; specific target organ toxicity-single exposure.
Benzene	Aspiration hazard; carcinogenicity; eye irritation; H225; H304; H315; H319; H340; H350; H372; germ cell mutagenicity.
Toluene	Aspiration hazard; flammable liquid; H225; H304; H315; H336; H361d; H373; reproductive toxicity; skin irritation; specific target organ toxicity-repeated exposure.
Styrene	Acute toxicity; eye irritation; flammable liquid.; H226; H315; H319; H332; H361d; H372; Skin irritation; Specific target organ toxicity-repeated exposure.
Biphenyl	Aquatic acute toxicity; aquatic chronic toxicity; eye irritation; H315; H319; H335; H400; H410.
Acrolein	Acute toxicity; aquatic acute toxicity; aquatic chronic toxicity; carcinogenicity; corrosive to the respiratory tract; eye damage; flammable liquid; H225; H300; H300 + H330; H302;H311;H314;H317;H318;H330;H341; H351; H400; H410; germ cell mutagenicity; skin corrosion; skin sensitization.
CO	Acute toxicity; flammable gases; H220; H280; H331; H360DM H372M gases under pressure; reproductive toxicity; specific target organ toxicity-repeated exposure.
COS	Acute toxicity; eye irritation; flammable gases; H220; H280; H315; H319; H331; H335; Gases under pressure.
Hydrogen fluoride	Acute toxicity; corrosive to the respiratory tract; H300; H310; H314; H330; skin corrosion.

As QMS and HF detection were not performed for Scenario 1, these data are missing within the graph. The entire list of components and individual concentrations for each scenario can be found in the Supplementary Materials, namely “GCMS Measurement, Activated Charcoal, Scenario 1.pdf”, “GCMS Measurement, Activated Charcoal, Scenario 2.pdf” and “GCMS Measurement, Activated Charcoal, Scenario 3.pdf”.

Even without further description, it can be clearly seen that the gas emission from Scenario 2 provokes the highest concentration for each of the selected species. Furthermore, the after filtration measurements show even lower concentrations compared to Scenario 1. For this scenario the lowest concentrations of organic components were expected due to their reaction with environmental oxygen (O₂) to CO₂ and H₂O. The reason for this behavior can be explained as follows: Scenario 1 was chosen to represent the event of a battery failure without any further security measures. In this case the cell expands until it bursts open and catches fire. As the outgassing of the cell within the barrel occurs abruptly (see the video “Experimental Setup Scenario 2.mp4” and freeze frame “Experimental Setup Scenario 2 Still.jpg” in online version in Supplementary Materials), it is assumed that the available quantity of O₂ is insufficient for an accomplished oxidation of all components, because the gas from the cell displaces the environmental air in the barrel. Therefore, only part of the volatile organic compounds feed the combustion, whereas a considerable amount still emerges as fume. This fume mainly consists of the electrolyte’s main constituents EMC and EC, with traces of the pollutants diethyl carbonate (DEC), benzene, toluene, styrene, and biphenyl.

As the case of a burning cell must be strictly avoided because of the cascaded inflammation of neighboring cells, which is most likely to occur, the first security measure is to suppress the inflammation of the emission gases, thus drastically reducing the amount of energy released. This was achieved by using a textile composite material enclosing the cell and thereby prohibiting flying sparks

while being permeable for the emission gases [16]. For this case (Scenario 2), almost no oxidation takes place. Consequently, a larger amount and a respective higher quantity of unburned organic substances were expected and could be verified by the analytical methods. All in all, 155 different constituents were found and particularly the concentration of the aforementioned components increased significantly (Figure 4). In addition to the mentioned constituents, a large number of several other organic substances can be seen, most of them are highly flammable and irritating and, thus, dangerous and unpredictable (Figure 3a,b). The results of the GC-MS from the silica gel tube do not show any subsidiary information, but nevertheless verify the results of the GC-MS from the activated charcoal tube. The reason for the large amount of different organic components that were found is mainly the lack of O₂ in combination with high temperatures. Under these conditions, pyrolysis leads to homolytic cleavage of the C–O single bonds to form free ethyl and methyl radicals, mainly from the electrolyte's main component EMC. Random combinations of these free radicals can end up in a recombination to EMC, as well as the combination to dimethyl carbonate (DMC) (although not detected here) and DEC (Figure 5).

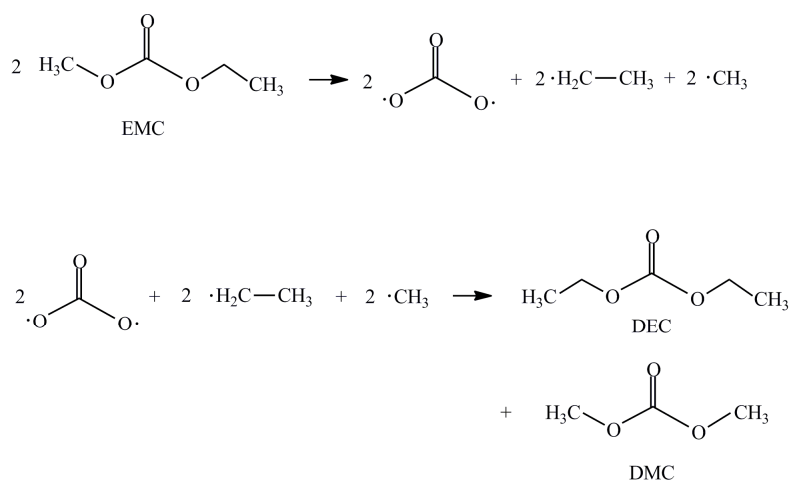


Figure 5. Homolytic cleavage and radical combination can form DEC and DMC from EMC.

Nevertheless the authors noticed DMC in further experiments with the same type of cell that are not part of this paper. For the GC-MS spectra shown in Figure 3, the detection of molecules started at a retention time of around 5 min to fade out the solvents. This retention time is too long for the detection of DMC that has its peak at around 4.85 min.

Alongside with free methyl and ethyl radicals, the formation of free vinyl and ethylene radicals is highly probable. The free vinyl radicals are able to combine to 1,3-butadiene. After radicalization butadiene, itself, can add an ethylene radical to form benzene. In a termolecular or stepwise reaction, benzene can also be formed from three free ethylene radicals. Additional reactions of benzene with free methyl and/or vinyl radicals lead to toluene, xylene, and styrene. Homolytic cleavage of a C–H bond in benzene forms the free phenyl radical C₆H₅ that can dimerize, forming biphenyl. Polycyclic aromatic compounds (PAH), like naphthalene, can be formed in similar reactions [17]. In Figure 6, a short overview of those reactions is shown.

Smaller molecules were detected via QMS. The corresponding spectrum (Figure 3c) shows that the major components of ambient air, such as nitrogen (N₂), O₂, water (H₂O), carbon monoxide (CO) and dioxide (CO₂), as well as argon (Ar), are still present, though at different fractions. Due to the experimental realization, several days of storage time occurred for the transfer from the gas emission experiment to the QMS. After this duration, the gas components with large molecular masses were expected already to be settled on the walls of the gas bag. Indeed, the EMC, DEC, EC, and biphenyl fractions found within the GC-MS spectra cannot be seen by QMS, even if they should be observable with both techniques. Toluene and benzene were found according to their major peaks at 91 u (115 ppm) and 78 u (505 ppm), respectively, while fragments of styrene can be ruled out due to the missing

peak at 89 u. In addition to the toluene and benzene, clear signs of carbonyl sulfide (COS), chlorine dioxide (ClO₂), sulfur dioxide (SO₂), and trifluoromethane (fluoroform) can be recognized according to their major fragments at 60 u, 66 u/67 u, 64 u, and 69 u, respectively. With its peak at 55 u/56 u, acrolein (46 ppm) is particularly critical because of its highly toxic properties (Table 1). The simplest unsaturated aldehyde acrolein is a common byproduct of oxidation processes. Its objectionable odor is e.g., created on the extinction of candles. It also occurs in tobacco smoke or in smoke from wild fires.

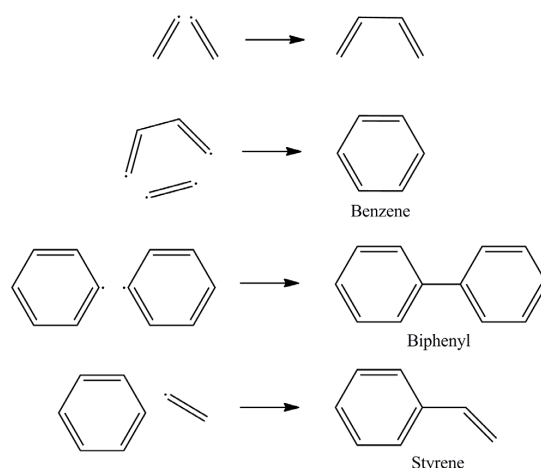


Figure 6. Four exemplary radical reactions that form benzene, biphenyl, and styrene. More reactions underlying similar principles lead to the large amount of different aromatic constituents that were found [17].

The detected fragments of substances with equal atomic mass, like N₂ and CO, are occasionally difficult to allocate with QMS. To verify these assigned values with QEPAS, an additional measurement method is available to retrieve additional information about the target gas mixture by addressing its absorption spectrum and its temporal behavior. The QEPAS measurement of CO gives a good idea of the temporal behavior of the processes involved. The measured concentration matches with the QMS data, considering the error assigned to the overlapping with N₂. For the measurement of reactive components, like substances with high electronegativity or large molecules that adsorb until their detection, QEPAS can be an additional analytical method. Especially, the use of a widely tunable laser in the mid infrared spectral region would provide an additional dataset for the whole gas mixture, thus increasing the accuracy of measurement [18].

Another hazardous substance of central importance is HF, which results mainly from the decomposition of the conducting salt LiPF₆; in Scenario 2 1640 ppm were found, which is more than 50 times higher than the immediately dangerous to life or health (IDLH) value. This concentration would lead to fatal consequences for a human being within a few minutes, since the reported emergency exposure limit (EEL) for 10 min is only 20 ppm [19].

As clarified by the evaluation and comparison of the experiments of Scenario 1 and 2, a suppression of the flame formation in the case of a thermal runaway is much more critical concerning the danger of the emerging gas. However, the ignition of the gas mixture in battery storages cannot be justified since it comes along with unpredictable risks. Therefore, in Scenario 3 an additional neutralization filter system for the emission gasses was tested to diminish the hazardous potential.

After passing the filter element, as described above, only three substances were found via GC-MS with significantly lower values, namely EMC, DEC, and toluene (Figure 4). Consistent with these results, the QMS also demonstrates that the concentrations of the hazardous gas components are strongly reduced by the filter system. In particular, the benzene, toluene, acrolein, and SO₂ contents were reduced to less than 20% of their initial fraction. The COS, ClO₂, and fluoroform emissions, however, dropped below the measurement range of the used spectrometer. For HF, a high filtration

efficiency could be achieved, too. In Scenario 3, the measured concentration was merely 3 ppm and, thus, significantly below the IDLH value of 30 ppm and more than 500 times lower than in Scenario 2. The majority of the organic compounds are removed by adsorption on activated charcoal. The efficiency of adsorption increases with molecule size and similarity to the graphite structure (aromatics). The major portion of acid gases, such as HF, is presumably filtered out by chemisorption of the alkaline part of the filter system, the activated alumina. Following Equation (1), the fluorine is trapped as aluminum fluoride under formation of H₂O [20]:



The measurements from Scenario 3 show highly-promising filtration rates for all hazardous components under test. It should be mentioned that a leak in the barrel-filter unit construction leads to a loss of some of the venting gas from the battery; the loss is estimated to be lower than 15%. However, the measured data should not be affected by this as the increased pressure in the barrel inhibited the influx of ambient air and, therefore, a decrease in the measured concentrations is unlikely. Furthermore, the gas was sucked from a gas collecting bag with a volume of nearly zero at the beginning; thus, only filtered gas was sucked to the measuring devices.

Even though the slight overcharging to 4.3 V could affect the gas within the cell due to a beginning decomposition, this effect can be neglected because a commercial cell at this voltage usually is far from a critical point. In addition, this paper is mainly focused on the reduction of risk potential by additional safety measures and less on the exact gas composition for different cell states.

4. Conclusions

By the outgassing of a lithium ion battery due to a thermal runaway, a dangerous gas mixture with highly explosive, hazardous, and carcinogenic components is released. If no counteractive measures are taken, the cell's failure leads most likely to an ignition, which must be excluded, as there is a great risk of a cascaded runaway of adjacent cells. However, with an inflammation of the battery gas, some of the hazardous substances get oxidized into harmless reaction products, as shown by the performed measurements. If the ignition of the cell is prevented, which can be done most effectively by a textile composite, the gas emission is far more dangerous. Consequently, a gas filtration system has been developed by which adsorption or neutralization processes reduce the concentration of the hazardous components. In a first trial, a selection of filtering materials and a subsequent analysis of the gases released by the filter unit showed very promising results, reducing the concentration of all relevant components well below the amount of the inflammation measurement. The success of these experiments conducted once, will be used in further investigations in order to realize a reliable and cost efficient filter unit which reaches IDLH, or comparable values, for all relevant emitted species.

The combination of the flame-inhibiting textile and the gas filter unit may be used in stationary systems for home storage, or even large scale storage applications, enhancing the security level of the state-of-the-art battery storage to the next level without changing the fundamental cell design.

Supplementary Materials: The following are available online at www.mdpi.com/2313-0105/2/1/5/s1, Experimental Setup Scenario 2.mp4, Experimental Setup Scenario 2 Still.jpg, GCMS Measurement, Activated Charcoal, Scenario 1.pdf, GCMS Measurement, Activated Charcoal, Scenario 2.pdf, GCMS Measurement, Activated Charcoal, Scenario 3.pdf.

Acknowledgments: Financial support from the investment and development bank of Lower Saxony (Project No. ZW3-80140889) is gratefully acknowledged.

Author Contributions: Antonio Nedjalkov and Jan Meyer were responsible for the project, the conducted experiments and the writing of the paper. Alexander Doering initialized the experiments and developed the principle filter design. Michael Köhring was responsible for the QEPAS measurements and helped writing the paper. Sebastian Dahle was responsible for the QMS measurements and assisted to analyze the data. Andreas Sander developed the Flotrex composite material and supported the performed experiments. Axel Fischer was responsible for the chemical analysis of HF, the GCMS measurements and helped writing the paper. Martin Angelmahr was the project manager and Wolfgang Schade supported the project as the head of the institute.

Conflicts of Interest: The authors declare no conflict of interest.

References

1. Leadbetter, J.; Swan, L.G. Selection of battery technology to support grid-integrated renewable electricity. *J. Power Sources* **2012**, *216*, 376–386. [[CrossRef](#)]
2. Beaudin, M.; Zareipour, H.; Schellenberg, A.; Rosehart, W. Energy storage for mitigating the variability of renewable electricity sources: An updated review. *Energy Sustain. Dev.* **2010**, *14*, 302–314. [[CrossRef](#)]
3. Rand, D.A.J.; Moseley, P.T. Energy Storage with Lead–Acid Batteries. In *Electrochemical Energy Storage for Renewable Sources and Grid Balancing*; Moseley, P.T., Garche, J., Eds.; Elsevier: Amsterdam, The Netherlands, 2015; Chapter 13; pp. 201–222.
4. Kurzweil, P. Lithium Battery Energy Storage: State of the Art Including Lithium–Air and Lithium–Sulfur Systems. In *Electrochemical Energy Storage for Renewable Sources and Grid Balancing*; Moseley, P.T., Garche, J., Eds.; Elsevier: Amsterdam, The Netherlands, 2015; Chapter 16; pp. 269–307.
5. Ren, G.; Ma, G.; Cong, N. Review of electrical energy storage system for vehicular applications. *Renew. Sustain. Energy Rev.* **2015**, *41*, 225–236. [[CrossRef](#)]
6. Wang, Y.; Liu, B.; Li, Q.; Cartmell, S.; Ferrara, S.; Deng, Z.D.; Xiao, J. Lithium and lithium ion batteries for applications in microelectronic devices: A review. *J. Power Sources* **2015**, *286*, 330–345. [[CrossRef](#)]
7. Lisboa, D.; Snee, T. A review of hazards associated with primary lithium and lithium-ion batteries. *Process Saf. Environ. Prot.* **2011**, *89*, 434–442. [[CrossRef](#)]
8. Wang, Q.; Ping, P.; Zhao, X.; Chu, G.; Sun, J.; Chen, C. Thermal runaway caused fire and explosion of lithium ion battery. *J. Power Sources* **2012**, *208*, 210–224. [[CrossRef](#)]
9. Doughty, D.H.; Crafts, C.C. *FreedomCAR Electrical Energy Storage System Abuse Test Manual for Electric and Hybrid Electric Vehicle Applications*; Sandia Report SAND2005-3123. Sandia National Laboratories: Albuquerque, NM; Livermore, CA, USA, 2006.
10. Abraham, D.P.; Roth, E.P.; Kostecky, R.; McCarthy, K.; MacLaren, S.; Doughty, D.H. Diagnostic examination of thermally abused high-power lithium-ion cells. *J. Power Sources* **2006**, *161*, 648–657. [[CrossRef](#)]
11. Larsson, F.; Andersson, P.; Blomqvist, P.; Lorén, A.; Mellander, B.-E. Characteristics of lithium-ion batteries during fire tests. *J. Power Sources* **2014**, *271*, 414–420. [[CrossRef](#)]
12. Ohsaki, T.; Kishi, T.; Kuboki, T.; Takami, N.; Shimura, N.; Sato, Y.; Sekino, M.; Satoh, A. Overcharge reaction of lithium-ion batteries. *J. Power Sources* **2005**, *146*, 97–100. [[CrossRef](#)]
13. Stein, S.E. “Mass Spectra” in NIST Chemistry WebBook: NIST Standard Reference Database Number 69. Available online: <http://webbook.nist.gov/> (accessed on 29 September 2015).
14. Kosterev, A.A.; Bakhirkin, Y.A.; Curl, R.F.; Tittel, F.K. Quartz-enhanced photoacoustic spectroscopy. *Opt. Lett.* **2002**, *27*, 1902–1904. [[CrossRef](#)] [[PubMed](#)]
15. Sigma-Aldrich. SDS Search and Product Safety Center. Available online: <http://www.sigmaaldrich.com/safety-center.html> (accessed on 31 August 2015).
16. K.TeX—Knein Technische Textilien GmbH. Insulation Materials for Lithium Ion Batteries. Available online: <http://www.ktex-gmbh.de/images/Anwendungen/Product-Portfolio-Insulation-Materials-for-Lithium-Ion-Batteries.pdf> (accessed on 29 September 2015).
17. Ballschmiter, K.; Bacher, R. *Dioxine: Chemie, Analytik, Vorkommen, Umweltoverhalten und Toxikologie der Halogenierten Dibenz-p-Dioxine und Dibenzofurane*; VCH: Weinheim, Germany; New York, NY, USA; Basel, Switzerland; Cambridge, UK; Tokyo, Japan, 1996. (In German)
18. Curl, R.F.; Capasso, F.; Gmachl, C.; Kosterev, A.A.; McManus, B.; Lewicki, R.; Pusharsky, M.; Wysocki, G.; Tittel, F.K. Quantum cascade lasers in chemical physics. *Chem. Phys. Lett.* **2010**, *487*, 1–18. [[CrossRef](#)]
19. Centers for Disease Control and Prevention. Hydrogen Fluoride (as F). Available online: <http://www.cdc.gov/niosh/idlh/7664393.html> (accessed on 26 February 2016).
20. Ingenieurbüro Oetzel. Aufnahmevermögen von Aktivkohle Gegenüber Chemischen Einzelverbindungen. Available online: <http://www.umweltanalytik.com/daten/aktivkohle.htm> (accessed on 26 February 2016). (In German)



Investigation on the fire-induced hazards of Li-ion battery cells by fire calorimetry

Perrine Ribière,^a Sylvie Grugeon,^a Mathieu Morcrette,^a Simeon Boyanov,^b Stéphane Laruelle^a and Guy Marlair^{*b}

Received 26th July 2011, Accepted 15th August 2011

DOI: 10.1039/c1ee02218k

The use of the high energy Li-ion battery technology for emerging markets like electromobility requires precise appraisal of their safety levels in abuse conditions. Combustion tests were performed on commercial pouch cells by means of the *Fire Propagation Apparatus* also called Tewarson calorimeter in the EU, so far used to study flammability parameters of polymers and chemicals. Well-controlled conditions for cell combustion are created in such an apparatus with the opportunity to analyse standard decomposition/combustion gases and therefore to quantify thermal and toxic threat parameters governing the fire risk namely the rate of heat release and the effective heat of combustion as well as the toxic product releases. Using the method of O₂ consumption, total combustion heats and its kinetic of production were determined as a function of the cell state of charge unveiling an explosion risk in the case of a charged cell. The resulting combustion heat is revealed to be consistent with cumulated contribution values pertaining to each organic part of the cell (polymers and electrolytes) as calculated from thermodynamic data. The first order evaluation of the dangerousness of toxic gases resulting from fire induced combustion such as HF, CO, NO, SO₂ and HCl was undertaken and stressed the fact that HF is the most critical gas originating from F-containing cell components in our test conditions.

1. Introduction

Today, it is crucial to find a source of alternative energy respecting the environment through the use of renewable

energies. The Li-ion battery is one of the emerging new systems of electric storage^{1–3} proposed in industries for innovative application (automobile, solar and wind energy, ...) according to its high energy density (approximately three times that of the Ni-MH battery). However, although these batteries have become quite common for consumer market applications like cell-phones or laptops, the widespread use of this technology for emerging markets like electromobility or smart grids requiring stronger energy and power capacities must be examined from a safety point of view. In general, most of the inherent hazards trigger

^aLaboratoire de Réactivité et Chimie des Solides, UMR CNRS 6007, Université de Picardie Jules Verne, 33 rue Saint Leu, 80039 Amiens, France

^bInstitut National de l'Environnement et des Risques (INERIS), Direction des Risques Accidentels, Parc Technologique Alata, BP2 60550 Verneuil en Halatte, France. E-mail: guy.marlair@ineris.fr; Fax: +33 3 44 55 65 65; Tel: +33 3 44 55 63 70

Broader context

Safety and safety management could remain for some time the hurdles to overcome before a sustainable development of lithium type electric storage systems is seen worldwide. Therefore, numerous initiatives have been launched by various organizations in the EU (CENELEC, UN Sub-Committee of experts on TDG in Geneva, Recharge, ...), and overseas (SAE, NFPA, ISO, ...) to learn more on technical aspects of safety issues and to improve—through testing and modelling—the resistance of such batteries to abuse conditions. However, fire, as rare an event it may become, remains a possibility. Therefore the consequences of fire scenarios involving lithium batteries need to be fully appraised for fire safety engineering purposes. This work is one of the earlier contributions in that direction, relying on the use of the so-called “*Fire propagation apparatus*”, internationally recognized as one of the most outstanding pieces of test equipment ever made available to fire scientists to produce scientifically sound data that can be extrapolated and in turn serve risk analysis in various contexts. Basic data allowing pertinent estimates of thermal and chemical threats following a burning Li-ion cell of the “pouch type” have been achieved and are discussed in a way that allows further evaluations regarding fire safety issues on the full value chain of electric energy storage.

accidental scenarios when batteries are misused or facing abnormal environmental conditions. In such a case, the contact of highly energetic active materials with flammable organic solvent-based electrolytes can lead to situations out of control. When working out of the stability domain of the system (in terms of temperature or voltage), a series of undesirable reactions (varying according to the type of electrochemistry involved) may occur such as electrolyte reduction at the negative electrolyte interfaces,⁴⁻⁶ lithium metal plating,^{7,8} oxidation of electrolyte at high potential *versus* Li⁺/Li⁰,^{9,10} These side reactions can lead to release of heat and gases, then subsequently cause thermal runaway¹¹ that entails significant threats such as explosion or fire phenomena such as the combustion of the electrolyte after rupture of battery confinement. Currently, tests are proposed to characterize the safety performance of the cell constituents of the batteries and appraise their safety levels in abuse conditions. They are determined from technical guidance documents and emerging standards are often under a revision process (UL,¹² ANSI, SEA, ISO and IEC, UN Manual of tests and criteria, ...). A recent compilation of these tests was recently proposed by Doughty.¹³ These tests can be classified into electrical (overcharge, internal short circuit, external short circuit, overdischarge, ...), mechanical (shock, nail penetration, crush, ...) or environmental (thermal cycling, ...) but hardly ever take account of fire conditions either resulting from a thermal runaway process or induced by external environment.

In particular, a fire event resulting from those abuse tests is considered as severe (rated as level 5 to 6) according to hazards rating schemes (level rating from 0 to 7) developed by various organisations (Table 1). However, severity may or may not be critical according to potential adverse effects of such a fire event in a given context, and this consideration has received so far little attention.

From a general survey of past fires that occurred in the last decades, it can be stated that a large proportion of fire injuries and fatalities can be attributed to the inhalation of smoke and toxic gases, so the identification and quantification of the released gases are of major interest as well as the determination of heat produced or onset temperature for thermal runaway. Researchers mainly focused so far on collecting the thermodynamic data, indeed the thermal abuse response of Li-ion cells has been studied at both the component and cell levels using differential scanning calorimetry (DSC)^{11,14-16} and accelerating rate calorimetry (ARC).¹⁷ In this paper, we report thermal tests performed with a fire calorimeter, namely the Fire Propagation Apparatus (ASTM E2058 & NFPA 287), also called the

Tewarson Apparatus in Europe.¹⁸⁻²⁰ This very versatile device originally developed by FM Global can give access to the most important fire parameters that are needed for qualifying actual accidental scenarios, such as the heat release rate (governing the thermal threat) and products release rate (governing the toxic threat). This calorimeter is routinely used to study the flammability parameters of polymers,²⁰⁻²² but is also relevant to learn on the fire behaviour of chemicals²³⁻²⁵ and electrical components.²⁶ The collected combustion thermal and chemical data are the basic input data required for performing thermal and toxic impact calculation to estimate the consequences of industrial fires. In particular, the on-line gas analysis instrumentation (including Fourier-Transform Infra Red equipment) conjugated to flow rate and mass loss rate measurements provides chemical data allowing the determination of the nature and the relating yields of toxic combustion or decomposition products.

In this article, a description of the Tewarson calorimeter and the heat rate calculation method is presented. Tests performed on commercial batteries with different states of charge are reported, supplemented by a discussion on possible mechanisms leading to the formation of the detected gases along with an evaluation of the human toxicity.

2. Experimental

Pretesting

First of all, to prevent the Tewarson calorimeter from being damaged by extreme fire scenarios, a preliminary test is performed to evaluate the explosion risk and relating effects. Hence, a sample of each battery to be studied in fire conditions in the Tewarson calorimeter was placed at first inside a concrete test chamber to undergo the impact of a pool fire of ethanol. In such conditions, no serious explosion risk was observed and adequate testing procedures were established according to further investigations making use of the Tewarson calorimeter.

The fire propagation apparatus (Tewarson calorimeter)

The working principle of the Tewarson apparatus is illustrated in Fig. 1. This apparatus comprises two main subsystems. The lower part of the equipment is used to set the sample in combustion configuration under well controlled conditions. The upper part conveys the smoke gases into the exhaust system through a ducting section where critical measurements are made. In particular, the set of instruments allows the quantification of main thermal and toxic threat parameters such as the rate of heat

Table 1 Toxicity threat and overall battery hazard rating according to various approaches (adapted from ref. 32)

Overall hazard level	EUCAR description	SAE J2464 description	IEC description	Toxicity issue
0	No effect	No effect	No effect	
1	Passive protection activated	Passive protection activated	Deformation	
2	Defect/damage	Defect/damage	Venting	Yes
3	Leakage ($\Delta m_{\text{mass}} < 50\%$)	Minor leakage/venting	Leakage	Yes
4	Venting ($\Delta m_{\text{mass}} \geq 50\%$)	Major leakage/venting	Leakage	Yes
5	Fire or flame	Rupture	Rupture	Yes
6	Rupture	Fire or flame	Fire	Yes
7	Explosion	Explosion	Explosion	Yes

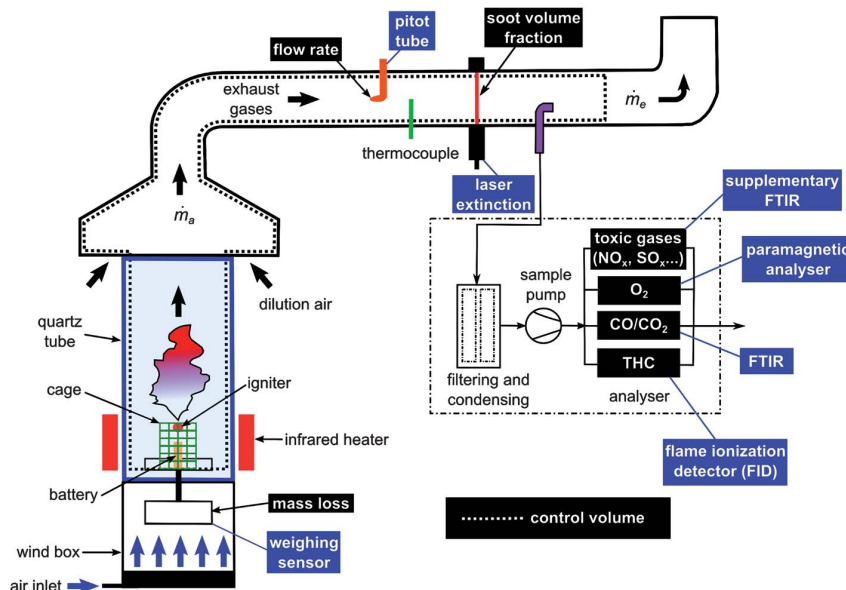


Fig. 1 Schematic of the INERIS fire propagation apparatus (Tewarson calorimeter).

release, the effective heat of combustion and the yields (or generation efficiencies) of the combustion products.

(i) Lower part details. The battery is placed in a tailored stainless steel cage which is laid onto a sample holder in the central axis of the system. The sample holder and its content are connected to a weighing sensor located inside the wind box, distributing evenly the combustion air (or any other oxidizing stream) in the combustor chamber delimited by a quartz tube. The oxidizing agent is injected at the bottom of the wind box. From this configuration, a well delimited area of combustion is thus created; it allows easy control of the degree of ventilation. The experiments were carried out under controlled air flow (350 L min^{-1}) simulating outside fire conditions.

An external heat flux is applied to the combustion chamber by four infrared heaters using tungsten filament quartz lamps inserted in both air-cooled and water-cooled reflectors (irradiance level impacting the sample in the order of 35 kW m^{-2}) placed around the battery (at around 10 cm) and whose efficiency depends on the matching between the emitted wavelength and the absorption spectrum of the material to be heated. The resulting flammable gas released from the battery can be ignited thanks to a pilot-flame placed at 30 mm above. Such infra-red heaters are desirable as they provide thermal aggression comparable to a fire environment and do not bring any additional fuel source needed to set fire conditions that would otherwise interfere with emissions of gases from the item under testing.

(ii) Upper part details. Fire products are totally captured and mixed with dilution ambient air, in the sampling duct, where the gas temperature and the product–air mixture flow rate are measured. The online analysis of the diluted smoke includes the quantification of O_2 by paramagnetic analyzer, CO and CO_2 by FTIR analyzer, soot using optical measurement and total

hydrocarbons by means of flame ionization detector. The volume fractions of these molecules will be utilized hereafter as input data to calculate thermodynamic and kinetic magnitudes. Note that these analyses are performed after preconditioning the gases by filtration and dewatering.

A supplementary FTIR Instrument was also implemented to provide data on “standard” toxic gases such as hydrogen halides, HCN, NO_x , SO_x , and aldehydes. Herein are reported the most significant concentrations detected with a Nicolet 6700 spectrometer using a 2 m gas cell ($V = 200 \text{ mL}$). It is worth noting that this fire calorimeter was recently listed as one of the rare lab-scale “fire physical models” capable of producing pertinent fire toxicity data at ISO level.²⁷

Determination of the heat release rate (HRR)

The rate at which energy is released from a fire is the most important factor which governs its behavior.²⁸ It is possible to determine the HRR experimentally in a convenient way using the method of oxygen consumption. During a combustion process that has gone to completion, it can be estimated by

$$\dot{q} = E(\dot{m}_{\text{O}_2}^0 - \dot{m}_{\text{O}_2}) \quad (1)$$

where \dot{q} is the heat release rate (kW), \dot{m}_{O_2} and $\dot{m}_{\text{O}_2}^0$ are the mass flow rates of oxygen from the entrained air when a combustion occurs or not, respectively (kg s^{-1}). E is the energy released per mass unit of O_2 consumed for a given fuel (kJ g^{-1} of O_2). For a large number of organic solids and liquids or gaseous compounds, this energy appears to be approximately constant (this is known as the Thornton principle). After having checked the values for all possible battery compounds that are able to burn, we took the averaged energy “ E ” of 13.1 kJ g^{-1} of O_2 . In most cases however, combustion in fire conditions is found to be incomplete implying carbon monoxide and soot particles

formation. This leads to an overestimation of the HRR calculated from eqn (1) that therefore requires the following corrections:

$$\dot{q} = E \left(\dot{m}_{\text{O}_2}^0 - \dot{m}_{\text{O}_2} + \Delta \dot{m}_{\text{O}_2(\text{CO} \rightarrow \text{CO}_2) + (\text{soot} \rightarrow \text{CO}_2)} \right) - \dot{q}_{\text{CO} \rightarrow \text{CO}_2} - \dot{q}_{\text{soot} \rightarrow \text{CO}_2} \quad (2)$$

where $\dot{q}_{\text{CO} \rightarrow \text{CO}_2}$ and $\dot{q}_{\text{soot} \rightarrow \text{CO}_2}$ are the HRR accounting for the CO and soot combustion respectively. They are defined as $\dot{q}_{\text{CO} \rightarrow \text{CO}_2} = \dot{m}_{\text{CO}} E_{\text{CO}}$ with $E_{\text{CO}} = 17.6 \text{ kJ g}^{-1}$ of O_2 required to convert CO to CO_2 , $\dot{q}_{\text{soot} \rightarrow \text{CO}_2} = \dot{m}_{\text{soot}} E_{\text{soot}}$ with $E_{\text{soot}} = 12.62 \text{ kJ g}^{-1}$ of O_2 required to convert soot to CO_2 .²⁹ The interested readers may refer to ref. 22,30 and 31 to learn about the applicability of these fire calorimetry equations which remain a complex issue according to actual material burning, gases measured and inherent limitations of the technique.

Batteries composition

For this study, 2.9 Ah (11 Wh) commercial pouch-type batteries were tested. Prior to being subject to the Tewarson test, a battery mass distribution (Fig. 2) has been established to subsequently compare with the combustion data resulting from the gas quantification. This mass distribution was assessed partially by support of physicochemical analysis of fully discharged battery components and by estimation from an industrial database. This battery was dismantled in an argon-filled glove box. The length, width, thickness and weight of the electrode and the separator were measured (Table 2). The electrode materials composition was determined by X-ray diffractometry (Bruker D8 with a PSD detector Cu K α). To do so, a fragment of electrode was cut and then examined without washing. The separator was rinsed in acetonitrile to recover the electrolyte whose composition was analyzed by ElectroSpray Ionisation High Resolution Mass Spectrometry (ESI-HRMS) and GC/MS techniques. The

conductive carbon content was estimated as representing 10% of the calculated electrodes weight and binder quantities were estimated at 10 and 5% of the negative and positive electrode mass respectively. The weight of the electrolyte was assessed by considering a density of 1.2 and a volume porosity of 50% for the separator and 30% for the electrodes.

Batteries state of charge

The calorimetric tests were undertaken at three different states of charge (100% SOC, 50% SOC and 0% SOC) and reproduced three times. All batteries were electrically preconfigured by initial cycling consisting of a galvanostatic charge/discharge cycle (C/10) between 2.0 and 4.1 V and then were brought to the wanted SOC (Fig. 2). In order to prevent self-discharge and storage effects, the cycling was carried out less than 24 hours before the calorimetric test. These cycling tests were performed with a VMP system (Biologic, Claix, France) equipped with an amplifier.

3. Results and discussion

From the physicochemical analysis, graphite carbon and LiMn_2O_4 materials were identified at the negative and positive electrode respectively and the ethylene, diethyl and dimethyl carbonate solvents (EC : DEC : DMC) with LiPF_6 salt were analyzed as electrolyte. The battery mass distribution is shown in Fig. 2. The active material represents 36% of the battery total mass while the current collectors weight percentage accounts for 30%. Other compounds namely the electrolyte, separator, binder and packaging materials that are mostly constituted of organic or polymers represent 27% (wt) in total.

a. Calorimetric and kinetic analysis

During testing, all batteries behave globally the same way; starting to swell around 90 seconds after the starting point of the external radiant heating process, then opening from the tabs, similar to the movement of an accordion.

(i) **Loss of mass.** Whatever the battery SOC was, the measured mass loss was found to be nearly identical (17, 17 and 16%) whereas the associated kinetics were quite different. As shown in Fig. 3, the discharged battery combustion process lasted longer than that of the fully charged battery (8 min vs. 3 min) and the half charged battery disclosed an intermediate behavior.

A visual observation of the cells after combustion clearly showed the exfoliated coiled copper foil and the presence of aluminium droplets due to Al melting. This observation indicates that the maximum temperature reached during the combustion test within the battery could be estimated between 660 and 1083 °C. At such temperature, all the organic and polymer compounds from separator, binder, packaging and electrolyte should have obviously burnt.

The packaging is comprised of an aluminium foil covered by polymer layers which can be roughly estimated at half the weight. So, the weight percentage of all organics and polymers deduced from this approximation and Fig. 2 data is about 23% which is comparable with the 17% mass lost during experiments. Visual observation of the battery after the test revealed that only the

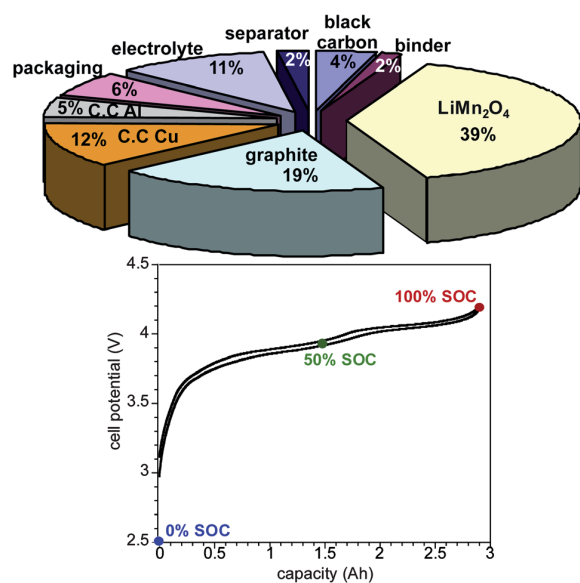


Fig. 2 Mass distribution ($m = 95 \text{ g}$) and potential-capacity curve (2.9 Ah) of the Li-ion battery.

Table 2 Component dimensions measured after 2.9 Ah pouch cell opening

	Cathode	Al current collector	Anode	Cu current collector	Separator
Length/cm	11.9		12.3		12.3
Width/cm	6.5		6.9		6.9
Thickness/cm	2 × 0.007	0.04	2 × 0.0065	0.02	0.0031
Number of electrodes	11		12		

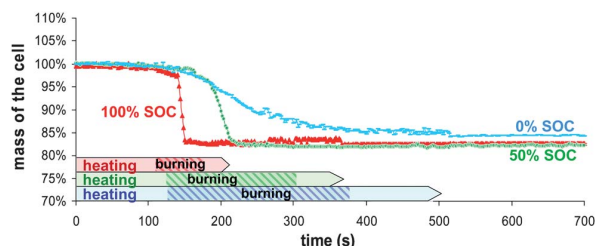


Fig. 3 Samples mass loss during combustion as a function of time for different battery SOC.

upper part of the packaging burnt that slightly decreases the organic compounds percentage to roughly 21%. Therefore, the decomposition and combustion of polymers and electrolytes are responsible for practically all the mass loss indicating such combustion conditions are optimal.

(ii) **Heat released rate (HRR).** The key data to consider are not only the energy value of the combustion but also the way this energy is released with time and the overall information can be extracted from the HRR profile (Fig. 4). In our case, HRR calculation is based on O₂ consumption, corrected for CO and soot production. Fig. 4 shows that the maximum HRR value increases with the SOC. This was found to reach approximately 21, 13 and 2.6 kW for 100, 50 and 0% SOC, respectively. Divided by the battery surface area, the resulting normalized HRR value (kW m⁻²) can be compared with those of other combustible compounds such as standard fuels and polymers that were previously tested using the same Tewarson calorimeter. The normalized HRR value for the 100% SOC batteries is slightly lower than that of gasoline (Fig. 5). For the 50% SOC battery, this is equivalent to that of fuel oil while the 0% SOC battery

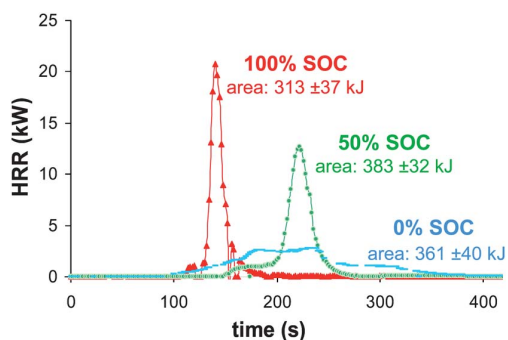


Fig. 4 Comparison of 100, 50 and 0% SOC batteries heat release rates measured from oxygen consumption calorimetry.

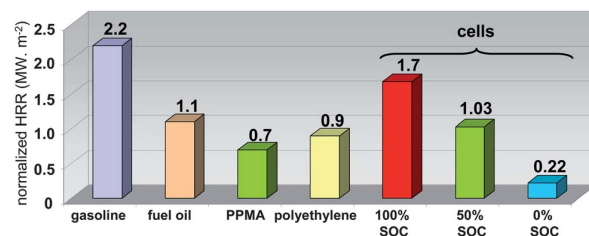


Fig. 5 Comparison of 100, 50 and 0% SOC batteries normalized HRR (MW m⁻²) with that of different combustibles.

presents the lowest value. Another point to consider is the kinetics of the combustion heat release. Fig. 4 clearly shows that the fully charged battery discloses the highest reaction rate; the combustion heat is very shortly released that could entail a potential risk of explosion. The 0% SOC battery is safer with a lower reaction rate. These kinetic changes may be explained either by exothermic redox processes occurring at the interface electrolyte/lithiated negative electrode upon heating or by a fire-induced short which may imply quite rapidly dissipation (by Joule effect) of the electric energy.³² Note that fire calorimetry techniques relying on mass balance (O₂ consumption) cannot, by principle, account for energy simply liberated by the Joule effect.

The HRR profile integration allows the estimation of the overall dissipated combustion heat. The calculated average values were 313 ± 37, 383 ± 32 and 361 ± 40 kJ for 100, 50 and 0% SOC, respectively, corresponding to a maximum effective combustion heat of 4.03 ± 0.34 MJ kg⁻¹ of cells (Fig. 6).

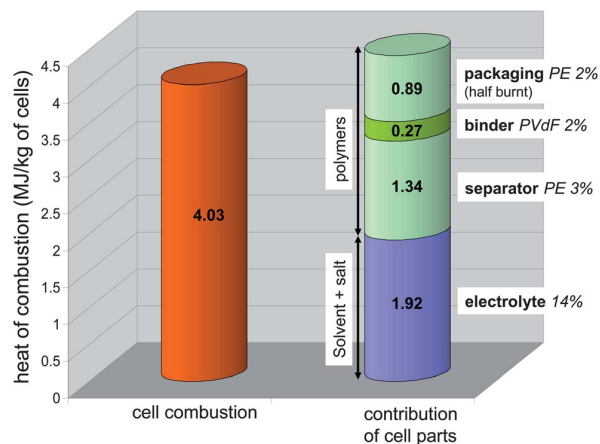


Fig. 6 Maximum experimental combustion heat (HRR integration) of the battery compared with cumulated contribution values pertaining to its organic parts calculated from thermodynamic data.

Compared to gasoline, the maximum volumetric energy of the battery (50% SOC) is three-fold lower (10 vs. 33.1 MJ L⁻¹). It can be noted that although the fully charged battery has the highest HRR values and reaction rates, the combustion energy displays the lowest value.

Thanks to the mass distribution of the battery that was previously estimated, we could predict the contribution of the combustion heat for organics namely the electrolyte and the polymers from separator, binder and packaging. The heat of combustion for PVdF as well as PE were found in the literature,^{33,34} and the heat of combustion of electrolyte was calculated using the heat of formation of solvents and salt³⁵⁻³⁷ and its assumed combustion products such as HF, Li₂O, P₄O₁₀, CO₂ and H₂O.³⁸ As shown in Fig. 6, the sum of these contributions compares well (91%) with the actual cell combustion heat deduced from Tewarson calorimeter data. The slightly higher value may indicate the yield of combustion is not quite complete as usually observed in fire conditions. It can be noticed the overall heat of combustion calculated for the polymers represents at least half the total heat.

Further discussion on uncertainties in HRR measurements. Apart from usual sources of uncertainties well described in the fire science literature (e.g. ref. 22,30, and 31), the brand new question here is the importance of energy that may be liberated through erratic electric discharge through external/internal shorts during the experiments (Joule effect), and that cannot indeed be related to O₂ consumption. Our estimate of the maximum contribution of such a process is about 10% of the overall energy content of a fully charged cell. This calculation confirms that the use of the oxygen consumption technique is reasonably relevant for the estimation of HRR in support of related fire safety engineering objectives.

b. Gas analysis and the toxic threat in abuse conditions leading to fire

The production of volatiles from the battery combustion could come from solids involving for the most part, thermal decomposition processes, or from liquids by a simple evaporation process. Also, as the temperature of a burning solid tends to be high, chemical reactions between the battery compounds or/and volatiles should be considered implying that the composition of gases which are ignited tends to be extremely complex. In this study, the gases we focused on allowed the assessment of the combustion overall efficiency (CO, THC), the HRR value (O₂, CO₂, CO) and the toxic risk (CO, HF, HCl, NO_x, SO₂).

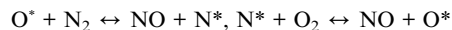
(i) **CO, CO₂ and total hydrocarbons (THC).** CO and CO₂ productions plotted in Fig. 7a and b reveal the combustion overall efficiency. Note that the CO production increases with the SOC of the battery; the combustion efficiency is reflected by nCO₂/nC_{total} molar ratio that reached 90, 98 and 99.5% for 100, 50 and 0% SOC of the tested batteries respectively. These values show that the more the battery stores energy the less the combustion goes to completion in our test conditions. This statement is also highlighted by the production of the total hydrocarbons (Fig. 7c) due to the fuel that has not burnt. Unlike

the 100% SOC case, the yield of THC for the two other batteries SOC is close to zero.

(ii) **SO₂, HCl, CO, NO and HF.** Uncontrolled combustion energy can cause material damage and thermal threat to people (burns), but attention has also to be paid to the reaction products, some of them having deleterious effects on humans, beyond the CO hazard.

During the experiments, “standard” toxic gases production was followed by means of the Infra-Red technique. The analysis revealed consequent yield for five of them: SO₂, HCl, CO, NO and HF.

In Fig. 8a, nitrogen oxide production is reported during combustion. This production depends on the SOC; when the SOC increases, the NO concentration increases and the production time is shortened. The origin of the nitrogen source was checked by testing different parts of the battery (packaging, separator, positive and negative electrodes) but no such source was identified. The nitrogen oxide might be produced as a reaction product of nitrogen (originating from air or fuel-bound N₂) and oxygen from air within the flame (thermal route of NO_x production). Usually, temperatures as high as 2500 K are necessary and radical processes as below are involved:



Visual observation of the combustion (video recording) confirms an apparent relationship between the flame intensity and the NO production measured: highly intense in a short time for the 100% SOC, less intense in a longer time for the 50% SOC and a dim flame for around 3 minutes in the case of 0% SOC. As far as the N₂ presence is concerned, further testing at larger scale would be needed to clarify its origin.

The yield of SO₂ was analyzed (Fig. 8b) and, surprisingly, was found to be in a higher concentration in the case of the fully charged battery. The origin of sulfur containing molecules arises from battery additives. Indeed, sulfur-based compounds are known to be used as additives for their property in facilitating SEI formation.³⁹⁻⁴¹ The heat release reaches a threshold for which the temperature is enough to initiate the degradation of the additive to form sulfur oxide. Unlike fully charged batteries, 50% and 0% SOC HRR values seem to be too low to allow such reaction.

Chlorine was detected through halide production (Fig. 8c). Polymers are chlorine potential sources and may be found in three components of the battery: binder, separator and packaging. The common binders used for commercial batteries, PVdF or CMC,⁴² do not contain chlorine; the sole halogen element which can be found is fluorine in PVdF. Combustion experiments on separator and packaging were undertaken and only the separator revealed the presence of chlorine. The HCl production kinetic for the 100% SOC batteries was different from the others for which the production spans at least two minutes. The quantity of this rejected halide has no SOC dependence and remains low (~25 mg).

From the gas effluents, hydrofluoric acid (HF) was also detected (Fig. 8d). The preliminary analyses of the battery components revealed that the major sources of fluorine were the

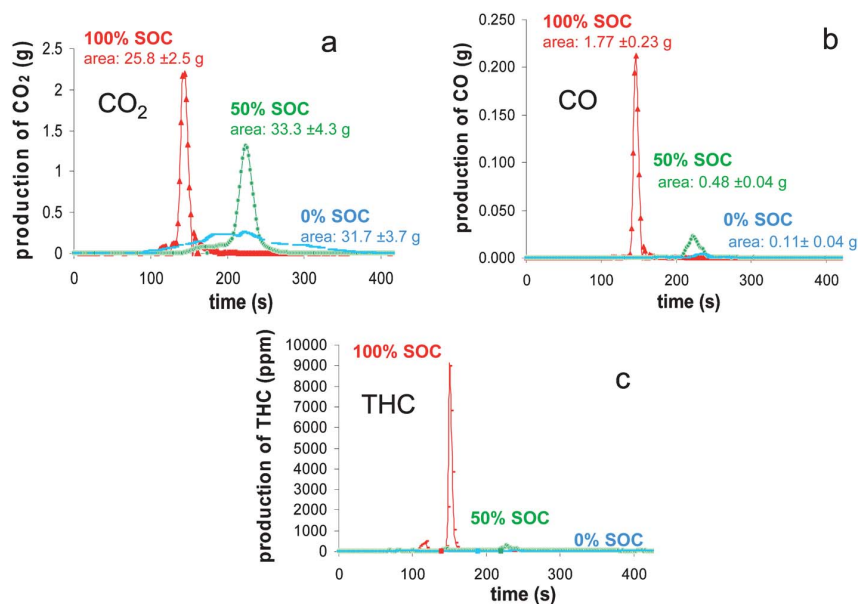


Fig. 7 Mass flux of CO₂ (a), CO (b) and THC (c) as a function of time during the combustion of the batteries at different SOC.

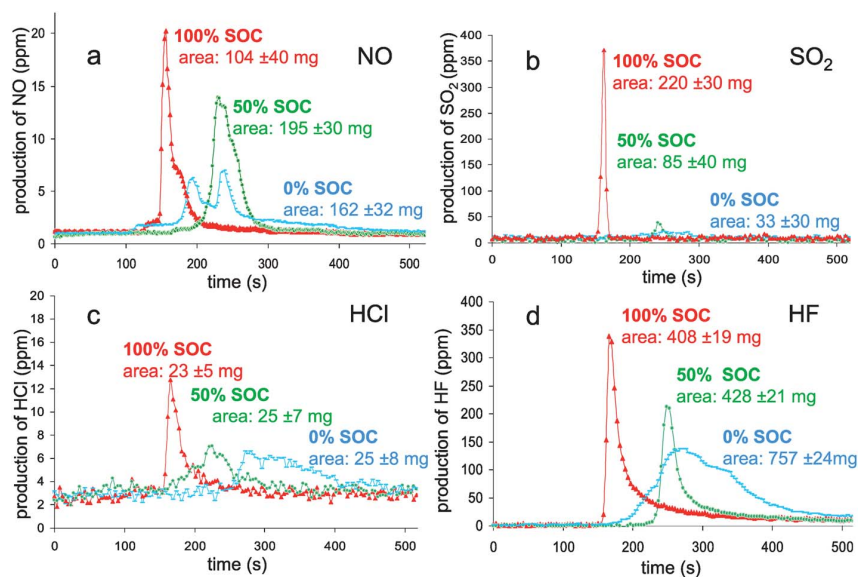


Fig. 8 Mass flux of NO (a), SO₂ (b), HCl (c) and HF (d) as a function of time during the combustion of the batteries at different SOC.

electrolyte salt (LiPF₆) and the binder (PVdF). Its production kinetic turned out to be different according to the battery SOC and followed the HRR profiles. Consequently, HF emission extends over a longer time (200 seconds) for a 0% SOC compared to 50 seconds for a 100% SOC. In accordance with the reaction rate, half-charged batteries behaved as an intermediate case.

Surprisingly, the HF cumulative masses calculated from the peak integration indicated quite different values; the higher one corresponding to the discharged batteries. From the mass distribution analysis, the HF equivalent mass could be estimated to be 1.21 g from the electrolyte and 1.23 g from the binder.

Hence, the detected maximum value (0.757 mg) only represents a third of the total equivalent mass of fluorine contained in the battery. It is worth noting here that, unlike the batteries, the combustion of a EC : DMC : DEC (1 : 1 : 1 wt) LiPF₆ (1 M) electrolyte tested alone in a pool burning mode by means of the same PFA apparatus entailed the release of nearly the total equivalent mass of HF (~98%). Hence, in the case of battery combustion, either a large part of HF is absorbed on battery components or fluorine is involved in complex chemistry^{43,44} so that other fluorine based compounds, not detected here, might be released.

c. Toxicity evaluation

A judicious question is the significance of toxic gas data from these combustion tests. A series of national and international standards give general guidance regarding the toxicity of gas as carbon dioxide, carbon monoxide, hydrogen halides (HCl, HBr, and HF), sulfur dioxide, hydrogen cyanide, nitrogen oxides, formaldehyde (CH₂O) and acrolein (C₃H₄O) gases. Based on the French standard,⁴⁵ the evaluation of the dangerousness⁴⁶ of the combustion gas products was undertaken. Two toxicity limit values were taken into account: the Irreversible Effects Threshold (IET) and the First Lethal Effects Threshold (FLET), as defined in the French regulatory context to perform toxic hazard studies in industrial environment. For a first order toxic hazard evaluation, we have considered the maximum quantity of gas released during all the combustion experiments in a fictive scenario where these gases are evenly distributed in a room of 50 m³ to compare experimental values with the mentioned thresholds.

From the experiments, the maximum values used were 0.22 g (4.4 × 10⁻³ g m⁻³), 0.025 g (5 × 10⁻⁴ g m⁻³), 1.77 g (3.54 × 10⁻² g m⁻³), 0.195 g (3.9 × 10⁻³ g m⁻³) and 0.757 g (1.5 × 10⁻² g m⁻³) for SO₂, HCl, CO, NO and HF, respectively. Fig. 9 plots the FLET and IET values as a function of both the exposure time and the maximum concentration of gas released from

the battery combustion tests. Whatever the exposure time, experimental values are far from IET limits. By basic extrapolation not taking account any scale-up effect on toxic species yields (which is indeed a very questionable assumption), we have evaluated the electrical energy of the batteries required for reaching the individual IET and FLET (Table 3) at a 60 minutes exposure time. Energies as high as 60 to 1320 Wh and 110 to 7880 Wh are announced to approach both the IET and FLET toxicity limits respectively, indicating that the hazard driven by those toxics would require full combustion of relatively large batteries to become critical. From this viewpoint, emerging e-mobility applications (hybrid electric vehicles, plug-in hybrid electric vehicles, full electric vehicles...) that require embarked electric energy storage systems in the range of 15 to 30 kWh would actually deserve dedicated studies focusing on toxicity impacts in the case of EV related fire scenarios. This is true in

Table 3 Estimated battery energy to reach the IET and FLET values for the NO, CO, HCl, SO₂ and HF toxic gases (exposure time of 60 minutes, fire occurring in a 50 m³ room)

(Wh)	HF	CO	NO	SO ₂	HCl
IET	60	290	280	530	1320
FLET	110	1140	2080	4710	7880

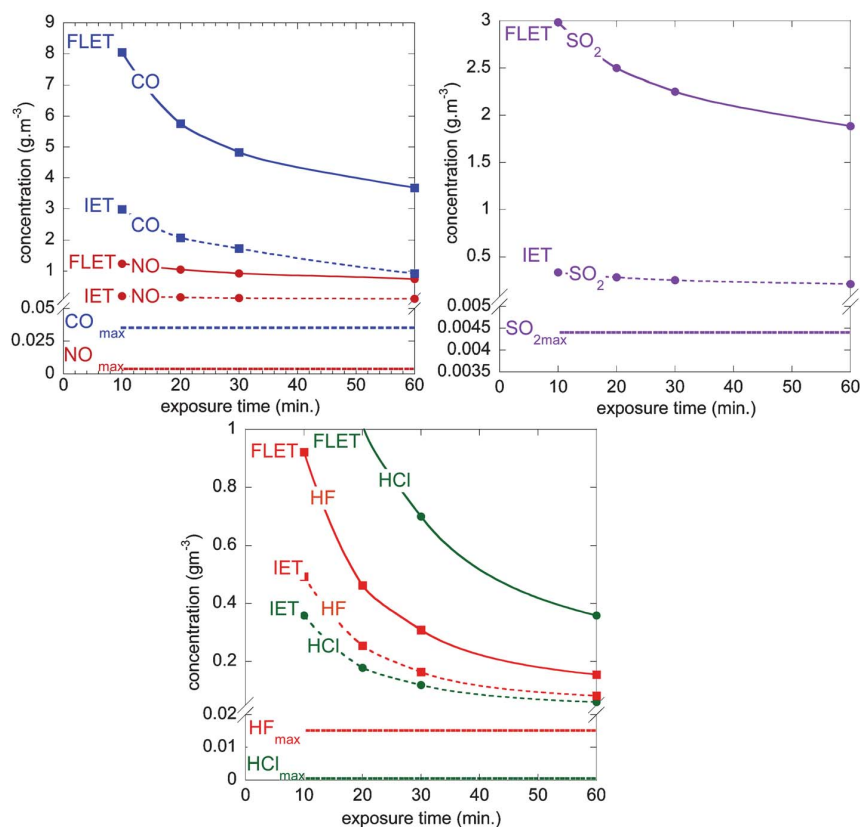


Fig. 9 FLET and IET concentration values as a function of exposure time with maximum concentration of CO, NO, SO₂, HCl and HF gases released from the batteries combustion (2.9 Ah pouch cell burning in a 50 m³ room). These graphs allow first-order evaluation of their dangerousness (see Table 3).

particular for storage fires and EV car fires, all the more in the latter case than the volume in which toxic smoke may be trapped could be far less than 50 m³ (e.g. car interior), or in case multiple car burning may be feared depending on the confinement taken into consideration (e.g. garage, underground park place, ...).

Note that CO toxicity is a common threat of any fire burning any carbon containing material. The actual threat being clearly related to the amount of material burning, combined (often additive) actions of individual gases, temperature and confinement conditions. More attention might be paid for hydrofluoric acid, since energies of 60 and 110 Wh (roughly equivalent to that of a laptop) are necessary to achieve the IET and FLET limits in these conditions. So, it can be deduced that fluorine based molecules are one of the key points for the battery security field. As it was mentioned above, fluorine sources are coming from the binder and the electrolyte. The removal of fluorine from the binder is conceivable and already exists with the use of binders such as carboxymethyl cellulose but replacement of fluorine containing salts in the electrolyte is a challenging situation for most applications. Reducing flammability of solvents might possibly serve fire toxicity management.

4. Conclusion

The calorimeter implementation for battery safety application was undertaken to add to the existing techniques, equipment able to provide more insight into the fire battery behaviour. This study has demonstrated the interest of the Tewarson calorimeter in the scope of battery safety field. This apparatus permits on-line analysis of mass loss and combustion gases production such as O₂, CO, CO₂, hydrogen halides, HCN, NO_x, SO_x, aldehydes, and THC. From these data, the heat released rate, the heat of combustion and the mass of burnt products from the combustion tests can be deduced. These data could be of great help for fire simulation. Moreover, the identification and quantification of toxic emissions from combustion gases can also be estimated. As a result, the whole data could have a part in the improvement of battery from safety point of view.

2.9 Ah pouch type batteries were tested at 100, 50 and 0% state of charge. Results showed that the masses lost during all the fire experiments were practically identical and roughly corresponded to the mass of organics. Nevertheless, depending on the SOC, the way of losing mass was different revealing the major role of the accumulated electrochemical energy.³¹ Upon heating (radiation of infrared heaters), this energy is released through different reaction pathways, leading to thermal runaway within the materials and production of fuel gas. The exact nature of these extra-reactions is beyond the scope of this paper but could be reactions of electrode materials with the electrolyte, electrolyte decomposition or positive active material decomposition. In the case of the fully charged batteries, the energy is rapidly released verging on explosion, and the phenomenon suddenness restricts the oxygen consumption leading to incomplete combustion. This can be noticed by the hydrocarbons detection, the highest carbon monoxide production and the lowest heat energy value. When the battery is half-charged, the thermal runaway is less important allowing the combustion to go nearly to completion. For the fully discharged case, the burning of the battery is relatively slow (8 minutes) leading to the complete combustion condition.

Quantification of O₂, CO and CO₂ gases allowed estimation of the cell combustion heat either by O₂ consumption or by CO and CO₂ releases. The maximum value (~4 MJ kg⁻¹ of the tested pouch 2.9 Ah batteries) was found to be close to the one calculated from thermodynamic data (combustion and formation heat of the organics). This quite good correlation brings to light that a battery heat of combustion can be estimated through simple addition of the contributions of all polymers and electrolyte combustion heats. Note that for the tested pouch cells, at least 50% of the combustion heat originates from polymers.

From the online analysis, significant concentrations of toxic gases are detected as HF, CO, NO, SO₂ and HCl. The production of these gases also depends on the cell SOC; carbon oxides and nitrogen oxide are the direct products of combustion and their kinetics follow the HRR profile. SO₂ is probably the reaction product of sulfur-based additive added into the electrolyte and its formation requires high heat that the fully charged battery is only able to release. The yield of HCl remains low and seems to have no SOC dependence. In contrast, HF results indicate a SOC dependence and the maximum concentration is achieved with the fully discharged battery. The evaluation of the dangerousness of the gaseous combustion products was undertaken by a simple extrapolation of the toxicity thresholds. The results stress the problem of fluorine-based compounds from a safety point of view and more precisely in the case of EV and HEV large-scale application. Despite the fact that experiments were conducted under high air flow and with high heat flux applied to the battery, it seems that future works have to be focussed on the replacement of LiPF₆ by a less fluorine-containing salt^{47,48} and by the removal of fluorine in the binder.

Acknowledgements

This work was supported by “Région de Picardie” through the BatteryNanosafe project. The authors are grateful to Jean-Pierre Bertrand for his technical assistance and to Alexandra Paillart and Michel Armand for helpful discussions.

References

- 1 M. Armand and J.-M. Tarascon, *Nature*, 2008, **451**, 652.
- 2 B. Scrosati, J. Hassoun and Y.-K. Sun, *Energy Environ. Sci.*, 2011, **4** (9), 3287.
- 3 V. Etacheri, R. Marom, R. Elazari, G. Salitra and D. Aurbach, *Energy Environ. Sci.*, 2011, **4**(9), 3243.
- 4 J. O. Besenhard, J. Gurtler and P. Komenda, *DEHEMA Monogr.*, 1987, **109**, 315.
- 5 A. Xiao, L. Yang, B. L. Lucht, S.-H. Kang and D. P. Abraham, *J. Electrochem. Soc.*, 2009, **156**(4), A318.
- 6 Z. Chen, Y. Qin, Y. Ren, W. Lu, C. Orendorff, E. P. Roth and K. Amine, *Energy Environ. Sci.*, 2011, DOI: 10.1039/c1ee01786a, Advance article.
- 7 S. S. Zhang, K. Xu and T. R. Jow, *J. Power Sources*, 2006, **160**(2), 1349.
- 8 M. C. Smart and B. V. Ratnakumar, *J. Electrochem. Soc.*, 2011, **158** (4), A379.
- 9 M. Pasquali, G. Pistoia, V. Manev and R. V. Moshtev, *J. Electrochem. Soc.*, 1986, **133**, 2454.
- 10 D. Aurbach, B. Markovsky, G. Salitra, E. Markevich, Y. Talyossef, M. Koltypin, L. Nazar, B. Ellis and D. Kovacheva, *J. Power Sources*, 2007, **165**, 491.
- 11 H. Yang, H. Bang, K. Amine and J. Prakash, *J. Electrochem. Soc.*, 2005, **152**(1), A73.

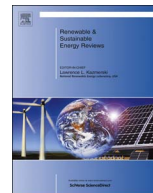
- 12 UL Standard for Safety for Lithium Batteries, UL 1642, Underwriters Laboratories Inc, Northbrook IL, 4th edn, 2005.
- 13 D. Doughty, *Proceedings of Battery Safety 2010*, Boston (USA), 2010, p. 347.
- 14 P. Biensan, B. Simon, J. P. Pérès, A. De Guibert, M. Broussely, J. M. Bodet and F. Pertou, *J. Power Sources*, 1999, **81–82**, 906.
- 15 E. P. Roth, D. H. Doughty and J. Franklin, *J. Power Sources*, 2004, **134**, 222.
- 16 D. Choi, J. Xiao, Y. J. Choi, J. S. Hardy, M. Vijayakumar, M. S. Bhuvaneswari, J. Liu, W. Xu, W. Wang, Z. Yang, G. L. Graff and J.-G. Zhang, *Energy Environ. Sci.*, 2011, DOI: 10.1039/c1ee01501j, Advance article.
- 17 H. Maleki and J. N. Howard, *J. Power Sources*, 2004, **137**, 117.
- 18 A. Tewartson and R. F. Pion, *Combust. Flame*, 1976, **26**, 85.
- 19 A. Tewartson, *J. Fire Sci.*, 1992, **10**(3), 188.
- 20 A. Tewartson, F. H. Jiang and T. Morikawa, *Combust. Flame*, 1993, **95** (1–2), 151.
- 21 A. Tewartson, *J. Fire Flammability*, 1977, **8**, 115.
- 22 G. Marlair and A. Tewartson, *Proceedings of the 7th International Symposium on Fire Safety Science*, Worcester (USA), 2002, p. 629.
- 23 C. Costa, G. Treand, F. Moineault and J.-L. Gustin, *Process Saf. Environ. Prot.*, 1999, **77 B3**, 154.
- 24 S. Brohez, G. Marlair and C. Delvosalle, *Fire Mater.*, 2006, **30**, 131.
- 25 S. Brohez, G. Marlair and C. Delvosalle, *Fire Mater.*, 2006, **30**, 35.
- 26 E. Thibert and B. Gauthier, *Polym. Degrad. Stab.*, 1999, **64**, 585.
- 27 Iso TR 16321-2, Geneva, 2007.
- 28 V. Babrauskas, *Fire Saf. J.*, 1985, **8**(3), 199.
- 29 S. Brohez, C. Delvosalle, G. Marlair and A. Tewartson, *J. Fire Sci.*, 2000, **18**(5), 327.
- 30 H. Biteau, PhD thesis, University of Edinburgh, 2009.
- 31 H. Biteau, T. Steinhaus, C. Schemel, A. Simeoni, G. Marlair, N. Bal and J.-L. Torero, *Fire Safety Science*, 2009, **9**, 1165.
- 32 B. Barnett, *Proceedings of Battery Safety 2010*, Boston (USA), 2010, p. 24.
- 33 A. Tewartson, F. Chu and F. H. Jiang, *Proceedings of the 4th International Symposium on Fire Safety Science*, Ottawa (Canada), 1994, p. 563.
- 34 R. N. Walters, S. M. Hackett and R. E. Lyon, *Fire Mater.*, 2000, **24** (5), 245.
- 35 W. L. Calhoun, *J. Chem. Eng. Data*, 1983, **28**, 146.
- 36 K. S. Gavritchev, G. A. Sharpataya, A. A. Smagin, E. N. Malys and V. A. Matyakha, *J. Therm. Anal. Calorim.*, 2003, **73**, 71.
- 37 S. J. Harris, A. Timmons and W. J. Pitz, *J. Power Sources*, 2009, **193**, 855.
- 38 *Handbook of Chemistry and Physics*, ed. D. R. Lide, CRC Press, 73rd edn, 1992, pp. 5–1.
- 39 M. W. Wagner, C. Liebenow and J. O. Besenhard, *J. Power Sources*, 1997, **68**, 328.
- 40 G. H. Wrodnigg, J. O. Besenhard and M. Winter, *J. Electrochem. Soc.*, 1991, **46**, 470.
- 41 G. H. Wrodnigg, J. O. Besenhard and M. Winter, *J. Power Sources*, 2001, **97–98**, 592.
- 42 J. H. Lee, U. Paik, V. A. Hackley and Y. M. Choi, *J. Electrochem. Soc.*, 2005, **152**(9), A1763.
- 43 A. Hammami, N. Raymond and M. Armand, *Nature*, 2003, **424** (6949), 635.
- 44 C. L. Champion, W. Li, W. B. Euler, B. L. Lucht, B. Ravdel, J. F. DiCarlo, R. Gitzendanner and K. M. Abraham, *Electrochem. Solid-State Lett.*, 2004, **7**, A194.
- 45 www.ineris.fr/substances/fr/page/23.
- 46 D. Lisbona and T. Snee, *Process Saf. Environ. Prot.*, 2011, DOI: 10.1016/j.psep.2011.06.022.
- 47 L. Li, S. Zhou, H. Han, H. Li, J. Nie, M. Armand, Z. Zhou and X. Huang, *J. Electrochem. Soc.*, 2011, **158**, A74.
- 48 L. Niedzicki, S. Grugeon, S. Laruelle, P. Judeinstein, M. Bukowska, J. Prejzner, P. Szczeciński, W. Wiczczonek and M. Armand, *J. Power Sources*, 2011, **196**(20), 8696.



Contents lists available at ScienceDirect

Renewable and Sustainable Energy Reviews

journal homepage: www.elsevier.com/locate/rser



A review of international abuse testing standards and regulations for lithium ion batteries in electric and hybrid electric vehicles



V. Ruiz^a, A. Pfrang^a, A. Kriston^a, N. Omar^b, P. Van den Bossche^b, L. Boon-Brett^{a,*}

^a European Commission, Joint Research Centre (JRC), Directorate for Energy, Transport & Climate, Energy Storage Unit, Westerduinweg 3, NL-1755 LE Petten, The Netherlands

^b Vrije Universiteit, MOBI, Pleinlaan 2, 1050 Brussels, Belgium

ARTICLE INFO

Keywords:

Battery safety
Standards
Lithium ion batteries
Abuse testing
Mechanical testing
Electromobility

ABSTRACT

Lithium ion batteries are a proven technology for automotive applications and their continued use in the future electric vehicle fleet is undeniable. In addition to battery performance and durability, battery safety is paramount to ensure confidence and widespread adoption of electromobility in our society. This comprehensive review aims at presenting the various international standards and regulations for safety testing of lithium ion batteries in automotive applications under various abusive environments. Safety tests are presented and analysed including mechanical, electrical, environmental and hazards of chemical nature. The intention of this review is compiling the most relevant standards and regulations to identify shortcomings and areas for future improvement.

1. Introduction

Reducing carbon dioxide emissions is a major driving force for the displacement of traditional internal combustion engines (ICE) based on fossil fuels by "greener" and more efficient alternatives. In this context, various measures within the policy framework are being established internationally to accelerate the development and adoption of vehicles based on alternative fuels. Based on these efforts, it is expected that the electrification of transport will make up a significant share of the near future automotive fleet [1]. According to the Report "Competitiveness of the EU Automotive Industry in Electric Vehicles" published in 2012 [2] the European Union (EU-27) will reach 14.8 million new light duty vehicle registrations (passenger cars and light commercial vehicles) by 2020, of which 7% will be electric vehicles (including Battery Electric Vehicles, BEVs, plug-in Hybrid Vehicles, PHEVs and Fuel Cell Vehicles, FCV). This market share is foreseen to rise to 31% by 2030 with Europe, Japan and U.S. expected to be leading markets. Other studies considering moderate policy support and technical advancement present 5–10% of the market share in the 2025–2030 time frame [3]. Global registrations of FCVs will still be under 1% in 2030, thus battery driven vehicles will dominate the EV market in the near future.

In 1991 Sony launched the first commercial lithium ion batteries (LIBs) [4]. Since then it has emerged as the dominant energy storage technology used in most consumer electronics (e.g. cell phones,

notebooks) [5]. Moreover, LIBs are used to power several electric vehicles available on the market, e.g. BMWi3, Tesla Model S, Nissan Leaf, Mitsubishi iMiEV, Chevrolet Volt, Renault Zoe. The widespread deployment of this technology is reinforced by its relatively high specific energy and power density and its progressive cost reduction, with estimations from ~ 800 \$ kW h⁻¹ per pack in 2010 down to ~ 248 \$ kW h⁻¹ by 2030 (for a 21 kW h BEV) [6] based on the current chemistries. Predictions assume that by 2020, LIBs will be used in 65% of the total EV systems, surpassing other technologies, including NiMH [7].

Many battery standards and regulations have been specifically developed to facilitate and regulate battery use in EVs. At this stage it is useful to differentiate between standards and regulations. Standards are in principle voluntary documents, drafted by non-governmental organisations such as the International Electrotechnical Commission (IEC), the International Organisation for Standardisation (ISO), the Society of Automotive Engineers International (SAE) at international level and the European Committee for Standardisation (CEN) and European Committee for Electrotechnical Standardisation (CENELEC) at European level. Standards can also be issued by National bodies (e.g. British Standards Institution (BSI), Japanese Industrial Standards Committee (JISC)) or regional organisations. Regulations, on the other hand, are issued by governmental authorities and have the force of law. For road vehicles, the most relevant regulations are type approval

* Corresponding author.

E-mail address: Lois.BRETT@ec.europa.eu (L. Boon-Brett).

<http://dx.doi.org/10.1016/j.rser.2017.05.195>

Received 15 June 2016; Received in revised form 10 April 2017; Accepted 21 May 2017

Available online 14 July 2017

1364-0321/© 2017 The Authors. Published by Elsevier Ltd. This is an open access article under the CC BY license (<http://creativecommons.org/licenses/by/4.0/>).

regulations issued by the United Nations Economic Commission for Europe (UNECE). These regulations define uniform technical prescriptions for wheeled vehicles, their parts and equipments, and state conditions for reciprocal recognition of type approvals by several countries. In the USA, the National Highway Traffic Safety Administration (NHTSA) issues regulations via the Federal Motor Vehicle Safety Standards (FMVSS), setting minimum safety performance requirements for motor vehicles or items of motor vehicle equipment.

Standards may be referred to by laws and regulations. For several technical domains, Europe now follows the so-called New Legislative Framework (NLF) adopted in July 2008, which built on the "New Approach", where directives only mention essential requirements, while technical details are specified in harmonized European standards referred to in these directives. Conformance to these standards subsequently implies conformity to the essential requirements of the directive. The NLF is used for example in the Low Voltage Directive, but not yet for road vehicles, for which UNECE type approval regulations are used. The Motor Vehicle Type Approval (EC Directives) allows national type approvals and subsequently ensures recognition of this approval in other EU member states, i.e. if one vehicle is type approved in one member state, it is allowed to be sold in any other member state.

In 2012, EU and US standards organisations agreed a Transatlantic Cooperation on Standards for Electric Vehicles to avoid proliferation of conflicting electric vehicle and battery safety standards. The cooperation sets the basis towards harmonisation and alignment of standards in the field of electromobility [8]. The need for such harmonisation of battery standards for automotive applications has been acknowledged by others who suggest that performance and safety can hence be improved [9].

Battery safety standards and regulations call for testing in abusive conditions. In these situations (e.g. overcharging, short circuit, physical deformation in a vehicle crash) exothermic reactions may be triggered (e.g. temperature rise of hundreds of degrees within seconds [10]) leading to thermal runaway. This can lead to the heating up of neighbouring cells within a module, which – if sufficient heat is generated – can lead to a chain reaction and propagation [11,12], and in a worst case scenario, develop into fire and explosion [13–15]. Most of the time LIBs behave as foreseen during their lifetime. However a number of highly publicized LIB safety events have led to hazardous situations making the evaluation of battery safety a key aspect in battery development. Events such as laptop fires [16], smoking cell phones [17], airplane incidents [18–21], the GM Volt fires [22], ground impacts leading to safety events on Tesla Model S [23], although scarce, reach the media much easier than events with established technologies (i.e. internal combustion engine fires). Such events have led to withdrawal of products from the market (e.g. Apple removed lithium ion power packs from their PowerBook 5300 line [24], CPSC and EV Global Motors Company announced the recall of 2000 batteries in their electric bicycles [25]) which may generate an increased concern from the general public towards lithium ion technologies in general. The link between safety related events and the market uptake of battery driven EVs is of concern to battery producers, vehicle original equipment manufacturers (OEMs) and transportation policy makers.

The objective of this review is to compile the most relevant standards and regulations dealing with abuse testing of LIBs. Safety risks specific to LIBs are summarized (Section 2). Test methods in these standards and regulations are classified according to the nature of the misuse conditions applicable (Section 3). Test parameters and conditions used in test methods are compared – commonalities and differences are highlighted (Section 3). Relevant forthcoming standards and regulation are listed (Section 4). Stemming from these comparisons, conclusions are drawn identifying areas for improvement with respect to the relevance and fitness for purpose of existing tests for

Table 1

List of typical components in lithium ion batteries (LIBs).

Cathode	LMO, LCO, NCA, NMC, LFP, ECPs
Anode	Graphitic carbons, Hard carbons, Synthetic graphite, LTO, Tin-based alloys, Silicon-based alloys
Electrolyte salts	LiPF ₆ , LiClO ₄ , LiAsF ₆ , LiCF ₃ SO ₃ , LiBF ₄
Electrolyte solvents	DMC, EC, DEC, PC, γ -GBL, RTIL's
Flame retardants	HMPN, TMP, TFP
Gel precursor	PEO, PAN, PVDF, PMMA, PTFE
Binder	PVDF, SBR, Glass Fibre, CMC, ACM
Separator	Polypropylene, Polyethylene, Cellulosic paper, Nonwoven fabrics, Ceramic

LMO: Lithium Manganese Oxide, LCO: Lithium Cobalt Oxide, NCA: Lithium Nickel Cobalt Aluminium Oxide, NMC: Lithium Nickel Manganese Cobalt Oxide, LFP: Lithium Iron Phosphate, ECPs: Electronic Conducting Polymers, LTO: Lithium Titanate, PVDF: Polyvinylidene Fluoride, SBR: Styrene Butadiene Rubber, CMC: Carboxymethyl Cellulose, ACM: acrylate-type copolymer, RTIL's: Room Temperature Ionic Liquids, DMC: Dimethyl Carbonate, EC: Ethylene Carbonate, DEC: Diethyl Carbonate, PC: Propylene Carbonate, γ -GBL: gamma-Butyrolactone, HMPN: hexamethoxycyclotriphosphazene, TMP: trimethyl phosphate, TFP: tris(2,2,2-trifluoroethyl)phosphate, PEO: Polyethylene Oxide, PAN: Polyacrylonitrile, PMMA: Poly Methyl Methacrylate, PTFE: Polytetrafluoroethylene.

electric vehicles (Section 5). Shortcomings and suggestions for future development are also identified (Section 5).

2. Safety issues and challenges related to lithium ion batteries

2.1. Battery materials and components

LIBs are rechargeable energy storage devices where Li ions move between the anode and cathode, which are electrically separated by a membrane. All components are fully soaked in an electrolyte. During charging, lithium ions move from the cathode towards the anode and in the discharge cycle the ions travel back. The electrons move via the external electrical circuit and lithium ions and solvent molecules travel within the electrolyte. When the battery is charged, the Solid Electrolyte Interface (SEI) is formed. This passivation layer, Li⁺ conducting and electronically insulating, is paramount for optimum battery performance as it allows Li intercalation and prevents further electrolyte decomposition [26,27].

As the risks associated with a certain battery technology depend highly on the cell constituents, it is important to consider all relevant components from a safety perspective. Table 1 summarizes typical components found in LIBs. A relatively high number of materials have been used in cathodes, including lithium manganese oxide (LMO), lithium cobalt oxide (LCO), lithium nickel cobalt aluminium oxide (NCA), lithium nickel manganese cobalt oxide (NMC) or olivine type materials, such as lithium iron phosphate (LFP). The latter has appeared as one of the safest chemistries due to its thermal stability and non-toxicity [28,29]. On the other hand the energy density in LFP batteries is lower compared to LCO alternatives, which have less desirable behaviour when a thermal event occurs [30,31].

Regarding the anode, carbon is commonly used in LIBs. It can reversibly accommodate significant amounts of lithium providing a theoretical capacity of 372 mA h g⁻¹ (LiC₆). More recently, lithium titanate (LTO) has attracted considerable attention due to its long cycle life without significant structural changes upon cycling [32,33] and its increased safety in terms of thermal stability and high potential which prevents dendrite formation [30] at the cost of a comparatively lower voltage [30].

Electrolytes used in LIBs are mainly based on aprotic organic solvents, often highly flammable [34]. The most commonly used electrolytes are mixtures of various carbonates (e.g. propylene carbonate) and a dissolved salt (e.g. lithium hexafluorophosphate (LiPF₆)). In the event of thermal runaway, the electrolyte decomposes leading to

the formation of gases. Consequently, significant overpressure is generated in the cell, which will eventually lead to venting and/or rupture. A major hazard is the presence of fluorinated compounds in the electrolyte, leading to the release of toxic and corrosive hydrogen fluoride (HF). Since some gases generated in such events are toxic [35,36] and may potentially cause severe harm to individuals in the surroundings, immediate medical attention is required after exposure to vented gases [16]. In order to reduce the flammability of these electrolytes various flame retardant additives have been explored giving rise to the concept of “non-flammable electrolytes” (e.g. Phosphate solvents [37], phosphazene derivatives [38,39], room temperature ionic liquids [40,41]). Safety performance of LIBs can be improved using alternative electrolytes such as more thermally stable, high flashpoint electrolytes [42] or room temperature ionic liquids (RTILs) [40,41], which show promise due to their low volatility, with virtually no vapour pressure (ca. 100 pPa at 298 K for 1-butyl-3-methylimidazolium hexafluorophosphate [43] compared with 3 kPa at 298 K for H₂O [44]), high flame resistance, thermal and chemical stability together with a wide window of electrochemical stability [45]. Electrolytes in the solid/gel form (solid polymer electrolytes), can also be utilized. On one hand their ionic conductivity is much lower than in liquid systems, but on the other hand their safety is improved (e.g. lower reactivity versus lithium, absence of risk of electrolyte release) [46,47].

The binder is essential for enabling electrode fabrication. Initially, most of the anodes were obtained by utilizing polyvinylidene fluoride (PVDF), however the current trend is to use styrene butadiene rubber (SBR), which yields more flexible electrodes, higher binding ability with a small amount of binder, larger battery capacity and higher cyclability [48]. SBR is unsuitable for the cathodes, which are prone to oxidation and consequently PVDF is still used. Electrode preparation with PVDF requires N-methyl pyrrolidone (NMP) for dissolution with a consequent toxicity concern. Water - soluble binders (e.g. carboxymethyl cellulose, CMC) are preferred from an environmental perspective. More recently, the highly flexible acrylate-type copolymer (ACM) has started to be used in some prismatic batteries [48].

The separator is a key element for preventing the electrical contact between electrodes while allowing ion transport [49]. Currently, thin microporous polyolefin membranes made of polyethylene (PE), polypropylene (PP), or laminates of both (e.g. PP/PE/PP [50]) are mostly used. In a hazardous situation when a temperature above the melting point of PE is reached (135 °C), PE will melt, whereas PP (melting point of 165 °C) will maintain its integrity. As the polymer melts, its pores are blocked resulting in an insulating layer, effectively shutting down the cell and providing a degree of protection against short circuit and overcharge [49]. Alternatively separators based on ceramic materials have also shown high-temperature stability, good chemical resistance, and wettability [51].

It is clear that many aspects influence the safety of LIBs and the evaluation of all battery design parameters (e.g. electrode material, particle size [52], separator) is needed in order to optimise safety. Furthermore, in order to achieve a safe system for a particular application a compromise in the selection of cell components with respect to safety, performance and cost is essential.

2.2. Battery cell and pack design

Industry experts estimate that between one in 10 million [11] or one in 40 million [34] cells fail during normal operation, if proper quality control is in place. Despite the low probability, the risk is not trivial and the consequences cannot be neglected. For this reason, efforts to improve the safety of the batteries are taken along the whole electric vehicle manufacturing chain [31], from safer components (see Section 2.1), smarter energy management [53] and battery management systems (BMS), and smarter vehicle designs (e.g. installation of battery pack away from crush zones [31] and other safety related

installation considerations [54]. An additional parameter influencing battery safety is cell design [16]). Vehicle manufacturers utilize prismatic (e.g. VW, Audi, Porsche, Citroen, Peugeot, Fiat), pouch (e.g. Mini, Mercedes, Renault) or cylindrical cells (e.g. Tesla). Cylindrical cells are cheap to manufacture, have good mechanical stability and high energy density. However, they have low packing efficiency [55]. They do not swell during operation, but when pressure builds up expulsion of the jelly roll (layers of anode/separator/cathode rolled up and inserted into a hollow cylinder casing) can occur [56]. Prismatic cells are mechanically robust with high packing efficiency, however, they have slightly lower energy density and are more expensive [55]. In case of pressure build up, the generated gases are released via the safety vent. When the opening of the safety vent is too small, or when it is clogged it can hinder the escape of gas. This situation can lead to rupture or explosion of the cell [16]. Soft pouch cells have a higher energy density than the other two designs, their fabrication cost is not very high, and they are much lighter. However, at system level this can be reversed due to the stronger mechanical constructions needed for their protection. They are prone to swelling during operation (e.g. ageing, exposure to > 60 °C [56]) and have no designated venting mechanism. In case of venting, gases are not directed towards a safety valve, as all the sealing points in the pouch cell impose small resistance to high pressure. Consequently, the release of gases occurs with smaller energy than for the other assemblies. The unconstrained nature of the pouch cells may be more effective preventing a thermal runaway reaction compared to cell designs where electrodes are forced to maintain close contact [57]. Additionally, pouch cells exhibit smaller internal temperature gradients compared to prismatic assemblies [55].

Another aspect associated to battery safety relates to the fact that cells within a pack exhibit non-uniform properties upon cycling. Consequently, there may be some unbalances (e.g. voltage variations between cells) that may trigger a safety hazard.

Battery ageing also needs to be evaluated. Battery cells degrade both by undergoing charge-discharge cycles and by time (calendar ageing). The application and safety of “second life” automotive batteries should be considered. In this application, decommissioned vehicle traction batteries may be used for stationary storage (e.g. electric grid support).

A final relevant aspect is the design of the battery pack. For example, standards such as SAE J2289:2008 [58] describe that material vented from the battery should not be directed into the passenger compartment where it may pose a hazard to passengers.

3. Relevant standards and regulations: abuse testing of lithium ion batteries for automotive applications

Lithium ion batteries must pass a series of safety tests to be certified for use in a particular application (e.g. portable electronics or automotive). Safety tests are described in international, national and regional standards, typically developed based upon pre-normative research and experience from industry, academia and regulatory bodies. These tests are performed to understand and identify potential battery weak points and vulnerabilities when the battery experiences real-life off-normal conditions and to determine how the battery will behave under severe abusive conditions, such as a car crash or thermal shock. In these situations, thermal runaway can develop. Other causes of a thermal runaway can be the presence of microscopic particles from manufacturing or impurities, which can pierce the separator creating an internal short circuit. Therefore, a thermal runaway can be initiated by both external and internal stimuli. The consequences that thermal runaway produces vary depending on several factors, including: state of charge (SOC), charging/discharging rate, cell-type, cell history, cathode/anode material, electrolyte composition, etc. [59].

Many tests presented in this review are devoted to the evaluation of the consequences of a short circuit, which might be followed by thermal

Table 2

Overview of tests in standards and regulations applicable to lithium ion batteries in automotive applications. Test level is indicated as C: Cell, M: Module, P: Pack and V: Vehicle.

Test	Region of applicability			International			EU and further countries ^a			USA			Korea	India	China
	Section	SAE	SAE	ISO 12405-1 (2)	ISO 12405-3	IEC 62660-2 (3)	UN/ECE-R100.02	UL 2580	USABC	FreedomCAR	KMVSS 18-	AIS-048			
Mechanical															
Mechanical shock	3.1.a	CMP	CMP	P	P	C	CMPV	CMP	MP	MP	MP	M			
Drop	3.1.b	P	P					CP	P	P	P				C
Penetration	3.1.c	CMP	CMP					CMP	CMP	CMP	CMP	CM			CP
Immersion	3.1.d	MP	MP	P	P			MP	MP	MP	P				CP
Crush/crash	3.1.e	CMP	PV	PV	C		CMPV	CMP	CMP	CMP	CMP	M			CP
Rollover	3.1.f	MP	P	P	P			P	MP	MP	MP	M			P
Vibration	3.1.g	CMP	CMP	P	P	C	CMP	CMP	CMP	CMP	CMP	M			P
Electrical															
External short circuit	3.2.a	CMP	P	P	P	C	CMP	CMP	CMP	CMP	P	CMP			CP
Internal short circuit	3.2.b					C									
Overcharge/overdischarge	3.2.c	CMP ^f	P	P	P	C	CMPV	CMP	CMP	MP	P	CMP ^g			CP
Environmental															
Thermal stability	3.3.a	C	C			C		C	CMP	CMP	P				CP
Thermal shock and cycling	3.3.b	CMP	CMP	P	P	C	CMP	CMP	CMP	CMP					CP
Overheat	3.3.c	MP	P						MP						
Extreme cold temperature	3.3.d								CMP						
Fire	3.3.e	MP	P	P ^b			CMPV	CMP	CMP	CMP	P				
Chemical															
Emissions	3.4.a	CMP	P					CMP	CMP	CMP					
Flammability	3.4.b	CMP	P					CMP	CMP	CMP					

^a Norway, Russia, Ukraine, Croatia, Serbia, Belarus, Kazakhstan, Turkey, Azerbaijan, Tunisia, South Africa, Australia, New Zealand, Japan, South Korea, Thailand and Malaysia.

^b Vehicle body may be included.

^c Also possible at battery pack subsystem: representative portion of the battery pack (energy storage device that includes cells or cell assemblies normally connected with cell electronics, voltage class B circuit, and overcurrent shut-off device, including electrical interconnections and interfaces for external systems).

^d Applicable to the LIB cell and pack whose rated voltage is 3.6 V and mx3.6 V (n: quantity of batteries), respectively.

^e At the module level for those electric energy storage assemblies intended for use in applications larger than passenger vehicles. The module level testing shall be representative of the electric energy storage assembly.

^f Overdischarge not at pack level.

^g Overdischarge not performed.

runaway, as this is one of the scenarios that may create a great risk, both for the vehicle occupants and first aid responders. In some tests the short circuit is induced externally, such as in the case of crush, penetration and drop tests, however other tests aim at inducing the short circuit internally. The development of tests representative of an internal short circuit is quite controversial due to the difficulty in emulating a true internal short circuit in a testing environment. For this reason, there is a lack of consensus regarding the "fit for purpose" of internal short circuit tests currently described in existing standards. There is little knowledge on how an internal short circuit within a battery pack develops. Most of the scientific literature refer to small batteries or cells [57,60], and analogous data at pack or full vehicle level is scarce due to the high cost of the tests and to the fact that the information is in most of the cases proprietary to the testing bodies or the OEM.

Table 2 presents a summary of the most frequently required abuse tests as described in international standards and regulations related to electric vehicles based on lithium ion technologies. Abuse tests are classified according to the nature of the misuse: mechanical, electrical, environmental and chemical. Tests that appear in only few standards or regulations will be mentioned but not explained in detail. In some circumstances, upon agreement between the manufacturer and the customer, the standard or regulation allows certain flexibility in the test conditions. The tests can be performed at various system levels: cell (C), module (M), pack (P) and vehicle (V). In general we will refer to the device under test (DUT). Definitions for each level follow SAE J2464:2009 [61] and can be summarized as:

- Cell (C): energy storage device composed of at least one cathode and one anode, and other necessary electrochemical and structural components.
- Module (M): grouping of interconnected cells in series and/or parallel into a single unit.
- Pack (P): interconnected modules including all auxiliary subsystems for mechanical support, thermal management and electronic control.

In general, standards and regulations set pass/fail requirements for each test. For example, UN/ECE-R100.02 [62], ISO 12405-3, UL 2580 [63] set "no fire", "no explosion", "no rupture", and "no leakage" as acceptance criteria for tests under reasonable foreseeable misuse (e.g. vibration, thermal shock, external short circuit), whereas the pass/fail criterion for fire resistance is "no explosion" only. Specific to automotive applications, the response of a technology to an abusive condition can be classified according to the EUCAR hazard levels [64,65]: from level 0 (no effect, system maintains its functionality) to level 7 (explosion, mechanical disintegration of the system). Battery and car manufacturers often utilize this classification to evaluate the response of a RESS to an abusive condition. For example, a level 3 or lower usually represents an acceptable level of performance.

Direct comparison of the value of each testing parameters should be performed prudently. Differences in test parameters may be rationalised by differences in the scope and purpose of the tests. For particular tests of interest the reader is advised to consult the reference texts directly.

3.1. Mechanical tests

3.1.1. Mechanical shock test

The mechanical shock test aims at evaluating the robustness of a battery in situation of sudden acceleration and/or deceleration of a vehicle. During the test a DUT is exposed to shock forces defined in terms of acceleration and shock duration adapted to different conditions; from normal in-use driving, driving at high speed over a kerbstone [67], to vehicle crash [62,65,72]. There is a great diversity in the test conditions (direction, peak acceleration, duration, state of

charge) in the various standards and regulations, as summarized in Table 3. To facilitate the comparison between the various parameters please refer to Fig. 1. Standards SAE J2464:2009 and SAE J2929:2013 [61,66] follow UN 38.3:2015 transportation regulation [76], and require the most stringent conditions of all the standards and regulations evaluated, in terms of peak acceleration (150g) for cells of < 0.5 kg. For heavier systems the conditions are eased [61,66].

Interestingly, ISO 12405 part 1:2011 and part 2:2012 [67,68], UL 2580:2013 [63] and ISO 62660-2:2011 [70] (which follow ISO 16750-3:2003 [77]) have the same requirements (500 m s⁻² (~ 51 g) and 6 ms) despite the fact that the test levels are different (P, P, C and C, respectively, see Table 3). It is reasonable to assume that the impact and outcome of the test is dependent on the DUT size, and that the test conditions should be dimensioned to each level.

Under the recently published ISO 12405-3:2014 [69], an optional mechanical shock test is included compared to parts 1 and 2 [67,68], adopting the shock parameters used by UN/ECE-R100.02:2013 [62]. This regulation specifies test parameters for batteries to be installed in road vehicles of categories M₁-N₁, M₂-N₂ and M₃-N₃¹ with varying acceleration profiles depending on orientation and vehicle type. A higher shock level and/or longer duration can be applied to the DUT if recommended by the manufacturer.

FreedomCAR and USABC standards [65,72] divide the shock test into low-level (no damage to the DUT) and mid-level (DUT may be inoperable after test). While all considered standards and regulations require a half-sine wave, FreedomCAR and USABC allow also other pulse shapes which would simulate actual decelerations more accurately. Also deviations from the specified shock parameters may be requested by the manufacturer. These two standards [65,72], as well as UN/ECE-R100.02:2013 [62], present significantly higher shock durations (ranging 55–120 ms) compared to the other standards (< 20 ms), presumably imposing harder conditions on the DUT.

Mechanical shock testing can also be performed at vehicle level, as mentioned in UN/ECE-R100.02:2013 [62], SAE J2929:2013 [66] and ISO 12405-3:2014 [69]. For UN/ECE-R100.02:2013 [62], batteries installed in a vehicle that has already been successfully subjected to vehicle crash testing in accordance with UN/ECE-R12:2012 – Annex 3 [78] for protection of the driver against the steering mechanism in the event of impact, with UN/ECE-R94:2012 – Annex 4 for frontal collision [79] and with UN/ECE-R95:2011 – Annex 4 for lateral collision [80] are considered to be compliant. SAE J2929:2013 [66] follows requirements described in FMVSS 305:2011 [81] (or equivalent regulation depending on the geographical region applicable to vehicle front, rear and side crash testing). Similarly ISO 12405-3:2014 [69] requires following relevant national or regional regulations on vehicle crash tests.

According to the FP7 project EVERS SAFE [82], the majority of real world crashes show acceleration values below 20–30g for frontal and side impacts with durations lower than 100 ms, and accelerations significantly lower (< 12g) in the case of rear impacts. However, when the aim of the test is to evaluate worst case scenarios, the parameters would need to be more stringent, particularly for standards and regulations investigating vehicle crash scenarios. For example, full-width barrier crash test (56 km h⁻¹) develops shock peaks up to 55g [83], only ISO 12405 part 1:2011 and part 2:2012 [67,68] approximate this value at pack level. Based on these examples, comparability of test conditions performed at vehicle level and component level would require deep evaluation. Another aspect pointed out by the project

¹ Vehicles designed for the carriage of passengers: (M₁: < 8 seats in addition to the driver's seat, M₂: > 8 seats in addition to the driver's seat, mass < 5 tonnes. e.g. small buses and minibuses, M₃: > 8 seats in addition to the driver's seat and a maximum mass > 5 tonnes. e.g. large buses) and vehicles designed and constructed for the carriage of goods: (N₁: having a maximum mass < 3.5 tonnes. e.g. light vans and trucks, N₂: having a mass between 3.5 and 12 tonnes e.g. mid-sized vans and trucks, and N₃: exceeding 12 tonnes. e.g. heavy vans and trucks).

Table 3
 Test conditions for the mechanical shock test at cell (C), module (M), pack (P) and vehicle (V) level.

Region of applicability Shock parameters	International			EU and further countries [#]		USA		India	China			
	SAE J2464 [61]	SAE J2929 [66]	ISO 12405-1(2) [67,68]*	ISO 12405-3 [69]*	IEC 62660-2(3) [70,71]**	UN/ECE-R100.02 [62]**	UL 2580 [63]			USABC [72]***	Freedom CAR [65]***	KMVSS 18-3 [73]
Level (C, M, P)	C M P	C M P	P	P	C	C M P	C M P	M P	M	M	M	M
Direction of shock	Positive and negative directions. 3 repeats on 3 axes	Positive and negative directions. L and lateral axes	L and T	L and T	***	L and T	*** (C), Positive and negative directions. 3 repeats on 3 axes (total 18 shocks) (M, P)	Axis that will cause the most potential damage	V and H axis	V and H axis	V and H axis	V and H axis
Peak acceleration (g)	150 (C), 50 (C > 0.5 kg M,P > 12 kg) or 25 (P)	150 (C M P), 50 (C > 0.5 kg M,P > 12 kg) or 25 (P)	51	51 or Vehicles ≤ 3.5 t: 10–28 (L)/4.5–15 (T), Medium-duty trucks and midi buses: 5–17 (L)/2.5–10 (T), Heavy-duty trucks and buses: 4–12 (L)/2.5–10 (T)	51	Vehicles ≤ 3.5 t: 10–28 (L)/4.5–15 (T), Medium-duty trucks and midi buses: 5–17 (L)/2.5–10 (T), Heavy-duty trucks and buses: 4–12 (L)/2.5–10 (T)	51 (C)	30 (mid-1) 20 (mid-2) 20 (low)	30	30	30	30
Shock duration (ms)	6 (C) 11 (C > 0.5 kg M,P > 12 kg) or 15 (P)	6 (C M P) 11 (C > 0.5 kg M,P > 12 kg) or 15 (P)	6	6 or 80–120	6	80–120	6 (C) 15 (M, P)	≤ 55 (low) ≤ 65 (mid-1) ≤ 110 (mid-2)	15	15	15	15
SOC (% rated capacity)	95–100 normal vehicle operation	95–100% max normal vehicle operation	50	50 or > 50% normal operating range	80 (HEV), 100 (BEV)	> 50% normal operating range	Max. operating SOC (M, P), 80 (HEV), 100 (BEV) (C)	100	100	100	100	100
Vehicle level (V)/collision speed	FMVSS 305 [81]: 48, 54, 80 km h ⁻¹	Relevant national or regional regulation on vehicle crash tests	UN/ECE-R95 [80]: 48, 3-53 km h ⁻¹ , UN/ECE-R94 [79]: 56 km h ⁻¹ , UN/ECE-R12 [78]: 50 km h ⁻¹	UN/ECE-R95 [80]: 48, 3-53 km h ⁻¹ , UN/ECE-R94 [79]: 56 km h ⁻¹ , UN/ECE-R12 [78]: 50 km h ⁻¹	UN/ECE-R95 [80]: 48, 3-53 km h ⁻¹ , UN/ECE-R94 [79]: 56 km h ⁻¹ , UN/ECE-R12 [78]: 50 km h ⁻¹	UN/ECE-R95 [80]: 48, 3-53 km h ⁻¹ , UN/ECE-R94 [79]: 56 km h ⁻¹ , UN/ECE-R12 [78]: 50 km h ⁻¹	UN/ECE-R95 [80]: 48, 3-53 km h ⁻¹ , UN/ECE-R94 [79]: 56 km h ⁻¹ , UN/ECE-R12 [78]: 50 km h ⁻¹	UN/ECE-R95 [80]: 48, 3-53 km h ⁻¹ , UN/ECE-R94 [79]: 56 km h ⁻¹ , UN/ECE-R12 [78]: 50 km h ⁻¹	UN/ECE-R95 [80]: 48, 3-53 km h ⁻¹ , UN/ECE-R94 [79]: 56 km h ⁻¹ , UN/ECE-R12 [78]: 50 km h ⁻¹	UN/ECE-R95 [80]: 48, 3-53 km h ⁻¹ , UN/ECE-R94 [79]: 56 km h ⁻¹ , UN/ECE-R12 [78]: 50 km h ⁻¹	UN/ECE-R95 [80]: 48, 3-53 km h ⁻¹ , UN/ECE-R94 [79]: 56 km h ⁻¹ , UN/ECE-R12 [78]: 50 km h ⁻¹	UN/ECE-R95 [80]: 48, 3-53 km h ⁻¹ , UN/ECE-R94 [79]: 56 km h ⁻¹ , UN/ECE-R12 [78]: 50 km h ⁻¹

Longitudinal (L), transversal (T), vertical (V), horizontal (H), * or according to a test profile determined by the customer and verified by the manufacturer. ** If more severe test parameters are requested by any regulation, such test conditions may be applied. *** It is in the interest of DUT manufacturers to keep the pulse duration as long as possible and still meet the specification. However, if the electrochemical storage system (ECSS) is robust, tests may exceed the peak acceleration, reduce the duration, reduce the test complexity, and hence, reduce the test cost. #Norway, Russia, Ukraine, Croatia, Serbia, Belarus, Kazakhstan, Turkey, Azerbaijan, Tunisia, South Africa, Australia, New Zealand, Japan, South Korea, Thailand and Malaysia. # A higher shock level and/or longer duration can be applied to the tested device if recommended by the manufacturer. *** Same direction as the acceleration of the shock that occurs in the vehicle. If the direction of the effect is not known, the cell shall be tested in all six spatial directions. * For those electric energy storage assemblies intended for use in applications larger than passenger vehicles. The module level testing shall be representative of the electric energy storage assembly.

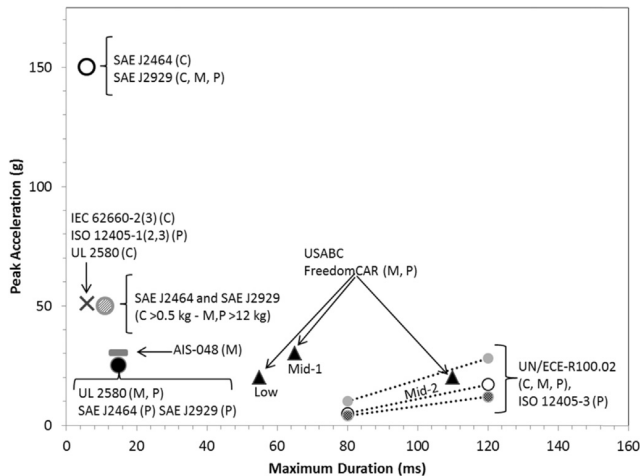


Fig. 1. Comparison of peak acceleration and shock duration for various standards and regulations.

EVERSAFE [82] is that the shock parameters defined in the standards and regulations are extracted from conventional car testing, however the accelerations experienced by the battery in the vehicle installation might be different for EVs. Investigations in this respect would be highly desirable to evaluate whether specific requirements for electric vehicles need to be imposed.

3.1.2. Drop test

This test simulates a situation when a battery is being removed from or installed in an electric vehicle and accidentally drops. Table 4 shows the requirements for surface type, drop height and SOC. During the test the DUT is let fall onto a rigid flat surface (e.g. concrete floor [63,73]) or onto a cylindrical object made of steel [65,72]. The shape of this cylindrical object is supposed to represent a telephone pole or a similar object. Alternatively, it is also possible to perform a horizontal impact of equivalent velocity as described in SAE J2464:2009 [61] or USABC:1999 [72]. The fall height varies considerably in the various standards (from 1 m [63] up to 10 m [65,72]). Consequently, the outcome of the test can be expected to vary.

Systems intended to be removed from the vehicle for charging (or replacement/swapping) are required to perform this test in UL 2580:2013 [63]. In this case, the test has to be repeated three times (on the same item) as the likelihood of dropping the battery is higher than if the battery does not need to be removed from the vehicle. This scenario seems very plausible, however, the drop test is not included in various automotive battery regulations and standards, such as UN/ECE-R100.02:2013 [62], ISO 12405-1: 2011, ISO 12405-2:2012, ISO 12405-3:2014 [67–69] and ISO 62660-2:2011 [70].

3.1.3. Penetration test

In this test, both mechanical and electrical damage is induced in the battery. A sharp steel rod – the 'nail' – is forced through the battery at a certain constant speed, generally 8 cm s^{-1} [65,72,74]. Although the consequence of the test is a short circuit, this short circuit is mechanically induced. For this reason, the penetration test is usually classified within the mechanical tests and not within electrical tests. As the nail penetrates through the cells and the integrity of the separator and electrodes is compromised, short circuits are created and consequently heat is released. Multiple electrode layers are in electrical contact, together with the shorting occurring on the nail, so relatively important damage occurs in a short period of time. Additionally, due to the fact that the deformation is localized in a relatively small area, the heat dissipation is quite limited.

Depending on the test level (cell, module or pack), the depth of penetration and the dimension of the nail vary as described in many of

Table 4
 Test conditions for the drop test at cell (C), module (M) and pack (P) level.

Region of applicability	International		USA		EU and further countries ^a		Korea		India		China	
	Drop parameters	SAE J2464 [61]	ISO 12405-1 (2)(3) [67–69]	ISO 62660-2 (3) [70,71]	IEC 62660-2 (3) [63]	UL 2580 [63]	USABC [72]	USABC [72]	FreedomCAR [65]	KMVSS 18-3 [73]	AIS-048 [74]	QC/T 743 [75]
Level (C, M, P)	P	P	P	P	C, P	P	P	P	C, M, P	P	P	C
Surface type	Flat surface	Flat surface	Flat surface	Flat surface	Flat concrete surface ^b	Cylindrical steel object (radius 150 mm)	Cylindrical steel object (radius 150 mm)	Concrete floor	Concrete floor	Concrete floor	Concrete floor	Hardwood floor 20 mm thick
Drop height (m)	2	maximum distance to ground or maximum possible drop distance which the battery system experiences when serviced according to documented procedures or ≥ 1	1	2	1	10	10	4.9	≤ 10	4.9	4.9	1.5
SOC (% rated capacity)	95–100	95–100% max. normal vehicle operation	Max. operating SOC	Max. operating SOC	Max. operating SOC	100	100	Max. operating range of a vehicle or 80% SOC	100	100	100	100

^aNorway, Russia, Ukraine, Croatia, Serbia, Belarus, Kazakhstan, Turkey, Azerbaijan, Tunisia, South Africa, Australia, New Zealand, Japan, South Korea, Thailand and Malaysia.

^bIf only one drop test is performed, it shall not be a flat drop. If the electric energy storage assembly is intended to be installed or removed in a horizontal direction, a drop with the DUT slanted at a 10° angle with pack edge impacted, should be considered.

Table 5
 Test conditions for the penetration test at cell (C), module (M) and pack (P) level.

Region of applicability	International		EU and further countries [#]	USA		Korea	India	China			
	SAE J2464 [61]	SAE J2929 [66]		ISO 12405-1 (2)(3) [67–69]	IEC 62660-2 (3) [70,71]				UN/ECE-R100.02 [62]	UL 2580 [63]	USABC [72]
Penetration parameters	SAE J2464 [61]	SAE J2929 [66]	ISO 12405-1 (2)(3) [67–69]	IEC 62660-2 (3) [70,71]	UN/ECE-R100.02 [62]	UL 2580 [63]	USABC [72]	Freedom CAR [65]	KMYSS 18-3 [73]	AIS-048 [74]	QC/T 743 [75]
Level (C, M, P)	C M P	C M P									
Speed (cm s ⁻¹)	≥ 8	≥ 8									
Diameter of Rod (mm)	3 (C) 20 (M, P)	3 (C) 20 (M, P)									
Minimum Depth of Penetration	Cell (C) 3 cells or 100 mm (M, P)	Cell (C) 3 cells or 100 mm (M, P)									
SOC (% rated capacity)	95–100	100									

[#]Norway, Russia, Ukraine, Croatia, Serbia, Belarus, Kazakhstan, Turkey, Azerbaijan, Tunisia, South Africa, Australia, New Zealand, Japan, South Korea, Thailand and Malaysia.

the standards (see Table 5). In most cases, a 3 mm diameter rod is required at cell level and a 20 mm diameter rod is required at module or pack level. The depth of penetration is at least through the entire cell for cell level testing and through cells or 100 mm (whichever is greater) for module or pack testing [61,65,72,74,75]. In all cases the rod remains in place during the post-test observation period (e.g. 1 h). For FreedomCAR:2005 [65] this is not explicitly mentioned.

The usefulness of this test is questioned by many in the research community [57,84], for three main reasons: first the test is not fully representative of an event that would likely occur in a real - situation (e.g. a sharp object penetrating inside the battery compartment within a vehicle), second it has been proven that the test does not represent a spontaneous internal short circuit [57,85,86] and finally there are many parameters that can strongly affect the outcome of the test, for example: nail speed, nail dimension and SOC of the battery [60,87,88]. Furthermore, it is uncertain as to the influence the quality and composition of the nail material may have on the outcome of the test and standards and regulations do not provide guidance on this. For all the reasons mentioned above it seems comprehensible that this test is not included in many of the automotive standards and regulations as displayed in Table 5.

3.1.4. Immersion test

The immersion test has been developed to simulate a situation where a battery is submerged or where battery assemblies installed in the underbody of the vehicle are partially flooded. In order to perform this test, the (fully charged) battery is completely submerged in salt water with a composition similar to seawater (e.g. 5 wt% NaCl (aq.)) at 25 °C for a period of at least 1–2 h or until any visible effects (e.g. bubbling) have stopped [61,63,65,66,72,73] (see Table 6). The immersion into other liquids, such as engine coolant or fuel, is also recommended in FreedomCAR:2005 [65].

In the latest version of ISO 12405, part 3 published in 2014 [69], the water immersion test is newly introduced (not included in parts 1 and 2 [67,68]). Unfortunately, the test is not described in much detail and it is merely pointing out that the consequence of the test is a short circuit with hazardous gases possibly being released.

It is important to evaluate the frequency or likelihood of an electric vehicle exposed to a flood situation. For example in the Netherlands around 700–800 car accidents per year result in vehicles flooded in a ditch or canal [89]. Around 1200 to 1500 vehicles end up submerged in water in the United States every year [90]. Additionally, there are quite frequent situations where hurricanes or storms cause numerous vehicles to be submerged. Just to mention some examples, up to 250,000 cars were destroyed in Hurricane Sandy in 2012 [91] and several incidents involving EVs occurred (e.g. 16 submerged Fisker Karma's in Hurricane Sandy leading to fire [92]). Another example where moisture led to a fire event was the BAE Systems HybriDrive incident [93]. Based on these incidents, it seems that the performance of the test would be of relevance, however many of the standards and regulations do not include this test (see Table 6).

3.1.5. Crush/crash test

In this test, the applied crush force emulates a vehicle accident or any external load force that may damage the battery enclosure and cause its deformation. In the crush test, also referred to as battery enclosure integrity test [66], an electrically insulated plate usually textured or ribbed [62,65,72] is pressed down onto the battery until a certain compression is reached (e.g. crush to 85% of initial dimension and after 5 min continue crushing up to 50% of initial dimension [61,65,72,75]) or until an abrupt voltage drop is observed (e.g. reduction by 1/3 of original cell voltage [70]). Two standardized crush surfaces are normally used, type A and type B whose characteristics and dimensions are displayed in Fig. 2. Typically, for cell level testing (cylindrical or prismatic), type B crushing bar (as described in IEC 62660-2:2011 [70]) is used. For module or pack assemblies crushing plate type A is generally recommended.

Table 6
 Test conditions for the immersion test at cell (C), module (M) and pack (P) level.

Region of applicability	International		EU and further countries [#]	USA		Korea	India	China
	SAE J2464 [61]	ISO 12405-1 (2) [67,68]		USABC [72]	FreedomCAR [65]			
Immersion parameters	SAE J2464 [61]	ISO 12405-1 (2) [67,68]	UN/ECE-R100.02 [62]	USABC [72]	FreedomCAR [65]	KMVSS 18-3 [73]	AIS-048 [74]	QC/T 743 [75]
Level (C, M, P)	M, P	P		M, P	C, M, P	P		
Immersion Fluid	5 wt% NaCl	Clear or salty water		Nominal composition of sea water		0.6 M NaCl		
Temperature (°C)	25 ± 5	25 ± 2		25 ± 2 ± 5% of reading		25 ± 5		
Immersion time	≥ 2 h or until any visible reactions have stopped	Not specified		≥ 2 h or until any visible reactions have stopped		1 h		
SOC (% rated capacity)	95–100	> 50% normal operating range (HP) Max. SOC at normal operation (HE)		100		Max. operating range of a vehicle or 80% SOC		

HP: High power applications. HE: high energy applications.

[#]Norway, Russia, Ukraine, Croatia, Serbia, Belarus, Kazakhstan, Turkey, Azerbaijan, Tunisia, South Africa, Australia, New Zealand, Japan, South Korea, Thailand and Malaysia.

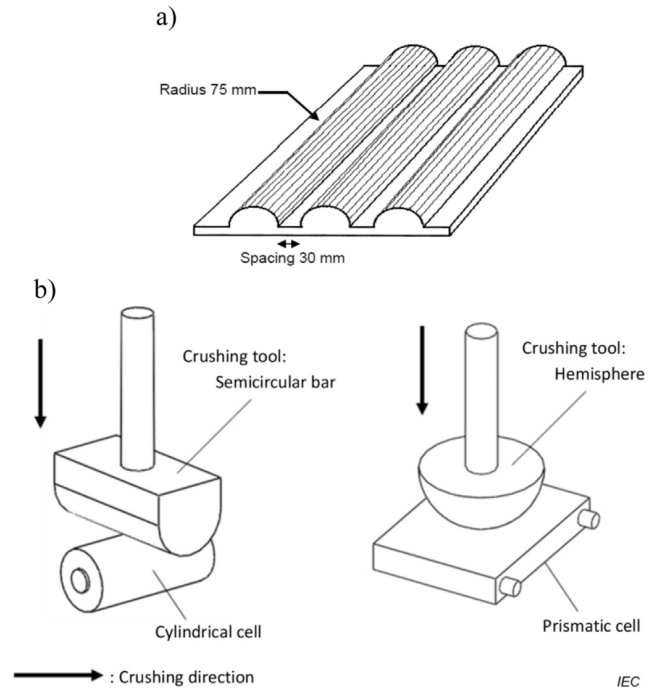


Fig. 2. Crushing plate a) type A and b) type B. Reprint from IEC 62660-2 ed.1.0 Copyright © 2010 IEC Geneva, Switzerland. www.iec.ch.^{3,3} “The author thanks the International Electrotechnical Commission (IEC) for permission to reproduce information from its International Standard IEC 62660-2 ed.1.0 (2010). All such extracts are copyright of IEC, Geneva, Switzerland. All rights reserved. Further information on the IEC is available from www.iec.ch. IEC has no responsibility for the placement and context in which the extracts and contents are reproduced by the author, nor is IEC in any way responsible for the other content or accuracy therein”.

Guidance on crush plate position is missing in most of the cases. SAE J2464:2009 [61] requires the test to be performed at the most vulnerable location to include the main cell area, whereas UN/ECE-R100.02:2013 [62] allows the manufacturer together with the technical service (e.g. certified testing body) to decide the plate position taking into consideration the direction of the travel of the DUT relative to its installation in the vehicle.

Some standards indicate that the force to be applied in the crush test has to be limited to 1000 times the weight of the battery [61,65,70,72] whereas others have a fixed force (e.g. 100 kN [62,63,66]) (Table 7), independent of the size of the battery to be tested. The implementation of the first option might lead to some issues testing traction batteries. As pointed out by Wech et al. [94] maximum forces of less than 1000 times the battery weight might not be sufficient to achieve the required compression (e.g. 50% of battery dimension [61,65,72,75]). This would be the case for pack level testing following USABC:1999 [72], FreedomCAR:2005 [65] and SAE J2464:2009 [61]. For example, in the case of the small battery (24 kg, 0.8 kW h) of the Mercedes-Benz S400 HYBRID, only 11% deformation would be achievable [94]. Applying this requirement to a full HEV battery pack with 1.5–3 kW h, or to an EV battery pack with 15–35 kW h, having weights ranging from 50 to 200 kg, would require a minimal load of 500–2000 kN. This is an unrealistic scenario, as maximum loads rarely exceed 200 kN based on crash test simulations [94].

Another aspect that can raise some concern is the comparability of results between tests performed at component and vehicle level. Investigations of real world accident scenarios on occurrence of deformations in selected positions of the vehicle, together with simulations on fuel cell vehicles equipped with a compressed hydrogen storage system lead to the conclusion that maximum contact loads are usually < 100 kN [95]. Applied crush force on the DUT at component and vehicle level might not be comparable as in the latter case the battery has extra

Table 7
 Test conditions for the crush test at cell (C), module (M) pack (P) and for the crush test at vehicle (V) level.

Region of applicability	International			EU and further countries [#]		USA			Korea	India	China	
	SAE J2464 [61]	SAE J2929 [66]	ISO 12405-1 (2) [67,68]	ISO 12405 (3) [69]	IEC 62660-2 (3) [70,71]	UN/ECE-R100.02 [62]	UL 2580 [63]	USABC [72]				FreedomCAR [65]
Level (C, M, P)	C M P	P	P	P	C	C M P	C M P	C M P	C M P	C M P	C M P	C P
Crush speed (mm min⁻¹)	0.5–1 (C) 5–10 (M, P)	5–10					5 – 10 (M, P)					
Crush force	≤ 1000 DUT weight	100 kN or expected intrusion as per FMVSS 305 [81]*	100–105 kN**	≤ 1000 DUT weight	100–105 kN***	≤ 1000 DUT weight (C) 100 ± 6 kN (M, P)	≤ 1000 DUT weight					
Crush plate type	B (cylindrical C) Parallel to crush surface (prismatic and pouch C) A (M, P)	A	A	B	A (≤ 600 mm × 600 mm)	B (C) A (M, P)	A	Solid cylindrical impactor half the cell average diameter (C) A (M, P)				Crush area > 20 m ² (C) A (30 mm × 150 mm) (P)
SOC (% rated capacity)	95–100	95–100% max. normal vehicle operation	> 50% normal operating range (HP) Max. SOC at normal operation (HE)	80 (HEV)	> 50% normal operating range	80 (HEV) 100 (BEV) (C)	80 (HEV) 100 (BEV) (C)	100				100
Vehicle level (V)		FMVSS 305 [81]**	Relevant national or regional regulation on vehicle crash test		UN/ECE-R12 [78], UN/ECE-R 94 [79], UN/ECE-R 95 [80]							

* If due to battery packaging location, no battery enclosure deformation is expected, this requirement is presumed to be met. The responsible organisation shall be responsible to make and document this conclusion. ** or a value determined by the customer depending on expected forces in vehicle crash tests. These values shall be based on appropriate analysis, e.g. vehicle crash tests or vehicle crash simulations. ***A higher crush force, a longer onset time, a longer hold time, or a combination of these, may be applied at the request of the manufacturer. # or equivalent regionally applicable for vehicle front, rear and side crash conditions. #Norway, Russia, Ukraine, Croatia, Serbia, Belarus, Kazakhstan, Turkey, Azerbaijan, Tunisia, South Africa, Australia, New Zealand, Japan, South Korea, Thailand and Malaysia.

protection provided by the chassis and battery enclosure. Additionally, there could be some disagreement centred around the fact that real world accidents have a dynamic nature, that is the battery is moving towards the impact zone, which is different from component level tests where the crush plate moves towards a static battery. Various published investigations have shown discrepancies between current standards and regulations and dynamic crash tests, and hence the authors of these investigations recommend appropriate modifications to the tests included in the regulatory framework [94,96].

The crush test can also be performed at vehicle level, the so-called *Crash test*. Electric vehicles shall comply with the crash safety requirements as for conventional vehicles. In Europe, vehicles have to pass the tests defined by the UNECE: steering mechanism, front impact, and side impact tests from UN/ECE-R12:2012, UN/ECE-R94:2012 and UN/ECE-R95:2011 [78–80] as described in UN/ECE-R100.02:2013 [62]. In the USA, vehicles need to comply with the test defined in the Federal Motor Vehicle Safety Standards, such as frontal rigid barrier, a side moving deformable barrier, a rear rigid barrier and a rear deformable barrier according to FMVSS 305:2011 [81]. Following the crush test, a roll over test, is performed in some cases. This is the case for SAE J2929:2013 [66], described in Section 4.1.f (Table 7).

3.1.6. Rollover test

This test, also referred to as rotation test, simulates overturn of a vehicle that might occur in an accident. Comparison of the different test parameters is presented in Table 8. In order to perform the test, the battery pack or module is slowly rotated (e.g. 6° s^{-1}) for one complete revolution (360°) in order to evaluate the presence of any leak (e.g. battery electrolyte, coolant liquid) or venting. Then, the DUT is rotated in 90° increments for another full rotation staying at each position for one hour [61,63,65,72,74].

The rollover test is usually performed after crash tests such as described in FMVSS 305:2011 [81] or after a crush test as described in SAE J2929:2013 [66]. In relation to the Korean standards, rollover testing is not part of Article 18-3, discussed in this review, but part of Article 91 (fuel system). The need for this testing is supported by the fact that around 220,000 light motor vehicles sustain rollover crashes in the US annually, which accounts for almost a third of all highway vehicle occupant fatalities [97]. Despite this fact, the rollover test is not included in various relevant standards and regulations, such as UN/ECE-R100.02:2013 [62].

It is interesting to point out the discrepancy between standards with respect to the applicability of the rollover test for certain types of battery chemistry: while UL 2580:2013 [63] mentions specifically that flooded lead acid batteries are not subjected to this test, AIS-048:2009 [74], on the contrary, states that the test is applicable only for flooded lead acid batteries.

3.1.7. Vibration test

Although vibration occurs in any driving environment under normal operating conditions, because it may be considered abusive to the battery, almost all of the standards and regulations evaluated in this review include a vibration test. The purpose of this test is to evaluate the effect of long-term vibration profiles – representative of driving – on the battery, both in terms of the durability and in terms of identification of design flaws. The vibration profiles vary quite considerably over a wide range of frequencies and amplitudes (see Table 9). In order to facilitate the comparison of the various vibration parameters, Fig. 3a and b display the sine wave and random profiles used in the evaluated standards and regulations. Sine swept testing is commonly used to identify product resonances, while random vibration simulates everyday life scenarios that a DUT would experience [98,99].

The vibration profiles in standards and regulations are derived from generic measurements from conventional vehicles at locations appropriate for mounting traction batteries in EVs. In fact, there are

Table 8
 Test conditions for the rollover test at module (M) and pack (P) level.

Region of applicability	International		EU and further countries ^a		USA		Korea	India	China			
	SAE J2464 [61]	SAE J2929 [66]	ISO 12405-1 (2)(3) [67–69]	IEC 62660-2 (3) [70,71]	UN/ECE-R100.02 [62]	UL 2580 [63] ^b				USABC [72]	Freedom CAR [65]	KMVSS 18-3 [73]
Rollover parameters												
Level (M, P)	M, P	P				P						
Rotation speed (continuous revolution)	$360^\circ \text{ min}^{-1}$					$360^\circ \text{ min}^{-1}$ in 3 mutually perpendicular directions						
Rotation steps incremental revolution/hold time per increment	90° h^{-1}	90° (within 60–180 s)/5 min										
SOC (% rated capacity)	95–100	95–100% max. normal vehicle operation				Max. operating SOC						

^aNorway, Russia, Ukraine, Croatia, Serbia, Belarus, Kazakhstan, Turkey, Azerbaijan, Tunisia, South Africa, Australia, New Zealand, Japan, South Korea, Thailand and Malaysia.

^b Except for flooded lead acid batteries.

^c Applicable only for flooded lead acid batteries.

Table 9
 Test conditions for the vibration test at cell (C), module (M), pack (P) and vehicle (V) level.

Region of applicability	International			EU and further countries [#]		USA		Korea	India	China	
	SAE J2464 [61]	SAE J2929 [66] ^c	ISO 12405-1 (2)(3) [67–69] ^e	IEC 62660-2 (3) [70,71]	UN/ECE-R100.02 [62]	UL 2580 [63]	USABC [72]				Freedom CAR [65]
Level (C, M, P)											
Type of profile	Random	C M P Sine wave	P Random	C Random	C M P Sine wave logarithmic sweep	C Random	M ^f P Random	C M P Sine wave or Random	M Sine wave	P Linear sweep	
Frequency range (Hz)	10–190 ^a	7–200 ^d	5–200 ^e	10–2000 ^e	7–50 ^b	10–2000 ^e	10–190 ^a	10–190 ^a	30–150	10–55	
PSD wave random (m s⁻²)²/Hz	0.4–11 ^a		0.02–5.8 ^e	0.14–20 ^e		0.14–20 ^e	0.4–11 ^a	0.4–11 ^a			
Loading range sine wave (m s⁻²)											
Axis	Vertical, longitudinal, lateral	Three mutually perpendicular mounting positions of the cell	Vertical, longitudinal, transversal	Vertical	Vertical	Vertical	Vertical, longitudinal, lateral	Vertical, longitudinal, lateral	Vertical axis and horizontal	Vertical	
SOC (% rated capacity)	95–100% max. normal vehicle operation		50	80 (HEV) 100 (BEV)	> 50% normal operating range	80 (HEV) 100 (BEV)	100 & 20 (Z-sine, random) 60 (X & Y-sine, random)	100 & 20 (Z-sine, random) 60 (X & Y-sine, random)	100		
Vehicle level (V)		SOC at normal vehicle operation									

PSD: Power spectral density

[#]Norway, Russia, Ukraine, Croatia, Serbia, Belarus, Kazakhstan, Turkey, Azerbaijan, Tunisia, South Africa, Australia, New Zealand, Japan, South Korea, Thailand and Malaysia.

^a Based on SAE J2380:2009 [102].

^b Higher can be requested by manufacturer.

^c A profile 'which reflects the application' may be used as alternative.

^d Based on UN 38.3:2015 [76].

^e Based on IEC 60068-2-64:1993 [101].

^f At the module level for those electric energy storage assemblies intended for use in applications larger than passenger vehicles. The module level testing shall be representative of the electric energy storage assembly.

^g Vibration endurance test in accordance with the anticipated end application vehicle vibration profile.

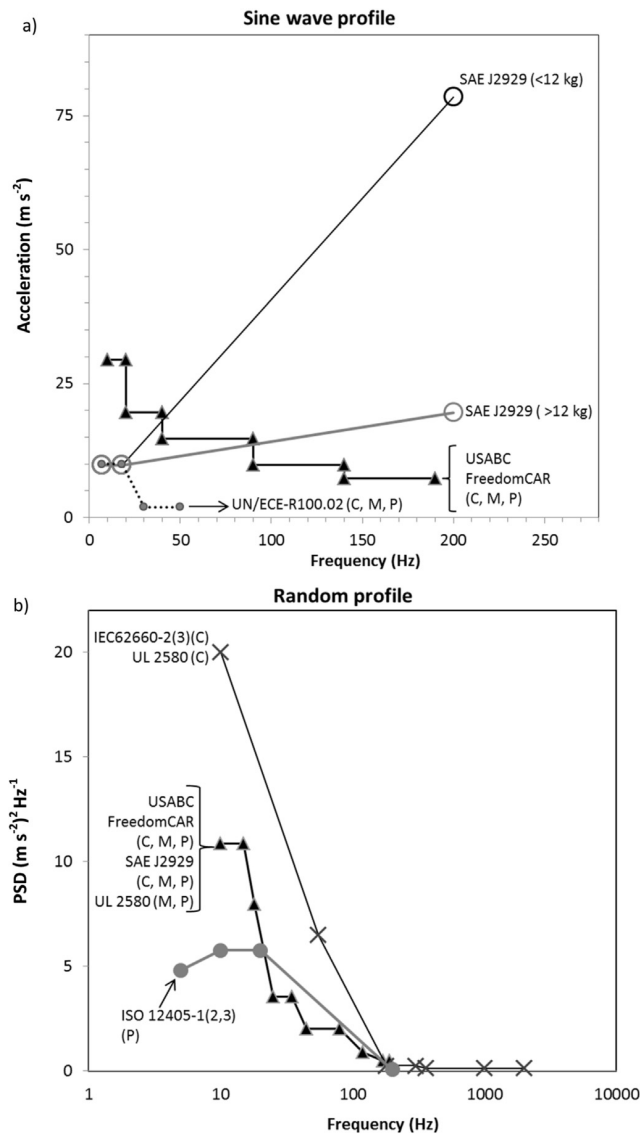


Fig. 3. Vibration profiles for the various standards and regulations requiring: a) sine wave profile and b) random profile.

very few works published on vibration profiles designed specifically to EVs and HEVs. Work published by Hooper et. al. pointed out that many of the vibration profiles described in the standards represent a short term abuse rather than a mechanical durability test to represent a battery life. Additionally it is suggested that battery packs may be exposed to vibration loads outside the range evaluated in existing standards [100].

Vibration test profiles in standards are adapted in most cases from UN 38.3:2015 [76], IEC 60068-2-64:1993 [101] or SAE J2380:2009 [102]. The vibration profile described in UN 38.3:2015 replicates vibrations during transport. This test is not considered relevant for the evaluation of battery resilience to vibration during driving conditions, since test conditions are not representative of the position of the battery and its fixture in the vehicle. For this reason the transport regulation is not discussed in detail in this review. Despite this, UN 38.3:2015 testing is provided as an alternative within SAE J2929:2013. On the other hand, standard IEC 60068-2-64:1993 [101] has been taken as the basis for IEC 62660-2(3):2011(2013): [70,71], ISO 12405-1(2):2011(2012) [67,68] and UL 2580:2013 [63]. It defines different test conditions for battery pack testing (up to 200 Hz) and for the electronic devices of the battery pack

(cell level testing, up to 2000 Hz) due to the difference in mass of the DUT.

Lastly, SAE J2380:2009 [102] is also widely used to define random vibration profiles. Actually this standard is the basis for SAE J2929:2013 [66], UL 2580:2013 [63] (module and pack level only), USABC:1999 [72] and related FreedomCAR:2005 [65] standards and it reflects rough-road measurements at locations where traction batteries are likely to be installed in EVs/HEVs, equivalent to 100,000 miles usage.

Interestingly, ISO 12405 part 1 and 2 [67,68] are to our knowledge the only standards, that require vibration testing at different ambient temperature conditions, namely at + 25 °C, + 75 °C and - 40 °C. The combined effect of vibration and temperature could certainly be relevant during in-use situations. However, a malfunction of the cooling and/or heating unit of the vehicle is required to observe such extreme temperatures.

Fig. 3a highlights how regulation UN/ECE-R100.02:2013 [62] requires significantly milder requirements compared to the other standards. Additionally, this regulation is one of the few documents that require performing the test in only one axis (vertical axis), whereas other standards require testing in two or three axes.

Vehicle level testing can also be performed as mentioned in SAE J2929:2013 [66] under conditions defined by the testing body.

3.2. Electrical tests

In this section the series of abusive tests to evaluate the electrical safety of the devices will be presented: external short circuit or short circuit protection test, internal short circuit test and overcharge/over discharge protection tests. Some other standards, which do not describe abusive tests, but still of relevance to electrical safety are also mentioned: general electrical functional safety requirements of electrically propelled road vehicles are specified in the international standard ISO 6469 series. Part 1 of this standard particularly covers the Rechargeable Energy Storage System (RESS) safety specification [103], while part 3 deals with general protection against electric shock [104] and part 4 deals with post-crash safety requirements, aimed at the protection of persons inside and outside the vehicle [105]. ISO 17409:2015 [106], deals with the safety of the electric vehicle during conductive charging. This document, which was initially part of the IEC 61851:2010 [107] series, focuses on electrical risks. Another document for wireless charging, ISO 19363 [108], is in an earlier stage of development (preparatory stage).

3.2.1. External short circuit test

The purpose of this test is to evaluate the safety performance of a DUT when applying an external short circuit. The test can evaluate the activation of the overcurrent protection device or the ability of cells to withstand the current without reaching a hazardous situation (e.g. thermal runaway, explosion, fire). The main risk factors are heat generation at cell level (thermal runaway [109]) and arcing which may damage circuitry or may lead to reduced isolation resistance.

The most relevant test parameters are presented in Table 10. During the test a low resistance element (e.g. 5 mΩ [62,70,72], 20 mΩ [63,68] or 100 mΩ [67]) is connected externally across the battery terminals in less than one second and maintained for a defined period of time (e.g. 10 min). As a consequence, current flows through the system until an overcurrent protection device – if present – limits the current [72]. Typically fuses, circuit breakers (passive elements) and contactors (active elements) are used to protect against over-currents at module or pack level. At cell level, built in current interruption devices (CID) or positive thermal coefficient (PTC) devices can be used, which disconnect the internal current collector from its terminal or limit the passage of current if the inside pressure and/or temperature reach a certain limit. All these protection devices have a time characteristic (e.g. for circuit breaker IEC 60898-1:2015 [110]) of how quickly they limit or interrupt the current. The higher the current,

Table 10
 Test conditions for the short circuit test at cell (C), module (M) and pack (P) level.

Region of applicability Short circuit parameters	International		EU and further countries ^a		USA		Korea	India	China		
	SAE J2464 [61] [70,71]	SAE J2929 [66] [67-69]	ISO 12405-1 (2) (3) [67-69]	IEC 62660-2 (3) [70,71]	UN/ECE-R100.02 [62]	UL 2580 [63]				USABC [72]	Freedom CAR [65]
Level (C, M, P)	C M P	P	P	C	C M P	C M P	C M P	C M P	C P		
Cooling medium	Operational	Operational if necessary for operation	Operational if necessary for operation		C M P	Operational	P	C M P	C P		
Passive short-circuit Protection device	Disabled or bypassed (C M P) or Operational (C M)	Operational	Operational		Operational if relevant to the outcome of the test	Operational		Operational	Operational		
Non-passive protective device						Disabled		Disabled	Disabled		
Resistance (mΩ)	Hard short: ≤ 5 and < < DUT DC impedance Soft short: ≥ 10 and resistance comparable to DUT DC resistance	100 (20) ^(c)	100 (20) ^(c)	≤ 5	≤ 5	≤ 5 ^a	50	≤ 5 ^b	< 5		
SOC (% rated capacity)	95–100	95–100% max. normal vehicle operation	100	100	> 50% max. operating SOC	Max. operating SOC	Max. operating range of a vehicle or 80% SOC	100	100		

^aNorway, Russia, Ukraine, Croatia, Serbia, Belarus, Kazakhstan, Turkey, Azerbaijan, Tunisia, South Africa, Australia, New Zealand, Japan, South Korea, Thailand and Malaysia.

^b For systems with ≤ 5 mΩ internal resistance, a conductor of 1/10 of the minimum resistance of the cell/module shall be used.

^c For systems with ≤ 0.9 mΩ V⁻¹ system voltage ± 0.1 mΩ internal resistance, a conductor of 1/10 of the minimum resistance of the cell/module shall be used.

^d ISO 12405-3: the test can be conducted at a lower resistance or higher temperature than specified in ISO 12405-1 (2), as appropriate for the DUT, according to agreement between the customer and the supplier.

^e Test temperature 55 ± 2 °C.

the faster they are typically able to interrupt it. If the current is not high enough (e.g. at low SOC) or if it drops quickly [111] the current may be not interrupted, potentially creating a hazardous situations. Therefore, standards require a hard short circuit when the external resistance is minimal [62,70,72] or a soft short circuit when the external resistance is comparable with of the internal resistance of the DUT. In this case, the soft short circuit will assure that the response of the cell is evaluated, rather than that of the protection device [61].

As mentioned, standards require a fixed external resistance irrespective of the size of the DUT. However, the initial short circuit current is influenced by the size of the DUT [112,113] as well as by its type of connection (i.e. parallel, serial or a combination thereof). Consequently, applying the same external resistance to DUTs having different sizes and types of connection, may result in not necessarily comparable initial short circuit currents per cell. Therefore some standards indicate for hard short conditions, that the external resistance needs to be much smaller than the DUT DC impedance [61] or 1/10 of the minimum resistance of the cell/module for systems with less than $0.9 \text{ m}\Omega \text{ V}^{-1}$ system voltage $\pm 0.1 \text{ m}\Omega$ internal resistance [74], as the initial short circuit current depends on the internal resistance of the DUT. For soft short conditions, when the external short circuit resistance is higher than that of the DUT, the initial short circuit current is governed primarily by the external resistance, therefore resulting in initial short circuit currents independent of the size of the RESS.

Temperature affects the internal resistance of a battery, i.e. the rate of electrochemical reactions and transport; therefore a higher initial current can be generated at elevated temperature, which creates more heat. Moreover the higher the temperature, the closer the DUT temperature is to the onset temperature of thermal runaway. At low temperature, the activation of the protecting device (e.g. fuse, circuit breaker) can be inhibited, or the time to interruption may increase. Only UN 38.3:2015 and UL 1642:2007 require a short circuit test to be performed at a temperature higher than room temperature ($55 \pm 5 \text{ }^\circ\text{C}$) [76,114]. Standards and regulations specific to electric vehicle applications (Table 10) do not require increased temperature testing. However, it may be considered reasonable that the short circuit test needs to be performed at temperatures higher than room temperature, which are likely to be reached during driving or when the cooling system is malfunctioning. In addition, none of the standards and regulations considers low temperature as a safety problem, where dendrite formation is prone to occur.

Another parameter that influences greatly the outcome of the test is the SOC. The worst case is achieved at high SOC, as the initial short circuit current created is maximum [112] and the onset temperature of thermal runaway is lowest [115]. Consequently, most of the standards require testing at 100% of the rated capacity (Table 10), however in the case of UN/ECE-R100.02:2013 [62], the test can be performed at 50% SOC (or above) of the maximum operating SOC value.

3.2.2. Internal short circuit test

Standardisation of the internal short circuit (ISC) test is under development, and no regulation dealing with batteries for automotive applications requires this test. The occurrence of internal short circuits, one of the main concerns for battery manufacturers, potentially leads to venting, thermal runaway, along with sparking which can ignite the electrolyte vapours escaping from the cell [57,116]. The generation of these internal shorts can be triggered by manufacturing imperfections, presence of impurities in the cells, dendritic growth of lithium etc. [57] and leads to most of in-field safety incidents [117]. Multiple internal short circuits scenarios are possible (e.g. electrical contact of cathode/anode, aluminium current collector/copper current collector, aluminium current collector/anode) each with a different contact resistance [117].

As mentioned previously, mechanical nail penetration tests aim at investigating the effects of an internal short circuit, however some

works suggest that nail penetration is not representative of real field situations [57,118]. For this reason, various alternative tests have been developed in order to represent a more realistic scenario; however these tests have not been widely implemented in the legislative landscape. We will summarize here three of the most relevant tests:

3.2.2.1. Separator shutdown integrity test. The purpose of this test is to evaluate the efficiency of the shutdown separator at high temperatures and the possible failure propagation within cells connected in series (in a module) as described in SAE J2464:2009 [61]. In this test the cell shall be heated to a temperature slightly above the shutdown temperature (i.e. $\geq 5 \text{ }^\circ\text{C}$). For detailed explanation on how to measure the shutdown temperature, please refer to the standard. Once the temperature is stable for 10 min, a voltage above (or equal to) 20 V is applied at a maximum current of 1 C and maintained for 30 min (or until separator failure).

3.2.2.2. Forced internal short circuit or nickel particle test. The international standards IEC 62133-2:2017 [119] and IEC 62660-3:2016 [71] provide detailed instructions for the internal short circuit test for cylindrical and prismatic type cells. The test, which is performed at two temperatures, $+10 \pm 2 \text{ }^\circ\text{C}$ and $+45 \pm 2 \text{ }^\circ\text{C}$, requires the disassembly, insertion of an L-shaped nickel particle (e.g. between positive coated area and negative coated area, between positive active material and separator) and reassembly of the cell. A short circuit is subsequently induced with a pressing machine at a speed of 0.1 mm s^{-1} .

This test has obvious drawbacks due to the need to manipulate the cell. As an alternative, the particle could be introduced during the manufacturing process.

3.2.2.3. Blunt rod indentation test. Another ISC variation, also referred to as Indentation-Induced ISC (IIISC) was developed by Underwriters Laboratories and NASA [120]. It entails the application of a mechanical force to the cell/battery, using a blunt rod instead of a sharp one, in order to deform the most outer electrode layers and eventually create a short circuit. The rod speed applied is several orders of magnitude lower than that used for the penetration tests (0.01 cm s^{-1} vs. 8 cm s^{-1}).

Overall, it can be concluded that these alternative tests exhibit uncertainties and difficulties, mostly from a practical point of view. Researchers are still actively looking for ways to evaluate the ISC hazard in a more realistic and practical way, allowing successful implementation of these tests in future automotive safety tests. Alternative approach taken by some battery manufacturers consists on designing systems where cell to cell propagation is hindered or designing packs able to contain a potential thermal runaway within.

3.2.3. Overcharge/overdischarge test

In order to evaluate the functionality of the overcharge/overdischarge protection system, the battery is charged or discharged beyond the limits recommended by the manufacturer, situations that could occur due to a charger failure, for example. The relevance of the test is underlined by the fact that almost all evaluated standards and regulations (with the exception of overdischarge in AIS-048:2009 [74]) require its application. A summary of test parameters is presented in Table 11.

The main safety risks during overcharge are the decomposition of the electrolyte [109,121], cathode and anode breakdown, exothermic decomposition of the SEI layer, separator degradation, and the Li plating [122], which can lead to self-heating of the battery and thermal runaway. Also fluorinated binders, such as polyvinylidene fluoride (PVDF), have been found to react exothermically with lithiated carbon

Table 11
 Test conditions for the overcharge/overdischarge test at cell (C), module (M), pack (P) and vehicle (V) level.

Region of applicability	International				USA		Korea		India		China	
	SAE J2464 [61]	SAE J2929 [66]	ISO 12405-1 (2)(3) [67–69] ***	IEC 62660-2 (3) [70,71]	UL 2580 [63]	USABC FreedomCAR [65]	KMVSS18-3 [73]	AIS-048 [74]	QC/T 743 [75]			
Overcharge Level (C, M, P, V)	C M P	P	P	C	C M P	C M P	M P	P	C M P	C P		
Passive overcharge Protection device	Operational	Operational	Operational		Operational	Operational	Operational			Electronic protection circuit removed ¹		
Non-passive protective device	Disabled	Disabled	Disabled		Disabled	Disabled						
Charge rate	a) 1C CC and b) at max. current supplied by regenerative braking or charging system (or 3C) (C) 1C CC (M, P)	Max. possible rate for the application	5C (HP) 2C (HE)	5I _t (HEV) 1I _t (BEV)	5I _t (HEV) (C) 1I _t (BEV) (C) Max. specified charging rate (M, P)	32 A CC* and < 450 Vdc		According to manufacturer's recommendation or 32 A CC until 1.5 x rated voltage followed by constant voltage	C/10	3I ₃ (= 9I ₃) (= 1C) 3C)		
End of charge	> 200% SOC or destructive factor (e.g. thermal runaway)	*	> 130% SOC, > 55 °C or **	2 V _{max} reached or 200% SOC	2 V _{max} reached or 200% SOC (C) *** or 110% rated capacity, or a manufacturer specified limit or DUT failure (explosion, fire) (M, P)	200% SOC or 4 h or 200% SOC (C) *** or 4 h	200% SOC or 4 h or DUT fail	150% SOC or 2.5 h after full charging	10 h	5 V or 10 V		
Overdischarge Level (C, M, P, V)	C M	P	P	C	C M P	C M P	M P	P	C M P	C P		
Passive overdischarge Protection device	Operational	Operational	Operational		Operational	Operational	Operational			Electronic protection circuit removed ¹		
Non-passive protection device	Disabled	Disabled	Disabled		Disabled	Disabled						
Discharge rate	Max. recommended current	1C (HEV/PHEV) C/3 (BEV)	1C (HP) C/3 (HE)	I _t	I _t (C) Max. specified discharge rate (M, P)	1C	1C			I ₃ (= C/3)		
End of discharge	-100% SOC (C) or 0.0 ± 0.2 V (M)	** or 0 ± 0.2 V	25% of nominal	90 min	** (M, P) 90 min (C)	1.5 h or until every subassemblies have	1.5 h or until 50% of subassemblies have	30 min		0 V (C) A cell is 0 V (P)	(continued on next page)	

Table 13
 Test conditions for the thermal shock test at cell (C), module (M) and pack (P) level.

Region of applicability	International				USA		Korea	India	China		
	SAE J2464 [61]	SAE J2929 [66]	ISO 12405-1 (2)(3) ^a [67–69]	IEC 62660-2 (3) ^a [70,71]	UN/ECE-R100.02 [62]	UL 2580 [63]	USABC [72]	Freedom CAR [65]	KMVSS 18-3 [73]	AIS-048 [74]	QC/T 743 [75]
Level (C, M, P)	C M P	C M P	P	C	C M P	C M P	C M P	C M P			
Protection device	Active thermal controls (primary and secondary) disabled Not defined in UN 38.3 alternative	Thermal controls disabled	Without electrical operation	With electrical operation	Protection devices shall be operational	Active thermal controls (primary and secondary) disabled	Thermal controls (primary and secondary) disabled				
T_{max} (°C)	+ 70 ± 2 or ± 5% of reading	+ 70 ± 2 or ± 5% of reading or + 72 ± 2	+ 85 ± 1 ^b	+ 65 ± 2	+ 60 ± 2	+ 85 ± 2	+ 80				
T_{min} (°C)	- 40 ± 2 or ± 5% of reading	- 40 ± 1	- 40 ± 1	- 20 ± 2	- 40 ± 2	- 40 ± 2	- 40				
Hold time (h)	≥ 1 (C) ≥ 6 (M) ^c (P)	≥ 1 (C) ≥ 6 (M) ^c (P) or ≥ 12 (C > 0.5 kg M, P > 12 kg)	≥ 1 (3)	1.5 (T _{min}) 1.83 (T _{max})	6	1.5 (T _{max}) (C) 1.83 (T _{min}) (C) ≥ 6 (M) ^c (P)	Appropriately adjusted (C) ≥ 6 (M) ^c (P)				
Repetitions	5	5 or 10	5	30	5	30	5				
SOC (% rated capacity)	95–100	95–100% max. normal vehicle operation	50 (HP) 80 (HE)	60 (HEV) 80 (BEV)	≥ 50% max. operating SOC	80/60 (HEV) 100/80 (BEV) (C)	50				

^aNorway, Russia, Ukraine, Croatia, Serbia, Belarus, Kazakhstan, Turkey, Azerbaijan, Tunisia, South Africa, Australia, New Zealand, Japan, South Korea, Thailand and Malaysia.

^b Or T_{min}, T_{max} as specified by manufacturer.

^c Part 3 of the standard allows: + 60 ± 2 °C with a hold time of 6 h.

^d As required to reach uniform temperature (± 5 °C).

Table 14
 Test conditions for the overheat test at cell (C), module (M), pack (P) and vehicle (V) level.

Region of applicability Over heat parameters	International		EU and further countries*		USA		Korea		India		China	
	SAE J2464 [61]	SAE J2929 [66]	ISO 12405-1 (2)(3) [67–69]	IEC 62660-2 (3) [70,71]	UN/ECE-R100.02 [62]	UL 2580 [63]	USABC [72]	FreedomCAR [65]	KMVSS 18-3 [73]	AIS-048 [74]	QC/T 743 [75]	
Level (C, M, P, V)	M P	P	C M P V	M P	M P							
Protection device	Active thermal controls (primary and secondary) disabled	Cooling system deactivated	Cooling system deactivated	Active thermal controls (primary and secondary) disabled								
Charge rate	As defined by the manufacturer	Max. normal rate	Steady current that will increase the temperature of cells as rapidly as possible within the range of normal operation defined by the manufacturer	IC	IC	IC	Manufacturer's recommended charge algorithm					
Discharge rate	Rate comparable to the intended application			IC	IC	Rate comparable to a 3 kW constant power rate for entire DUT						
Number of cycles	20											
SOC (% rated capacity)	95–100	Max. normal operating SOC										

*Norway, Russia, Ukraine, Croatia, Serbia, Belarus, Kazakhstan, Turkey, Azerbaijan, Tunisia, South Africa, Australia, New Zealand, Japan, South Korea, Thailand and Malaysia.

if sufficient temperature is reached (e.g. 200 °C [60]). Factors affecting the outcome of the test are amongst others, the charging rate and the finally reached SOC.

For the overcharge test, a controlled current is applied to the battery (e.g. 1/3 I_t^2 -rate) up to a set charge limit (e.g. 200% SOC [61,62,70,72], 110% SOC [63], 130% [67]) or until the tested-device (automatically) interrupts or limits the charging. Although most of the standards provide a general description for all types of energy storage devices, others describe specific tests for EVs, HEVs and PHEV applications (e.g. charging rate at 5 I_t [123] for HEV and 1 I_t for BEV [70,71]). Some other standards recommend much lower C-rate (e.g. C/10 in AIS-048:2009 [74], C/3 rate in UN/ECE-R100.02:2013 [62]). Tobishima et al. showed that cells overcharged at low rates did not show any venting whereas those cells overcharged at a 2C rate did [124]. Golubkov et al. showed that NCA cells with SOC ≤ 100% had a thermal runaway onset temperature in the range 136–160 °C, whereas overcharged cells (SOC > 100%) showed much lower onset temperatures (ranging 65–80 °C). Although serious events occur at cell level with significant overcharge (e.g. 2 times the rated capacity), repeated charge/discharge cycling at moderate overcharge (110% SOC) can also lead to internal short and failure of the cell in only 10 cycles [125].

To address another scenario of great importance, an over-discharge (or forced discharge) test is generally required. Safety risks during overdischarge are polarity reversal leading to oxidation of the anode current collector (Copper) and to plating on the cathode side. Even minor over-discharge may cause dendrite formation and finally short circuit [126]. During the overdischarge test, a fully charged battery is discharged (e.g. 1C rate for 1.5 h [65], C/3 rate) until the tested-device interrupts or limits the discharging [62]. The great variability in test parameters found in the various evaluated documents (Table 11) can lead to the conclusion that the outcome of the tests might be dependent on the standard or regulation followed. For this reason harmonisation of testing parameters is required to allow comparable testing.

3.3. Environmental tests

Environmental testing aims at evaluating the safety performance of a system under conditions of temperature change, such as an accident scenario involving fire, or extreme weather exposure in certain geographic areas. In this section, the most common environmental tests, thermal stability, thermal shock, overheat and extreme cold temperature and fire tests are described.

3.3.1. Thermal stability test

This test evaluates the stability of a battery at an elevated temperature to identify the temperature where thermal runaway begins. For this test, the temperature of the cell is increased sequentially in 5 °C steps with a holding time of 30 min at each incremental step, until the temperature reaches 200 °C [65,72] above the maximum operating temperature of the battery (or until a catastrophic event occurs such as venting or major damage to the DUT). For modules and packs, the increments of temperature are set to 10 °C with a longer holding time of 120 min [65,72]. Standard SAE J2464:2009 [61] has a higher threshold temperature of 300 °C above the maximum operating temperature. These tests require a second execution in order to refine the exact start temperature of the thermal event. During the second execution, the temperature is increased in 2 °C increments and held for a minimum of one hour at each incremental step [61,65,72].

Some other standards evaluate the performance of the system at elevated temperature, not aiming at reaching thermal runaway, but at the

² The current I_t represents the discharge current in amperes during one hour discharge and C is the measured capacity of a battery pack (or a cell): I_t (A) = Cn (Ah)/1 (h); n is the time base (hours) for which the rated capacity is declared.

Table 15
 Test conditions for the fire test at cell (C), module (M), pack (P) and vehicle (V) level.

Region of applicability	International		EU and further countries [#]	USA		Korea	India	China	
	SAE J2464 [61]	ISO 12405-1 (2) [67,68]		ISO 12405 (3) [69]	IEC 62660-2 (3) [70,71]				UN/ECE-R100.02 [62]
Level (C, M, P, V)	M, P	P	P, V ^a	C, M, P, V	C, M, P	C, M, P	C, M, P	P	
Heat source	Radiant heat	Flame	Flame	Flame	Radiant heat	Flame	Flame	Flame	
Set-up	Cylindrical metallic fixture	Wire mesh screen (Fig. 4a)	Grating table (Fig. 4b)	Grating table (Fig. 4b)	Cylindrical metallic fixture	Cylindrical metallic fixture	Cylindrical fixture	Not specified	
T_{max} (°C)	890 °C	To be defined by responsible testing organisation	Not specified	Not specified	890 °C	890 °C	890 °C	890–900 °C	
Holding time at T_{max}	10 min		70 s	70 s	10 min	20 min	10 min	2 min	
SOC (% rated capacity)	100	> 50% normal operating range (HP) Max. SOC at normal operation (HE)	> 50% max. operating SOC	> 50% max. operating SOC	≥ 80	Fully charged (C) Max. operating SOC (M, P)	100	Max. operating range of a vehicle or 80% SOC	

[#]Norway, Russia, Ukraine, Croatia, Serbia, Belarus, Kazakhstan, Turkey, Azerbaijan, Tunisia, South Africa, Australia, New Zealand, Japan, South Korea, Thailand and Malaysia.

^a The vehicle body may be included.

^b The overall dimensions of the projectile test aluminium test screen may be increased to accommodate cells with dimensions larger than 127 mm (5 in.), but shall not exceed a distance of 305 mm (12 in.) from the cell in any direction.

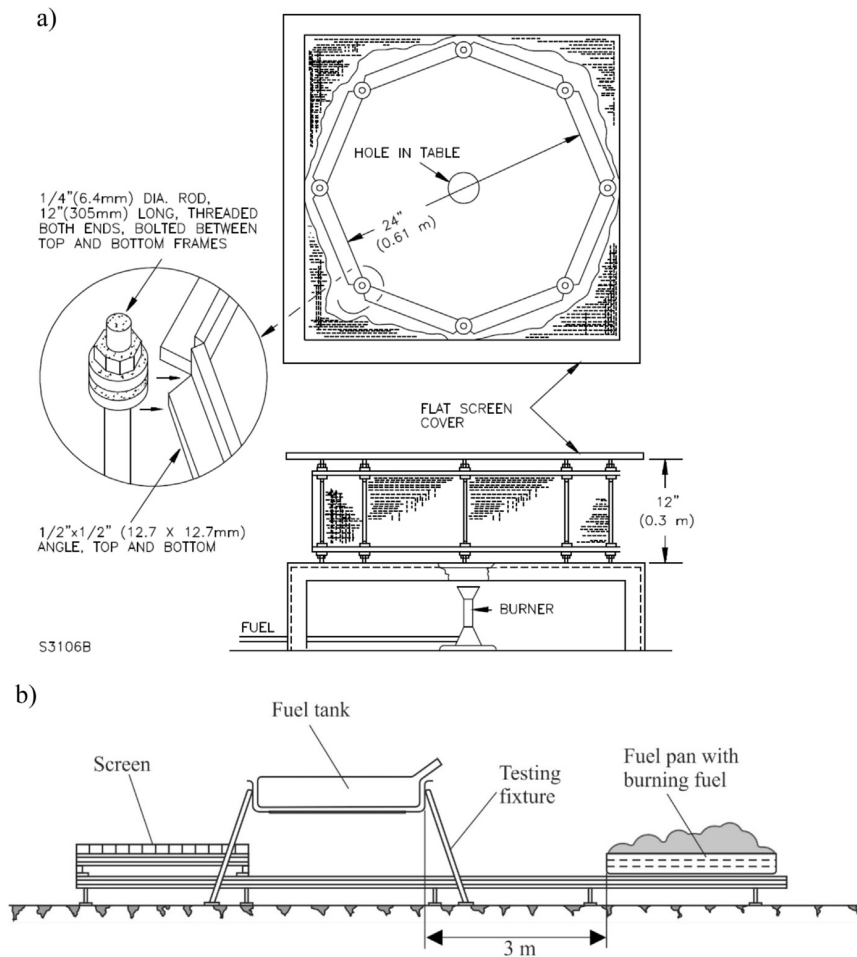


Fig. 4. Examples of fuel fire test set ups: a) wire mesh screen (copied from UL 1642 [112]) and b) grating table (copied from UN/ECE-R34 [127]). Copyright © Underwriters Laboratories Inc. UL 1642, 4th edition, 2007.

assessment of the thermal stability of the DUT at this temperature. Examples include ISO 62660-2:2011 (*High temperature endurance test*) [70], QC/T 743:2006 (*heat test*) [75] and KMVSS18-3:2009 (*Heat exposure test*) [73] as they require placing the battery in a chamber and increasing the temperature to only 130 °C, 85 °C and 80 °C, respectively.

Although it seems that both variants of the test provide useful insight into the safety of the energy storage system, they are not widely required as can be seen in Table 12.

3.3.2. Thermal shock test

This test is designed to evaluate changes in the integrity of the DUT arising from expansion and contraction of cell components upon exposure to extreme and sudden changes in temperature (e.g. the vehicle is entering or exiting a heated garage, during transport [63]) and potential consequences of such changes. During a thermal shock the DUT is exposed to two temperature limits and held at each temperature limit for a specified period of time. The thermal shock tests described in standards have different maximum temperature limits (see Table 13). ISO 12405-1:2011 [67], ISO 12405-2:2012 [68], IEC 62660-2:2011 [70] and UL 2580:2013 [63] have set the highest upper limit at +85 °C, while the lowest upper limit is set at +60 °C in UN/ECE-R100.02:2013 [62]. The lower temperature limit is – 40 °C in all the cases.

Noteworthy is that amongst all the documents evaluated, only UN/ECE-R100.02:2013 [62] permits operation of the protection devices during this test. In the other standards the protection device is disabled, which imposes harder testing conditions.

3.3.3. Overheat test

The overheat test, also referred to as *rapid charge/discharge, cycling without thermal management, single point thermal control system failure, over-temperature protection* test, aims at evaluating the effect of temperature control failure or failure of other protection features against internal overheating during operation. Test parameters required in this test are displayed in Table 14.

For this test, a fully charged DUT, whose active thermal control system (e.g. cooling system) is disabled, is cycled (e.g. 20 cycles with no resting period between charge and discharge [61,66]). As a consequence, the temperature of the DUT will increase. According to some standards, the test must be performed in a closed volume in order to evaluate the flammability of any materials being released from the battery during the test [61,65,66,72]. In this case, a spark source has to be present to ignite any potentially flammable gases or vapours from the DUT or, alternatively, a gas concentration measuring device can be utilized as suggested by SAE J2929:2013 [66].

In the case of UN/ECE-R100.02:2013 [62], the test is stopped when either: (a) the DUT interrupts the charging/discharging to prevent temperature increase, (b) the temperature of the DUT is stable (i.e. variation < 4 °C in 2 h) or (c) there is evidence of DUT damage (e.g. electrolyte leakage, rupture, fire or explosion).

3.3.4. Extreme cold temperature test

The rationale behind this test is the effect of possible exposure of the DUT to low temperatures (e.g. vehicle parked in a cold environment). At low temperatures, the electrolyte has poor ionic conductivity

and the anode experiences high over-potentials [127] which can lead to dendrite formation. Metallic plating can be a safety concern because growing dendrites could short circuit the cell. Despite these issues, only one standard deals with this topic. USABC:1999 [72] describes a matrix for charging at the normal primary charge rate for the specific system and discharging at 1C down to various DOD's (depths of discharge): 20, 50, 60, 80, 100% at the following temperatures: -40, -20, 0 and 25 °C [72]. The liquid coolant is present, but not circulating during the test. The test shall be stopped if abnormal conditions (e.g. voltage, temperature) or physical damage to the DUT becomes evident.

3.3.5. Fire test

The objective of the fire test is to expose a battery or a vehicle to a fire and assess the risk of explosion. The source of the fire can be spilled fuel either from the vehicle itself or a nearby vehicle. This test is often termed *Fuel fire test* but can be also called: *Radiant heat*, *Projectile fire*, *External fire simulation*, *Exposure to simulated vehicle fire*, *High-temperature hazard* or *Fire resistance* test. Table 15 displays test parameters. Three types of the test are described:

- i) *Radiant-heat test*: the battery (e.g. $\geq 80\%$ SOC [72], 100% SOC [61,65]) is placed inside a cylindrical metallic fixture, which is externally heated by means of radiant heat (e.g. quartz lamps, tube furnace and conveyor mechanism). A temperature of 890 °C shall be reached in less than 90 s and held for 10 min. Hazardous substance monitoring (e.g. EPA Methods TO-15 [128] and TO-17 [129]) is performed by sampling of combustion products to determine the possible presence of hazardous gas species released during the test [61,65].
- ii) *Projectile test*: in this case the DUT, exposed to a uniform fire, is surrounded by a steel wire mesh screen in a way that no part of an exploding cell or battery can penetrate through the mesh (e.g. 0.25 mm diameter wire and grid density of 6–7 wires cm^{-1}) (Fig. 4a) [63,66].

UL 2580:2013 requires testing at least at 590 °C for a duration of 20 min [63]. In this case, the use of a mesh screen is not mandatory and as alternative the DUT can be placed within a circular inner perimeter area (e.g. < 1 m marked on the floor). No explosion of the DUT that results in projectiles falling outside of this perimeter is allowed. A second outer perimeter (around 1.5 m from inner perimeter) made of a non-combustible material surrounds the inner perimeter.

- i) *Grating table configuration test*: this test as described in UN/ECE-R100.02:2013 [62] is an adaptation from UN/ECE-R34:2012 - Annex 5 [130], where a flame is created by burning fuel in a pan. The DUT shall be placed on a grating table positioned above the pan (Fig. 4b). The different steps of the test require first the preheating of the DUT during 60 s by placing the burning fuel pan at a distance of 3 m. Then, the DUT is directly exposed to the flame for another 70 s. Immediately after, a screen of refractory material is placed in between the pan and the DUT in order to reduce the flame for further 60 s as depicted in Fig. 4b. This test is passed if there is no evidence of explosion during the test.

Only two standards, SAE J2464:2009 [61] and UL 2580:2013 [63] highlight the importance of quantifying toxic and determining flammable emissions providing suitable testing procedures (see Section 3.4 for further details). Although it has been proven by various authors that significantly higher amounts of, for example HF, are generated in EV fires compared to ICE vehicle fires (e.g. 1500 g compared to 600–800 g, respectively [131–133]), the implementation of analysis of emissions is not widely adopted. Moreover, with such a variation of conditions and requirements for the fire test, it seems clear that the comparability of test results is not ensured.

3.4. Chemical hazards evaluation tests

Lithium ion batteries contain, as mentioned in the introduction, significant amounts of potentially hazardous materials (e.g. highly flammable electrolytes, corrosive and toxic components [16,134,135]). If exposed to certain conditions, it is expected that the integrity of the battery is compromised which may lead to electrolyte leakage, venting, rupture or even fire and explosion. Amounts of gas released from various 18650 cells during a thermal runaway event have been measured to be around $1.21 (\text{A h})^{-1}$ [87,136] for various cathode materials. Golubkov et al. found higher amounts of vented gas on LCO/NMC batteries (e.g. $2.31 (\text{A h})^{-1}$ as calculated from 0.27 mol of gas released) [10]. The gases being released are composed of a mixture of species: carbon monoxide, carbon dioxide, methane, hydrogen, oxygen, ethane, ethylene, hydrofluoric acid as measured in various studies [10,35,131,137,138]. The exposure of persons in the vicinity of such compromised batteries can lead to serious injuries (e.g. eye irritation, chemical burns, poisoning, abrasion, skin injuries). Thus, it is of importance to identify and quantify substances being released from the battery during tests representing misuse and abuse events and to ensure that the amounts released are not hazardous to vehicle occupants and first aid responders. Within this context, the development of warning sensors for passengers, first aid responders and rescue workers has been advised [82]. For example, fire brigades include in their guidelines advice related to the chemical risks of batteries for EVs and HEVs (i.e. gas and liquid releases) such as: use of full PPE (personal protective equipment), avoid standing close to hot battery remnants and avoid inhaling the fumes under any circumstances [139–141].

3.4.1. Emissions related tests

Some standards require hazardous substances measurements (e.g. gas, smoke, flames, and particulates) and for this analytical techniques or gas sensors are recommended. Moreover, many standards require that the amounts measured need to be below certain concentrations [61,63,65,66,72], such as those defined by the Emergency Response Planning Guidelines ERPG-2 [142], from the American Industrial Hygiene Association [143] or other industry practice documents or standards such as from the Occupational Safety and Health Administration (OSHA) [144], Acute Exposure Guidelines Levels from the Environmental Protection Agency (EPA) [145], Short-Term Exposure Limits (STEL) [146].

SAE J2464:2009 [61] points out that the concentration of the released hazardous substances shall be scaled to the full pack for quantitative comparison and scaled to a volume appropriate to human exposure in the vehicle (e.g. below ERPG-2 level: maximum airborne concentration levels below which most individuals could be exposed for up to one hour without experiencing or developing serious or irreversible health effects or symptoms which could impair an individual's ability to take protective action).

When manufacturers indicate the possibility that toxic gases can be released during abusive conditions, gas monitoring is needed during the tests by utilizing one of the following techniques (or equivalent) as described in UL 2580:2013 [63] and SAE J2464:2009 [61]:

- ASTM (the American Society for Testing and Materials) D4490: standard practice for measuring concentrations of toxic gases of vapours using detector tubes [147].
- ASTM D4599: standard practice for measuring concentrations of toxic gases of vapours using length-of-stain dosimeters [148].
- OSHA: Evaluation guidelines for air sampling methods utilizing spectroscopic analysis [149].
- NIOSH (The National Institute for Occupational Safety and Health): Manual for analytical methods [150].
- EPA Methods TO-15 [128] for the determination of VOC's (volatile organic compounds) in air analysed by Gas Chromatography and Mass spectrometry.

- EPA Methods TO-17 [129] for the determination of VOC's in air using active sampling onto sorbent tubes.

More sophisticated devices for gas detection of evaporated compounds can be Fourier Transformed Infrared Spectroscopy (FTIR) and mobile detection systems (e.g. detection of O₂, CO, H₂, C₂H₄O, HF and of toxic VOC's as used by German fire brigades [82]).

Standard SAE J6469-1:2009 [103] requires that potentially dangerous concentration of hazardous gases or other hazardous substances shall not be allowed anywhere in the driver, passenger and load compartments. The maximum allowable quantity accumulated during testing of hazardous gases and other substances (for normal operating and environmental conditions) shall refer to the latest version of applicable National/International standards or regulations.

UN/ECE-R100.02:2013 [62] regulates emissions from open-type traction batteries, which may produce hydrogen gas during normal operation. The quantification of hydrogen during normal charging follows the protocol indicated in the regulation and must remain below certain limits (i.e. below 25 x h (g)). Other gases are not considered. Systems with a closed chemical process, such as LIBs, are considered 'emission free' (i.e. do not emit gases under normal operation). In the case of abusive conditions, this regulation does not enforce any requirements or limitations for emissions of hazardous gases (e.g. venting) from any type of rechargeable energy storage systems. An improvement of the regulation in this regard could be of high importance to ensure the safety of users and first aid responders.

3.4.2. Flammability tests

In abusive conditions, it is possible that LIBs emit flammable gases (e.g. methane, ethane, hydrogen, carbon monoxide). SAE J2929:2013 [66], for example, highlights this hazard and recommends that consideration should be given to preventing the build-up of flammable gases that could get in contact with vehicle ignition sources (e.g. sparks from a short circuit, fire in the vicinity). Determination of the flammability of any substance (e.g. liquid, solid materials) emitted from the battery is mandatory in many standards [61,63,65,66,72]. One method is to incorporate one or several spark ignition source(s) in the testing area, located close to the DUT. Alternatively, gas monitors can also be used, as mentioned in UL 2580:2013 [63]. On the contrary, some other standards do not give indications on how to assess this property, e.g. UN/ECE-R100.02:2013 [62].

Overall it can be concluded that the evaluation of chemical hazards is tackled very differently in the various standards and regulations. In some cases, such as in SAE J2464:2009 [61], SAE J2929:2013 [66] and UL 2580:2013 [63], detailed information on quantifying and determining toxicity and flammability of LIB emissions is provided, while in other cases this issue is only slightly mentioned, such as in UN/ECE-R100.02:2013 [62]. In some instances chemical hazards are not even considered, such as in ISO 12405-1(2,3):2001(2012,2014) [67–69], IEC 62660-2(3):2001(2013) [70,71], KMVSS 18-3:2009 [73], AIS-048:2009 [74] and QC/T 743:2006 [75]. Taking into consideration the importance of the issue, it would be advisable that future standardisation/regulation developments consider a harmonized testing guidance or protocol to ensure that chemical hazards of automotive batteries are appropriately assessed.

4. Current evolutions and future perspectives

International standards on lithium traction battery safety are being developed by ISO and IEC, focusing respectively on system and cell level. Documents already published by ISO include ISO 12405-1:2011 and 12405-2:2012 [67,68], defining test specifications for high-power (for hybrids) and high-energy batteries (for battery electric vehicles), respectively. Both these documents were complemented with the recently published ISO 12405-3:2014 [69], which sets pass/fail requirements to the precedent documents. Chinese counterparts were

published in 2015 under GB/T 31467.1, GB/T 31467.2 and GB/T 31467.3. Within IEC, IEC62660-2 [70] was published in 2011, describing safety tests for propulsion cells. IEC 62660-3:2016 [71], defining cell safety specifications was published in 2016. Also a new standard, IEC 62485-6 [151], on safety requirements for lithium-ion batteries and battery installations is proposed.

On vehicle safety, ISO 6469-4 [105] on post-crash safety has been published in 2015.

Once published, standards go into a maintenance cycle with periodic revision at least every five years. Topics for revision may include consideration of upcoming battery technologies such as lithium sulfur, lithium air as well as lithium ion capacitors for which specific test procedures may be required. Furthermore, the use of batteries in a "second life" application will require specific test regimes to determine their state of health and their cycling in stationary applications, taking into account the specific safety requirements of the operating environment.

A Global Technical Regulation on Electric Vehicle Safety (GTR-EVS) has been submitted for a vote to the UNECE World Forum for Harmonization of Vehicle Regulations (WP.29). A decision on the adoption of this regulation is expected in November 2017.

5. Conclusions

This work presents a comprehensive review of the various standards and regulations dealing with the safety performance of lithium ion batteries to be used in electrified transport. Test parameters and conditions adopted in the test methods which are described in these standards and regulations are compared. From the analysis performed the following conclusions are drawn:

- Most of the existing standards and regulations impose test requirements derived from regulatory documents originally intended for conventional vehicles. It is clear that more analysis and data evaluation specific to EVs and HEVs is highly desirable to cover the specificities of electrified technologies. For example, recent research has indicated that battery pack installations may be exposed to vibration loads outside the range evaluated by existing standards [100].
- Another concern is whether the tests performed at component level are comparable to those carried out at vehicle level. For example, the force experienced by a DUT in a crush test (component level) or crash test (vehicle level) is expected to depend on the presence and - if present, on the properties of - mechanical protection (such as the chassis or battery enclosure).
- Comparability of component testing at cell, module and pack level should also be examined. For example, it has been proven that the initial current created in the short circuit test is influenced by the size of the DUT [112,113] as well as by its type of connection (i.e. parallel or serial). Similar influence on test outcome may be expected when applying a single crush force and crushing plate to DUTs of different sizes.
- Dispersion in test conditions (e.g. SOC, temperature) is rather wide for most tests (e.g. overcharge, thermal shock, short circuit). This has an important impact in the comparability of data obtained utilizing various standards, while in some cases differences in parameters might be due to different considered scenarios. Alignment of parameters is advisable in order to perform fair and equivalent tests. As the worst case typically corresponds to maximum SOC, it is logical that abuse testing is performed in such condition. For example, in the short circuit test, the higher the SOC value of the DUT, the higher the short circuit current generated [112] and the lower the onset temperature of thermal runaway [115]. Most standards already require 100% SOC, however regulation UN/ECE-R100.02:2013 [62] allows testing at ≥ 50% SOC.

- Real world accidents are dynamic events i.e. the battery moves towards the impact zone. However, testing at component level is carried out using static assemblies where the impactor moves towards the battery. Investigations have shown discrepancies in mechanical loads between current standards and regulations and dynamic crash tests [94,96], and for this, appropriate modifications within the regulatory framework are advisable.
- Systems intended to be removed from the vehicle for charging, swapping or replacement may be accidentally dropped during handling. Although this scenario seems plausible, the drop test is not included in various automotive battery regulations and standards, such as UN/ECE-R100.02:2013 [62], ISO 12405-1(2,3):2011(2012,2014) [67–69] and ISO 62660-2:2011 [70].
- The occurrence of internal short circuits is one of the main concerns for battery manufacturers; however these tests have not been widely implemented in the legislative landscape. It is recognized, though, that the practicalities of this test are complex and implementation of such testing would require significant research for test method development.
- Only SAE J2464:2009 [61], SAE J2929:2013 [66] and UL 2580:2013 [63] highlight the importance of determining toxic and flammable emissions and provide suitable testing procedures. The implementation of specific analysis is not widely adopted by other bodies. Taking into consideration the importance of this issue, it is advisable that future standardisation/regulation developments consider a harmonized testing guidance and protocols to ensure that chemical hazards of automotive batteries are appropriately assessed in order to ensure the safety of vehicle occupants and surrounding persons.
- In relation to safety testing, the evaluation of realistic scenarios is greatly recommended in order to ensure a safe future for the use of lithium ion battery technologies. To ensure this, the addition of some tests, such as roll over, drop, immersion, low temperature hazards, toxicity, flammability, etc. into future standards and regulations should be considered.
- Finally, clear and unambiguous testing guidelines should be provided as part of the test method and rationale description. Examples include descriptions of the method for setting the SOC, the location of temperature sensors, the exact position of the DUT in the various tests, in addition to the minimum tolerance required for the testing equipment. Such guidelines facilitate the correct and harmonized interpretation of the standard or regulation by the testing bodies and comparability of results would be improved.

Acknowledgements

Authors thank Marc Steen for his excellent support reviewing this manuscript.

References

- [1] Electric Vehicle Market Forecasts . Global forecasts for light duty hybrid, plug-in hybrid, and battery electric vehicle sales and vehicles in use: 2014–2023. Nav Res 2014.
- [2] Proff H, Kilian D. Competitiveness of the EU automotive industry in electric vehicles. Duisburg: University of Duisburg-Essen; 2012.
- [3] Lutsey N. Transition to a global zero-emission vehicle fleet: a collaborative agenda for governments, international council on clean transportation transition to a global zero-emission vehicle fleet: a collaborative agenda for governments. Int Council Clean Transp 2015.
- [4] Lithium ion rechargeable batteries technical handbook. Sony Corporation. (https://www.4project.co.il/documents/doc_286_2661.pdf).
- [5] Lowe M, Tokuko S, Trigg T, Gereffi G. Lithium-ion batteries for electric vehicles: the US value chain. Centre on Globalization, Governance & Competitiveness Duke University; 2010.
- [6] Cluzel C, Douglas C. Cost and performance of EV batteries. final report. Elem Energy Ltd Comm Clim Change 2012.
- [7] Lache R, Galves D, Nolan P, et al. Autos & auto parts electric cars: plugged in 2. A mega-theme gains momentum. FITT Res 2009.
- [8] American and European standards organisations agree to strengthen transatlantic cooperation on standards for electric vehicles. The European Committee for Standardization (CEN) and the European Committee for Electrotechnical Standardization (CENELEC); 2012. Available Online: (http://www.cenelec.eu/news/press_releases/pages/PR-2012-18.aspx).
- [9] Opitz A, Badami P, Shen L, Vignaroban K, Kannan AM. Can Li-ion batteries be the panacea for automotive applications?. *Renew Sustain Energy Rev* 2017;68(Part1):685–92.
- [10] Golubkov AW, Fuchs D, Wagner J, Wiltsche H, Stangl C, Fauler G, et al. Thermal-runaway experiments on consumer Li-ion batteries with metal-oxide and olivine-type cathodes. *RSC Adv* 2014;4:3633–42.
- [11] Jacoby M. Burning batteries, chemical & engineering news. *C & EN Chem Eng News* 2007;85:26–8.
- [12] Lamb J, Orendorff CJ, Steele LAM, Spangler SW. Failure propagation in multi-cell lithium ion batteries. *J Power Sources* 2015;283:517–23.
- [13] von Sacken U, Nodwell E, Sundler A, Dahn JR. Comparative thermal stability of carbon intercalation anodes and lithium metal anodes for rechargeable lithium batteries. *Solid State Ion* 1994;69:284–90.
- [14] Chen Y, Evans JW. Thermal analysis of lithium-ion batteries. *J Electrochem Soc* 1996;143:2708–12.
- [15] Bandhauer TM, Garimella S, Fuller TF. Temperature-dependent electrochemical heat generation in a commercial lithium-ion battery. *J Power Sources* 2014;247:618–28.
- [16] Levy SC, Bro P. Battery hazards and accident prevention. New York and London: Plenum Press; 1994.
- [17] Mikolajczak MK C, White K, Long RT. Lithium-ion batteries hazard and use assessment. Menlo Park, CA: Exponent Failure Analysis Associates, Inc, Springer; 2011.
- [18] Boeing 787 battery fire. National Transportation Safety Board (NTSB) Accident Investigations; 2013. (http://www.ntsb.gov/investigations/pages/boeing_787.aspx).
- [19] Hazardous materials accident reports. National Transportation Safety Board. (<http://www.ntsb.gov/investigations/AccidentReports/Pages/hazardous.aspx>).
- [20] Lithium battery fire risk linked to Dubai plane crash. *The National*; 2010. (<http://www.thenational.ae/news/uae-news/lithium-battery-fire-risk-linked-to-dubai-plane-crash>).
- [21] Air accident investigation report: uncontained cargo fire leading to loss of control inflight and uncontrolled descent into terrain. General Civil Aviation Authority of the United Arab Emirates; 2010. (<https://www.gcaa.gov.ae/en/ePublication/admin/iradmin/Lists/Incidents%20Investigation%20Reports/Attachments/40/2010-2010%20-%20Final%20Report%20-%20Boeing%20747-44AF%20-%20N571UP%20-%20Report%2013%202010.pdf>).
- [22] Smith B. Chevrolet volt battery incident overview report, 2012th ed.. Washington, DC: National Highway Traffic Safety Administration (NHTSA); 2012. (http://www.nhtsa.gov/staticfiles/nvs/pdf/Final_Reports.pdf).
- [23] On-site electric vehicle fire investigation. US Department of Transportation – National Highway Traffic Safety Administration; 2013.
- [24] Apple says product shortage will hurt quarterly earnings: computers: company unable to keep up with consumer demand. It also is recalling new PC because of fire concern. *Times, Los Angeles*; 1995. (http://articles.latimes.com/1995-09-15/business/ft-46242_1_many-apple-computers).
- [25] CPSC and EV Global Motors Co. Announce recall of lithium batteries in electric bikes. United States: Consumer Product Safety Commission; 2002. (<https://www.cpsc.gov/Recalls/2002/CPSC-and-EV-Global-Motors-Co-Announce-Recall-of-Lithium-Batteries-in-Electric-Bikes-/>).
- [26] Ogumi Z, Wang H. Chapter 3: carbon anode materials. In: Yoshio Masaki, Brodd Ralph J, Kozawa A, editors. *Lithium-ion batteries science and technologies*. New York, NY: Springer; 2009. p. 51.
- [27] Zhang SS. A review on electrolyte additives for lithium-ion batteries. *J Power Sources* 2006;162:1379–94.
- [28] Illig J, Chrobak T, Ender M, Schmidt JP, Klotz D, Ivers-Tiffée E. Studies on LiFePO₄ as cathode material in Li-ion batteries. In: *Proceedings of the batteries and energy technology joint general session – 217th ECS meeting*, 30 ed. Vancouver, BC; 2010, p. 3-17.
- [29] Saw LH, Ye Y, Tay AAO. Electrochemical–thermal analysis of 18650 lithium iron phosphate cell. *Energy Convers Manag* 2013;75:162–74.
- [30] Nitta N, Wu F, Lee JT, Yushin G. Li-ion battery materials: present and future. *Mater Today* 2015;18:252–64.
- [31] Balakrishnan PG, Ramesh R, Prem Kumar T. Safety mechanisms in lithium-ion batteries. *J Power Sources* 2006;155:401–14.
- [32] Zhu G-N, Du Y-J, Wang Y-G, Yu A-S, Xia Y-Y. Electrochemical profile of lithium titanate/hard carbon composite as anode material for Li-ion batteries. *J Electroanal Chem* 2013;688:86–92.
- [33] Nowack LV, Waser O, Yarema O, Wood V. Rapid, microwave-assisted synthesis of battery-grade lithium titanate (LTO). *RSC Adv* 2013;3:15618–21.
- [34] Reddy T. *Linden's handbook of batteries*, 4th edition. New York, NY: McGraw-Hill, Inc.; 2011.
- [35] Campion CL, Li W, Lucht BL. Thermal decomposition of LiPF₆-based electrolytes for lithium-ion batteries. *J Electrochem Soc* 2005;152:A2327–A2334.
- [36] Lebedeva N, Boon-Brett L. Considerations on the chemical toxicity of contemporary Li-ion battery electrolytes and their components. *J Electrochem Soc* 2015;163:A821–A830.
- [37] Ue M. Fire-resistant electrolyte for lithium battery JP1992–184870A; JP3274102B [in Japanese]. Japan: Mitsubishi Petrochem; 1992.
- [38] Ue M, Sasaki Y, Tanaka Y, Morita M. Chapter 2: nonaqueous electrolytes with advances in solvents. *Electrolytes for lithium and lithium-ion batteries*. In: *Join*

- TR, Xu K, Borodin O, Ue M, editors. *Modern aspects of electrochemistry*. Springer; 2014.
- [39] Lee CW, Venkatachalapathy R, Prakash J. A novel flame retardant additive for lithium batteries electrochemical and solid-state letters, Vol. 3; 2000, p. 63–5.
- [40] Damen L, Lazzari M, Mastragostino M. Safe lithium-ion battery with ionic liquid-based electrolyte for hybrid electric vehicles. *J Power Sources* 2011;196:8692–5.
- [41] Balducci A, Jeong SS, Kim GT, Passerini S, Winter M, Schmuck M, et al. Development of safe, green and high performance ionic liquids-based batteries (ILLIBATT project). *J Power Sources* 2011;196:9719–30.
- [42] Kerner M, Lim D-H, Jeschke S, Rydholm T, Ahn J-H, Scheers J. Towards more thermally stable Li-ion battery electrolytes with salts and solvents sharing nitrile functionality. *J Power Sources* 2016;332:204–12.
- [43] Paulechka YU, Kabo GJ, Blokhin AV, Vydrov OA, Magee JW, Frenkel M. Thermodynamic properties of 1-butyl-3-methylimidazolium hexafluorophosphate in the ideal gas state†. *J Chem Eng Data* 2003;48:457–62.
- [44] Lemmon EW, McLinden MO, Friend DG. Thermophysical properties of fluid systems. In: Linstrom PJ, Mallard WG, editors. *NIST chemistry WebBook, NIST standard reference database number 69*. (<http://webbook.nist.gov>).
- [45] Ohno H. Chapter 1: importance and possibility of ionic liquids. *Electrochemical aspects of ionic liquids*. New Jersey: John Wiley & Sons, Inc., Publication; 2005. p. 1–4.
- [46] Daigle JC, Vijn A, Hovington P, Gagnon C, Hamel-Pâquet J, Verreault S, et al. Lithium battery with solid polymer electrolyte based on comb-like copolymers. *J Power Sources* 2015;279:372–83.
- [47] Janek J, Zeier WG. A solid future for battery development. *Nat Energy* 2016;1:16141.
- [48] Yamamoto H, Mori H. Chapter 7: SBR binder (for negative electrode) and ACM binder (for positive electrode). In: Yoshio Masaki, Brodd Ralph J, Kozawa A, editors. *Lithium-ion batteries science and technologies*. New York: Springer; 2009.
- [49] Zhang Z, Ramadass P. Chapter 20: lithium-ion battery separators. In: Yoshio Masaki, Brodd Ralph J, Kozawa A, editors. *Lithium-ion batteries science and technologies*. New York: Springer; 2009.
- [50] Yu WC, Hux SE. Method of making a trilayer battery separator. US Patent, 5,952, 120; 1999.
- [51] Hying C. Separation separators for lithium batteries – safety & performance. Batteries. Paris; 2004.
- [52] Pfrang A, Kriston A, Ruiz V, Lebedeva N, di Persio F. Chapter eight – safety of rechargeable energy storage systems with a focus on Li-ion Technology A2 – Rodriguez-Martinez, Lide M. In: Omar N, editor. *Emerging nanotechnologies in rechargeable energy storage systems*. Boston: Elsevier; 2017. p. 253–90.
- [53] Kumar MS, Revankar ST. Development scheme and key technology of an electric vehicle: an overview. *Renew Sustain Energy Rev* 2017;70:1266–85.
- [54] Arora S, Shen W, Kapoor A. Review of mechanical design and strategic placement technique of a robust battery pack for electric vehicles. *Renew Sustain Energy Rev* 2016;60:1319–31.
- [55] Yeow K, Teng H, Thelliez M, Tan E. 3D thermal analysis of Li-ion battery cells with various geometries and cooling conditions using abaqus. In: *Proceedings of the SIMULIA community conference*; 2012. p. 1–16.
- [56] Mikolajczak C, Kahn M, White K, Long RT. Lithium-ion batteries hazard and use assessment. In: Exponent failure analysis associates IPRPF, editor. *Exponent Failure Analysis Associates, Inc., Fire Protection Research Foundation*; 2011.
- [57] Lamb J, Orendorff CJ. Evaluation of mechanical abuse techniques in lithium ion batteries. *J Power Sources* 2014;247:189–96.
- [58] SAE J2289. Electric-drive battery pack system: functional guidelines; 2008.
- [59] Lisbona D, Snee T. A review of hazards associated with primary lithium and lithium-ion batteries. *Process Saf Environ Prot* 2011;89:434–42.
- [60] Spotnitz R, Franklin J. Abuse behavior of high-power, lithium-ion cells. *J Power Sources* 2003;13:81–100.
- [61] SAE J2464. Electric and hybrid electric vehicle rechargeable energy storage system (RESS) safety and abuse testing; 2009.
- [62] UN/ECE Regulation No. 100.02. Uniform provisions concerning the approval of vehicles with regard to specific requirements for the electric power train; 2013.
- [63] UL 2580. Batteries for use in electric vehicles; 2013.
- [64] Ashtiani CN. Analysis of battery safety and hazards' risk mitigation. 19th ed. Washington, DC; 2008. p. 1–11.
- [65] Doughty DH, Crafts CC. SAND 2005–3123: freeDomCAR electrical energy storage systems abuse test manual for electric and hybrid electric vehicle applications; 2005.
- [66] SAE J2929. Safety standards for electric and hybrid vehicle propulsion battery systems utilizing lithium-based rechargeable cells; 2013.
- [67] ISO 12405-1. Electrically propelled road vehicles – test specification for lithium-ion traction battery packs and systems Part 1: high-power applications; 2011.
- [68] ISO 12405-2. Electrically propelled road vehicles – test specification for lithium-ion traction battery packs and systems Part 2: high-energy applications; 2012.
- [69] ISO 12405-3. Electrically propelled road vehicles – test specification for lithium-ion traction battery packs and systems Part 3: Safety performance requirements; 2014.
- [70] IEC 62660-2. Rechargeable cells standards publication secondary lithium-ion cells for the propulsion of electric road vehicles Part 2: reliability and abuse testing; 2011.
- [71] IEC 62660-3. Rechargeable cells standards publication secondary lithiumion cells for the propulsion of electric road vehicles Part 3: safety requirements of cells and modules; 2016.
- [72] Unkelhaeuser T, Smallwood D. SAND99-0497-USABC: United States advanced battery consortium electrochemical storage system abuse test procedure manual; 1999.
- [73] KMVSS Article18-3. Traction battery; 2009.
- [74] AIS-048. Battery operated vehicles – safety requirements of traction batteries; 2009.
- [75] QC/T 743. Lithium-ion batteries for electric vehicles Chinese voluntary standards for automobiles; 2006.
- [76] UN 38.3; Recommendations on the transport of dangerous goods manual of test and criteria, 6th revised edition; 2015.
- [77] ISO 16750-3. Road vehicles – environmental conditions and testing for electrical and electronic equipment Part 3: mechanical loads; 2003.
- [78] UN/ECE Regulation No. 12. Uniform provisions concerning the approval of vehicles with regard to the protection of the driver against the steering mechanism in the event of impact; 2012.
- [79] UN/ECE Regulation No. 94. Uniform provisions concerning the approval of vehicles with regard to the protection of the occupants in the event of a frontal collision; 2012.
- [80] UN/ECE Regulation No. 95. Uniform provisions concerning the approval of vehicles with regard to the protection of the occupants in the event of a lateral collision; 2011.
- [81] FMVSS 305. Electric powered vehicles: electrolyte spillage and electrical shock protection; 2011.
- [82] Wisch M, Ott J, Thomson R, Léost Y, Abert M, Yao J. EVERSAFE. Recommendations and guidelines for battery crash safety and post-crash safe handling. In: *Proceedings of the 7th framework programme era-net transport electromobility+*; 2014.
- [83] Adolph T, Edward M, Thomson R, Stein M, Lemmen P, V N, et al. FIMCAR full width test procedures: updated protocol in FIMCAR-frontal impact and compatibility assessment research , Bd VIII. Berlin: Universitatverslag der TU Berlin; 2015. p. 1–85.
- [84] Dubaniewicz TH, DuCarme JP. Are lithium ion cells intrinsically safe? In: *Proceedings of the industry applications society annual meeting (IAS)*. IEEE; 2012. p. 1–10.
- [85] Maleki H, Howard JN. Internal short circuit in Li-ion cells. *J Power Sources* 2009;191:568–74.
- [86] Cai W, Wang H, Maleki H, Howard J, Lara-Curzio E. Experimental simulation of internal short circuit in Li-ion and Li-ion-polymer cells. *J Power Sources* 2011;196:7779–83.
- [87] Dubaniewicz TH, Jr., DuCarme JP. Further study of the intrinsic safety of internally shorted lithium and lithium-ion cells within methane-air. *J Loss Prev Process Ind* 2014;32:165–73.
- [88] Spek EJ. Lithium ion abuse test methods improvement IEEE symposium on product compliance engineering (IEEE PSES). Portland, Oregon; 2012.
- [89] Bierens JJLM. Handbook on drowning: prevention, rescue, treatment; 2006.
- [90] Florida leads the nation in car crash drownings; 2014. (<http://touch.orlandosentinel.com/#section/-/1/article/p2p-81915801>)
- [91] Hurricane sandy destroyed up to 250,000 cars; 2012. (http://www.huffingtonpost.com/2012/11/07/hurricane-sandy-cars_n_2090916.html)
- [92] Fisker loses over 300 karmas in sandy floods at Port Newark; 2012. (<http://www.autoblog.com/2012/11/07/fisker-loses-over-300-karmas-in-sandy-floods-at-port-newark/>)
- [93] Brecher A. Chapter 9: transit bus applications of lithium-ion batteries. In: Pistoia G, editor. *Lithium-ion batteries: advances and applications*; 2014. p. 194.
- [94] Wech L, Richter R, Justen R, Schöneburg R. Crash safety aspects of HV batteries for vehicles. In: *Proceedings of the international technical conference on the enhanced safety of vehicles ESV-22*. Washington, USA; 2011.
- [95] Bakker J, Sachs J, Otte D, Justen R, Hannawald L, Friesen F. Analysis of fuel cell vehicles equipped with compressed hydrogen storage systems from a road accident safety. *Perspect SAE Int J Passeng Cars – Mech Syst* 2011;4:332–42.
- [96] Justen R, Schöneburg R. Crash Safety of Hybrid and Battery Electric Vehicles. In: *Proceedings of the international technical conference on the enhanced safety of vehicles ESV-22*. Washington, USA; 2011.
- [97] El-Hennawy HM, El-Menyar A, Al-Thani H, Tuma M, Parchani A, Abdulrahman H, et al. Epidemiology, causes and prevention of car rollover crashes with ejection. *Ann Med Health Sci Res* 2014;4:495–502.
- [98] Baren JV. What is random vibration testing?. *Sound Vib Instrum Ref Issue* 2012;9–12.
- [99] Jayahari L. Correlation of sinusoidal sweep test to field random vibrations [Master's degree thesis]. Karlskrona, Sweden: Blekinge Institute of Technology; 2005.
- [100] Hooper JM, Marco J. Characterising the in-vehicle vibration inputs to the high voltage battery of an electric vehicle. *J Power Sources* 2014;245:510–9.
- [101] IEC 60068-2-64. Environmental testing Part 2: test methods – test Fh: vibration, broad-band random (digital control) and guidance; 1993.
- [102] SAE J2380. Vibration testing of electric vehicle batteries; 2009.
- [103] ISO 6469-1. Electrically propelled road vehicles – safety specifications Part 1: on-board rechargeable energy storage system (RESS); 2009.
- [104] ISO 6469-3. Electrically propelled road vehicles – safety specifications – Part 3: protection of persons against electric shock; 2011.
- [105] ISO 6469-4. Electrically propelled road vehicles – safety specifications Part 4: post crash electrical safety requirements; 2015.
- [106] ISO 17409. Electrically propelled road vehicles – connection to an external electric power supply – safety requirements; 2015.
- [107] IEC 61851. Electric vehicle conductive charging system; 2010.
- [108] ISO PAS 19363. Electrically propelled road vehicles – magnetic field wireless power transfer – safety and interoperability requirements.
- [109] Wang Q, Ping P, Zhao X, Chu G, Sun J, Chen C. Thermal runaway caused fire and explosion of lithium ion battery. *J Power Sources* 2012;208:210–24.

- [110] IEC 60898-1. Electrical accessories – circuit-breakers for overcurrent protection for household and similar installations Part 1: circuit-breakers for ac operation; 2015.
- [111] Okazaki S, Higuchi S, Kubota N, Takahashi S. Measurement of short circuit current for low internal resistance batteries. *J Appl Electrochem* 1986;16:513–6.
- [112] Conte FV, Gollob P, Lacher H. Safety in the battery design: the short circuit. *World Electr Veh J* 2009;3.
- [113] Okazaki S, Higuchi S, Kubota N, Takahashi S. Predicted and observed initial short circuit current for lead-acid batteries. *J Appl Electrochem* 1986;16:631–5.
- [114] UL 1642. UL standard for safety for lithium batteries; 2007.
- [115] Mendoza-Hernandez OS, Ishikawa H, Nishikawa Y, Maruyama Y, Umeda M. Cathode material comparison of thermal runaway behavior of Li-ion cells at different state of charges including over charge. *J Power Sources* 2015;280:499–504.
- [116] Wu A, Tabaddor M, Wang C, Jeevarajan J. Simulation of internal short circuits in lithium-ion cells. *Corp Res UL LLC* 2014.
- [117] Zhao W, Luo G, Wang C-Y. Modeling internal shorting process in large-format Li-Ion cells. *J Electrochem Soc* 2015;162:A1352–A1364.
- [118] Orendorff CJ, Roth EP, Nagasubramanian G. Experimental triggers for internal short circuits in lithium-ion cells. *J Power Sources* 2011;196:6554–8.
- [119] IEC 62133-2. Secondary cells and batteries containing alkaline or other non-acid electrolytes – safety requirements for portable sealed secondary cells, and for batteries made from them, for use in portable applications - Part 2: Lithium systems; 2017.
- [120] Jones HP, Chapin JT, Tabaddor M. Critical review of commercial secondary lithium-ion battery safety standards. European Space Agency, (Special Publication). In: Proceedings of the ESA SP 4th IAASS conference 'making safety matter'; 2010.
- [121] Feng X, Fang M, He X, Ouyang M, Lu L, Wang H, et al. Thermal runaway features of large format prismatic lithium ion battery using extended volume accelerating rate calorimetry. *J Power Sources* 2014;255:294–301.
- [122] Lu W, López CM, Liu N, Vaughey JT, Jansen A, DW D. Overcharge effect on morphology and structure of carbon electrodes for lithium-ion batteries. *J Electrochem Soc* 2012;159:A566–A570.
- [123] IEC 61434. Secondary cells and batteries containing alkaline or other non-acid electrolytes – guide to designation of current in alkaline secondary cell and battery standards; 1996.
- [124] Tobishima S, Sakurai Y, Yamaki J. Safety characteristics of rechargeable lithium metal cells. *J Power Sources* 1997;68:455–8.
- [125] Xu F, He H, Liu Y, Dun C, Ren Y, Liu Q, et al. Failure investigation of LiFePO₄ cells under overcharge conditions. *J Electrochem Soc* 2012;159:A678–A687.
- [126] He H, Liu Y, Liu Q, Li Z, Xu F, Dun C, et al. Failure investigation of LiFePO₄ cells in over-discharge conditions. *J Electrochem Soc* 2013;160:A793–A804.
- [127] Zhang SS, Xu K, Jow TR. Study of the charging process of a LiCoO₂-based Li-ion battery. *J Power Sources* 2006;160:1349–54.
- [128] U.S. Environmental Protection Agency (EPA) method TO-15. Determination of volatile organic compounds (VOCs) in air collected in specially-prepared canisters and analyzed by gas chromatography/mass spectrometry (GC/MS); 1999. <http://www.epa.gov/ttnamti1/files/ambient/airtox/to-15r.pdf>.
- [129] U.S. Environmental Protection Agency (EPA) method TO-17. Determination of volatile organic compounds in ambient air using active sampling onto sorbent tubes; 1999. <https://www3.epa.gov/ttnamti1/files/ambient/airtox/to-17r.pdf>.
- [130] UN/ECE Regulation No. 34. Uniform provisions concerning the approval of vehicles with regard to the protection of fire risks; 2012.
- [131] Lecocq A, Bertana M, Truchot B, Marlair G. Comparison of the fire consequences of an electric vehicle and an internal combustion engine vehicle. In: Proceedings of the international conference on fires in vehicles – FIVE. Chicago, United States; 2012. p. 183–94.
- [132] Andersson P, Blomqvist P, Lorén A, Larsson F. Investigation of fire emissions from Li-ion batteries. SP technical research institute of Sweden; 2013.
- [133] Sturk D, Hoffmann L, AT A. Fire tests on e-vehicle battery cells and packs. *Traffic Inj Prev* 2015;16:159–64.
- [134] Vimmerstedt LJ, Ring S, Hammel CJ. Current status of environmental, health and safety issues of lithium ion electric vehicle batteries. Golden, CO: National Renewable Energy Laboratory (NREL); 1995.
- [135] Lebedeva N, Ruiz V, di Persio F, Kriston A, Pfrang A, Kosmidou T, et al. Evaluation of volume of free electrolyte in various cell types – method and preliminary results. EVS-07-24e – (JRC) free electrolyte. Working Party on Passive Safety (GRSP) – Electric Vehicle Safety (EVS) 7th session in (<https://www.unece.org/wiki/display/trans/EVS+7th+session>); 2015.
- [136] Roth EP, Orendorff CJ. How electrolytes influence battery safety. *Electrochem Soc Interface* 2012;21:45–9.
- [137] Roth EP, Crafts CC, Doughty DH, McBreen J. Thermal abuse performance of 18650 Li-ion cells; 2004.
- [138] Ohsaki T, Kishi T, Kuboki T, Takami N, Shimura N, Sato Y, et al. Overcharge reaction of lithium-ion batteries. *J Power Sources* 2005;146:97–100.
- [139] Wargelou D. Extrication from cars during road traffic accidents. Swedish Civil Contingencies Agency (MSB); 2011.
- [140] Casey C, Grant PE. Fire fighter safety and emergency response for electric drive and hybrid electric vehicles. *Fire Prot Res Found* 2010.
- [141] Accident assistance and recovery of vehicles with high-voltage systems. German Association of the Automotive Industry (VDA); 2013.
- [142] Emergency Response Planning Guidelines: ERPG level 2. (<https://www.aiaa.org/get-involved/AIHAGuidelineFoundation/EmergencyResponsePlanningGuidelines/Documents/2014%20ERPG%20Introduction.pdf>).
- [143] American industrial hygiene association. (<https://www.aiaa.org/Pages/default.aspx>).
- [144] Occupational safety and health administration (OSHA). (<https://www.osha.gov/>).
- [145] Acute exposure guidelines levels from the environmental protection agency (EPA). (<http://www.epa.gov/oppt/aegl/pubs/chemlist.htm>).
- [146] Short-term exposure limits (STEL). (<http://www.acgih.org/store/>).
- [147] ASTM D4490. Standard practice for measuring concentrations of toxic gases of vapours using detector tubes; 2011.
- [148] ASTM D4599. Standard practice for measuring concentrations of toxic gases of vapours using length-of-stain dosimeters; 2014.
- [149] OSHA. Evaluation guidelines for air sampling methods utilizing spectroscopic analysis. (<https://www.osha.gov/dts/sltc/methods/spectroguide/spectroguide.pdf>).
- [150] NIOSH. Manual for analytical methods. (<http://www.cdc.gov/niosh/docs/2003-154/>).
- [151] IEC 62485-6. Safety requirements for secondary batteries and battery installations Part 6: lithium-ion batteries for traction applications PNW.


Glossary

ASTM: The American Society for Testing and Materials
 CC: Constant Current
 CV: Constant Voltage
 ERPG: Emergency Response Planning Guidelines
 EPA: Environmental Protection Agency
 EV: Electric Vehicle
 DUT: Device Under Test
 BEV: Battery Electric Vehicle
 FMVSS: Federal Motor Vehicle Safety Standards
 HP: High Power
 HE: High Energy
 HEV: Hybrid Electric Vehicle
 NIOSH: The National Institute for Occupational Safety and Health
 NLF: New Legislative Framework
 LIB: Lithium Ion Battery
 OSHA: Occupational Safety and Health Administration
 PSD: Power Spectral Density
 STEL: Short-Term Exposure Limits
 SOC: State of Charge
 VOC's: Volatile Organic Compounds



Article

Analysis of Li-Ion Battery Gases Vented in an Inert Atmosphere Thermal Test Chamber

David Sturk ¹, Lars Rosell ², Per Blomqvist ²  and Annika Ahlberg Tidblad ^{3,*}

¹ Autoliv Sverige AB; SE-447 37 Vårgårda, Sweden

² Research Institute of Sweden (RISE), Box 857, SE-501 15 Borås, Sweden

³ Volvo Car Corporation, SE-405 31 Gothenburg, Sweden

* Correspondence: annika.ahlberg.tidblad@volvocars.com; Tel.: +46-709-613424

Received: 6 January 2019; Accepted: 1 August 2019; Published: 4 September 2019



Abstract: One way to support the development of new safety practices in testing and field failure situations of electric vehicles and their lithium-ion (Li-ion) traction batteries is to conduct studies simulating plausible incident scenarios. This paper focuses on risks and hazards associated with venting of gaseous species formed by thermal decomposition reactions of the electrolyte and electrode materials during thermal runaway of the cell. A test set-up for qualitative and quantitative measurements of both major and minor gas species in the vented emissions from Li-ion batteries is described. The objective of the study is to measure gas emissions in the absence of flames, since gassing can occur without subsequent fire. Test results regarding gas emission rates, total gas emission volumes, and amounts of hydrogen fluoride (HF) and CO₂ formed in inert atmosphere when heating lithium iron phosphate (LFP) and lithium nickel-manganese-cobalt (NMC) dioxide/lithium manganese oxide (LMO) spinel cell stacks are presented and discussed. Important test findings include the large difference in total gas emissions from NMC/LMO cells compared to LFP, 780 L kg⁻¹ battery cells, and 42 L kg⁻¹ battery cells, respectively. However, there was no significant difference in the total amount of HF formed for both cell types, suggesting that LFP releases higher concentrations of HF than NMC/LMO cells.

Keywords: Li-ion batteries; gas emission; acid gases; hydrogen fluoride (HF); thermal runaway; venting; safety; firefighting; electric vehicles

1. Introduction

The number of vehicles with electrified drivetrains produced annually increase every year as the market penetration rises steadily, although still at very low volumes. Electric vehicles (EV) comprise hybrid vehicles (HEV), plug-in hybrid vehicles (PHEV) and pure electric vehicles (PEV). The latter can either be battery powered, also referred to as battery electric vehicle BEV or powered by a fuel cell, fuel cell electric vehicle (FEV). Increasing restrictions on carbon dioxide (CO₂) and nitrogen oxide (NO_x) emissions from the transport sector as well as more aggressive political strategies for fuel economy and reduced fossil fuel dependence contribute to this trend. The transition from conventional internal combustion engine (ICE) vehicles to EV implies exposure to new risk scenarios and hazards inherent with the rechargeable electrochemical energy storage systems (REESS).

A consequence of this development is that vehicle manufacturers, test institutes, and other organizations who perform assessments of vehicle crash worthiness are experiencing a rising demand to perform such tests on EVs as well as component testing on propulsion batteries and battery systems. Crash testing of EVs introduces a significant difference compared to testing of conventional ICE vehicles [1]. Testing of ICE vehicles with liquid or gas fuels are performed with an “empty tank”, hence with its fuel removed, whereas the energy storage of the EVs is in place during the test and is

typically at a relatively high state of charge (SOC) at the time of the impact. Even a partly or “fully” depleted lithium-ion (Li-ion) EV battery, i.e., when the battery indicator shows that the traction battery is fully discharged, can have substantial energy content, depending on the operational SOC window defined by the vehicle application. Additionally, the size of the battery pack depends on the level of electrification and vehicle model. A BEV would be expected to have significantly more battery power available onboard than a HEV of the same vehicle model, both because the BEV is likely to have a wider SOC operational window than a HEV, but also because the battery itself is expected to be larger for range purposes. Furthermore, there are various different cell chemistries which exhibit varying safety performance characteristics. This challenges the existing safety routines of the test operators, who must update their safety practice to accommodate for the new risks implied in crash testing of hybridized and/or fully EVs. For the same reason, new safety routines for first and second responders performing rescue work at traffic incidents involving EVs are in the process of evaluation around the globe.

Comprehensive studies on plausible critical failure scenarios and their consequences for the automotive traction battery is one way of supporting development of new safety practices in testing and field situations. This paper focuses on risks and hazards associated with venting from Li-ion batteries, currently the battery technology of choice for EV propulsion. Venting occurs when the Li-ion batteries experience internal pressure build-up due to increased vapor pressure and formation of gaseous degradation products inside the battery cell [2]. The liquid electrolytes used in Li-ion batteries are unstable and will react with the graphite anode, as the solid-electrolyte interface (SEI) layer degrades, to form a gaseous species when heated above a threshold temperature, typically temperatures greater than 80–120 °C [3] and the battery experiences what is commonly referred to as a “thermal event”. There are several failure modes that can result in a thermal event. Some conditions are initiated internally in the battery system, e.g., shorting of the battery cell, either externally or internally, or improper battery management leading to overcharge, overcurrent, or overdischarge, and some are caused by conditions external to the battery, e.g., severe mechanical abuse (crash) and external heat exposure (fire) [3]. In extreme cases, the thermal event turns into a state of “thermal runaway”. The thermal runaway is characterized by rapid gas evolution from one or more cells, as the alkyl carbonate electrolytes used in most Li-ion cells start to break down in the temperature range from 150–200 °C to form different organic and inorganic species, including CO₂, CH₄, C₂H₄, C₂H₆, C₂H₅F, H₂, and hydrogen fluoride (HF) [4]. This is when the rate of the decomposition reactions continually accelerate and the temperature of the cell increases uncontrollably to extreme levels, often well above 200–300 °C. Barnett et al. reported [3] that the total release of the electrochemical energy can raise the temperature to 700 °C and exothermic reactions between the anode and cathode materials under adiabatic conditions can also elevate cell temperatures by 700 °C. There are different definitions for when the onset of thermal runaway occurs. Roth defines this as the time when the cathode material starts to release oxygen [5]; however, for testing purposes, thermal runaway is often defined by a combination of measurable parameters, including the cell temperature or rate of temperature increase. The total amount of heat energy that can be released from a Li-ion battery can exceed 10 times the amount of electric energy stored in the battery if all combustible materials react with air [3]. However, the oxygen available inside the cell is not sufficient for full combustion of the electrolyte solvent even in Li-ion cell chemistries with metal oxide cathodes. Hence, a major fraction of solvent combustion must take place external to the cell [3].

Conditions of venting, the amount of gas released, and the composition of gases formed by heating two types of automotive grade Li-ion cells in an oxygen free environment were studied experimentally. The test was designed to prevent ignition of vented gases, and thus testing was performed in an inert atmosphere. The Li-ion chemistries represented in the study was lithium iron phosphate (LFP) and lithium nickel manganese cobalt (NMC) dioxide/lithium manganese oxide (LMO) spinel (NMC/LMO). In this study, each test sample comprised a bundle of five cells clamped together and placed on a heating plate that provoked the bottom cell into the thermal runaway, which then propagated through the other four

cells. Gas analysis of selected major and minor gases was performed. Major gases comprise combustion gases, carbon dioxide (CO₂), carbon monoxide (CO), and volatile organic compounds (VOCs). The minor gases selected were acid gases (HF and phosphorous oxyfluoride (POF₃)) due to their high toxicity.

2. Results

2.1. Gas Volumes and Emission Rates

2.1.1. Gas Volumes Produced

A measurable gas flow was detected from the NMC/LMO cells. However, the LFP cells did not produce enough gas to get a reading on the flow sensor, and, therefore, the volume was calculated based on the gas concentration levels measured for VOCs CO₂ and HF; see Section 4.3 for details. The total gas volumes are summarized in Table 1. The amount of gas formed from the NMC/LMO cells was 30 times greater than for the LFP cells. Normalized to battery weight, the relative amount of gas formed from the NMC/LMO cells was almost 20 times that of LFP.

Table 1. Gas volumes produced by battery stacks comprising five cells when heated to thermal runaway in an oxygen-free environment.

Test Number	Cell Type	Total Gas Volume	Normalized Gas Volume
1	LFP	50 L ¹	42 L/kg
2	NMC/LMO	1500 L	780 L/kg

¹ Calculated value from measured amounts of volatile organic compounds (VOCs), carbon dioxide (CO₂), and hydrogen fluoride (HF).

2.1.2. Emission Rates

Figures 1 and 2 show the emission rates of CO₂ and HF for the LFP and NMC/LMO cells, respectively. $t = 0$ is the time when the first sign of venting is detected. Note the different scales on the axes, showing that the rate of gas release for NMC/LMO is accelerated by a factor 100 compared to LFP in terms of CO₂ release. The venting times of the five cells are clearly separated for LFP, whereas only three distinct peaks can be seen for NMC/LMO. The gassing process for the NMC/LMO cells is also completed very much faster. The duration of gassing in NMC/LMO cells is approximately one-tenth of the total venting time of the LFP cells. Furthermore, it is worth noting that, for LFP, the emission rate of CO₂ is one order of magnitude greater than that of HF, whereas, for the NMC/LMO cells, the difference in emission rate between these two gases is two orders of magnitude.

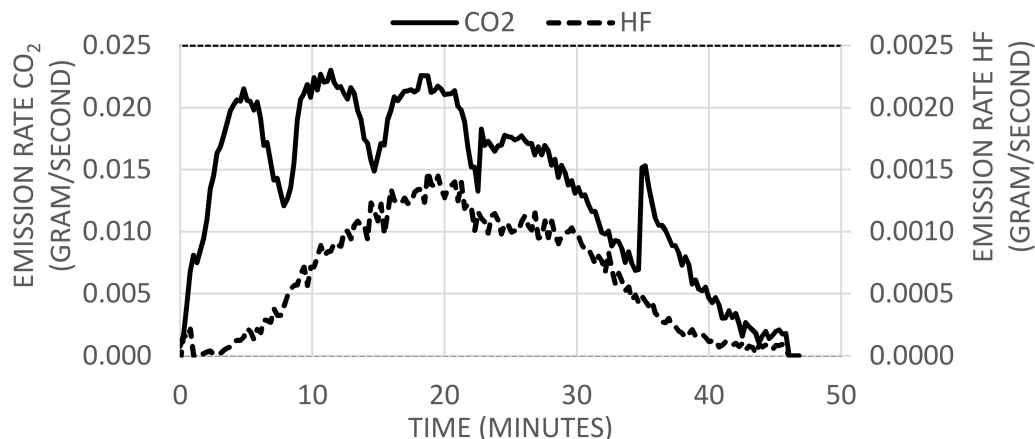


Figure 1. Rate of CO₂ and HF release after a thermal event in lithium iron phosphate (LFP cells). $t = 0$ is the time when the first sign of venting is detected. Note that the order of magnitude is different for CO₂ (left) and HF (right) in the diagram.

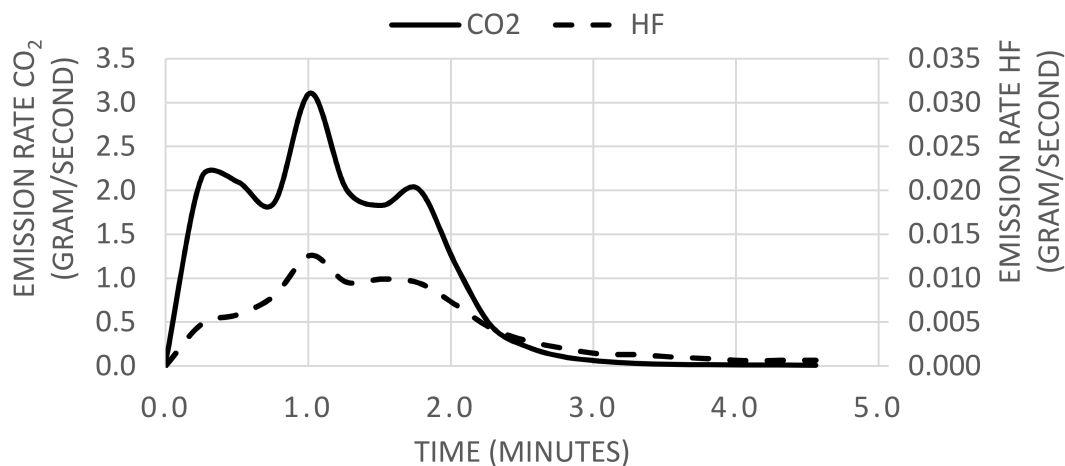


Figure 2. Rate of CO₂ and HF release after a thermal event in lithium nickel manganese cobalt (NMC) dioxide/lithium manganese oxide (LMO) spinel (NMC/LMO) cells. $t = 0$ is the time when the first sign of venting is detected. Note that the order of magnitude is different for CO₂ (left) and HF (right) in the diagram.

Figures 3 and 4 show the gas emission rates of hydrocarbon compounds for the LFP and NMC/LMO cells, respectively. Unfortunately, some data points are lost for the NMC/LMO case, where the flame ionization detector (FID) was over-loaded at the sensitivity range used during the first 20–25 s. However, the general peak shape was recovered using the available data recordings. Two NMC/LMO cells vented in the first 30–40 s and hence the missing data is from both of these cells. The hydrocarbon gas peaks are more distinct than the CO₂ peaks for the NMC/LMO cells and can be used for time resolved cell venting determination.

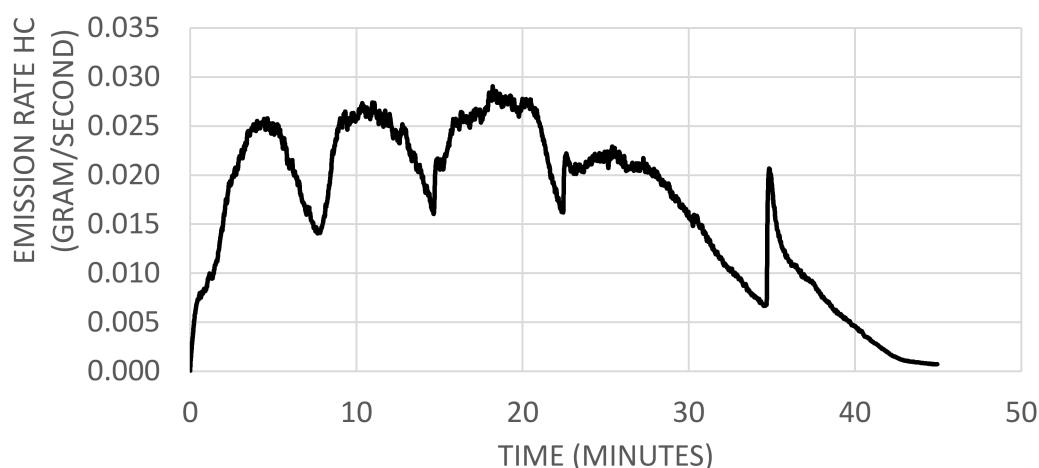


Figure 3. Rate of hydrocarbon (HC) release after a thermal event in LFP cells. $t = 0$ is the time when the first sign of venting is detected. HC measured as propane equivalents.

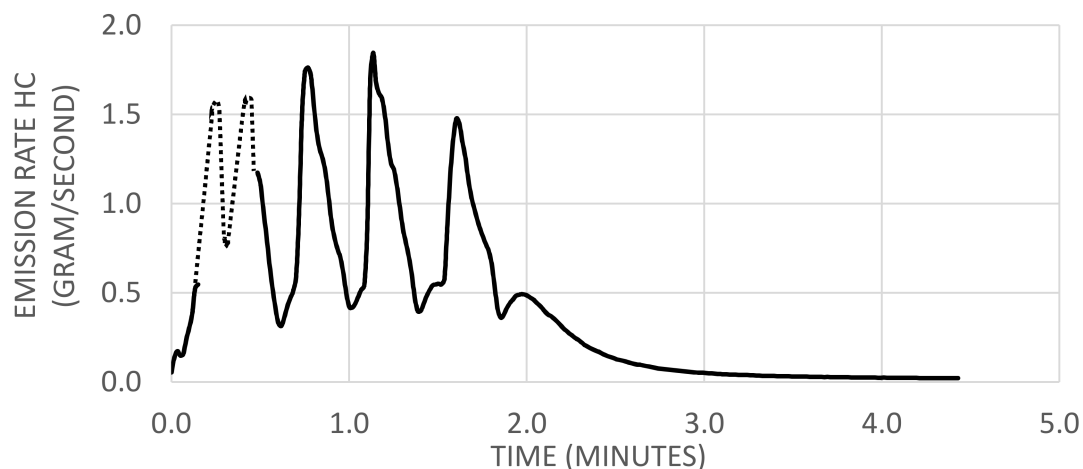


Figure 4. Rate of hydrocarbon (HC) release after a thermal event in NMC/LMO cells. $t = 0$ is the time when the first sign of venting is detected. HC measured as propane equivalents. The dotted line represents reconstructed data in place of missing data in the initial part of the graph due to over-loading of the flame ionization detector (FID) at the used sensitivity range.

2.1.3. Temperatures at Venting

Figure 5 shows the temperatures in the LFP cell stack as a function of test time. Figure 6 is the corresponding temperature curves for NMC/LMO. The peak temperature in the NMC/LMO stack is reached almost immediately following the thermal event, while it ramps up over a period of approximately 30 min in the LFP test. The average temperature slopes during heating are $11.7\text{ }^{\circ}\text{C}/\text{min}$ for LFP and $1390\text{ }^{\circ}\text{C}/\text{min}$ for NMC/LMO, respectively. The peak temperature for the NMC/LMO cells, $615\text{ }^{\circ}\text{C}$, is approximately $230\text{ }^{\circ}\text{C}$ higher than the highest measured temperature in the LFP cells, $386\text{ }^{\circ}\text{C}$. Note that the inflection point at $400\text{ }^{\circ}\text{C}$ in the initial temperature peak for NMC/LMO in Figure 6 suggests that two cells vent in very quick succession during the first 30 s. This supports the assumption that the reconstructed part of Figure 3 comprises the venting of two cells.

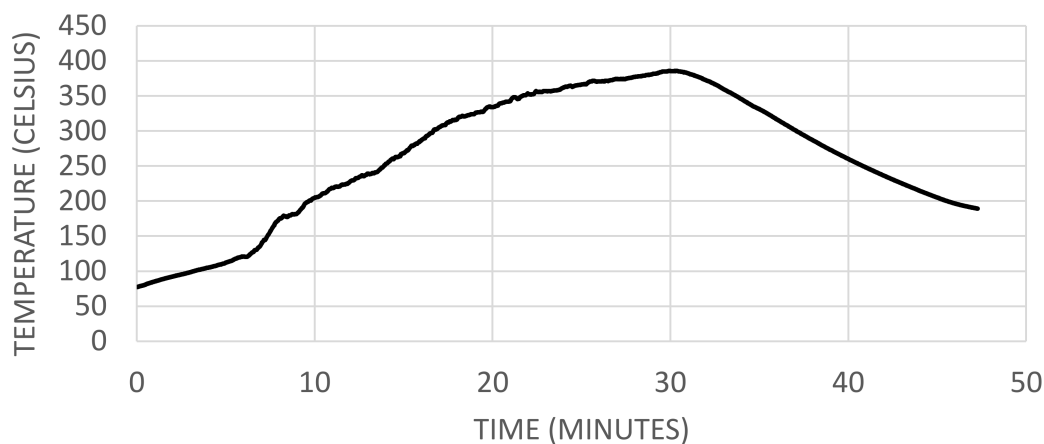


Figure 5. The temperature measured between the two bottom cells in the LFP cell stack. $t = 0$ is the time when the first sign of venting is detected. The average slope, dT/dt , from onset to peak temperature is $11.7\text{ }^{\circ}\text{C}/\text{min}$.

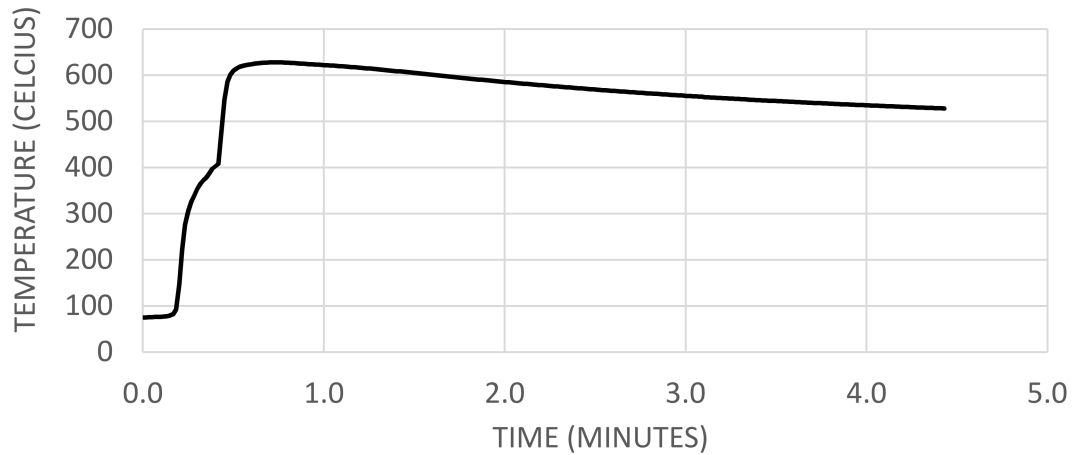


Figure 6. The temperature measured between two bottom cells in the NMC/LMO cell stack. $t = 0$ is the time when the first sign of venting is detected. The average slope, dT/dt , from onset to peak temperature is $1390\text{ }^{\circ}\text{C}/\text{min}$.

The temperatures of the measured gas flows are shown in Figures 7 and 8 for LFP and NMC/LMO cells, respectively. These temperatures are much lower and about the same for both cell types. This is due to the cooling effect of the nitrogen carrier gas. The venting of the five LFP cells takes approximately 45 min, as shown in Figure 7, but it is difficult to determine the exact venting times of the individual cells. Figure 8 shows that all five NMC/LMO cells have vented in less than 4 min. The 5 cells venting events are clearly discernable in the temperature measurement of the gas flow leaving the test vessel.

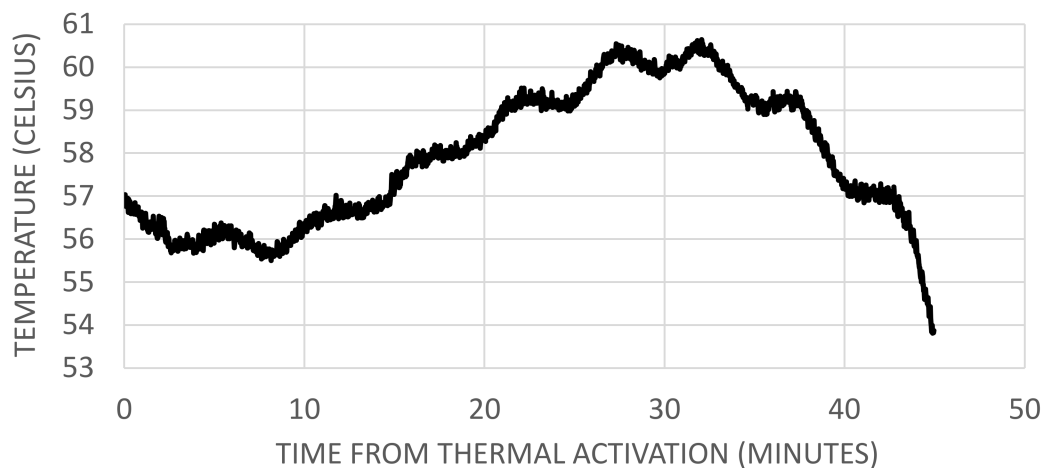


Figure 7. The temperature in the gas flow leaving the test vessel for the LFP cells. $t = 0$ is the time when the first sign of venting is detected.

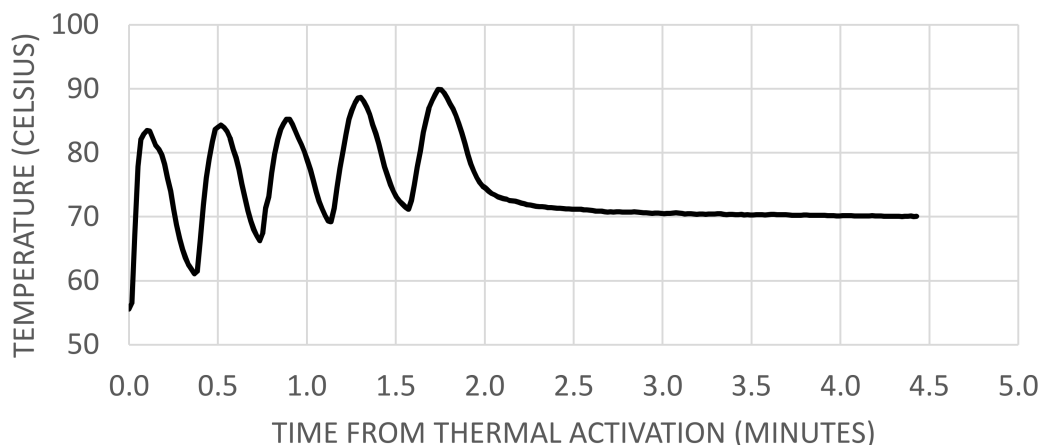


Figure 8. The temperature in the gas flow leaving the test vessel for the NMC/LMO cells. $t = 0$ is the time when the first sign of venting is detected.

2.2. Gaseous Species

2.2.1. HF Emissions

Table 2 shows the HF amounts detected in the vent gases of the two cell types using wash bottles and Fourier-transform infrared spectroscopy (FTIR), respectively. The wash bottle method consistently has significantly higher amounts of HF, due to treating all soluble fluorinated species as HF. The measured amounts of HF indicate that the amount of HF released is comparable for both cell types, but since the total gas volume of LFP is significantly smaller compared to NMC/LMO, the relative concentration of HF is very much higher in the fumes from the former.

Table 2. Total amount of HF measured in the vent gas streams for LFP and NMC cells using two different methods; wash bottles and FTIR. The HF amounts have been normalized to battery mass (g/kg) and energy density (g/kWh), respectively.

Cell Type	Wash Bottles ¹	FTIR	Normalized Amounts: Wash Bottles		Normalized Amounts: FTIR	
LFP	4.2 g	1.8 g	3.6 g/kg	36 g/kWh	1.5 g/kg	16 g/kWh
NMC/LMO	6.5 g	1.7 g	3.4 g/kg	23 g/kWh	0.9 g/kg	6.0 g/kWh

¹ Calculated from the total fluoride ion concentration in the solution.

2.2.2. FTIR and Gas Chromatography-Mass Spectrometry (GC-MS) Analysis

Most of the main absorption peaks in the FTIR spectra from both cell types are from carbonates, which is expected since different mixes of organic carbonates constitute the electrolyte solvents used in commercial Li-ion cells. A summary of the absorption peaks used for quantitative analysis is found in Table 3. Major absorption peaks are found around 1770 cm^{-1} and 1280 cm^{-1} , which are characteristic for diethyl carbonate (DEC), dimethyl carbonate (DMC) and ethyl methyl carbonates (EMC). Absorption bands at 1870 cm^{-1} and 1100 cm^{-1} are most likely propylene carbonate (PC). However, the absorption band at 1100 cm^{-1} can also represent unknown organic fluorinated substances. A typical bond stretching wavenumber for a fluorine atom bounded to a tertiary carbon is 1100 cm^{-1} [6]. The wave number for the fluorine carbon bond stretching varies with the configuration of the carbon, e.g., the wave number for the fluorine bond with a primary carbon in 1-fluoropropane is 1018 cm^{-1} [7]. CO_2 , an electrolyte decomposition product, was observed with a peak around 2350 cm^{-1} , which is the major CO_2 peak. However, this peak is not suitable for quantitative analysis, and for this purpose 2392 cm^{-1} was used instead. HF bands were seen between 4000 cm^{-1} and 4200 cm^{-1} . POF_3 was not

conclusively identified in any of the two cell types, but cannot be completely excluded. CO could not be conclusively determined due to interference in the spectral region of the C-O bond.

Table 3. Summary of FTIR absorption peaks used for quantitative analysis of emitted gas composition. The gas species reported include: carbon dioxide (CO₂), carbon monoxide (CO), diethyl carbonate (DEC), dimethyl carbonate (DMC), ethyl methyl carbonates (EMC), propylene carbonate (PC), hydrogen fluoride (HF) and phosphorous oxyfluoride (POF₃).

Type of Gases	Gas Species	Absorption Band (cm ⁻¹)	LFP	NMC/LMO
Combustion gases	CO ₂	2392	Strong peak	Strong peak
	CO	2134	Not conclusive due to interference	Not conclusive due to interference
Organic carbonates	DEC	1770 and 1280	Major peaks	Major peaks
	DMC			
	EMC	1870 and 1100	Major peaks	Major peaks
	PC			
Fluorinated hydrocarbons		1100	Major peak but cannot separate from PC	Major peak but cannot separate from PC
Acid gases	HF	4075 ^a	4000–4200 band clearly identified	4000–4200 band clearly identified
	POF ₃	1416, 991, and 871 ^b	Not conclusively identified	Not conclusively identified

^a Wave number used for quantification. ^b Wave numbers used for qualitative assessment.

The presence of significant amounts of non-reacted electrolyte solvent was confirmed by the gas chromatography-mass spectrometry (GC-MS) analysis of collected gas bag samples, as shown in Figures 9 and 10 for LFP and NMC/LMO cells, respectively.

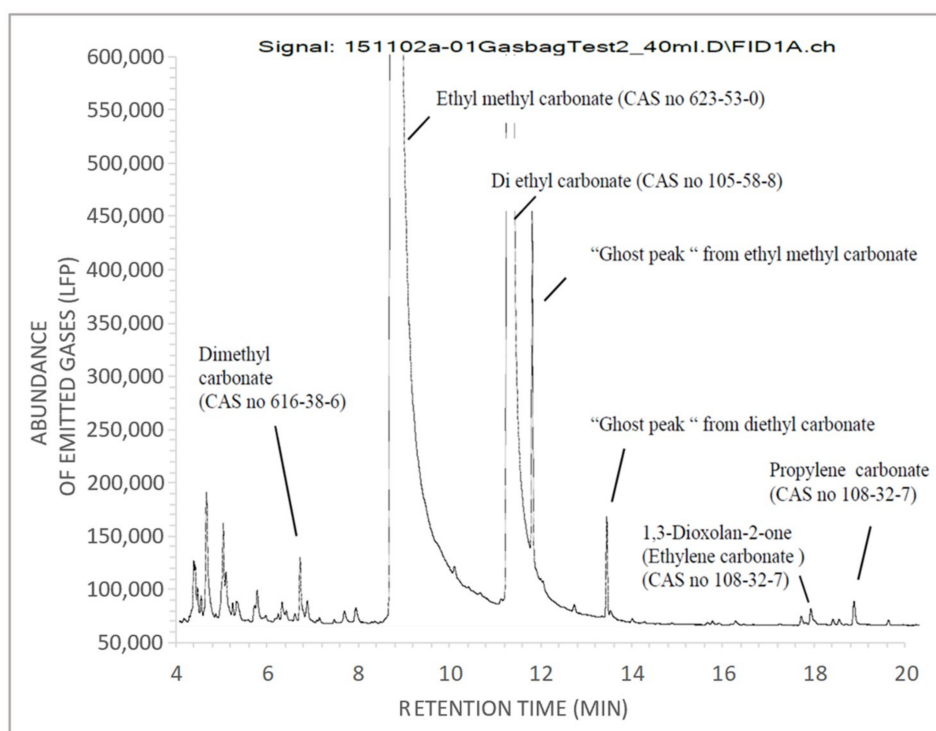


Figure 9. Gas chromatogram (FID signal) of gas volume sampled from LFP cells.

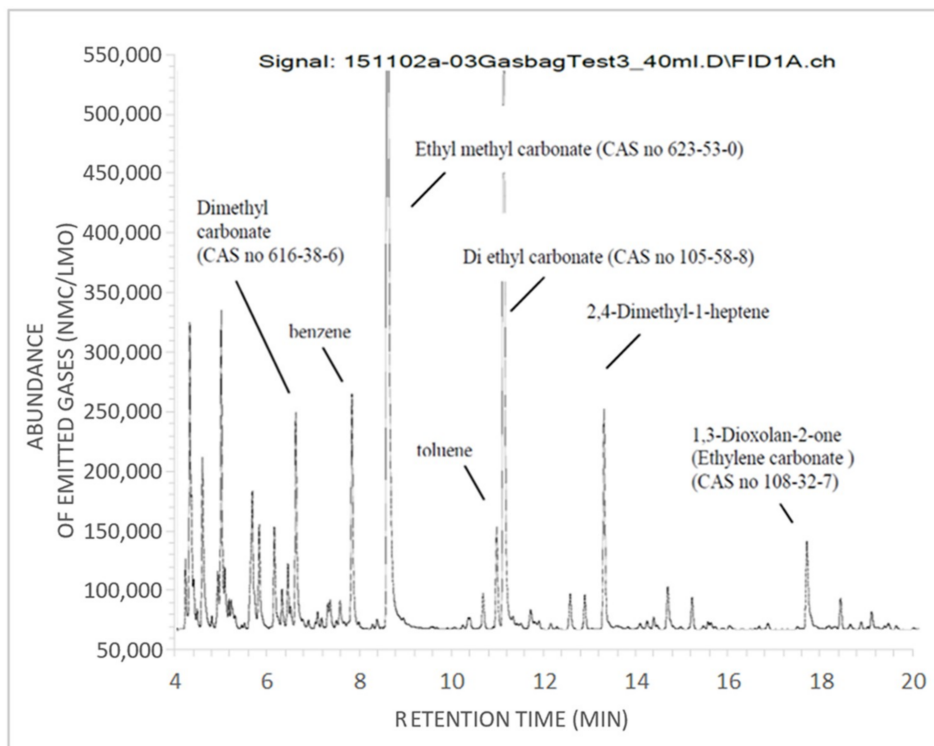


Figure 10. Gas chromatogram (FID signal) of gas volume sampled from NMC/LMO cells.

3. Discussion

3.1. Gas Volumes and Emission Rates

The huge difference in the total gas volumes emitted from the LFP cells compared to the NMC/LMO cells was surprising. Although the weight difference between the two cell types, 0.236 g/cell for LFP and 0.385 g/cell for NMC/LMO, can account for a small part of the difference in total gas volume, it is far from explaining a difference of more than an order of magnitude. A plausible explanation for the large gas volumes formed by the NMC/LMO cells is that the cathode material releases oxygen readily, as the material decomposes with increasing temperature, leading to combustion of a significant proportion of the electrolyte solvent. It is a well-known fact that the LFP crystalline structure is resistant to oxygen release [8], and hence combustion reactions of the electrolyte and the graphite anode to form CO and CO₂ is dependent on the availability of oxygen releasing species in the electrolyte itself when there is no external supply of oxygen available for the reactions. The NMC/LMO cells were completely consumed at the end of the test, whereas the LFP cells had only suffered minor damage. If full combustion of the LFP cells had been achieved, the total gas volume would likely have been larger. Roth has concluded that gas volumes and composition are related to the electrolyte mixture and different thermal stages during thermal runaway [5]. His results were achieved under fully aerated conditions and an externally regulated temperature profile as determined by the accelerated rate calorimeter (ARC) with a steady temperature increase, which is the same for all tests performed. Lei et al. [9] have also conducted ARC studies on 18650 cells with different cathode materials. Their data shows that LFP generates less gas than NMC and lithium cobalt dioxide (LCO)/NMC and ratios are reported as 1:3:5.5 [9]. The difference in gas volumes is not as large as the results in this study. This can be explained by the difference in the experimental set up. In the case when ARC is used, the ambient temperature is increasing at a linear rate and constantly contributing to the heating of the battery cells. In this study, the nitrogen carrier gas had a cooling effect on the reaction chamber and the temperature increase of the Li-ion cells was dependent on the capability and rate of self-heating of the respective cell chemistries. In an EV battery, the cooling system will respond to an increasing cell and battery temperature to suppress the

self-heating process. Dependent on the balance between applied cooling and the rate of self-heating, the maximum temperatures reached, and the time spent in the different runaway stages are going to vary for different cell chemistries. This will have an impact on the gas composition and, consequently, the influence of gas volumes and the level of cell combustion achieved. The relationship between cooling and self-heating used in this test set-up intended to replicate a thermal balance. However, the same cooling effect was applied to both cell types and, since LFP has both a lower heat of reaction as well as a lower maximum temperature than NMC/LMO [9], the LFP cell stack did not reach as high temperature ranges as NMC/LMO. However, this simulates a realistic field scenario, since the safety advantage of LFP relies on these properties [10].

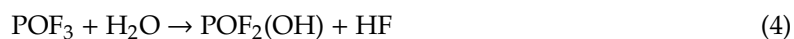
3.2. Gaseous Spec

The chemical species detected in the vented gases in this study are consistent with reports from other authors [11–14]. HF detection was prioritized in this study, since this is a gas with high toxicity at low concentrations. Two conclusions can be drawn from the gas measurements in this study: The total amount of HF released from the LFP and the NMC/LMO cells are comparable, despite the huge difference in the total amounts of gas volumes, and the measurement method chosen to quantify the amount of HF impacts significantly on the measured values. Furthermore, the results indicate that the concentration of HF in gases released from LFP cells is more than an order of magnitude higher than for NMC/LMO cells. This emphasizes the necessity to not just focus on the total amount of gas released from a Li-ion EV battery, but to also take account of the composition and relative concentration of problematic species and the total time frame of gassing when assessing the risk of unwanted chemical exposure.

In this study, there is little difference in the total HF amounts released by the two cell types. This seems to contradict the assumption that the relative amounts of electrolyte in the two cells is proportional to the weight. Since the weight of the NMC/LMO cells is approximately 60% greater than that of the LFP cells, the former should contain more electrolyte than the latter. However, the results seem to suggest that the total amount of lithium hexafluorophosphate (LiPF₆) that reacted to form HF in the two cell types is about the same despite the difference in weight and electric capacity. Yang et al. [15] have described the reaction mechanism by which the electrolyte salt LiPF₆ reacts to form HF:



Kawamura et al. [16] suggest that POF₃ will readily react with moisture according to:



Wilken et al. [17] have studied initial stages of thermal decomposition of LiPF₆-based Li-ion battery electrolytes. Their investigations conclude that the decomposition of LiPF₆ to form HF follows the path of pyrolysis of the salt, forming PF₅, which then reacts with water to form HF. The water can either be moisture contamination inside the cell or external moisture. [17].

The results obtained in this study may suggest that conditions for formation of HF are favoured when the thermal event develops over a longer time, as in LFP, compared to the very fast temperature raise and accompanying gas production and ventilation rates that was characteristic for the NMC/LMO cells. A plausible explanation is that the intermediate PF₅ predominantly forms inside the cell at the onset of the thermal event and early into the thermal runaway, which is consistent with the shielding effect observed in a previous study [2]. According to Hammami et al. [18], the nickel and manganese found in the NMC/LMO cells will catalyse the formation of a different organic fluoro compound, such as fluoroethanol ether, and this is the reason for the lower HF concentration in the vented gases.

These findings are consistent with Sun et al. [19] and Sturk et al. [20], who report different identifications of organic combustion products from NMC and LFP cells. NMC appear to generate significantly lower concentrations of HF than LFP [19].

In this study, the nitrogen gas served three purposes: It was a carrier gas and it created a dry inert oxygen-free atmosphere that prevented outbreak of fire in the reaction vessel. The gas flow kept the temperature of the gases released from the reaction vessel at manageable levels for chemical analysis and quantification. The results show another important difference between the LFP and NMC/LMO cell types: The temperature of the vented gases increased significantly faster and reached higher levels for the NMC/LMO cells compared to LFP. This is attributed to the higher reactivity of the transition metal oxide materials compared to the metal phosphate. Previous studies showed that the reactivity of the Li-ion cells at thermal runaway increased significantly when the cells were fully charged [2]. Therefore, the cells in this study were charged to the highest possible SOC level in order to have the highest possible energy available in the cells at the onset of thermal runaway.

Since the trend in the automotive industry is to move from LFP to NMC cell technologies in order to benefit from the higher energy density of these chemistries, it is important that construction engineers are aware of and consider that different Li-ion technologies have different gassing behaviors. Since the emitted gas contains toxic species, e.g., CO and HF, as well as volatile and flammable organic carbonates, it is necessary to take care of gas emissions in a controlled way so that the vehicle occupants are protected from exposure. When changing from LFP to NMC cells, the potential total gas volume that can be released is not only increased by an order of magnitude, but the gas release rate is also increased at the same time. In a worst-case scenario, the results from this study imply that the gas management system of a battery pack with NMC/LMO based cells would need to handle a gas emission rate that is two orders of magnitude higher compared to LFP. This ratio is obtained by dividing the total gas volume by the gas release time and cell stack mass. For the NMC/LMO cells, this becomes $1500 \text{ L}/(4 \text{ min} \times 1.925 \text{ kg}) = 190 \text{ L min}^{-1} \text{ kg}^{-1}$. Similarly, for LFP cells, the result is $50 \text{ L}/(45 \text{ min} \times 1.180 \text{ kg}) = 0.94 \text{ L min}^{-1} \text{ kg}^{-1}$. Clearly, this will have an implication on both dimensioning and placement of vents to avoid uncontrolled leakage of gases through seals in the pack casing, since the expected rate and amount of gas released from thermal decomposition of NMC/LMO exceeds that of LFP [9]. However, the difference will be less pronounced for a battery pack where the self-heating rate of failing cells is managed with a well-balanced cooling system. In this study, the steady cooling provided by the nitrogen carrier gas appears to have been excessive for LFP, since the cell stack was not fully combusted.

3.3. Test Method and System Considerations

The results of the HF measurements shown in Table 2 highlights the importance of the chosen method of quantification. It is always challenging to measure small volume gases (ppm and ppb level) and the measurement uncertainty can be quite high. In this case, the amount of HF obtained using wash bottles was more than double that measured with FTIR. There are two probable reasons for this discrepancy. The wash bottle result over-estimates the actual amounts of HF formed since it is assumed that all F^- captured originates from HF. The gas measurement showed that a large portion of the vented gases is made up from vaporized electrolyte solution. It cannot be excluded that the vented gases contain some electrolyte aerosols, including the electrolyte salt LiPF_6 , due to the high pressure and emission rate. Additionally, the FTIR spectra indicate possible formation of fluorinated hydrocarbons as well as other inorganic fluoro-gases, such as POF_3 . All inorganic fluoro-gases will also be captured in the wash bottles and incorrectly contribute to the HF estimate. Another important reason for the lower amount detected by the FTIR is that the gas has to travel longer before reaching the detection system. HF is a very reactive substance, and it is not unlikely that some reacted with other species in the gas or with the surfaces in the (externally insulated) gas ducts on the way to the FTIR spectrometer. In the current measurement set-up, it was not practically possible to saturate all surfaces with HF prior to heating the cell stacks, since the system was continually purged with nitrogen gas.

However, it is important to note that the gas emission rate varied with time and that, during part of the venting episodes for NMC/LMO cells, the gas emission rate was very high. There is, therefore, a possibility that the wash bottle method underestimates the total HF amount for NMC/LMO cells compared to the amount for the LFP cells in this study due to fast short term variations in the relative sampled volume portion of the gas flow in the NMC/LMO test, since the sample gas flow to the wash bottles was kept constant at 1.0 L min^{-1} . Despite this limitation, the amount of HF determined for NMC/LMO cells with the wash bottle method is still expected to be an overestimation compared to the actual amount of HF due to contributions from other fluoro containing substances, which is reflected by the lower value obtained with the FTIR spectroscopy measurement.

One has to be cautious about drawing too far-reaching conclusions about the composition of venting gases from Li-ion cells and batteries based on the results of this type of test. The measurements are made on gas emissions from Li-ion cells in a dry inert atmosphere. While it is desirable to create a test environment where the vented gases do not ignite, the lack of oxygen may significantly impact on what species will form, and it is not unlikely that chemical substances form in oxygen-starved systems would not be stable in a normal atmosphere. The lack of moisture in the nitrogen carrier gas may also have limited formation of HF. Yang et al. [15] have shown that HF formation from a Li-ion electrolyte will be limited in case the humidity is too low. Their results show that no HF is formed at 10 ppm water content while significant production occurs at 300 ppm water vapor. They also show that the survival time for the intermediate PF_5 increased significantly when the humidity was very low [15]. The humidity in the nitrogen carrier gas in the current study was 40 ppm, or <10% RH. HF was detected by both FTIR and water-filled wash bottles. If large amounts of intermediate PF_5 did not react due to lack of humidity in the test environment, one would expect that the detected amount would be much higher for the water bottles, where there is an abundance of available moisture. Table 2 shows that the total difference between the wash bottle and the FTIR measurement was 1:2 for LFP and 1:3 for NMC/LMO, which is within the same order of magnitude, and the present results indicate that comparable amounts of HF formed in the gas ducts before reaching the FTIR detector.

Another limitation with this type of test system is that the gases that will be detected are dependent on the assumptions made when setting up the measurement system; the choice of analytical methods as well as the chosen detectors. Unexpected gas species may therefore be overlooked, which impacts both on the determined composition of the gas mixture and the relative concentrations/amounts of the various constituents.

One of the strengths of this method is its ability to provide time-resolved information of the propagation of thermal runaway spreading from one cell to the next. In this test, temperature measurements of the vented gases successfully identified the time of rupture of each cell in the stack and hence the rate of propagation for the NMC/LMO cells. For the LFP cells, measurements of changes in temperature were not sensitive enough as a consequence of much lower thermal activity by these cells. However, since the amount of gas was much lower, measurements of CO_2 did offer detailed information about the propagation of thermal runaway spreading from cell to cell in the stack. An additional method to acquire time-resolved propagation data on both cell chemistries is by means of total hydrocarbon quantification using FID. This technique worked for both the NMC/LMO and LFP cells. Consequently, different sensors can be considered for detection of activated thermal runaway within a battery, but their ability for good time resolution may differ depending on circumstances, e.g., high or low thermal activity and large or limited production of vent gases. A recent study of different sensors to detect thermal runaway in Li-ion battery packs conducted by Koch et al. [21] showed that thermal runaway detection based on gas, pressure, and force sensors was faster than temperature sensors and very reliable, which supports the results presented in this paper.

3.4. Application Perspectives

The results in this study indicate that gas sensors may be more appropriate to give early detection of a thermal event in progress in a Li-ion battery than temperature sensors. The closer the sensor is to the gas emitting cell, the earlier the potential time of detection.

This study shows that gas emitted from the slow reacting LFP cells contains the same total amounts of HF as the faster reacting NMC/LMO cells. Due to the much smaller gas volumes released from LFP compared to NMC/LMO, it may appear as if the concentration of HF is higher from venting LFP cells. However, it is important to also factor in the total time of gas release in order to estimate the average concentration over time for the two cell types. The FTIR measurements indicate that both cell types release just below 2 g HF (see Table 2), but that the total gas volumes are 50 L from LFP and 1500 L for NMC/LMO, respectively. Considering that it takes 40 min for all cells to vent for LFP vs. 2 min for NMC/LMO, this implies that the average concentration in the gas emissions during the venting is about the same order of magnitude in both cases; $0.9 \text{ mg L}^{-1} \text{ min}^{-1}$ for LFP and $0.3 \text{ g L}^{-1} \text{ min}^{-1}$ for NMC/LMO, respectively. Which of these two outcomes that is the most problematic will depend very much on the conditions of the incident. Outside, in free air, there will be little risk of HF and other lighter species accumulating near or around the vehicle, since these will rise and rapidly dissipate. A short emission duration may be an advantage in this case (if such dissipation is sufficient), since it means that the total time to handle the incident is notably less. In closed spaces, slow gas emission rates may be easier to manage with existing gas evacuation capability of the surrounding space, and a prolonged emission period may be desirable. However, it is important to remember that studies of vehicle fires show little difference in the amount of toxic gas release from an EV compared to an ICE, and recent data from Truchot et al. [22] shows that an ICE will release a total of 0.4 kg HF compared to 0.7 kg for the EV. Furthermore, their data shows that the initial HF gas release, with the highest concentration, is identical to and independent of the energy carrier and is released from sources that are common to both ICE and EV, e.g., fluorinated plastics and air conditioning refrigerant. The Li-ion battery contribution to HF did not appear until 30 min into the fire. The conclusion was that it would not affect the toxicity level at the time of evacuation of occupants from the vehicle, at least when the fire incident is initiated outside of the battery itself, e.g., an external heat source, such as a fire starting in another part of the vehicle or somewhere in the proximity of the vehicle [22].

Fire studies show that several toxic gases form during combustion of both ICE vehicles and EVs [22]. The acid gases, i.e., HF, hydrogen chloride (HCl), and hydrogen cyanide (HCN), make up a very low volume in terms of total amounts, but deserve consideration for the toxic impact due to their low toxicity thresholds [22]. However, the strong polar nature of these acid gases, as well other halogenated compounds, can be used as an advantage, since it is possible to reduce the concentration of such gases significantly by spraying water and “washing out” the acid and halogenated gaseous species from the emissions [23]. This method is not an established practice by firefighters when fighting fires in EVs, however, it is commonly practiced when mitigating effects of acid gas emissions from chemical fires [24]. Information to fire-fighting authorities about the acid nature of the Li-ion gas emissions during a thermal incident should greatly enhance the opportunity to reduce some of the challenges of handling an EV fire incident in the field by means of water “washing” the Li-ion battery gas emissions. Water can also be used to effectively reduce concentrations of a wide range of harmful substances with lower solubility by diluting the combustion gases [24].

4. Materials and Methods

4.1. Test Set-Up

Figure 11 shows a photo and a schematic of the experimental set up developed for the vented gas measurements. The 60 L test vessel was insulated and its walls were electrically heated to approximately $70 \text{ }^\circ\text{C}$ in order to limit condensation of gaseous substances released from the battery cells during the test. A plate heater was installed at the bottom of test vessel to be used to heat the Li-ion cells.

The heater was controlled and turned on/off from the outside of the test vessel. The heater power was 1500 W, generating a maximum temperature of 350 °C at a rate of 7 °C/min.

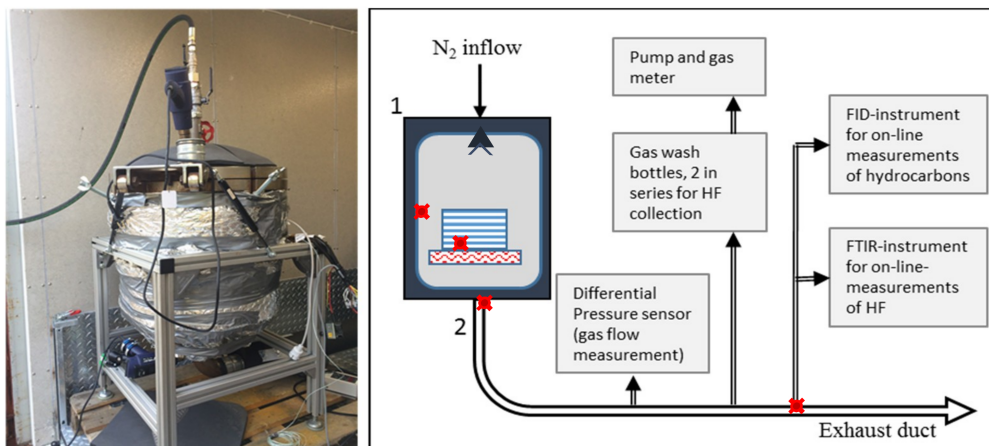


Figure 11. A schematic representation of the test set-up shown to the right. The cell stack was placed on the heating plate in the test vessel (1), and the exhaust duct (2) collected the vented gases and lead them to the measurement equipment. Thermocouples were placed at locations illustrated by the red-crossed circles.

The top of the test vessel was fitted with an inlet for nitrogen gas in order to be able to establish an inert oxygen-free atmosphere inside the reaction chamber. The humidity of the nitrogen gas was 40 ppm. The objective of the nitrogen was to avoid ignition, and violent combustion reactions with the volatile gases expected to be emitted by the battery cells during tests. A nozzle was installed in the vessel lid in order to distribute the nitrogen gas evenly over the test items. The volume flow rate of the nitrogen gas was nominally 10 L min⁻¹. Thermocouples were mounted on the vessel's inside wall, between the bottom two cells of the stack at the gas outlet of the test vessel and the gas sampling point. The thermocouples are of K type, and have a thickness of 0.5 mm.

At the bottom of the vessel, a heated outlet was connected to an insulated and similarly heated ventilation duct. The duct system was designed to make it possible to measure the gas flow, to sample gases for measurements, and to ventilate gases to an external smoke stack. The gas flow in the duct was measured using a flow sensor (Mecatrone MFS-C80) from AB Mecatrone, Solna, Sweden, that was connected to a manometer and a data logger. This arrangement enabled study of any changes in the primary flow of nitrogen, originating from gas evolved from the batteries during heating.

Two sampling lines were connected to the heated duct. The first one was a heated sampling probe with a ceramic filter. The gas was directed through heated polytetrafluoroethylene PTFE tubing to the FTIR and FID for on-line measurements. The FTIR was heated and had a sampling flow rate of 4.2 L min⁻¹ and was calibrated for HF and a range of other gases, e.g., CO and CO₂. The heated FID (SICK/Maihak model 3006) was calibrated against a gas mix of 800 ppm propane in synthetic air and had a sampling flow rate of 1.2 L min⁻¹. The other sampling line conducted non-filtered gas at a flow rate of 1.0 L min⁻¹ to a series of 2 gas wash bottles containing a buffer solution for sampling of HF and other water-soluble fluorinated species. The accumulated fluoride concentration in the solution was determined using ion chromatography (IC). The accuracy of the FTIR measurement is assessed to be within 10%-relative. Internal references were used to calibrate the FTIR for CO₂, CO, HF, and POF₃. A certified gas mixture of HF was used for quantification of the absorption peaks. A detailed description of the calibration procedure is found in the paper by Andersson et al. [25]. The measurement uncertainty for the gas washing bottle method is largely determined by the precision in the gas sampling.

Gas samples for later identification of VOCs were taken on selected occasions during the test. The sampling time was about 1 min and occurred mainly after the main peak flow. The gas samples

were collected using Tedlar type gas bags. From these, small volumes of gas were transferred onto multisorbent tubes containing three types of sorbents (Tenax, Carboxen, and Carbograph as adsorbents) for a broad spectrum of organic species. The adsorbed samples were later thermally desorbed into a gas chromatograph system, using FID and mass selective detection (MSD), using the NIST 08 mass spectra library for identification.

4.2. Test Objects

The test was performed on automotive grade LFP and NMC/LMO pouch cells, shown in Figure 12a. These are mass production grade EV cells and are used in commercial EVs on the market. Table 4 summarizes weight and capacity of the test objects. Prior to testing, the cells were charged to about 100% SOC for the respective chemistry, which corresponds to 4.1 V/cell for NMC/LMO cells and 3.3 V/cell for LFP cells, respectively, in order to have a high onset reactivity in the cells when heating. In each test, a stack of five pouch cells was clamped between metal plates, as shown in Figure 12b, and placed onto the heating plate inside the test vessel. The vented gases were examined as they passed through the duct.



Figure 12. (a) Li-ion pouch cells used for the test. All NMC/LMO cells were charged to 4.1 V/cell and the LFP cells to 3.3 V/cell, respectively, before the test. (b) Stacks of 5 cells were clamped between metal plates with thermocouples placed between the bottom cell, nearest the heating plate, and the second cell in the stack.

Table 4. Test object data.

Cell Type	Cell Weight	Weight of Tested Cell Stack (5 Cells)	Rated Capacity
LFP	0.236 kg	1.180 kg	7 Ah
NMC/LMO	0.385 kg	1.925 kg	14 Ah

4.3. Method for Calculating Gas Volume

In the test with LFP, there was no increase in the flow rate inside the duct detected by the MFS-C80 gas flow sensors, since the emitted gas flow from the battery cells was too small compared to the primary flow rate of nitrogen. Consequently, the total gas volume could not be calculated directly from the measured flow rate. Instead, the measured volume concentrations of emitted gaseous species were used by applying the ideal gas law in combination with gas temperature and the total gas flow rate, as measured by the MFS-C80. The composition of the gas was determined to be 50% VOCs, 45% CO₂, and 5% HF. Other potential gases in the emissions, such as H₂, were not included in the calculation. For the VOCs, the total hydrocarbon concentration was measured, and the detector was calibrated against propane. Thus, the assumption was that the hydrocarbons were in the form of propane, which gives an uncertainty in the volume calculation, depending on the average number of carbon atoms in the VOCs. The GC-MS analysis of the collected gas bag samples showed that the dominating organic

gas species was methyl ethyl carbonate ($C_4H_8O_3$). This indicates that it is valid to select propane as a representative hydrocarbon, since the 4 carbon atoms in $C_4H_8O_3$ would result in a similar or lower FID signal compared to propane because the carbonyl carbon does not contribute to the FID signal [26] and the remaining oxygen atoms will reduce the signal further.

5. Conclusions

The gas and temperature measurements confirm studies stating that there is a great difference in chemical reactivity between different types of Li-ion cell chemistries. The NMC/LMO-based technologies are significantly more reactive than LFP, which is seen by a much faster venting period during self-heating and combustion of the NMC/LMO cells; i.e., approximately 2 min venting duration compared to 45 min for LFP cells in this study. The maximum temperatures measured between cells is also much higher for the NMC/LMO cells than for LFP; i.e., about 600 °C and 400 °C, respectively.

The LFP cells released 50 L of gas and the NMC/LMO cells released 1500 L of gas in total, and the corresponding difference in emission rate of CO_2 is two orders of magnitude higher for the NMC/LMO cells. However, the absolute amount of HF released from both test series is about the same, whereas the amounts of CO_2 differs significantly. For the LFP cells, the HF/ CO_2 ratio is 1/10, and for the NMC/LMO cells, the ratio is 1/100. However, due to the lower energy density of the LFP cells, the normalized amount of HF and its corresponding gas concentration is notably higher for this chemistry compared to NMC/LMO.

Temperature and hydrocarbon sensors used in the test system were able to provide time-resolved information on the on-set timing and propagation of thermal runaway from cell to cell in the stack. The hydrocarbon sensor was more sensitive than the temperature sensors in the gas duct where the gas temperatures had dropped. Hence, hydrocarbon sensors monitoring gases accumulating inside the battery pack may effectively detect the presence of critical cell failure in a Li-ion battery system, regardless of the rate of temperature increase occurring inside the battery.

Extrapolation of these test results needs to be done cautiously. Venting in an inert atmosphere may impact on the gaseous species formed, since it is possible that chemical species form that are unstable in normal atmospheres. However, the test method is useful for making comparative studies of the amount of gas released from different cell chemistries and relative amounts of major gas constituents. Quantitative determination of small volume gases depends strongly on the detection method used, and the measurement uncertainties are rather high.

Author Contributions: D.S. conceived and designed the experiments; L.R. and P.B. performed the experiments and consolidated the data; D.S. and A.A.T. analyzed the data and wrote the paper.

Funding: Autoliv Sverige AB kindly provided funding to design and execute the tests and compile test results. This research received no external funding.

Conflicts of Interest: The authors declare no conflict of interest.

References

1. Sturk, D.; Näsman, Y.; Hoffmann, L.; Gustafson, H.; Östrand, L.; Björnstig, U. E-vehicle safe rescue. Investigation of risk factors and rescue tactics in a traffic incident event involving an e-vehicle. In *Proceedings of the Third International Conference on Fire in Vehicles – FIVE 2014*; Andersson, P., Sundström, U., Eds.; SP Technical Research Institute of Sweden: Berlin, Germany, 2014; pp. 255–265.
2. Sturk, D.; Hoffmann, L.; Ahlberg Tidblad, A. Fire on e-vehicle battery cells and packs. *Traff. Inj. Prev.* **2015**, *16*, S159–S164. [[CrossRef](#)]
3. Barnett, B.; Ofer, D.; Sriramulu, S.; Stringfellow, R. Li-ion batteries, safety. In *Batteries for Sustainability. Selected Entries for the Encyclopedia of Sustainability Science and Technology*; Brodd, R.J., Ed.; Springer: New York, NY, USA, 2013; pp. 285–318. ISBN 978-1-4614-5790-9.
4. Roth, E.P.; Orendorff, C.J. How electrolytes influence battery safety. *ECS Interface* **2012**, *21*, 45–49. [[CrossRef](#)]
5. Roth, E.P. Abuse response of 18650 Li-Ion cells with different cathodes using EC:EMC/LiPF6 and EC:PC:DMC/LiPF6 Electrolytes. *ECS Trans.* **2008**, *11*, 19–41. [[CrossRef](#)]

6. Hollas, J.M. *Modern Spectroscopy*, 3rd ed.; John Wiley & Sons Ltd.: Chichester, UK, 1996; p. 139. ISBN 0471965235.
7. Giurgis, G.A.; Zhu, X.; Durig, J.R. Conformational and structural studies of 1-fluoropropane from temperature dependant FT-IR spectra of rare gas solutions and ab initio calculations. *Struct. Chem.* **1999**, *10*, 445–461. [[CrossRef](#)]
8. Xiang, H.F.; Wang, H.; Chen, C.H.; Ge, X.W.; Guo, S.; Sun, J.H.; Hu, W.Q. Thermal Stability of LiPF₆-based Electrolyte and Effect of Contact with Various Delithiated Cathodes of Li-ion Batteries. *J. Power Sources* **2009**, *191*, 575–581. [[CrossRef](#)]
9. Lei, B.; Zhao, W.; Ziebert, C.; Uhlmann, N.; Rohde, M.; Seifert, H.J. Experimental analysis of thermal runaway in 18650 cylindrical Li-Ion cells using an accelerating rate calorimeter. *Batteries* **2017**, *3*, 14. [[CrossRef](#)]
10. Barai, A.; Uddin, K.; Chevalier, J.; Chouchelamane, G.H.; McGordon, A.; Low, J.; Jennings, P. Transportation safety of lithium iron phosphate batteries—A feasibility study of storing at very low states of charge. *Sci. Rep.* **2017**, *7*, 5128. [[CrossRef](#)]
11. Eshetu, G.G.; Bertrand, J.-P.; Lecocq, A.; Grugeon, S.; Laruelle, S.; Armand, M.; Marlair, G. Fire behavior of carbonates-based electrolytes used in Li-ion rechargeable batteries with a focus on the role of the LiPF₆ and LiFSI salts. *J. Power Sources* **2014**, *269*, 804–811. [[CrossRef](#)]
12. Lecocq, A.; Eshetu, G.G.; Grugeon, S.; Martin, N.; Laruelle, S.; Marlair, G. Scenario-based prediction of Li-ion batteries fire-induced toxicity. *J. Power Sources* **2016**, *316*, 197–206. [[CrossRef](#)]
13. Bergström, U.; Gustafsson, Å.; Häggglund, L.; Lejon, C.; Sturk, D.; Tengel, T. *Vented Gases and Aerosol of Automotive Li-ion LFP and NMC Batteries in Humidified Nitrogen Under Thermal Load*; Försvarets Forskningsinstitut FOI-R-4166—SE; Försvarets Forskningsinstitut: Umeå, Sweden, 2015.
14. Abert, M. Analysis of gases emitted in safety events. In *Electrochemical Powers Sources: Fundamentals, Systems, and Applications. Li-Battery Safety*; Garche, J., Brandt, K., Eds.; Elsevier: Amsterdam, The Netherlands, 2019; pp. 196–215. ISBN 978-0-444-63777-2.
15. Yang, H.; Zhuang, G.V.; Ross, P.N., Jr. Thermal stability of LiPF₆ Salt and Li-ion battery electrolytes containing LiPF₆. *J. Power Sources* **2006**, *161*, 573–579. [[CrossRef](#)]
16. Kawamura, T.; Okada, S.; Yamaki, J.I. Decomposition reaction of LiPF₆-based electrolytes for lithium ion cells. *J. Power Sources* **2006**, *156*, 547–554. [[CrossRef](#)]
17. Wilken, S.; Treskow, M.; Scheers, J.; Johansson, P.; Jacobsson, P. Initial stages of thermal decomposition of LiPF₆-based lithium ion battery electrolytes by detailed Raman and NMR spectroscopy. *RSC Adv.* **2013**, *3*, 16359–16364. [[CrossRef](#)]
18. Hammami, A.; Raymond, N.; Armand, M. Lithium-ion batteries: Runaway risk of forming toxic compounds. *Nature* **2003**, *42*, 635–636. [[CrossRef](#)] [[PubMed](#)]
19. Sun, J.; Li, J.; Zhou, T.; Yang, K.; Wei, S.; Tang, N. Toxicity, a serious concern of thermal runaway from commercial Li-ion battery. *Nano Energy* **2016**, *27*, 313–319. [[CrossRef](#)]
20. Sturk, D.; Häggglund, L.; Lejon, C.; Tengel, T.; Gustafsson, Å. Analysis of emitted gases from Li-ion LFP and NMC batteries at elevated temperatures. In *Proceedings of the EVS29 Symposium, Montreal, QC, Canada, 19–22 June 2016*.
21. Koch, S.; Birke, K.P.; Kuhn, R. Fast thermal runaway detection for Lithium-ion cells in large scale traction batteries. *Batteries* **2018**, *4*, 16. [[CrossRef](#)]
22. Truchot, B.; Fouillen, F.; Collet, S. An experimental evaluation of toxic gas emissions from vehicle fires. *Fire Saf. J.* **2018**, *97*, 111–118. [[CrossRef](#)]
23. Larsson, F.; Andersson, P.; Blomqvist, P.; Mellander, B.-E. Toxic fluoride gas emissions from lithium-ion battery fires. *Sci. Rep.* **2017**, *7*, 10018. [[CrossRef](#)] [[PubMed](#)]
24. Eriksson, T. (International Association of Fire and Rescue Services (CTIF), Karlstad, Sweden). Personal communication, 2019.
25. Andersson, P.; Blomqvist, P.; Loren, A.; Larsson, F. Using FTIR to determine toxic gases in fires with Li-ion batterie. *Fire Mater.* **2016**, *40*, 999–1015. [[CrossRef](#)]
26. Scanlon, J.T.; Willis, D.E. Calculation of flame ionization detector relative response factors using the effective carbon number concept. *J. Chromatogr. Sci.* **1985**, *23*, 333–340. [[CrossRef](#)]



See discussions, stats, and author profiles for this publication at: <https://www.researchgate.net/publication/350175794>

Particles Released by Abused Prismatic Ni-rich Automotive Lithium-ion Batteries

Article in *WSEAS Transactions on Systems and Control* · March 2020

DOI: 10.37394/23203.2020.15.4

CITATION

1

READS

104

5 authors, including:



Hewu Wang
Tsinghua University

130 PUBLICATIONS 3,492 CITATIONS

[SEE PROFILE](#)



Weifeng Li
Jilin University

28 PUBLICATIONS 451 CITATIONS

[SEE PROFILE](#)



Cheng Li
Tsinghua University

11 PUBLICATIONS 108 CITATIONS

[SEE PROFILE](#)

Some of the authors of this publication are also working on these related projects:



Adsorption [View project](#)



fuel cell hybrid tram [View project](#)

Particles released by abused prismatic Ni-rich automotive lithium-ion batteries

HEWU WANG

State Key Laboratory of Automotive Safety and Energy
Tsinghua University
Haidian District, Beijing
P. R. CHINA
wanghw@tsinghua.edu.cn

YAJUN ZHANG

State Key Laboratory of Automotive Safety and Energy
Tsinghua University
Haidian District, Beijing
P. R. CHINA
zhyj032469@163.com

WEIFENG LI

State Key Laboratory of Automotive Safety and Energy
Tsinghua University
Haidian District, Beijing
P. R. CHINA
lwfsearch@126.com

CHENG LI

State Key Laboratory of Automotive Safety and Energy
Tsinghua University
Haidian District, Beijing
P. R. CHINA
2317351211@qq.com

MINGGAO OUYANG

State Key Laboratory of Automotive Safety and Energy
Tsinghua University
Haidian District, Beijing
P. R. CHINA
ouymg@tsinghua.edu.cn

Abstract: The particulate matter released by lithium-ion batteries during eruption and combustion caused by thermal runaway may contain heavy metal pollution elements. The aim of this study is to reveal four heavy metal element content and size distribution of particulate matter released by abused prismatic Ni-rich automotive lithium-ion batteries. A fully charged commercial 50 Ah $\text{Li}(\text{Ni}_{0.6}\text{Mn}_{0.2}\text{Co}_{0.2})\text{O}_2$ cell was triggered by

heating in a sealed chamber at nitrogen environment. The particulate matter with size being below $500\ \mu\text{m}$ were divided into three samples using sieves. Four soil pollution elements, including nickel, copper, zinc, chromium, were detected, and sizes were analyzed. The results show that all these four elements are found, and nickel and copper are found in all samples. Among the four elements, Ni had the largest mass percentage, followed by Cu, Zn and Cr. These particulate matter account for 1.7% of the cell mass, with the minimum size and median size being approximately $1.45\ \mu\text{m}$ and $162.9\ \mu\text{m}$. The element content reveals the pollution from LIBs and the size distribution provides a basis for the design of the particle filter pore.

Key-Words: lithium-ion batteries, settleable particulate matter, heavy metal element, particle size

Received: September 22, 2019. Revised: February 1, 2020. Accepted: February 13, 2020. Published: February 28, 2020.

1 Introduction

In recent years, regulatory restrictions on emissions and environmental awareness have prompted a surge in zero or partial-aero emission electric vehicles, which including battery electric vehicles (BEV) and plug-in hybrid electric vehicles (PHEV), and have led to reductions in the usage of traditional petroleum internal combustion engine vehicles, which including gasoline and diesel vehicles [1-5]. Electric car deployment has been growing rapidly over the past ten years, with the global stock of electric passenger cars passing 5 million in 2018, an increase of 63% from the previous year [6].

However, when a fire occurs in a BEV or PHEV, similar to a traditional petroleum vehicle, it also causes pollution to the environment [7-9]. Amandine. et al [7] compared the fire consequences of BEV and the corresponding gasoline vehicle and found that the cumulative masses of carbon dioxide (CO₂), carbon monoxide (CO), total hydrocarbons, nitric oxide (NO), nitrogen dioxide (NO₂), hydrogen chloride (HCl) and hydrogen cyanide (HCN) were similar for both types of vehicles. The types of toxic gases released by BEV and gasoline vehicle in fires were similar, including CO, HCl and HF [7-9], but cumulative mass of HF was higher for BEV due to the combustion of the Li-ion battery pack [7].

Because the main difference between electric vehicles and petroleum vehicles is the power system, it is necessary to focus on the environmental pollution of electric vehicle power systems in the event of a fire accident. After many years of development, lithium-ion batteries (LIBs) have become increasingly acceptable as one of the main electricity storage sources in vehicles due to their largely increasing in energy density, calendar or cycle life, and reliability [10].

The LIB releases various gases during the eruption and combustion processes [11-19]. These gases primarily form from the decomposition of negative solid-electrolyte interface film [11, 12], reactions between the anodes and electrolytes [11], decomposition of cathode materials [11, 13-15], decomposition of electrolytes [16], decomposition of binders [17], and reactions between various material decomposition products. Somandepalli et al. [18] studied variations in the composition, concentration, and volume of these gas during eruption under different SOC. They placed the battery in a sealed 6-L chamber filled with argon

(Ar) and heated it until vent. The results showed that gases erupted mainly included carbon dioxide (CO₂), carbon monoxide (CO), hydrogen (H₂), and hydrocarbons with different numbers of carbon atoms such as methane (CH₄), ethylene (C₂H₄), and ethane (C₂H₆). As the SOC increased, the CO₂ concentration decreased, the CO and CH₄ concentrations increased, the H₂ concentration remained relatively unchanged, and total hydrocarbons varied between 20% and 30%. Perrine et al. [19] found CO₂, CO, THC, NO, SO₂, HCl and HF in the emissions of 2.9 Ah pouch type batteries during combustion.

Regarding the PM released by LIBs, researchers are more concerned about their impact on fire. With gases, these PM are released from the inside of the battery with the eruption flow. These high-temperature PM are often accompanied by sparks with temperatures as high as 1,200°C [20]. Once the combustible mixture and high-temperature PM have been simultaneously released into the external environment and exposed to oxygen, fire or even explosion could occur according to the combustion theory [20]. In addition, because high-temperature particulate has large kinetic energy, it is easily scattered and exposed to combustible materials, making it vulnerable to catching fire.

Few studies reported soil pollution caused by particulate matter released by lithium-ion batteries [21,22]. Soil environmental quality affects directly the quality of arable land, the safety of agricultural products and the health of the human environment. Soil heavy metal pollution has been one of the major environmental issues facing countries around the world [23-25]. As soil environmental issues become more prominent and public awareness of environmental protection increases, China's work on soil environmental protection is getting heavier. National Survey of Soil Pollution in China's Ministry of Ecology and Environment reported that heavy metal pollution elements in China's soil mainly include nickel (Ni), copper (Co), zinc (Zn), chromium (Cr), cadmium (Cd), mercury (Hg), lead (Pb) and arsenic (As) [26, 27].

Since the LIB material contains a variety of metal elements [9], such as nickel (Ni), Co, manganese (Mn) and other metal elements. The particulate matter (PM) released by lithium-ion batteries (LIBs) during eruption and combustion may contain these elements and pollute the soil. For example, when an electric car fire caused by thermal

runaway of a LIB occurs, PM vented by the battery during the firefighting process may be released directly or with the water to the surrounding environment and deposited in the soil. They can be enriched thousands of times by biomagnification of the food chain before they finally enter the human body [28].

LIBs probably will be one of heavy metal soil pollution element sources in the future due to their large-scale application on vehicles and an increasing number of electric vehicle fires.

In our previous research [21, 22], the composition of the PM released by a LIB was given in a relatively macroscopic view. A fully charged commercial 50 Ah $\text{Li}(\text{Ni}_{0.6}\text{Mn}_{0.2}\text{Co}_{0.2})\text{O}_2$ cell was triggered by heating in a sealed chamber. The main elements were carbon, nickel, cobalt, etc. The content of metallic elements was approximately 40%. The emissions also contained potentially toxic elements, including aluminum, lithium, fluorine, etc. However, the content of soil pollution elements in the small particles was not given. Small particles are more likely to enter the natural environment and it is more difficult to suppress them. Therefore, soil pollution elements in small particles need to be studied. In addition, the common method of trapping PM is to use microporous filtration, so it is necessary to study the size of these PM.

It should be noted that the release of particulate matter by lithium-ion batteries is an accidental event, and there is a large difference in the magnitude of continuous release of particulate matter under normal operating conditions of traditional vehicles.

The aim of this study is to reveal four heavy metal element content and size distribution of vent PM from abused prismatic Ni-rich automotive lithium-ion batteries. With this in mind, a 50 Ah, 3.65 V, commercial prismatic LIB cell with lithium nickel manganate cobalt (NMC) oxide cathode at 100% SOC was used, and it was placed in a sealed chamber and heated by a 1 kW heater to trigger the thermal runaway. At the termination of the experiment, the PM scattered throughout the sealed chamber during the battery eruption caused by thermal runaway were collected. The settleable PM with size below 500 μm were divided into three samples—a, b and c—with sizes ranging from 0–50 μm , 50–100 μm , and 100–500 μm , respectively. The Ni, Co, Zn, and Cr content and size distribution were measured. These results will reveal the potential harm of the settleable PM released by LIBs to the soil.

2 Experimental Procedure

2.1 Experimental setup

A commercial cell based on NMC cathodes was tested, which is especially for electric automotive. According to the manufacturer's data, the cell nominal capacity and voltage is 50 Ah and 3.65 V, respectively. More information is shown in Table 1. The cell was composed of a lid, a shell and a core. The safety valve, tab and terminal of the cell were installed on the lid. The cathode, separator, and anode were curled to form the core. The cathode was composed of a cathode active material and a cathode current collector. The cathode active material of the cell in this research was mainly $\text{Li}(\text{Ni}_{0.6}\text{Mn}_{0.2}\text{Co}_{0.2})\text{O}_2$, and the current collector was an aluminum foil. Similarly, the anode was composed of an anode active material and the anode current collector. The anode active material of the cell in this research was mainly graphite, and the current collector was a copper foil.

Table 1 Detailed technical specifications of the test cell.

Parameters	Specifications
Cell mass (g)	900
Nominal capacity (Ah)	50
Nominal voltage (V)	3.65
Minimum voltage (V)	2.75
Maximum voltage (V)	4.25
Cathode active material	$\text{Li}(\text{Ni}_{0.6}\text{Mn}_{0.2}\text{Co}_{0.2})\text{O}_2$
Cathode coating thickness (μm)	61
Anode active material	Graphite
Anode coating thickness (μm)	73
Cathode current collector	Aluminum foil
Cathode current collector thickness (μm)	16
Anode current collector	Copper foil
Anode current collector thickness (μm)	10
Shell Material	Aluminium alloy

The thermal runaway was triggered by a heater. During the experiment, the cell was placed above the heater and fixed, as shown in Fig. 1. In order to ensure safety and collect the settleable PM released by the cell, the thermal runaway experiment was conducted in a self-made sealed chamber. Using this device, we have conducted studies on the eruption process, the identifications of LIB gas emissions at inert atmosphere and LIB particulate matter emissions at air atmosphere [21, 22, 29]. The air in

the chamber can be replaced by nitrogen (N₂). To observe the vent PM during thermal runaway of the cell, a visualization window was installed in the wall of the sealed chamber. The outer surface of the sealed chamber was covered with insulating cotton to reduce heat transfer.

2.2 Experimental methods

The cell SOC for this research was set to 100%, which is the most typical operation. The cell was fully charged under standard conditions before the test was started. The experiment consisted of the following steps. The cell underwent an open circuit voltage check, was charged to the selected SOC, then placed on top of the heater and fixed with hard refractory cottons. The heater was attached inside the sealed chamber and then the air in the chamber was replaced with N₂. The thermal runaway experiment was initiated by turning on the heater. The cell inside the chamber was heated with a heating power of 5 kW. The cell transitioned into thermal runaway and PM were released along with the ejection flow.

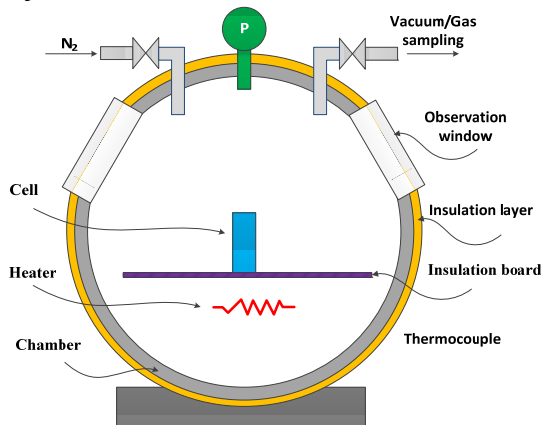


Fig. 1. Schematic diagram of the experimental setup [21, 22, 29].

All settleable PM in the chamber were collected after the thermal runaway reaction. The PM with size being below 500 μm was selected by a sieve. To get the mass distribution, these PM were divided into 5 samples by filters with mesh diameter of 30 μm, 50 μm, 100 μm, and 250 μm, as shown in Fig. 2. Then they were divided into three samples (a, b, and c), with the sizes ranging from 0–50 μm, 50–100 μm, and 100–500 μm to detect the element content. It should be noted that the threshold for each sample is determined based on the classification of soil particles [30], shown as Table 2. The size below 50 μm was defined as silt and clay, between 50–100 μm was defined as very fine sand, between 100–250 μm was defined as fine

sand, and between 250–500 μm was defined as medium sand.

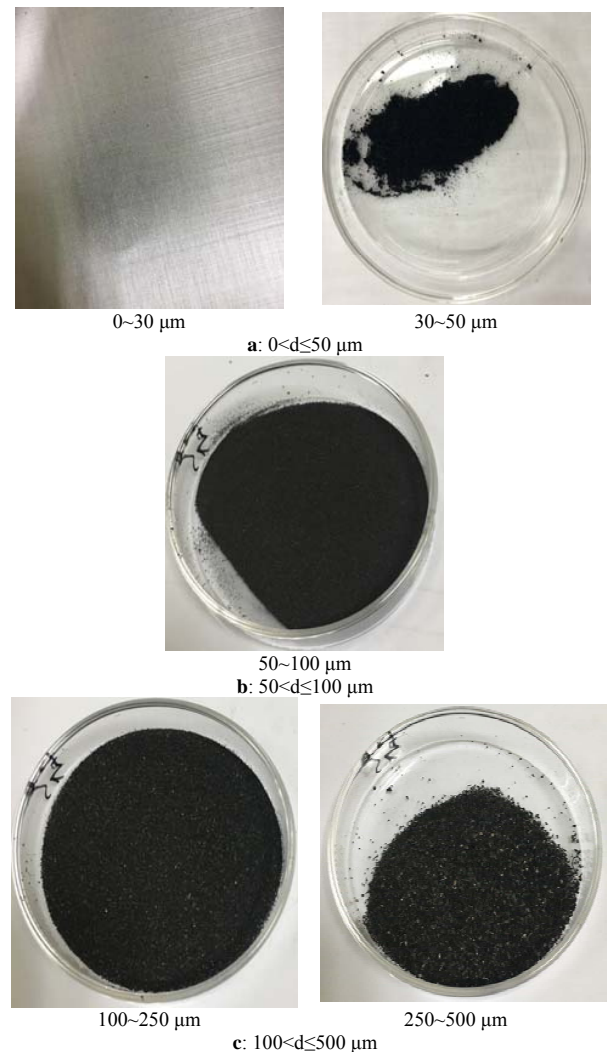


Fig. 2. Photograph of samples.

Table 2 Partial soil particle classification method.

Size interval (μm)	Classification
<50	Silt and clay
50~100	Very fine sand
100~250	Fine sand
250~500	Medium sand

The mass was detected by a million-point electronic balance (Sartorius, Germany; BSA224S). The particle size distribution was analyzed by a Malvern particle size analyzer (Malvern Panalytical, United Kingdom; Hydro2000MU). The Ni, Co, Zn, and Cr content were detected by an inductively coupled plasma mass spectrometer (Thermo Fisher Scientific., America; ICP-6000). The inductively coupled plasma mass spectrometry are widely used methods and have high precision. The Analysis and detection process were shown as Fig. 3.

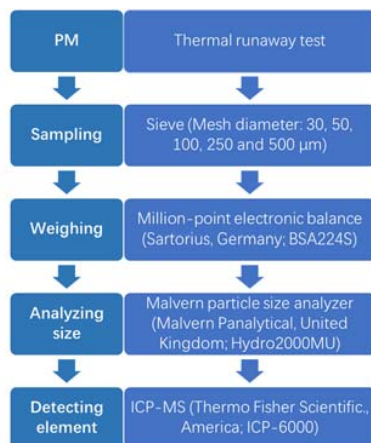


Fig. 3. Analysis and detection process.

3 Results and Discussion

3.1 Element Content

Table 3 shows the content of the four elements, including Ni, Cu, Zn and Cr, in these three samples. The role of the four elements in the battery is as follows [31]. Ni mainly comes from Li (Ni_{0.6}Mn_{0.2}Co_{0.2})O₂, which is the cathode material of the battery. This positive electrode material is a layered crystal. During the charging process, lithium ions can be de-intercalated from the crystal, and the metal ions in the positive electrode material undergo an oxidation reaction due to the principle of electrical neutrality, and the valence state increases. During discharge, lithium ions are released from the negative electrode to the positive electrode and re-embedded in the crystal. At the same time, the metal ions undergo a reduction reaction and the valence state decreases. The development of positive electrode materials is to increase nickel, because increasing the content of Ni helps to increase the capacity of the battery, and Ni is cheaper. Cu comes mainly from the negative current collector of the battery. The current collector is the base metal used to attach the active material. The current collector is in contact with the active material, and its function is to collect the current generated by the active material and output the current to the outside. The negative electrode current collector generally uses copper foil. Copper foil is generally required to have electron conduction and very stable electrochemical characteristics. Because the organic electrolyte used in lithium ion batteries is highly corrosive, copper foils are required to have strong corrosion resistance. In addition, the copper foil surface must ensure good adhesion to the negative electrode

material, and the tensile strength must be sufficiently high. Zn and Cr are mainly derived from additives. The role of additives is mainly to improve battery performance.

To describe the contents of these elements in each sample clearly, these four elements are classified according to their mass percentages, i.e. the overall mass percentage, from high to low, above 1% as shown in Fig. 4(a), and below 1% as shown in Fig. 4(b).

As shown in Fig. 4(a), the constituent elements with an overall mass percentage of more than 1% include Ni, and Cu, which account for 41.422%, and 6.537%, respectively. The content of nickel is about 7 times that of copper. As shown in Fig. 4(b), the constituent elements with an overall mass percentage below 1% are Zn, and Cr, and both corresponding percentages are 0.002%.

Table 3 Elemental mass percentage in each sample.

	Overall	a	b	c
	0<d≤500	0<d≤50	50<d≤100	100<d≤500
Ele.	(%)	(%)	(%)	(%)
Ni	41.422	41.725	38.050	44.142
Cu	6.537	11.208	6.502	5.776
Zn	0.002	0.000	0.005	0.000
Cr	0.002	0.000	0.001	0.003

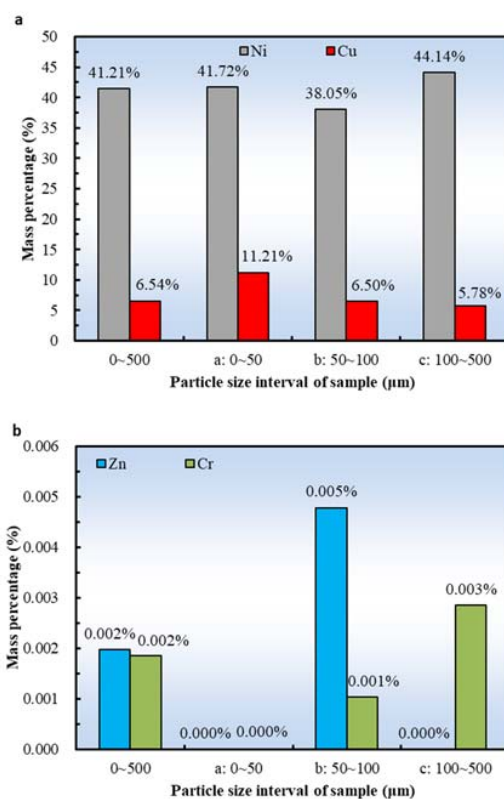


Fig. 4. Elemental composition of each sample.

Among the four samples, sample a has the smallest size of PM, followed by samples b and c, and sample d is the largest. The content of each element has different trend with increasing particle size. As the particle size increases, the Ni content increases first and then increases, the Cu content increases monotonically. The Zn has an opposite trend with Ni, and Cr has an opposite trend with Cu with increasing particle size, as shown in Fig. 4.

These PM are mainly derived from the internal material of the cell, so the correspondence between the PM and cell parts can be established depending on the element source. Ni and Cu are mainly from the cathode active material and anode current collector, resulting that they have relatively high mass percentage in the PM. Zn and Cr are from the cathode material additives, so their contents are lower than those of Ni and Cu.

It should be noted that soil polluted by heavy metals will affect crop growth and reduce production [27]. Crops may absorb and enrich certain pollutants and affect the quality of agricultural products. The loss of China's annual agricultural output reduction caused by heavy metal soil pollution reaches 20 billion yuan [27]. Soil pollution affects the survival and reproduction of plants, soil animals and microorganisms, and endangers normal soil ecological processes and ecosystem service functions [27]. Pollutants in the soil may undergo transformation and migration, and then enter surface water, groundwater, and the atmospheric environment, affecting the quality of surrounding environmental media. In addition, these elements can be enriched thousands of times by biomagnification of the food chain before they finally enter the human body [28]. Although elements such as Ni, Cu, Cr and Zn are necessary elements for plant growth and human nutrition, they can also cause harm to animals and humans at high concentrations [32]. The higher incidence of liver cancer in the Yangtze River Delta region of China is related to the high levels of Cu and Zn in soil, water and food [33]. The incidence of esophageal cancer in Henan, Shanxi, and other places in China is also related to the high content of Cu, Zn, V, and Zr in the soil of the affected area. There is a clear relationship between trace element imbalances and high incidence of regional tumors [32].

Therefore, the PM released by the LIB after the thermal runaway must be collected and treated to avoid entering the ecological environment, such as water and soil. It is necessary to capture these PM. One of the methods is to use a particle filter. The pore size of the particle filter needs to be determined

based on the size distribution of the particle size, shown as in 3.2 section.

3.2 Size Distribution

Fig. 5 shows variation in mass vs. particle size interval. The total mass of these PM is 14.57 g, accounting for 1.67% of the cell mass, wherein PM with size being 0~30 μm , 30~50 μm , 50~100 μm , 100~250 μm , and 250~500 μm accounted for 0.005%, 8.477%, 41.288%, 34.456% and 15.774% respectively. The results show that if a filter with a pore size below 100 μm is used, more than 50% in mass of the particle with size below 500 μm will be filtered.

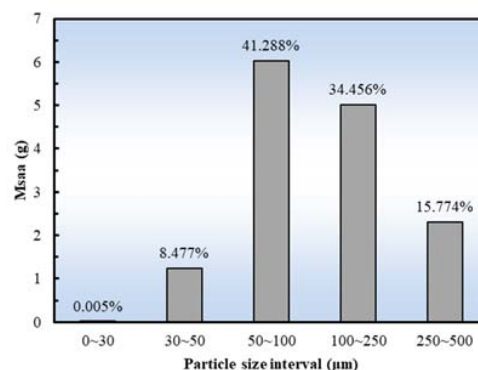


Fig. 5. Schematic diagram of the experimental setup.

Fig. 6 shows the particle size distribution of the settleable particle with size below 500 μm . The measuring lower range is 0.1 μm , and the minimum diameter of the particle is 1.45 μm . As the particle equivalent particle size increases, the particle volume first increases, then decreases, peaking at 198.5 μm of the equivalent particle size. The D10 value is 43.8 μm , i.e., PM with an equivalent particle diameter of less than 43.8 μm account for 10% of the total volume of the PM. Similarly, D50 and D90 are 162.9 μm and 485.6 μm , respectively. The above results indicate that 90%, 50%, and 10% of the PM can be filtered when sample a is filtered using filter holes with diameters of 485.6 μm , 162.9 μm , and 43.8 μm , respectively.

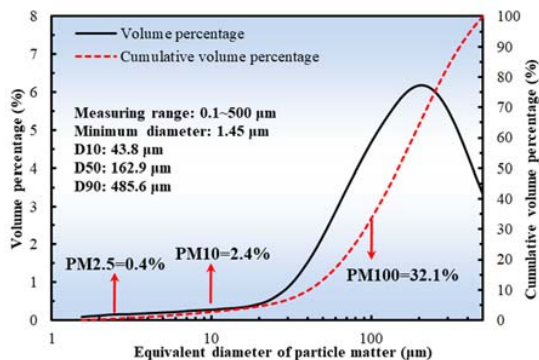


Fig. 6. Schematic diagram of the experimental setup.

3.3 Contribution of this research

The academic and engineering significance of the research are as follows:

There are currently very few literatures reporting the characteristics of battery PM emissions. This study gives and four heavy metal element content, the mass distribution and particle-size distribution of the settleable PM emissions with size below 500 µm. The results of the study tell us that electric vehicles not only have safety problems, such as fire, but also potential harm to the ecological environment. This is because once the soil is contaminated, the surrounding farmland, animals, and people will be harmed, and the contaminated soil will be difficult to treat. In addition, once these heavy metal-containing particles enter the water environment, they are more harmful due to the fluidity of the water. Therefore, in the long run, the legislative branch should pay attention to this. This study provides a theoretical basis for further standardizing electric vehicle regulations and can also provide guidance for the rational disposal of lithium-ion battery particles.

4 Conclusions

The elemental composition and size distribution of the settleable solid PM with size being below 500 µm released by a 50 Ah lithium-ion battery with an NMC cathode during thermal runaway were studied. The main conclusions are summarized as follows:

1) Among the four elements, Ni had the largest mass percentage, followed by Cu, and then Zn and Cr, with corresponding mass percentages of 41.422%, 6.537%, 0.002% and 0.002%, respectively.

2) The mass percentage of each element had different trend with increasing particle size.

3) The mass of PM with size being below 500 µm was 14.57 g, accounting for 1.67% of the cell mass, wherein PM with size being 0~30 µm, 30~50 µm, 50~100 µm, 100~250 µm, and 250~500 µm accounted for 0.005%, 8.477%, 41.288%, 34.456% and 15.774% respectively.

4) The minimum diameter of the settleable PM was 1.45 µm. The particle volume first increased, then decreased with increasing particle size, peaking at 198.5 µm. The D10, D50 and D90 value was 43.8 µm, 162.9 µm and 485.6 µm, respectively.

Acknowledgment

This research was supported by the Ministry of Science and Technology of the People's Republic of China under the Grant No. 2016YFE0102200 and 2019YFE0100200, the China Postdoctoral Science Foundation under the Grant No. 2018M631464, and the National Natural Science Foundation of China under the Grant No. U1564205.

References:

- [1] Xuebing Han, Languang Lu, Yuejiu Zheng, Xuning Feng, Zhe Li, Jianqiu Li, Minggao Ouyang. A review on the key issues of the lithium ion battery degradation among the whole life cycle. *eTransportation* 1 (2019) 100005.
- [2] Minggao Ouyang. Meet the new era of new energy intelligent electric vehicles. *Science and technology review* 2019, 37 (7): 1-1.
- [3] Graham Mills, Iain MacGill. Assessing electric vehicle storage, flexibility, and distributed energy resource potential. *Journal of Energy Storage*, 2018, 17: 357-366.
- [4] Xiao Shi, Jian Pan, Hewu Wang, Hua Cai. Battery electric vehicles: What is the minimum range required? *Energy* 2019, 166: 352-358.
- [5] Korakianitis T, Namasivayam AM, Crookes RJ. Natural-gas fueled spark-ignition (SI) and compression-ignition (CI) engine performance and emissions. *Prog Energy Combust Sci* 2011, 37: 89-112.
- [6] IEA, Global Electric Vehicle (EV) Outlook 2019. <https://www.iea.org/reports/global-ev-outlook-2019/>.
- [7] Amandine Lecocq, Marie Bertana, Benjamin Truchot, Guy Marlair. Comparison of the fire consequences of an electric vehicle and an internal combustion engine vehicle. 2. *International Conference on Fires In Vehicles -*

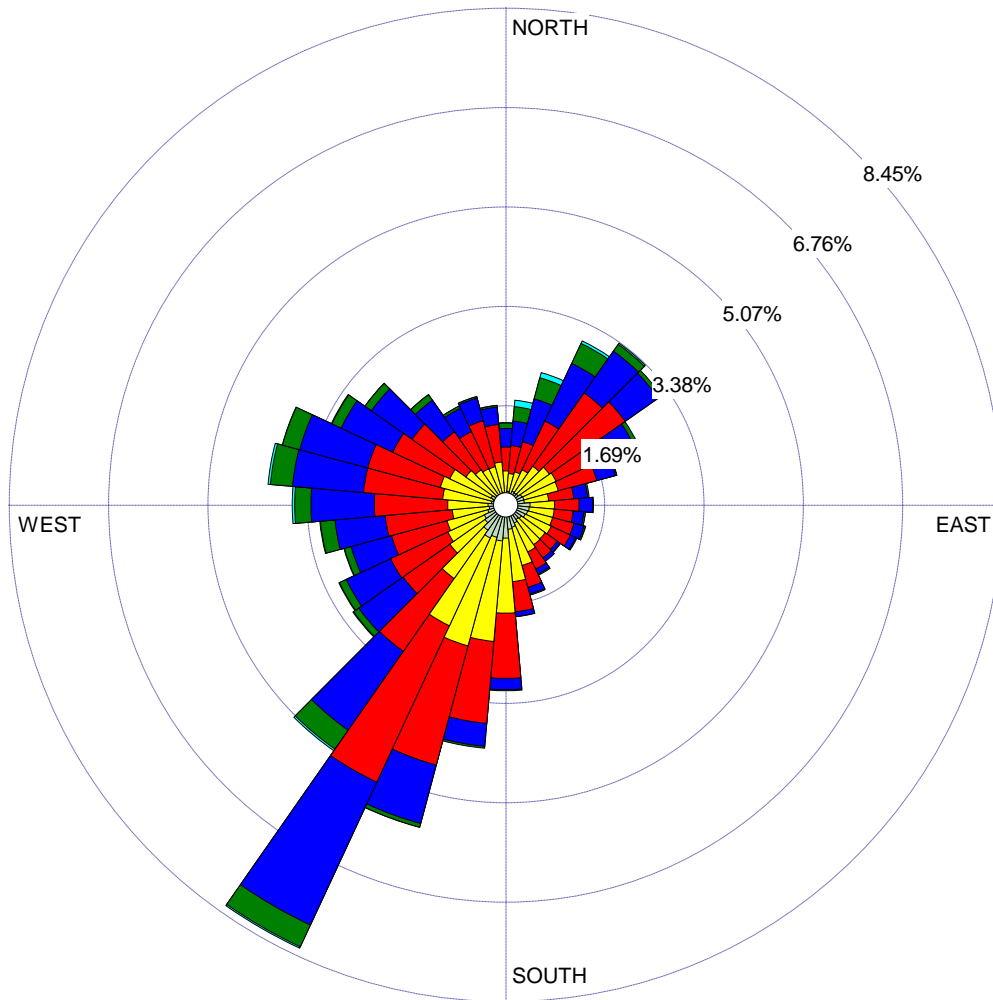
- FIVE 2012, Sep 2012, Chicago, United States. SP Technical Research Institute of Sweden. Boras, pp.183-194, 2012.
- [8] Masashi Takahashi, Masayuki Takeuchi, Kiyotaka Maeda, and Shouma Nakagawa. Comparison of Fires in Lithium-Ion Battery Vehicles and Gasoline Vehicles, 2014-01-0428.
- [9] Yajun Zhang, Hewu Wang, Xuning Feng, Minggao Ouyang, Anjian Zhou, Ling Su, Huiqian Yang. Research progress on thermal runaway combustion characteristics of power lithiumion batteries, *Journal of Mechanical Engineering*, 55(20): 17-27.
- [10] Z. Wang, F. Sun, P. Liu, Electric vehicle battery systems, China machine press, Beijing, 2017.
- [11] R. Spotnitz, J. Franklin, Abuse behavior of high-power, lithium-ion cells, *J. Power Sources* 113 (2003) 81-100.
- [12] M.N. Richard, J.R. Dahn, Accelerating rate calorimetry study on the thermal stability of lithium intercalated graphite in electrolyte. I. Experimental, *Fuel Energ. Abs.* 41 (1999) 2068-2077.
- [13] H. Wang, A. Dang, K. Huang, Oxygen evolution in overcharged $\text{Li}_x\text{Ni}_{1/3}\text{Co}_{1/3}\text{Mn}_{1/3}\text{O}_2$ electrode and its thermal analysis kinetics, *Hubei Elec. Power* 29 (2011) 1583-1588.
- [14] D.D. MacNeil, J.R. Dahn, The reaction of charged cathodes with nonaqueous solvents and electrolytes: I. $\text{Li}_0.5\text{CoO}_2$. *J. Electrochem. Soc.* 148 (2001) A1205-A1210.
- [15] Q. Wang, J. Sun, C. Chen, Thermal stability of delithiated with electrolyte for lithium-ion batteries, *J. Electrochem. Soc.* 154 (2007) A263-A267.
- [16] S.E. Sloop, J.K. Pugh, S. Wang, J.B. Kerr, K. Kinoshita, Chemical reactivity of PF_5 and LiPF_6 in ethylene carbonate/dimethyl carbonate solutions, *Electrochem. Solid St.* 4 (2001) 357-364.
- [17] A.D. Pasquier, F. Disma, T. Bowmer, A.S. Gozdz, G. Amatucci, J.M. Tarascon, Differential scanning calorimetry study of the reactivity of carbon anodes in plastic Li-ion batteries, *J. Electrochem. Soc.* 145 (1998) 472-477.
- [18] V. Somandepalli, K. Marr, Q. Horn, Quantification of combustion hazards of thermal runaway failures in lithium-ion batteries, *SAE Int. J. Alt. Power.* 3 (2014) 98-104.
- [19] Perrine Ribiere, Sylvie Grugeon, Mathieu Morcrette, Simeon Boyanov, Stphane Laruelle and Guy Marlair. Investigation on the fire-induced hazards of Li-ion battery cells by fire calorimetry. *Energy Environ. Sci.*, 2012, 5, 5271–5280.
- [20] T. Xu, S. Hui, Combustion Science, China machine press, Beijing, 2017.
- [21] Y. Zhang, H. Wang, W. Li, C. Li, Y. Ouyang, Size distribution and elemental composition of vent particles from abused prismatic Ni-rich automotive lithium-ion batteries. *J. Energy Storage* 26 (2019) 100991.
- [22] Y Zhang, H Wang, W Li, C Li. Quantitative identification of emissions from abused prismatic Ni-rich lithium-ion batteries. *eTransportation* 2 (2019) 100031.
- [23] PANDEY G, JAIN R, BUDHIRAJA R et al. Phytoremediation: an overview of metallic ion decontamination from soil[J]. *Applied Microbiology and Biotechnology*, 2014, 61(5-6): 405-412.
- [24] Dermont G, Bergeron, Mercier G M, Richer L M. Soil washing for metal removal: A review of physical/chemical technologies and field applications[J]. *Journal of Hazardous Materials*, 2008, 152(1):1-31.
- [25] Ping Chen, Yan Chen, Lu Bai. Environmental quality standards for soil and state of soil pollution in Japan [J] . *Environmental Monitoring in China* 20(4) (2004) 63-67.
- [26] Bulletin of National Survey of Soil Pollution [EB/OL]. (2014-04-17). <http://www.gov.cn/foot/site1/20140417/782bcb88840814ba158d01.pdf>.
- [27] G. Zhuang, Current situation of national soil pollution and strategies on prevention and control, *Soil and Ecological Environment Safety* 30 (4) (2015) 477-482.
- [28] J.Y. Hu, J.Y. Dai, Advance in studies on human distribution and toxic effects of perfluoroalkyl and polyfluoroalkyl substances, *Asian J. Ecotoxicol.* 8 (2013) 650-657.
- [29] H. Wang, Y. Zhang, C. Li, W. Li, M. Ouyang. Venting process of lithium-ion power battery during thermal runaway under medium state of charge, *Energy Storage Science and Technology* 8(6) (2019) 1043-1048.
- [30] Y. Lu, Soil Science, Beijing: China Agricultural Press, 2006.
- [31] Reiner Korthauer. Handbuch Lithium-Ionen-Batterien. Beijing: China machine press, 2018.
- [32] Taizhong Gao, Jingyin Li. Study on the heavy metal-contaminated soil and status of the treatment. *Soil and Environmental sciences* 8(2) (1999) 137-140.

- [33] Xiaonan Lu, Cifu Ment, Wanzhu Ma, Review on heavy metals, soil environment quality and food safety. Chinese Journal of Eeo-Agriculture 15(2) (2007) 197-200.

EXHIBIT 7

WIND ROSE PLOT:
Station #54769

DISPLAY:
**Wind Speed
 Direction (blowing from)**



WIND SPEED (m/s)

- >= 11.10
- 8.00 - 11.10
- 5.00 - 8.00
- 3.00 - 5.00
- 1.50 - 3.00
- 0.50 - 1.50

Calms: 1.38%

COMMENTS:

DATA PERIOD:
**Start Date: 1/1/2017 - 00:00
 End Date: 12/31/2021 - 23:59**

COMPANY NAME:
PN01847-0001

MODELER:
ALL4

CALM WINDS:
1.38%

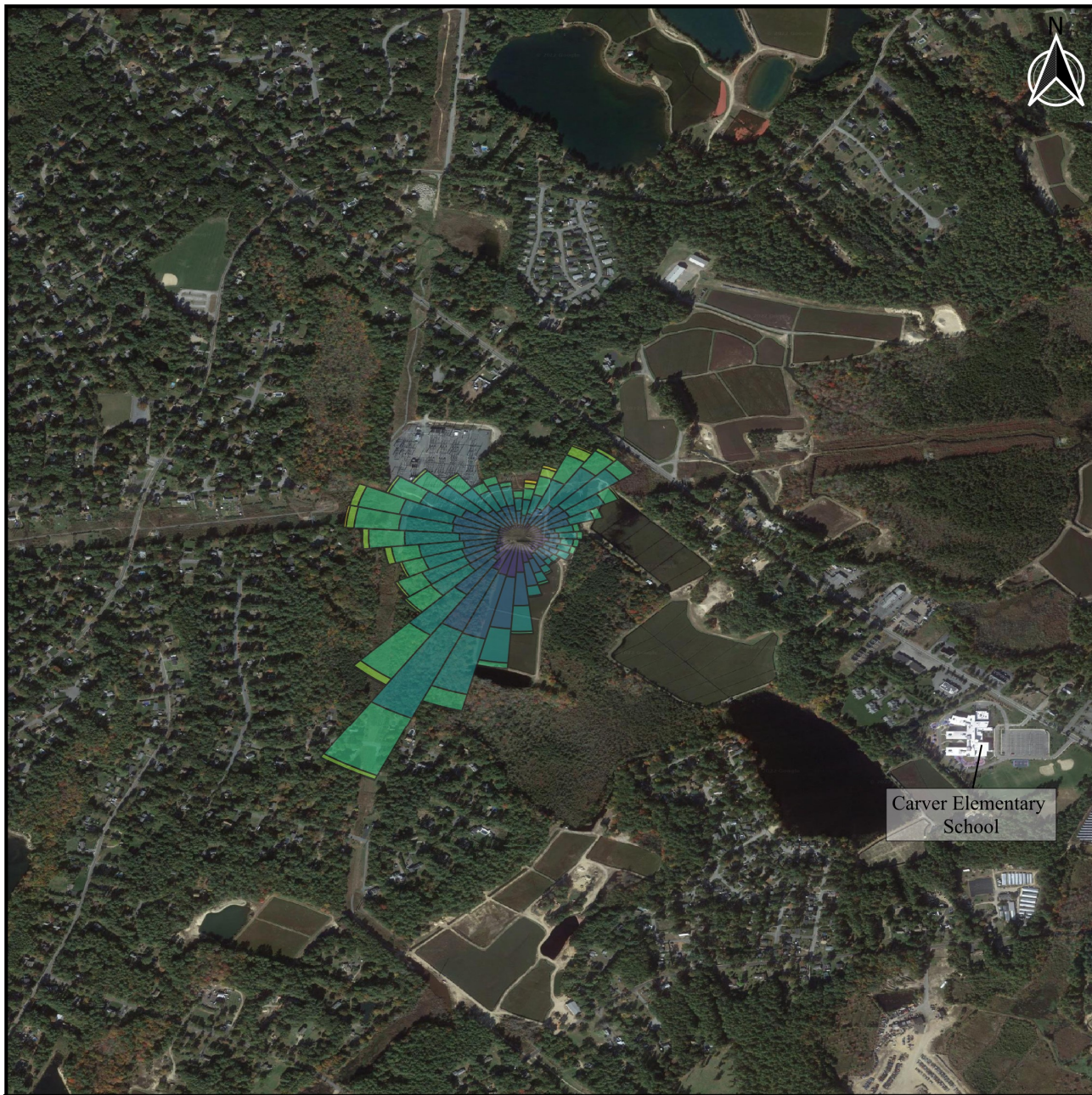
TOTAL COUNT:
43561 hrs.

AVG. WIND SPEED:
3.90 m/s

DATE:
9/7/2022

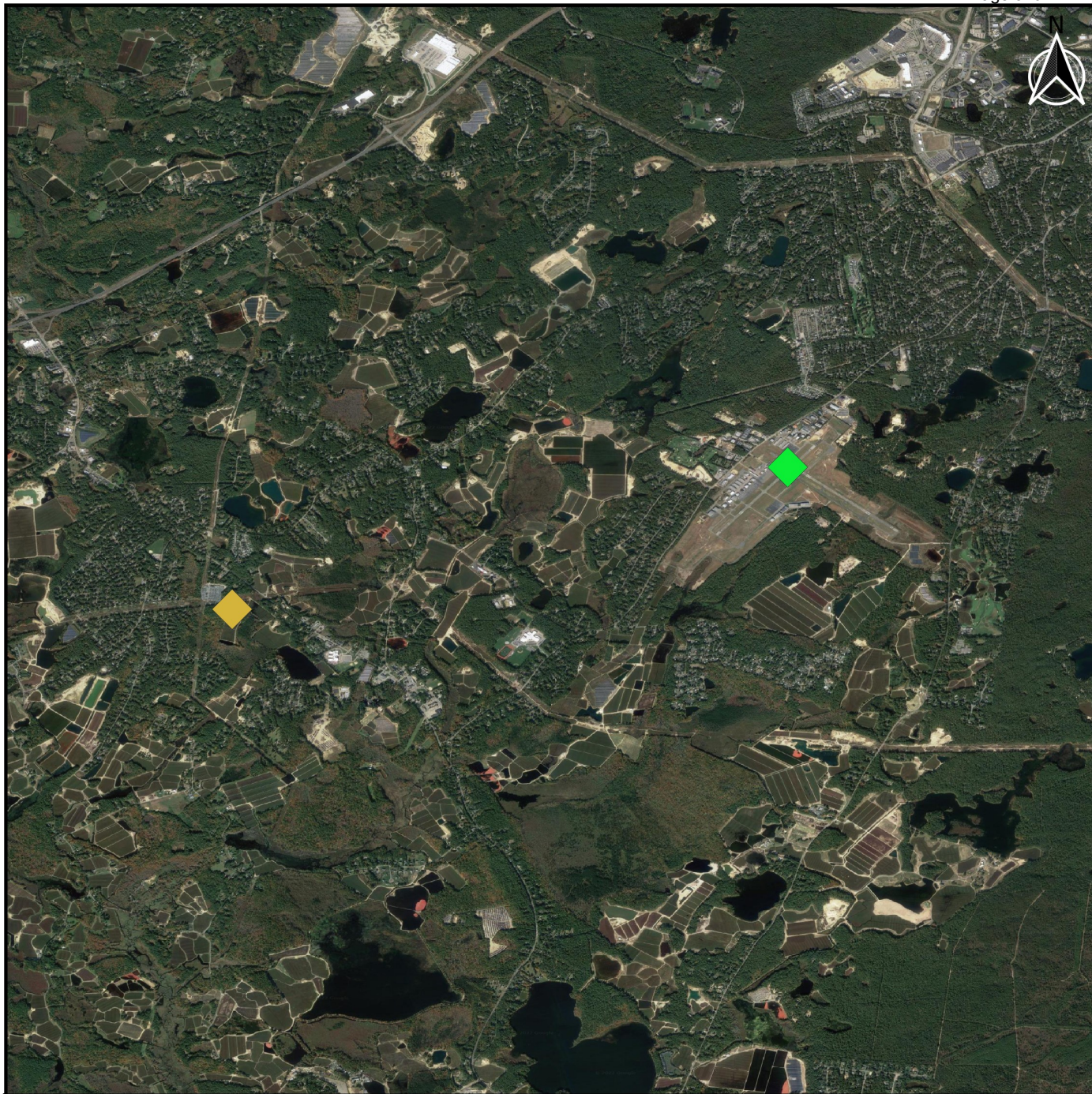
PROJECT NO.:
Carver, MA

EXHIBIT 8



<p>Legend</p> <p>Wind Speed (mph)</p> <table border="0"> <tr> <td></td> <td>1.1 - 4.7</td> <td></td> <td>8.1 - 12.8</td> <td></td> <td>19.7 - 24.8</td> </tr> <tr> <td></td> <td>4.7 - 8.1</td> <td></td> <td>12.8 - 19.7</td> <td></td> <td>>= 24.8</td> </tr> </table> <p>Calms: 1.38% Average Wind Speed: 8.7 mph</p> <p>1,000 0 1,000 2,000 ft</p>		1.1 - 4.7		8.1 - 12.8		19.7 - 24.8		4.7 - 8.1		12.8 - 19.7		>= 24.8	<p>Cranberry Point Energy Storage Wind Rose</p>	
		1.1 - 4.7		8.1 - 12.8		19.7 - 24.8								
	4.7 - 8.1		12.8 - 19.7		>= 24.8									
<p>Save the Pine Barrens Plymouth, MA</p>		<table border="1"> <tr> <td>DRAWN BY: C.Q.</td> <td>CHECKED BY: J.H.</td> </tr> <tr> <td>DATE: September 2022</td> <td>PROJ NO.: 01847-0001.00</td> </tr> </table>	DRAWN BY: C.Q.	CHECKED BY: J.H.	DATE: September 2022	PROJ NO.: 01847-0001.00								
DRAWN BY: C.Q.	CHECKED BY: J.H.													
DATE: September 2022	PROJ NO.: 01847-0001.00													

EXHIBIT 9



Legend

- ◆ Plymouth Municipal Airport
- ◆ Cranberry Point Energy Storage Facility

Distance from Cranberry Point to
 Plymouth Airport: 3 Miles



Proximity to Plymouth Municipal Airport

Save the Pine Barrens
 Plymouth, MA

DRAWN BY:	C.Q.	CHECKED BY:	J.H.
DATE:	September 2022	PROJ NO.:	01847-0001.00

